ALB-242
2.2.4.21

VIA ELECTRONIC MAIL ONLY

Memorandum

To: Ann Demint
Middle Rio Grande Project Manager

From: Mark Nemeth \s\
Manager, Technical Services Division

Subject: Geomorphic and Hydraulic Assessment of the Isleta to San Acacia Reach

The Albuquerque Area Office Technical Services Division has completed our assessment on the reach between Isleta Diversion Dam and San Acacia Diversion Dam and it is presented in the attached reports. The geomorphic and hydraulic assessments present historic trends and current conditions, and also provide recommendations on needs for river maintenance and opportunities for habitat restoration in the reach. Those findings are described below:

- The geomorphic and hydraulic reports found that in the last century the annual volume of water and sediment passing through this reach has decreased, and in response the main channel has narrowed and slightly deepened.
- In the last few decades (1992-2012), the channel's mean bed elevation has incised on average less than one foot and the 5,000 cfs water surface elevation has increased on average less than one foot with the exception of the vicinity around the Rio Puerco down to the San Acacia Diversion Dam where the bed has had alternating periods of aggradation and degradation. These minimal changes are indicative of bed stability.
- The main channel conveyance capacity has had varying trends over the years as the channel adjusted to wetter and drier hydrologic periods. Based on 2015 data, the bank overtops on average at 4,600 cfs in the Isleta to Rio Puerco reach, and on average at 5,500 cfs in the Rio Puerco to San Acacia Reach. Some areas begin to overbank as low as the 2,000 to 3,000 cfs range.
- Based on 2015 data, the high water threat to the levees was greatest in the Isleta to Highway 309 (Belen) reach. The water surface is at the same elevation as the levee toes at an average flow of 3,100 cfs in the Isleta to Rio Puerco reach. The water surface is at the same elevation as the levee toes at an average flow of 8,800 cfs in the Rio Puerco to San Acacia reach.
- The banks are higher than the levee toes (perched condition) from Isleta to Highway 309, and in the rest of the reach the banks are similar in elevation to the levee toes.

Subject: Assessment of the Isleta to San Acacia Reach

The recommendations developed from the assessment are described below:

- Channel narrowing and the increased channel velocities are detrimental for fish habitat. Channel velocities can be decreased by lowering floodplains, widening the channel including the use of side channels, or decreasing the energy slope.
- Perched channel conditions combined with overbanking at lower flows can be a potential threat to the levees through avulsion and prolonged saturation, and overbanking with no return path can strand fish. Side channels and strategic bank lowering should be created to provide preferred paths for the fish and water to return to the main channel in the Isleta to Belen reach.
- A very steep zone immediately downstream of the Rio Salado may limit fish migration. The slope and velocity in this zone should be investigated to determine the impacts, if any, to fish migration.

If you have any questions or comments on this document, please contact me at (505) 462-3615, Robert Padilla at (505) 462-3626, or Michelle Klein at (505) 462-3628, of my staff.

Attachments (4):
Geomorphic Report-Final.pdf
Geomorphic Report-Final-Appendix A.pdf
Geomorphic Report-Final-Appendix B.pdf
Hydraulic Modeling Report-Final.pdf

cc: ALB-600 (LWoodruff), ALB-200 (MNemeth), ALB-240 (RPadilla), ALB-242 (MKlein) (w/att to all)

RECLAMATION

Managing Water in the West

Isleta to San Acacia Hydraulic Modeling Report

Middle Rio Grande Project, NM

Upper Colorado Region

U.S. Department of the Interior
Bureau of Reclamation

December 2018

Mission Statements

The mission of the Department of the Interior is to protect and manage the Nation's natural resources and cultural heritage; provide scientific and other information about those resources; and honor its trust responsibilities or special commitments to American Indians, Alaska Natives, and affiliated island communities.

The mission of the Bureau of Reclamation is to manage, develop, and protect water and related resources in an environmentally and economically sound manner in the interest of the American public.

Isleta to San Acacia Hydraulic Modeling Report

Middle Rio Grande Project, NM

Upper Colorado Region

Report Prepared by
Michelle Klein, PE, Hydraulic Engineer
Jonathan AuBuchon, PE, Hydraulic Engineer
Tony Lampert, PE, Hydraulic Engineer
Cameron Herrington, EIT, Hydraulic Engineer

Report Reviewed by
Ari Posner, PhD, Physical Scientist
Aubrey Harris, PE, Hydraulic Engineer

Reclamation River Analysis Group,
Technical Services Division

Cover Photographs. Rio Grande looking downstream near agg-deg line 1091 by Suzanne Devergie on July 28, 2016

U.S. Department of the Interior
Bureau of Reclamation

December 2018

CONTENTS

Executive Summary

The Bureau of Reclamation (Reclamation) has authority for river channel maintenance on the Rio Grande between Velarde, New Mexico, and the headwaters of the Caballo Reservoir. Reclamation regularly monitors changes in the river channel and evaluates channel and levee capacity in an effort to identify river maintenance sites where there is concern about possible damage to riverside facilities. The Rio Grande between Isleta and San Acacia Diversion Dams was identified as an area of river maintenance concern due to confinement by spoil levees on both sides and the increasing vegetation encroachment. This reach is approximately 53 river miles in length and flows through the communities of Isleta Pueblo, Los Lunas, and Belen. This report subdivided the 53 mile reach into two separate reaches based on their similar geomorphic conditions and trends.

This report provides an analysis of channel hydraulics, channel equilibrium, and bank stability within the Isleta Dam to Rio Puerco and Rio Puerco to San Acacia reaches. This assessment helps evaluate river system changes and aids in understanding and identifying future work needs.

Major findings associated with channel hydraulics, channel equilibrium, and bank stability between Isleta and San Acacia are summarized as follows:

- The energy grade slope of the Rio Grande through the Isleta to San Acacia reach has decreased from the 1980s to early 2010s. The slope of the Rio Grande from Isleta to the Rio Puerco has decreased from the 2000s to the early 2010s, while the slope of the Rio Grande from Rio Puerco to San Acacia has increased during the same time period.
- The average energy grade slope between 1962 and 2012 for Isleta to Rio Puerco was 0.00083 ft/ft while the average energy grade slope for Rio Puerco to San Acacia was 0.00085 ft/ft.
- Reclamation (2012) 1-D mobile bed modeling estimated that the 20-year future equilibrium slope for the Isleta to Rio Puerco and Rio Puerco to San Acacia reaches as 0.00077 ft/ft and 0.00076 ft/ft respectively. (Section 4.1 Energy Slope p.15).
- The river cross sectional flow area and wetted perimeter on the Rio Grande through the Isleta to San Acacia reach have decreased from the 1970s to early 2010s. (Sections 4.2 Flow Area p.16 and 4.3 Wetted Perimeter p.17).
- The hydraulic radius (surrogate for channel depth) on the Rio Grande through the Isleta to San Acacia reach has increased from 2002 to 2012. Between 1962 and 2002 the changes in the hydraulic depth were minimal (Section 4.4 Hydraulic Radius p.18).

- The mean velocity on the Rio Grande through the Isleta to San Acacia reach remained relatively constant between 1962 to 2002 and then increased from 2002 to 2012 (Section 4.5 Mean Velocity p.19).
- The width to depth ratio on the Rio Grande through the Isleta to San Acacia reach has decreased from the 1970s until the early 2010s. The rate of decrease for the Rio Puerco to San Acacia reach is five times greater than the observed decrease in the Isleta to Rio Puerco reach (Section 4.6 Width/Depth Ratio p.20).
- For Isleta to San Acacia, the reach average distance between the minimum channel elevation and the bank ("bank height") has increased between 2002 and 2012. This likely indicates channel incision, and is supported by results from the 2018 Isleta to San Acacia Geomorphic Analysis (Klein et al 2018). However, this has not always been the trend, with alternating trends of increasing and decreasing bank heights since 1962 (Section 4.7 Bank Height, p. 21).
- For Isleta to San Acacia, the reach average distance between the 5,000 cfs water surface elevation and the bank ("freeboard") has had alternating trends of increasing and decreasing distances between 1962 and 2012 (Section 4.7 Bank Height, p. 21).
- More recently, between 2002 and 2012 the reach average distance between the 5,000 cfs water surface elevation and the bank ("freeboard") decreased for the Isleta to Rio Puerco reach, and increased for the Rio Puerco to San Acacia reach. If the freeboard is used as a surrogate for conveyance capacity, then between 2002 and 2012 the conveyance capacity is decreasing between Isleta and Rio Puerco, and increasing between Rio Puerco and San Acacia. However, since these trends have not held steady since 1962, there is a reasonable likelihood of changing trends in the near future (Section 4.7 Bank Height, p. 21).
- The normal shear stress on the Rio Grande channel bed and banks through the Isleta to San Acacia reach has increased between 2002 and 2012 (Section 4.8 Normal Shear Stress, p. 23).
- The bankfull discharge for Isleta to San Acacia has varying trends between 1962 and 2012, which indicates the channel's adjustment to both wetter and drier hydrologic periods. 2012 has the lowest bankfull discharge value than the earlier evaluated years, likely indicating a drier hydrologic period. (Section 4.9 Bankfull Discharge, p. 24).
- The water surface elevation (WSE) at 5,000 cfs has remained relatively stable (fluctuations of about two feet) from 1962 to 2015 between Isleta and the HWY-346 Bridge (Section 4.10 Water Surface Elevation at 5,000 cfs, p. 25).
- The 5,000 cfs WSE dropped between HWY-346 and San Acacia Diversion Dam from 1972 to 1992 (as much as 10 feet at the Rio Puerco confluence). This drop in WSE was not seen in the vicinity of the Rio Salado, suggesting that the Rio Salado may have acted as a localized grade control. Since 1992 the 5,000 cfs WSE has been slowly increasing (Section 4.10 Water Surface Elevation at 5,000 cfs, p. 25).

- The 5,000 cfs WSE profiles at the Rio Salado and just below its confluence with the Rio Grande show a dramatic drop in water surface elevation over a short longitudinal distance. This steep zone may limit fish migration given the large drop.
- In the 2014/2015 current geometry model, banks are overtopped at an average of 4,600 cfs in the Isleta to Rio Puerco reach, and banks are overtopped at an average of 5,500 cfs in the Rio Puerco to San Acacia reach (Section 4.11 Current Hydraulic Profile, p. 30).
- In the 2014/2015 current geometry model, the main channel's average water surface elevation reaches the same elevation as the levee toes at an average flow of 3,100 cfs in the Isleta to Rio Puerco reach, and an average flow of 8,800 cfs in the Rio Puerco to San Acacia reach (Section 4.11 Current Hydraulic Profile, p. 30).
- Banks throughout the reach are susceptible to toe erosion, although the current vegetation and soil material indicates bank stability up to discharges of 20,000 cfs. (Section 5.3 BSTEM Results, p.35).
- The bank areas identified as having the highest risk for lateral migration include the following: around Los Lunas, NM; downstream of Abo Arroyo (near Veguita, NM), and just upstream of the Rio Puerco confluence. (Section 5.3 BSTEM Results, p.35).
- Current channel conditions in the Isleta to San Acacia Reach are close to the stable channel dimensions (slope, depth, and width) predicted by the Copeland Method for discharges between 4,000 and 7,500 cfs. This suggests the geomorphic influence of peak flow conditions during the spring snow-melt runoff (Section 6.1.2 Results for Copeland Method, p.40).
- The Rio Grande within the Isleta to San Acacia reach doesn't fit the predicted stable channel conditions of the regime equations, suggesting more of a dependence on the suspended sediment load than the bed load (Section 6.1.3 Results for the Regime Method, p. 42).
- Tractive Force estimates for a stable channel suggest that sand bed particles will be mobile at discharges as low as 750 cfs (Section 6.1.4 Results for Tractive Force Method, p. 44).
- Measured total sediment loads on the Rio Grande through the Isleta to San Acacia reach ranged from around 19,000 tons/day during the peak discharges of the 2017 spring snow-melt runoff to around 400 tons/day as measured at the tail-end of the runoff (Section 7.1.2 Measured Total Load Results, p.46).
- Physical measurements of total load on the Rio Grande during the 2017 spring snow-melt runoff generally indicate the total sediment load decreases with distance downstream for the Isleta to San Acacia reach. Peak measured total sediment loads are correlated with the peak discharge, while there is a larger scatter in the measured total sediment loads on the falling limb than the rising limb of the spring snow-melt runoff (Section 7.1.2 Measured Total Load Results, p.46).

- Sediment within the Isleta to San Acacia reach moves in suspension and along the bed, except at very low discharges (Section 7.1.3 Comparison of BORAMEP Calculations with Field Estimates, p.48).
- Sediment load measurements during the 2017 spring snow-melt runoff indicate sediment was depositing between Isleta Diversion Dam and Belen, NM in an amount larger than the following sub reaches. The river sub reach between Belen, NM and the Abo Arroyo confluence tended to be more erosional. The Rio Grande between Abo Arroyo and below the Rio Puerco tends to be more depositional; however, sediment was observed to be mobilized out of this sub reach during the falling limb of the 2017 spring snow-melt runoff (Section 7.1.4 Comparison of Total Load Measurements between Rangelines, p. 51).
- Nominal riprap size required for bank protection within the Isleta to San Acacia reach primarily range between 4 and 18 inches. Larger riprap is estimated to be needed at the Drain Unit 7 river maintenance site (Section 8.2 Riprap Results, p.56).
- Estimated scour within the Isleta to San Acacia reach ranges from 0 to 10 feet for a design discharge of 4,000 cfs. The highest potential scour occurs around the U.S. Highway 60 Bridge and near the Rio Puerco RM 127.9, La Joya, and Drain Unit 7 river maintenance sites (Section 9.2 Scour Results, p. 59).

1.0 Introduction

The Isleta Dam to Rio Puerco and the Rio Puerco to the San Acacia reaches are classified as a Maintenance Class 3B river maintenance reach (Maestas et al., 2014). There are currently ten (10) river maintenance sites identified by Maestas et al. (2014) within these two reaches– one (1) Maintenance Class 3A sites (RM 121), seven (7) Maintenance Class 3B sites (NM 6 Bridge, Highway 309 Bridge, Rio Puerco 127.9, Rio Puerco 127.5, Rio Puerco 127.0, La Joya, and Bernardo Arroyo), and two (2) class 4 sites (Los Trujillos and DU7). The scope of this analysis focuses on channel hydraulics, bank stability, and stable channel conditions for these two reaches.

The two reaches being assessed are shown in Figure 1. The two reaches combined span a little over 53 miles from river mile (RM) 169.3 at the Isleta Diversion Dam to RM 116.2 at the San Acacia Diversion Dam.

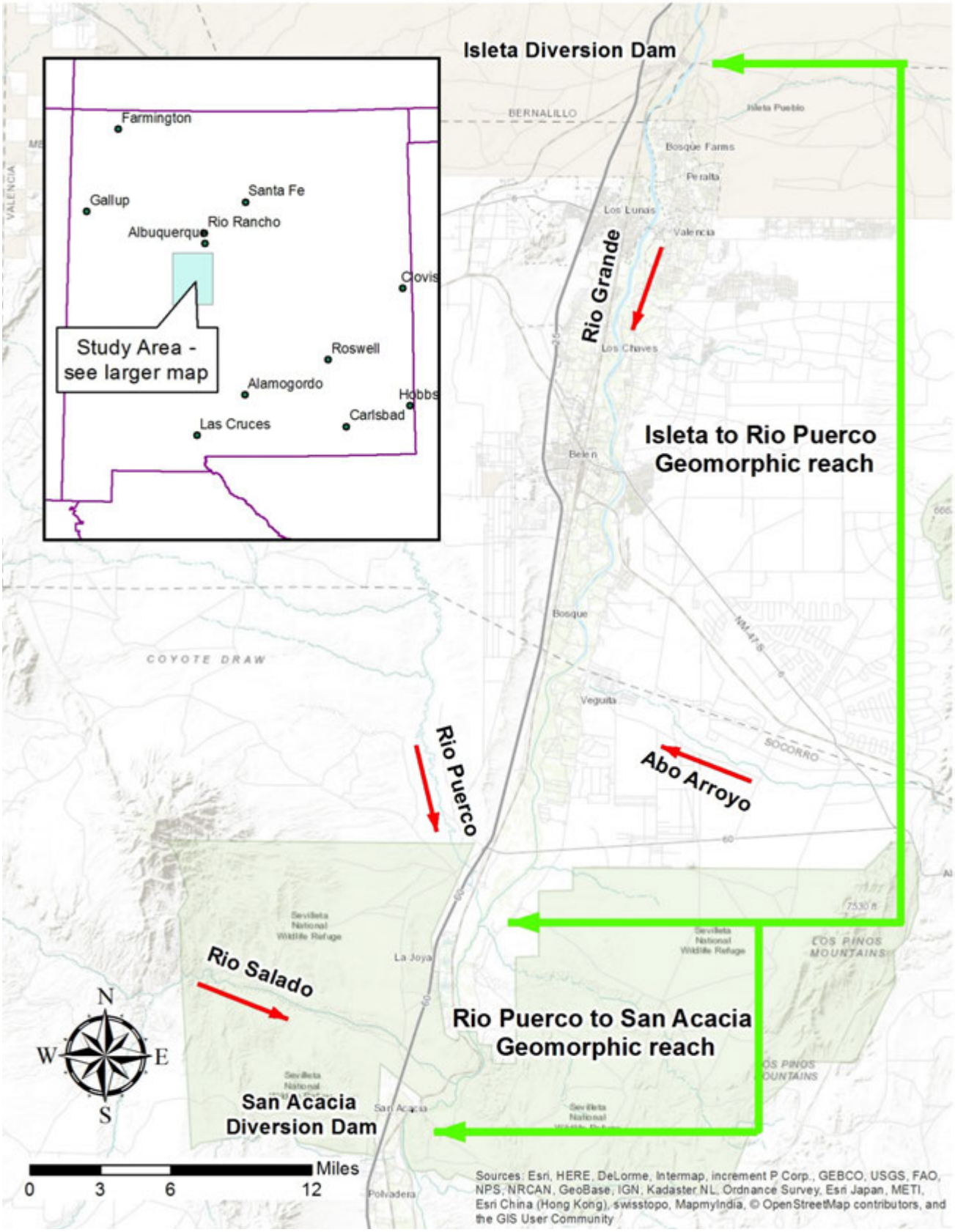

Figure 1. Isleta to San Acacia Study Area and geomorphic reach designation.

2.0 Background Information

Over the years a number of studies have occurred on the Rio Grande between the Isleta and San Acacia Diversion Dams and two of its primary tributaries– the Rio Puerco and the Rio Salado. An overview of these studies can be found in Aubuchon's 2015 report "Isleta to San Acacia Reach Overview of Previous Work." In the early 1960s Culbertson and Dawdy (1964) performed river measurements on the Rio Grande in the Casa Colorado reach. This study reported a range in roughness (Manning's n values) from 0.0122 to 0.028 over a discharge range of 800 to 8,300 cfs. Culbertson and Dawdy suggested that a distinctive roughness change occurred between upper-regime and lower-regime flows (high flow versus low flows), with the roughness of the upper-regime flows primarily a function of the bed material size. Culbertson and Dawdy also recorded a change in the water surface elevation in association with the regime change from lower to upper regime flows. Nordin and Beverage (1965) also suggested that the bed configuration played a role in the roughness. While studying the Rio Puerco, Nordin (1963) found that Manning's n values were independent of the suspended sediment concentration and independent of whether the antecedent bed condition was cohesive or noncohesive.

Simons et al. (1981) looked at the flood routing effects on the Rio Grande from large floods on the Rio Salado and Rio Puerco tributaries. Their analysis showed the possibility of sediment deposition from these tributaries at each of the confluences that could raise the water surface elevation as much as 5.5 feet, with an average around 2.2 feet. In the early 2010s, Tetra Tech (2014a; 2014b) performed 2-dimensional numerical modeling between the Isleta and San Acacia Diversion Dams and estimated the following inundated areas outside the active channel that met the low velocity (< 1.5 ft/sec) and low depth (< 1.5 ft) criteria for the Rio Grande Silvery Minnow:

- At 2,000 cfs – No inundation
- At 3,500 cfs – ~50 acres are inundated
- At 5,000 cfs – ~2,100 to 2,800 acres are inundated
- At 7,000 cfs – ~3,270 acres are inundated
- At 10,000 cfs – ~3,300 acres are inundated

This report is meant to augment and build upon these studies, assessing contemporary channel dynamics in the reach. The scope of this report evaluates channel hydraulics, bank stability, and stable channel design. The development and analyses performed using these models are described in the sections that follow.

3.0 Hydraulic Modeling Development

One-dimensional numerical hydraulic modeling is useful to estimate average hydraulic conditions, such as velocity and shear stress, through a study area. The geomorphic analysis (Klein et al., 2018) also utilizes results from the one-dimensional numerical hydraulic modeling to assess energy grade slope and bed material stability. One-dimensional numerical hydraulic modeling was accomplished using the U.S. Army Corps of Engineers (USACE) HEC-RAS River Analysis System (version 5.1.0). The details of that model are described in the following sections.

3.1 Current Geometry Model (2015)

A HEC-RAS model was developed to simulate the river conditions found in 2015 based on river cross section geometry from 2014 and 2015. The geometry for the model was first developed in USACE's HEC-GeoRAS extension for ESRI's ArcMap (version 10.1), and then later refined after importation into USACE's HEC-RAS (version 5.1.0). Additional cross sections were interpolated for numerical stability. A Manning's n value was calibrated for both base and high flow conditions.

3.1.1 Geometry Development

The channel geometry for this model was collected between 2014 and 2015 through hydrographic field surveys as shown in Table 1. One hundred and two river cross sections between Isleta Diversion Dam and San Acacia Diversion Dam were surveyed during this time frame. Figure 2 through Figure 4 show the locations of the surveyed cross sections used in the generation of this hydraulic model. Twenty eight cross sections downstream of San Acacia Diversion Dam were also included in the model to create stability in the model's area of study.

Collection time frames and references for each data collection effort are shown in Table 1. Only six cross sections in this reach were not surveyed in 2014 or 2015. The modeled cross sections are listed in Table 1.

Table 1: Data Sources for cross sections used in the model. 102 cross sections are between Isleta and San Acacia Diversion Dams, and 28 cross sections are downstream of San Acacia Diversion Dam.

Cross Sections	Dates Collected	Report Citation
IS-684 through CO-877 (36 cross sections)	March 2014	(Southwest Water Design, 2014)
IS-880 through RP-1205.8 (66 cross sections)	May-Aug 2015	(Easterling, 2015)
SA-1207 through SA-1246 (28 cross sections)	November 2014	(Southwest Water Design, 2015)

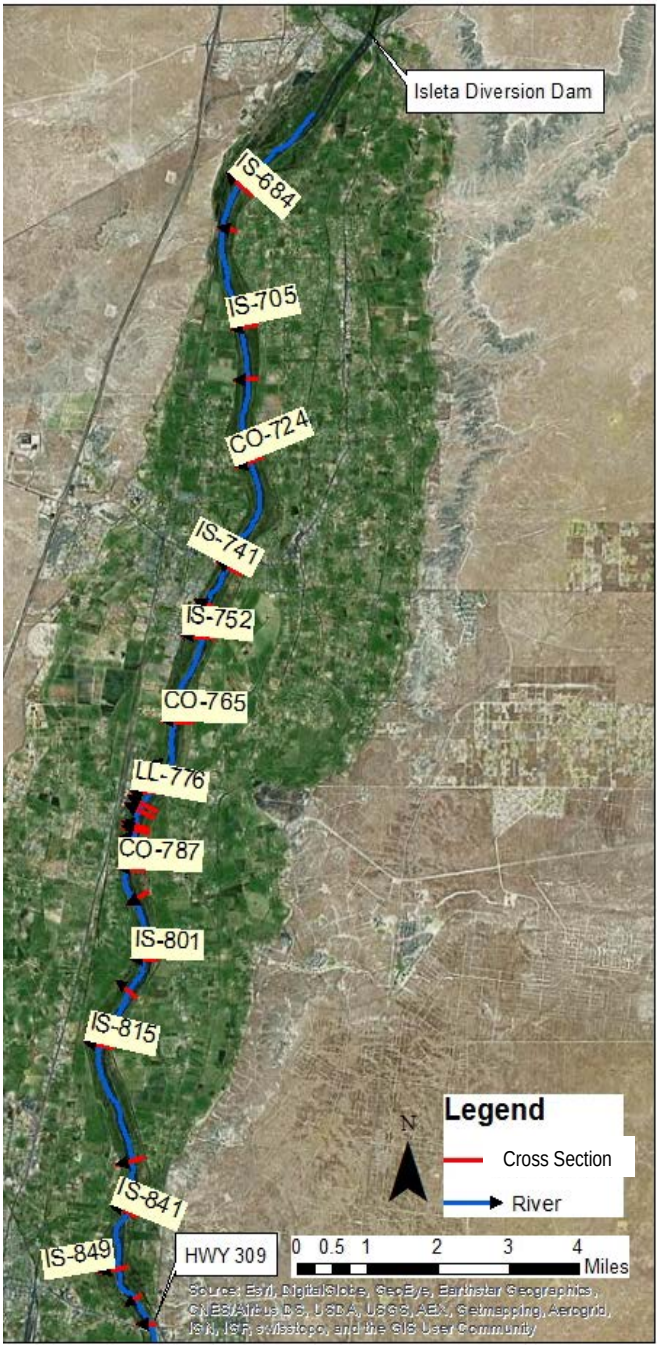

Figure 2: Cross sections used to develop HEC-RAS 1D model geometry, from Isleta Diversion Dam to Highway 309 in Belen, NM.

Figure 3: Cross sections used to develop HEC-RAS 1D model geometry, from Highway 309 to Highway 60.

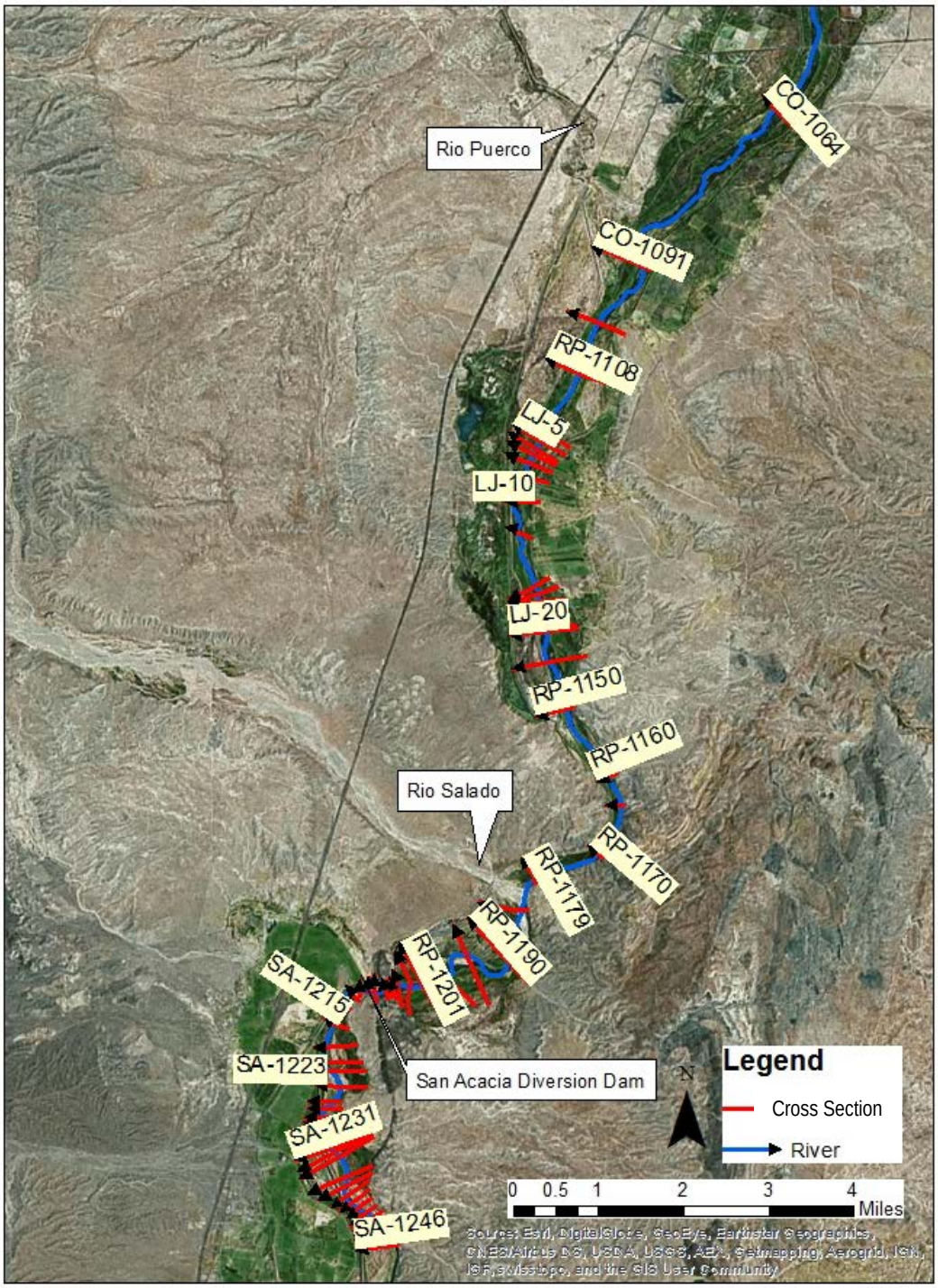

Figure 4: Cross sections used to develop HEC-RAS 1D model geometry, from Highway 60 to San Acacia Diversion Dam.

Neither Isleta nor San Acacia Diversion Dams were included in the model, since the objective was to look at average hydraulic characteristics for this 53 mile stretch of river. To facilitate numerical model convergence within the study area, the model was extended approximately four miles (28 cross sections) downstream

of San Acacia Diversion Dam. This made a total of 130 cross sections in the model.

The floodplain elevation data for this model is a subset of data that was collected aerially in February 2012 for the entire Middle Rio Grande (Woolpert, 2012). The data included LiDAR and 4-band aerial photography. The NSSDA vertical accuracy at the 95% confidence level was 1.1 feet (Benoit, 2013).

While developing the cross sections in HEC-GeoRAS, the 2014-2015 field-collected data points were given preference over the 2012 LiDAR data by filtering out all LiDAR points located within 10 feet of the field-collected data points.

The left, channel, and right reach lengths were determined in HEC-GeoRAS using the "flow path" feature. The HEC-GeoRAS 4.2 User's Manual instructs, "A flow path line should be created in the center-of-mass of flow in the main channel, left overbank, and right overbank for the water surface profile of interest." (USACE, 2009, p. 8-10) Thus the right and left flow path lines were hand-drawn by looking at aerial imagery and using engineering judgement to determine the center-of-mass of flow. For the channel flow path, the line was copied from the 2012 river centerline shapefile created from the 2012 aerial imagery (Reclamation, unpub. data, 2013).

The bank stationing (where Manning's n changes from an overbank value to a channel roughness value) was assigned in HEC-GeoRAS from the 2012 LIDAR bank line shapefile (Woolpert, unpub. data, 2012).

Levees were created in HEC-RAS by visual examination, according to the following principle from the HEC-RAS 4.1 User's Manual: "When levees are established, no water can go to the left of the left levee station or to the right of the right levee station until either of the levee elevations is exceeded." (USACE, 2010a, p. 6-17). Thus high areas adjacent to the bank were established as the levee since it is assumed that low areas past the channel will not be flowing until those high elevations adjacent to the channel are exceeded.

To ensure that no flow went past the spoil levees in the interpolated cross sections (interpolations are described below), areas past the designated HEC-RAS levees were modeled as obstructions. The HEC-RAS 4.1 User's Manual gives the definition: "Obstructions decrease flow area and add wetted perimeter when the water comes in contact with the obstruction." (USACE, 2010a, p. 6-19).

Additional cross sections were interpolated at a 100 foot spacing for the entire reach to minimize numerical modeling errors.

3.1.2 Boundary Conditions

The model is run as subcritical steady flow. The downstream boundary condition is normal depth with a slope of 0.000773 which is the slope between SA-1207

(the first rangeline downstream of San Acacia Diversion Dam) and SA-1246 (the last cross section of the model).

3.1.3 Manning's n Calibration

The overbank or floodplain roughness was assumed to be 0.1, as suggested by Vensel et al. (2006).

The channel roughness was used to calibrate the model. A single Manning's channel n value was assessed for the entire reach for two discharge scenarios. Since Manning's n values change based on the magnitude of flow, one value was determined for flows < 5,000 cfs and one value was determined for flows >5,000 cfs.

The goal of the calibration was to provide a best fit between the model's computed water surface elevation and the observed water surface elevation at established rangeline locations. The channel Manning's n value for the 2015 model was then adjusted until the root mean square error (RMSE) of the water surface elevations (WSEL) was minimized. The RMSE is defined in Equation 1.

Equation 1 (ASPRS, 2015).

$$RMSE = \sqrt{\frac{1}{n}\sum_{i=1}^{n}(WSEL_{i-model} - WSEL_{i-measured})^2}$$

Where RMSE = the root mean square error,
n = the number of analyzed cross sections,
i = the ith location of the analyzed cross sections,
$WSEL_{i\text{-}model}$ = the HEC-RAS modeled water surface elevation (NAVD88 datum, feet) at the i^{th} location, and
$WSEL_{i\text{-}measured}$ = the field measured water surface elevation (NAVD88 datum, feet) at the i^{th} location.

Flows <5,000 cfs

When the model's 130 cross sections were surveyed in 2014 and 2015, the water surface elevations were observed and recorded with the cross section data. The surveys took place on 23 different dates. The corresponding flow data for these 23 dates was pulled from USGS gages including the gage on the Rio Grande at Bosque Farms (USGS 08331160), Bosque (USGS 08331510), and San Acacia (USGS 08354900), and the gage on the Rio Puerco (USGS 08353000). Table 2 shows which gage data was used for each group of cross sections.

The calibration of cross sections is usually based on the flow data from the nearest gage, but there are some exceptions. The gage at Bernardo did not have 2015 flow data at the time of the analysis and was not used. The gage at San Acacia is downstream of the water withdrawals at San Acacia Diversion Dam; thus the flow from this gage was only applied to cross sections downstream of the dam. The

cross sections downstream of the Rio Puerco are calibrated based on combined flows from the Rio Grande at Bosque and the Rio Puerco.

Table 2: USGS gage flow data used for each cross section group

Cross Sections	USGS Gage	USGS Gage Number
IS-684 to IS-801	Bosque Farms	08331160
CO-806 to CO-1091	Bosque	08331510
RP-1100 to RP-1205.8	Bosque + Rio Puerco	08331510 + 08353000
SA-1207 to SA-1246	San Acacia	08354900

Flow data for each of the 23 survey dates was entered in the model in the steady flow file. When examining model results, it was found that the ten cross sections upstream from San Acacia Diversion Dam had significant differences between the computed and observed water surface elevations. These discrepancies are likely due to the hydraulics affected by the dam. Thus, those ten cross sections were not included with the other 92 cross sections in the Manning's n value calibration. The ten cross sections extend approximately 2 river miles upstream of the dam.

The calibrated model channel Manning's n value was found to be 0.032. This value was used in the model for discharges below 5,000 cfs.

Flows > 5,000 cfs

To calibrate Manning's n for high flows, water surface elevations from the 2005 high flow event were used. The data and collection methods are described in Tetra Tech's report (2005). Fifty one cross sections in the reach were surveyed over three days in 2005 during this high flow event. Only 42 of these cross sections were included in the RMSE calculation, since the seven cross sections just upstream of San Acacia Diversion Dam were excluded due to the hydraulic uncertainty surrounding San Acacia Diversion Dam.

The flows corresponding to the three survey days in 2005 were submitted to the model in the steady flow file. These flow values are shown below in Table 3.

The calibrated model channel Manning's n value was found to be 0.025. This value was used in the model for discharges above 5,000 cfs.

Table 3: High Flow Data used in High Flows Calibration

Reach	USGS Gage	USGS Gage Number	May 25, 2005 Flow (cfs)	May 26, 2005 Flow (cfs)	May 27, 2005 Flow (cfs)
IS-684 to IS-815	Isleta	08330875	6,000	5,770	5,710
CO-833 to CO-1091	Bernardo	08332010	5,570	5,720	5,690
RP-1100 to SADD	Bernardo + Rio Puerco	08332010 + 08353000	5,635	5,791	5,754

3.2 Historical Geometry Models (1962, 1972, 1992, 2002, and 2012)

In the 1960s, a set of lines known as the Aggradation/Degradation (Agg/Deg) lines was set up on the Rio Grande. These lines spanned from the Cochiti Diversion Dam to the headwaters of Elephant Butte Reservoir. The lines are set at 500 foot spacing to help evaluate repeat cross section changes roughly every decade. Because of the large scale nature of this data collection effort, photogrammetry has been employed to collect the necessary elevation data. Data collection efforts have occurred in 1962, 1972, 1985, 1992, 2002, and 2012, with an extraction of elevation data using photogrammetry techniques. Between 1962 and 2002 this has primarily involved the use of stereo models using aerial photography. In 2012, Light Detection and Ranging (LiDAR) sensors were used to collect elevation data remotely from reflected light pulses. The locations of the Agg/Deg lines for this study area are shown in Figure 5 through Figure 7.

3.2.1 Geometry Development

For each of the photogrammetry/LiDAR collection years, station and elevation data are extracted along the Agg/Deg lines. The extracted data typically has a vertical accuracy of +/- 1 foot (Woolpert, 2012; Benoit, 2013). The extracted data, however, does not capture the underwater channel prism, since photogrammetry techniques (both aerial photography and LiDAR) collect the elevation at the water surface. Reclamation's Technical Service Center (TSC) has developed an iterative program to approximate the underwater channel prism, generating HEC-RAS geometry files along the Agg/Deg lines that reflect the mean bed elevation at the time of the data collection (Holmquist-Johnson and Makar, 2006; Varyu, 2013). Every decadal year was used for this study, except 1985. There were inaccuracies in the collected data for 1985 that render it unusable for evaluating channel changes.

Bank and levee stations were assigned for this analysis to the HEC-RAS geometry models developed by TSC (1962, 1972, 1992, and 2002). The bank and levee stations were already assigned in the prepared 2012 model.

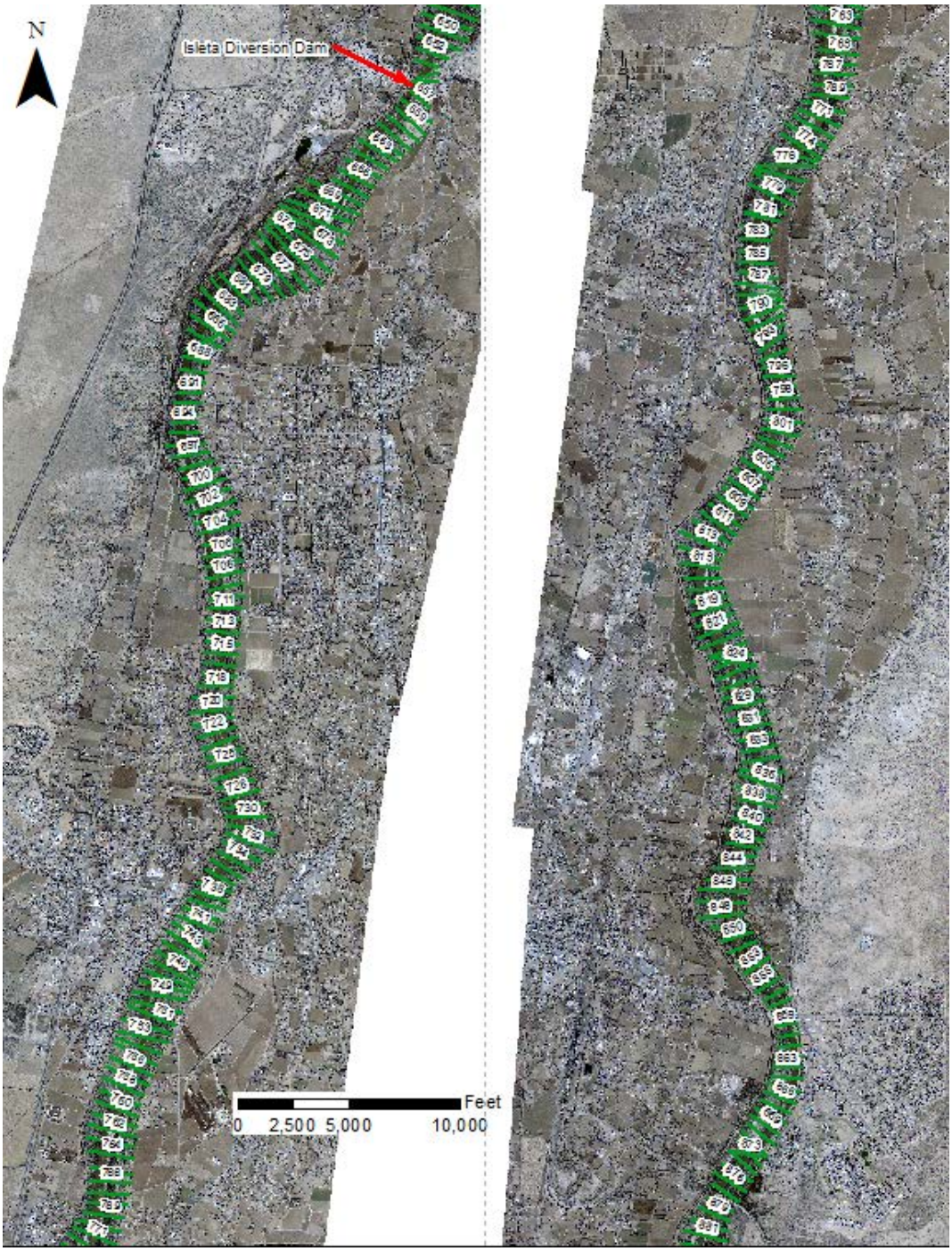

Figure 5: Study Area: Agg/Deg lines 655-880

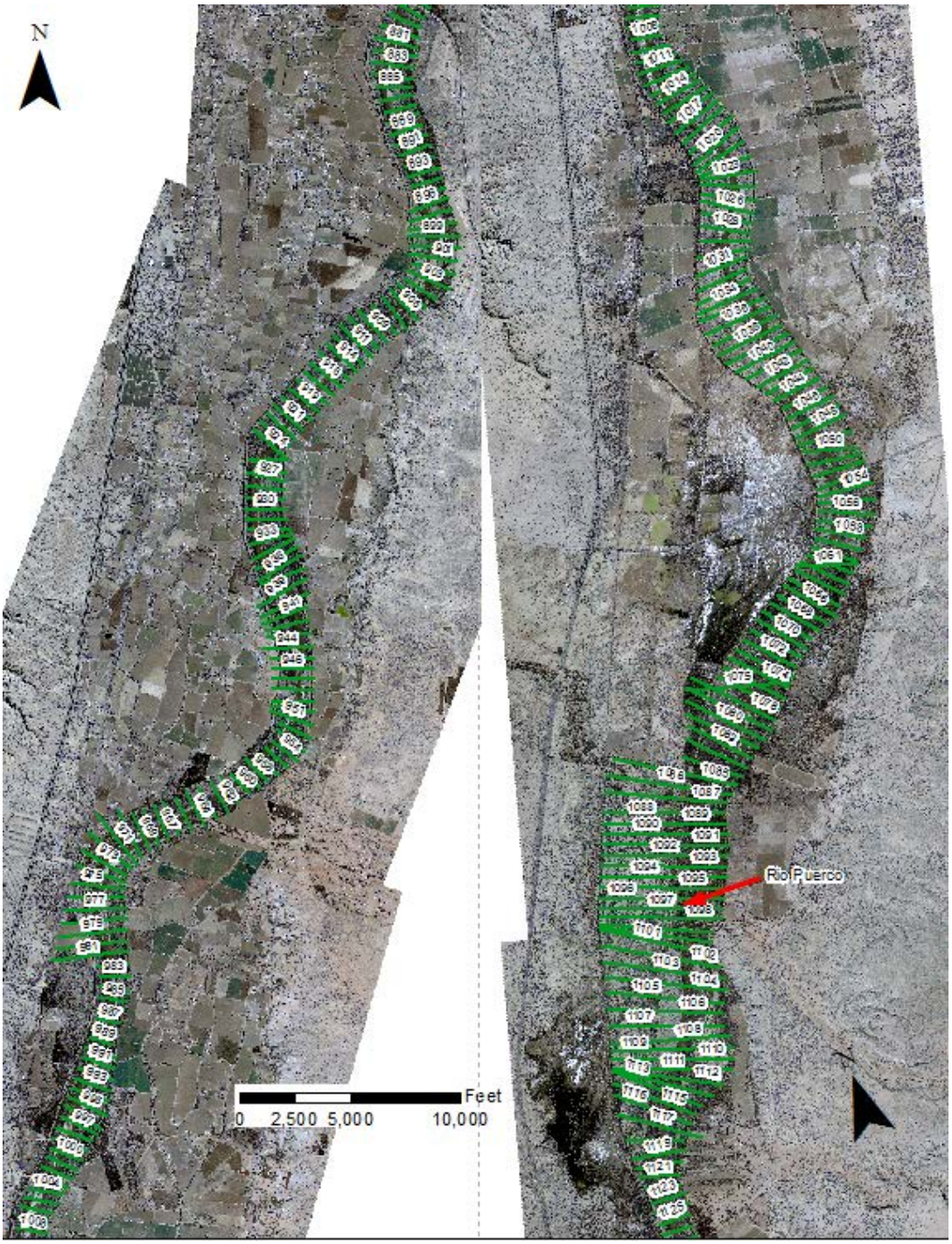

Figure 6: Study Area: Agg/Deg lines 881-1125

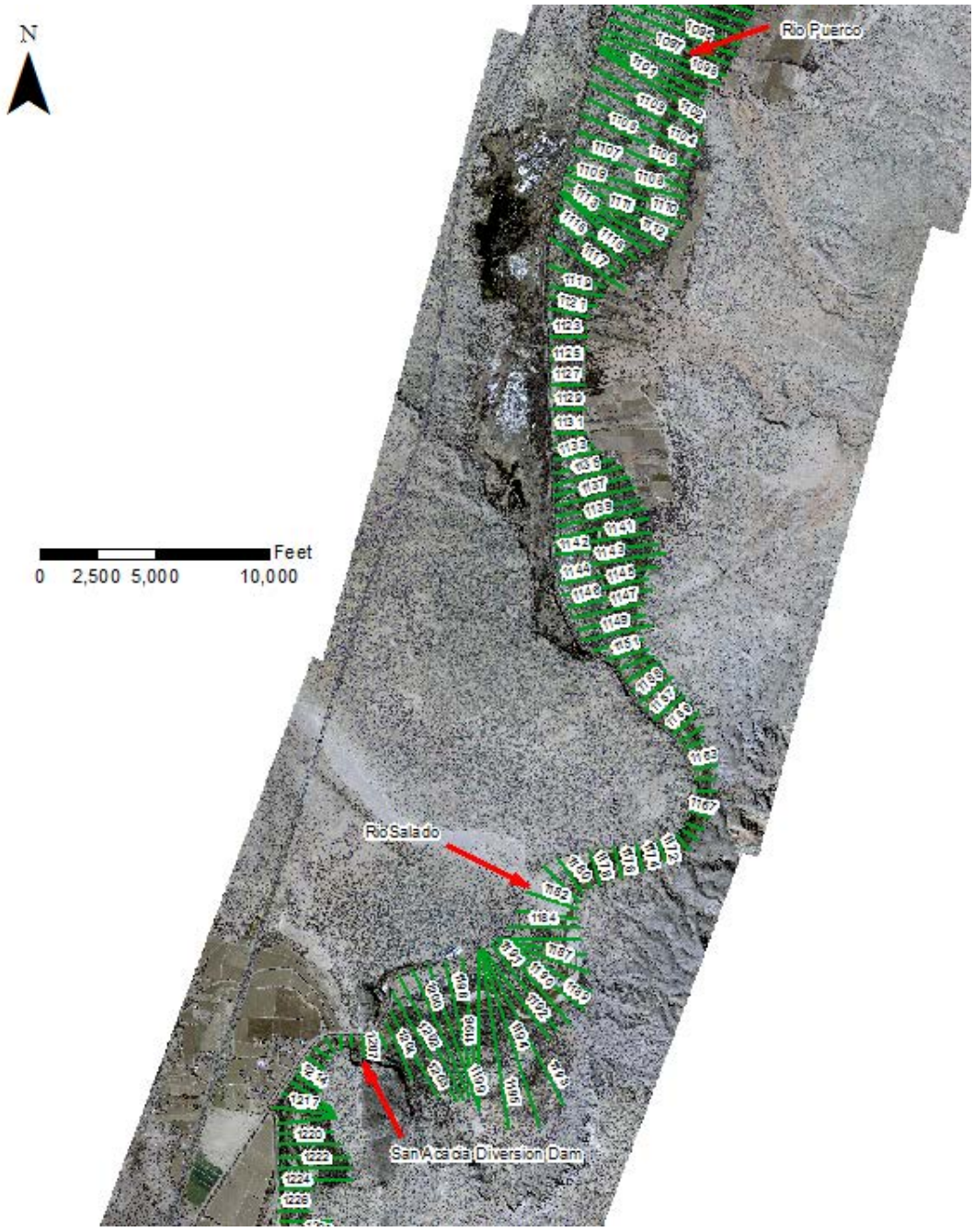

Figure 7: Study Area: Agg/Deg lines 1097-1206

3.2.2 Flow and Boundary Conditions

For each of the model geometries, the flow and boundary conditions listed in Table 4 were assigned. The model extents were not adjusted for this study, so modeled river lengths varied as follows: The 1962 and 1972 models spanned from Cochiti Diversion Dam to the San Acacia Diversion Dam. The 1992 and 2002 models spanned the extents of the study reach (Isleta Diversion Dam to San Acacia Diversion Dam). The 2012 model covered the distance from the Cochiti Flood Control Dam (1973) to the headwaters of Elephant Butte Reservoir.

The Manning's n values are based on values used by a Colorado State University study (Vensel et al., 2006) that evaluated channel changes on the Rio Grande between the Rio Puerco and the San Acacia Diversion Dam. For each of these models, cross-section averaged hydraulic information is extracted from the model runs within the study reach (between Agg/Deg line 655 and Agg/Deg line 1206).

A discharge value of 5,000 cfs was used to provide a consistent reference point between the years and be similar to the previous Colorado State University Studies (Vensel et al., 2006). This discharge value is close to the 2-year regulated peak flow values calculated by Wright (2010) for the USGS gage at Bernardo (4,900 cfs) and is of a similar magnitude to the USGS gages at Albuquerque (4,000 cfs) and San Acacia (7,800 cfs).

Table 4. Flow and Boundary Conditions for historical hydraulic modeling

Condition	Assigned Value
Flow Condition	Steady state, subcritical, constant flow (5,000 cfs)
Downstream boundary condition	Normal Depth (slope based on an average for that year's underwater channel prism)
Channel Manning's n value	0.019
Floodplain Manning's n value	0.1

4.0 Hydraulic Modeling Results

Hydraulic modeling results from the one-dimensional numerical models (HEC-RAS) for the historical model geometry were extracted into a Microsoft Excel spreadsheet (version 2013) for further analysis. The following hydraulic parameters were extracted from the HEC-RAS models at a discharge of 5,000 cfs: minimum channel elevation, water surface elevation, energy grade elevation, energy grade slope, channel velocity, cross sectional flow area, top width, hydraulic depth, hydraulic radius, total wetted perimeter, total and channel shear stress, and the right and left channel bank elevations.

The slope (energy grade line), flow area, wetted perimeter, hydraulic radius (as a surrogate for mean depth), mean channel velocity, width/depth ratio, total bank height, bank height above 5,000 cfs, and normal shear stress were evaluated for each of the two reaches within the study area: Isleta to Rio Puerco and Rio Puerco to San Acacia. The width/depth ratio was calculated by taking the wetted top width at 5,000 cfs divided by the hydraulic depth. Total bank height in this analysis represents the distance from the river bed to the top of the bank. The total bank height was calculated by taking the assigned elevation of both the right and left channel bank location and subtracting the minimum channel elevation. This gives two bank heights, one for the right bank and one for the left bank. By taking

the arithmetic average of the two heights a total bank height was calculated for each Agg-Deg line.

The bank height above the 5,000 cfs water surface elevation is calculated by taking the assigned elevation of both the right and left channel bank location and subtracting the water surface elevation, and then averaging the result from the two banks.

Each of the evaluated parameters are weighted by distance based on the applicable Agg-Deg line distances. Some models included all of the Agg-Deg lines, other models were missing a few lines that were infeasible to create during the model development. The downstream distances were used to weight each parameter value. The weighted distance was determined by taking half of the distance to the listed Agg-Deg line upstream and half of the distance to the listed Agg-Deg line downstream. A reach averaged value was then obtained by summing the distance-weighted value of each parameter for the Agg-Deg lines within that reach and dividing by the reach length. For the Isleta to Rio Puerco reach this included parameter values between Agg-Deg lines 655 and 1097. For the Rio Puerco reach this included parameter values between Agg-Deg lines 1098 and 1206. Observed trends in the hydraulic parameters are similar to results found in previous investigations by Richard et al. (2001) and Vensel et al. (2006).

4.1 Energy Slope

Changes in the reach averaged energy grade line slope between 1962 and 2012 are shown in Figure 8. The average energy grade slope for the Isleta to Rio Puerco reach is 0.00083 ft/ft between 1962 and 2012, while the average slope for the Rio Puerco to San Acacia reach is slightly steeper at 0.000851 ft/ft. Slope changes in the Isleta to Rio Puerco reach seem to lag behind the slope changes occurring in the Rio Puerco to San Acacia reach. The Rio Puerco to San Acacia reach appears to have gone through a period of a steepening slope from 1962 to 1992, slope flattening between 1992 and 2002, and then a slight flattening of the slope again from 2002 to 2012. The Isleta to Rio Puerco reach has a period of slope flattening from 1962 to 1972, a period of slope steepening from 1972 to 2002, and then a period of slope flattening from 2002 to 2012. Reclamation (2012) performed 1-dimensional numerical sediment and hydraulic modeling, estimating the equilibrium slope for the Isleta to Rio Puerco and Rio Puerco to San Acacia reaches as 0.00077 ft/ft and 0.00076 ft/ft, respectively. This would indicate that the future slope trend would be one of flattening compared to the estimated energy grade slopes.

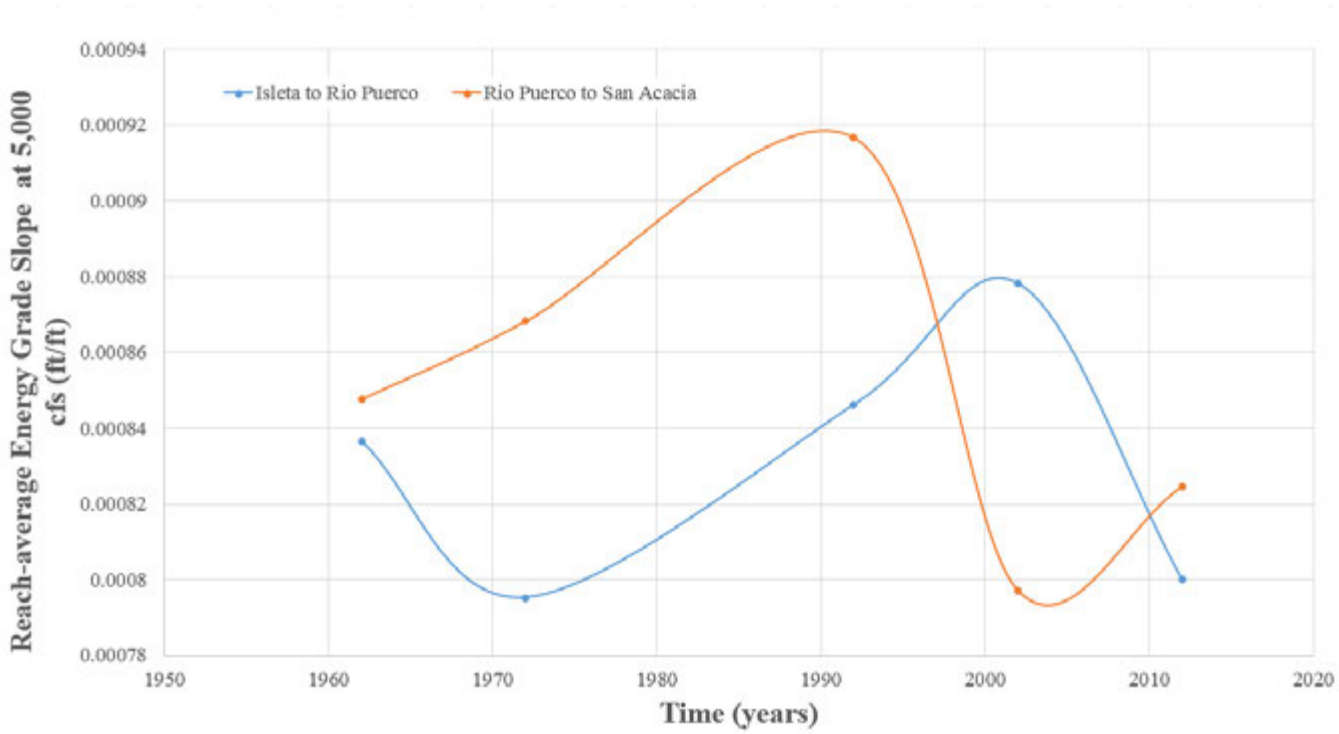

Figure 8. Reach Average Energy Grade Slope values for Isleta to Rio Puerco and Rio Puerco to San Acacia between 1962 and 2012

4.2 Cross Sectional Flow Area

Changes in the channel flow area at a discharge of 5,000 cfs are shown in Figure 9. The general trend for both the Isleta to Rio Puerco and Rio Puerco to San Acacia reach is a decrease in the cross sectional flow area at a discharge of 5,000 cfs between the early 1960s and early 2010s. The reach averaged cross sectional flow area decreased for both reaches between 1962 and 2012 is about 500 square feet at a discharge of 5,000 cfs.

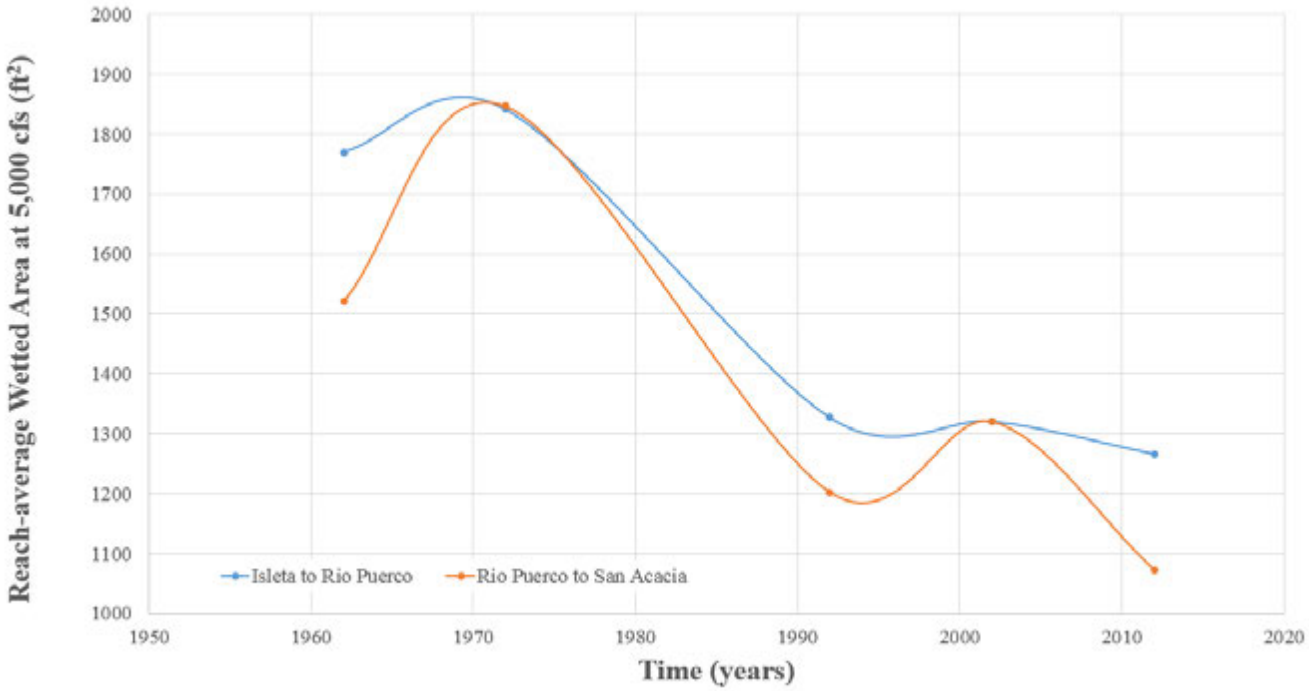

Figure 9. Reach Average Flow Area values for Isleta to Rio Puerco and Rio Puerco to San Acacia between 1962 and 2012

4.3 Wetted Perimeter

Changes in the wetted perimeter are shown in Figure 10. The reach averaged wetted perimeter trends mirror the cross sectional flow area trends for each time period and reach, although to different magnitudes. Like the cross sectional flow area, the general trend for wetted perimeter shows a decreasing trend for both the Isleta to Rio Puerco and Rio Puerco to San Acacia reaches. The reach averaged wetted perimeter decrease at a discharge of 5,000 cfs is about 370 feet for the Isleta to Rio Puerco reach during the period from 1962 to 2012 and 470 feet for the Rio Puerco to San Acacia reach for the same period.

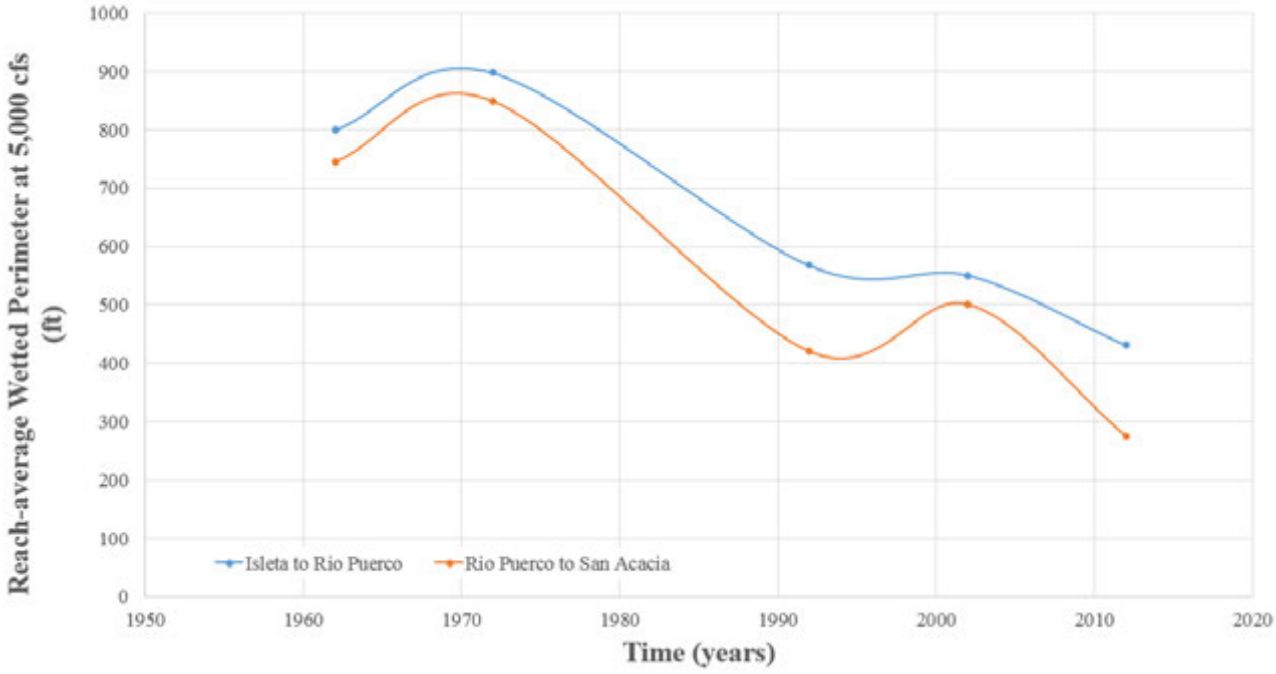

Figure 10. Reach Average Wetted Perimeter values for Isleta to Rio Puerco and Rio Puerco to San Acacia between 1962 and 2012

4.4 Hydraulic Radius

Changes in the reach averaged hydraulic radius, calculated as the cross sectional flow area divided by the wetted perimeter (USACE, 2010b), are shown in Figure 11. While not necessarily representing a specific channel depth at a given location in a river cross section, the hydraulic radius can be thought of as a surrogate for a mean cross sectional depth.

In the early 1960s, Culbertson and Dawdy (1964) measured a range of hydraulic radii between 1.6 and 5.5 on the Rio Grande in the Casa Colorado area (within the Isleta to Rio Puerco reach) for discharges ranging from 800 to 8,300 cfs. This is a similar range observed over time from the hydraulic modeling at 5,000 cfs. Between 1962 and 2002 the hydraulic radius between Isleta to Rio Puerco decreased about 0.4 feet. During the same time period the hydraulic radius for the Rio Puerco to San Acacia reach increased about 0.7 feet. Both reaches saw an increase in the hydraulic radius between 2002 and 2012 of around 1.3 feet. Considering the decreasing cross sectional flow area between 2002 and 2012, the increase in hydraulic radius indicates that the wetted perimeter is decreasing at a greater rate than the flow area is decreasing.

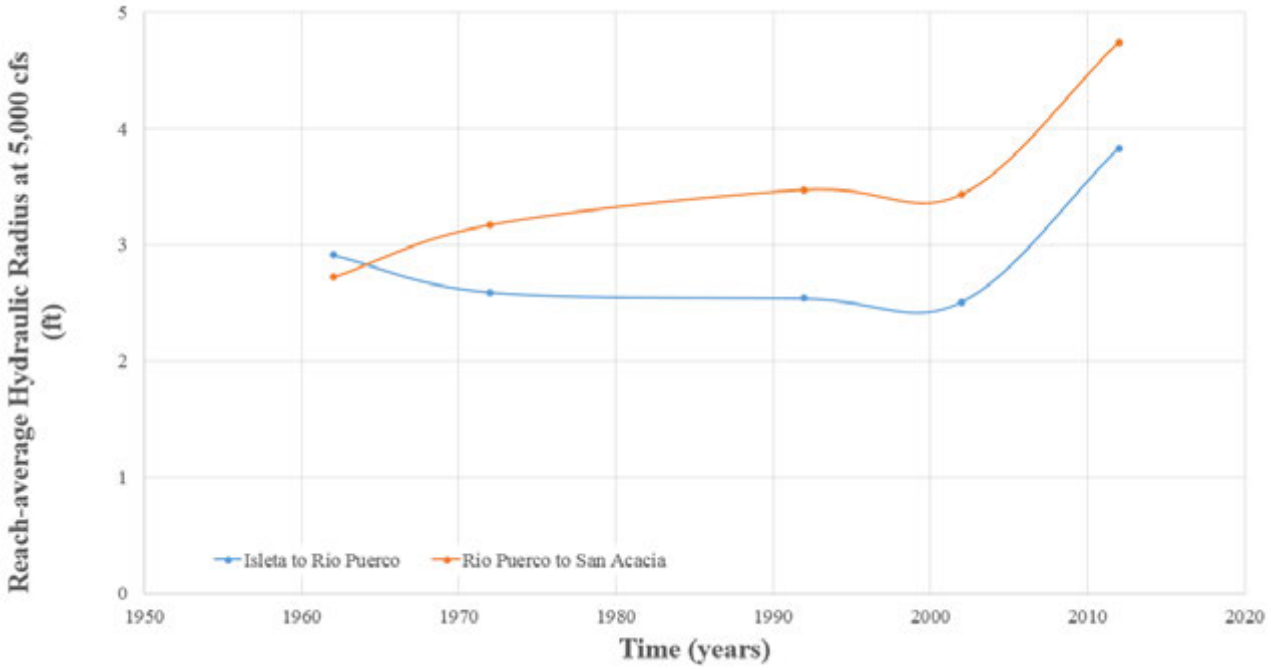

Figure 11. Reach Average Hydraulic Radius values for Isleta to Rio Puerco and Rio Puerco to San Acacia between 1962 and 2012.

4.5 Mean Velocity

Changes in the reach averaged mean channel velocity are shown in Figure 12. The mean channel velocity in the Isleta to Rio Puerco reach shows a slight reduction between 1962 and 2002, while the mean velocity within the Rio Puerco to San Acacia reach shows a slight increase. The mean channel velocity in both reaches increases a little over a foot per second between 2002 and 2012, which is consistent with the trend of decreasing reach average cross sectional flow area satisfying continuity. Culbertson and Dawdy (1964) measured velocity ranges in the early 1960s on the Rio Grande between 2 and 7 ft/sec in the Casa Colorado area (within the Isleta to Rio Puerco reach). These velocity measurements were over a discharge range of 800 to 8,300 cfs.

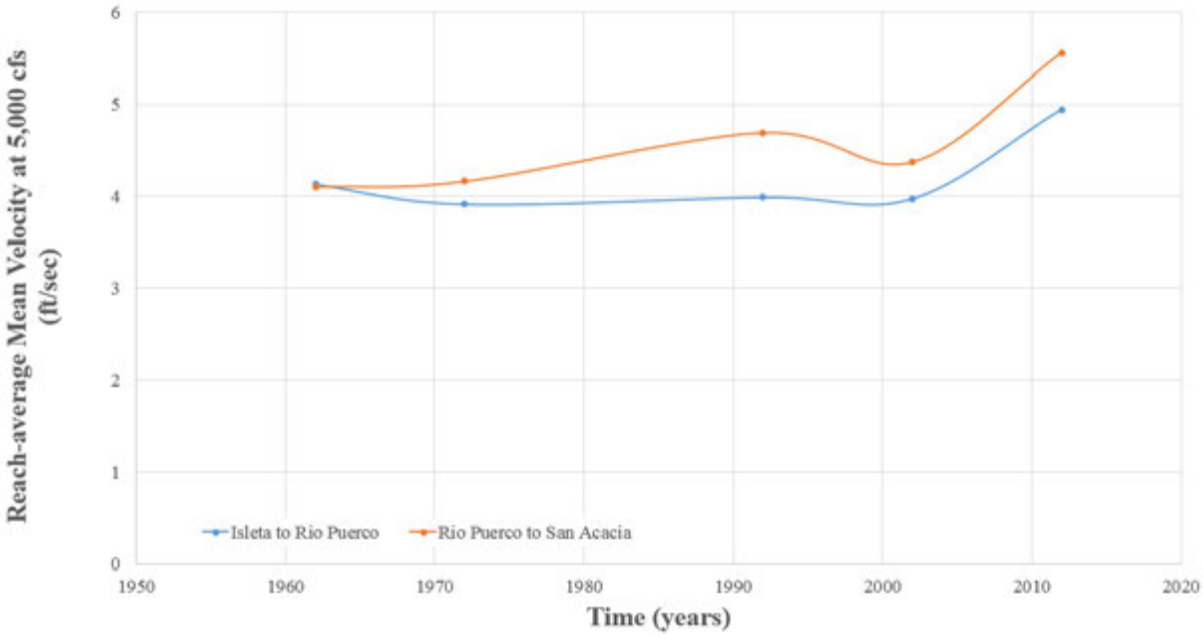

Figure 12. Reach Average Mean Velocity values for Isleta to Rio Puerco and Rio Puerco to San Acacia between 1962 and 2012

4.6 Width/Depth Ratio

Changes in the width/depth ratio are shown in Figure 13. Higher values indicate a wide, shallow river, while lower values indicate a narrow, deep river. The general trend between 1962 and 2012 is a decreasing ratio, indicating a deeper and/or narrower channel on average. In the Isleta to Rio Puerco reach the 2012 width/depth ratio is less than half of the 1962 width/depth ratio. In the Rio Puerco to San Acacia reach the 2012 width/depth ratio is approximately one fifth of the 1962 width/depth ratio.

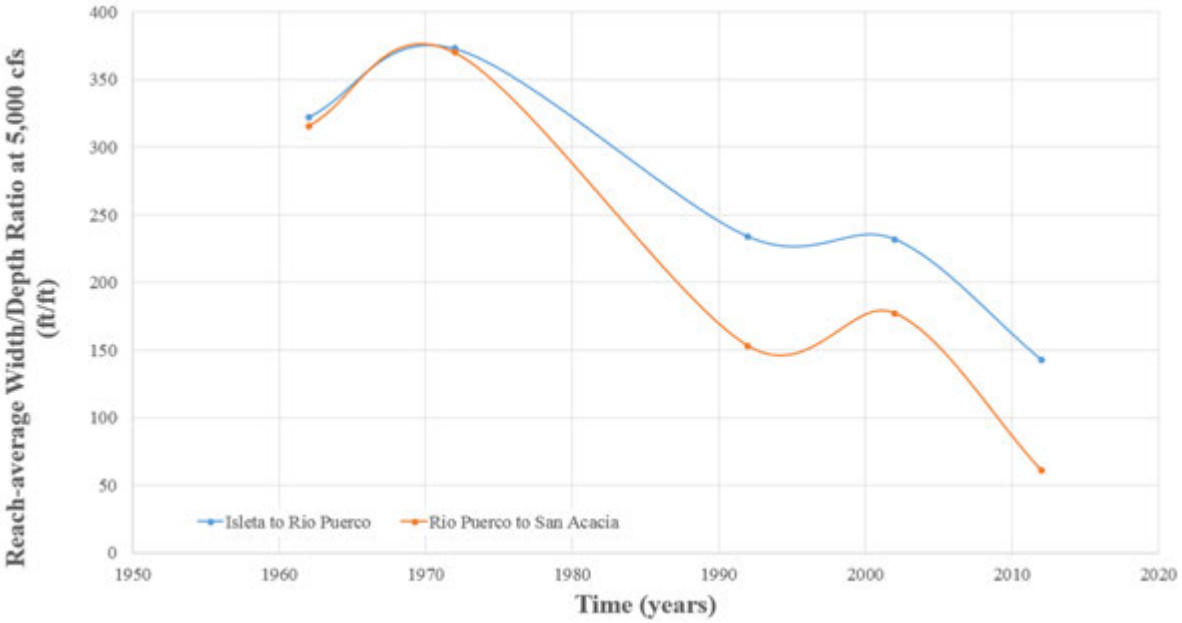

Figure 13. Reach Average Width/Depth ratios for Isleta to Rio Puerco and Rio Puerco to San Acacia between 1962 and 2012

4.7 Bank Height

Changes in the bank height are shown in Figure 14 and Figure 15. The bank height was illustrated graphically by two means.

Figure 14 shows the difference between the elevation of the bank locations and the minimum channel elevation in the estimated underwater prism. This would be representative of the entire bank height from the channel bed. Since there is a transverse slope in the river it is likely that the actual bank height is less than this value. Figure 15 provides the difference between the elevation of the bank locations and the water surface elevation at a discharge of 5,000 cfs. Positive values indicate feet of freeboard between the 5,000 cfs water surface elevation and the top of the bank. Negative values indicate how far above the bank the 5,000 cfs water surface is overbanking. It should be noted that for this analysis the hydraulic model bank locations were used. The bank locations within the model were chosen based on changes in slope and vegetation breaks shown in the aerial photography. There is some uncertainty as to the actual value, but when averaged over the reach they provide an indication of reach trends that are occurring.

Between 1962 and 1992 the decrease in the reach averaged bank height to minimum channel elevation in the Isleta to Rio Puerco reach indicates that channel aggradation is likely occurring. From 1992 to 2012 there is an increase in this bank height that is on the same magnitude of the preceding decrease, and it likely indicates that either channel incision is occurring or bank elevations are increasing. Section 4.3.3. Longitudinal River Profiles from the 2018 Isleta to San

Acacia Geomorphic Analysis Report confirms that the channel has incised over most of the reach between 1992 and 2012.

The Rio Puerco to San Acacia reach shows an increasing reach averaged bank height to minimum channel elevation from 1972 to 1992 and 2002 to 2012. There are periods where there is a decreasing bank height from 1962 to 1972 and again between 1992 and 2002, but the decrease is much less than the increase. This likely indicates an overall trend of incision and/or bank elevations increasing. Section 4.3.3. Longitudinal River Profiles from the 2018 Isleta to San Acacia Geomorphic Analysis Report confirms that the channel aggraded over most of the reach between 1992 and 2002, and incised over most of the reach between 2002 and 2012.

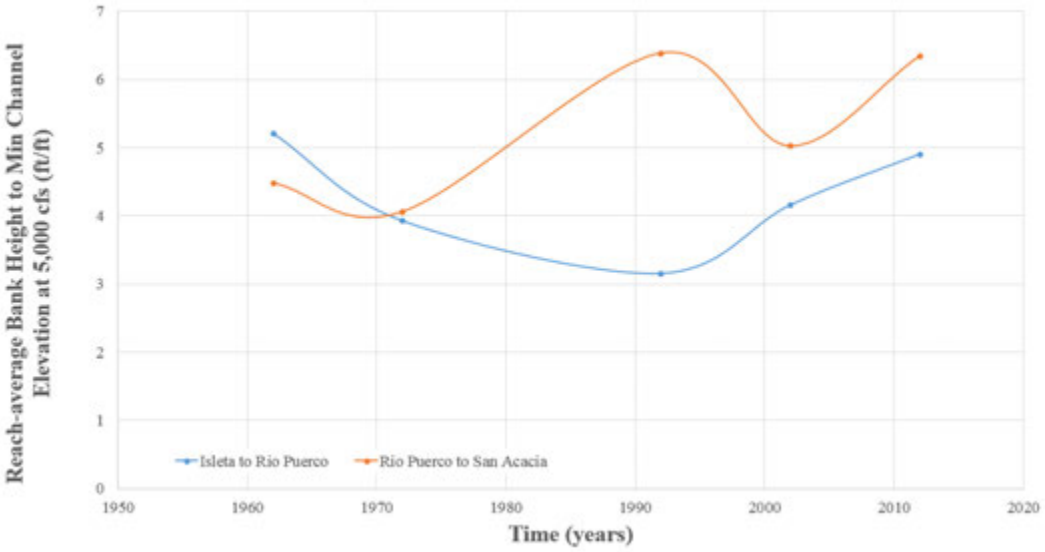

Figure 14. Reach Average Bank Height to Minimum Channel Elevation for Isleta to Rio Puerco and Rio Puerco to San Acacia between 1962 and 2012

Figure 15 indicates that the reach average bank freeboard above the 5,000 cfs water surface elevation ranges from near zero to two feet over the years. The Isleta to Rio Puerco and Rio Puerco to San Acacia reaches are often trending oppositely, but both show a trend towards a lower reach average freeboard elevation. This may indicate a general aggradation in the reaches or the establishment of a lower inset floodplain developing in the channel. This also may indicate lower conveyance capacity than in the past.

Figure 14 and Figure 15 show that both types of bank height (bank height to minimum channel elevation and bank height to 5,000 cfs water surface elevation) trend the same direction for each time period and reach except the Isleta to Rio Puerco reach between 2002 and 2012. In this instance the bank height to minimum channel elevation increases, but the bank height to 5,000 cfs water surface elevation goes the opposite direction and decreases. This may indicate that

even though the channel incised during this time, it also narrowed rapidly and decreased the conveyance capacity.

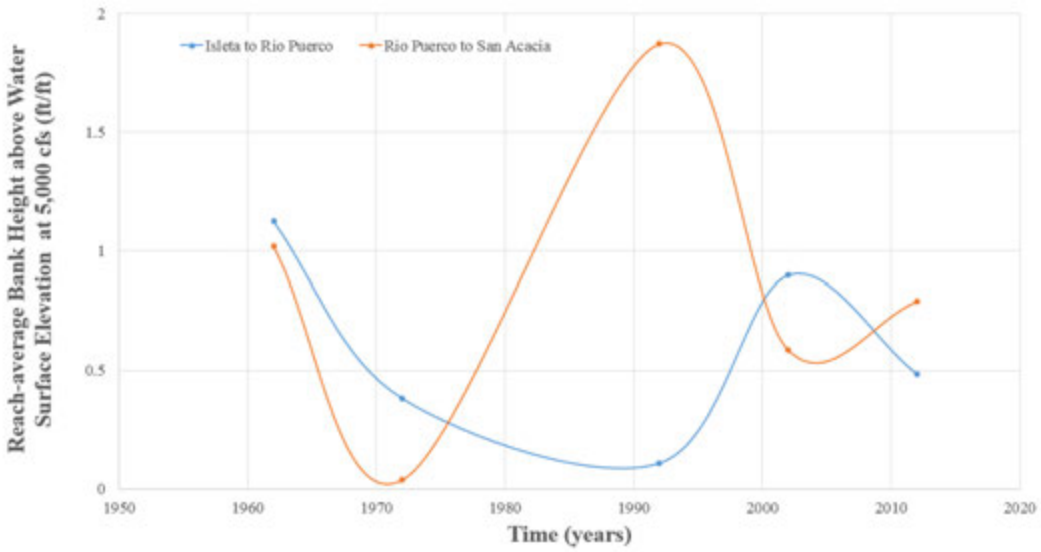

Figure 15. Reach Average Bank Height to 5,000 cfs Water Surface Elevation for Isleta to Rio Puerco and Rio Puerco to San Acacia between 1962 and 2012

4.8 Shear Stress

Changes in the channel shear stress, calculated as the unit weight of water times the channel hydraulic radius times the friction slope (USACE, 2010b), are shown in Figure 16. The trend in the shear stress is similar to the mean velocity trends and indicates that the shear stress is increasing over time, with the most dramatic increase between 2002 and 2012. This would also be expected to increase the bed material size through the reach since the shear stress increase is an indication of an increased ability of the channel to do work.

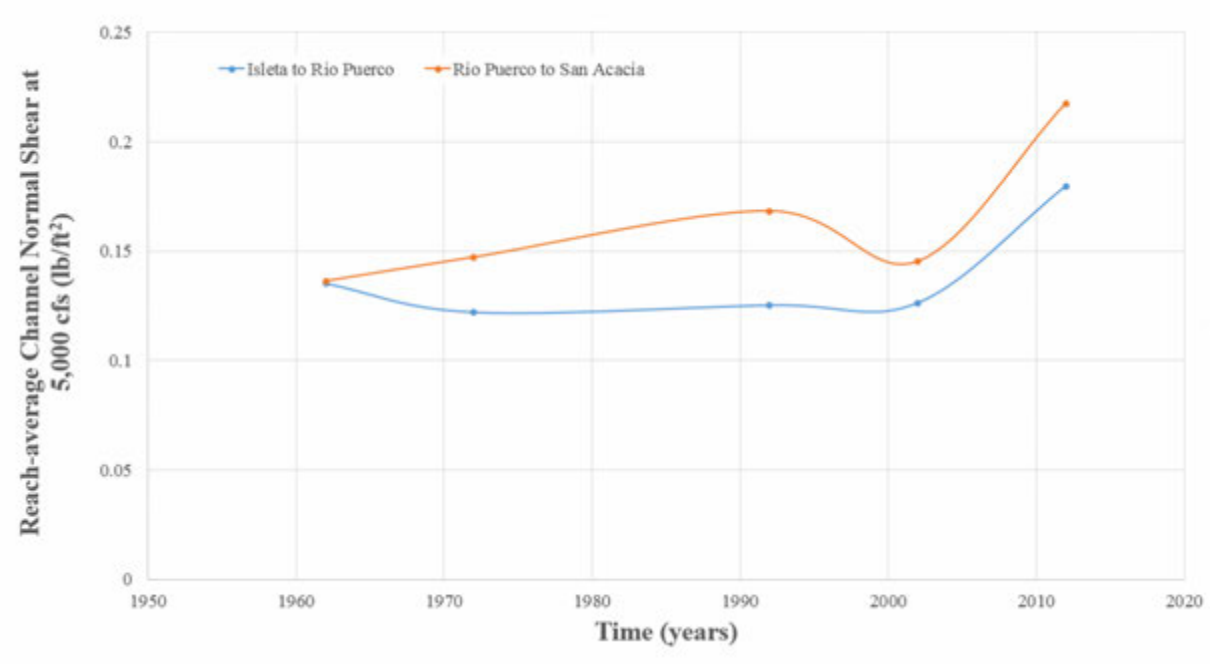

Figure 16. Reach Average Normal Shear Stress in the channel for Isleta to Rio Puerco and Rio Puerco to San Acacia between 1962 and 2012.

4.9 Bankfull Discharge

Bankfull discharge is defined as the discharge at which the river's water surface elevation equals the elevation of the lower of the right or left top of bank. The historical geometry models were run at 1000 cfs intervals to determine the bankfull discharge at each agg/deg line, and the bankfull discharge values were distance-weighted and averaged for each reach. Changes over time in the distance-weighted average bankfull discharge are shown in Figure 17. The Isleta to Rio Puerco and Rio Puerco to San Acacia reaches are often trending oppositely, but both culminate in a lower bankfull discharge value in 2012 than in the earlier evaluated years. A decreasing bankfull discharge value likely indicates a hydrologic regime with decreasing flows.

It should be noted that these results depend on how each historical geometry model defines the bank stationing. The 2012 model has many more topography data points in a cross section than the 1962 to 2002 models, and thus the 2012 bank stationing is more precise than the earlier models. In most cross sections, the 2012 bank stationing is lower in elevation than the earlier models simply because of the additional topography points available to choose from. This difference in bank selection results in a lower bankfull discharge for the 2012 model than the earlier models, independent of any channel geometry changes.

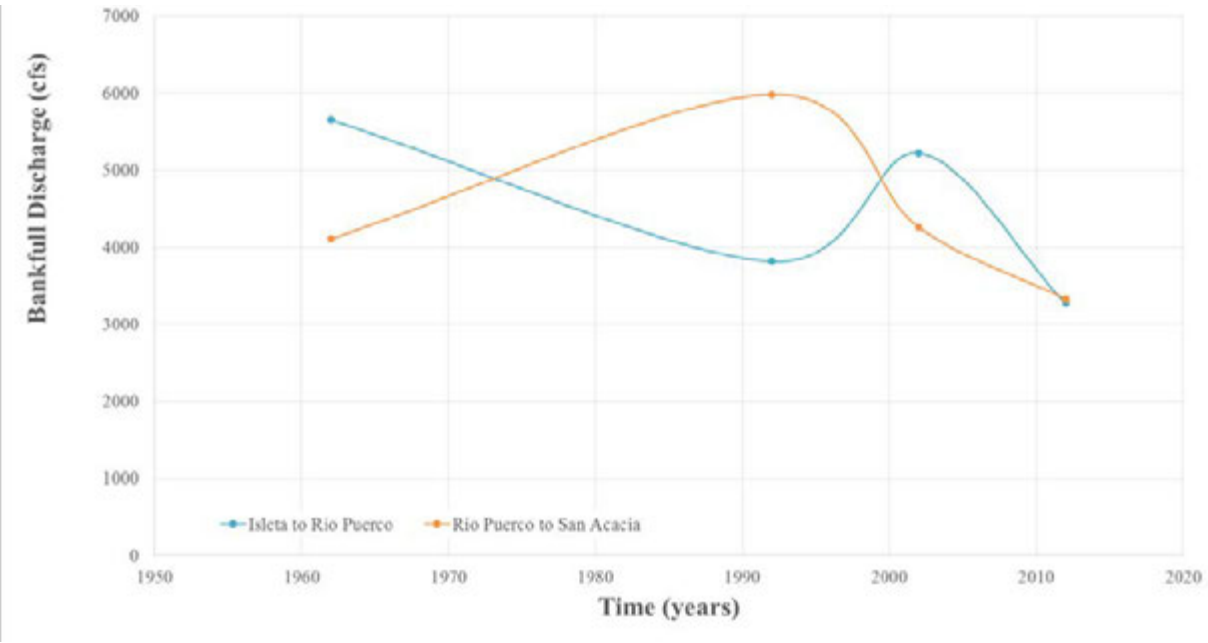

Figure 17: Reach Average Bankfull Discharge for Isleta to Rio Puerco and Rio Puerco to San Acacia between 1962 and 2012.

4.10 Water Surface Elevation at 5,000 cfs

Changes in water surface elevation (WSE) at 5,000 cfs are shown in Figure 18 through Figure 21. The figures show that the WSE at 5,000 cfs has remained relatively stable (fluctuations of about two feet between 1962 and 2015) between Isleta and the HWY-346 Bridge. Between 2002 and 2012, the 5,000 cfs WSE for the entire reach increased on average 0.9 feet. Between 2012 and 2015, the 5,000 cfs WSE had no change on average for the entire reach.

Between HWY-346 and approximately two miles upstream of the Rio Salado, it appears that there was a severe drop in WSE at 5,000 cfs between 1972 and 1992, sometimes as much as 10 feet. Since 1992 in this segment, the 5,000 cfs WSE has been slowly increasing but has only returned to 1972 levels downstream of Arroyo los Alamos.

The 5,000 cfs WSE between the Rio Salado and San Acacia Diversion Dam also dropped significantly between 1972 and 1992, in some places as much as 6 feet. By 2015 the 5,000 cfs WSE returned to 1972 levels.

In 1962 and 1972 the 5,000 cfs WSE slope was fairly constant through the location of the Rio Salado. Starting in 1992, the slope of the 5,000 cfs WSE increasingly flattens out as it approaches the Rio Salado, and after the Rio Salado the 5,000 cfs WSE experiences a rapid drop. This likely indicates that the Rio Salado acted as a grade control and prevented the significant decrease in 5,000 cfs WSE that occurred between 1972 and 1992 downstream of HWY-346.

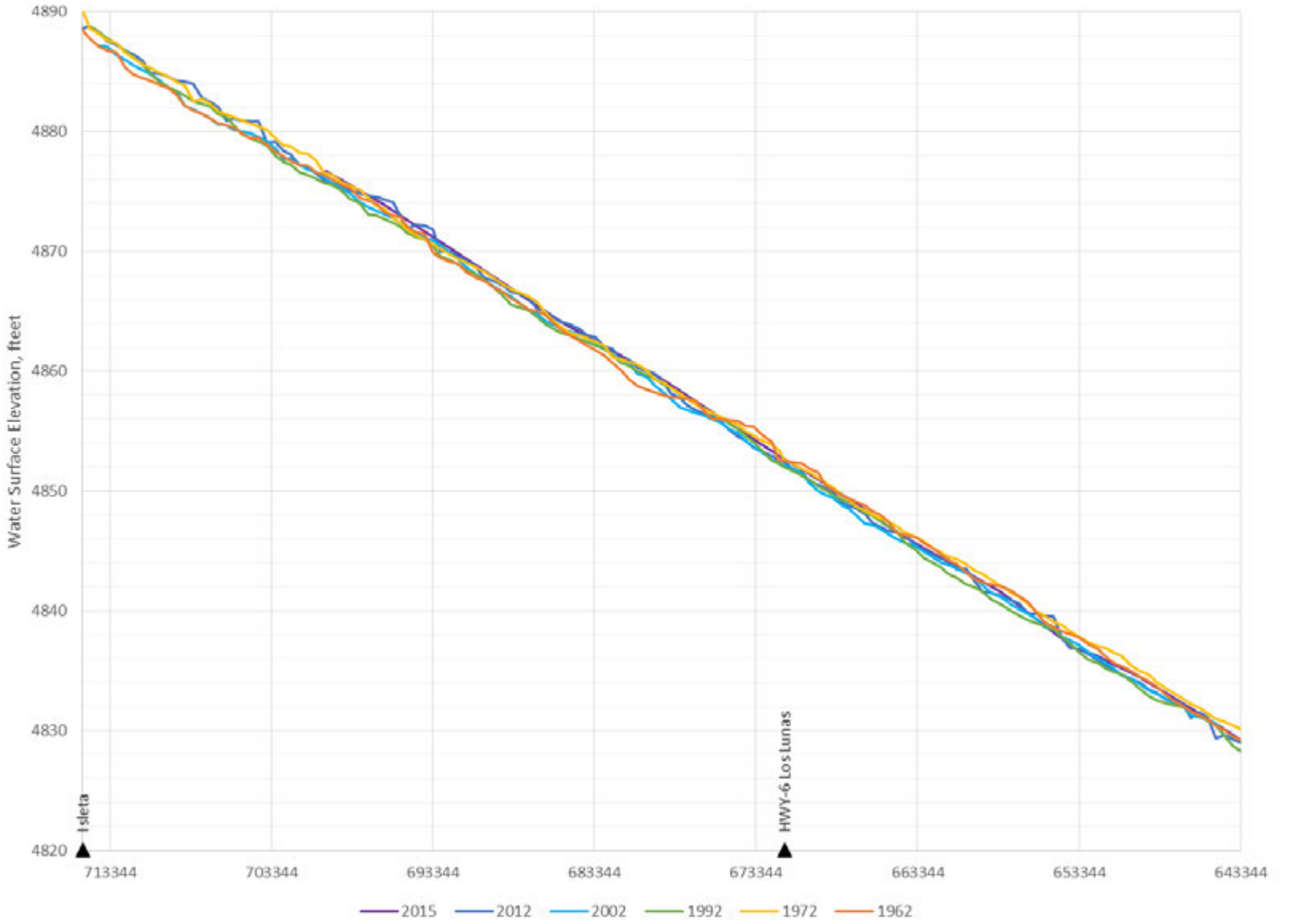

Figure 18: Isleta to Los Chavez Water Surface Elevation at 5,000 cfs

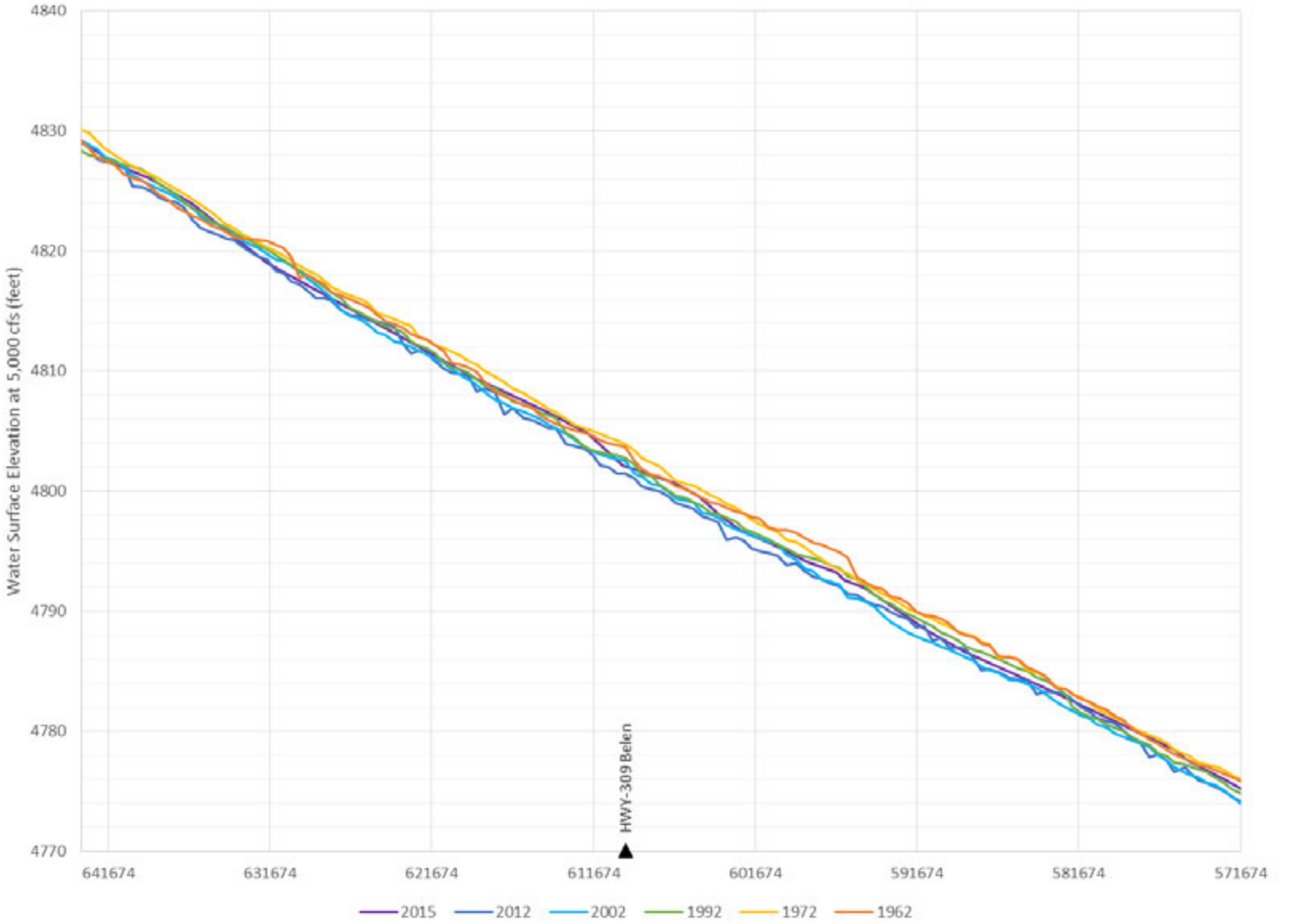

Figure 19: Los Chavez to Jarales Water Surface Elevation at 5,000 cfs

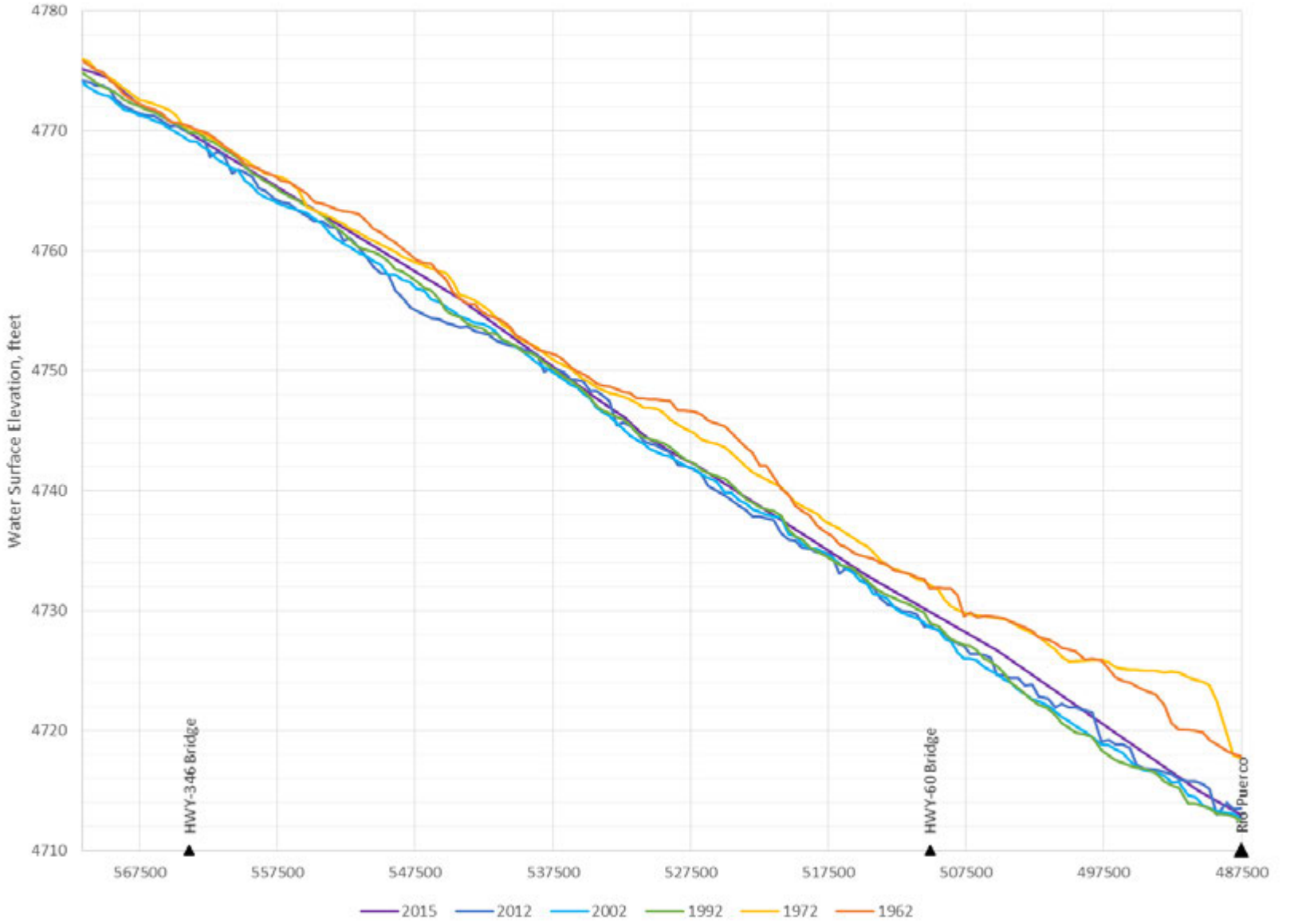

Figure 20: Jarales to Rio Puerco Water Surface Elevation at 5,000 cfs

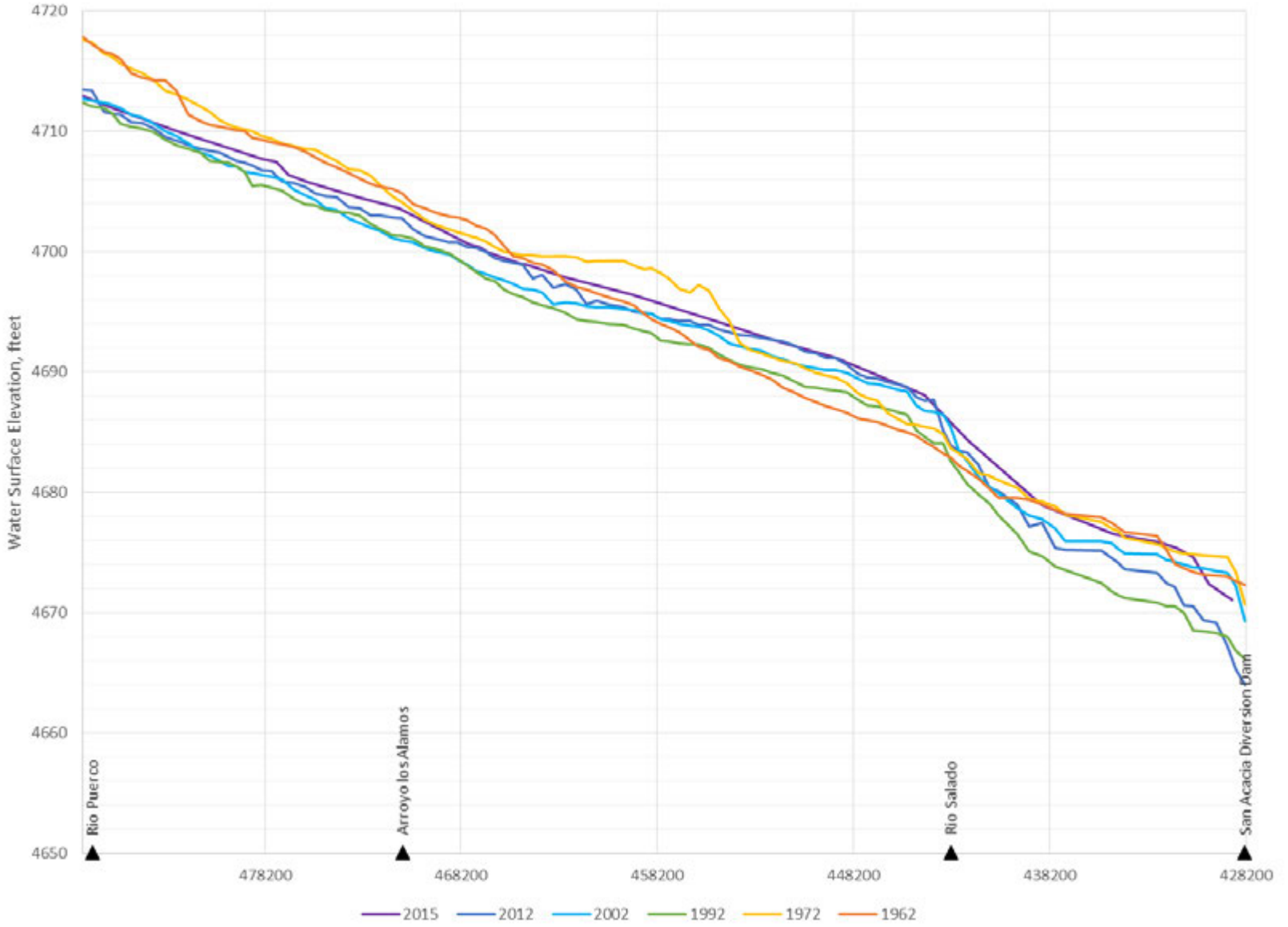

Figure 21: Rio Puerco to San Acacia Water Surface Elevation at 5,000 cfs

4.11 Current Hydraulic Profile

Hydraulic profiles for the current geometry model (2014/2015) are shown in Figure 22, Figure 23, and Figure 24 for Isleta to Highway 309, Highway 309 to Rio Puerco, and Rio Puerco to San Acacia, respectively. The figures include profiles of the minimum channel elevation, water surface elevation at 5,000 cfs, right and left top of banks, right and left toe of levees, and right and left top of levees.

Due to intermittent perched channel conditions in this reach, the channel water may or may not be physically against the levees when the 5,000 cfs WSE is above the elevation of the levee toes. The distances between the 5,000 cfs WSE and the levee toe elevations are shown below for the three river sections shown in Table 5. These river sections were split based on similar trends.

Table 5: 5,000 cfs WSE in relation to levee toe elevation

River Section	5,000 cfs WSE
Isleta to HWY-309	Always above levee toe (as high as 4 feet)
HWY-309 to HWY-60	Usually above levee toe (as high as 4 feet) Occasionally below levee toe (as low as 1 foot)
HWY-60 to San Acacia	Usually below levee toe (as low as 8 feet) Occasionally above levee toe (as high as 3 feet)

Table 6 shows the distances between the 5,000 cfs WSE and the lower of the right or left top of bank. The river was split into two sections at the Railroad Bridge based on similar overbanking trends.

Table 6: Distances between 5,000 cfs WSE and the lower of the right or left top of bank.

River Section	5,000 cfs WSE Max Overbanking	5,000 cfs WSE Max Freeboard
Isleta to Railroad Bridge	1 foot	1 foot
Railroad Bridge to San Acacia	2 feet	6 feet

An analysis of water surface elevations for varying flow rates in the Isleta to Rio Puerco reach found that for the 2014/2015 channel geometry, banks are overtopped at an average of 4,600 cfs. In the Rio Puerco to San Acacia reach, overtopping occurred at an average flow of 5,500 cfs. These bankfull numbers were not included in Section 4.9 Bankfull Discharge because the historic models and the current model were developed slightly differently and thus may not be comparable (see Section 3.0 Hydraulic Modeling Development).

The water surface is at the same elevation as the levee toes at an average flow of 3,100 cfs in the Isleta to Rio Puerco reach. The water surface is at the same elevation as the levee toes at an average flow of 8,800 cfs in the Rio Puerco to

San Acacia reach. Due to intermittent perched channel conditions, when the water surface is at the same elevation as the levee toes, the levee toes may or may not be wet.

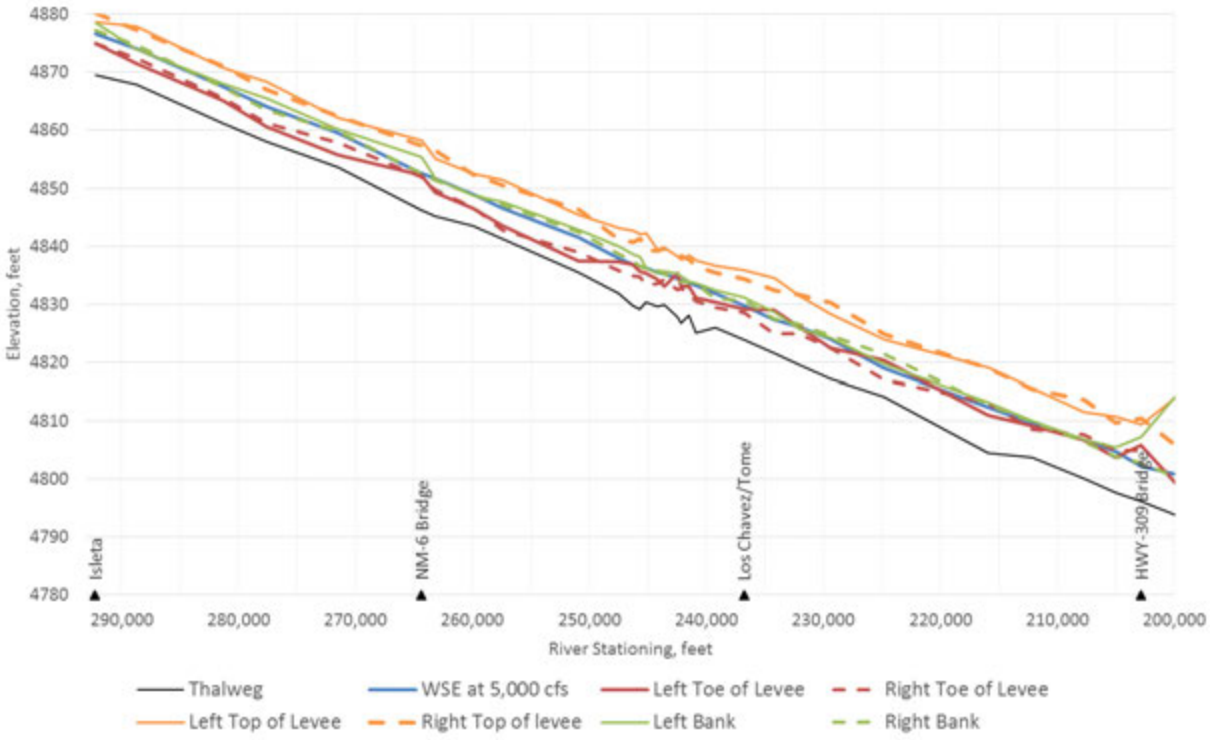

Figure 22: Current Hydraulic Profile from Isleta Diversion Dam to Highway 309

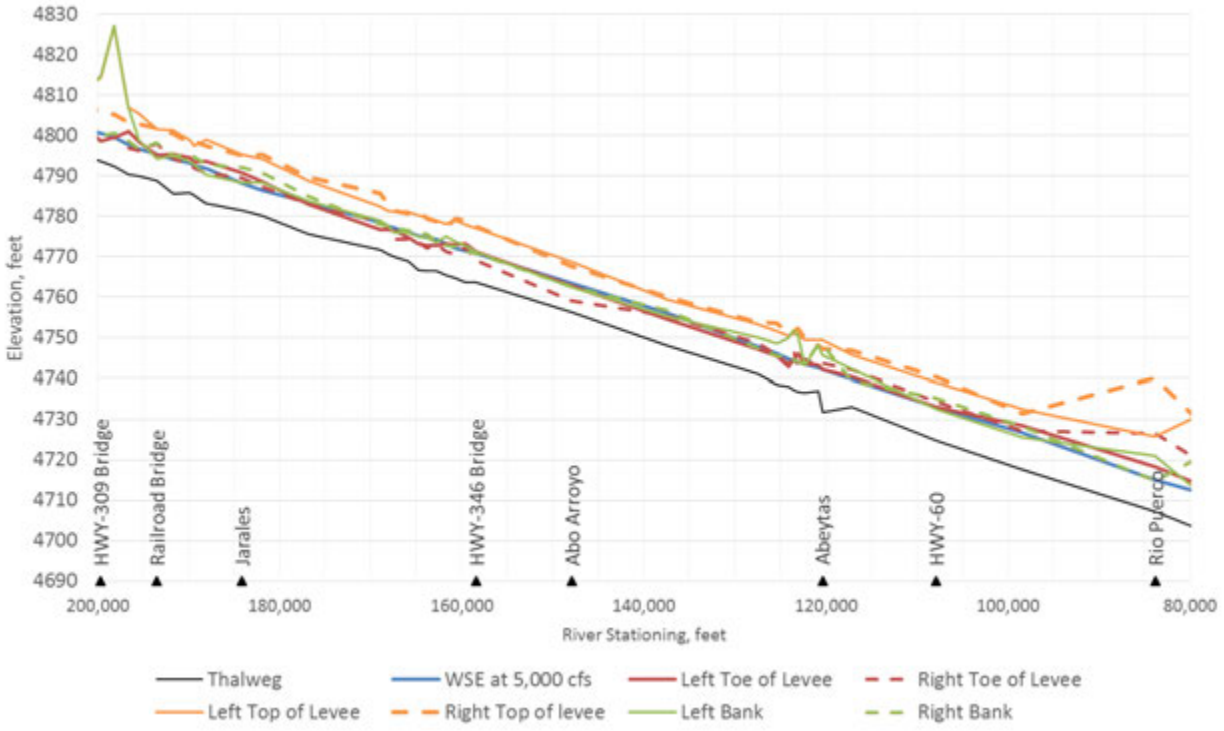

Figure 23: Current Hydraulic Profile from Highway 309 to Rio Puerco

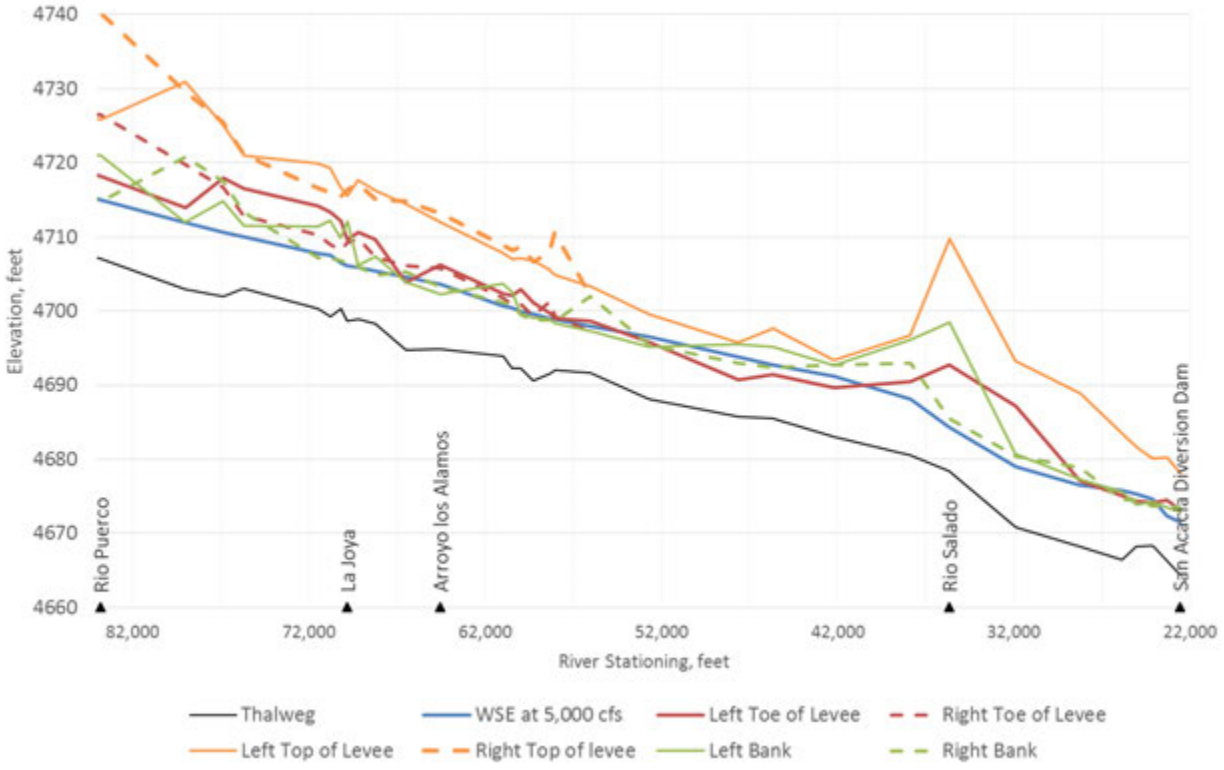

Figure 24: Current Hydraulic Profile from Rio Puerco to San Acacia Diversion Dam

5.0 Bank Stability Analysis

Bank and toe stability was examined at ten cross sections within the Isleta to San Acacia study reach using the one-dimensional HEC-RAS hydraulic model results, cross section geometry, and measured soil characteristics from bank samples collected by Reclamation in 2016 (Klein et al, 2018). This information, coupled with a Microsoft Excel based model, Bank Stability and Toe Erosion Model (BSTEM version 5.4), developed by the Agricultural Research Service (ARS) of the United Stated Department of Agriculture, was used to evaluate bank stability. The BSTEM model accepts user-defined input that describes the geometry of the river bank and toe of the study cross section, the bank's nominal grain size (D_{50}) value, as well as hydraulic information such as the water surface elevation of the target flow to determine the resistance of the bank and normal shear stress forces generated by the channel flow.

5.1 Bank Samples

One of the targeted interests of this reach study was to identify the propensity of key channel sections for lateral migration of the main river channel towards riverside infrastructure. Ten channel cross sections were identified within the limits of the Isleta to San Acacia reach. Cross sections were identified based on major bend locations within the study reach and composite bank samples were taken at these locations (Klein et al., 2018). These cross sections are listed in Table 7 sorted from upstream to downstream sampling location.

The 2016 bank samples (Klein et al., 2018) were used to determine the grain size distribution of the soil for input into the BSTEM model. Each bank sample was obtained from a representative bank area located on the outside channel bend, which is the section that will experience maximum shear forces within the cross section of interest. If the soil material and bank vegetation are insufficient to stabilize the bank, lateral migration of the river channel at these locations may be possible. The 2016 sampled bank materials were fairly homogenous, so only one sample was collected at each location (Klein et al., 2018). The primary bank material is derived from qualitative descriptors written in the laboratory sheets and the gradation analysis to assess the soil characteristic that would most influence erodibility. For instance, if the gradation analysis indicated a nominal bank material of fine sand, but the physical description on the laboratory sheets indicated the presence of clay material, then clay was entered as the primary material because the cohesive nature of the soil was assumed to drive the bank erodibility. Descriptions of the soil material from this assessment were based on the available soil materials within BSTEM.

Table 7. Locations of river bank samples for BSTEM analyses.

Sample No.	Lab Sample No.	River Mile	Agg/Deg Line	Date Acquired	Primary Material
1	731070616	162	731	7/6/2016	Clay
2	863071416	149	863	7/11/2016	Clay
3	974072816	138.2	974	7/28/2016	Clay
4	CO1061070716	130.4	1061	7/7/2016	Clay
5	1086072816	127.9	1086	7/28/2016	Clay
6	1088070716	127.5	1088	7/7/2016	Clay
7	1094072816	127	1094	7/28/2016	Angular Sand
8	LJ10070116	124.2	1124	7/1/2016	Clay
9	RP1170070716	119.8	1170	7/7/2016	Clay
10	RP1202_5071916	116.5	1202.5	7/19/2016	Clay

5.2 Procedure

The initial step within the BSTEM model is to define the cross section input geometry that identifies the bank profile of the target section. There are multiple options available to the user to input this information, and for more detailed explanation of this process the reader is referred to the ARS website for more detailed documentation of the modeling process (USDA, 2016). Once the bank profile geometry was defined for the cross section, the following hydraulic information was inputted into the BSTEM model:

- Discharge — For this analysis, model flows of 4k-, 7.5k-, and 20k-cfs were simulated using the 2015 model described in section 3.1. A discharge of 4,000 cfs is approximately the 2-yr regulated peak at Albuquerque estimated by Wright (2010). A discharge of 7,500 cfs is approximately the 10-yr regulated peak at Albuquerque and close to the 2-yr regulated peak at San Acacia, and 20,000 cfs is close to the 10-yr unregulated peak at San Acacia (Wright, 2010).
- Flow duration —Duration of modeled flow was selected to be 72 hours in order to simulate a sustained peak runoff flow on the bank section.
- Bend length – Input reach length was defined in the model as the entire bend distance. This distance was measured within ESRI's ArcGIS software (version 10.2) for each study bend.
- Slope — Reach slope was calculated by extracting the simulated energy grade line (EGL) slope from the HEC-RAS model along with the distance between cross sections through the bend and then weighting the EGL over the total distance through the bend section.

After defining the input geometry for the modeled cross section it is then necessary to enter bank material information. The BSTEM Bank Material tab contains five separate bank material profiles as well as a required input for the toe material information. For this analysis, the primary material description, as listed in Table 7, was entered into BSTEM. Most of the bank lab results

indicated the presence of clay material. These were entered into BSTEM with the bank material descriptor of "erodible soft clay". Sample No. 7 in Table 5 was the only sample that departed from this descriptor, and thus a "coarse angular sand" descriptor within BSTEM was used for this bank material.

If a particular cross section was found to be either unstable or conditionally stable (further discussion of model results is described in more detail in the following section of this report), a second bank stability run was performed in BSTEM using its Bank Vegetation and Protection module. This module allows the user to input bankline vegetation information in order to simulate the influence of the vegetation's root mass on the bank's structural stability. Vegetation type, density, and age are used to estimate the increase in bank stability by estimating the soil cohesion value (measured in kPa) that is factored into the model's erosion calculations. The higher this value, corresponding to a higher volume of root mass within the bank, the more erosive resistance the bankline is. If the modeled cross section was found to become stable after performing the vegetative stability run this was then recorded in the BSTEM results summary.

Finally, toe erosion is analyzed using the Toe Model Output of the BSTEM model. This module applies hydraulic normal shear stresses to the toe of the study cross section and reports estimated erosion to the user through the model's output interface. These results estimate a maximum lateral retreat as well as the eroded area of both the bank and toe material from the model simulation.

5.3 BSTEM Results

The BSTEM analysis of the ten chosen cross sections within the Isleta to San Acacia reach indicates that toe erosion is the primary cause for bankline lateral migration throughout the study reach. All modeled sample sections experienced at least some toe erosion under the simulated flow conditions, which may lead to lateral bank migration. The one notable exception was at sample No. 9. Here the coarser bed material helped stabilizes the toe and resulted in minimal estimated toe erosion.

Using BSTEM to evaluate hydraulic and geotechnical forces acting on the bank, outside of toe erosion and subsequent geotechnical failure, almost all of the evaluated cross sections predicted stable banks. BSTEM estimates streambank stability through calculating the shear strength of a saturated soil as described by the Mohr-Coulomb criterion (USDA, 2016). The resistance of the bank soils to shear is then considered against the driving forces of the river flow and this ratio is output from the model as a factor of safety. When this value is less than unity the bank is considered to be unstable. Out of the ten sampled cross sections, the BSTEM simulations resulted in only one model run with a slightly unstable bank condition at a flow of 4,000 cfs (sample No.

8 from Table 7). This same bank section when evaluated with the vegetative module from BSTEM is predicted to be stable under the tested flow scenario. Results from BSTEM are provided in Table 8 to Table 10.

To further classify the magnitude of predicted toe erosion and subsequent lateral migration, toe erosion at the ten evaluated bank sections was classified into four categories: Very High, High, Moderate and Minimal. This was done in order to better define the severity of erosion predicted by the model. The classifications correlate to the following definitions of lateral bank retreat.

- Very High–indicates that the model predicted a lateral bank retreat of 10 feet or greater over a 72 hour period (>3 ft/day).
- High–indicates lateral bank retreat between 5 and 10 feet in this period
- Moderate–results in a lateral retreat of between 2 and 5 feet in 72 hours
- Minimal–results in a lateral retreat of less than 2 feet over a 72 hour period.

The sampled sections with the greatest propensity for lateral bank retreat (migration) were located around RM 127 (Sample No. 5 and No. 6, which are around the confluence with the Rio Puerco). These locations had an estimated maximum retreat rate of 8.6 ft/day under the highest simulated flow condition (20,000 cfs). Bank profiles at each evaluated bank section can be found in Appendix A. The bank profiles show erosion impacts estimated from the BSTEM model runs for each cross section.

Table 8. BSTEM results from 4,000 cfs flow simulation, 72-hour duration.

4,000 cfs				
Sample No.	**River Mile**	**Bank Erosion**	**Toe Erosion**	**Max. Lateral Retreat (ft)**
1	RM 162	None	High	8.5
2	RM 149	Stable	Moderate	4.1
3	RM 138.2	None	High	5.0
4	RM 130.4	Stable	High	5.6
5	RM 127.9	None	Very High	14.8
6	RM 127.5	None	Very High	14.1
7	RM 127	None	Minimal	0.6
8	RM 124.2	Conditionally Stable	Minimal	1.5
9	RM 119.8	*Stable	Minimal	0.0
10	RM 116.5	Stable	High	5.3

*Denotes that Vegetation module was necessary to run in order to achieve a stable bank section.

Table 9. BSTEM results from 7,500 cfs flow simulation, 72-hour duration.

7,500 cfs				
Sample No.	**River Mile**	**Bank Erosion**	**Toe Erosion**	**Max. Lateral Retreat (ft)**
1	RM 162	None	High	6.7
2	RM 149	Stable	High	5.7
3	RM 138.2	None	High	8.9
4	RM 130.4	Stable	High	5.3
5	RM 127.9	None	Very High	16.2
6	RM 127.5	None	Very High	15.7
7	RM 127	None	Minimal	0.9
8	RM 124.2	Conditionally Stable	Moderate	3.3
9	RM 119.8	Stable	Minimal	0.0
10	RM 116.5	Stable	High	5.5

Table 10. BSTEM results from 20,000 cfs flow simulation, 72-hour duration.

20,000 cfs				
Sample No.	**River Mile**	**Bank Erosion**	**Toe Erosion**	**Max. Lateral Retreat (ft)**
1	RM 162	None	Very High	17.5
2	RM 149	Stable	High	5.4
3	RM 138.2	None	Very High	15.7
4	RM 130.4	Stable	Moderate	3.2
5	RM 127.9	None	Very High	25.9
6	RM 127.5	None	Very High	25.4
7	RM 127	None	Moderate	2.0
8	RM 124.2	Conditionally Stable	Moderate	4.4
9	RM 119.8	Stable	Minimal	0.3
10	RM 116.5	Stable	Moderate	4.1

6.0 Stable Channel Design Analysis

Hydraulic modeling, when coupled with relationships that describe stable channel dimensions (slope, width, depth, etc.), is useful to help understand current channel dynamics and potential future trends. A stable channel analysis was pursued for the Isleta to San Acacia reach to estimate the range of channel dimensions that are able to transport the estimated sediment supply in relationship to a given discharge. The USACE's channel stability module (SAM) within HECRAS (Thomas et al., 2002; USACE, 2010b) was used for this analysis.

6.1 SAM Hydraulic Design Module

SAM provides a means to estimate stable channel dimensions for known channel inputs and was developed primarily as a qualitative evaluation tool for preliminary planning. Three options for estimating stable channel dimensions are offered: Copeland, Regime, and Tractive Force methods. A summary of these methods is given by the HEC-RAS Reference Manual (USACE, 2010b) below:

> *"The Copeland method uses an analytical approach to solve stable channel design variables of depth, width and slope. Stability is achieved when the sediment inflow to a particular reach equals the sediment outflow. The Regime method is purely empirical, and, within HEC-RAS, uses equations developed by Blench (1975). The Regime method defines a channel as being stable when there is no net annual scour or deposition in the design reach. The Tractive Force method is an analytical scheme that defines channel stability as no appreciable bed load movement." (USACE, 2010b, p. 12-12)*

6.1.1 Input Variables for Analysis

All three methods within SAM require or have the option to input the following variables: discharge, specific gravity, sediment gradation, water temperature, bank side slope, bank Manning's n, inflow sediment concentration, valley slope, median channel width, default regime (upper or lower), side factor, and the angle of repose. The specific input requirements for each method are listed in Table 11.

The discharge values analyzed within the SAM hydraulic design module are 750, 4,000, 7,500, and 20,000 cfs. The discharge value of 750 cfs was chosen as this was estimated to be the effective discharge for suspended sediment at San Acacia (Klein et al., 2018). A discharge of 4,000 cfs is approximately the 2-yr regulated peak at Albuquerque estimated by Wright (2010). A discharge

of 7,500 cfs is approximately the 10-yr regulated peak at Albuquerque and close to the 2-yr regulated peak at San Acacia, with 20,000 cfs being close to the 10-yr unregulated peak at San Acacia (Wright, 2010).

Table 11: Input variables used for each of the three Stable Channel Design methods

Input Variable	Copeland	Regime	Tractive Force
Discharge	✓	✓	✓
Specific Gravity	✓		✓
Sediment Gradation	✓	✓	✓
Water Temperature	✓	✓	✓
Bank Side Slope	✓		✓
Bank Manning's n	✓		✓
Inflow Sediment Concentration	✓	✓	
Valley Slope	*Optional*		✓
Median Channel Width	*Optional*		
Default Regime (Upper or Lower)	*Optional*		
Side Factor		✓	
Angle of Repose			✓

The sediment gradation used in this analysis was the average of all bed material samples collected between 2014 and 2016 from Isleta Diversion Dam to just upstream of the Rio Salado. Two of the bed material samples were collected by Easterling (2014) in 2013 and were processed by Reclamation. The remaining 21 bed material samples were collected and processed by Reclamation in 2016. These bed material soil samples indicate that the primary bed substrate is sand between Isleta Diversion Dam to just upstream of the Rio Salado. From the Rio Salado and downstream, the bed material samples have a nominal (D_{50}) gradation in the gravel and cobble range (Klein et al., 2018). The Copeland and Regime methodologies were primarily developed for sand bed systems, so applying these relationships to the reach downstream of the Rio Salado was not pursued to keep within the identified limits of applicability for these methods.

While the bank side slopes vary greatly through the study reach, a single bank slope of 2:1 (horizontal:vertical) was used. This slope was selected because a comparison of SAM results from a few select cross sections using the actual bank slopes showed reasonable comparison with the assumption of a single bank slope. So while the SAM results are highly sensitive to the bank slope, the use of a single bank slope value was used to provide a reasonable representation of the qualitative predictions from SAM.

The stable channel results were also highly sensitive to the angle of repose, which is discussed in the Tractive Force Method results section.

The Manning's n used for this analysis was 0.032 for discharges of 750 and 4,000 cfs and 0.025 for discharges of 7,500 and 20,000 cfs. This is based on the results of the channel Manning's n calibration (Section 3.1.3 on p. 8).

The inflow suspended sediment concentration used for this analysis was a value of 2,408 mg/L. This is the average suspended sediment concentration at the Albuquerque and San Acacia USGS gages based on the most recent (late 2000s to early 2010s) slope between breaks of the double mass curves for these gages (Klein et al., 2018). The SAM program requires a concentration input in parts per million (ppm), which for the assessed concentrations has a conversion factor of one (USGS, 1993).

It should be noted that the Copeland and Regime Method results are sensitive to the inflow suspended sediment concentration. Slightly lower concentrations result in much lower slope values required for equilibrium. Considering that the only concentration data available is for the Albuquerque and San Acacia gages, and considering that the concentration at these gages may be higher than the concentration seen between Isleta Diversion Dam and the Rio Puerco, it is possible that the Copeland and Regime Method results dictate higher slopes than necessary to achieve stable channel conditions.

The bank side factor, only utilized for the Regime analysis, was chosen based on guidance from Blench (USACE, 2010b). The value used is 0.2 for silty, clay, loam banks, which is the best category for the assessed banks in the Isleta to San Acacia reach (Klein et al., 2018).

6.1.2 Results for Copeland Method

The Copeland Method estimates a stable width, depth, and slope values for the given inputs in Table 11. A number of values are provided for each discharge, providing a range of various combinations of width, depth, and slope that are expected to be stable for the reach of the Rio Grande between Isleta Diversion Dam and the confluence with the Rio Salado. Figure 25 and Figure 26 show the variations of width vs. slope and depth vs. slope for various flow discharges. As discharge increases, the slope generally decreases and there is a greater range of width and depth options that result in a stable channel.

The average channel bed slope and average valley slope for the Rio Grande within the Isleta to San Acacia reach, as described by Klein et al. (2018) is plotted on Figure 25 and Figure 26. Theoretically, river channels which plot above the set of stable curves predicted using the Copeland Method would indicate a tendency towards degradation, while those which plot below the set of stable curves indicate a tendency towards aggradation. This assumes that the set of stable channel curves represents an equilibrium condition for which the channel has a tendency to move towards.

Figure 25 and Figure 26 show the valley slope as a gray dashed line and the average channel bed slope as an orange dashed line. These lines representing

the Rio Grande tend to plot between the curves representing the 4,000 and 7,500 cfs discharge conditions on these figures. This suggests that the discharge range of 4,000 cfs to 7,500 cfs has played a critical role in defining the current channel condition. These discharge values are within the range of the peak snow-melt runoff discharges observed in the last several decades (Klein et al., 2018). These figures also suggest that the for the given suspended sediment concentration the lower evaluated discharge (750 cfs) may result in some channel aggradation, while channel degradation is likely with the higher evaluated discharge (20,000 cfs). Essentially if the slope, width and depth values plot above each respective curve for 750 cfs, 4,000 cfs, 7,500 cfs, and 20,000 cfs then there will be a tendency for degradation to reach a stable channel condition. The converse is also true associated with the slope, width and depth values plotting below each curve for aggradation. Based on the intersection with the current reach average channel bed slope, the range of estimated stable channel widths from the Copeland method is 75 to 175 feet. This is similar to the current reach averaged channel widths reported by Klein et al. (2018). For the same conditions, the estimated stable channel depths range from 4 to 7 feet, which concurs with the range of hydraulic radii shown in Figure 11.

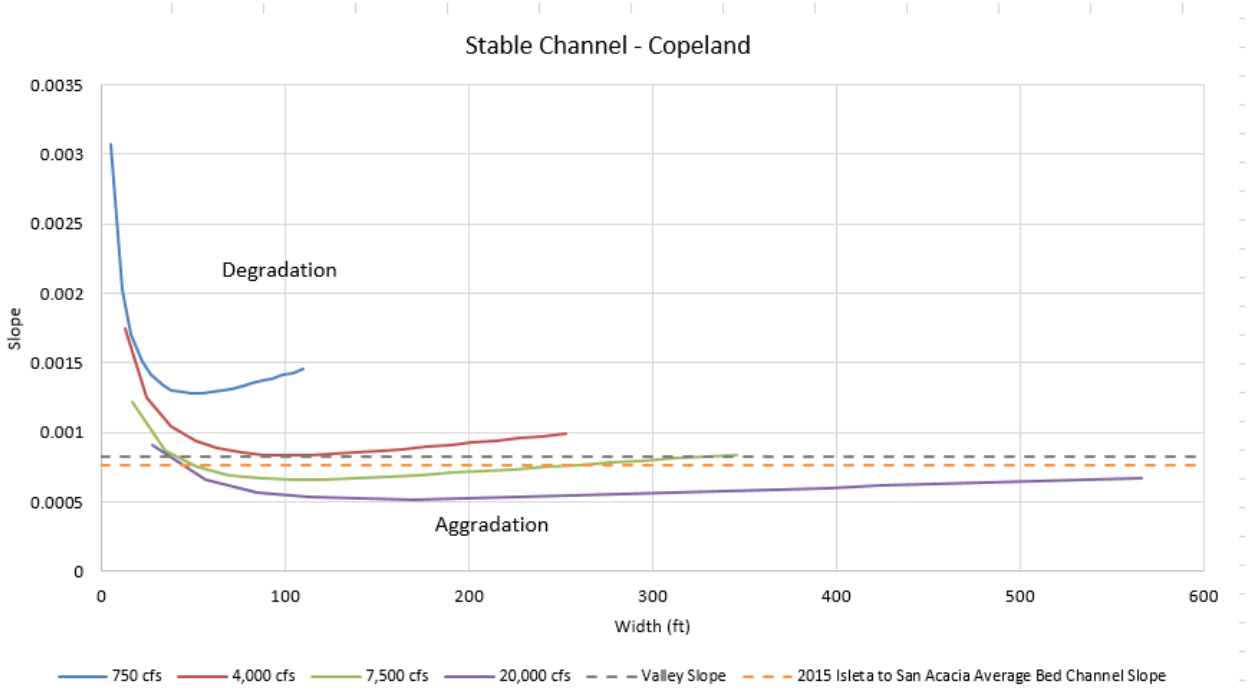

Figure 25: Stable Channel Width using the Copeland Method

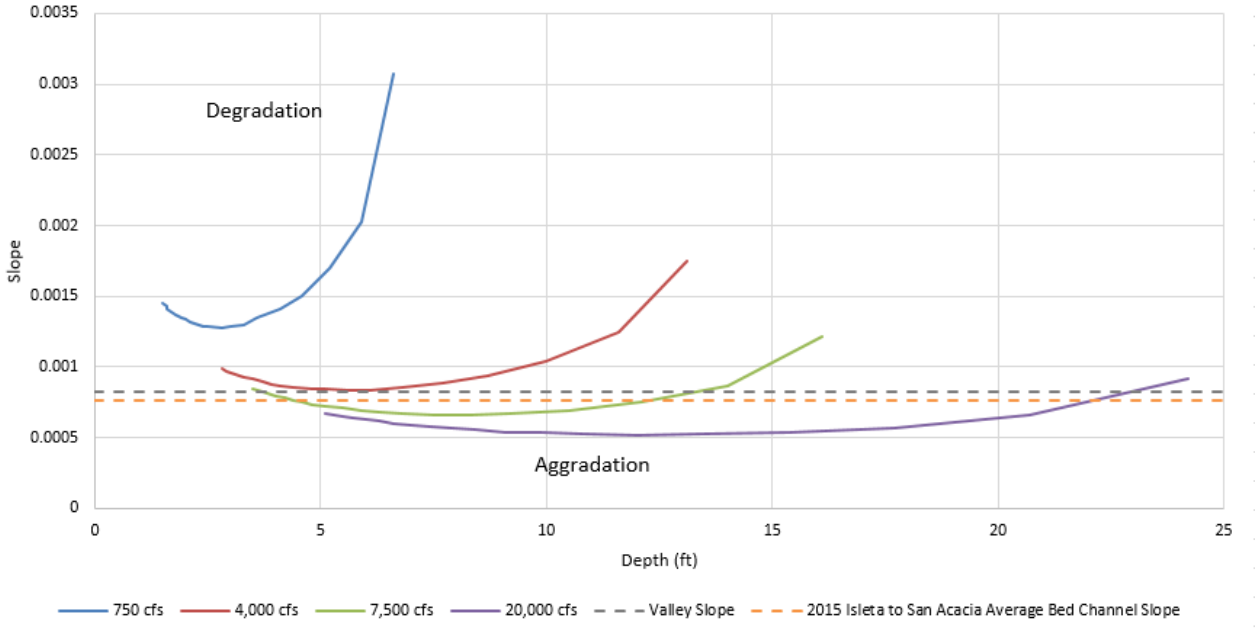

Figure 26: Stable Channel Depth using the Copeland Method

6.1.3 Results for Regime Method

The Regime Method provides one value of width, depth, and slope for each evaluated discharge, as shown in Figure 27 and Figure 28. As the discharge increases, the estimated stable width and depth both increase, while the estimated stable slope decreases. Figure 27 plots the current channel bed and valley slopes for the Rio Grande within the Isleta to San Acacia reach. These slopes indicate that the Rio Grande is currently not in equilibrium, at least not according to the Blench equation, which is the regime equation used within SAM (USACE, 2010b). Blench regression equations came from Indian canals with sand beds and slightly cohesive-to-cohesive banks. Assuming that the regime methodology reflects an equilibrium condition to which the Rio Grande is adjusting, then the expectation would be to see an increased slope develop from existing conditions between the Isleta and San Acacia reach based on the slope values predicted in Figure 27 for the corresponding discharges.

Figure 28 plots the 1965 and 2012 distance-weighted average values of top width and hydraulic depth alongside the stable channel results. Based on 2012 values of channel width and depth, the channel would be need to widen considerably and become shallower to find equilibrium. This wider and shallower condition was documented to exist prior to 1949 on the Middle Rio Grande (Crawford et al., 1993; Klein et al., 2018), but current observation in the slope, width, and depth of the Rio Grande (Klein et al., 2018) suggest that the opposite trends are occurring, implying that the conditions upon which the Blench regime equation were based are not applicable to the Rio Grande within the Isleta to San Acacia reach. Since Blench's regime equation assumes

that sediment is primarily moved via bed load (USACE, 2010b), this may suggest that the Rio Grande is more influenced by the suspended sediment load, a suggestion also made by Klein et al. (2018) based on a planform analysis following Schumm's methodology.

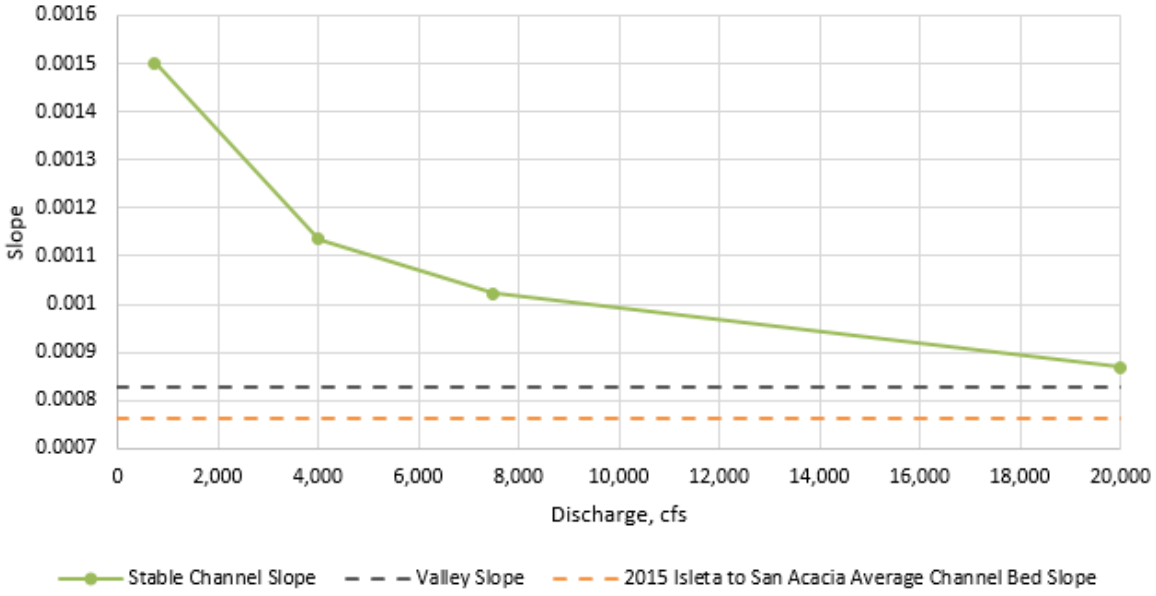

Figure 27: Stable Channel Slope using the Regime Method

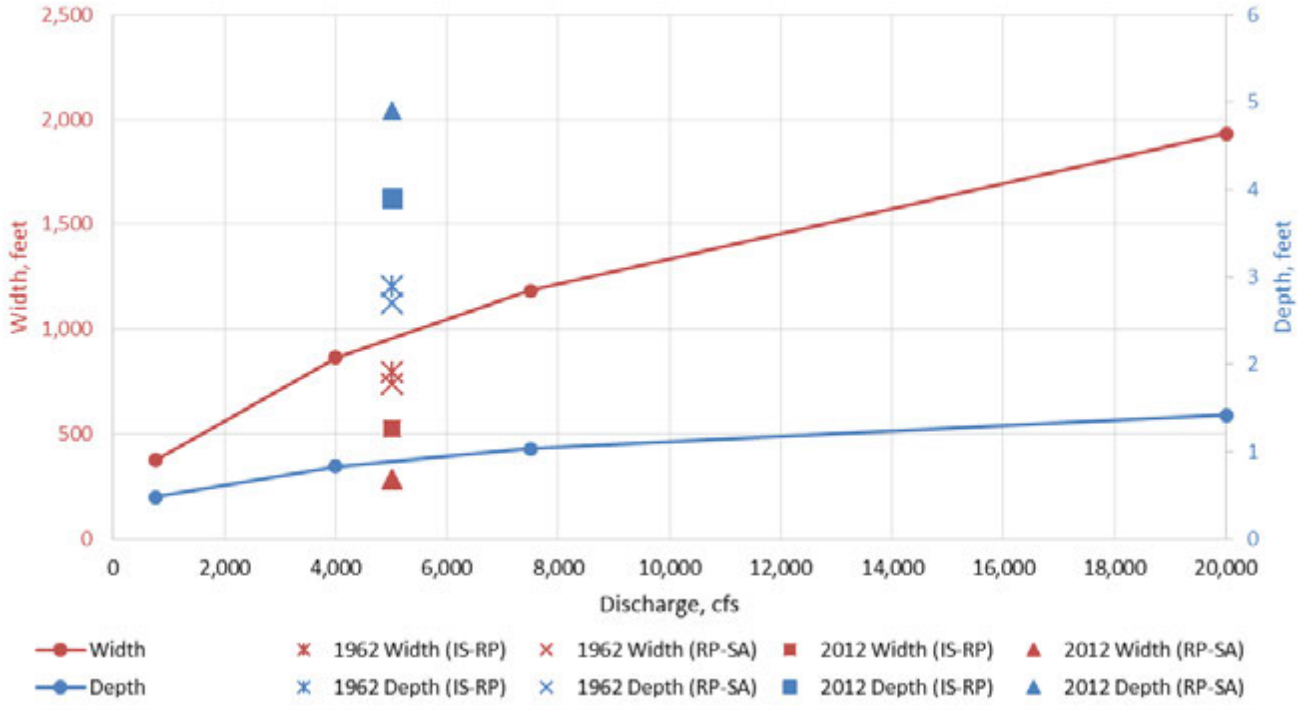

Figure 28: Stable Channel Width and Depth using Regime Method, compared with 1962 and 2012 values of top width and hydraulic depth

6.1.4 Results for Tractive Force Method

Unlike the Copeland and Regime methods, which consider the channel to be stable when there is no net aggradation or degradation, the Tractive Force Method considers a channel to be stable if there is zero movement of the bed particles, or when the channel shear stress is less than the critical shear stress required to initiate particle movement. Considering that the bed material in the reach (Isleta Diversion Dam to just upstream of the Rio Salado) has a median grain size (D_{50}) of 0.431 mm and the valley slope in this reach is 0.000838, this requires the channel shear stress to be extremely small to achieve a stable channel condition, which is only possible with an extremely high width to depth ratio, as shown in Table 12. Thus, this analysis is inconclusive for stable channel design.

The HEC-RAS stable channel design module allows the selection of the Lane Method or the Shields Method to calculate the critical shear stress. The Lane method was empirically developed in a canal with coarse particle sizes (USACE 2010b) and thus may not be highly suited for this sandy reach. The Shields Method was developed based on a wider range of data including sand (USACE, 2010b) and thus is better suited for this reach. An analysis of bed particle stability using the Shields method was conducted in the 2018 Isleta to San Acacia Geomorphic Analysis Report and can be referred to for more detailed calculations. That analysis confirmed that the bed material is unstable at the evaluated discharges except around the Rio Salado confluence where the bed material is coarser (Klein et al 2018).

Discharge values larger than 4,000 cfs were not included in the analysis because the width to depth ratios tend to increase with discharge and the values for the lower discharges were already extremely high.

Table 12: Tractive Force Method for Stable Channel Design

	750 cfs (Lane Method)	4,000 cfs (Lane Method)	750 cfs (Shields Method)	4,000 cfs (Shields Method)
Depth (feet)	0.18	0.18	0.09	0.09
Width (feet)	9,727	51,878	33,068	176,366
Width/Depth	~54,000	~288,000	~367,000	~1,960,000

7.0 Sediment Deposition and Erosion

7.1 Total Load Measurement for 2017

7.1.1 Total Load Procedure

In spring 2017, Reclamation's contractors measured a variety of hydraulic and sediment parameters within the Isleta to San Acacia reach for the purpose of determining the total sediment load being transported through the reach (Southwest Water Design, 2017).

The measurements were conducted in five "rounds" of measurements at four different rangelines on the Rio Grande between the Isleta Diversion Dam and the Rio Puerco confluence. The relationship of the measurement dates to the 2017 spring snow-melt hydrograph is shown in Figure 29. Round 1 and 2 were conducted on the rising limb of the hydrograph, while round 4 and 5 were conducted on the falling limb. Round 3 occurred near the peak flow condition. Round 5 was conducted around base flow conditions at the end of the spring runoff.

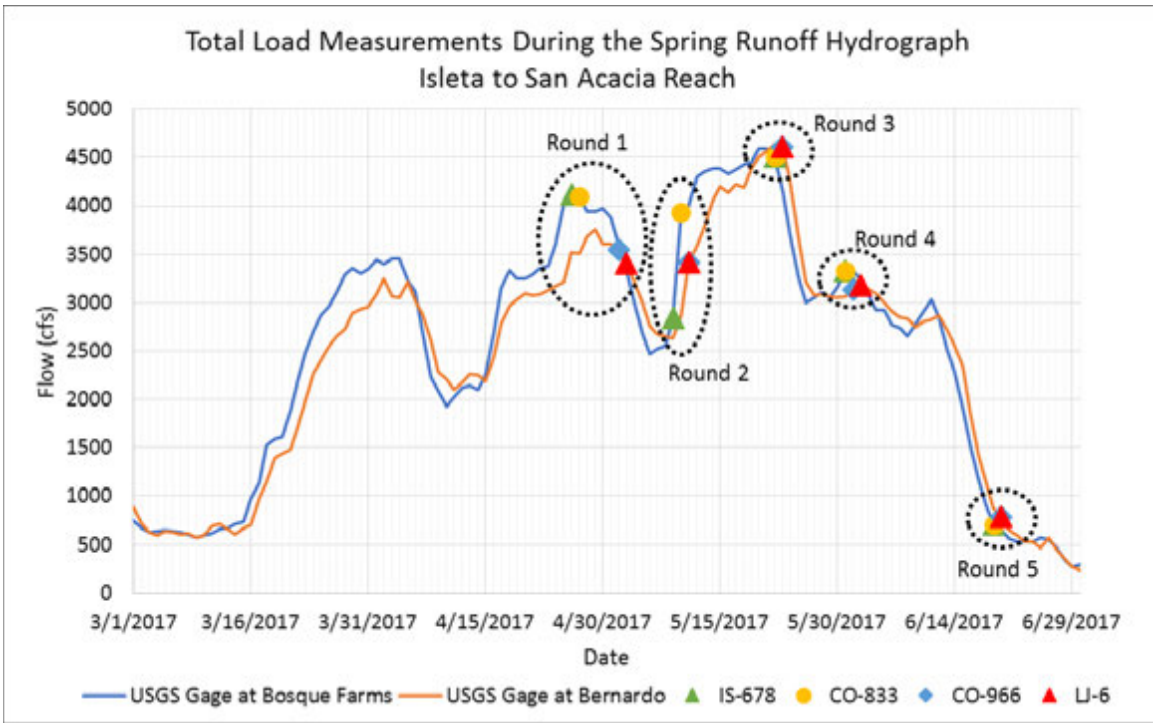

Figure 29: Timing of total load measurements during the spring runoff hydrograph

The four rangelines where measurements took place are described in Table 13.

Table 13: Total load measurement locations

Rangeline	2012 River Mile Demarcation	Location Description
IS-678	RM 167	Approx. 2 mi downstream of Isleta Diversion Dam
CO-833	RM 152	Immediately upstream of Belen, NM
CO-966	RM 130	Immediately downstream of Abo Arroyo confluence
LJ-6	RM 125	Between the Rio Puerco and the Rio Salado confluences

The collection procedure followed the USGS' Equal Discharge Interval (EDI) methodology for field measurements (Edwards and Glysson, 1999).

The total load was estimated using two different methods. The first method calculated total load by combining physical measurements of the suspended sediment load and the bed load (not available for the first round of measurements since bed load measurements were not taken at that time). The bed load was calculated as the weight of the dry bed load sample over the time that it took to collect the sample (between 60 and 180 seconds) resulting in a bed load flow rate of lbs/second. With the appropriate unit conversions, this provides a bed load flow rate in tons/day. The suspended sediment load was calculated as the weight of the dry suspended sediment sample per volume of sample (mg/L), multiplied by the river flow rate (ft^3/s). With the appropriate unit conversions, this provides a suspended sediment flow rate in tons/day. To determine the total load, the suspended sediment and bed load flow rates were combined.

The second method used physical measurements of the suspended sediment load and the bed material to estimate the total load utilizing the Bureau of Reclamation's Automated Modified Einstein Procedure (BORAMEP) software. BORAMEP provides a calculated total load value based on the overlapping of sediment size bins associated with the bed and suspended sediment material (Holmquist-Johnson et al., 2009). This methodology requires at least two overlapping size classes, which is not always possible, especially when the flows are low and the suspended sediment is dominantly fines. In the case of the 2017 measurements, which totaled 100 pairs of bed material and suspended sediment samples, BORAMEP calculated total load values on 76 of the pairs. The inability to successfully calculate a sediment load due to a lack of overlapping sediment size classes has been noted by previous studies (Shah, 2006; Shah-Fairbank, 2009).

7.1.2 Total Load Results from Field Measurements

The measured total load (total load estimated from measured suspended sediment and bed material load) was plotted versus river discharge (Figure 30). The range of sediment moving during the 2017 spring snow-melt runoff

is between 400 and approximately 19,000 tons/day. Also, there is more than twice as much sediment moving at the largest measured discharge than the other discharges.

Figure 31 and Figure 32 show the same total load data points, but the data points have been color-coded and the axes have been modified to highlight differences due to the location in the reach (Figure 31) and differences due to the timing on the spring hydrograph (Figure 32). Figure 31 shows that generally there is less sediment being transported per unit of river discharge as you move downstream. This likely indicates that sediment is depositing onto the bed and banks throughout the reach. Figure 32 shows that the total load is not distinctly higher or lower for measurements acquired on the rising limb (round 2) versus the falling limb (round 4), but the range of sediment load is greater on the falling limb than the ascending limb of the hydrograph. Also, the peak discharge measurements (round 3) are correlated with the highest sediment loads per unit of river discharge. The sediment load is the lowest when the river discharge returns to base flow levels (round 5).

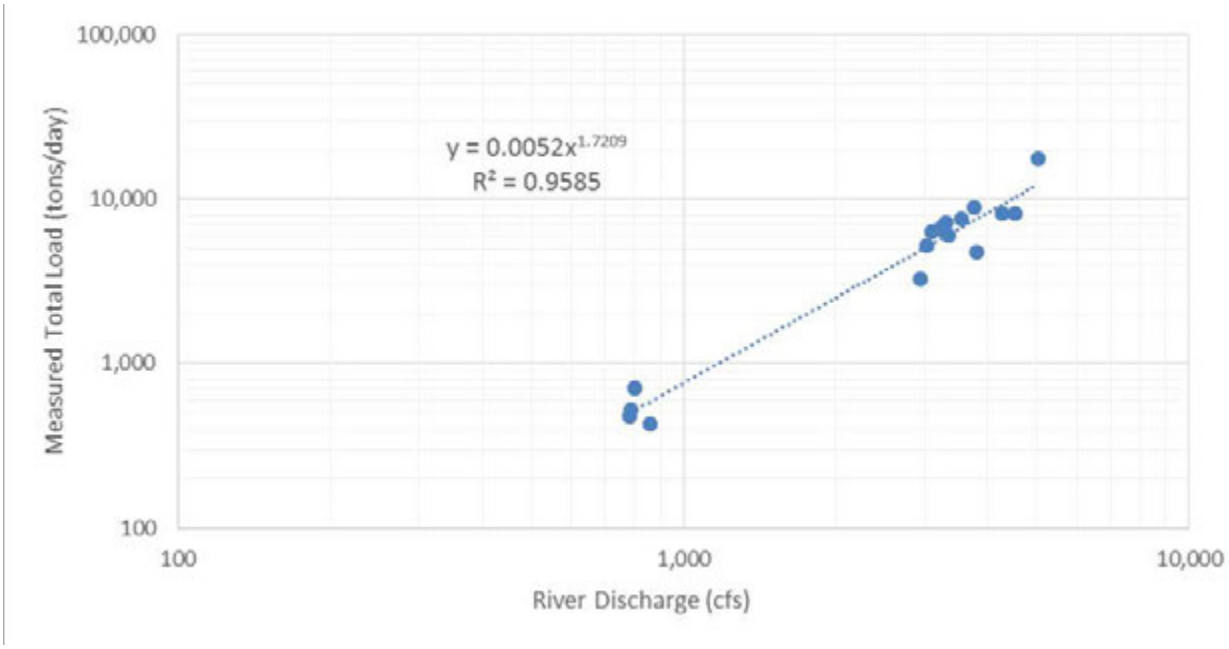

Figure 30: River discharge versus measured total load

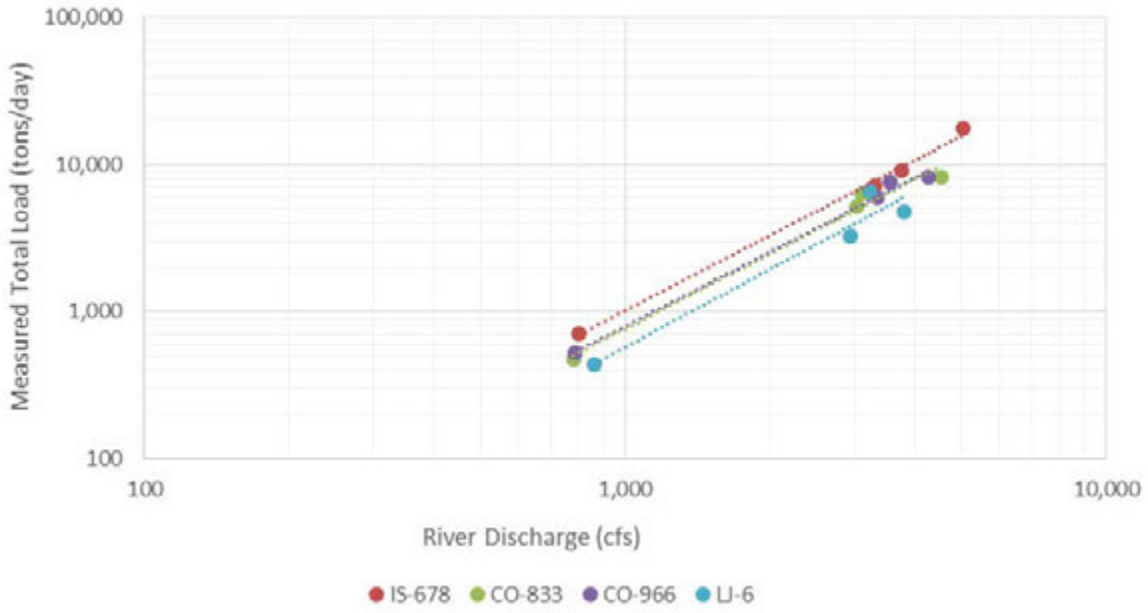

Figure 31: River discharge vs measured total load for each rangeline

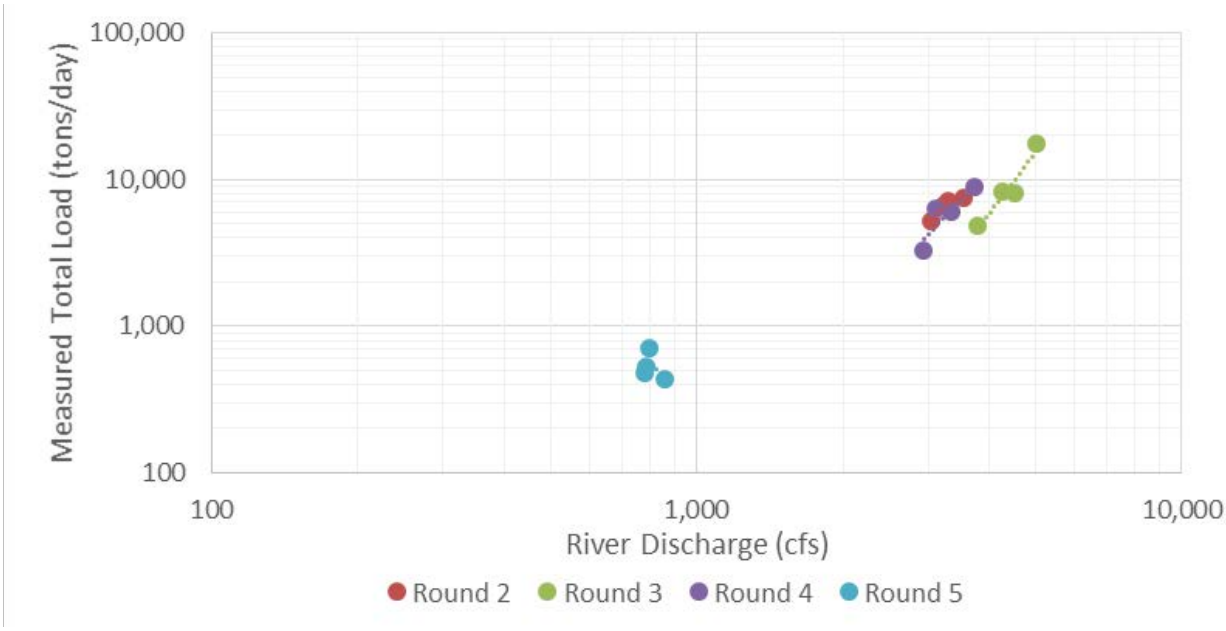

Figure 32: River discharge vs measured total load for each measurement round

7.1.3 Comparison of BORAMEP Calculations with Field Estimates

Since the 2017 field data collection captured data for both a physical measurement of total load and a BORAMEP calculation of total load, a comparison can be made (Figure 33). In general, the BORAMEP estimates tend to be higher than the physical measurements.

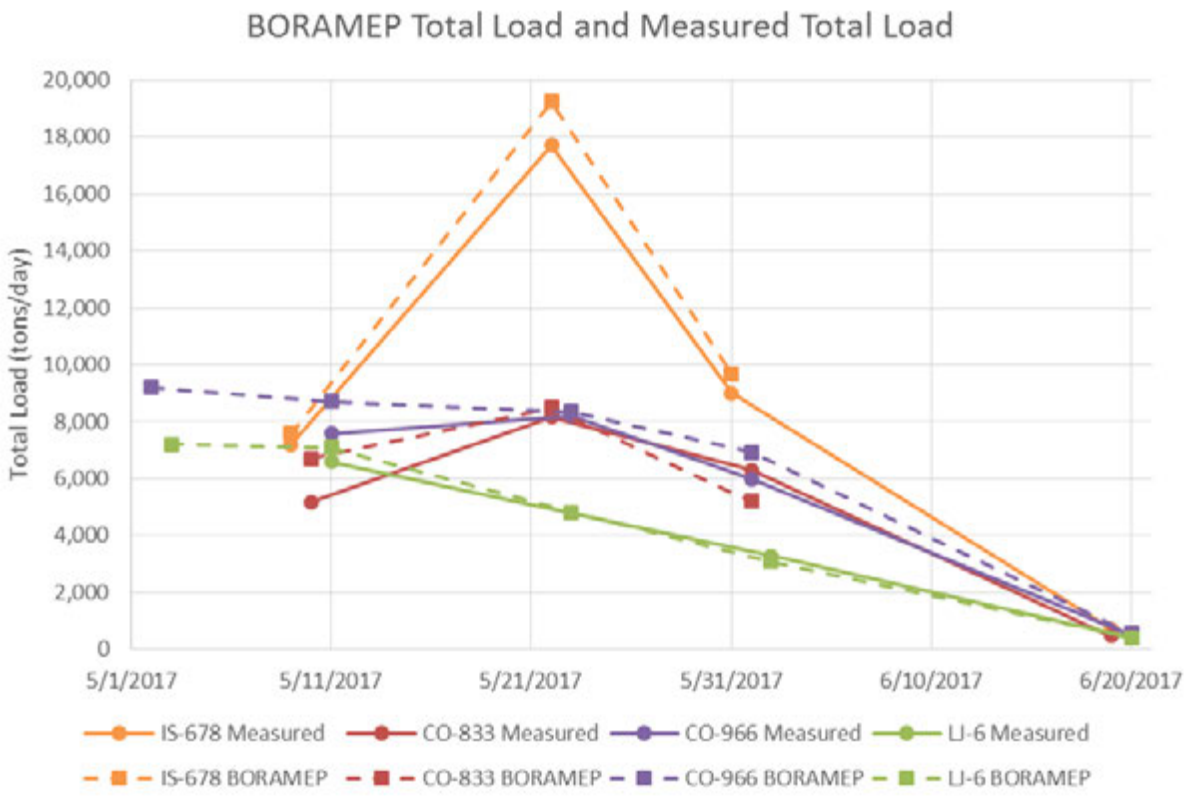

Figure 33. Total Load estimates from 2017 physical measurements and BORAMEP estimates

Bed load can be defined as movement of sediment at or near the bed that relies on what Bagnold (1966) describes as "solid-transmitted stress" (p. I4). Einstein (1950), however, defined bed material load as being the movement of sediment within the same size classification as the bed material. This would include both those sediment particles that previously were on the bed and now are moving in suspension or through various processes along the bed. The BORAMEP calculation utilizes the Einstein (1950) definition of bed material load (Holmquist-Johnson et al., 2009), calculating a bed load from sampled bed material and suspended sediment measurements.

The field estimate based on Helley Smith measurements captures an estimate of the bed load that is closer to the definition provided by Bagnold (1966). This estimate does not include former bed material that now may be moving in suspension, unlike BORAMEP's estimate. It is therefore reasonable to assume that the bed material load calculated using BORAMEP calculations, which may include a portion of the measured suspended load, would be greater than the direct field measurement for the bed load.

As previously described, field measurements for total load employed the Equal Discharge Interval (EDI) sampling methodology (Southwest Water Design, 2017). This is a methodology developed by the USGS which

minimizes sampling error when using the approved Federal Interagency Sedimentation Project (FISP) samplers, but there is still a zone that is unmeasured despite using paired samplers (Edwards and Glysson, 1999). The 2017 data collection effort on the Rio Grande used the FISP approved D-74 suspended sediment and BLH-84 bed load samplers (Southwest Water Design, 2017). The D-74 measures suspended sediment in the water column with a 4.1 inch zone near the bed that is unmeasured (Davis, 2005). The BLH-84 bed load sampler has a 3 inch entrance nozzle that rests on the river bed (Davis, 2005), covering part, but not all of the zone left unmeasured by the suspended sediment sampler. This would also tend to make the field measured bed load estimate less than the BORAMEP estimate.

Given these uncertainties, both in the definition of bed load versus bed material load and the unmeasured sediment quantity between the field sediment samplers, it seems there is a reasonable correlation between the two total load methodologies used to assess the 2017 data collection effort (Figure 33). The BORAMEP estimates for bed material and total load are greater than the estimate derived from the physical measurements, implying that a significant portion of the total load consists of bed material carried in suspension.

Table 14 shows the portion of the total load attributable to bed load as measured by Helley Smith measurements, and the portion of the total load attributable to bed material load as calculated by BORAMEP. The remainder of the total load consists of the measured suspended sediment load. Figure 34 also shows the portion of the total load attributable to bed load as measured by Helley Smith measurements plotted against discharge (USGS gage 8331160 near Bosque Farms).

Table 14: Portion of Total Load Attributable to Bed Load

Location on Hydrograph	Round	Portion of Total Load Attributable to Bed Load (Helley Smith) (Averaged for All Locations)	Portion of Total Load Attributable to Bed Material Load (BORAMEP) (Averaged for All Locations)
Rising Limb	R2	18%	20%
Peak	R3	18%	22%
Falling Limb	R4	23%	18%
Falling Limb (Base Flows)	R5	42%	23%

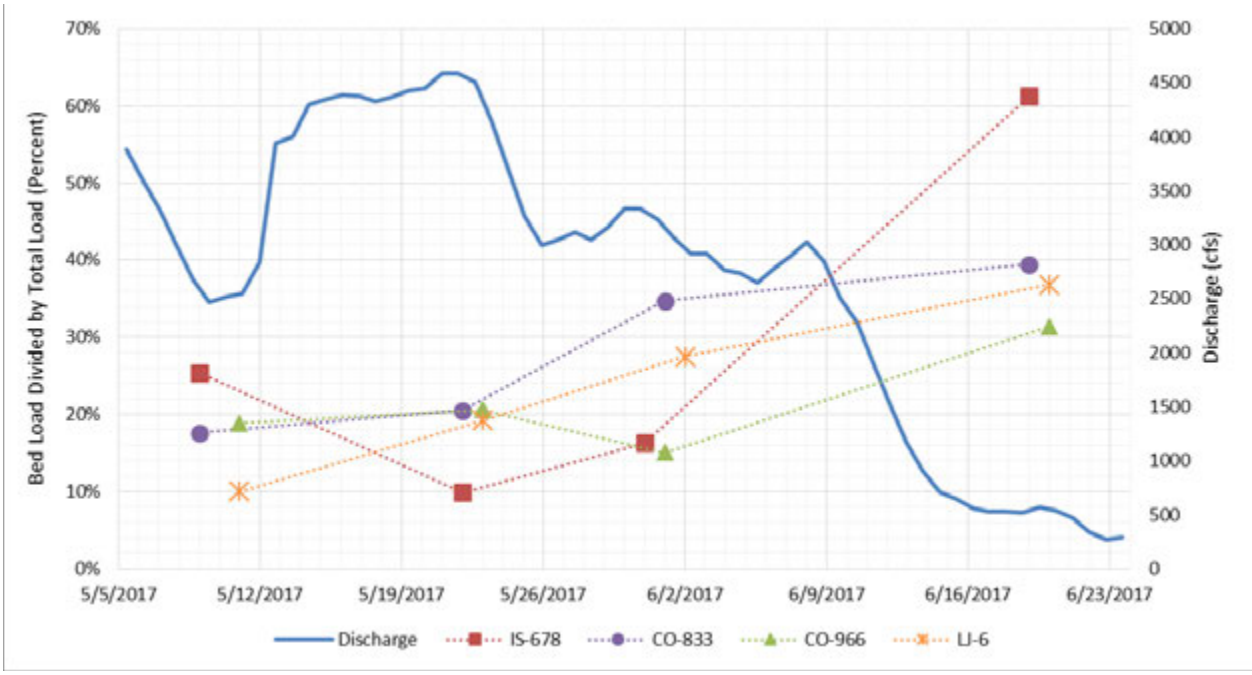

Figure 34: Bed load as a percent of total load for each of the field measurements

7.1.4 Comparison of Total Load Measurements between Rangelines

Insight into how sediment moves within the Isleta to San Acacia reach can be assessed by evaluating the differences in the total load between the measurements at the four rangelines. It should be noted that evaluated differences are simply a subtraction of the estimated volumetric sediment transport and do not take into account transit time or measurement delays. Often the four rangelines were collected over a 2 to 3 day interval, so this may have an effect on the observed differences. The total load estimates used to calculate the difference are the BORAMEP values at each rangeline. Sampling at CO-833 and IS-678 did not result in sufficient overlapping bins for a BORAMEP calculation during round 5, so the estimates from direct measurements were used instead. Insufficient data was available during the round 1 measurements to calculate a total load estimate from either the direct measurements or BORAMEP at IS-678 and CO-833, so no round 1 comparisons are available for these two rangelines.

The IS-678 rangeline is near river mile 167 (2012 river mile demarcations), which is in the Bosque Farms, NM area. CO-833 is about 15 river miles downstream, just upstream of Belen, NM. The rangeline is near river mile 152 (2012 river mile demarcations). CO-966 is downstream of the Abo Arroyo confluence around river mile 130 (2012 river mile demarcations). This gives around a 22 river mile stretch of the Rio Grande. Finally, LJ-6 is located

around river mile 125 (2012 river mile demarcations), which is about two miles downstream of the Rio Puerco confluence.

Figure 35: Total Load Measurement Locations

Table 15: Description of sub reaches as divided by measurement locations

Measurement Locations	Reach Identifiers	Approximate River Miles
IS-678 to CO-833	Bosque Farms to Belen	15
CO-833 to CO-966	Belen to Abo Arroyo	13
CO-966 to LJ-6	Abo Arroyo to downstream of Rio Puerco	14

Table 16 provides a summary of the total load field measurement results (bed load values obtained by Helley Smith measurements) including gains and losses between measurement locations. Positive values indicate a decrease in sediment load from the upstream measurement location to the downstream

measurement location; this may indicate deposition in the channel or floodplain. Negative values may indicate channel erosion or tributary inputs between measurement locations.

In the reach between IS-678 and CO-833, each of the measurements saw a decrease in total load, likely indicating that deposition was more prominent than erosion and tributary inputs. In the reach between CO-833 and CO-966, tributary inputs and/or bank and bed erosion was likely more prominent, and between CO-966 and LJ-6, deposition was likely more prominent.

Table 16: Total load field measurement results

Measurement Location	Date	Discharge (cfs)	Susp. Load (tons/day)	Bed Load (tons/day)	Total Load (tons/day)	Total Load Gain/Loss (tons/day)
IS-678	5/9/2017	3,308	5,376	1,828	7,204	--
CO-833	5/10/2017	3,037	4,265	911	5,176	2,028
CO-966	5/11/2017	3,550	6,159	1,433	7,592	(2,415)
LJ-6	5/11/2017	3,215	5,927	660	6,587	1,005
IS-678	5/22/2017	5,030	15,965	1,748	17,713	--
CO-833	5/22/2017	4,535	6,485	1,678	8,163	9,549
CO-966	5/23/2017	4,263	6,616	1,595	8,212	(49)
LJ-6	5/23/2017	3,805	3,879	921	4,799	3,412
IS-678	5/31/2017	3,748	7,531	1,468	8,999	--
CO-833	5/31/2017	3,100	4,118	2,189	6,308	2,691
CO-966	6/1/2017	3,348	5,091	900	5,991	317
LJ-6	6/2/2017	2,940	2,378	903	3,281	2,710
IS-678	6/19/2017	800	277	438	714	--
CO-833	6/19/2017	780	289	188	477	237
CO-966	6/20/2017	788	361	165	527	(49)
LJ-6	6/20/2017	860	274	160	433	93

7.2 One-Dimensional Sediment Modeling

A one-dimensional numerical sediment model was developed for the Isleta to San Acacia reach using Reclamation's Sedimentation and River Hydraulics – One Dimension (SRH-1D) mobile boundary hydraulic and sediment transport numerical model (Greimann, 2018). The goal of the modeling effort was to predict future channel response to different hydrologic regimes (Huang, 2018). A brief summary of this modeling effort is described below:

- Cross section geometry is based on the underwater bathymetry generated from the 2002 aggradation-degradation aerial photography data collection effort (Holmquist-Johnson and Makar, 2006).
- The numerical model was calibrated using the underwater bathymetry generated from the 2012 aggradation-degradation LiDAR data

collection effort (Varyu, 2013) using actual hydrographs from 2002 to 2012.

- Sediment transport was estimated by using the Parker (1990) sediment transport equation combined with Engelund-Hanson sediment transport equation. This provided the best calibration of the 2002 geometry to the 2012 geometry.
- Three 20-year, unsteady state, hydrologic regimes were used to forecast the future channel response for wet, average, and dry climatic sequence were used representing the 10%, 50%, and 90% exceedance, respectively.

Conclusions from the modeling effort provided the following predictions for the future 20 year channel response (Huang, 2018):

- The subreaches with the greatest deposition will be from Isleta to Bosque Farms, and from Rio Salado to San Acacia.
- The subreach with the greatest degradation will be from Bosque Farms to the northern side of Belen.
- Median sediment size will be relatively stable in the study reach, ranging from 0.38 mm at the upstream end to 0.33 at Rio Salado and 0.37 at San Acacia.

The areas of deposition and erosion predicted by the 1-dimensional model are roughly similar to the areas of deposition and erosion identified by the total load field measurements during the 2017 spring snow-melt runoff.

8.0 Riprap Sizing

8.1 Riprap Procedure

Riprap sizing was calculated for nine river maintenance sites within the Isleta to San Acacia Reach. These sites included Highway 309, Los Trujillos, Rio Puerco RM 127.9, Rio Puerco RM 127.5, Rio Puerco RM 127, La Joya, Bernardo Arroyo, RM 121, and Drain Unit 7. The nominal (D_{50}) riprap size required for traditional bank protection at each of these sites was calculated using two different rip rap sizing methodologies. Guidance from de Almeida and Martin-Vide (2009) was used to estimate riprap sizes for transverse feature placement from the bank protection estimates. A multiplication factor of 2.5 (de Almeida and Martin-Vide, 2009) was used for this estimation of the riprap size required at the tip of the transverse feature. Abt et al. (2016) have also suggested a need to increase the riprap size when placement is not parallel to the direction of flow. Abet et al. suggested multiplying the design velocity by a factor of 1.7 which results in a riprap size that is around or slightly more conservative than the de Almeida approach (2009). The 2014/2015 HEC-RAS 1-dimensional numerical model was used to generate the necessary inputs for the riprap calculations. The design flow was 20,000 cfs. Equations and calculations for the riprap sizing are provided in Appendix B.

The first riprap methodology employed for estimating bankline riprap size is the Army Corps of Engineers (USACE) method described in the Hydraulic Design of Flood Control Channels (USACE, 1994). The USACE method is a velocity-based method derived from physical scale modeling of riprap stability that took into account bend curvature. The method is based on using graded riprap material. An independent review (Lagasse et al., 2006) of sites where riprap was placed found this equation to be the most comprehensive. The USACE requires inputs that varied between each of the sites, including average velocity at the upstream end of the bend, the local depth of flow, the center-line radius of curvature of the bend, the water-surface width, the angle of side slope with horizontal, and the location of riprap within the channel (e.g. inside bend, outside bend, straight). The method also requires inputs that did not vary between the nine evaluated sites. These values included the channel type, specific weight of water and riprap, stability coefficient, blanket thickness coefficient, and safety factor.

The second riprap method utilized the California Department of Transportation (Caltrans) methodology published in a guide on rock slope protection (Racin, 2000). The Caltrans method is also a velocity-based method based on the layered rock slope protection. The equation provides the minimal weight needed for the outer layer to be stable, provided the inner layers are included in the design. An independent study (Lagasse et al., 2006)

found this method to be acceptable if the appropriate layers were used. It was found that this approach typically uses more riprap than a graded riprap mixture. The equation is also based on physical scale models. The Caltrans method uses a smaller subset of the factors employed by the USACE method. These factors include velocity, angle of side slope, and specific weight of water and riprap. In addition, the Caltrans Method requires a binary input of designating whether the flow is impinging or parallel to the bank.

8.2 Riprap Results

Figure 36 shows the results of the riprap size calculations. The figure compares the riprap sizing resulting from both the USACE and Caltrans methodology for each of the nine sites. A secondary axis on Figure 36 shows the riprap sizing for transverse features which incorporates the multiplication factor suggested by de Almeida and Martin-Vide (2009). For all sites, the USACE method prescribes larger riprap sizing than the Caltrans method, which is expected since the USACE equation is more comprehensive than the Caltrans equation.

The required riprap D_{50} size at the northern eight sites ranges between about 4 to 18 inches for continuous bank protection and from about 10 to 45 inches for transverse riprap placement. The Drain Unit 7 river maintenance site requires the largest nominal riprap sizes of the tested sites, around a 60 inch nominal riprap size needed for continuous bank protection. The Drain Unit 7 river maintenance site is close to San Acacia Diversion Dam, and in an area where there was known numerical uncertainties in the model results since the HEC-RAS model didn't simulate operation at San Acacia Dam. It is therefore possible the riprap sizes at Drain Unit 7 may be more conservative than needed, especially for a checked water condition.

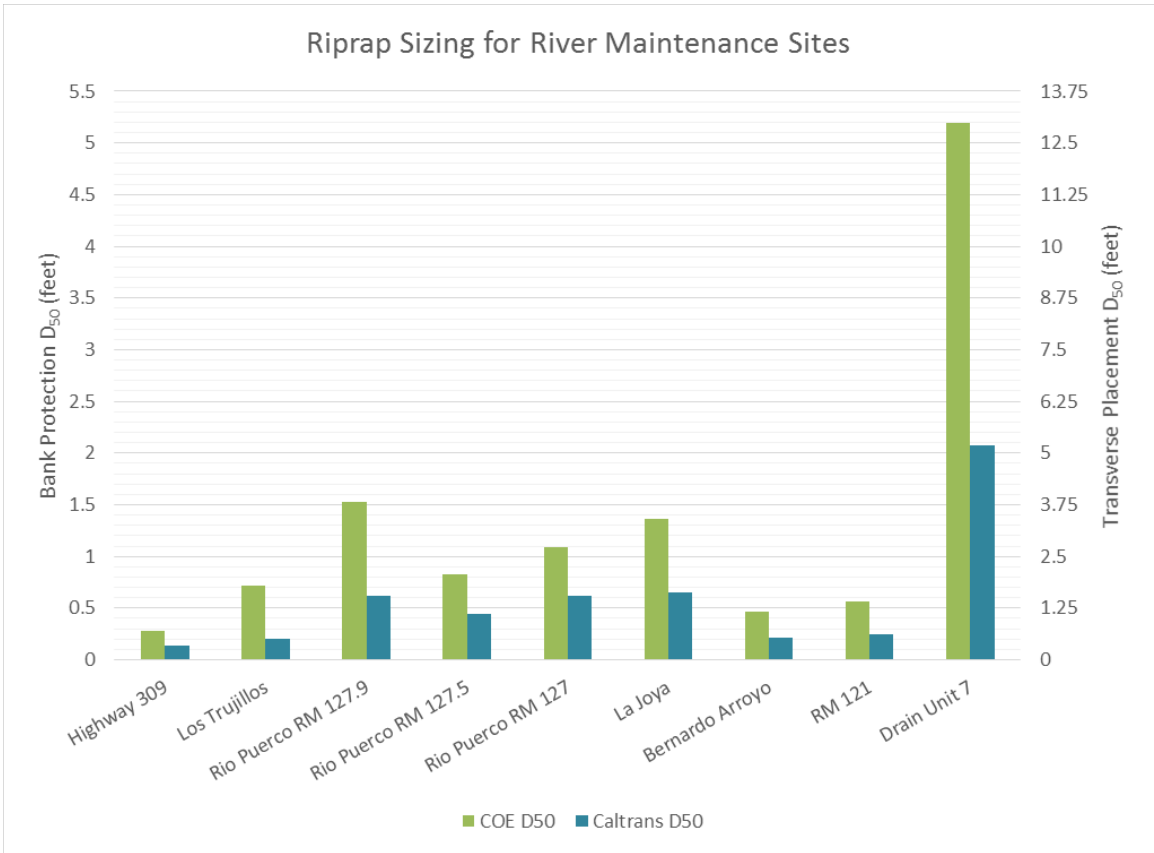

Figure 36: Riprap sizing for longitudinal bank protection (primary axis) and transverse placement (secondary axis) as determined by the USACE methodology and the Caltrans methodology for river maintenance sites

9.0 Scour Estimate

9.1 Scour Procedure

Scour was calculated at ten locations within the Isleta to San Acacia Reach. These locations were closest to the following 2012 river mile (RM) demarcations: RM 162, RM 149 (near Los Trujillos and Highway 309 Bridge), RM 138.2, RM 130.4, RM 127.9, RM 127.5, RM 127.0, RM 124, RM 120, and RM 116.5 (near Drain Unit 7 river maintenance site). Evaluated scour equations were from Pemberton and Lara (1984), ASCE (2004a), and ASCE (2004b). The 2014/2015 HEC-RAS 1-dimensional numerical model, measurements within ESRI's ArcMap software (version 10.4.1), and field collected data were used to generate the necessary inputs for the scour calculations. The design flow was 4,000 cfs. Equations, calculations, and input values for the scour analysis are provided in Appendix C for each site.

Since the ten sites rarely aligned perfectly with one of the HEC-RAS model cross sections, results were extracted from either the closest input cross section or from the nearest interpolated cross section.

Since the HEC-RAS model did not include San Acacia Diversion Dam, the cross sections near the dam have a high level of uncertainty. Site RM 116.5 utilizes inputs from cross sections near the dam, and thus the scour estimates from this site also have a high level of uncertainty.

Aerial photography was used in conjunction with drawing tools within ESRI's ArcMap software (version 10.4.1) to provide estimates of the radius of curvature for a site's river bend. Aerial photography was also used to determine whether the evaluated site was on a straight reach, moderate bend, or severe bend.

Many equations also required information about the site's bed material size. Sediment samples were collected throughout the reach in 2016 (Klein et al., 2018), and the required bed material sizes for the scour equations were derived from the nearest bed material sampling site. Because the collected samples were spread uniformly throughout the reach, they were not always immediately adjacent to the ten locations chosen for the scour analysis. Table 17 provides the bed material location and collection year for each of ten evaluated scour locations. Near RM 116.5, the nearest 2016 bed material sample was from a location miles away at the confluence of the Rio Salado Arroyo, where material was much coarser than expected at this location. In 2012 (Tetra Tech, 2012) bed material was collected at a closer location and was therefore used in the scour calculations.

Table 17: Bed material information used in scour equations

Site name	Bed Material Sample Location (year)	Bed material size D_{50} (mm)
RM 162	Agg/Deg 732 (2016)	0.60
RM 149	Agg/Deg 857 (2016)	0.43
RM 138.2	Agg/Deg 976 (2016)	0.46
RM 130.4	Agg/Deg 1061 (2016)	0.39
RM 127.9	CO-1091 (2016)	0.40
RM 127.5	CO-1091 (2016)	0.40
RM 127	CO-1091 (2016)	0.40
RM 124	LJ-18 bed (2016)	0.38
RM 120	CO-1164 (2016)	0.41
RM 116.5	RP-1203.7 (2012)	0.55

9.2 Scour Results

The scour depths calculated for each of ten locations for all of the evaluated scour equations are shown in Appendix C. Table 18 provides a range of the calculated scour depths. The results show that the sites with the highest potential scour include RM 130.4, RM 127.9, RM 124, and RM 116.5 (2012 river mile demarcations).

Table 18: Range of scour values which can be applied based on design needs

Site name	Minimum Scour Estimate, feet (Equation)	Maximum Scour Estimate, feet (Equation)
RM 162	1.1 (Zeller)	5.5 (Lacey)
RM 149	0 (Zeller)	5.4 (Thorne)
RM 138.2	0.7 (Neill)	4.5 (Thorne)
RM 130.4	1.6 (Zeller)	9.6 (USACE)
RM 127.9	1.3 (Neill)	9.3 (USACE)
RM 127.5	1.1 (Neill)	7.1 (USACE)
RM 127	1.1 (Neill)	5.5 (USACE)
RM 124	1.6 (Neill)	10.6 (USACE)
RM 120	0.6 (Zeller)	6.8 (Thorne)
RM 116.5	3.4 (Neill)	7.9 (USACE)

Conclusions

This report has provided an analysis of channel hydraulics, channel equilibrium, and bank stability within the Isleta to Rio Puerco and Rio Puerco to San Acacia reaches to aid in understanding and identifying future work needs.

In conclusion, the Rio Grande from Isleta to San Acacia has narrowed and become deeper, leading to greater velocities and channel shear stress. This is supported by this report's findings that the river's cross sectional flow area, wetted perimeter, and width-depth ratio have an overall decreasing trend, while the hydraulic radius (surrogate for channel depth), mean velocity, and shear stress have a recently increasing trend.

The 5,000 cfs WSE has increased on average 0.9 feet between 2002 and 2012, indicating a likely decrease in main channel conveyance capacity during that time. Between 2012 and 2015, the 5,000 cfs WSE and conveyance capacity have remained stable.

Bankfull discharge has had varying trends between 1962 and 2012. The varying trends indicate the channel's adjustment to both wetter and drier hydrologic periods. Based on 2015 data, the bank overtops on average at 4,600 cfs in the Isleta to Rio Puerco reach, and on average at 5,500 cfs in the Rio Puerco to San Acacia Reach. Some areas begin to overbank as low as the 2,000 to 3,000 cfs range.

Based on 2015 data, the high water threat to the levees was greatest in the Isleta to Highway 309 (Belen) reach, and lowest in the Highway 60 to San Acacia reach. The banks are higher than the levee toes (perched condition) from Isleta to Highway 309, and in the rest of the reach the banks are similar in elevation to the levee toes.

Overall, this is a fairly stable reach with relatively minor changes in the floodplain accessibility and conveyance capacity. There are specific areas where various changes historically have been more significant, and these areas include near the Rio Puerco, the Rio Salado, and upstream of San Acacia Diversion Dam. All these changes have been so variable that future trends are not easily predictable from the past changes.

Recommendations

The following recommendations have been generated to address the negative aspects of the current conditions and trends in the Isleta to San Acacia reach.

- The increased channel velocities are detrimental for fish habitat. Channel velocities can be decreased by lowering floodplains, widening the channel including the use of side channels, or decreasing the energy slope.

- Perched channel conditions combined with overbanking at lower flows can be a potential threat to the levees through avulsion and prolonged saturation, and overbanking with no return path can strand fish. Side channels and other drains should be created to provide preferred paths for the fish and water to return to the main channel in the Isleta to Belen reach.

- The 5,000 cfs WSE profiles downstream of the Rio Salado show a dramatic drop in water surface elevation over a short longitudinal distance. This steep zone, which is almost twice the slope of the rest of the reach, may limit fish migration given the large drop. The slope and velocity should be investigated and a biologist should be consulted to see how significant the slope and velocity are as a potential fish migration constraint.

Acknowledgments

This work has been greatly benefited by the persistent data collection of the U.S. Geological Survey, technical work members of the River Analysis Group in Reclamation's Albuquerque Area Office, and historical work to date on the Rio Grande through this reach, much of which has been cited throughout this report.

References

Abt, S.R., Scurlock, S.M., Thornton, C.I., Cox, A.L., and Holste, N.J. 2016. Bendway Weir Riprap Sizing Criteria. Journal of Hydraulic Engineering, American Society of Civil Engineers, Volume 142, Issue 12, Reston, VA. 5 pp.

ASCE. 2004a. Stream Investigation, Stabilization, and Restoration Workshop by David Derrick, U.S. Army Corps of Engineers, and Gary Freeman, WEST Consultants, American Society of Civil Engineers, Tempe, AZ. 253 pp.

ASCE. 2004b. Predicting Bed Scour for Toe Protection Design for Bank Stabilization Projects Workshop by Dennis Richards, WEST Consultants, American Society of Civil Engineers, Tempe, AZ. 146 pp.

ASPRS. 2015. ASPRS Positional Accuracy Standards for Digital Geospatial Data, Edition 1, Version 1.0 – November 2014. Photogrammetric Engineering and Remote Sensing, Vol 81, No. 3, March 2015, ASPRS, Bethesda, MD, pp. A1-A26

AuBuchon, Jonathan. 2015. Isleta to San Acacia Reach Overview of Previous Work. U.S. Department of the Interior, Bureau of Reclamation, Upper Colorado Region, Albuquerque, NM. 31 pp.

Bagnold, R.A. 1966. An Approach to the Sediment Transport Problem from General Physics. U.S. Department of the Interior, Geological Survey Professional Paper 422-1, United States Government Printing Office, Washington, D.C. 37 pp.

Benoit, V. 2013. 2012 Aggradation/Degradation LiDAR Data of Historic Range Lines. U.S. Department of the Interior, Bureau of Reclamation, Upper Colorado Region, Albuquerque, NM. 17 pp.

Culbertson, J.K. and Dawdy, D.R. 1964. A Study of Fluvial Characteristics and Hydraulic Variable Middle Rio Grande New Mexico. U.S. Geological Survey, Professional Paper 1498-F, Washington, D.C. 82 pp

Crawford, C.S., Cully, A.C., Leutheuser, R., Sifuentes, M.S., White, L.F., and Wilber, J.P. 1993. Middle Rio Grande Ecosystem: Bosque Biological Management Plan. Middle Rio Grande Biological Interagency Team, Albuquerque, NM. 320 pp.

Davis, B.E. 2005. A Guide to the Proper Selection and Use of Federally Approved Sediment and Water-Quality Samplers. U.S. Geological Survey and the Federal Interagency Sedimentation Project, Reston, VA. 26 pp.

de Almeida, G.A. and Martin-Vide, J.P. 2009. Riprap Stability: Transverse and Longitudinal versus Continuous Protections. Journal of Hydraulic Engineering, American Society of Civil Engineers, Volume 135, issue 6, Reston, VA. pp. 447-456

Easterling. 2014. Middle Rio Grande Project Hydrographic Data Collection, Hydrographic Data Collection Report Cross-Section Survey and GPS Surveys, Montaño Bridge to Isleta Dam, December 2013-February 2014. Easterling Consultants, LLC, Albuquerque, NM 594 pp.

Easterling. 2015. Middle Rio Grande Project Hydrographic Data Collection Field Data Collection Report Cross-Section Surveys, 2015 Belen RR Bridge to San Acacia Rangeline Surveys. Easterling Consultants LLC in collaboration with Tetra Tech, Inc. Albuquerque, NM 34 pp.

Edwards, T.K. and Glysson, G.D. 1999. Field Methods for Measurement of Fluvial Sediment. U.S. Geological Survey, Denver, CO. 97 pp.

Einstein, H.A. 1950. The Bed-Load Function for Sediment Transportation in Open Channel Flows. U.S. Department of Agriculture, Soil Conservation Service, Technical Bulletin No. 1026, Washington D.C. 81 pp.

Greimann, B. 2018. SRH-1D Fact Sheet. U.S. Department of the Interior, Bureau of Reclamation, Sedimentation and River Hydraulics Group, Technical Service Center, Denver, CO. ftp://aidea.org/AEASuWaEnvironmental/Protocols_&_Models/FluvialGeomorphology/SRH-1D/SRH-1D%20Fact%20Sheet.pdf, last accessed March 12, 2018.

Holmquist-Johnson, C.L., and Makar, P. 2006. Draft 2002 Cross Section Geometry Generation and Validation. U.S. Department of the Interior, Bureau of Reclamation, Technical Service Center. Denver, CO. 11 pp.

Holmquist-Johnson, C., Raff, D., and Russell, K. 2009. Bureau of Reclamation Automated Modified Einstein Procedure (BORAMEP) Program for Computing Total Sediment Discharge. U.S. Department of the Interior, Bureau of Reclamation, Technical Service Center. Denver, CO. 52 pp.

Huang, V.J. 2018. SRH-1D Numerical Model for the Middle Rio Grande. U.S. Department of the Interior, Bureau of Reclamation, Technical Service Center, Sedimentation and River Hydraulics Group, Denver, CO. 53 pp.

Klein, M., Herrington, C., AuBuchon, J., and Lampert, T. 2018. Isleta to San Acacia Geomorphic Analysis. U.S. Department of the Interior, Bureau of Reclamation, Albuquerque, NM. 451 pp.

Lagasse, P.F., Clopper, P.E., Zevenbergen, L.W., and Ruff, J.F. 2006. Riprap Design Criteria, Recommended Specifications and Quality Control, National Cooperative Highway Research Program Report 568. Transportation Research Board, National Academies of Science, Washington, D.C. 226 pp.

Maestas, J., Padilla, R., Nemeth, M., AuBuchon, J., Casuga, J., Makar, P., and Varyu, D. 2014. Determination of River Maintenance Need at Individual Sites and Reaches on the Middle Rio Grande, NM. U.S. Department of the Interior, Bureau of Reclamation, Upper Colorado Region, Albuquerque, NM. 32 pp.

Nordin, C.F. 1963. A Preliminary Study of Sediment Transport Parameters Rio Puerco near Bernardo, New Mexico. U.S. Geological Survey, Professional Paper 462-C, Washington, D.C. 26 pp.

Nordin, C.F. and Beverage, J.P. 1965. Sediment transport in the Rio Grande New Mexico. U.S. Geological Survey, Professional Paper 462-F, Washington, D.C. 42 pp.

Parker, G. 1990. Surface-Based Bedload Transport Relationship for Gravel Rivers. Journal of Hydraulic Research, Vol 28, p. 417-436.

Pemberton, E.L. and Lara, J.M. 1984. Computing Degradation and Local Scour, technical Guideline for Bureau of Reclamation. U.S. Department of the Interior, Bureau of Reclamation, Technical Service Center, Denver, CO. 48 pp.

Racin, J. H. 2000. California Bank and Shore Rock Slope Protection Design, Practitioner's Guide and Field Evaluations of Riprap Methods. Caltrans Engineering Service Center, Federal Highway Administration (FHWA), California Department of Transportation (Caltrans), Sacramento, CA. pp. 154

Reclamation. 2012. Middle Rio Grande River Maintenance Program Comprehensive Plan and Guide: Appendix B: One-dimensional Modeling and Indicator Results for the Middle Rio Grande. U.S. Department of the Interior, Bureau of Reclamation, Upper Colorado Region, Albuquerque, NM. 135 pp.

Richard, G., Leon, C., and Julien, P. 2001. Hydraulic Modeling on the Middle Rio Grande, New Mexico: Rio Puerco Reach. Colorado State University, Fort Collins, CO. 102 pp

Shah, S.C. 2006. Thesis: Variability in Total Sediment Load using BORAMEP on the Rio Grande Low Flow Conveyance Channel. Colorado State University, Fort Collins, CO. 209 pp.

Shah-Fairbank, S.C. 2009. Dissertation: Series Expansion of the Modified Einstein Procedure. Colorado State University, Fort Collins, CO. 263 pp.

Simons, D.B., Li, R., Li, L., and Ballantine, M.J. 1981. Summary of Results for the Sedimentation Study of the Rio Grande between Cochiti Reservoir and Elephant Butte Reservoir with Special emphasis on Rio Puerco and Rio Salado. Simons, Li, and Associates, Inc. 71 pp.

Southwest Water Design. 2014. Middle Rio Grande Project Hydrographic Data Collection Final Report - Cross Section Surveys, Isleta to Belen - Range Lines March 2014. Southwest Water Design, LLC, Albuquerque, NM. 309 pp.

Southwest Water Design. 2015. Middle Rio Grande Project Hydrographic Data Collection Final Report - Cross Section Surveys, San Acacia Reach - Range Lines Nov/Dec 2014. Southwest Water Design, LLC, Albuquerque, NM. 331 pp.

Southwest Water Design. 2017. Middle Rio Grande Project Hydrographic Data Collection Final Report – 2017 Total Load Data Collection, April 26 to June 20 IS-678, CO-833, CO-966, and LJ-6. Southwest Water Design, LLC, Albuquerque, NM. 621 pp.

Tetra Tech. 2005. Middle Rio Grande Hydrographic Data Collection Report: Overbank Monitoring of the 2005 High Flow Spring Release from Cochiti Dam. Tetra Tech, Inc. Albuquerque, NM. 484 pp.

Tetra Tech. 2012. Middle Rio Grande Hydrographic Data Collection: Field Data Collection Report Cross-Section Surveys and River Profile Survey – Rio Puerco (RP) Line Surveys, La Joya (LJ) Line Surveys, and Cochiti (CO) line Surveys, February – April 2012. Tetra Tech, Inc., Albuquerque, NM. 218 pp.

Tetra Tech. 2014a. Draft Report: Habitat Relationships along the Middle Rio Grande in New Mexico for the Endangered Southwestern Willow Flycatcher. Tetra Tech, Inc., Albuquerque, NM. 96 pp.

Tetra Tech. 2014b. Final Report: Ecohydrological Relationships along the Middle Rio Grande of New Mexico for the Endangered Rio Grande Silvery Minnow. Tetra Tech, Inc. Albuquerque, NM. 115 pp.

Thomas, W.A., Copeland, R.R., and McComas, D.N. 2002. SAM Hydraulic Design Package for Channels. U.S. Army Corps of Engineers, Engineer, Research and Development Center, Coastal and Hydraulics Laboratory, Washington, D.C. 232 pp.

USACE. 1994. Engineering and Design, Hydraulic Design of Flood Control Channels, Engineer Manual 1110-2-1601. U.S. Army Corps of Engineers, Department of the Army, Washington, D.C. 183 pp.

USACE. 2009. HEC-GeoRAS GIS Tools for Support of HEC-RAS using ArcGIS Users' Manual, Version 4.2. U.S. Army Corps of Engineers, Institute for Water Resources, Hydrologic Engineering Center (HEC), Davis, CA. 246 pp.

USACE. 2010a. HEC-RAS River Analysis System User's Manual, Version 4.1. U.S. Army Corps of Engineers, Institute for Water Resources, Hydrologic Engineering Center (HEC), Davis, CA. 790 pp.

USACE. 2010b. HEC-RAS River Analysis System Hydraulic Reference Manual, Version 4.1. U.S. Army Corps of Engineers, Hydrologic Engineering Center (HEC), Davis, CA. 417 pp.

USDA. 2016. BSTEM Overview. United Stated Department of Agriculture, Agricultural Research Service, Oxford, MS. https://www.ars.usda.gov/southeast-area/oxford-ms/national-sedimentation-laboratory/watershed-physical-processes-research/research/bstem/overview/, last accessed March 7, 2018.

USGS. 1993. Policy and technical guidance for conversion of sediment concentration from parts per million (ppm) to milligrams per liter (mg/L), Technical Memorandum No. 93-21. U.S. Geological Survey, Office of Surface Water. https://water.usgs.gov/admin/memo/SW/sw93.21.html, last accessed March 9, 2018.

Varyu, D. 2013. Aggradation/Degradation Volume Calculations: 2002-2012. U.S. Department of the Interior, Bureau of Reclamation, Technical Service Center, Denver, CO. 455 pp.

Vensel, C, Richard, G., Leon, C., and Julien, P. 2006. Hydraulic Modeling on the Middle Rio Grande, New Mexico Rio Puerco Reach. Colorado State University, Ft. Collins, CO. 112 P.

Wentworth, C.K. 1922. A scale of grade and class terms for clastic sediments. Journal of Geology, volume 30, Chicago, IL. pp 377-392.

Woolpert. 2012. Aerial Triangulation Project Report. Woolpert for the U.S. Department of the Interior, Bureau of Reclamation, Englewood, CO. 7 pp.

Wright, J.M. 2010. Middle Rio Grande Peak Discharge Frequency Study. U.S. Department of the Interior, Bureau of Reclamation, Technical Service Center, Denver, CO. 151 pp.

Appendix A

BSTEM Bank and Toe Erosion Profiles

Bank Sample No. 1 (RM 162)

Bank Results:

4000 cfs

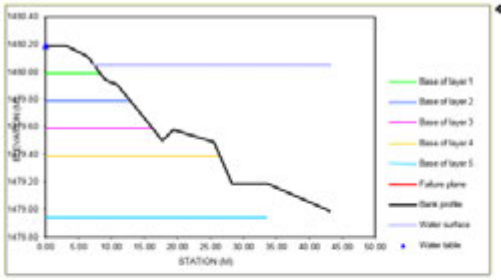

7500 cfs

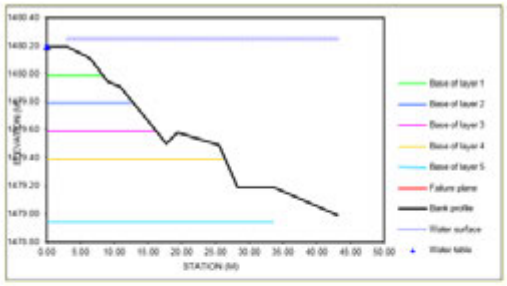

20000 cfs

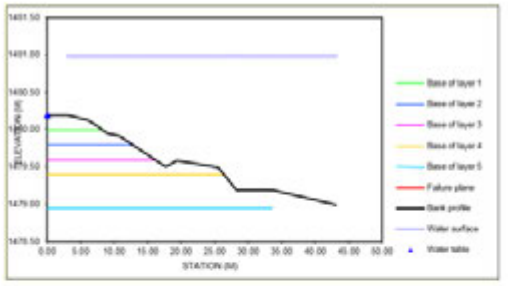

Toe Results:

4000 cfs

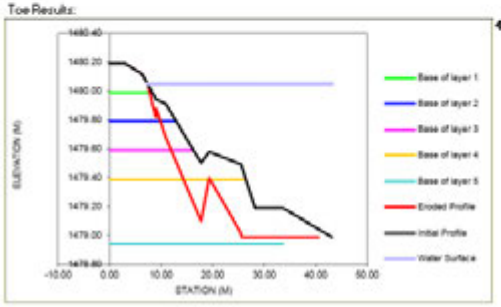

7500 cfs

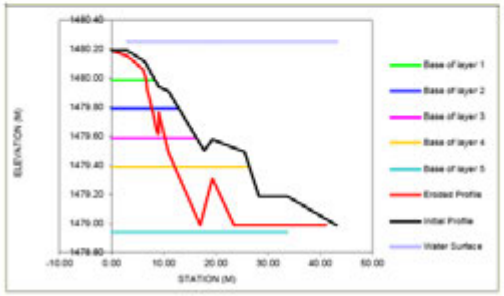

20000 cfs

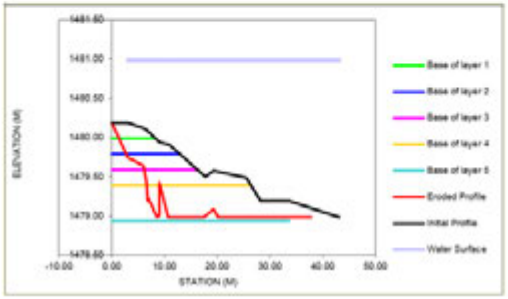

Bank Sample No. 2 (RM 149)

Bank Results:

4000 cfs

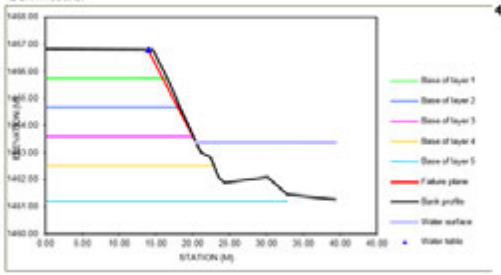

7500 cfs

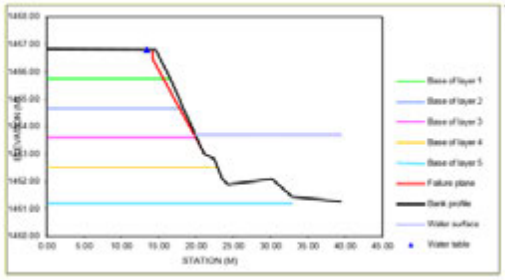

20000 cfs

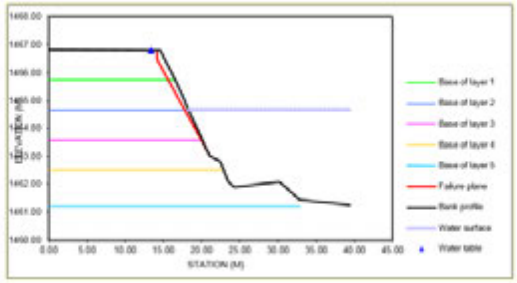

Toe Results:

4000 cfs

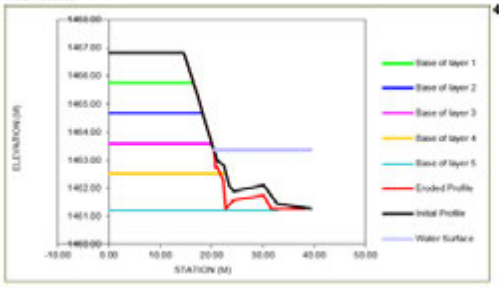

7500 cfs

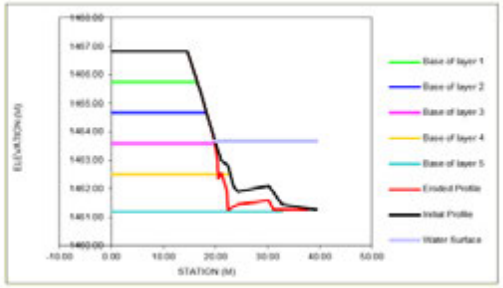

20000 cfs

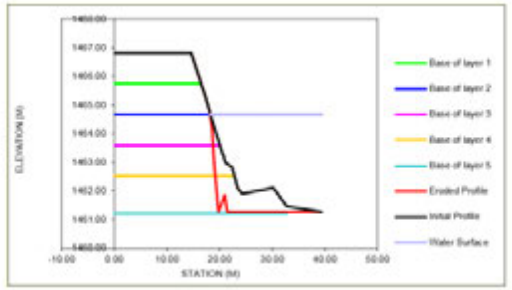

Bank Sample No. 3 (RM 138.2)

Bank Results:

4000 cfs

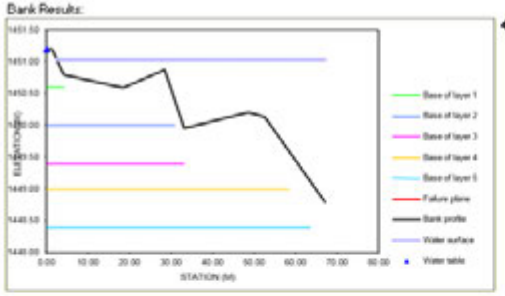

7500 cfs

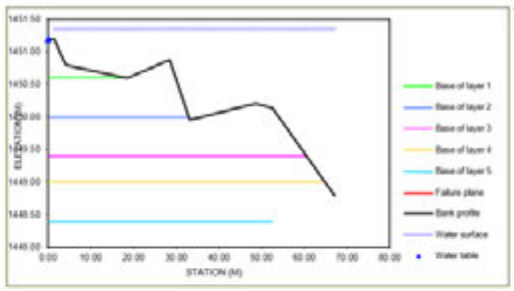

20000 cfs

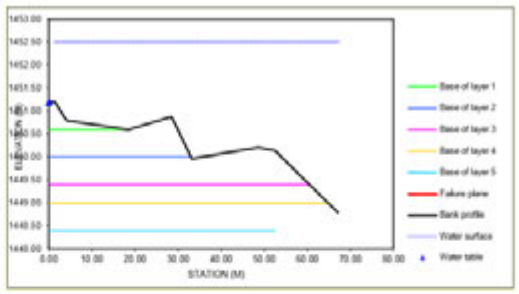

Toe Results:

4000 cfs

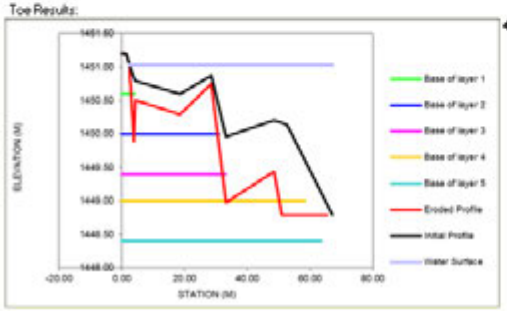

7500 cfs

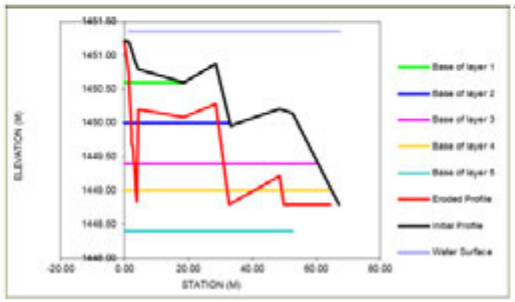

20000 cfs

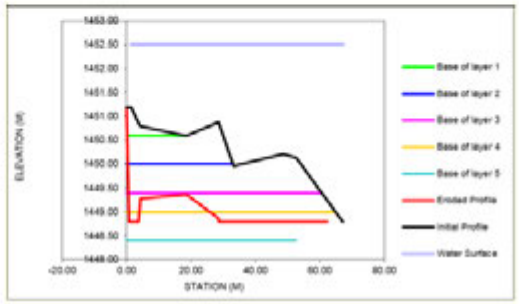

Bank Sample No. 4 (RM 130.4)

Bank Results:

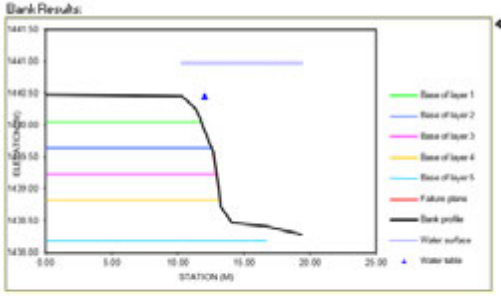

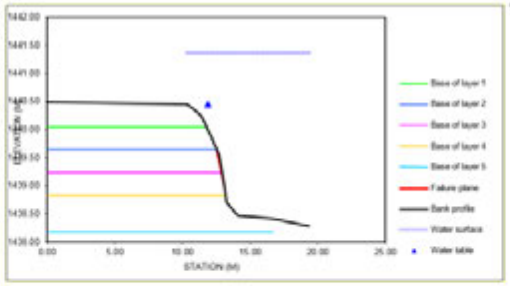

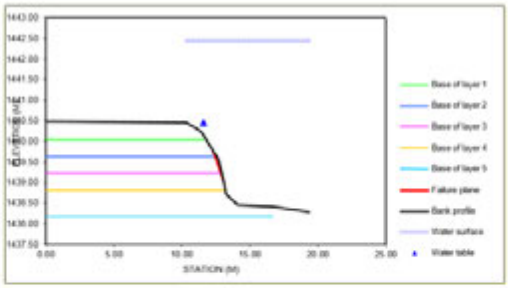

Toe Results:

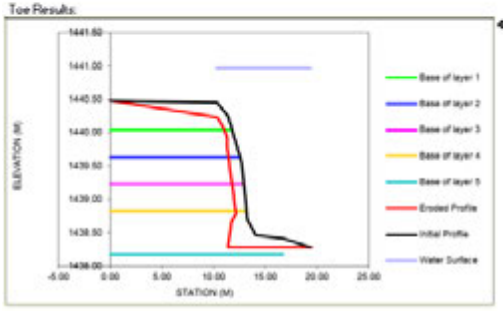

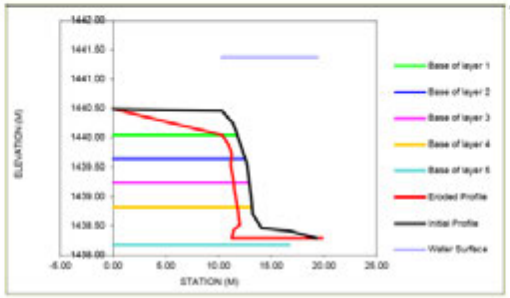

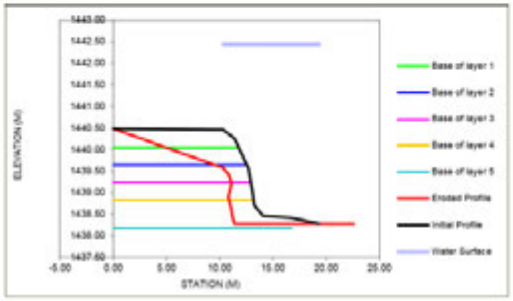

Bank Sample No. 5 (RM 127.9)

Bank Results:

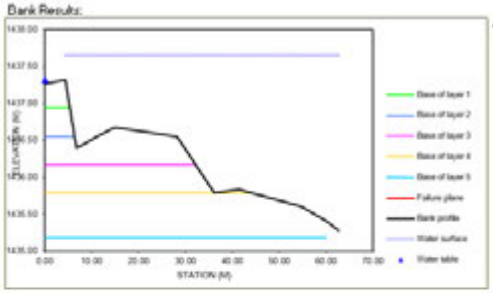

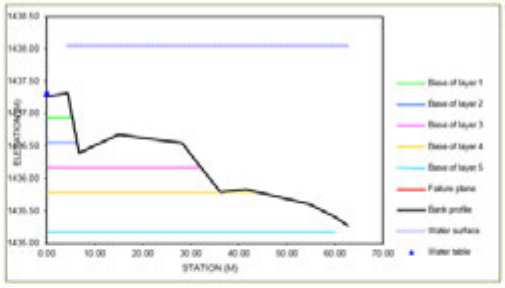

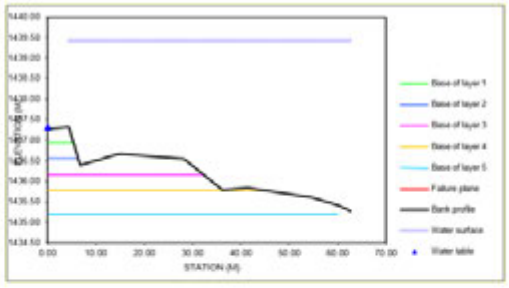

Toe Results:

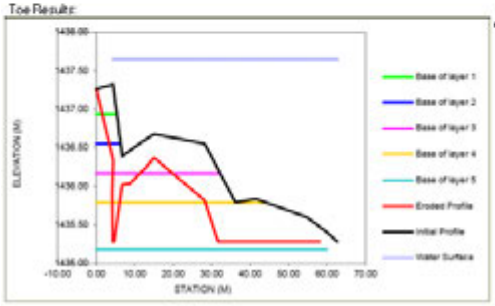

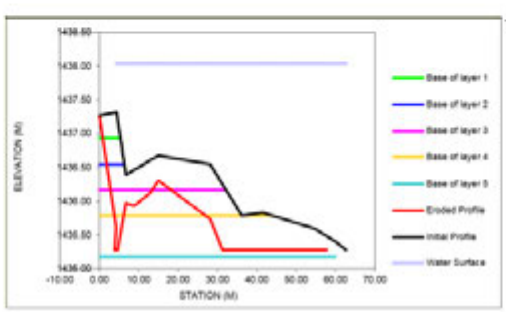

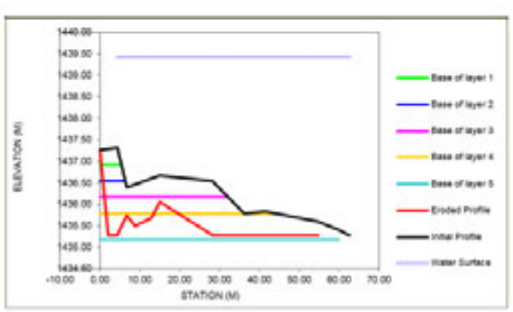

Bank Sample No. 6 (RM 127.5)

Bank Results:

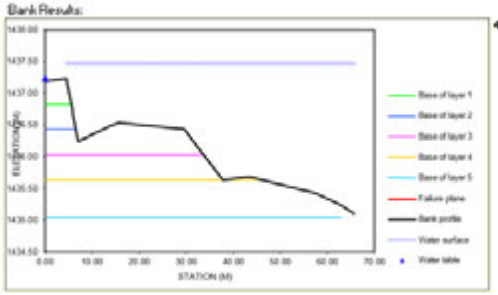

4000 cfs

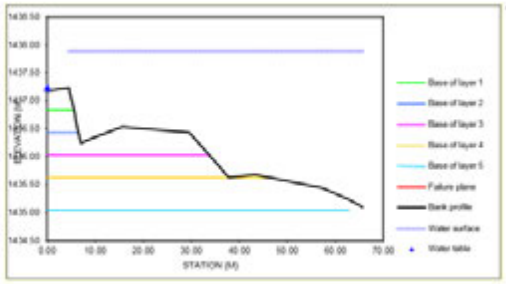

7500 cfs

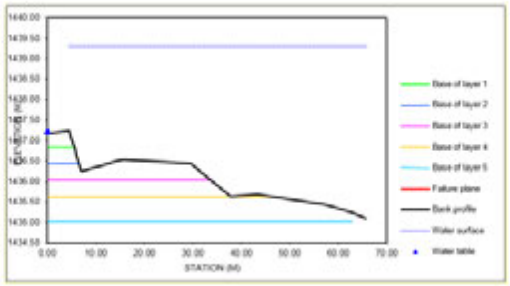

20000 cfs

Toe Results:

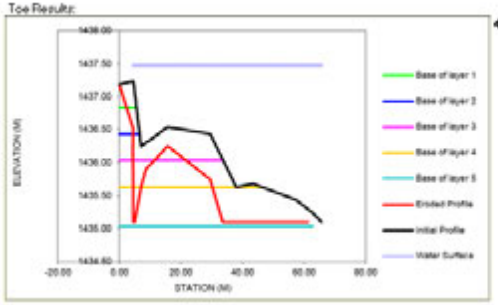

4000 cfs

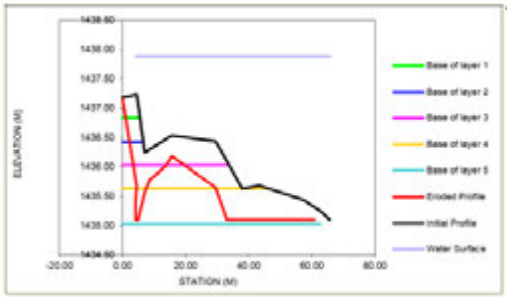

7500 cfs

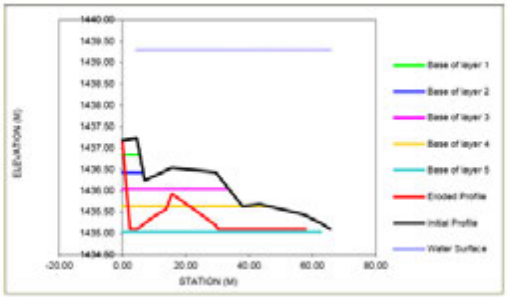

20000 cfs

Bank Sample No. 7 (RM 127)

Bank Results:

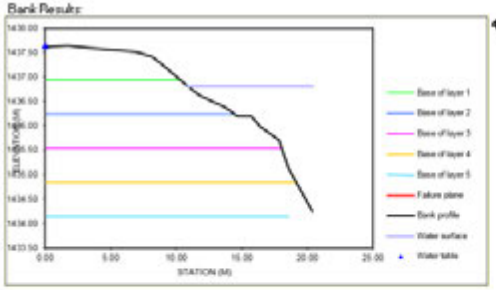

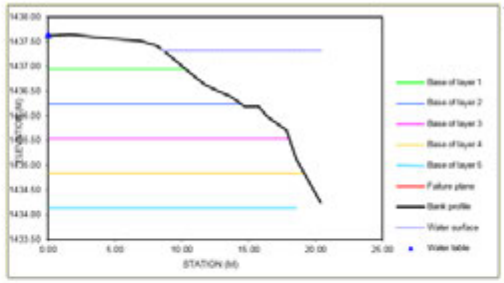

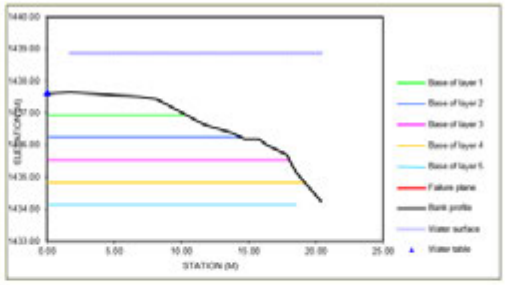

Toe Results:

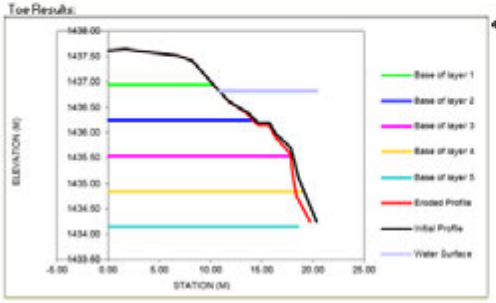

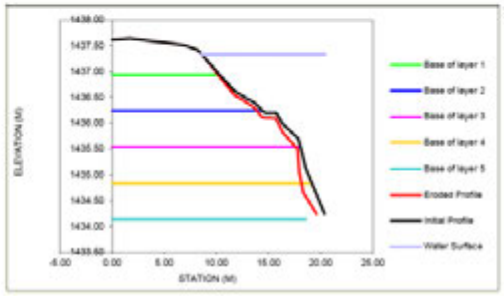

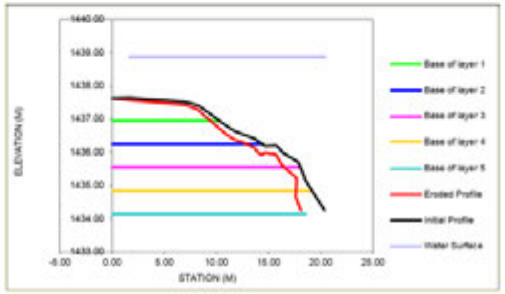

Bank Sample No. 8 (RM 124.2)

Bank Results:

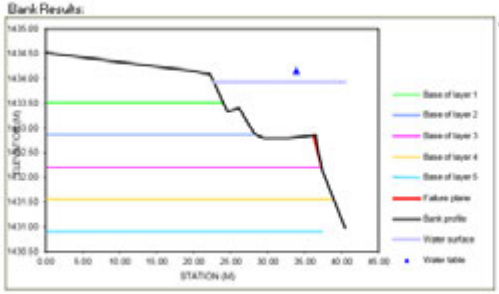

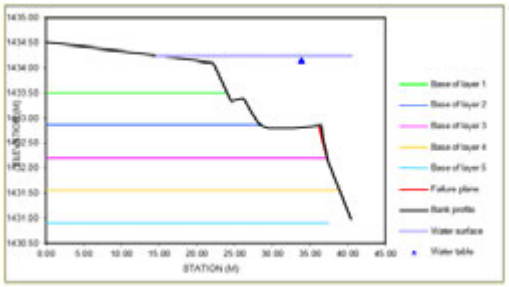

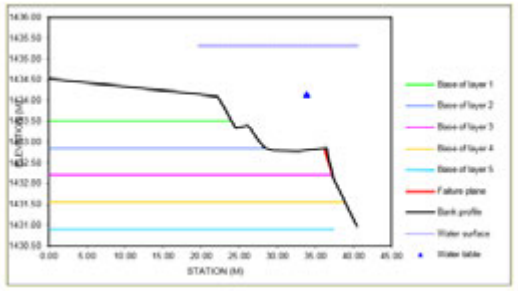

Toe Results:

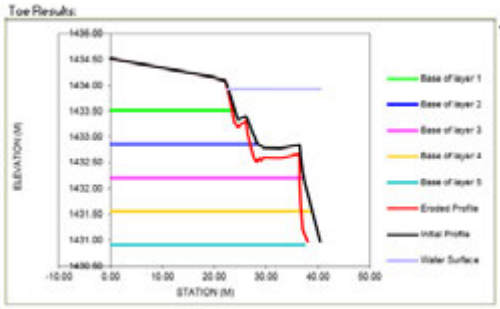

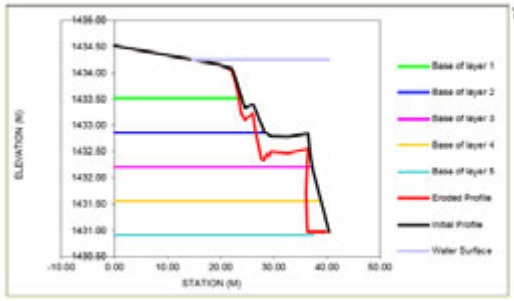

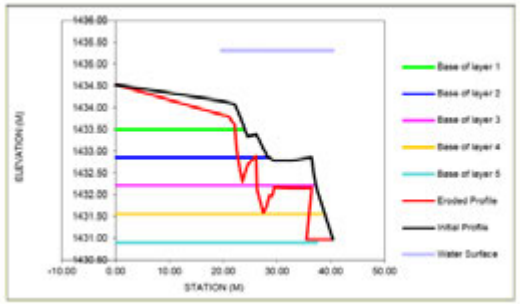

Bank Sample No. 9 (RM 119.8)

Bank Results:

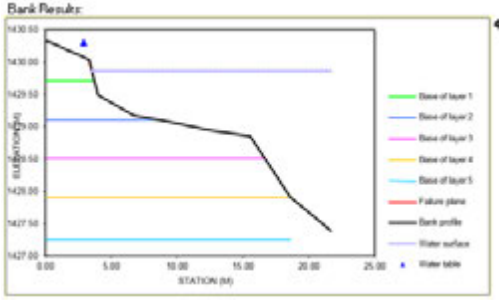

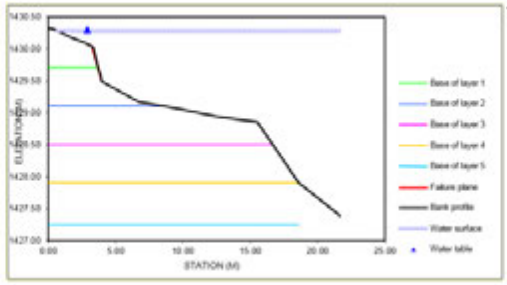

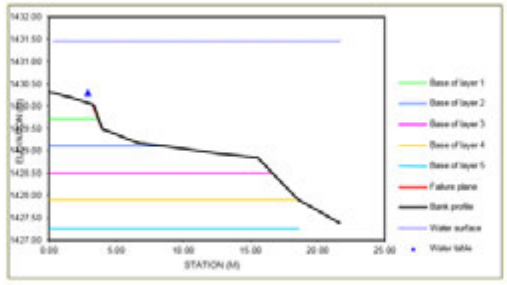

Toe Results:

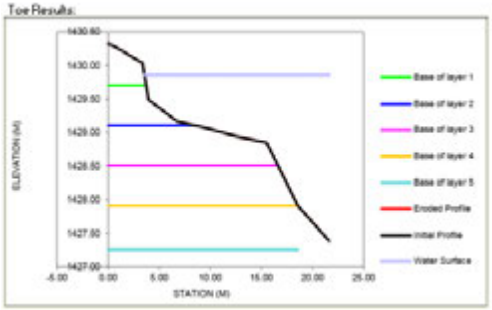

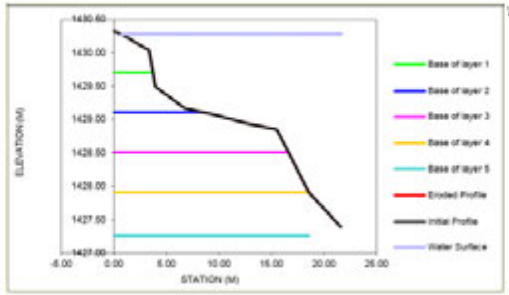

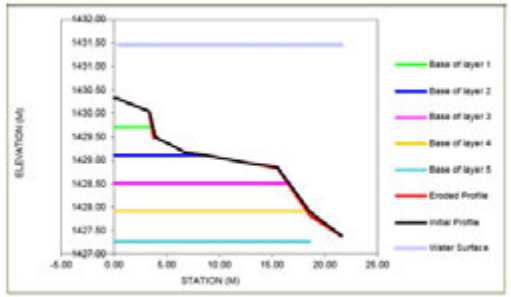

Bank Sample No. 10 (RM 116.5)

Bank Results:

4000 cfs

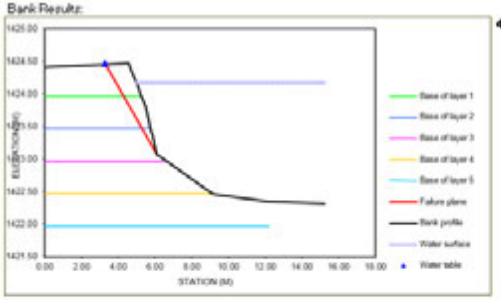

7500 cfs

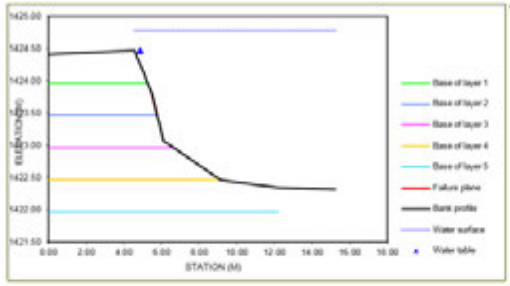

20000 cfs

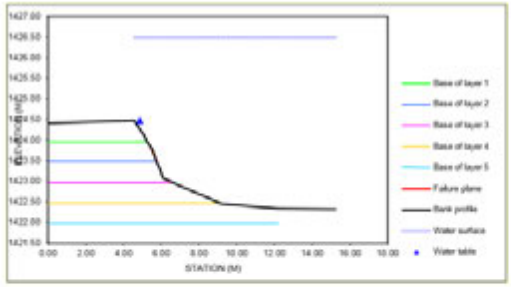

Toe Results:

4000 cfs

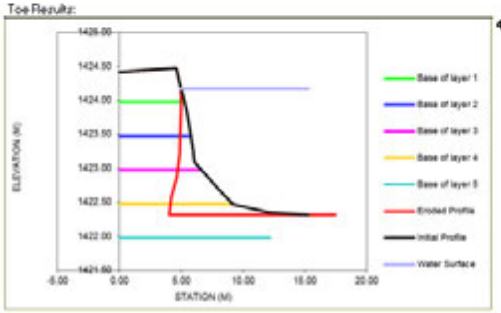

7500 cfs

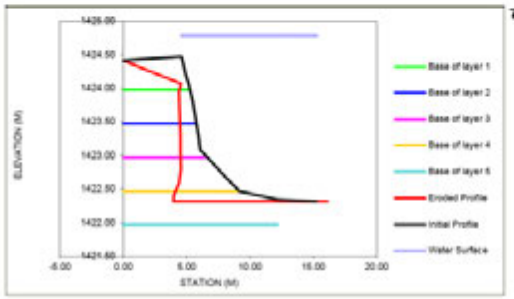

20000 cfs

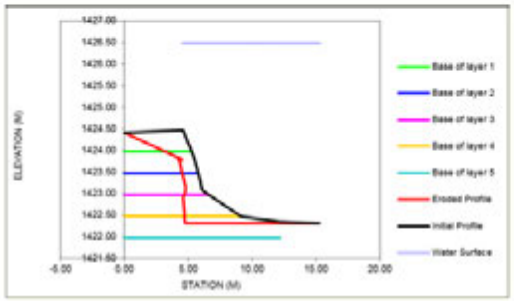

Appendix B

Rip Rap Sizing Equations and Inputs

USACE Method

A spreadsheet was used which was developed based on the concepts of the Army Corps of Engineer's Engineer Manual (EM) 1601, "Hydraulic Design of Flood Control Channels" (USACE, 1994). The equation for the USACE method is shown in Equation 2.

Equation 2.USACE equation (USACE, 1994)

$$D_{30} = S_f C_s C_v C_t d \left(\left(\frac{\gamma_w}{\gamma_s - \gamma_w} \right)^{0.5} \frac{V_{des}}{\sqrt{K_{1gd}}} \right)^{2.5}$$

Where:
D_{30} = riprap size of which 30 percent is finer by weight,
S_f = Safety factor (1.2),
C_s = Stability coefficient for incipient failure (0.3 for angular rock),
C_v = vertical velocity distribution coefficient (outside of bends = 1.283-0.2 log(R/W) or 1 for R/W > 26),
C_t = thickness coefficient (1),
γ_w = Specific weight of water (62.4 pcf),
γ_s = Specific weight of riprap (165 pcf),
g = gravitation constant (32.2 ft/s^2),
V_{des} = local depth-averaged velocity (ft/sec) at a point 20% upstream from the toe
or $V_{des} = V_{avg}$ * [function (R_c/W, ChanType = Natural)],
d = local depth of flow, and
K = side slope correction factor

$$K_1 = \sqrt{1 - \frac{\sin^2 \theta}{\sin^2 \phi}}$$

where θ = angle of side slope with horizontal and
φ = angle of repose of riprap material (40 deg)

The equation is limited to longitudinal slopes that are 2% or flatter with a bank slope of 1.5H:1V (67%) or flatter. For the nine river maintenance sites, Table 19 shows the input values used in calculating D_{30}. The median riprap size D_{50} was calculated as 1.2*D_{30} (assuming a target gradation D_{85}/D_{15} of approximately 1.75 to 2.00).

Table 19: Input variables generated by HEC-RAS for riprap sizing for nine river maintenance sites

Site	V_{avg} -Local depth-averaged velocity (ft/s)	R_c/W - Bend Curvature	d -Local depth of flow (ft)	θ -Angle of side slope with horizontal
Highway 309	5.8	8.2	11.1	25°
Los Trujillos	7.0	4.2	11.1	27°
Rio Puerco RM 127.9	5.8	0.3	14.4	33°
Rio Puerco RM 127.5	5.8	0.5	14.4	14°
Rio Puerco RM 127	5.8	0.8	14.4	33°
La Joya	6.9	0.5	14.3	17°
Bernardo Arroyo	4.1	0.3	11.9	14°
RM 121	8.2	8.2	14.0	19°
Drain Unit 7	10.3	0.7	16.3	36°

Caltrans Method

A spreadsheet was used which was developed based on the concepts of the Caltrans guide to rock slope protection (Racin, 2000). The equation for the Caltrans method is shown in Equation 3.

Equation 3. Caltrans equation (Racin, 2000)

$$W = \frac{0.00002\, V^6 \left(\frac{\gamma_s}{\gamma_w}\right)}{\left(\frac{\gamma_s}{\gamma_w} - 1\right)^3 \sin^3(r - \theta)}$$

Where:
W = computed minimum standard rock weight (lbs), assumed to be the 30% riprap weight,
V = average channel velocity (ft/s),
θ = angle of side slope with horizontal,
r = angle for randomly placed riprap (70°),
γ_w = Specific weight of water (62.4 pcf), and
γ_s = Specific weight of riprap (165 pcf).

The limitations for this equation are:

- Calculates minimum standard rock weight for outer layer of RSP
- Layered RSP design uses a more uniform rock size placed in multiple layers, decreasing in size from the outer to inner layer(s)
- Relationship between size and weight assumes spherical shape

The conversion from the calculated rock weight from the Caltrans equation to a nominal riprap diameter (D_{30}) is based on National Cooperative Highway Research Program Report 568 (Lagasse et al, 2006) and shown in Equation 4.

The median riprap size D_{50} was calculated as 1.2*D_{30} (assuming a target gradation D_{85}/D_{15} of approximately 1.75 to 2.00).

Equation 4. Approximation of riprap size from riprap volume, assuming a spherical shape (Lagasse et al., 2006)

$$W = \gamma_s\left(\frac{\pi D_{30})}{6}\right)$$

Where:
W = computed minimum standard rock weight (lbs),
γ_s = Specific weight of riprap (165 pcf),
π = Pi (3.1456), and
D_{30} = riprap size of which 30 percent is finer by weight.

Appendix C

Scour Estimate Equations and Inputs

Ten different scour equations were assessed for the Isleta to San Acacia reach hydraulic analysis. The equations are derived from Pemberton and Lara (1984), ASCE (2004a), and ASCE (2004b). The evaluated scour equations include the mean velocity, competent velocity, Zeller general, Regime, and bend scour estimates from Thorne, Maynord, Zeller, and USACE. These are each described in the sections below.

C.1 Mean Velocity

The mean velocity from field measurement methodology (Pemberton and Lara, 1984) is based on determining the mean channel depth. The depth is determined by using a series of at least 4 cross sections and using a 1-dimensional numerical model to compute a mean channel depth. The scour is estimated by applying the appropriate multiplying factor (Z) developed for the Lacey regime equation. The equation used for the Isleta to San Acacia reach assessment is shown in Equation 5.

Equation 5. Mean Depth from field measurements (Pemberton and Lara, 1984)

$$y_s = Z y_m$$

Where y_s = predicted depth of scour (feet),
Z = Lacey multiplying factor (0.75 is a severe bend and 0.5 is a moderate bend), and
y_m = mean channel depth (feet).

This approximation includes general and bend scour (ASCE, 2004a). Mean depth values were extracted from the 2015 1-dimensional model described in Section 3.1, Current Geometry Model (2015). Specific values for the mean channel depth are listed in Table 20. Table 20 also provides the specific multiplication factor used in the equation and the resultant estimate for scour depth.

Table 20: Mean Velocity equation variables and input values

Site	y_m Mean Depth (ft)	Z_L Lacey adjustment factor	**y_s Depth of Scour (ft)**
RM 162	2.6	0.75	**1.9**
RM 149	6.0	0.50	**3.0**
RM 138.2	4.7	0.50	**2.4**
RM 130.4	5.1	0.50	**2.6**
RM 127.9	5.0	0.75	**3.7**
RM 127.5	5.0	0.50	**2.5**
RM 127	5.0	0.50	**2.5**
RM 124	6.0	0.75	**4.5**
RM 120	5.1	0.50	**2.6**
RM 116.5	5.7	0.75	**4.2**

C.2 Competent Velocity

The competent or limiting velocity control to scour methodology (Pemberton and Lara, 1984) assumes that the scour depth is dependent upon an adjustment in the channel bed until there is no more bed material movement. This is considered to be an upper limit on the estimation of scour that would occur in the deepest scour holes. The methodology relies on a comparison of the mean channel velocity to a velocity that is competent to move certain materials. The equation was developed for bed material that is sand or coarser (>0.3 mm) (Pemberton and Lara, 1984). The equation used for the Isleta to San Acacia reach assessment is shown in Equation 6.

Equation 6. Competent velocity scour method (Pemberton and Lara, 1984)

$$y_s = y_m\left(\frac{V_m}{V_c} - 1\right)$$

Where y_s = predicted depth of scour (feet),
V_m = competent velocity (ft/sec) based on table in Pemberton and Lara (1984) of competent velocities for erosion of material or local experience,
V_c = mean channel velocity (ft/sec), and
y_m = mean channel depth (feet).

This approximation includes general and thalweg formation scour (ASCE, 2004a). Mean depth and velocity values were extracted from the 2015 1-dimensional model described in Section 3.1, Current Geometry Model (2015). Specific values for the mean channel depth and velocity are listed in Table 21. Table 21 also provides the selected competent velocity based on the mean flow depth and the closest bed material samples collected in the Isleta to San Acacia reach.

Table 21: Competent Velocity equation variables and input values

Site	y_m Mean Depth (ft)	V_m Mean Channel Velocity at Design (ft/s)	V_c competent mean velocity for significant bed movement (ft/s)	**y_s Depth of Scour (ft)**
RM 162	2.6	3.2	2.1	**1.3**
RM 149	6.0	3.3	2.5	**2.0**
RM 138.2	4.7	3.5	2.3	**2.4**
RM 130.4	5.1	3.8	2.4	**2.9**
RM 127.9	5.0	3.3	2.4	**1.8**
RM 127.5	5.0	3.3	2.4	**1.8**
RM 127	5.0	3.3	2.4	**1.8**
RM 124	6.0	3.2	2.5	**1.6**
RM 120	5.1	2.9	2.4	**1.1**
RM 116.5	5.7	5.6	2.5	**7.0**

C.3 Zeller, General

A sand-bed equation for scour was developed by Mike Zeller in the 1980s based on an investigation of sand-bed intermittent streams in southern Arizona (ASCE, 2004b). The equation is for general scour only. It is possible that this scour equation may result in negative estimated scour depths, in which guidance (ASCE, 2004b) suggests assuming that the general scour is zero or negligible. The equation used for the Isleta to San Acacia reach assessment is shown in Equation 7.

Equation 7. Zeller equation for general scour (ASCE, 2004b)

$$y_{gs} = y_{max}\left(\frac{0.0685 V_m^{0.8}}{y_h^{0.4} S_e^{0.3}} - 1\right)$$

Where y_{gs} = predicted general scour depth (feet),
Y_{max} = maximum flow depth (feet),
V_m = mean channel velocity (ft/sec),
y_h = mean hydraulic depth (feet), and
S_e = energy slope or bed slope for uniform flow conditions (feet/feet).

Max depth, mean channel velocity and hydraulic depth, and energy grade slope were extracted from the 2015 one-dimensional model described in Section 3.1, Current Geometry Model (2015 and listed in Table 22. Table 22 also provides the computed general scour depth.

Table 22: Zeller general scour equation variables and input values

Site	Y_{max} Max depth (ft)	V Mean velocity (ft/s)	y_h Mean Hydraulic depth (ft)	S_e Energy grade slope (ft/ft)	**Y_{gs} Depth of general scour (ft)**
RM 162	6.0	3.2	2.6	0.0014	**0**
RM 149	7.1	3.3	6.0	0.0005	**0**
RM 138.2	7.1	3.5	4.7	0.0007	**0**
RM 130.4	8.1	3.9	5.8	0.0007	**0**
RM 127.9	7.9	3.3	5.0	0.0006	**0**
RM 127.5	7.9	3.3	5.0	0.0006	**0**
RM 127	7.9	3.3	5.0	0.0006	**0**
RM 124	7.1	3.5	6.0	0.0005	**0**
RM 120	8.1	3.6	6.8	0.0005	**0**
RM 116.5	6.1	7.2	4.8	0.0030	**0.1**

C.4 Regime Equations

Three different regime equations (Neill, Lacey, and Blench) were used to estimate scour within the Isleta to San Acacia reach. The regime methodologies rely on obtaining field measurements (Pemberton and Lara, 1984). From these measurements a mean flood depth is obtained and an estimate of the maximum predicted scour depth is determined by using a multiplying factor to account for the probable concentration of flood flows within the river. All three of these equations are assumed to include general, bend, and thalweg formation scour (ASCE, 2004a).

C.4.1 Neill

The Neill equation is based on field measurements (bankfull discharge and mean channel depth) within an incised reach (Pemberton and Lara, 1984). The equations used for the Isleta to San Acacia reach assessment are shown in Equation 8 and Equation 9.

Equation 8. Neill regime scour method (Pemberton and Lara, 1984)

$$y_f = y_i \left(\frac{q_f}{q_i} \right)^m$$

Where y_f = depth of scour below the design discharge water surface (feet),
y_i = average depth (feet) at bankfull discharge,
q_f = design discharge per unit width (ft^2/sec),
q_i = bankfull discharge per unit width (ft^2/sec), and
m = exponent related to bed material type (0.67 for sand and 0.85 for coarse gravel).

Equation 9. Neill predicted scour from multiplying factor (Pemberton and Lara, 1984)

$$d_s = Z * y_f$$

Where d_s = predicted maximum depth of scour (feet),
Z = Neill multiplying factor (0.7 is a severe bend and 0.6 is a moderate bend), and
y_f = depth of scour below the design discharge water surface (feet) from Equation 8.

Average bankfull depths were extracted from the 2015 1-dimensional model described in Section 3.1, Current Geometry Model (2015). Estimated bankfull discharges, average bankfull depth, and discharges per unit width are listed inTable 23. Table 23 also provides the estimated flood scour depth below the design discharge's water surface elevation and the predicted maximum scour depth within the Isleta to San Acacia reach.

Table 23: Neill equation variables and input values

Site	Bankfull Discharge (cfs)	Y_i Average Depth at Bankfull Discharge (ft)	q_f Design flood discharge* per unit width (ft^2/s)	q_i Bankfull discharge per unit width (ft^2/s)	m Bed material exponent **	Y_f Scour depth below design floodwater level (ft)	Z Neill adjustment factor	**y_s Depth of scour below streambed**
RM 162	2,000	1.8	6.9	9.8	0.67	1.4	0.7	**1.0**
RM 149	1,000	3.1	5.5	7.0	0.67	2.6	0.6	**1.6**
RM 138.2	1,000	2.4	2.9	10.2	0.67	1.1	0.6	**0.6**
RM 130.4	3,000	4.5	5.3	12.5	0.67	2.5	0.6	**1.5**
RM 127.9	2,000	3.0	7.1	17.1	0.67	1.7	0.7	**1.2**
RM 127.5	2,000	3.0	7.1	17.1	0.67	1.7	0.6	**1.0**
RM 127	2,000	3.0	7.1	17.1	0.67	1.7	0.6	**1.0**
RM 124	2,000	4.5	5.6	17.7	0.67	2.1	0.7	**1.5**
RM 120	1,000	2.8	6.9	8.7	0.67	2.4	0.6	**1.4**
RM 116.5	6,000	6.7	26.2	49.8	0.67	4.3	0.7	**3.0**

*Design discharge is 4,000 cfs for all sites
**Varying from 0.67 (sand) to 0.85 (coarse gravel)

C.4.2 Lacey

The Lacey equation is derived from an empirical relationship relating an estimated mean depth to a design discharge and bed material size (Pemberton and Lara, 1984). The equations used for the Isleta to San Acacia reach assessment are shown in Equation 10 and Equation 11.

Equation 10. Lacey regime scour method (Pemberton and Lara, 1984)

$$y_m = 0.47\left(\frac{Q_d}{f}\right)^{\frac{1}{3}}$$

Where y_m = mean depth (feet) at the design discharge,
Q_d = design discharge (ft^3/sec), and
f = Lacey silt factor, calculated as $1.76*(D_{50})^{0.5}$, where D_{50} is the median bed material size in mm (Pemberton and Lara, 1984).

Equation 11. Lacey predicted scour from multiplying factor (Pemberton and Lara, 1984)

$$d_s = Z * y_m$$

Where d_s = predicted maximum depth of scour (feet),
Z = Lacey multiplying factor (0.75 is a severe bend and 0.5 is a moderate bend), and
y_m = mean depth (feet) at the design discharge from Equation 10.

Median bed material sizes (D_{50})were derived field measurements (Klein et al., 2018). The D_{50}, Lacey silt factor, design discharge, and calculated mean depth

are listed in Table 24. Table 24 also provides the predicted maximum scour depth within the Isleta to San Acacia reach.

Table 24: Lacey equation variables and input values

Site	D_{50} (mm)	f Lacey's silt factor:	y_m Mean water depth at design discharge* (ft)	Z Lacey adjustment factor	**y_s Depth of scour below streambed (ft)**
RM 162	0.6	1.4	6.7	0.75	**5.0**
RM 149	0.43	1.2	7.1	0.50	**3.6**
RM 138.2	0.46	1.2	7.0	0.50	**3.5**
RM 130.4	0.39	1.1	7.2	0.50	**3.6**
RM 127.9	0.4	1.1	7.2	0.75	**5.4**
RM 127.5	0.4	1.1	7.2	0.50	**3.6**
RM 127	0.4	1.1	7.2	0.50	**3.6**
RM 124	0.38	1.1	7.3	0.75	**5.4**
RM 120	0.41	1.1	7.2	0.50	**3.6**
RM 116.5	0.55	1.3	6.8	0.75	**5.1**

*Design discharge is 4,000 cfs for all sites

C.4.3 Blench

The Blench equation is a regime equation derived from a zero-bed sediment transport (Pemberton and Lara, 1984). The equations used for the Isleta to San Acacia reach assessment are shown in Equation 12 and Equation 13.

Equation 12. Blench regime scour method (Pemberton and Lara, 1984)

$$y_{f_0} = \frac{q_f^{\frac{2}{3}}}{F_{b_0}^{\frac{1}{3}}}$$

Where y_{fo}= depth (ft) for zero bed sediment transport at the design discharge,
q_f = design discharge per unit width (ft^2/sec), and
F_{bo} = Blench's "zero bed factor", derived from chart based on the median (D_{50}) bed material size in feet (Pemberton and Lara, 1984).

Equation 13. Blench predicted scour from multiplying factor (Pemberton and Lara, 1984)

$$d_s = Z * y_{fo}$$

Where d_s = predicted maximum depth of scour (feet),
Z = Blench multiplying factor (0.6 for bends), and
y_{fo}= depth (ft) for zero bed sediment transport at the design discharge from Equation 12.

Median bed material sizes (D_{50})were derived field measurements (Klein et al., 2018). The design discharge and "zero-bed factor" are listed in Table 25. Table 25 also provides the estimated depth for zero bed sediment transport at

the design discharge and the predicted maximum scour depth within the Isleta to San Acacia reach.

Table 25: Blench equation variables and input values

Site	q_f Design flood discharge per unit width (ft^2/s)	F_{bo} Blench's "zero bed factor"	y_{fo} Depth for zero bed sediment transport (ft)	Z_B Blench adjustment factor for severe bend	**y_s Depth of scour below streambed (ft)**
RM 162	6.9	1.4	3.2	0.6	**1.9**
RM 149	5.5	1.3	2.8	0.6	**1.7**
RM 138.2	2.9	1.3	1.9	0.6	**1.1**
RM 130.4	5.3	1.3	2.8	0.6	**1.7**
RM 127.9	7.1	1.3	3.4	0.6	**2.0**
RM 127.5	7.1	1.3	3.4	0.6	**2.0**
RM 127	7.1	1.3	3.4	0.6	**2.0**
RM 124	5.6	1.3	2.9	0.6	**1.7**
RM 120	6.9	1.3	3.3	0.6	**2.0**
RM 116.5	26.2	1.4	7.9	0.6	**4.7**

C.5 Thorne, bend

This is an empirical scour equation developed by C.R. Thorne in the 1990s (ASCE, 2004a; ASCE, 2004b). The equation is for general, bend and thalweg formation. The equation is limited to ratios of the radius of curvature over top width greater than two. The equation used for the Isleta to San Acacia reach assessment is shown in Equation 14. The equation predicts a maximum water depth from which a scour depth can be estimated as shown in Equation 15.

Equation 14. Thorne bend scour equation (ASCE, 2004a)

$$\frac{y_{max}}{y_u} = 2.07 - 0.19 \log\left(\frac{r_c}{W_u} - 2\right)$$

Where y_{max} = maximum water depth in the bend (feet),
y_u = average depth in the upstream crossing (feet) at the design discharge,
r_c = radius of curvature(ft), and
W_u = water surface width at the upstream bend (feet) at the design discharge.

Equation 15. Equation to predict Thorne bend scour

$$y_s = y_{max} - y_u$$

Where y_s = predicted maximum depth of scour (feet),
y_{max} = maximum water depth in the bend (feet), and
y_u = average depth in the upstream crossing (feet) at the design discharge.

Channel widths and depths, required for the equation, were extracted from the 2015 one-dimensional model described in section 3.1, Current Geometry Model (2015. These values, along with the estimated max depth and predicted scour depth are shown in Table 26.

Table 26: Thorne equation variables and input values

Site	r_c Radius of curvature (ft)	W_u Upstream bankfull top width (ft)	y_u Avg flow depth in crossing upstream of bend (ft)	y_{max} Maximum water depth in bend (ft)	**y_s Max scour depth in bend (ft)**
RM 162	3,076	297	2.6	4.8	**2.3**
RM 149	5,022	198	6.0	10.9	**4.9**
RM 138.2	3,002	209	4.7	8.8	**4.1**
RM 130.4	614	164	5.8	11.8	**6.0**
RM 127.9	703	235	5.0	10.3	**5.3**
RM 127.5	1,282	235	5.0	9.8	**4.8**
RM 127	1,802	235	5.0	9.6	**4.6**
RM 124	615	191	6.0	12.3	**6.3**
RM 120	3,330	370	6.8	12.9	**6.1**
RM 116.5	592	160	4.8	9.7	**4.9**

C.6 Maynord, bend

This is an empirical scour equation developed by S.T. Maynord in the 1990s (ASCE, 2004a; ASCE, 2004b). The equation is for general, bend and thalweg formation. The equation is limited to ratios of the radius of curvature over top width between 1.5 and 10. The equation should also only be used when the ratio of the top width to the upstream bend mean flow depth at the design discharge is between 20 and 125. The equation used for the Isleta to San Acacia reach assessment is shown in Equation 16. The equation predicts a maximum water depth from which a scour depth can be estimated as shown in Equation 17

Equation 16. Maynord bend scour equation (ASCE, 2004a; ASCE, 2004b)

$$\frac{y_{mbx}}{y_u} = 1.8 - 0.051\left(\frac{r_c}{W_u}\right) + 0.0084\left(\frac{W_u}{y_u}\right)$$

Where y_{mbx} = maximum water depth in the bend (feet),
y_u = average depth in the upstream crossing (feet) at the design discharge,
r_c = centerline radius of curvature(ft), and
W_u = water surface width at the upstream bend (feet) at the design discharge.

Equation 17. Equation to predict Maynord bend scour

$$y_s = y_{mbx} - y_u$$

Where y_s = predicted maximum depth of scour (feet),
y_{mbx} = maximum water depth in the bend (feet), and
y_u = average depth in the upstream crossing (feet) at the design discharge.

Channel widths and depths, required for the equation, were extracted from the 2015 one-dimensional model described in section 3.1, Current Geometry

Model (2015. Radius of curvature was measured along the centerline within ESRI's ArcMap (vserion 10.4.1). These values, along with the estimated max depth and predicted scour depth are shown in Table 27.

Table 27: Maynord equation variables and input values

Site	r_c Radius of curvature (ft)	W_u Upstream bankfull top width (ft)	y_u Avg flow depth in crossing upstream of bend (ft)	y_{mbx} Maximum water depth in bend (ft)	**y_s Max scour depth in bend (ft)**
RM 162	3,076	297	2.6	5.7	**NA***
RM 149	5,022	198	6.0	4.7	**NA***
RM 138.2	3,002	209	4.7	6.8	**NA***
RM 130.4	614	164	5.8	10.8	**NA***
RM 127.9	703	235	5.0	10.2	**5.2**
RM 127.5	1,282	235	5.0	9.6	**4.6**
RM 127	1,802	235	5.0	9.0	**4.0**
RM 124	615	191	6.0	11.4	**NA***
RM 120	3,330	370	6.8	12.2	**5.4**
RM 116.5	592	160	4.8	9.0	**NA***

*Not applicable because the input variables are outside the equation limitations

C.7 Zeller, bend

This is an empirical scour equation developed by M. Zeller in the 1980s (ASCE, 2004a; ASCE, 2004b). The equation is for a maximum bend scour in a sand-bed river. The equation used for the Isleta to San Acacia reach assessment is shown in. The equation predicts a maximum water depth from which a scour depth can be estimated as shown in Equation 17

Equation 18. Zeller bend scour equation (ASCE, 2004a; ASCE, 2004b)

$$y_{bz} = \frac{.0685\, y_{max}\, V^{0.8}}{y_h^{0.4}\, S_e^{0.3}} \left[2.1 \left(\frac{\sin^2\left(\frac{\alpha}{2}\right)}{\cos \alpha} \right)^{0.2} - 1 \right]$$

Where y_{bs} = predicted bend scour depth (feet),
y_{max} = maximum upstream flow depth (feet) at the design discharge,
V = mean upstream channel velocity (ft/sec),
y_h = mean upstream hydraulic depth (feet),
S_e = upstream energy slope (feet/feet), and
α = angle formed by a line projected from the channel centerline at the point of curvature to a line tangent to the outer bankline (°)

Max depth, mean channel velocity and hydraulic depth, and energy grade slope were extracted from the 2015 one-dimensional model described in

section 3.1, Current Geometry Model (2015. These are also listed in Table 28. Table 28 also provides the predicted bend scour.

Table 28: Zeller bend scour equation variables and input values

Site	Y_{max} Max depth of upstream flow at design discharge (ft)	V Mean velocity of upstream flow at design discharge (ft/s)	y_h Mean hydraulic depth of upstream flow (ft)	S_e Upstream energy slope	α angle formed between a line projected from channel centerline and a line tangent to outer bank (radians)	**y_{bs} Depth of bend scour (ft)**
RM 162	6.0	3.2	2.6	0.0014	0.47	**1.0**
RM 149	7.1	3.3	6.0	0.0005	0.26	**0**
RM 138.2	7.1	3.5	4.7	0.0007	0.66	**2.5**
RM 130.4	8.1	3.9	5.8	0.0007	0.47	**1.4**
RM 127.9	7.9	3.3	5.0	0.0006	0.49	**1.5**
RM 127.5	7.9	3.3	5.0	0.0006	0.49	**1.5**
RM 127	7.9	3.3	5.0	0.0006	0.44	**1.1**
RM 124	7.1	3.5	6.0	0.0005	0.72	**2.9**
RM 120	8.1	3.6	6.8	0.0005	0.37	**0.6**
RM 116.5	6.1	7.2	4.8	0.0030	1.05	**5.1**

C.8 USACE, bend

This is an empirical scour relationship developed by USACE in the 1990s (ASCE, 2004a; ASCE, 2004b). The relationship is determined by reading nomographs for both gravel and sand bed systems developed from data collected on natural fluvial systems. The nomographs relate the ratio of the centerline radius of curvature divided by the water surface width at the design discharge (R_c/W) to the ratio of the max water depth divide by the mean water depth in the approach channel. The developed relationship is an upper envelope fit for maximum bend scour for the evaluated fluvial systems. Because all of the evaluated bends are primarily composed of sand bed material, only the sand nomograph was used for the Isleta to San Acacia scour assessment.

Channel widths and depths, required for the nomograph ratios, were extracted from the 2015 one-dimensional model described in section 3.1, Current Geometry Model (2015. Radius of curvature was measured along the centerline within ESRI's ArcMap (vserion 10.4.1). These are listed in Table 29. The maximum water depth is determined by using Equation 19 and the predicted scour is determined by

Equation 19. Equation to predict max water depth from USACE nomograph

$$y_{max} = \frac{y_{max}}{y_u} * y_u$$

Where y_{max} = maximum water depth in the bend (feet),
y_{max}/y_u = ratio read from the USACE nomograph for sand bed channels (ASCE, 2004a; ASCE, 2004b), and
y_u = mean water depth in the upstream crossing (feet) at the design discharge.

Equation 20. Equation to predict max bend scour from USACE max water depth

$$y_s = y_{max} - y_u$$

Where y_s = predicted maximum depth of scour (feet),
y_{max} = maximum water depth in the bend (feet) estimated by Equation 19, and
y_u = average depth in the upstream crossing (feet) at the design discharge.

The estimated maximum water depth and bend scour are also listed in Table 29.

Table 29: USACE equation variables and input values

Site	r_c Radius of curvature (ft)	W_u Upstream bankfull top width (ft)	y_{max}/y_u Max water depth in bend / mean water depth in approach channel*	y_u Mean water depth in approach channel (ft)	y_{max} Maximum water depth in bend (ft)	**y_s Max scour depth in bend (ft)**
RM 162	3,076	297	1.8	2.6	4.6	**2.0**
RM 149	5,022	198	1.2	6.0	7.2	**1.2**
RM 138.2	3,002	209	1.6	4.7	7.6	**2.8**
RM 130.4	614	164	2.5	5.8	14.6	**8.7**
RM 127.9	703	235	2.7	5.0	13.5	**8.5**
RM 127.5	1,282	235	2.3	5.0	11.2	**6.2**
RM 127	1,802	235	2.0	5.0	10.0	**5.0**
RM 124	615	191	2.6	6.0	15.6	**9.6**
RM 120	3,330	370	1.9	6.8	12.8	**6.1**
RM 116.5	592	160	2.5	4.8	11.9	**7.2**

*Value from USACE nomograph for sand bed channel (ASCE, 2004a; ASCE, 2004b).

C.9 Scour Results by Site

The following tables show the calculated scour for each of the above scour equations at each site. The estimates for the Zeller bend and general scour are coupled together for an overall Zeller scour estimate. A safety factor of 1.1 is also calculated for each of the sites. The tables show that the sites with the highest potential scour include RM 130.4, RM 127.9, RM 120, and RM 116.5.

Table 30: Site RM 162 scour calculation results

Scour Component	Mean Velocity	Competent Velocity	Neill	Lacey	Blench	Maynord	Zeller	Thorne	USACE
General only	incl.	incl.	incl.	incl.	incl.	incl.	0	incl.	incl.
Bend only	incl.		incl.	incl.	incl.	incl.	1.0	incl.	incl.
General & Thalweg	n/a	1.3	n/a	n/a	n/a	n/a	n/a	n/a	n/a
General, Bend, Thalweg	1.9	1.3	1.0	5.0	1.9	*NA	1.0	2.3	2.0
Total Scour	1.9	1.3	1.0	5.0	1.9	*NA	1.0	2.3	2.0
Total Scour w/SF = 1.1	2.1	1.4	1.1	5.5	2.1	*NA	1.1	2.5	2.2

*Not applicable because the input variables are outside the equation limitations

Table 31: Site RM 149 scour calculation results

Scour Component	Mean Velocity	Competent Velocity	Neill	Lacey	Blench	Maynord	Zeller	Thorne	USACE
General only	incl.	incl.	incl.	incl.	incl.	incl.	0	incl.	incl.
Bend only	incl.		incl.	incl.	incl.	incl.	0	incl.	incl.
General & Thalweg	n/a	2.0	n/a	n/a	n/a	n/a	n/a	n/a	n/a
General, Bend, Thalweg	3.0	2.0	1.6	3.6	1.7	*NA	0	4.9	1.2
Total Scour	3.0	2.0	1.6	3.6	1.7	*NA	0	4.9	1.2
Total Scour w/SF = 1.1	3.3	2.2	1.7	3.9	1.9	*NA	0	5.4	1.3

*Not applicable because the input variables are outside the equation limitations

Table 32: Site RM 138.2 scour calculation results

Scour Component	Mean Velocity	Competent Velocity	Neill	Lacey	Blench	Maynord	Zeller	Thorne	USACE
General only	incl.	incl.	incl.	incl.	incl.	incl.	0	incl.	incl.
Bend only	incl.		incl.	incl.	incl.	incl.	2.5	incl.	incl.
General & Thalweg	n/a	2.4	n/a	n/a	n/a	n/a	n/a	n/a	n/a
General, Bend, Thalweg	2.4	2.4	0.6	3.5	1.1	*NA	2.5	4.1	2.8
Total Scour	2.4	2.4	0.6	3.5	1.1	*NA	2.5	4.1	2.8
Total Scour w/SF = 1.1	2.6	2.6	0.7	3.9	1.2	*NA	2.8	4.5	3.1

*Not applicable because the input variables are outside the equation limitations

Table 33: Site RM 130.4 scour calculation results

Scour Component	Mean Velocity	Competent Velocity	Neill	Lacey	Blench	Maynord	Zeller	Thorne	USACE
General only	incl.	incl.	incl.	incl.	incl.	incl.	0	incl.	incl.
Bend only	incl.		incl.	incl.	incl.	incl.	1.4	incl.	incl.
General & Thalweg	n/a	2.9	n/a	n/a	n/a	n/a	n/a	n/a	n/a
General, Bend, Thalweg	2.6	2.9	1.5	3.6	1.7	*NA	1.4	6.0	8.7
Total Scour	2.6	2.9	1.5	3.6	1.7	*NA	1.4	6.0	8.7
Total Scour w/SF = 1.1	2.8	3.2	1.7	4.0	1.8	*NA	1.6	6.6	9.6

*Not applicable because the input variables are outside the equation limitations

Table 34: Site RM 127.9 scour calculation results

Scour Component	Mean Velocity	Competent Velocity	Neill	Lacey	Blench	Maynord	Zeller	Thorne	USACE
General only	incl.	incl.	incl.	incl.	incl.	incl.	0	incl.	incl.
Bend only	incl.		incl.	incl.	incl.	incl.	1.5	incl.	incl.
General & Thalweg	n/a	1.8	n/a	n/a	n/a	n/a	n/a	n/a	n/a
General, Bend, Thalweg	3.7	1.8	1.2	5.4	2.0	5.2	1.5	5.3	8.5
Total Scour	3.7	1.8	1.2	5.4	2.0	5.2	1.5	5.3	8.5
Total Scour w/SF = 1.1	4.1	2.0	1.3	5.9	2.2	5.7	1.7	5.9	9.3

Table 35: Site RM 127.5 scour calculation results

Scour Component	Mean Velocity	Competent Velocity	Neill	Lacey	Blench	Maynord	Zeller	Thorne	USACE
General only	incl.	incl.	incl.	incl.	incl.	incl.	0	incl.	incl.
Bend only	incl.		incl.	incl.	incl.	incl.	1.5	incl.	incl.
General & Thalweg	n/a	1.8	n/a	n/a	n/a	n/a	n/a	n/a	n/a
General, Bend, Thalweg	2.5	1.8	1.0	3.6	2.0	4.6	1.5	4.8	6.5
Total Scour	2.5	1.8	1.0	3.6	2.0	4.6	1.5	4.8	6.5
Total Scour w/SF = 1.1	2.7	2.0	1.1	4.0	2.2	5.0	1.7	5.3	7.1

Table 36: Site RM 127 scour calculation results

Scour Component	Mean Velocity	Competent Velocity	Neill	Lacey	Blench	Maynord	Zeller	Thorne	USACE
General only	incl.	incl.	incl.	incl.	incl.	incl.	0	incl.	incl.
Bend only	incl.		incl.	incl.	incl.	incl.	1.1	incl.	incl.
General & Thalweg	n/a	1.8	n/a	n/a	n/a	n/a	n/a	n/a	n/a
General, Bend, Thalweg	2.5	1.8	1.0	3.6	2.0	4.0	1.1	4.6	5.0
Total Scour	2.5	1.8	1.0	3.6	2.0	4.0	1.1	4.6	5.0
Total Scour w/SF = 1.1	2.7	2.0	1.1	4.0	2.2	4.4	1.2	5.1	5.5

Table 37: Site RM 124 La Joya scour calculation results

Scour Component	Mean Velocity	Competent Velocity	Neill	Lacey	Blench	Maynord	Zeller	Thorne	USACE
General only	incl.	incl.	incl.	incl.	incl.	incl.	0	incl.	incl.
Bend only	incl.		incl.	incl.	incl.	incl.	2.9	incl.	incl.
General & Thalweg	n/a	1.6	n/a	n/a	n/a	n/a	n/a	n/a	n/a
General, Bend, Thalweg	4.5	1.6	1.5	5.4	1.7	*NA	2.9	6.3	9.6
Total Scour	4.5	1.6	1.5	5.4	1.7	*NA	2.9	6.3	9.6
Total Scour w/SF = 1.1	5.0	1.7	1.6	6.0	1.9	*NA	3.2	7.0	10.6

*Not applicable because the input variables are outside the equation limitations

Table 38: Site RM 120 scour calculation results

Scour Component	Mean Velocity	Competent Velocity	Neill	Lacey	Blench	Maynord	Zeller	Thorne	USACE
General only	incl.	incl.	incl.	incl.	incl.	incl.	0	incl.	incl.
Bend only	incl.		incl.	incl.	incl.	incl.	0.6	incl.	incl.
General & Thalweg	n/a	1.1	n/a	n/a	n/a	n/a	n/a	n/a	n/a
General, Bend, Thalweg	2.6	1.1	1.4	3.6	2.0	5.4	0.6	6.1	6.1
Total Scour	2.6	1.1	1.4	3.6	2.0	5.4	0.6	6.1	6.1
Total Scour w/SF = 1.1	2.8	1.2	1.6	3.9	2.2	6.0	0.6	6.8	6.7

Table 39: Site RM 116.5 scour calculation results

Scour Component	Mean Velocity	Competent Velocity	Neill	Lacey	Blench	Maynord	Zeller	Thorne	USACE
General only	incl.	incl.	incl.	incl.	incl.	incl.	0.1	incl.	incl.
Bend only	incl.		incl.	incl.	incl.	incl.	5.1	incl.	incl.
General & Thalweg	n/a	7.0	n/a	n/a	n/a	n/a	n/a	n/a	n/a
General, Bend, Thalweg	4.2	7.0	3.0	5.1	4.7	*NA	5.2	4.9	7.2
Total Scour	4.2	7.0	3.0	5.1	4.7	*NA	5.2	4.9	7.2
Total Scour w/SF = 1.1	4.7	7.7	3.4	5.6	5.2	*NA	5.7	5.4	7.9

*Not applicable because the input variables are outside the equation limitations

RECLAMATION

Managing Water in the West

Isleta to San Acacia Geomorphic Analysis

Middle Rio Grande Project, NM

Upper Colorado Region

U.S. Department of the Interior
Bureau of Reclamation

March 2018

Mission Statements

The mission of the Department of the Interior is to protect and manage the Nation's natural resources and cultural heritage; provide scientific and other information about those resources; and honor its trust responsibilities or special commitments to American Indians, Alaska Natives, and affiliated island communities.

The mission of the Bureau of Reclamation is to manage, develop, and protect water and related resources in an environmentally and economically sound manner in the interest of the American public.

Isleta to San Acacia Geomorphic Analysis

Middle Rio Grande Project, NM

Upper Colorado Region

Report Prepared by
Michelle Klein, PE, Hydraulic Engineer
Cameron Herrington, EIT, Hydraulic Engineer
Jonathan AuBuchon, PE, Hydraulic Engineer
Tony Lampert, PE, Hydraulic Engineer

Report Reviewed by
Ari Posner, PhD, Physical Scientist
Chi Bui, PE, Hydraulic Engineer

Reclamation River Analysis Group,
Technical Services Division

Cover Photographs. Rio Grande looking downstream from ~RM 118 (2002 river miles) by Jonathan AuBuchon on May 17, 2016

U.S. Department of the Interior
Bureau of Reclamation

March 2018

CONTENTS

Acknowledgments

This work has been greatly benefited by the persistent data collection of the U.S. Geological Survey, technical work members of the River Analysis Group in Reclamation's Albuquerque Area Office, and historical work to date on the Rio Grande through this reach, much of which has been cited throughout this report. Also many thanks to Chi Bui, Ari Posner, and Robert Padilla for their review of this work.

Executive Summary

The Bureau of Reclamation (Reclamation) has authority for river channel maintenance on the Rio Grande between Velarde, New Mexico, and the headwaters of the Caballo Reservoir. Reclamation regularly monitors changes in the river channel and evaluates channel and levee capacity in an effort to identify river maintenance sites where there is concern about possible damage to riverside facilities. The Rio Grande between Isleta and San Acacia Diversion Dams was identified as an area of river maintenance concern due to confinement by spoil levees on both sides and the increasing vegetation encroachment. This reach is approximately 53 river miles in length and flows through the communities of Isleta Pueblo, Los Lunas, and Belen.

This report provides an analysis of geomorphic and hydraulic observations within the Isleta Dam to Rio Puerco and Rio Puerco to San Acacia reaches. This helps evaluate changes that have and are occurring in the riverine system and aids in understanding future channel responses and identifying viable future activities.

Flow and sediment supply are the two main drivers of geomorphic change on the Rio Grande (Makar and AuBuchon, 2012). An analysis of the magnitude, frequency, and duration of discharge in the Rio Grande and sediment supply provide indications of how the drivers have changed. Major findings related to the drivers of geomorphic changes between Isleta and San Acacia are summarized as follows:

- The annual water volume on the Rio Grande between Isleta to San Acacia has reduced in recent years (from late 2000s to early 2010s) from about 0.8 million acre-feet per year to 0.4 million acre-feet per year (3.1.1.1 *Single Mass Curves p. 11).*
- Rio Grande is primarily driven by the spring snow-melt runoff, but there is also high, flashy peaks from rainfall-runoff during the late summer-early fall monsoon season. The tributaries to the Rio Grande through this reach are primarily influenced by the monsoon rainfall-runoff period (3.1.1.2 *Water Magnitude Plots* p. 23).
- Peak discharges during the spring snow-melt from Isleta to San Acacia have decreased from the mid-1980s until the early 2010s. Peaks from the 1990s are similar to peaks in the 2000s. (3.1.1.2 *Water Magnitude Plots* p. 23).
- The depth to the shallow groundwater aquifer has been increasing over the last decade, likely due to thalweg incision. There is a strong correlation between the shallow groundwater aquifer depth fluctuations and fluctuations in the river discharge (3.1.1.3 *Groundwater Flows* p.28).

- Local precipitation, annual average between 6 and 8 inches, primarily occurs from July through September via high magnitude but short duration events (3.1.1.4 *Precipitation Data* p. 43).
- The frequency of high flow events has decreased during the 1990s and 2010s compared to the mid-1970s through the late 1990s (3.1.2 *Frequency* p.49).
- Frequency of low flow events has increased at the Albuquerque USGS gage from the 1990s to the early 2010s, but decreased slightly for the Bernardo and San Acacia USGS gages (3.1.2 *Frequency* p.49).
- Duration of flow events > 500 cfs has decreased between 1995 and 2015. (3.1.3 *Duration* p.51).
- Annual suspended sediment discharge has decreased since the early 1970s on the Middle Rio Grande upstream of the Rio Puerco. Below the Rio Puerco confluence the sediment discharge has fluctuated with a relatively constant trend between 2 and 5 million tons/year. (3.2.1.1 *Single Mass Curves* p.11).
- The Rio Puerco annual suspended sediment yield has decreased since the late 1970s (3.2.1.1 *Single Mass Curve*s p. 55).
- The mean annual suspended sediment concentration measured at San Acacia tends to be twice that measured at Albuquerque. The average suspended sediment concentration at Albuquerque between 2012 and 2014 was 1,262 mg/L, while at San Acacia the average concentration between 2007 and 2014 was 3,554 mg/L (3.2.1.2 *Double Mass Curves* p. 61).
- Highest suspended sediment concentrations within this study reach occur in the months of July through September. The largest suspended sediment discharge (tons/day), however, occurs in May at the upstream end of this reach (Albuquerque USGS gage) and in August at the downstream end of this reach (San Acacia USGS gage). (3.2.1.3 *Average Monthly Histograms,* p.68).
- Since the 2000s, the Rio Grande appears to be storing suspended sediment in the reach between Albuquerque and Bernardo based on the decrease in suspended sediment mass observed between the USGS gages. However, in the reach between Albuquerque and San Acacia the Rio Grande appears to be mining suspended sediment based on the increase in suspended sediment mass observed between the USGS gages. The Rio Puerco, Rio Salado, and other tributaries between Bernardo and San Acacia are likely the main factors contributing to this observation (3.2.1.4 *Difference Mass Curves*, p. 72).
- The effective discharge for suspended sediment (discharge at which the most suspended sediment is moved) has increased in recent decades between Albuquerque and Bernardo from around 900 cfs to just over 1,000 cfs. The effective discharge for suspended sediment between Bernardo and San Acacia however, has decreased from around 900 cfs to about 750 cfs (3.2.1.5 *Effective Suspended Sediment Discharge Curves*, p. 74.

- The predominant sediment moved through the reach are sands and finer material (silts/clays), being almost two orders of magnitude higher yield than gravels. (3.2.2.2 *Total Load Curves,* p. 80).
- Based on total load calculations from collected samples from the early 1990s through 2010 at the San Acacia USGS gage, the predominant material transported by the river is sand (~68%). Finer material (silts and clays) constitutes around 32% of the total load at the San Acacia gage. (3.2.2.2 *Total Load Curves,* p. 80).
- The effective discharge for total load (discharge at which the most total load is moved) has decreased at San Acacia in recent decades from 940 cfs to around 750 cfs (3.2.2.2 *Total Load Effective Discharge Curves* p. 86).

Geomorphic change within the Isleta to Rio Puerco and the Rio Puerco to San Acacia reaches have also been assessed using six parameters: width, slope, sinuosity, planform, channel topography, and bed material size. A summary of the major observations for the six analyzed geomorphic parameters are as follows:

- The average and range of the active channel width has decreased throughout the Isleta to San Acacia reach of the Rio Grande since the 1960s. The average active channel width in 2016 for the Isleta to Rio Puerco reach was just under 180 feet, while the Rio Puerco to San Acacia reach was just over 150 feet (4.1 *Channel Width* p. 90 and 4.6 *Channel and Floodway Topography* p. 136).
- The Rio Grande planform between Isleta and San Acacia Diversion Dams has shifted from a multi-threaded channel to a primarily single thread channel between the 1990s and early 2010s (4.2.1 *Planform Classification on the Rio Grande* p. 95).
- Potential exists for the river to deepen and narrow in the Isleta to Rio Puerco reach, potentially creating conditions for lateral migration of the banklines. A higher terrace adjacent to the active channel in the Rio Puerco to San Acacia reach may also create a tendency for banks to laterally migrate. (4.2.1 *Planform Classification on the Rio Grande* p. 95)
- Vegetation cover has increased as much as 20% on the Rio Grande since the 1990s, which has affected the local sinuosity and reach width. (4.2.1 *Planform Classification on the Rio Grande* p. 95 and 4.2.3 *Vegetation Trends* p.111) .
- The number and area of mid-channel bars has decreased as mid-channel bars have become attached to the banklines. (4.2.4 *Island Trends* p.116)
- The slope of the Rio Grande through the Isleta to San Acacia reach has decreased from the 1980s to early 2010s. The slope of the Rio Grande from Isleta to the Rio Puerco has decreased from the 2000s to the early 2010s, while the slope of the Rio Grande from Rio Puerco to San Acacia has increased during the same time period (4.3 *Channel Slope* p. 119).
- The sinuosity of the Isleta to Rio Puerco geomorphic reach is currently increasing. The sinuosity of the Rio Puerco to San Acacia geomorphic

reach is currently experiencing a slight increase (4.4 Channel *Sinuosity* p. 126).

- Bed material, primarily sands, tends to be coarsening between the Isleta and San Acacia Diversion Dams. Shear stress and particle stability analysis on the bed materials indicate that bed material is unstable except around the Rio Salado confluence, where bed material is gravel (4.5 *Bed Material Size and Type* p. 127).
- An assessment of the channel and floodway topography between the mid-1990s and mid-2010s indicates that in some areas (between Los Lunas, NM and Casa Colorado, NM and upstream of San Acacia Diversion Dam) the river has incised. But there are other areas (Isleta Diversion Dam to Los Lunas, NM and Casa Colorado, NM to just upstream of San Acacia Diversion Dam) where the river has aggraded. The change in the bank height follows a similar trend. The increase in bank height is due to a combination of channel incision and vertical accretion of sediment on mid-channel bars and at the bankline. (4.6 Channel and Floodway Topography p. 136).
- The Rio Grande between Isleta and San Acacia has various terrace surfaces. Between Isleta Diversion Dam and Tome, NM the active channel is slightly perched relative to the adjacent floodplain. From Abeytas, NM to San Acacia Diversion Dam a majority of the floodplain surfaces are high and elevated above the active channel. The area between Tome, NM and Abeytas, NM has a mix of these two characteristics (4.7 Terrace Mapping p. 150).

The Rio Grande between Isleta and San Acacia Diversion Dams is generally shifting to a single thread channel, becoming narrower, decreasing in slope, and becoming more sinuous over the last 10-15 years. The two portions of the reach experiencing deepening along the channel thalweg include the Rio Grande from the Los Lunas, NM to Casa Colorado, NM and just immediately upstream of the San Acacia Diversion Dam. The rest of the Rio Grande through this reach has experienced channel aggradation along the thalweg. Most of the Rio Grande has also experienced significant floodplain deposition from the 1990s until the mid-2010s.

River trends expected to continue within the Isleta to San Acacia reach are channel depth increasing (channel incision and/or bank height increase), active channel width narrowing, slope decreasing, bed material coarsening, meander wavelength decreasing, and sinuosity increasing. The channel depth increase, plus sedimentation in the floodplain will continue to diminish floodplain connectivity and increase channel uniformity. The absence of higher river flows will also likely promote the continued vegetation encroachment along river banks and within inter-channel sand bars, further decreasing the active channel width. If the channel incision, however, extends below the root zones of riparian species, banks would likely be more susceptible to bank erosion. If the river begins to laterally

migrate from active bank erosion, the active channel width in local areas could increase.

Potential river maintenance concerns within the Isleta to Rio Puerco reach include increased risk of infrastructure adjacent to the active channel and ineffective transport of sediment and water downstream. Areas between Los Lunas, NM and Casa Colorado, NM are currently the most at risk for lateral migration of the active channel. Isleta Diversion Dam to Tome, NM, and to a lesser extent Tome, NM to Abeytas, NM are the reaches most susceptible to ineffective transport of sediment and water as the floodplain adjacent to the active channel tends to be higher than terrain adjacent to the constraining infrastructure (e.g. perched channel conditions). Improving active channel-floodplain connection would likely be beneficial, as would providing streambank protection paralleling the constraining infrastructure. This would help hydraulically protect the adjacent infrastructure while still providing the river some freedom to make adjustments. Mechanical intervention, through the removal of vegetation and re-connection of lower terraces or lowering of higher terrace adjacent to the active channel, may temporarily provide improved floodplain connection. If fluvial processes are able to continually remove newly established vegetation, sinuosity may increase, further improving the morphological diversity within the active channel. These effects, however, would not be sustainable unless longer term changes in the sediment and water discharge loads were experienced (5.0 *Future Channel Response* p. 164).

River trends expected to continue within the Rio Puerco to San Acacia reach are channel depth decreasing (channel aggradation), active channel width narrowing, slope increasing, bed material fining, meander wavelength decreasing, and sinuosity increasing. If channel aggradation continues floodplain connectivity may increase. This would be controlled to a large extent by the influence of larger bed material around the Rio Salado acting like a grade control. Since this reach currently has high terraces adjacent to the active channel, the majority of the reach is currently susceptible to bank erosion on these surfaces through lateral migration. The future expectation would be for small aggradational changes within the active channel, with a tendency towards lateral migration and increased channel sinuosity. If the sediment supply increases or the grade control at the Rio Salado is more pronounced then floodplain connectivity to the high terrace may increase and reduce the lateral migration. This potential future lateral connection to the floodplain would tend to decrease the channel uniformity and increase the morphological channel complexity and diversity.

Within the Rio Puerco to San Acacia Reach, potential river maintenance concerns include the increased risk of infrastructure adjacent to the active channel, especially where the valley is narrow downstream of the Rio Salado, ineffective transport of sediment and water downstream, and increased risk of flooding. Removal of vegetation near the bank may exacerbate the lateral migration and provide an opportunity for an inset floodplain to develop adjacent to the active

channel. Vegetation growth, naturally or through bio-engineering methods, would tend to provide additional stability near infrastructure. The establishment of an inset floodplain, through encouraging lateral migration or by creating floodplain surfaces in the higher terrace, would help convey the effective transport of water and sediment downstream. Methods that rehabilitate the active channel capacity and/or strengthen/raise the adjacent spoil levee are likely the most suitable options for addressing the risk of flooding. Observations of the future morphological responses within this reach may also provide opportunities for additional habitat rehabilitation efforts that augment the natural fluvial processes occurring within this reach (5.0 *Future Channel Response* p. 164).

1.0 Introduction

The Isleta Dam to Rio Puerco and the Rio Puerco to the San Acacia reaches are classified as Class 3b river maintenance reaches (Maestas et al., 2014). There are currently ten (10) river maintenance sites identified by Maestas et al. (2014) within these two reaches– one (1) class 3a sites (RM 121), seven (7) class 3b sites (NM 6 Bridge, Highway 309 Bridge, Rio Puerco 127.9, Rio Puerco 127.5, Rio Puerco 127.0, La Joya, and Bernardo Arroyo), and two (2) class 4 sites (Los Trujillos and DU7). In evaluating the channel dynamics in this reach, an updated analysis on the geomorphic, hydraulic, hydrologic, and sediment transport of these two reaches was performed.

The two reaches being assessed are shown in Figure 1. The reach spans a little over 53 miles from river mile (RM) 169.3 at the Isleta Diversion Dam to RM 116.2 at the San Acacia Diversion Dam.

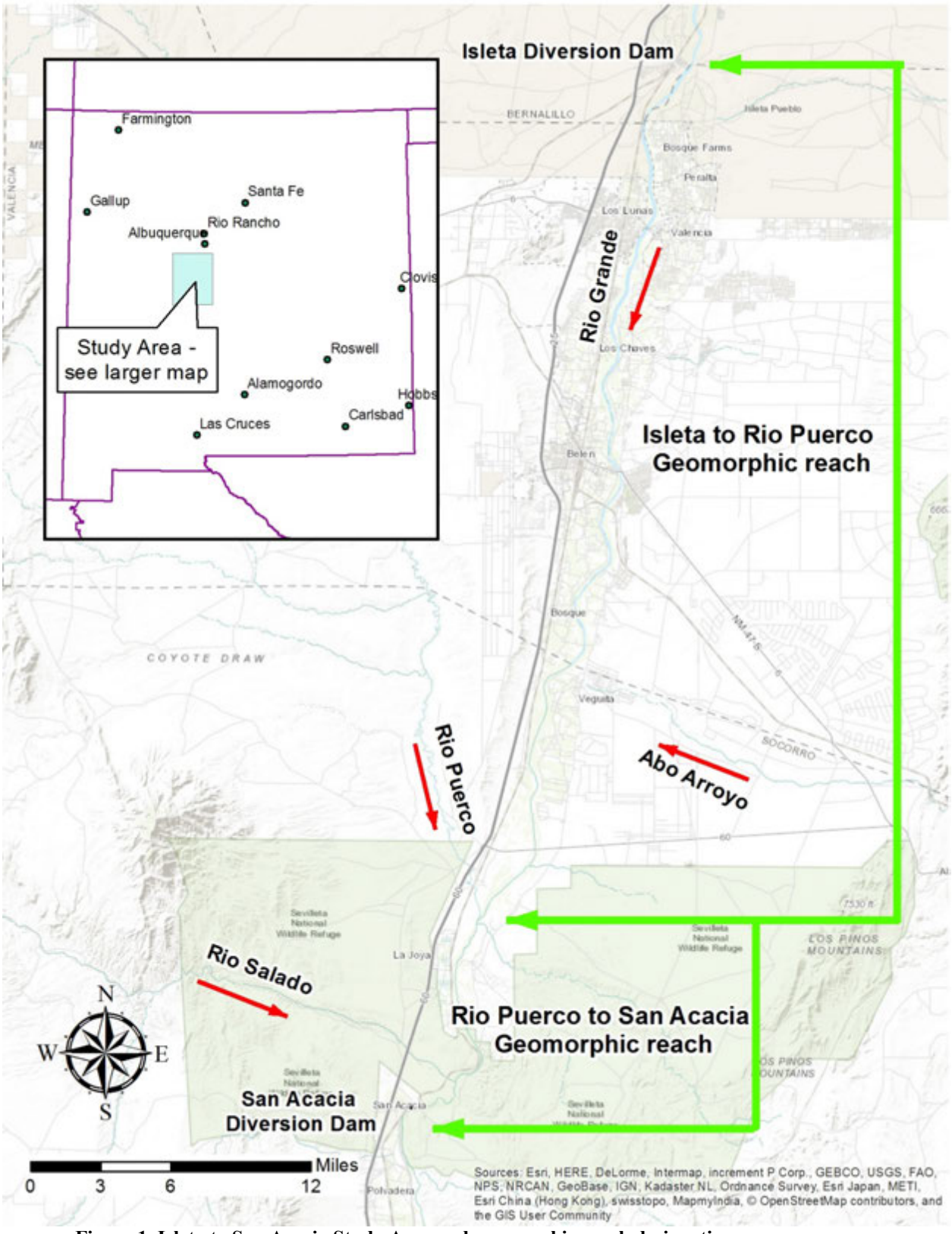

Figure 1. Isleta to San Acacia Study Area and geomorphic reach designation.

2.0 Background Information and Project Purpose

A variety of geomorphic, hydrologic, and sediment studies have been conducted on the Rio Grande and its tributaries, namely the Rio Puerco and the Rio Salado. A summary of these studies is provided in AuBuchon (2015). The intent of this geomorphic study was to update some of the analyses from these studies, with the specific intention of evaluating recent decades. This report looks at geomorphic trends occurring in the Isleta to San Acacia reaches to facilitate future river maintenance and habitat rehabilitation projects. The desire for this undertaking is to provide an understanding of the geomorphic processes at work in the Middle Rio Grande between Isleta and San Acacia.

Some of the historical information summarized in AuBuchon (2015) is repeated in this report, within the pertinent section, to provide some historical context. Relevant information from Makar (2015) is also included where applicable.

3.0 Assessment of Geomorphic Drivers

There are two main drivers of geomorphic change on the Rio Grande, as defined by Makar and AuBuchon (2012). The two main drivers include flow (magnitude, frequency, and duration) and sediment supply. Ascertaining changes in the drivers over time helps provide links to understanding observed geomorphic changes (historically and contemporaneously). The majority of the information for the analyses of the drivers is derived from collected data at the USGS gages. A

Major findings related to the drivers of geomorphic changes between Isleta and San Acacia are summarized as follows:

- There are cycles of wet and dry periods reflected by the average annual volume of water recorded passing the USGS gage stations. Generally the reach between Isleta to San Acacia loses water as it moves downstream. The Rio Puerco, one of the largest tributaries to the Rio Grande in this reach, contributes less than 15% of the total volume of water in the Rio Grande (3.1.1.1 *Single Mass Curves* p. 11).
- The annual water volume on the Rio Grande between Isleta to San Acacia has reduced in recent years (from late 2000s to early 2010s) from about 0.8 million acre-feet to 0.4 million acre-feet (3.1.1.1 *Single Mass Curves p. 11).*
- Rio Grande is primarily driven by the spring snow-melt runoff, but there is also high, flashy peaks from rainfall-runoff during the fall. The tributaries to the Rio Grande through this reach are primarily influenced by the fall rainfall-runoff period (3.1.1.2 *Water Magnitude Plots* p. 23)

- Peak discharges during the spring snow-melt from Isleta to San Acacia have decreased from the mid-1980s until the early 2010s. Peaks from the 1990s are similar to peaks in the 2000s. (3.1.1.2 *Water Magnitude Plots* p. 23).
- The depth to the shallow groundwater aquifer has been increasing over the last decade. There is a strong correlation between the shallow groundwater aquifer depth fluctuations and fluctuations in the river discharge (3.1.1.3 *Groundwater Flows* p. 28)
- Local precipitation, annual average between 6 and 8 inches, primarily occurs from July through September via high magnitude but short duration events (3.1.1.4 *Precipitation Data* p. 43).
- Frequency of low flow events has increased since the mid-1980s. The frequency of high flow events has decreased over the last decade or so (3.1.2 *Frequency* p. 49)
- Duration of flow events > 500 cfs has decreased between 1995 and 2015. (3.1.3 *Duration* p. 51).
- Annual suspended sediment discharge has decreased since the 1970s on the Middle Rio Grande north of the Rio Puerco (USGS gage at Bernardo), from between 7 and 4 million tons per year to around 0.5 to 1 million tons per year. Below the Rio Puerco's confluence with the Rio Grande (USGS gage at San Acacia) the annual sediment discharge has fluctuated with a relatively constant trend between 2 and 5 million tons/year. (3.2.1.1 *Single Mass Curves* p. 55).
- The Rio Puerco annual suspended sediment discharge has decreased from around 2.5 million tons/year in the late 1970s (roughly about 80% of the suspended sediment volume in the Rio Grande as recorded at the San Acacia gage) to about 1 million tons/year in 2014 (or roughly 30% of the suspended sediment volume in the Rio Grande as recorded at the San Acacia gage) (3.2.1.1 *Single Mass Curve*s p. 55)
- The suspended sediment concentration has decreased through the study reach, with the largest decrease in magnitude occurring in the 1970s and 1980s (depending on the gaging station) (3.2.1.2 *Double Mass Curves* p. 61).
- The mean annual suspended sediment concentration measured at San Acacia tends to be twice that measured at Albuquerque (3.2.1.2 *Double Mass Curves* p. 61).
- Highest suspended sediment concentrations within this study reach occur in the months of July through September. The largest suspended sediment discharge (tons per day), however occur in May at the upstream end of this reach (Albuquerque USGS gage) and in August at the downstream end of this reach (San Acacia USGS gage). Just upstream of the Rio Puerco confluence the Bernardo USGS gage shows an equally high sediment discharge in May and July, indicating the increasing impact of tributary flows moving downstream in this reach (3.2.1.3 *Average Monthly Histograms,* p. 68).

- Since the 2000s the Rio Grande appears to be storing suspended sediment in the reach between Albuquerque and Bernardo based on the difference in suspended sediment mass observed between the USGS gages. Between Albuquerque and San Acacia the river may be transporting, storing, or mining suspended sediment as there is a greater mass of suspended sediment flowing past the USGS gage at San Acacia, then at the Albuquerque USGS gage. The additional suspended sediment load added by the Rio Puerco, the Rio Salado, and other tributaries in the reach is likely contributing to this observation (3.2.1.4 *Difference Mass Curves*, p. 72).
- The effective discharge for suspended sediment (discharge at which the most suspended sediment is moved) has increased in recent decades between Albuquerque and Bernardo from around 900 cfs to just over 1,000 cfs. The effective discharge for suspended sediment between Bernardo and San Acacia however, has decreased from around 900 cfs to about 750 cfs (3.2.1.5 *Effective Suspended Sediment Discharge Curves*, p. 74.
- The predominant sediment moved through the reach are sands and finer material (silts/clays), being almost two magnitudes higher yield than gravels. Rainfall-runoff events tend to move more sediment per day (up to 5 times greater) than a spring runoff event for events up to 2,000 cfs. Above this discharge there is not enough information to quantify the difference. (3.2.2.2 *Total Load Curves,* p. 80).
- Based on total load calculations from collected samples from the early 1990s through 2010 at the San Acacia USGS gage, the predominant material transported by the river is sand (~68%). Finer material (silts and clays) constitutes around 32% of the total load at the San Acacia gage. The percentage of the total load moved by the Rio Grande past San Acacia that is sand has decreased from an average percentage of 73% in the 1990s to about 64% in the 2000s. The average percentage of finer material increased from about 27% in the 1990s to about 35%. The percentage of gravel moving also increased, but it is still had an average percent of the total load less than 1% (3.2.2.2 *Total Load Curves,* p. 80).
- The effective discharge for total load (discharge at which the most total load is moved) has decreased at San Acacia in recent decades from 940 cfs to around 750 cfs (3.2.2.2 *Total Load Effective Discharge Curves* p. 86).

3.1 Flow

The Rio Grande exhibits two distinct flow patterns through a given year (Bauer, 2009). During the spring/early summer there is a peak in the river flow due to snow-melt runoff. The flow is typically characterized by a gradual rise and fall of the hydrograph, with a high runoff volume spread out over 1-2 months. The second flow pattern occurs in the late summer/early fall and is derived from intense rain events. The flow associated with the rainfall-runoff events is

characterized by a sharp rise and fall of the hydrograph, with a low runoff volume that is typically measured in hours.

Between the Isleta Diversion Dam and the Rio Puerco confluence there are about 15 tributaries, most of which are canal or drain returns. Between the Rio Puerco and San Acacia Diversion Dam there are 13 tributaries most of which are braided sandy washes (Varyu and Fox, 2014). Two of the principal tributaries between Isleta and San Acacia Diversion Dams (the Rio Puerco and the Rio Salado) are primarily driven by rainfall-runoff events (Mosley, 2000).

3.1.1 Magnitude

Peaks of both the snow-melt and rainfall-runoff flow events have been curtailed in recent decades due to upstream reservoirs (MEI, 2002). Rainfall-runoff events primarily originating in unregulated watersheds like the Rio Puerco and Rio Salado are the exception and production of high peak discharges are still possible (e.g. the USGS San Acacia gage on the Rio Grande (# 08354900) recorded an instantaneous peak of 9,020 cfs on September 16, 2013 at 11:30 am. A gage on the Rio Puerco, near Bernardo, NM (#08353000) showed a similar peak discharge on September 15, 2013 at 10:30 pm). This observed flow peak is still smaller than Rio Grande flood peaks from the late 1920s until early 1940s with magnitudes between 18,000 cfs and 47,000 cfs. Many of these events had significant discharge contributions from the Rio Puerco and the Rio Salado (MEI, 2002).

3.1.1.1 Single Mass Curves

Single mass curves are used to show annual changes in water conveyance (flow volume) over time. The total flow discharged in a year is added to the previous years' discharge to provide a cumulative total. Single mass curves (Figure 2 through Figure 9) were created for the following USGS gage locations: Albuquerque, Isleta, Bosque Farms, Bosque, Bernardo, San Acacia, Rio Puerco near Bernardo, and Rio Salado near San Acacia.

Figure 2 shows the single mass curve for the Rio Grande in Albuquerque at the Central Avenue Bridge. The flow data was obtained from USGS gage 08330000 "Rio Grande at Albuquerque, NM."

Figure 3 shows the single mass curve for the Rio Grande just below the I-25 bridge on the northern side of Isleta Pueblo. The flow data was obtained from USGS gage 08330875 "Rio Grande at Isleta Lakes near Isleta, NM."

Figure 4 shows the single mass curve for the Rio Grande near Bosque Farms around river mile 166 (2012 demarcations). The data comes from USGS gage 08331160 "Rio Grande near Bosque Farms, NM."

Figure 5 shows the single mass curve for the Rio Grande near Bosque, NM at the State Highway 346 Bridge. The data comes from the USGS gage 08331510 "Rio Grande at State HWY 346 near Bosque, NM." Data for 2006 was only available

for days after February 23, so the “Cumulative Water Discharge” does not accurately reflect the entire water year.

Figure 6 shows the single mass curve for the Rio Grande near Bernardo at the U.S. Highway 60 Bridge. The flow data between 1958 and 2014 was obtained from USGS gage 08332010 “Rio Grande Floodway near Bernardo, NM.” The data prior to 1958 was obtained from the USGS gage 08332000 “Rio Grande near Bernardo, NM.” However, there are many gaps in this data: 1939-1941, 1943, 1954, and 2006-2011. Data is also missing for part of the year in 1956 and 2005, so the “Cumulative Water Discharge” does not accurately reflect the entire water year.

Figure 7 shows the single mass curve for the Rio Grande just downstream of the San Acacia Diversion Dam. The data for years 1937-1958 comes from the USGS gage 08355000 “Rio Grande at San Acacia NM.” The data for years 1959-2014 comes from the USGS gage 08354900 “Rio Grande Floodway at San Acacia, NM.” The flow values at the San Acacia gages reflect discharge in the main channel and do not include flow from the Low Flow Conveyance Channel (LFCC).

The low slope period at San Acacia between 1958 and 1981, shown in Figure 7, can be partially attributed to the operation of the LFCC since this time period corresponds to the time of highest diversions to the LFCC. However, this period of low slope is also seen in Figure 6 at Bernardo. Since the LFCC only begins diversions from the main channel at San Acacia Diversion Dam, this period of low slope must also be attributed to other diversions besides the LFCC. This period of low slope is not seen at the Albuquerque gage (see Figure 2).

Figure 8 shows the single mass curve for the Rio Puerco near Bernardo. The data comes from USGS gage 08353000 “Rio Puerco near Bernardo, NM.” Figure 9 shows the single mass curve for the Rio Salado near San Acacia. The data comes from USGS gage 08354000 “Rio Salado near San Acacia, NM.” Figure 10 shows the total flow each year in acre feet at each of the USGS gages between Albuquerque and San Acacia.

Areas of each graph with similar slopes of the single mass curves (slopes represent a mean annual discharge) were grouped together and labeled with the years and mean annual discharge. The single mass curves show a wetter period (demonstrated by a steeper curve) from the late 1970s/early 1980s to the mid-1990s, with annual flow volumes ranging between 0.6 and 1.6 million acre-feet. The mean annual flow volume during this time period was almost double the mean annual volume recorded prior to this time frame at the Albuquerque gage (about 0.7 million acre-feet), and almost 5x greater as recorded at the Bernardo and San Acacia gages (about 0.2 million acre-feet). From the mid-1990s to around 2000 (0.7 to 1.0 million acre-feet per year at Albuquerque, Bernardo, and San Acacia) and then again from the mid-2000s to around 2010 (0.2 to 0.8 million

acre-feet per year at Albuquerque, Isleta, Bernardo, and San Acacia), the annual flow volume was about the same as that prior to the late 1970s. The early 2000s and early 2010s show an even drier period with annual flows ranging from 0.2 to 0.4 million acre-feet at Albuquerque, Isleta, Bernardo, and San Acacia.

Gages on the Rio Puerco and Rio Salado (last operated in 1984) watersheds tend to add less than 15% of the annual flow volume as recorded by the USGS gages on the Rio Grande. The flow events on the Rio Puerco may be high magnitude events, but are typically short-lived and therefore do not add significant volumes of water on an annual basis to the Rio Grande. During the period of record the Rio Salado and Rio Puerco do not indicate the same wet/dry cycles as shown for the Rio Grande, except in the early 2000s where annual flow volumes on the Rio Puerco drop from about 20 to 80 thousand acre-feet to about 8 to 9 thousand acre-feet.

Figure 10 shows the annual flow volumes at the Albuquerque, Bernardo, and San Acacia gages. There seems to be a slight reduction in the downstream direction of the annual volume of water. The difference between the annual flow volume at Albuquerque and the two southern gages is more noticeable between 1960 and 1980. The LFCC was operated during this period which may explain differences at San Acacia, but the diversion point for the LFCC is downstream of the Bernardo gage. Drains were also connected together during this period, such as tying the Socorro Main Canal being tied into the Drain Unit 7 Extension and Drain Unit 7 facilities. This may have influenced the Bernardo gage as well.

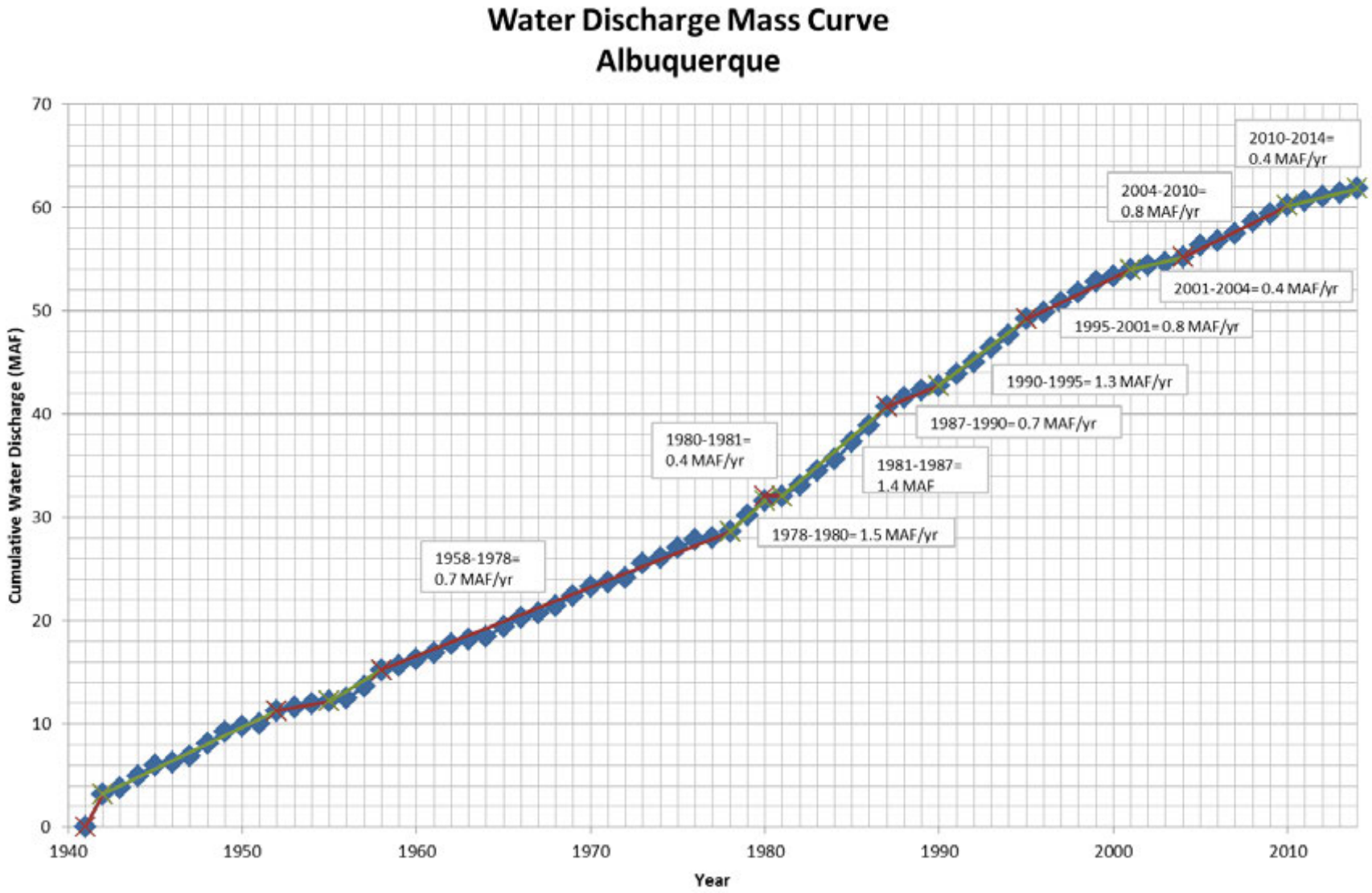

Figure 2: Water Discharge Mass Curve for the Albuquerque USGS gage: 1941 - 2014

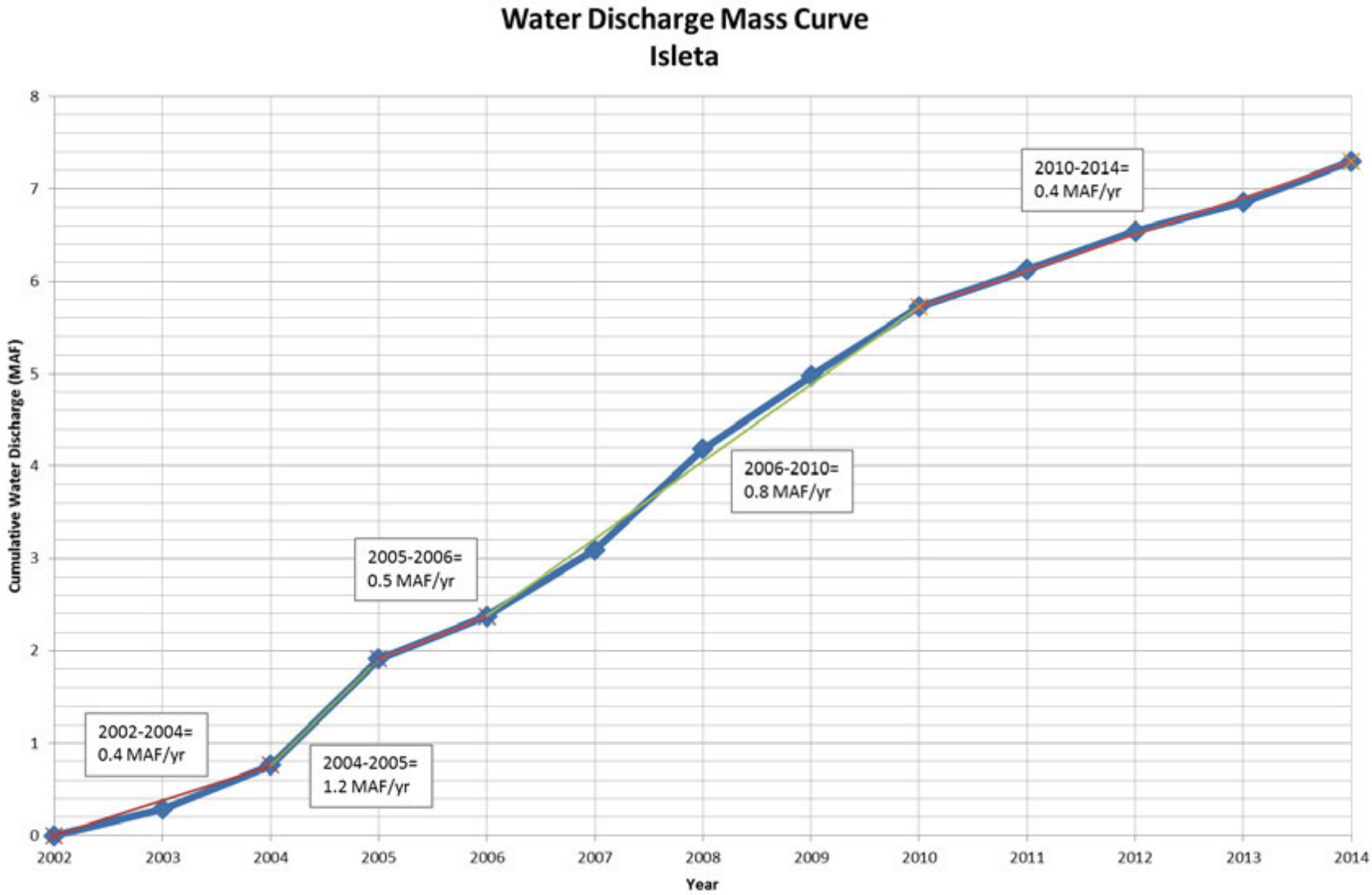

Figure 3: Water Discharge Mass Curve for the Isleta USGS gage: 2002 - 2014

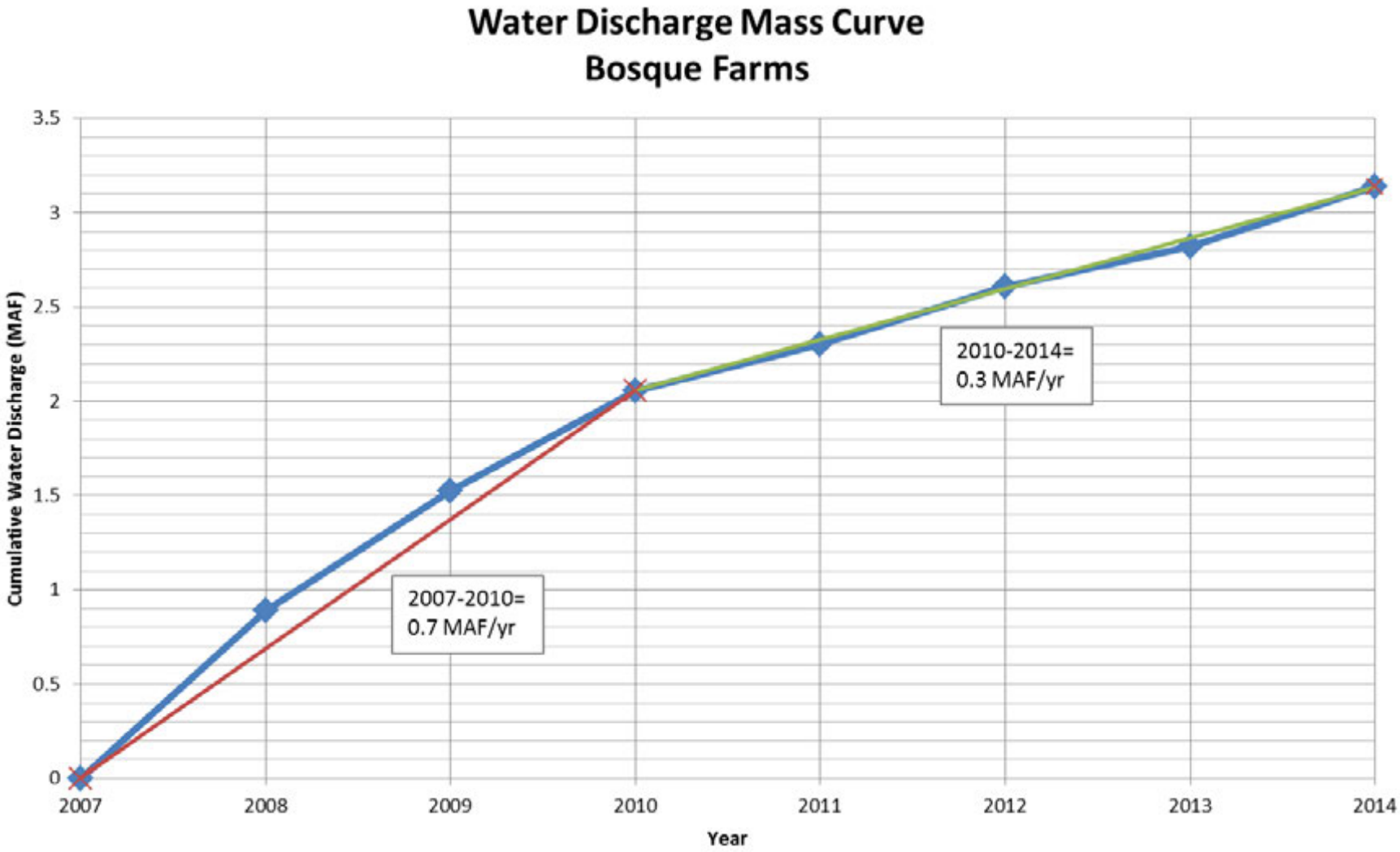

Figure 4: Water Discharge Mass Curve for the Bosque Farms USGS gage: 2007 to 2014.

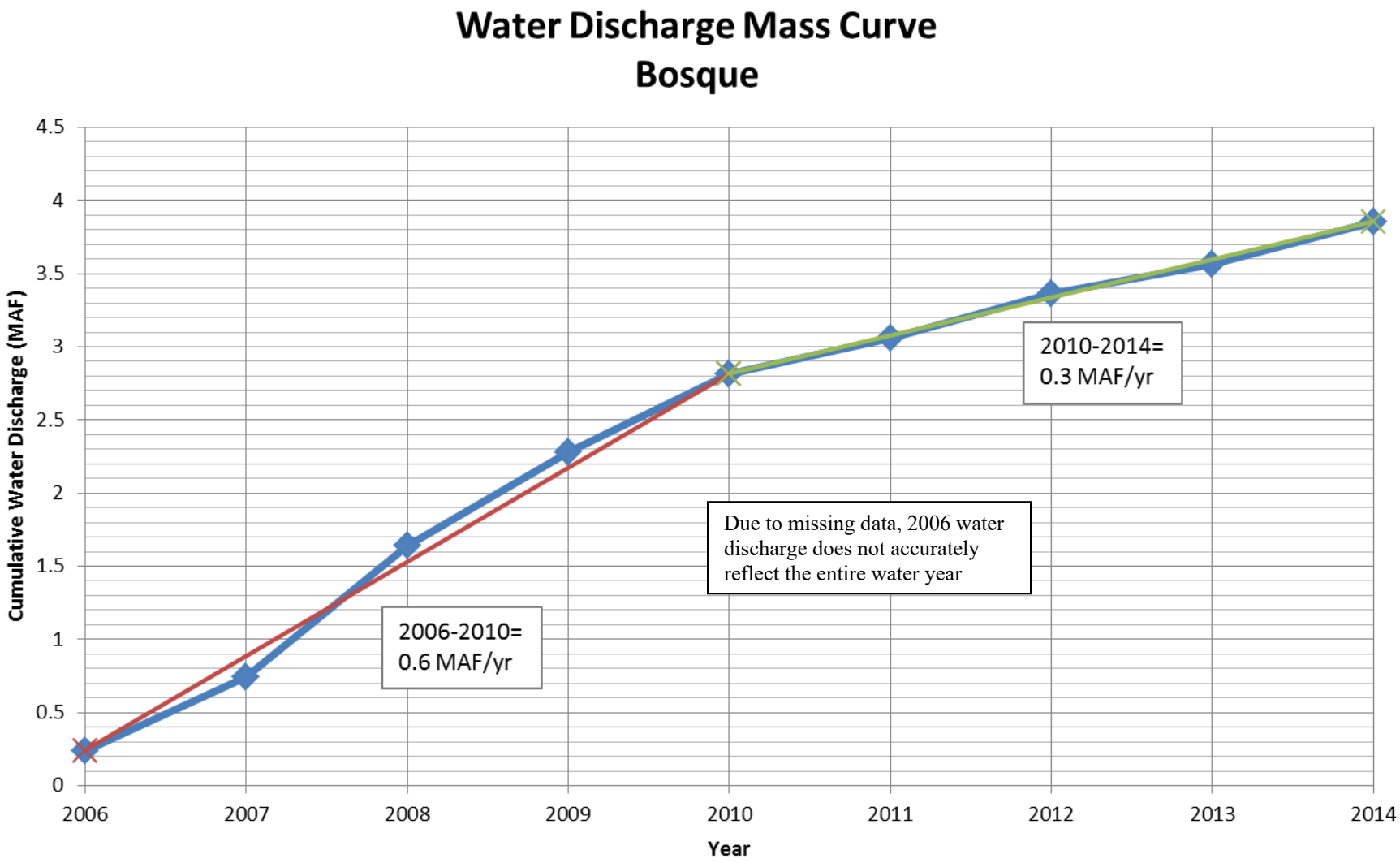

Figure 5: Water Discharge Mass Curve for the Bosque USGS gage: 2006 to 2014

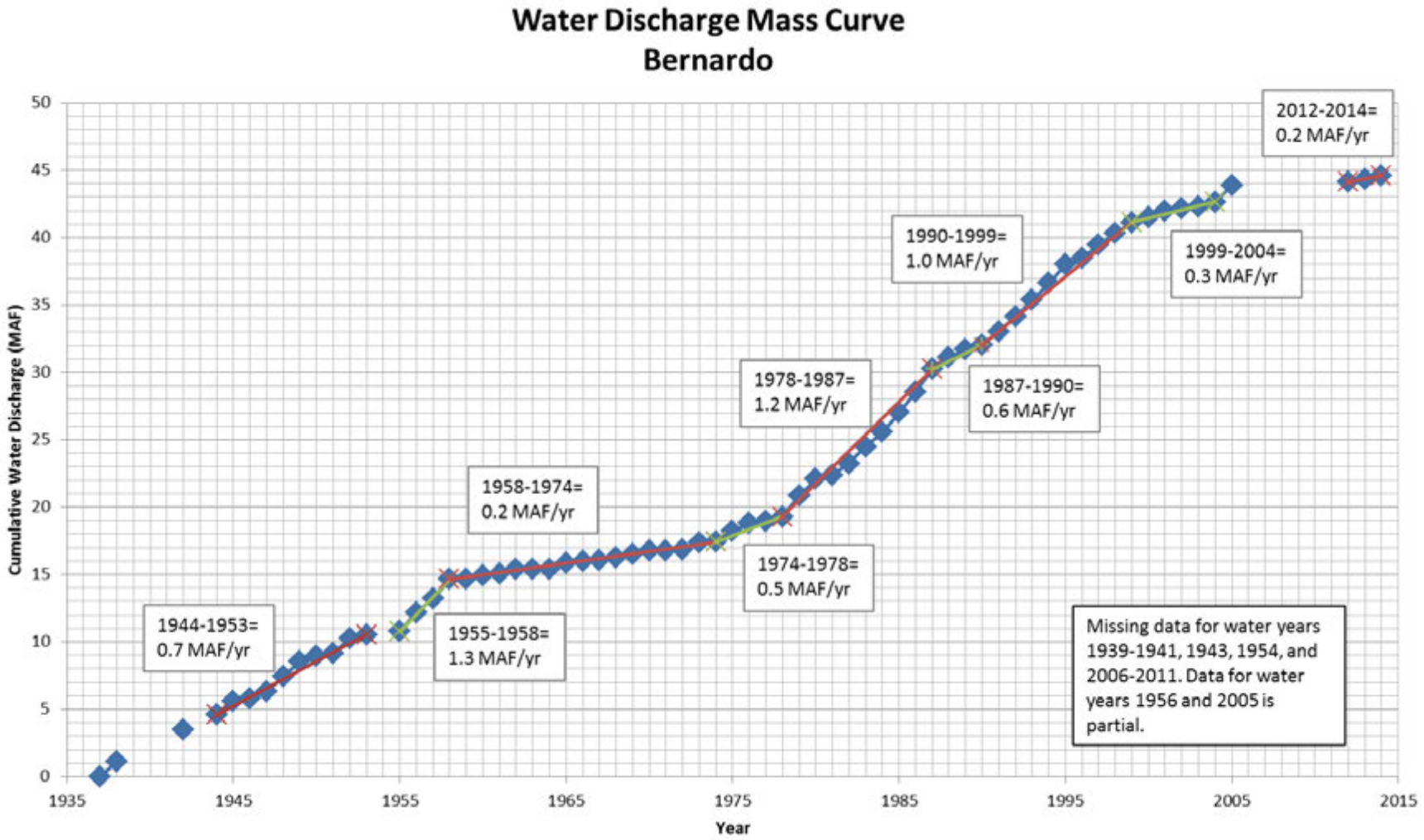

Figure 6: Water Discharge Mass Curve for the USGS Bernardo gage: 1937 to 2014.

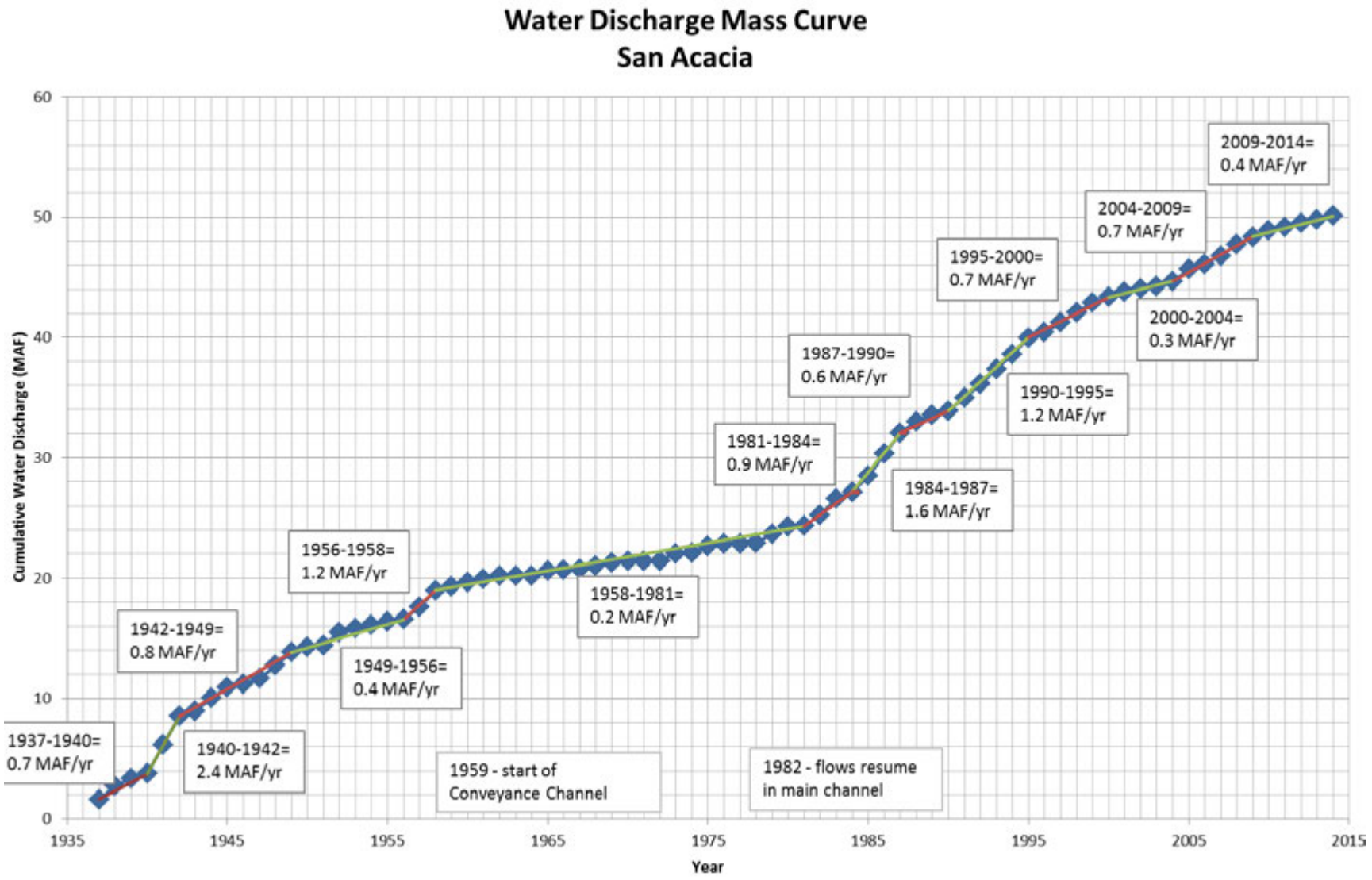

Figure 7: Water Discharge Mass Curve for the San Acacia USGS gage: 1937 to 2014.

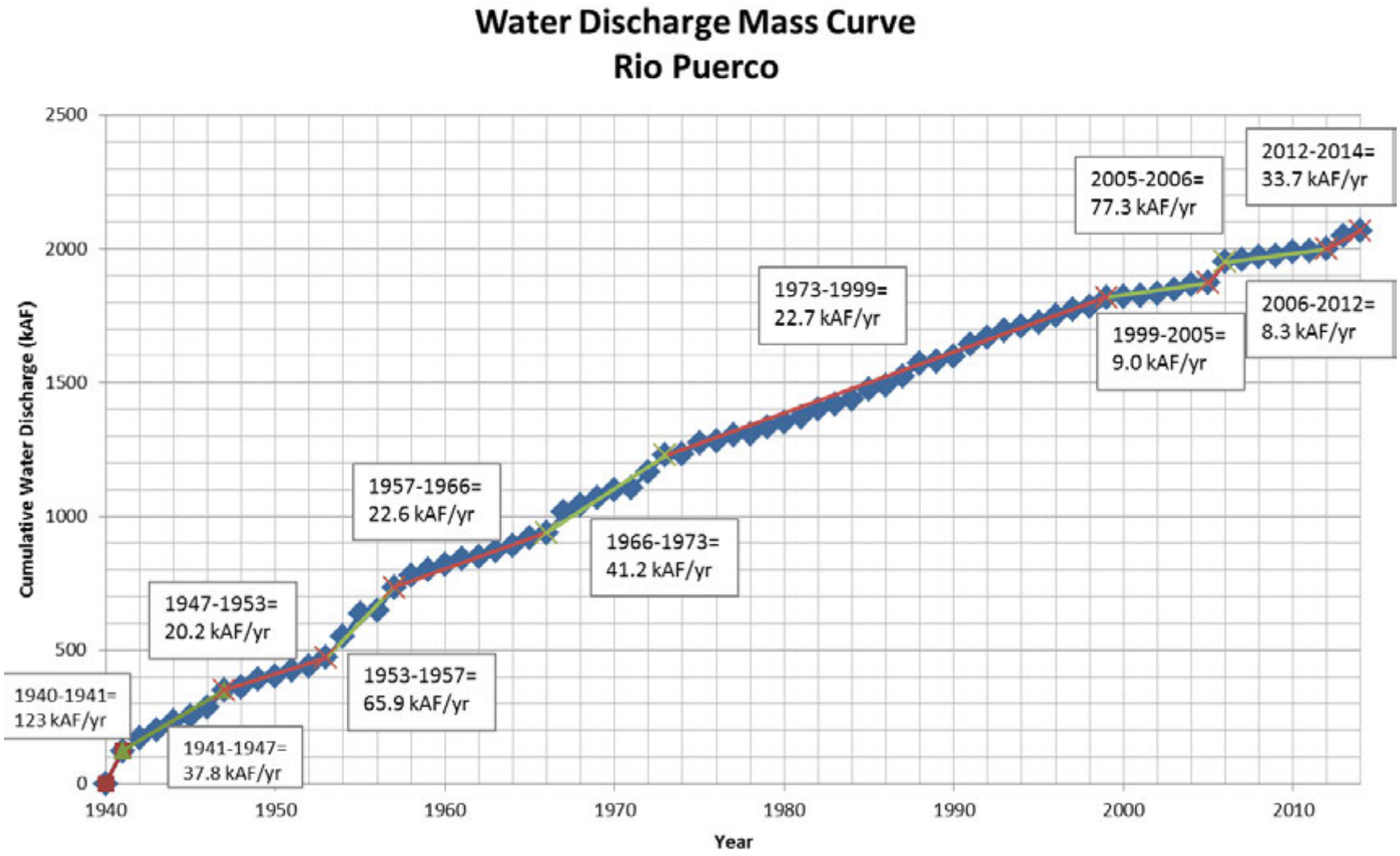

Figure 8: Water Discharge Mass Curve for the Rio Puerco USGS gage near Bernardo: 1940 to 2014

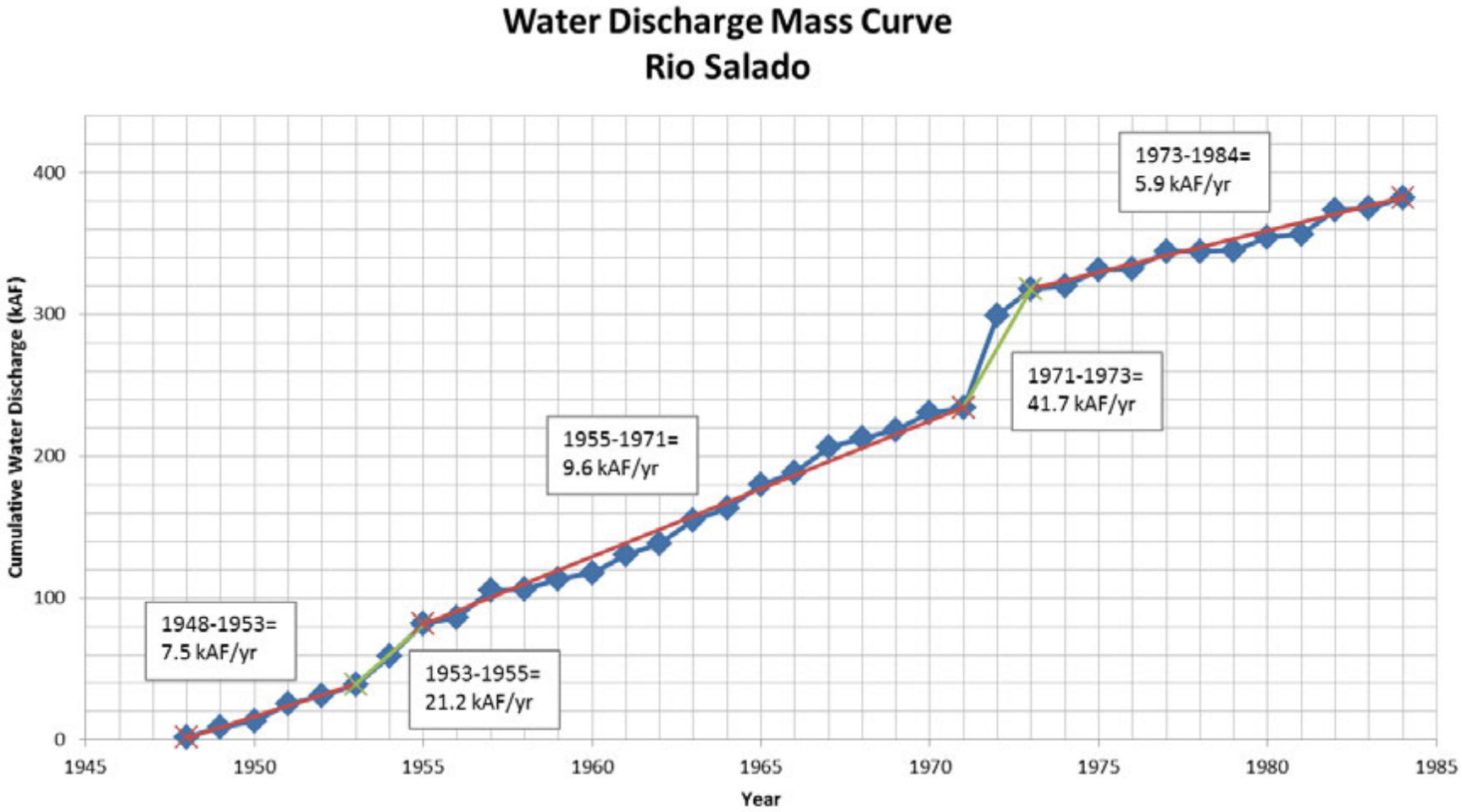

Figure 9: Water Discharge Mass Curve for the Rio Salado USGS gage near San Acacia: 1948 to 1984

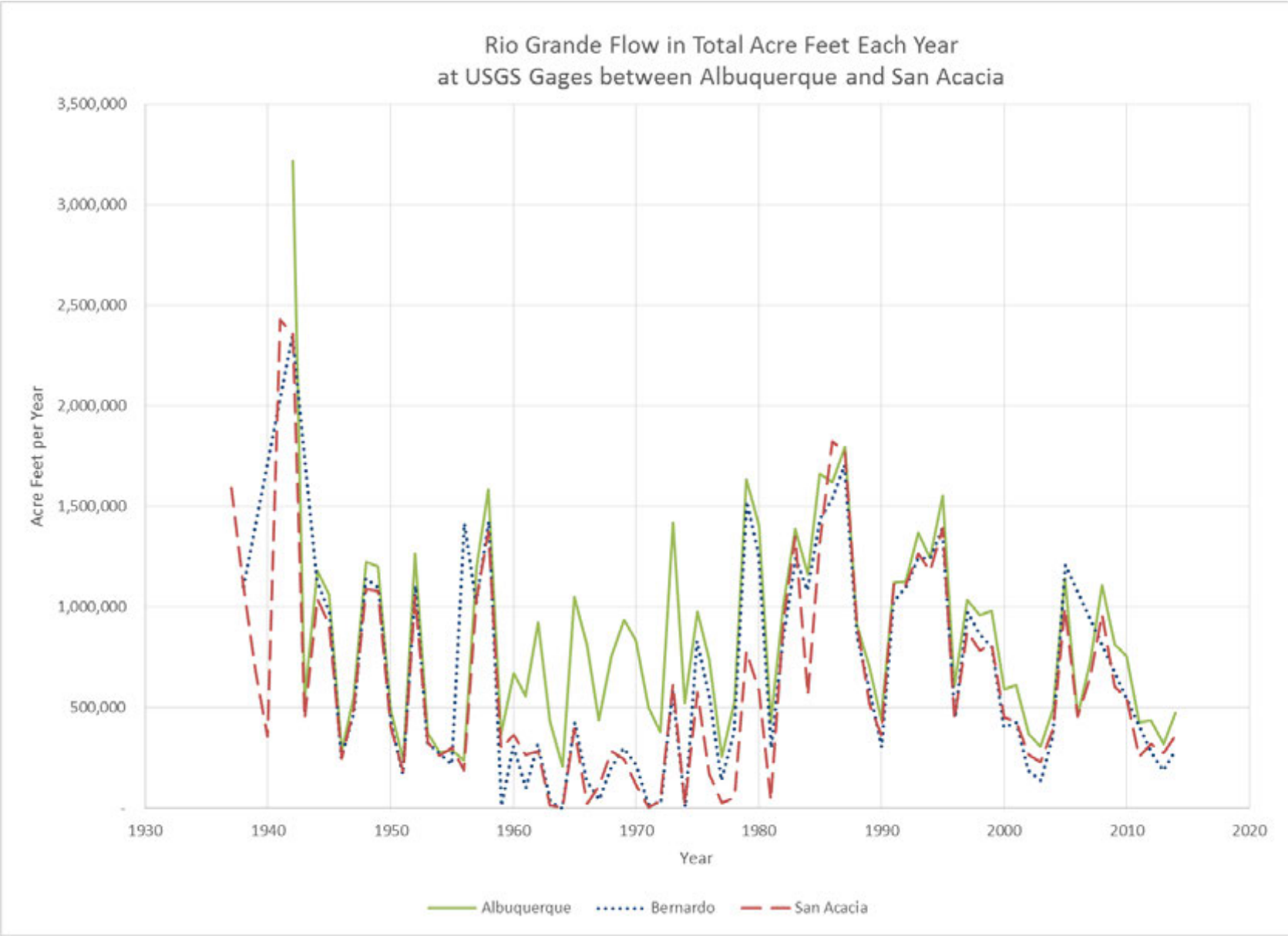

Figure 10: Total flow each year in acre feet between Albuquerque and San Acacia

3.1.1.2 Water Magnitude Plots

The following mean monthly discharge plots (herein referred to as water magnitude plots) graphically show the temporal variations in flow, both annually and seasonally of the Rio Grande and the Rio Puerco. The plots were made for the following gages on the Rio Grande: Albuquerque, Bernardo, and San Acacia. The Rio Puerco plot used the gage near Bernardo. The plots were created by using the monthly mean discharge values calculated by the USGS, which are based on the approved daily-mean discharge values. The data on each graph is displayed in calendar years, not water years. The reduction in mean monthly discharges on the Rio Grande since the 1940s is evident from these plots. For the Albuquerque, Bernardo, and San Acacia gages, the plots show the spring peaks in the back and the monsoonal peaks in the front, since the spring peaks are generally larger than the monsoonal peaks at these gages. However, for the Rio Puerco gage, the plot shows the monsoonal peaks at the back and the spring peak at the front, since the monsoonal peaks are generally larger than the spring peaks on this river.

Figure 11 shows the water magnitude plot for the Rio Grande in Albuquerque at the Central Avenue Bridge. The data from this plot comes from the USGS gage 08330000 “Rio Grande at Albuquerque, NM.”

Figure 12 shows the water magnitude discharge plot for the Rio Grande near Bernardo at the U.S. Highway 60 Bridge. The data for June 1937 through September 1958 comes from the USGS gage 08332000 “Rio Grande near Bernardo, NM.” The data from October 1958 through November 2014 comes from the USGS gage 08332010 “Rio Grande Floodway near Bernardo, NM.” Data is missing for water years 1939-1941, 1943, and1954. Other periods where no data was available include September 1956, and July 2005 through September 2011. These periods appear as zero values on the 3D graph.

Figure 13 shows the water magnitude discharge plot for the Rio Grande just downstream of the San Acacia Diversion Dam. The monthly data for May 1936 through the end of water year 1958 comes from the USGS gage 08355000 “Rio Grande at San Acacia, NM.” The data for water years 1958 through 2014 comes from USGS gage 08354900 “Rio Grande Floodway at San Acacia, NM.”

Figure 14 shows the water magnitude discharge plot for the Rio Puerco near Bernardo. The monthly data for this plot comes the USGS gage 08353000 “Rio Puerco near Bernardo, NM.”

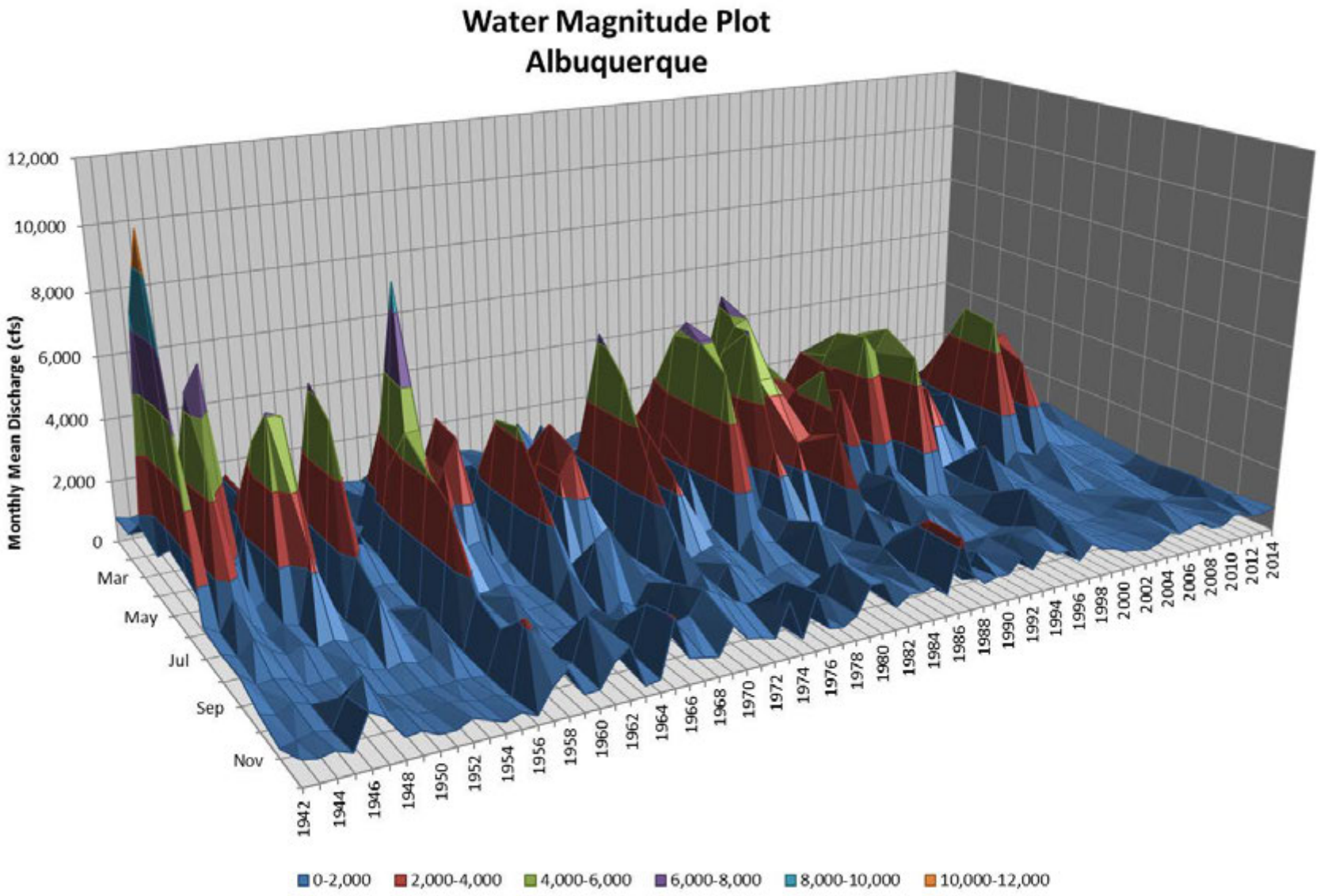

Figure 11: Water Magnitude Plot for the Rio Grande at Albuquerque: 1942 to 2014. Discharge values are the USGS reported mean monthly discharge values derived from the approved mean daily flows.

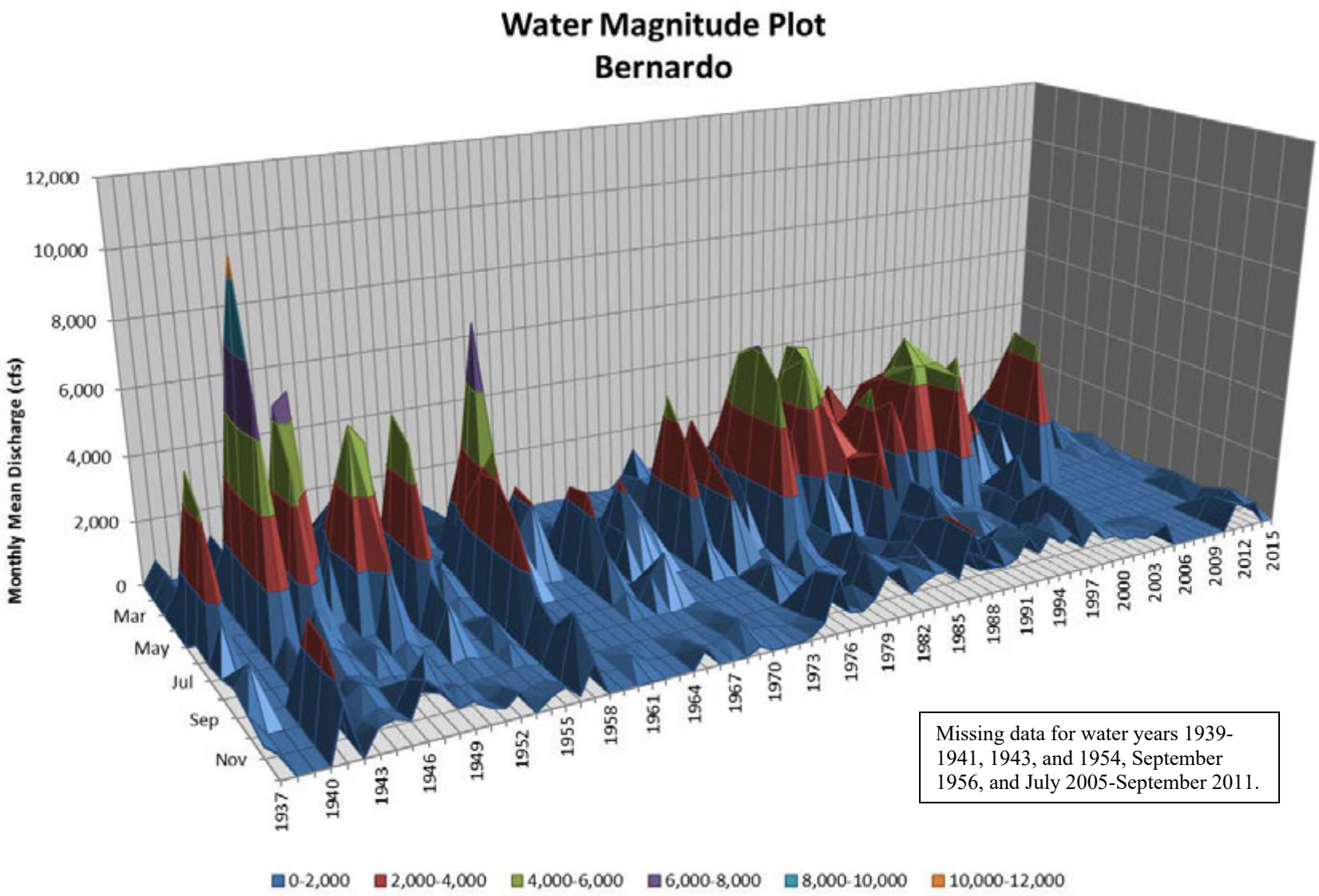

Figure 12: Water Magnitude Plot for the Rio Grande at Bernardo: 1937 to 2014. Discharge values are the USGS reported mean monthly discharge values derived from the approved mean daily flows.

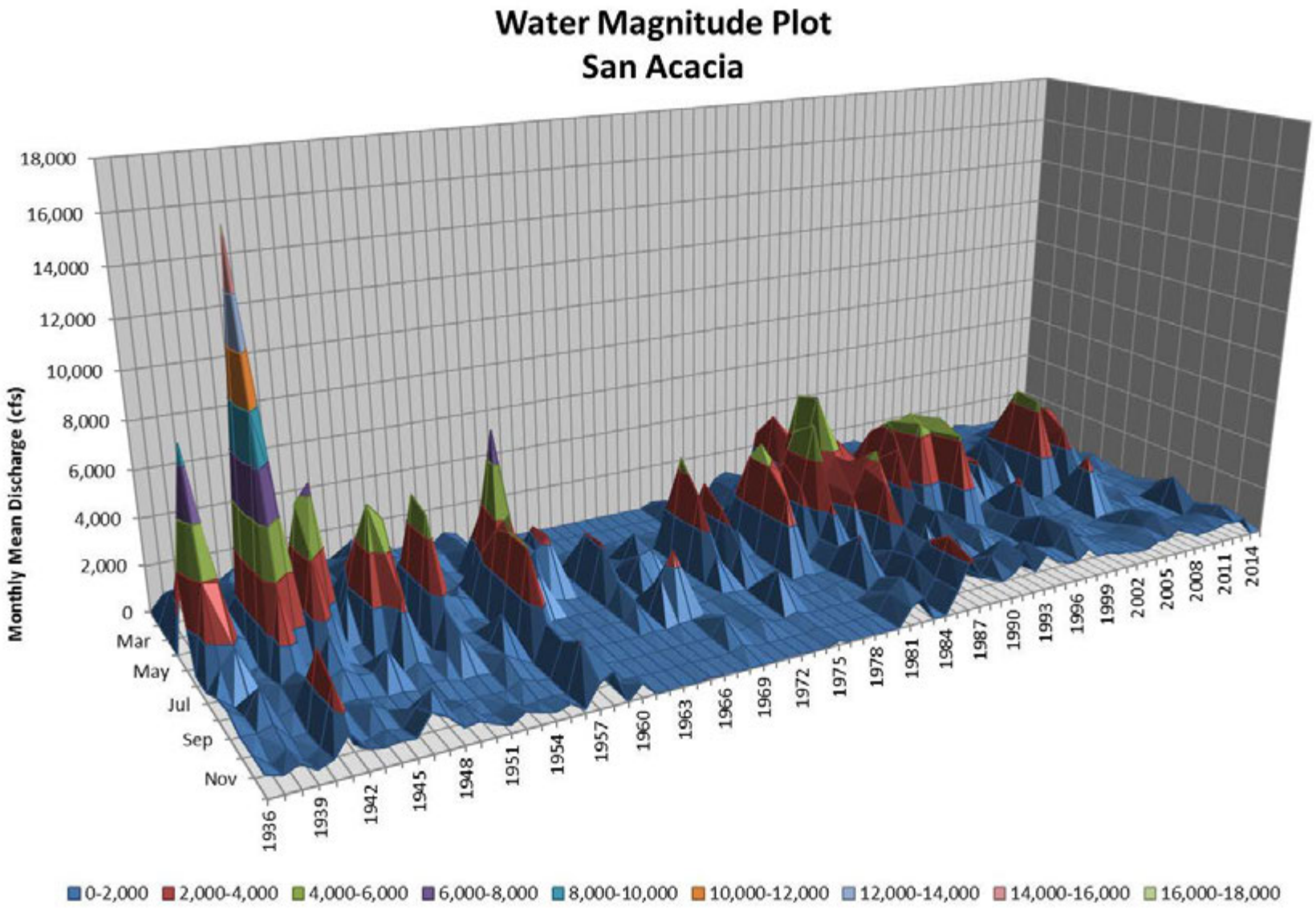

Figure 13: Water Magnitude Plot for the Rio Grande at San Acacia: 1936 to 2014. Discharge values are the USGS reported mean monthly discharge values derived from the approved mean daily flows.

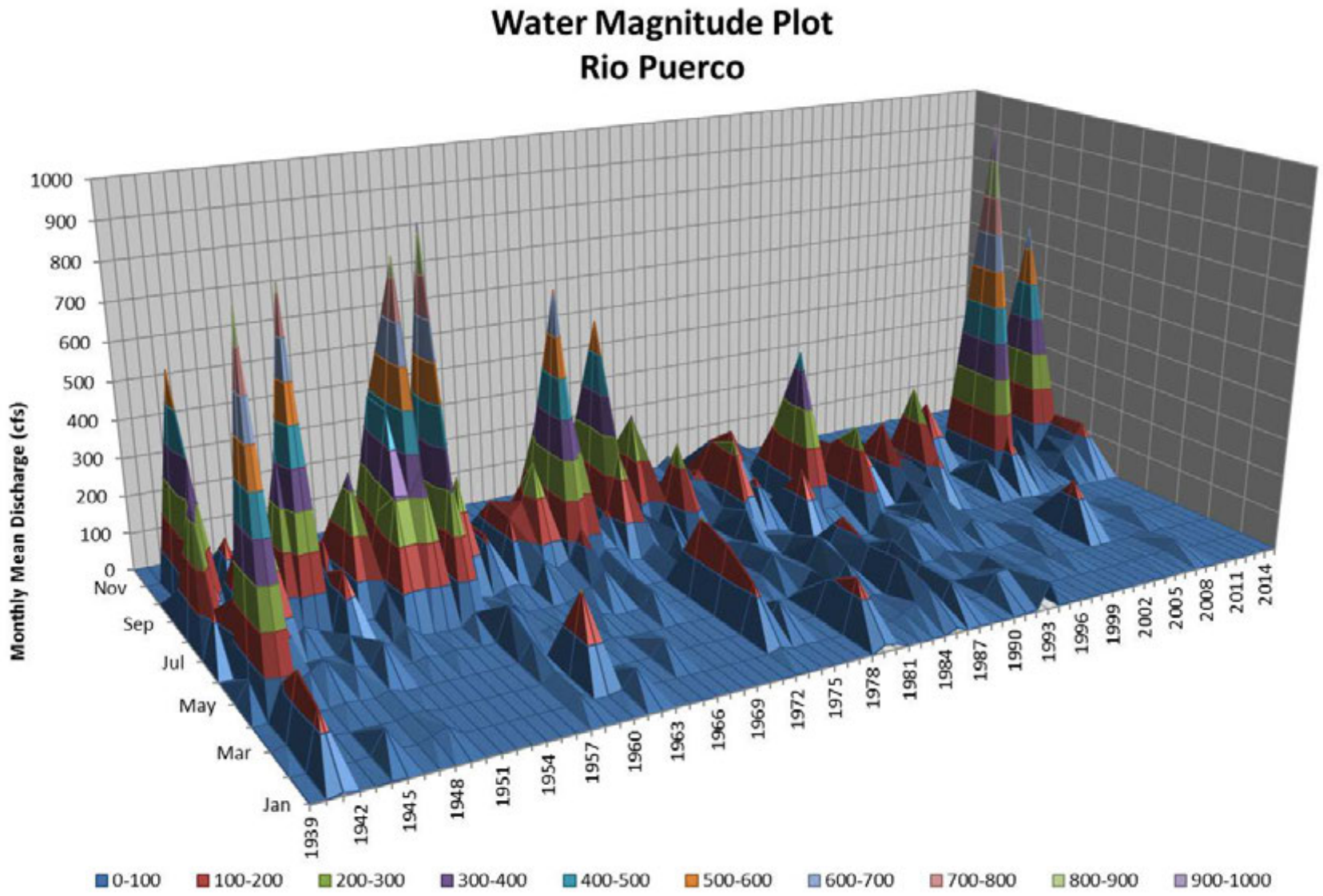

Figure 14: Water Magnitude Plot for the Rio Puerco: 1939 to 2014. Discharge values are the USGS reported mean monthly discharge values derived from the approved mean daily flows.

3.1.1.3 Groundwater Flows

Groundwater data has been collected and plotted with surface water data. These plots help identify the groundwater/surface water interactions and trends over time.

Groundwater data was obtained from a spreadsheet available on the Bosque Ecosystem Monitoring Program (BEMP) website along with a location map of the sites (Figure 15) (Bosque Ecosystem Monitoring Program, 2016). The sites, from upstream to downstream on the Rio Grande within the Isleta to San Acacia reach are Los Lunas, Reynolds Forest, Reynolds Cleared, Valencia Cleared, Belen, Valencia Forest, Crawford, and Sevilleta. The BEMP spreadsheet also provided corresponding USGS flow data for the Rio Grande, although the exact gage was not cited.

Figure 16 through Figure 23 show the groundwater/surface water interaction for each BEMP site. The figures include a trend line of average depth to the shallow groundwater aquifer. The trend lines reveal an increase in the depth to the ground water table over the last decade on the order of 0.5 to 1.5 feet. The slope of the trend lines also indicate that certain sites (Los Lunas, Reynolds Forest, Crawford and Sevilleta) show a rate of increase in the depth to groundwater almost twice that of the other sites. For the period of record (most are over a decade) the shallow groundwater averages between 3 to 5 feet beneath the ground surface, which is a similar range found by Parametrix (2008). Anecdotal accounts of the Middle Rio Grande valley from the late 1880s (waterlogged) and early 1910s (depth of around 2 feet) indicate that the trend of increasing depth to groundwater has been occurring for some time (Berry and Lewis, 1997). Currently the groundwater levels at the BEMP sites between Isleta and San Acacia Diversion Dams ranges from 0.5 feet to 8 feet.

Figure 24, Figure 25, and Figure 26 compare all the sites on one graph for water years 2005, 2008, and 2011, respectively. Examining the sites on a single year basis reveals more than is easily noticeable on a multi-year scale. These graphs show that most sites are similar to each other in that they are influenced by the river. Since most of the BEMP groundwater wells are within the shallow floodplain aquifer a strong correlation with the river discharge is suggested, rising and fallings at about the same rate as the Rio Grande. An assessment of the channel and floodway topography between the mid-1990s and mid-2010s (see section 4.6) indicates that in some areas (between Los Lunas and Casa Colorado) the river has incised on the same order of magnitude as the observed drop in groundwater between the early 2000s and mid-2010s, suggesting that drops in the groundwater may be a response to morphological changes on the Rio Grande. But there are other areas (Isleta Diversion Dam to Los Lunas and Casa Colorado to just upstream of San Acacia Diversion Dam) where the river has aggraded the same order of magnitude, indicating that there are other confounding issues besides river morphological changes that are influencing changes in the groundwater levels. These may include aquifer responses to low water years, groundwater pumping, increased vegetation growth, etc.

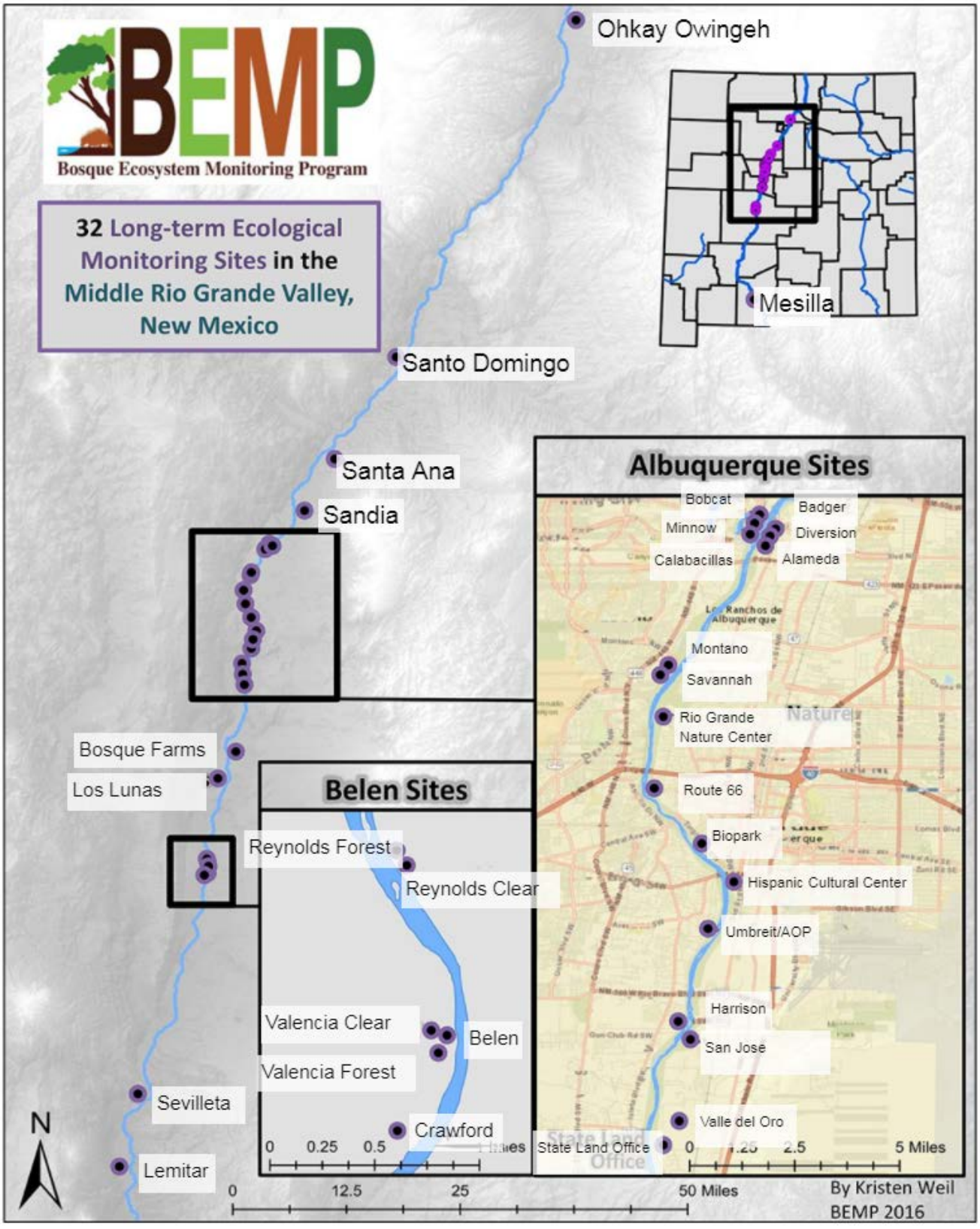

Figure 15: Location of the BEMP data collection sites (Bosque Ecosystem Monitoring Program, 2016)

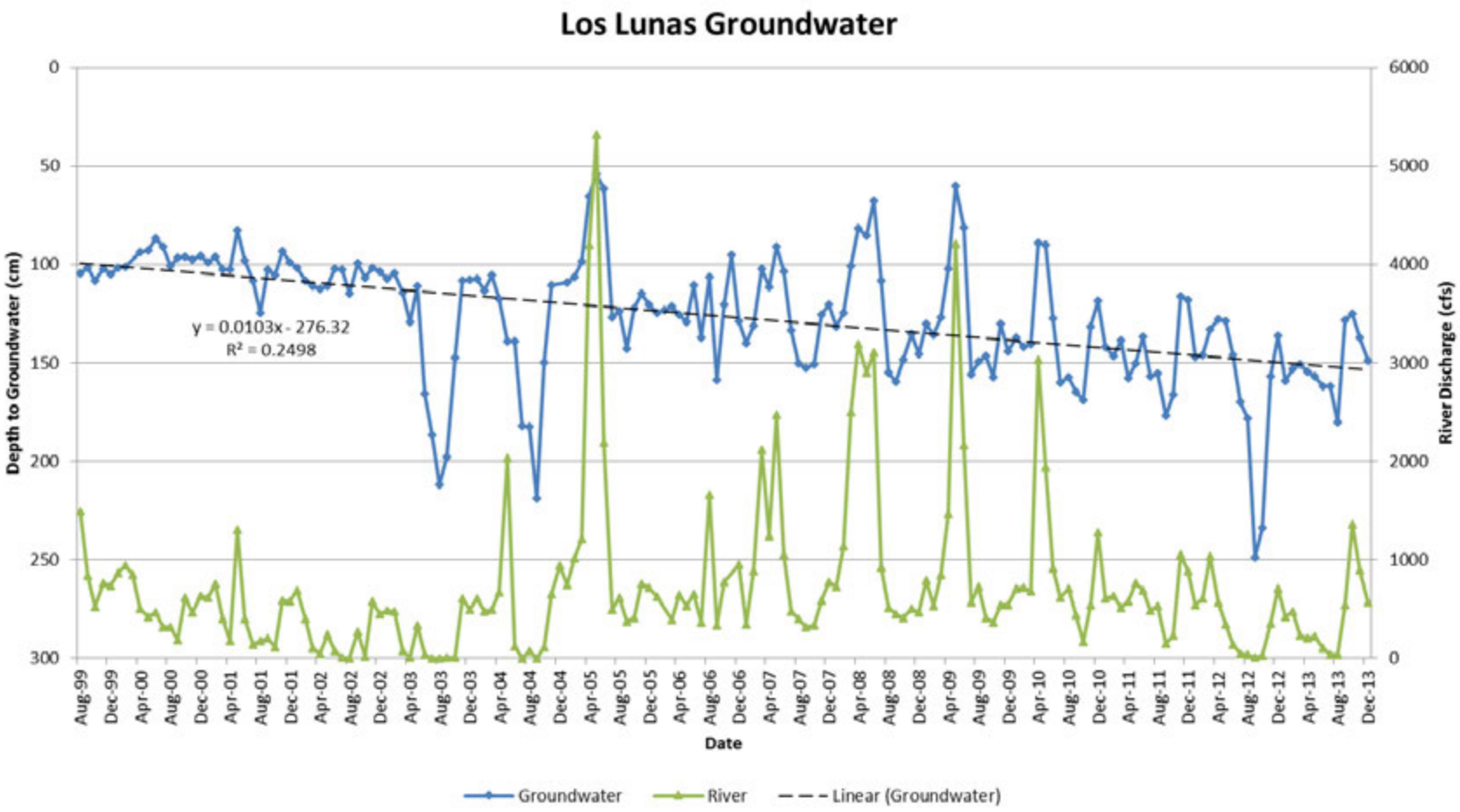

Figure 16: Depth to groundwater at Los Lunas BEMP site compared to flow in the Rio Grande as recorded on BEMP's website

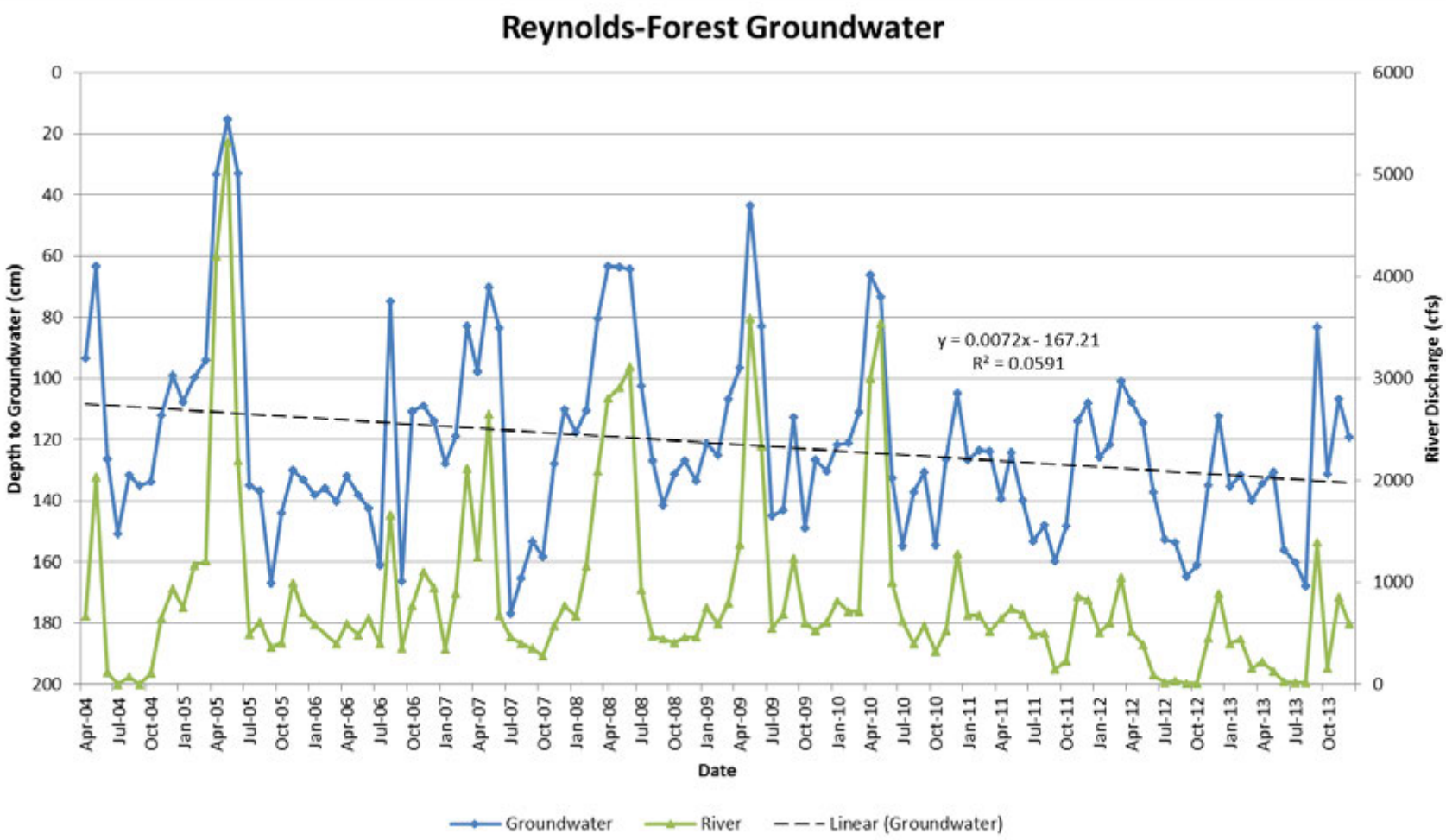

Figure 17: Depth to groundwater at Reynolds Forest BEMP site compared to flow in the Rio Grande as recorded on BEMP's website

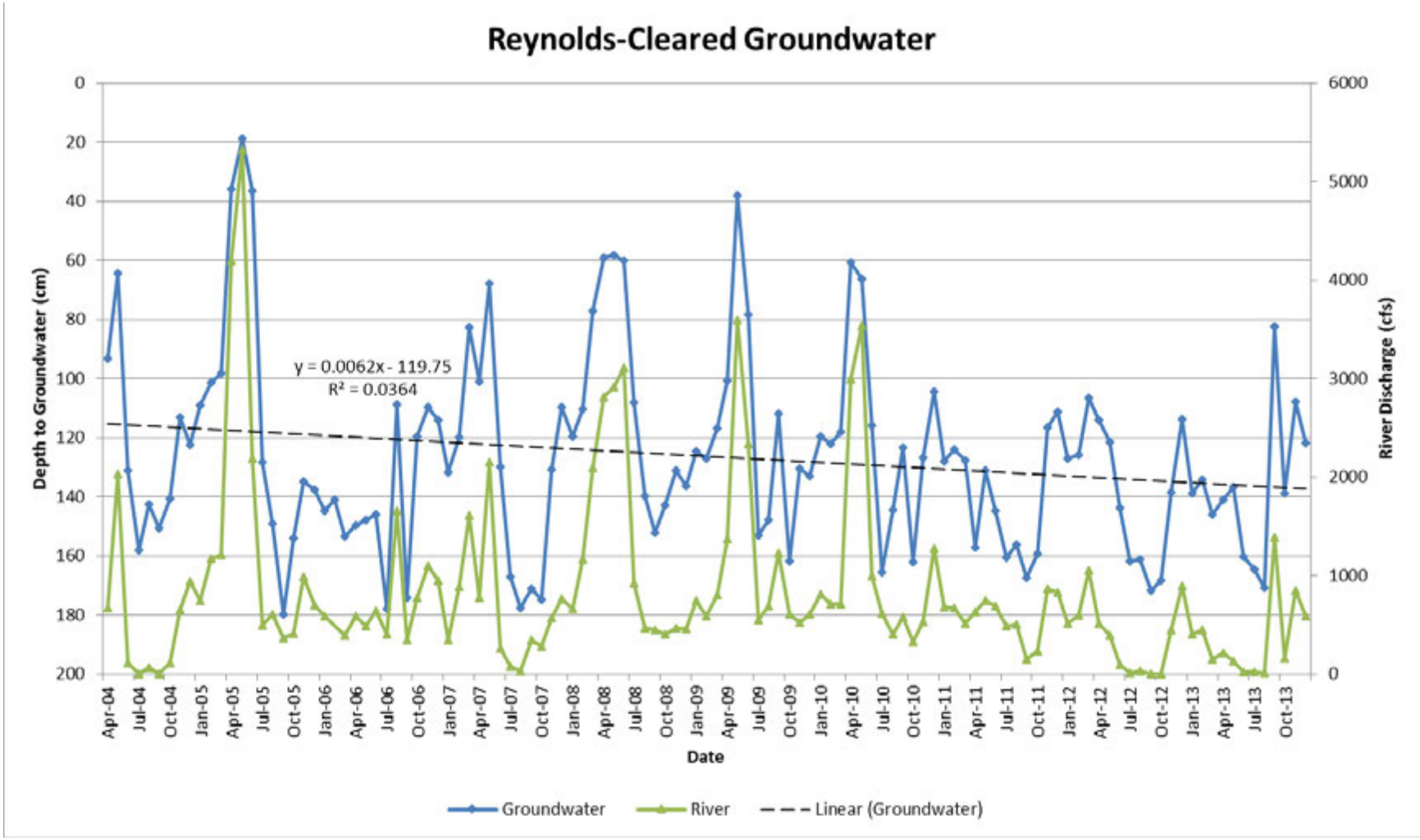

Figure 18: Depth to groundwater at Reynolds Cleared BEMP site compared to flow in the Rio Grande as recorded on BEMP's website

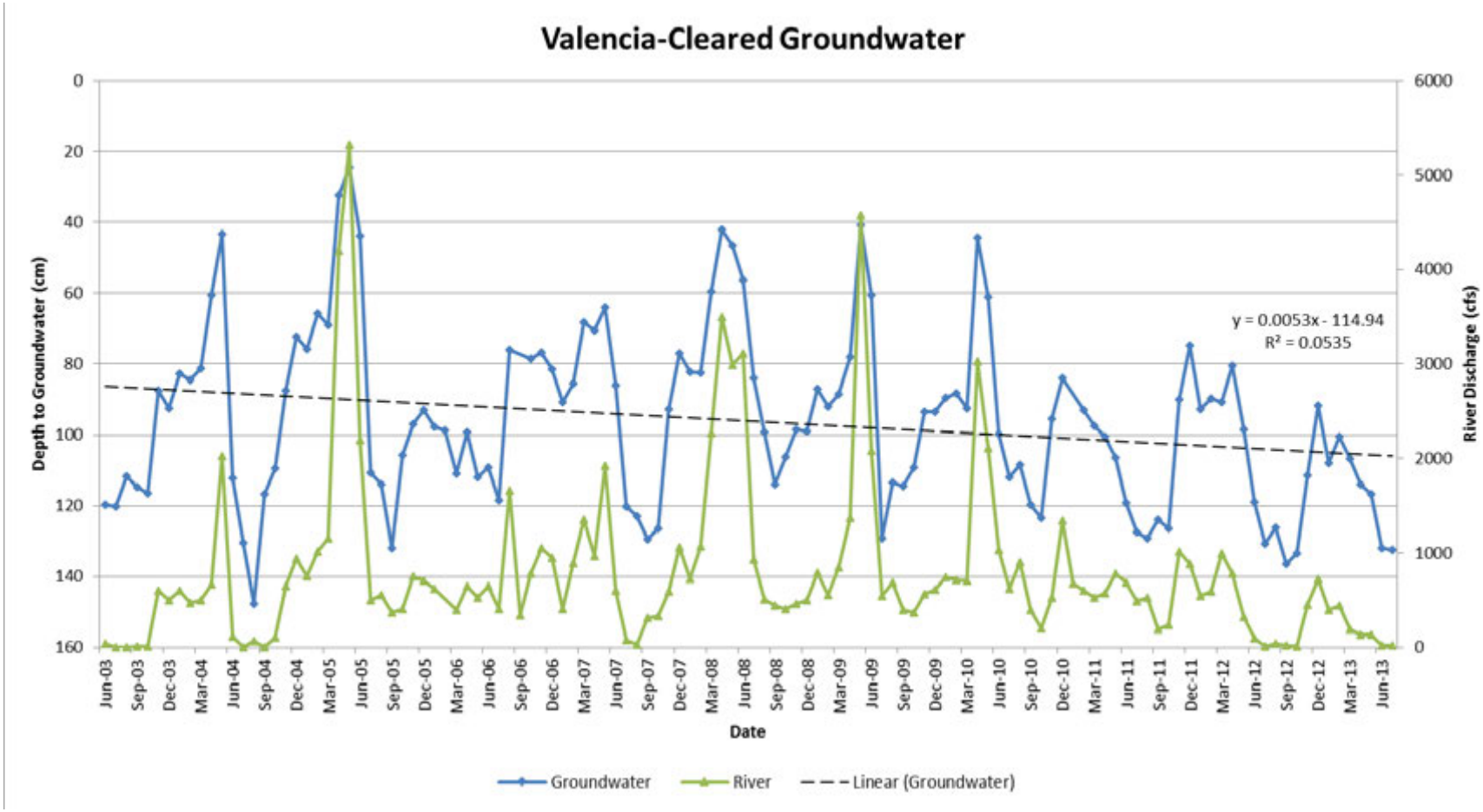

Figure 19: Depth to groundwater at Valencia Cleared BEMP site compared to flow in the Rio Grande as recorded on BEMP's website

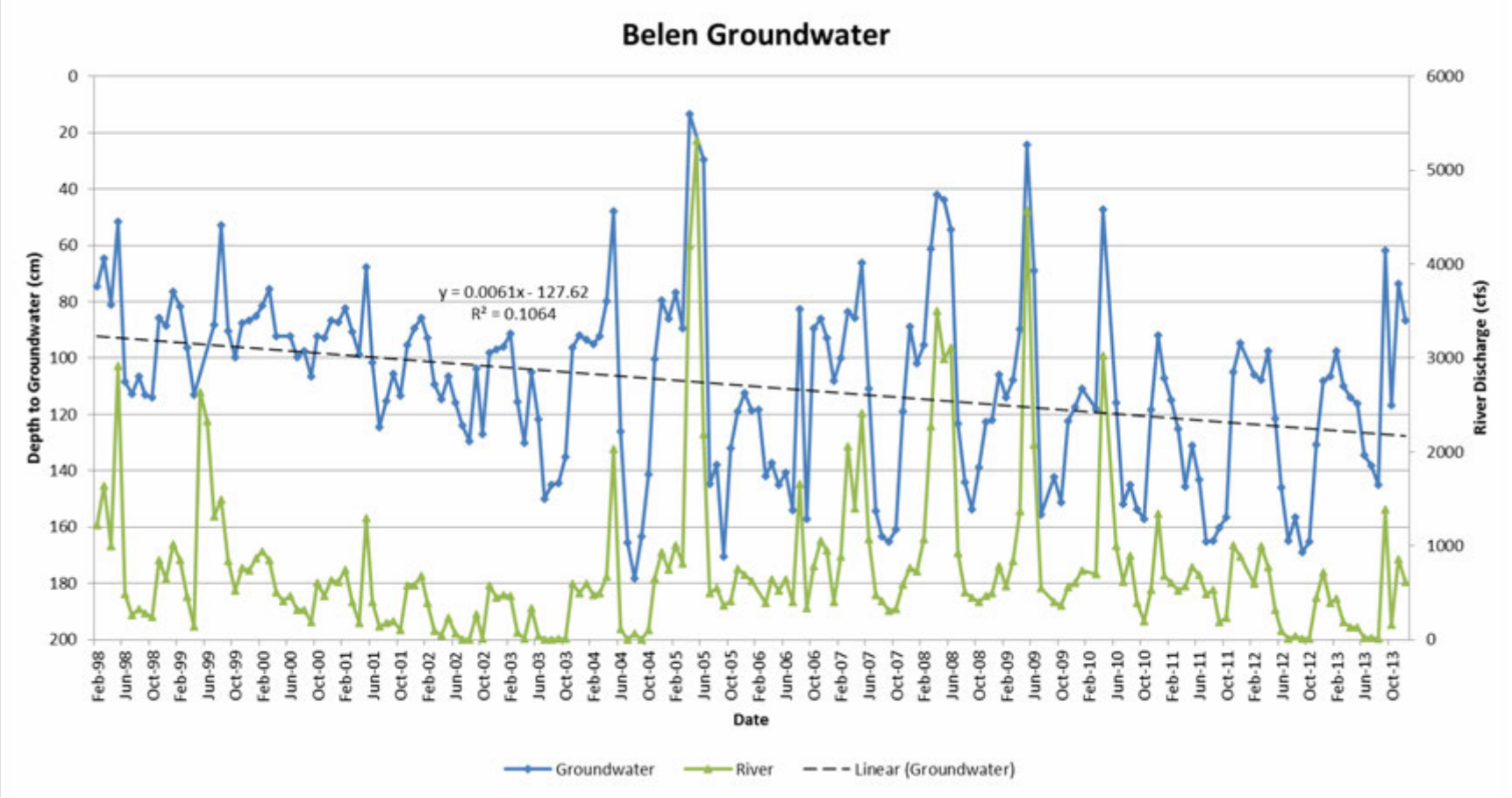

Figure 20: Depth to groundwater at Belen BEMP site compared to flow in the Rio Grande as recorded on BEMP's website

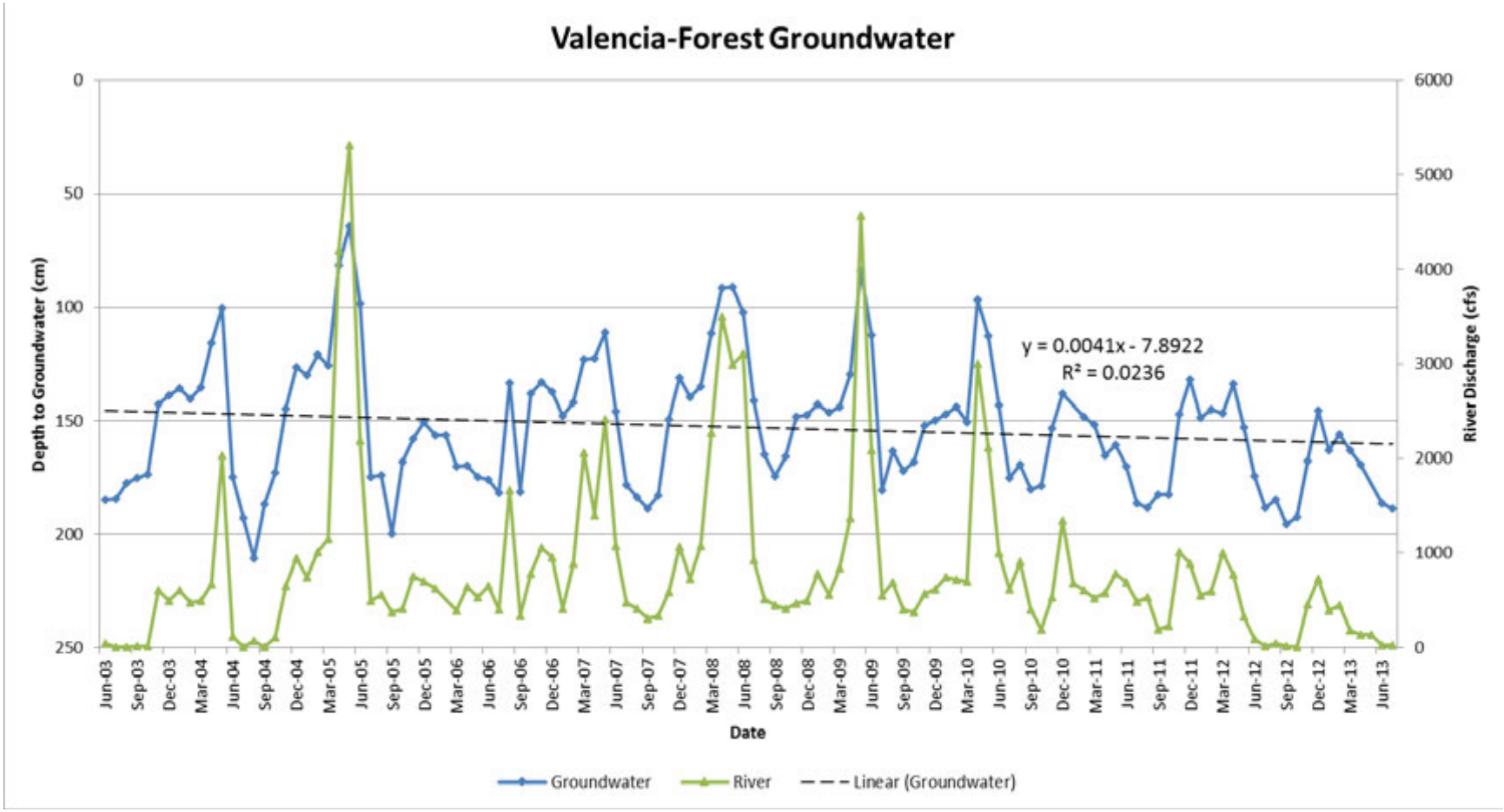

Figure 21: Depth to groundwater at Valencia Forest BEMP site compared to flow in the Rio Grande as recorded on BEMP's website

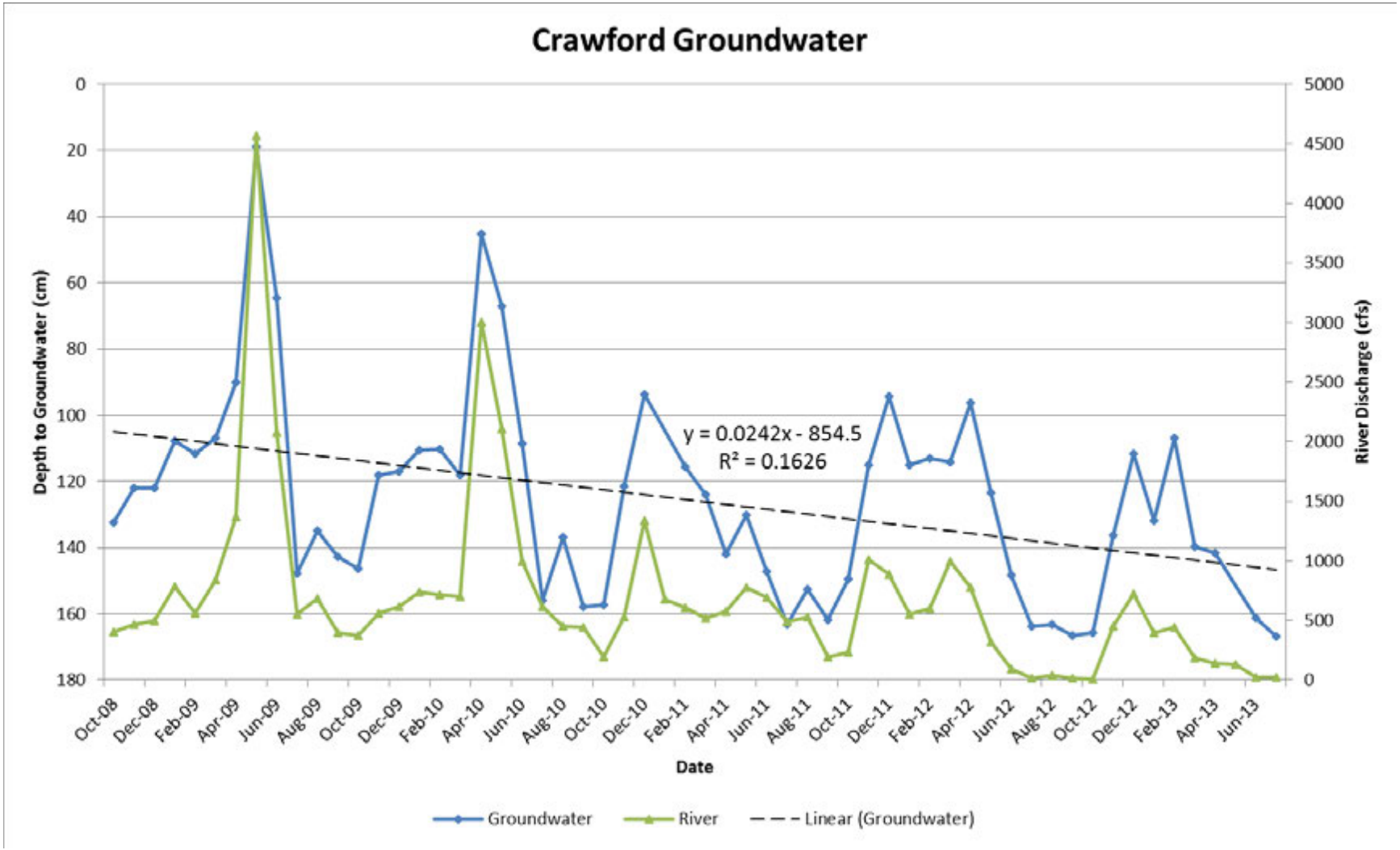

Figure 22: Depth to groundwater at Crawford BEMP site compared to flow in the Rio Grande as recorded on BEMP's website

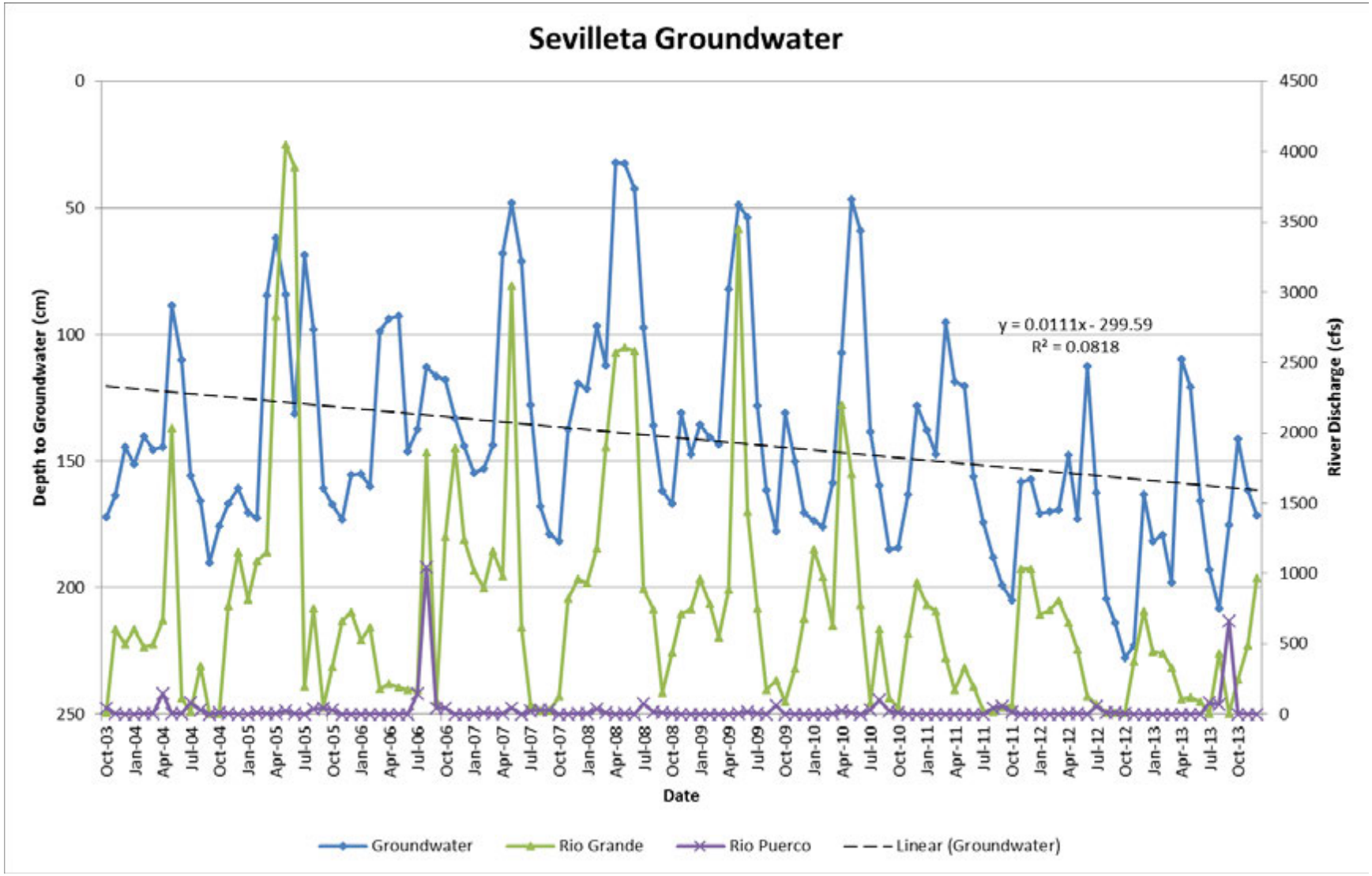

Figure 23: Depth to groundwater at Sevilleta BEMP site compared to flow in the Rio Grande as recorded on BEMP's website and the Rio Puerco (USGS 08353000 RIO PUERCO NEAR BERNARDO, NM)

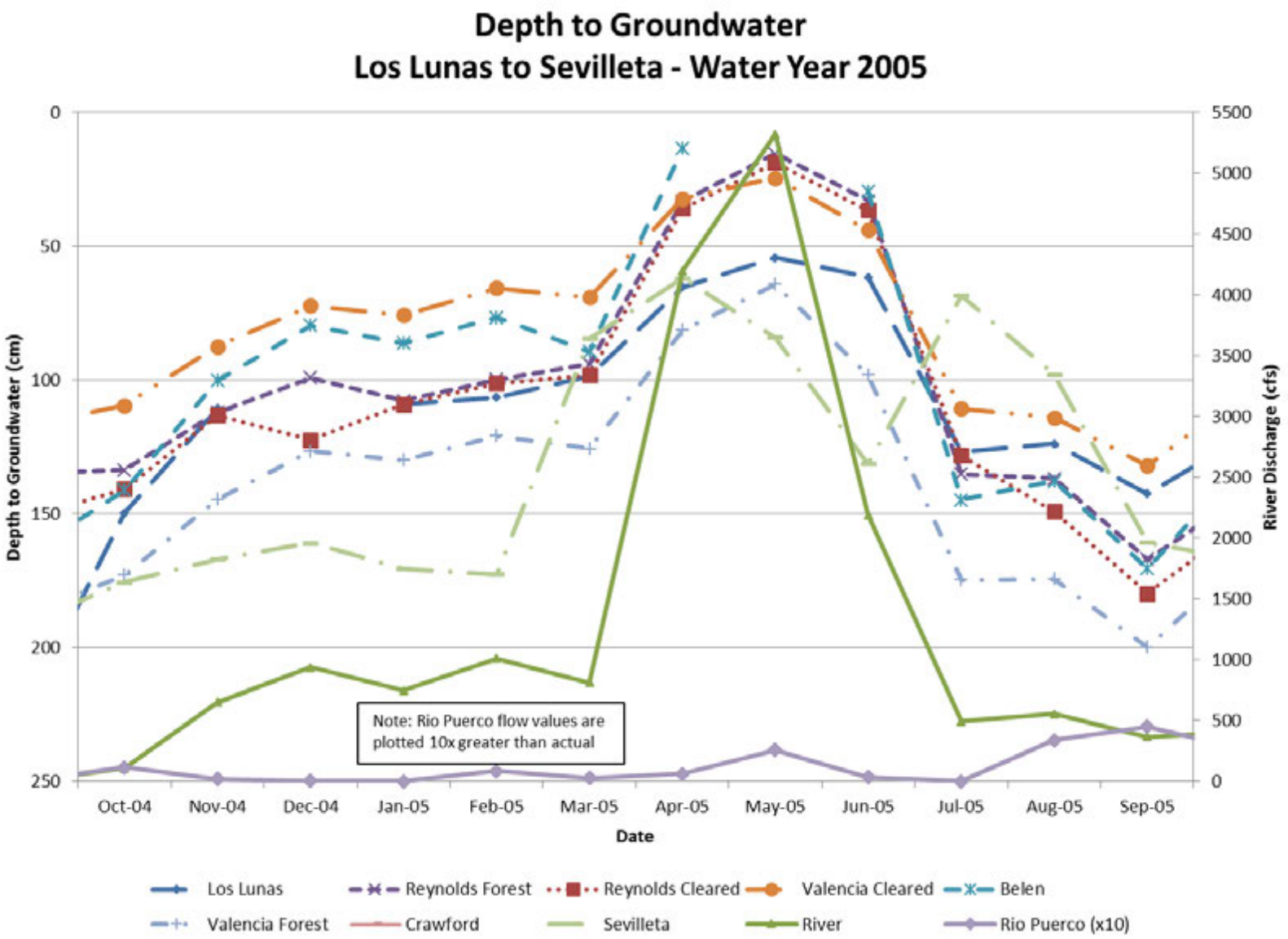

Figure 24: Depth to groundwater at BEMP sites Los Lunas to Sevilleta compared to flow in the Rio Grande as recorded on BEMP's website and the Rio Puerco (USGS 08353000 RIO PUERCO NEAR BERNARDO, NM) for water year 2005

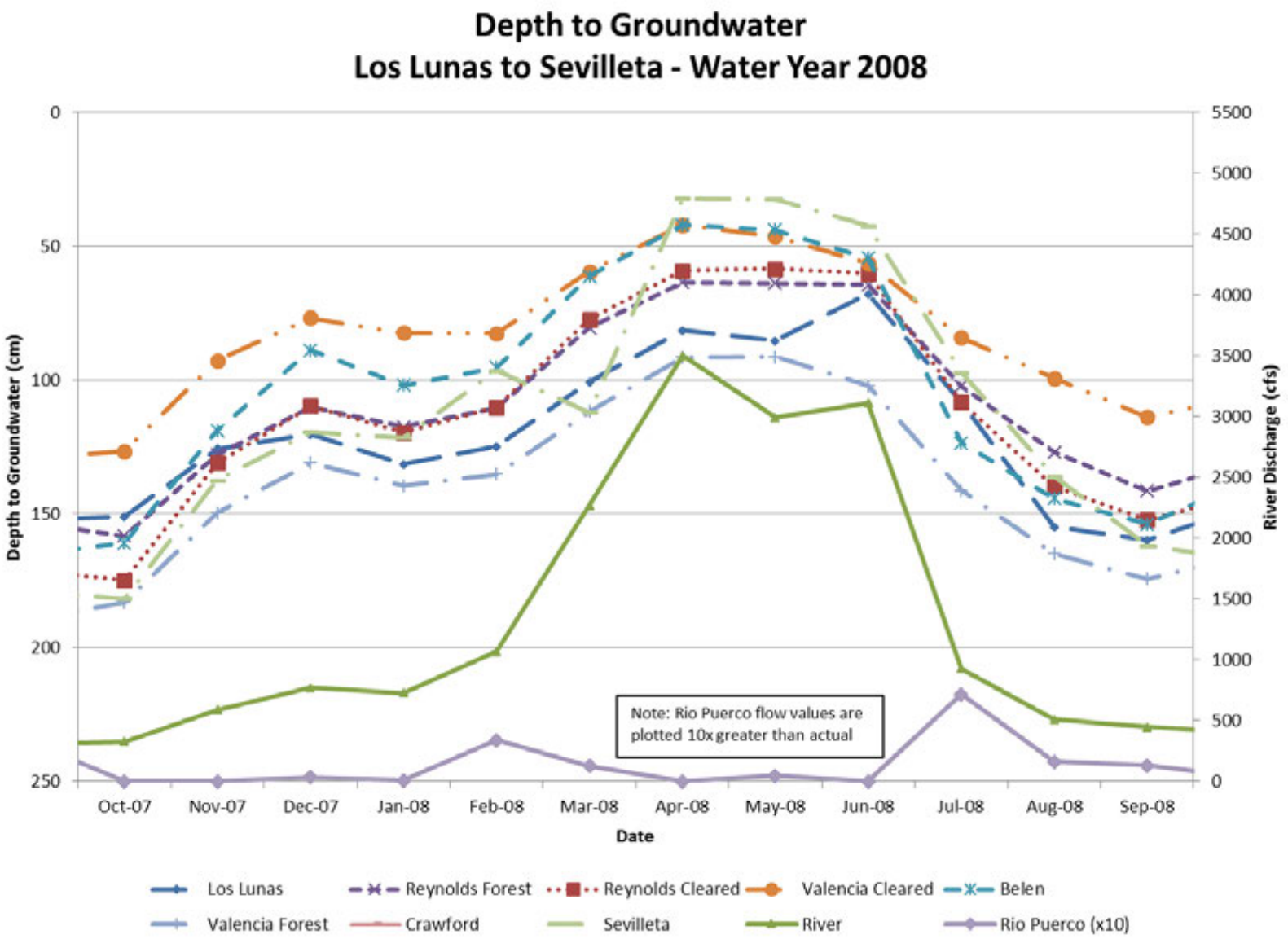

Figure 25: Depth to groundwater at BEMP sites Los Lunas to Sevilleta compared to flow in the Rio Grande as recorded on BEMP's website and the Rio Puerco (USGS 08353000 RIO PUERCO NEAR BERNARDO, NM) for water year 2008

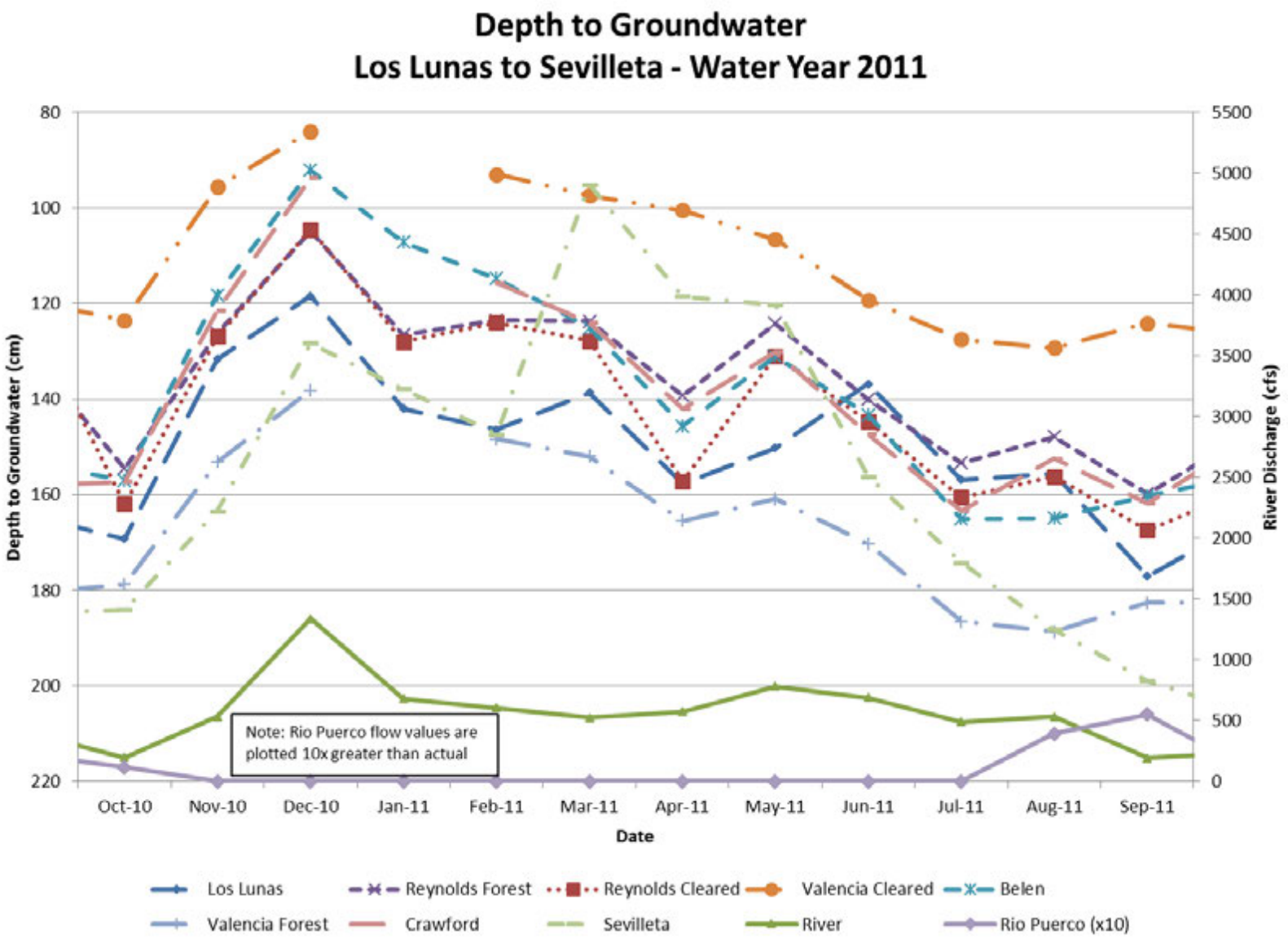

Figure 26: Depth to groundwater at BEMP sites Los Lunas to Sevilleta compared to flow in the Rio Grande as recorded on BEMP's website and the Rio Puerco (USGS 08353000 RIO PUERCO NEAR BERNARDO, NM) for water year 2011

Figure 27 shows the minimum, maximum, and mean depths to groundwater for the entire time period available for each site. For all of the sites the groundwater depths fluctuate throughout the period of record with a mean depth to groundwater between 100 and 160 cm (around 3 to 5 feet).

Figure 28 shows by year the minimum, maximum, and average depth for all sites. While there is a considerable amount of fluctuations in the observed groundwater levels there does appear to be a trend towards increased depth to groundwater. This trend though may be influenced by the drier years in the early 2010s which was the closing date range for this analysis.

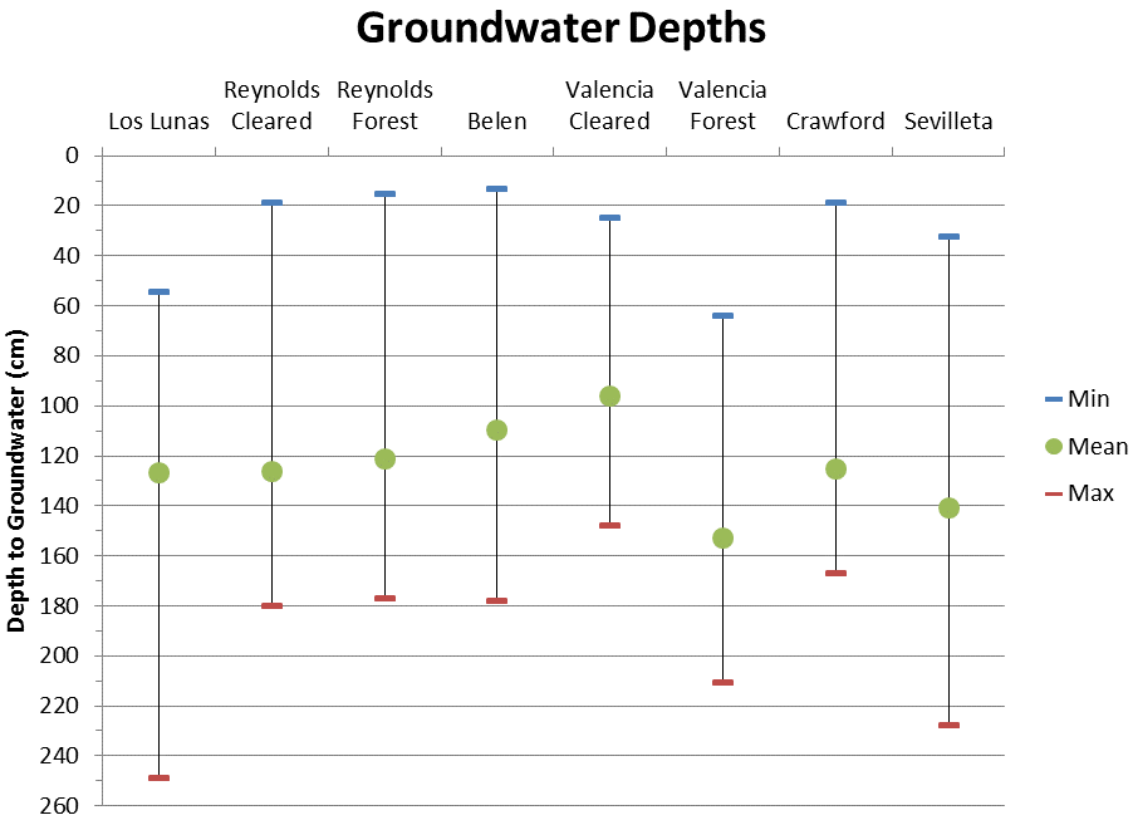

Figure 27: Minimum, Maximum, and Mean depths to groundwater for Los Lunas to Sevilleta for the period of record

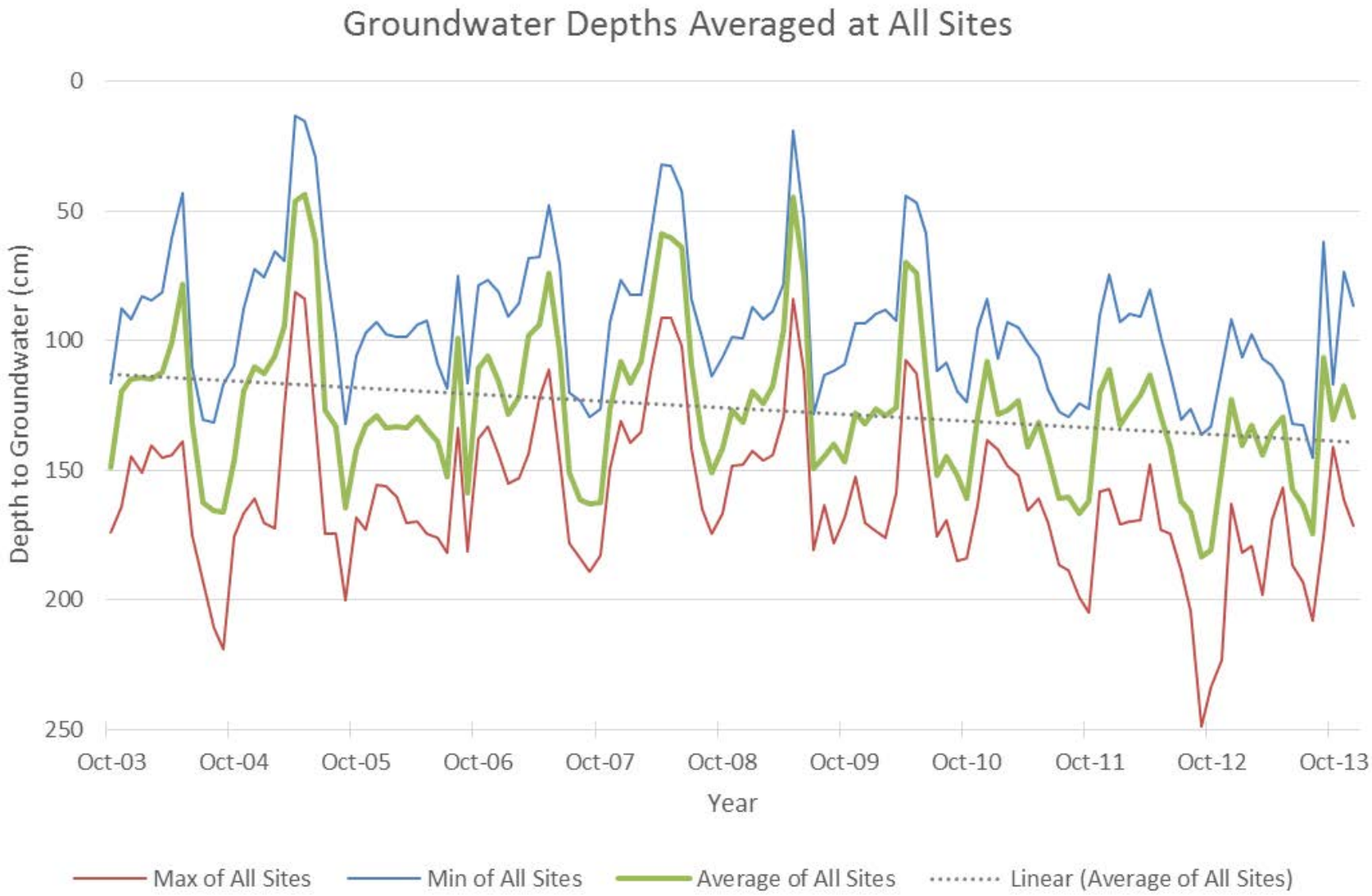

Figure 28: Depth to Groundwater - Minimum, Maximum, and All Sites Average

3.1.1.4 Precipitation Data

Precipitation data has been collected and plotted with surface water data for the following locations, from upstream to downstream: Los Lunas, Reynolds Forest, Reynolds Cleared, Valencia Cleared, Belen, Valencia Forest, Crawford, and Sevilleta. The data for each site is monthly and is available as "canopy precipitation" and "open precipitation." The precipitation data was obtained from a spreadsheet available on the Bosque Ecosystem Monitoring Program (BEMP) website (Bosque Ecosystem Monitoring Program, 2013). These plots provide a variety of information including how precipitation varies from site to site, how it varies from open areas to areas under the canopy, and which months generally have the most precipitation.

Figure 29 shows the annual mean precipitation for each site. These values represent the average of the monthly Open Precipitation and Canopy Precipitation data, and the data is averaged over each water year (October 1 through September 30). It should be noted that the BEMP data set frequently has missing data, although it is less than five percent of the time (Eichorst et al., 2012). Thus for items such as annual precipitation where precipitation is summed, the actual value is likely higher.

Precipitation data from the BEMP sites indicates an annual range between 50 to 290 mm (2 to 11 inches). The average annual rainfall of all sites is typically between 140 and 200 mm (6 and 8 inches). Similar precipitation trends have been found in historical studies of the Middle Rio Grande valley through this reach (Nordin, 1963; Eichorst et al., 2004; Parametrix, 2008; Eichorst et al., 2012). While rainfall-runoff events have an effect on the streamflow, there is less correlation between specific rain events and the groundwater fluctuation than the river discharge and the groundwater fluctuation. The data does show that while precipitation events have occurred at various times during the year, typically the higher events occur during the fall, coinciding with the monsoon season. This indicates a minimal water volume added from the adjacent landscape during the spring snow-melt runoff. It also suggests that rainfall-runoff events in the adjacent landscape during the monsoonal season can have an appreciable effect on the river's discharge.

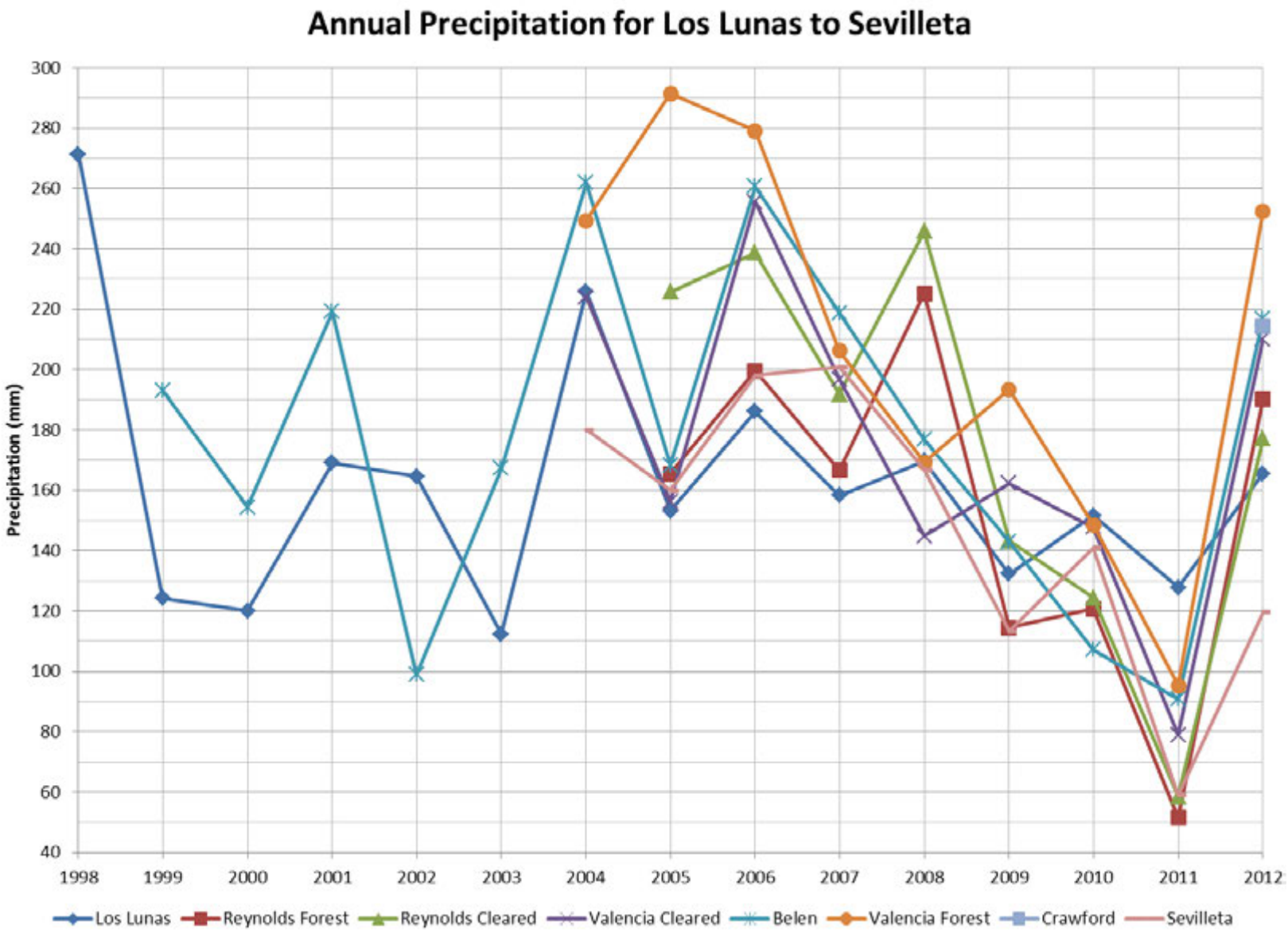

Figure 29: Annual Precipitation for Los Lunas to Sevilleta

Table 1 shows the average annual precipitation for each site for the available time period. The site with the longest time period is Los Lunas (1998-2012) and the site with the shortest time period is Crawford (2012 only).

Table 1: Average Annual Precipitation for Los Lunas to Sevilleta

Site	Average Annual Precipitation (mm)	Average Annual Precipitation (inches)
Los Lunas	160	6
Reynolds Forest	150	6
Reynolds Cleared	180	7
Valencia Cleared	180	7
Belen	180	7
Valencia Forest	210	8
Crawford	210	8
Sevilleta	150	6

Figure 30 shows the total annual canopy precipitation and total annual open precipitation for 2005-2012 for each of the sites except Crawford, since Crawford only has data for 2012. The period 2005-2012 was chosen since each of the sites' data encompasses at least those years. The forest sites are simply the untouched sites adjacent to their counterpart "cleared" sites that have been mechanically cleared. Reynolds and Valencia were both cleared in 2003 (Eichorst et al., 2012). At the Reynolds Forest site, the precipitation is lower than at the Reynolds Cleared site. This suggests a higher interception ratio where vegetation is established. However, this isn't always the case. At the Valencia Forest site, the precipitation is higher than at the Valencia Cleared site.

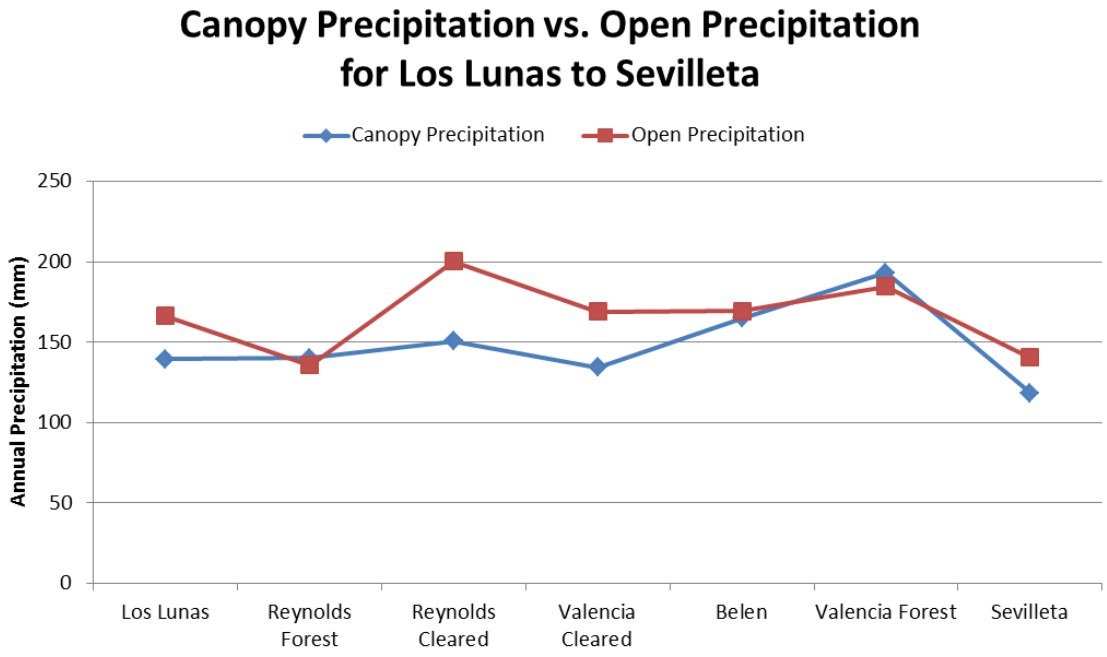

Figure 30: Canopy precipitation and open precipitation for Los Lunas to Sevilleta except Crawford

Figure 31 shows an average of each of the sites' monthly precipitation. In 2003 there were only a few sites with data available, but by 2012 all the sites had data. The figure also identifies the month of the highest six peaks on the graph. Three of the six highest peaks occurred in August, and five of the six peaks occurred in the second half of the year.

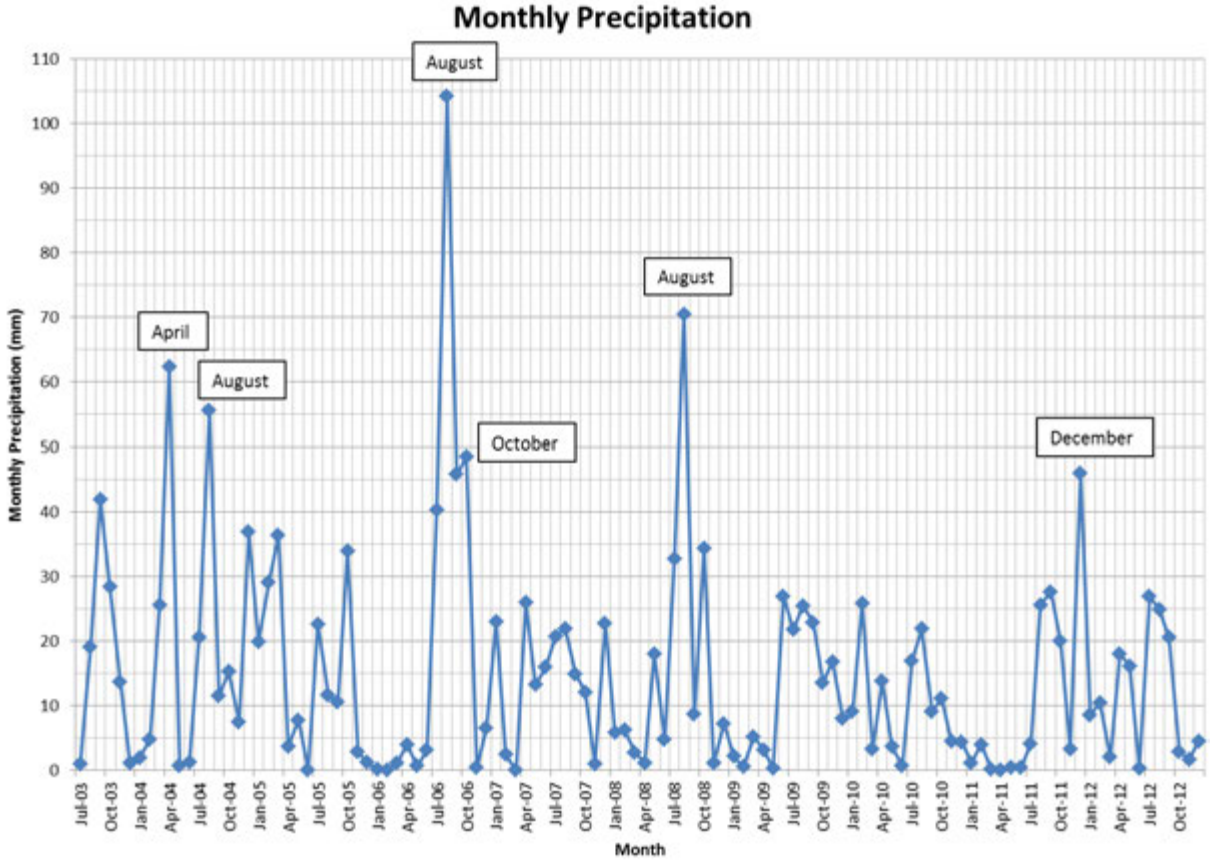

Figure 31: Monthly precipitation for Los Lunas to Sevilleta

Figure 32 and Figure 33 compare precipitation data, groundwater data, and river flows for Los Lunas to Sevilleta for two periods of time. The precipitation data and groundwater data are an average of all these sites.

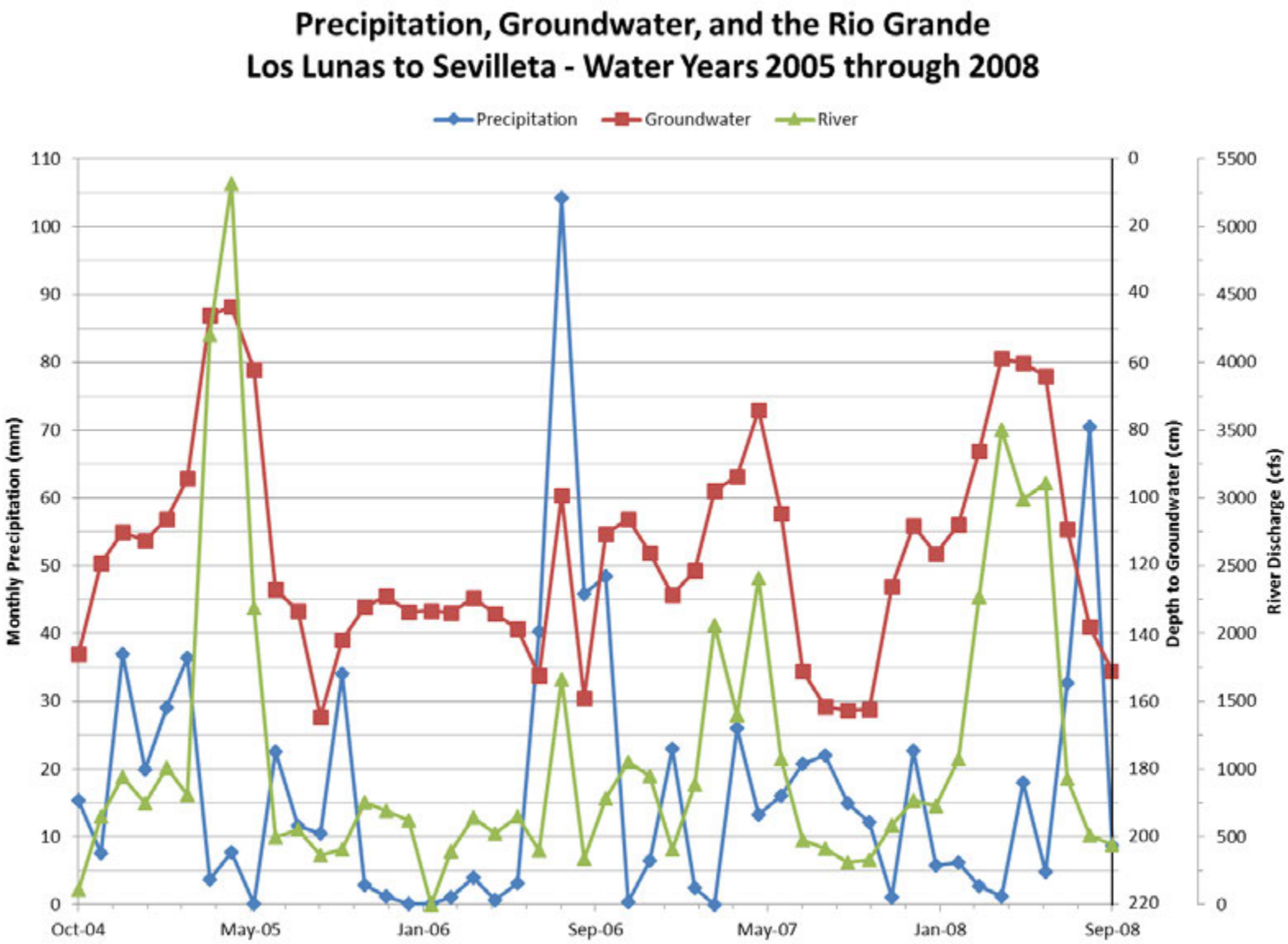

Figure 32: A comparison of precipitation, groundwater, and the Rio Grande as recorded on BEMP's website for Los Lunas to Sevilleta sites, water years 2005 through 2008

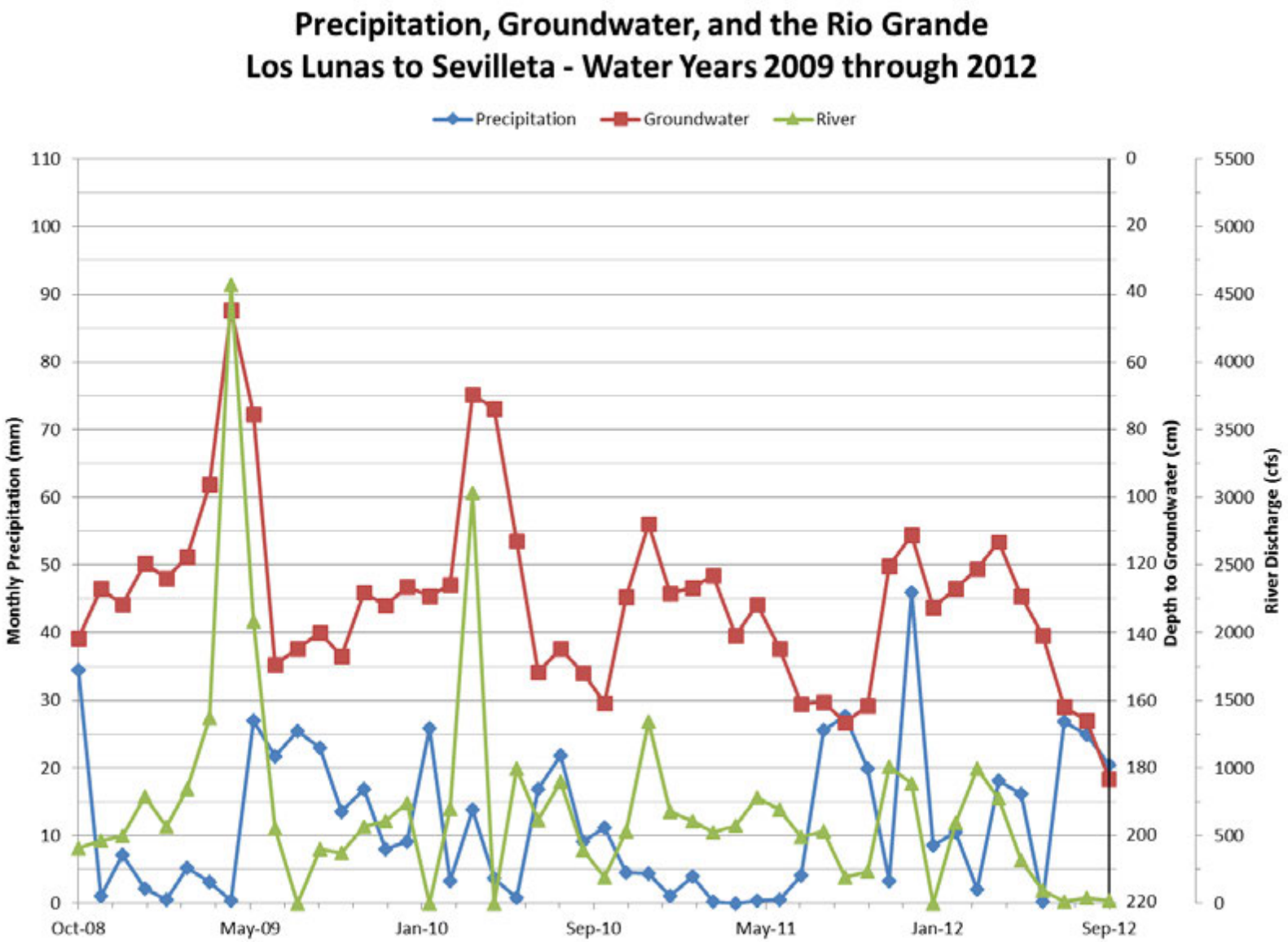

Figure 33: A comparison of precipitation, groundwater, and the Rio Grande as recorded on BEMP's website for Los Lunas to Sevilleta sites, water years 2009 through 2012

3.1.2 Frequency

Flood frequency indicates the magnitude and frequency of discharge events that happen between specific time periods. Flow frequency/flow duration analyses for the study area can be summarized from four reports: Harris and AuBuchon (2016), Bui (2014), Wright (2010), and MEI (2002). MEI and Wright extracted the annual peak flow from available USGS gage data to estimate return period flow. All three assumed a log Pearson Type III probability distribution. Wright used the same analysis approach and combined potential flows from tributary inputs with flows on the Rio Grande to develop flood frequencies that represented a maximum potential flow condition. MEI (2002) produced flow duration curves for Albuquerque, Bernardo, and San Acacia within their study period, but a return period analysis was only conducted for the Albuquerque gaging station. Harris and AuBuchon (2016), Bui (2014), and MEI (2002), performed statistical analyses based on the historical USGS gage observations of mean daily flows, resulting in a percent exceedance for the period of analysis. MEI (2002) also analyzed the Bernardo and San Acacia gages pre and post LFCC diversion cessation, which occurred around 1985. Bui's work provides probabilities and potential return intervals for particular discharges, but her original analysis was intended to help characterize seasonal flow regimes within a year, corresponding to the life cycle of the Silvery Minnow. Bui (2014) does not fit a probability distribution. Table 2 provides the various analyses periods for each of the sources cited in this review.

Table 2. Analysis period for USGS gaging stations for flood frequency analysis.

Citation Source	**Albuquerque***	**Bernardo****	**San Acacia*****
MEI (2002)	1974-1999	1974-1999	1974-1999
Wright (2010)	1936-2008	1936-2008	1936-2008
Bui (2014)	1993-2013	1993-2013	1993-2013
Harris and AuBuchon (2016)	--	--	1993-2013

Notes: * – Albuquerque and Bernalillo USGS gage stations 08330000 and 08329500, respectively
** – Bernardo USGS gage stations 08332000 and 08332010
*** – San Acacia USGS gage stations 08355000 and 08354900

For this analysis three of the USGS gages from Bui's (2014) analysis and MEI's (2002) analysis were reviewed. These include the gages at Albuquerque (USGS 08330000), Bernardo (USGS 08332010), and San Acacia (USGS 08354900). The ninety ninth percentile of discharge represents the maximum discharge that occurs within the reach over the observation period. The percent exceedance is obtained as 100% minus the discharge percentile.

The 99th percentile flows are similar when comparing MEI's (2002) flow duration analyses to Bui's (2014). There is a notable increase in the flows at the 25th and 75th discharge percentile after 1985 and the statistical analyses performed by MEI (2002) for the period after LFCC diversion cessation and Bui (2014) both capture

this flow increase. This is likely due to the discontinuation of the LFCC (Reclamation, 1985; Reclamation, 2000). Bui's analysis shows a decrease in the frequency of the 75th percentile flows over the last two decades, which may be attributed to the drought that began in 1999. The bottom 25th percentile during Bui's (2014) analysis period also decreases, but not as significantly as the 75th percentile flows, indicating an increase in the low flow frequency. Because this analysis is based on daily average flows, it probably does not reflect high, flashy peaks that have a short temporal duration.

Table 3. Discharge at different discharge percentiles for an entire years flow within the study area (modified from Bui 2014 and MEI 2002). The daily percent exceedance for the study period can be assessed by taking 100% minus the stated discharge percentile.

Discharge (cfs)	Bottom 25th Percentile	75th Percentile	99th Percentile
Albuquerque 1974-1999 (MEI 2002)	500	~1,800	~6,000
Albuquerque (Bui 2014)	~1,400	~3,500	~5,000
Bernardo 1974-1985 (MEI 2002)	40	~1,500	~5,000
Bernardo 1986-1999 (MEI 2002)	~450	~2,000	~5,000
Bernardo (Bui 2014)	~400	~1,400	~5,000
San Acacia 1974-1985 (MEI 2002)	5	800	~6,000
San Acacia 1986-1999 (MEI 2002)	500	2,000	~6,000
San Acacia (Bui 2014)	200	800	5,500

Table 4 shows return period discharges from Wright (2010), MEI (2002), Harris and AuBuchon (2016) and a new analysis using the same time period (1993-2013) as Bui (2014) at Albuquerque and Bernardo. The new analysis was performed with input data from annual peak flows from USGS gages at Albuquerque (skew coefficient = -0.415) and Bernardo (skew coefficient = -0.718). Each analysis represented in Table 4 assumes a log Pearson type III probability distribution, but evaluates a different period from the flow record. Wright calculated regulated peak flows at the USGS gages in Albuquerque (USGS 08330000), Bernardo (USGS 08332010), and San Acacia (USGS 08354900) incorporating the influence of reservoir regulation and potential tributary inputs on discharge for the MRG. The operations at dams and reservoirs affect the rivers' discharge and therefore the peak flood intensity. Wright also considered input from tributaries to estimate a maximum peak flows on the Rio Grande. Only the regulated peak discharges from Wright's work is shown in Table 4. MEI (2002), Harris and AuBuchon (2016), and the current analyses evaluated the period of time after the closure of Cochiti Dam using just the USGS data. The current analysis also looks at a period of time after the cessation of flows in the LFCC (Reclamation, 1985; Reclamation, 2000).

Table 4: Discharge at different regulated flood frequencies for the study area modified from Wright (2010), MEI (2002), and Harris and AuBuchon (2016). Annual peak flow from the USGS was used in analysis.

Discharge (cfs)	2 Year	5 Year	10 Year	25 Year	50 Year	100 Year
Albuquerque (MEI (2002))	5,410	7,600	8,940	10,100	11,600	12,600
Albuquerque (Wright (2010))	4,000	6,200	7,500	9,000	10,000	10,000
Albuquerque, 1993-2013	3,370	5,280	6,550	8,100	9,230	10,300
Bernardo (Wright (2010))	4,900	7,700	9,300	11,200	12,500	12,700
Bernardo, 1993-2013	3,290	5,610	7,090	8,820	10,000	11,100
San Acacia (Wright (2010)	7,800	12,000	14,500	17,400	19,300	20,100
San Acacia (Harris, 2016)	4,410	6,380	7,570	8,920	9,820	10,600

For all return periods (except the 100 year at Albuquerque) the discharge decreases with each subsequent analysis over time. For instance MEI (2002) determined the two-year return period flow at the Albuquerque gage to be 5,410 cfs, based on an evaluation of data between 1974 and 1999. The 1980s and 1990s were wetter compared to more recent years. An analysis of data from 1993 to 2013 shows that a similar sized discharge event on the Rio Grande at the Albuquerque gage would have a five-year return period. MEI's analysis was performed prior to a number of dry years that occurred in the 2000's and thus it is expected that the return period values are higher. Wright's analysis used a longer time period, incorporated regional skew coefficients, and focused on the larger flow magnitudes across the valley.

3.1.3 Duration

Prior to 1973 the Rio Grande has been documented to dry about 70% of the time, while between 1986 and 1999 drying occurred about 1% of the time (MEI, 2002). An analysis of the daily data available between 1995 and 2015 from USGS provides the number of days per water year that the flow in the Rio Grande is above the specified flow value. This is total days in the water year, not number of consecutive days. This analysis is provided for Albuquerque (USGS 08330000), Bernardo (USGS 08332010), and San Acacia (USGS 08354900). The Bernardo gage is missing daily data for July 20, 2005 through September 29, 2011. Table 5 through Table 7 show the number of days exceeding a given flow value at the Albuquerque, Bernardo, and San Acacia gages. Figure 34 through Figure 36 also show number of days exceeding a given flow value, but in a graphical format. The number of days exceeding a given discharge between 1995 and 2015 is generally decreasing for all three USGS gage stations. It is also apparent from the figures that discharge has often been less than 500 cfs for a portion of the year on the Rio Grande, except in the late 1990s at the Albuquerque gage.

Table 5: Days exceeding target flow values at Albuquerque USGS gage

	500 cfs	1,000 cfs	2,000 cfs	3,000 cfs	4,000 cfs	5,000 cfs	6,000 cfs
1995	348	232	130	96	85	59	2
1996	264	150	0	0	0	0	0
1997	332	150	66	43	35	15	0
1998	365	226	49	23	0	0	0
1999	359	163	72	33	13	0	0
2000	366	27	0	0	0	0	0
2001	310	68	21	2	2	0	0
2002	209	4	0	0	0	0	0
2003	73	4	0	0	0	0	0
2004	187	65	27	5	0	0	0
2005	265	117	81	73	65	38	11
2006	266	18	1	0	0	0	0
2007	290	117	41	9	0	0	0
2008	322	147	109	79	21	3	0
2009	276	99	51	36	12	0	0
2010	290	87	58	30	5	0	0
2011	255	21	0	0	0	0	0
2012	259	35	1	0	0	0	0
2013	132	7	4	0	0	0	0
2014	253	33	2	0	0	0	0
2015	285	83	21	0	0	0	0

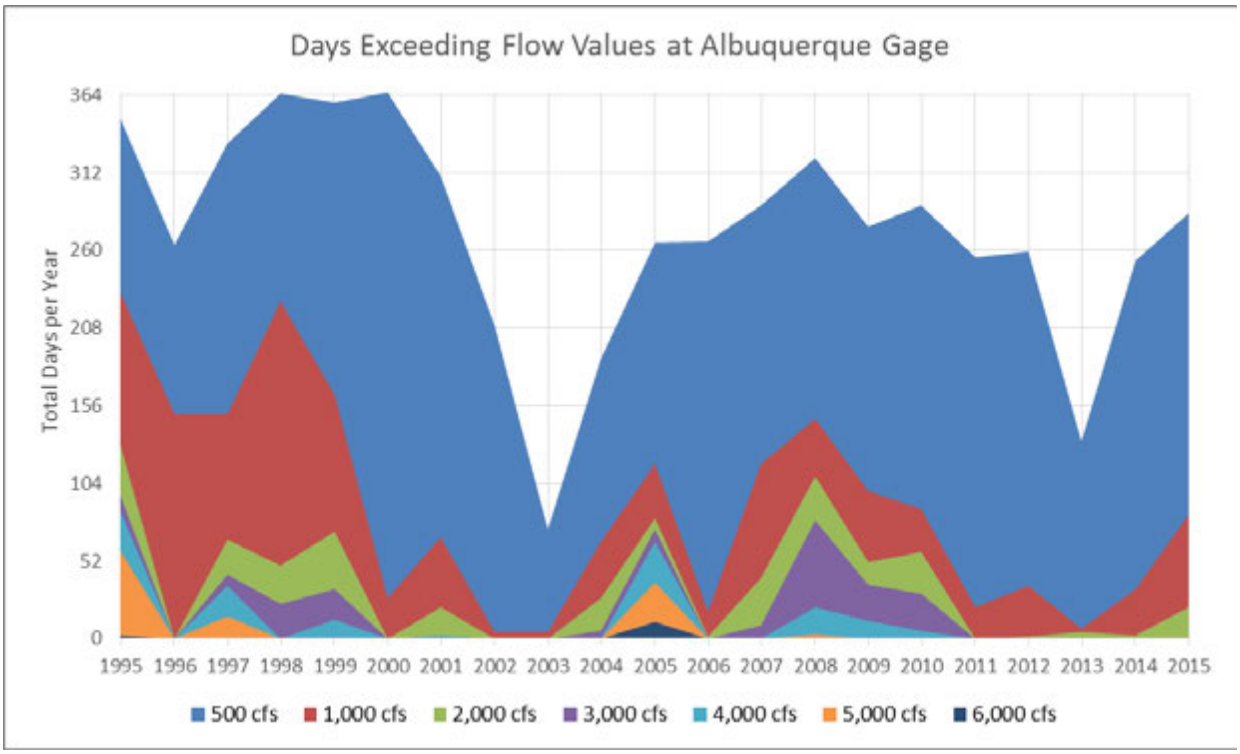

Figure 34: Days exceeding target flow values at Albuquerque USGS gage

Table 6: Days exceeding target flow values at Bernardo USGS gage

	500 cfs	1,000 cfs	2,000 cfs	3,000 cfs	4,000 cfs	5,000 cfs	6,000 cfs
1995	306	233	119	93	77	4	0
1996	182	122	0	0	0	0	0
1997	300	127	56	41	35	21	10
1998	281	226	48	11	0	0	0
1999	283	106	53	24	6	0	0
2000	167	30	0	0	0	0	0
2001	199	38	7	2	2	0	0
2002	97	3	0	0	0	0	0
2003	13	0	0	0	0	0	0
2004	161	42	14	0	0	0	0
2005	232	114	74	70	51	25	2
2006	NO DATA						
2007							
2008							
2009							
2010							
2011							
2012	156	10	1	0	0	0	0
2013	57	6	2	1	0	0	0
2014	161	9	0	0	0	0	0

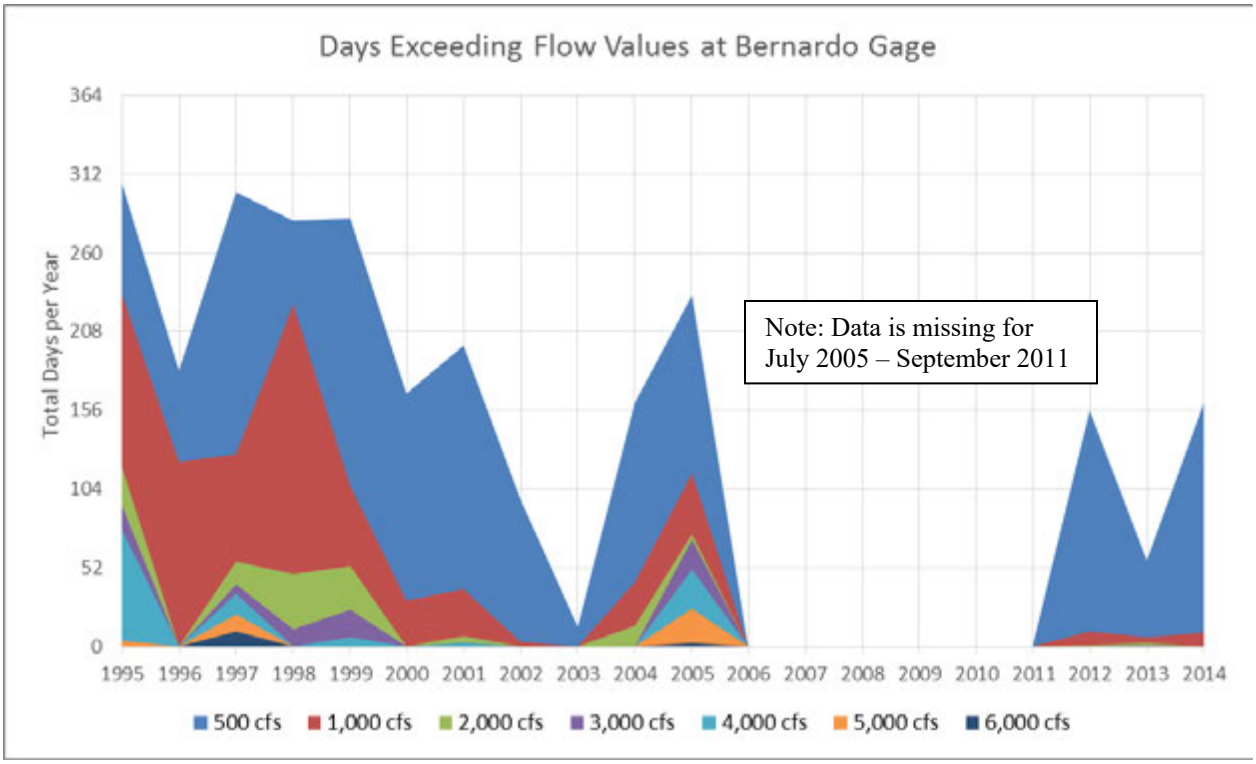

Figure 35: Days exceeding target flow values at Bernardo USGS gage

Table 7: Days exceeding target flow values at San Acacia USGS gage

	500 cfs	1,000 cfs	2,000 cfs	3,000 cfs	4,000 cfs	5,000 cfs	6,000 cfs
1995	305	253	122	90	68	9	0
1996	185	92	1	1	1	1	0
1997	295	123	60	37	16	1	0
1998	278	219	26	2	0	0	0
1999	287	151	48	20	6	0	0
2000	174	60	0	0	0	0	0
2001	232	25	2	0	0	0	0
2002	121	6	0	0	0	0	0
2003	135	2	1	0	0	0	0
2004	182	49	17	2	0	0	0
2005	242	111	75	70	48	24	0
2006	171	36	23	9	4	0	0
2007	257	157	22	2	0	0	0
2008	280	149	91	47	5	0	0
2009	229	68	43	19	1	0	0
2010	221	65	46	3	0	0	0
2011	131	1	0	0	0	0	0
2012	169	13	1	0	0	0	0
2013	95	11	6	4	3	2	2
2014	181	32	0	0	0	0	0
2015	222	52	19	5	0	0	0

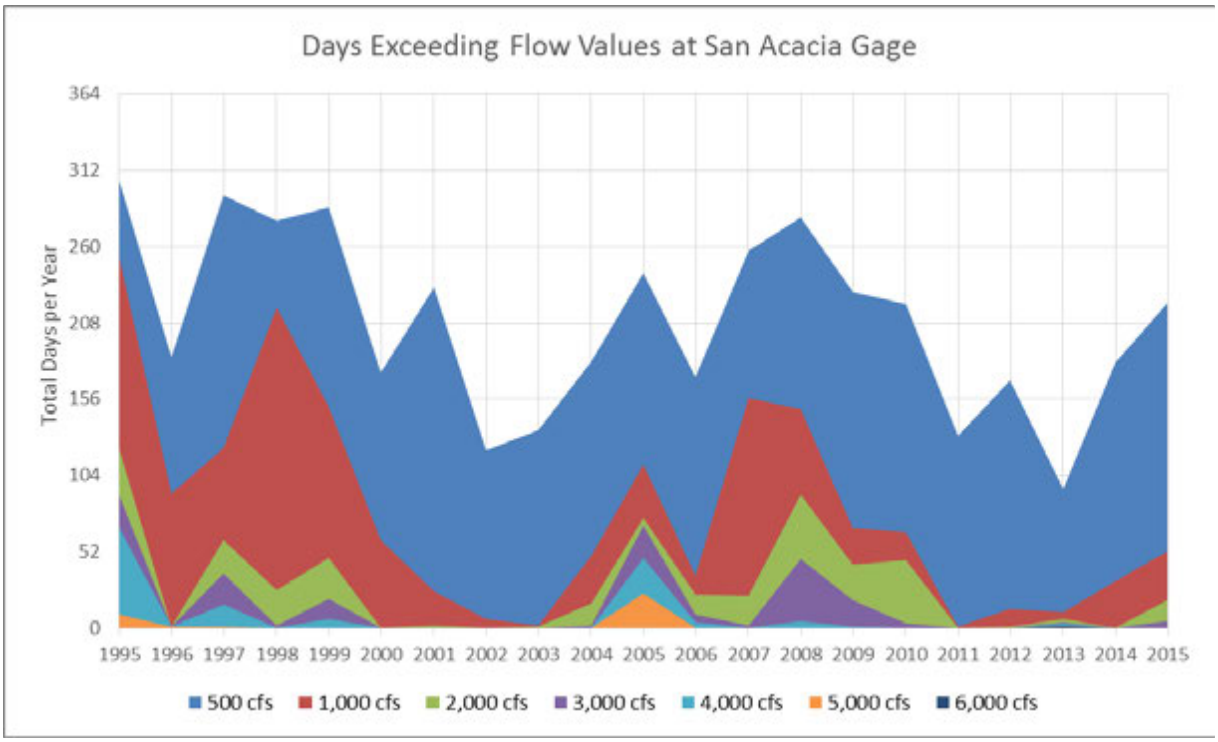

Figure 36: Days exceeding target flow values at San Acacia USGS gage

3.2 Sediment supply

One of the other primary drivers of geomorphic change on the Middle Rio Grande is sediment. Unlike flow, sediment tends to move irregularly through the system, with accumulations moving in and out of storage on the floodplain (MEI, 2002). Culbertson and Dawdy (1964) measured an 8 to 10 fold increase in the suspended sediment supply between the lower and upper regime flows. Historical studies have indicated the significant role that tributaries, especially the Rio Puerco and the Rio Salado (Bryan and Post, 1927; Gorbach, 1996; MEI, 2002; Crawford et al., 1993; Scurlock, 1998; Bauer, 2009), have had on the Rio Grande.

3.2.1 Suspended sediment

3.2.1.1 Single Mass Curves

Single mass curves show the volume of suspended sediment transported over time. Changes in slope indicate decreases or increases in suspended sediment transported over time.

Single mass curves were made using available USGS data for the Rio Grande at Albuquerque (USGS 08330000), Bernardo (USGS 08332000 and 08332010), and San Acacia (USGS 08354900). A single mass curve was also developed for the Rio Puerco near Bernardo (USGS 0853000). The data is presented in water years (October 1 through September 30). The data for Albuquerque was obtained as annual statistics for the water years 1970 through 2014. The data is plotted in Figure 37.

The sediment data for Bernardo was obtained as daily data for water years 1956 through 1966. The data wasn't available as an annual statistic because there were many days of data missing from July, August, October, and November 1956; July 1958, June 1959, all of July 1959, sections of September 1959, all of September 1960, and sections of September 1962 and September 1964. Thus the data shown in Figure 38 for water years 1956 through 1966 should be evaluated with the consideration that it is partial data. The data for Bernardo for water years 1967 through 2014 was obtained as annual statistics as well. The data is plotted in Figure 38. The data for San Acacia was obtained as annual statistics for water years 1964 through 2014. The data is plotted in Figure 39. The data for the Rio Puerco near Bernardo was obtained as annual statistics for water years 1956 through 2014. However, water year 1994 is entirely missing from the dataset. The available data is plotted in Figure 40.

The information from the single mass curves indicate that there was considerably more suspended sediment moving through the Middle Rio Grande prior to the early 1970s. Gellis (1991) suggests that arroyos along the Rio Grande underwent a period of incision between 1880 and 1920 that contributed large volumes of sediment to the Rio Grande. Scurlock (1998) estimated that in the early 1900s almost 40 million tons of sediment were transported by the Rio Grande per year. Finch and Tainter (1995) estimated the annual sediment load between 1936 and

1941 was around 32 million tons per year. During the same period the Rio Puerco was estimated to add about 25 million tons of suspended sediment to the Rio Grande (Bryan and Post, 1927; Scurlock, 1998; Finch and Tainter, 1995). This is about 62% of the suspended sediment load to the Rio Grande in the early 1900s and about 78% of the sediment load later in the twentieth century. From the single mass curve in Figure 40 it can be seen that the Rio Puerco in the late 1950s produced an average annual suspended volume of about 18 million tons per year. During this same time period the Rio Grande at the Bernardo gage (about 4 miles upstream of the confluence with the Rio Grande) recorded around 7 million tons per year (see Figure 38) and the Rio Grande at the San Acacia gage (about 11 miles downstream) recorded around 1 million tons per year (see Figure 39). Since the late 1950s, both the Rio Grande at Bernardo gage and the Rio Puerco near Bernardo gage have shown a decreasing annual yield of suspended, while the Rio Grande at the San Acacia gage has shown an increasing suspended sediment yield.

A decrease in the annual production of suspended sediments (see Figure 37) is noticeable in the Albuquerque gage starting in the late 1970s. The San Acacia gage, while showing some fluctuations, has had an annual suspended sediment yield ranging between 2 and 5 million tons per year since the early 1970s. Between the Albuquerque and Bernardo gages the fluctuations in annual suspended sediment yield are similar. Between the 1970s and mid -1980s the suspended sediment yield at Bernardo was about half or less of that recorded at the Albuquerque gage. A similar reduction in sediment yield is occurring currently (mid-2000s through the mid 2014s, which was the extent of this analysis) between the Albuquerque and Bernardo gages. Between the mid-1980s and early 2000s the Bernardo gage recorded more suspended sediment yield than at the Albuquerque gage, despite a loss of suspended sediment around the Isleta Diversion Dam.

The San Acacia gage (see Figure 39) records an increase in suspended sediment yield from the Albuquerque and Bernardo gage (Figure 37 and Figure 38, respectively), ranging between 2 to 8 times the annual volume between the early 1970s through 2014 (end of analysis period). The annual suspended sediment yield from the Rio Puerco gage at Bernardo (see Figure 40) is decreasing with time. Between the late 1970s through the early 1980s the Rio Puerco contributed about 70% of the annual suspended sediment volume (around 2.5 million tons) recorded at the San Acacia gage (about 3 million tons). This percentage decreased to about 60% between the mid-1980s and early 1990s, with the Rio Grande increasing to about 4 million tons per year. Currently (2006 to 2014) the annual suspended sediment yield from the Rio Puerco (about 0.9 million tons) is about 38% of that recorded at the San Acacia gage (about 2.4 million tons per year). Others have also observed lower sediment yields with time on the Rio Puerco and have documented channel filling on the lower Rio Puerco (Friedman et al., 2015).

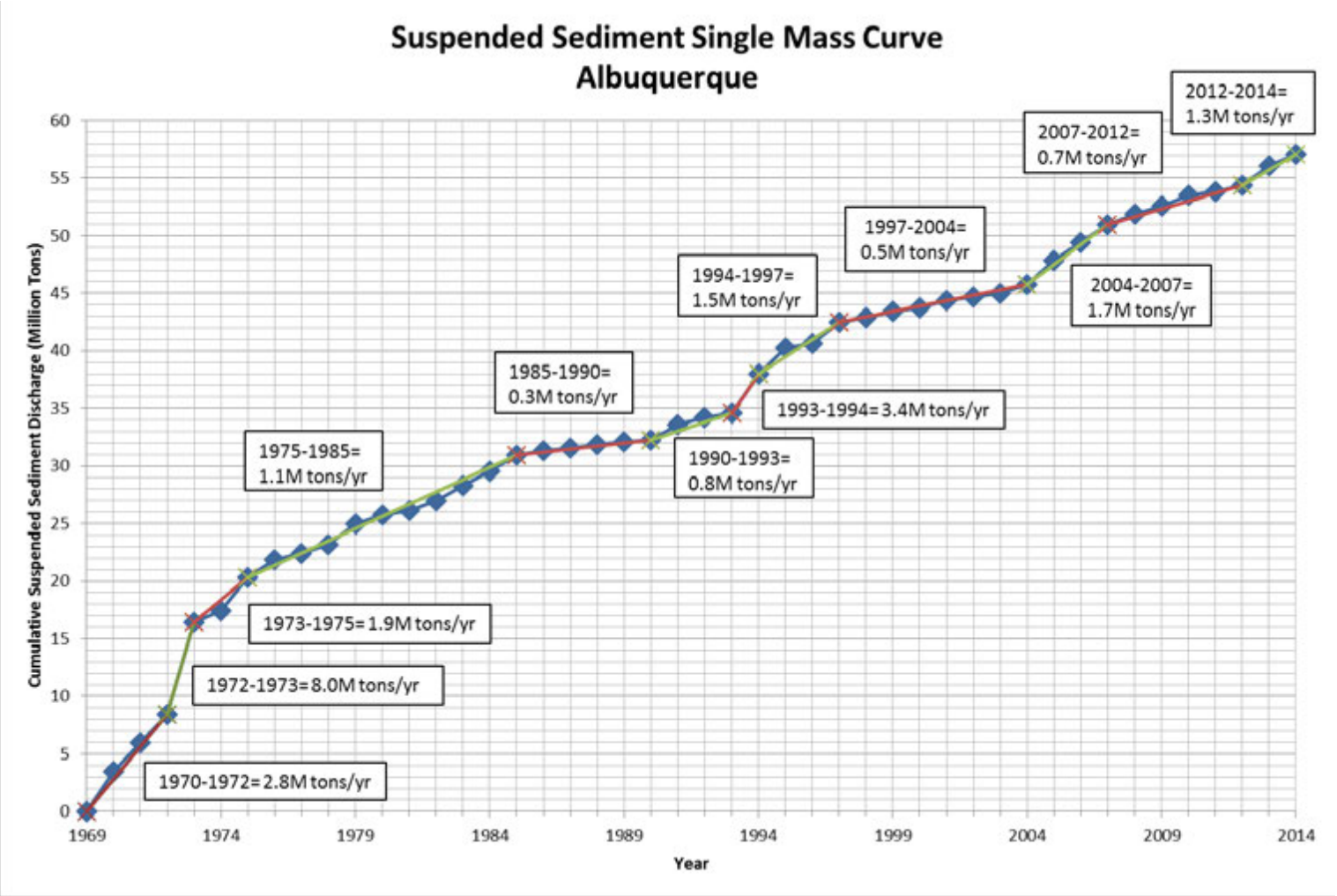

Figure 37: Rio Grande at Albuquerque Single Mass Curve for Suspended Sediment

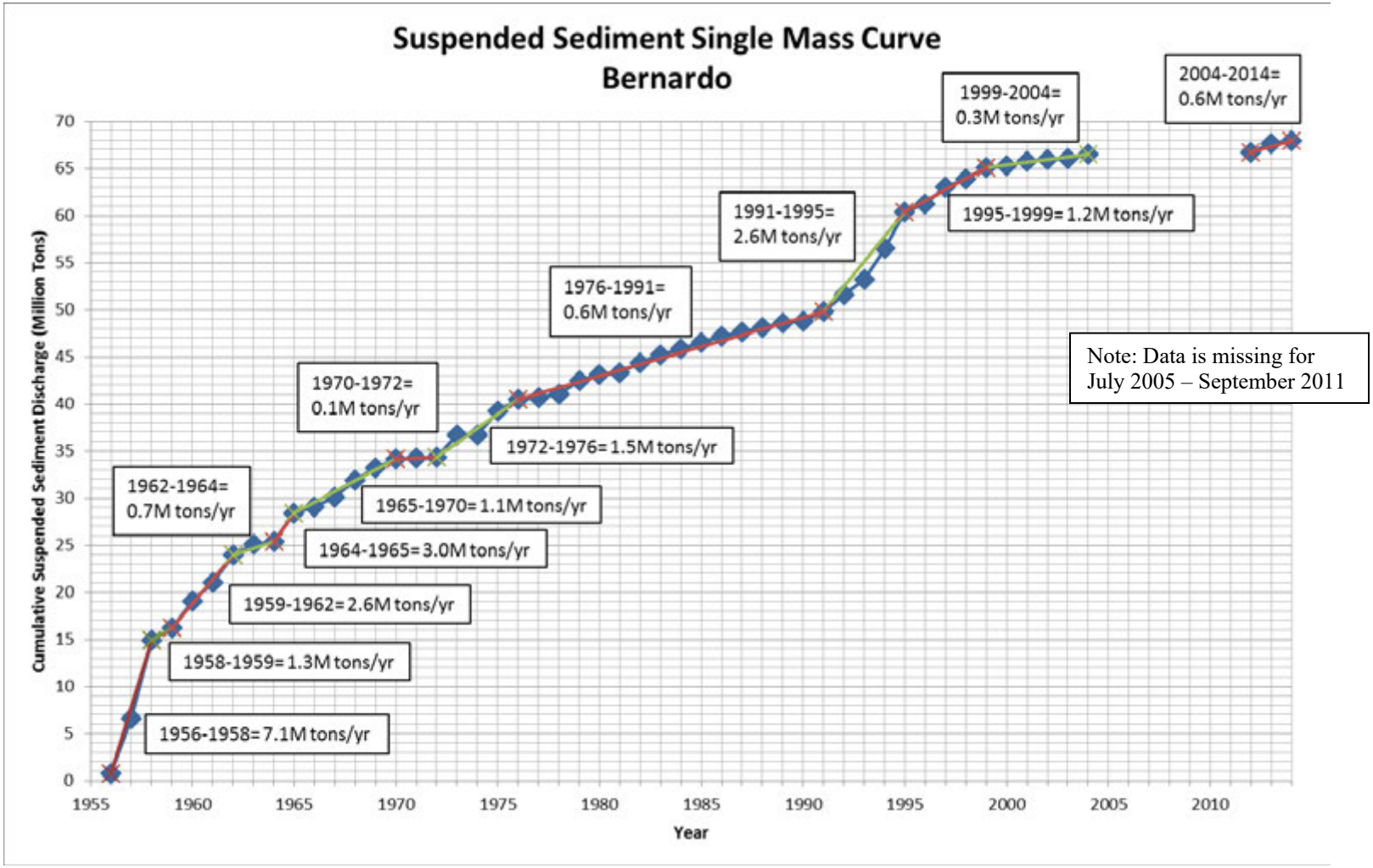

Figure 38: Rio Grande near Bernardo Single Mass Curve for Suspended Sediment

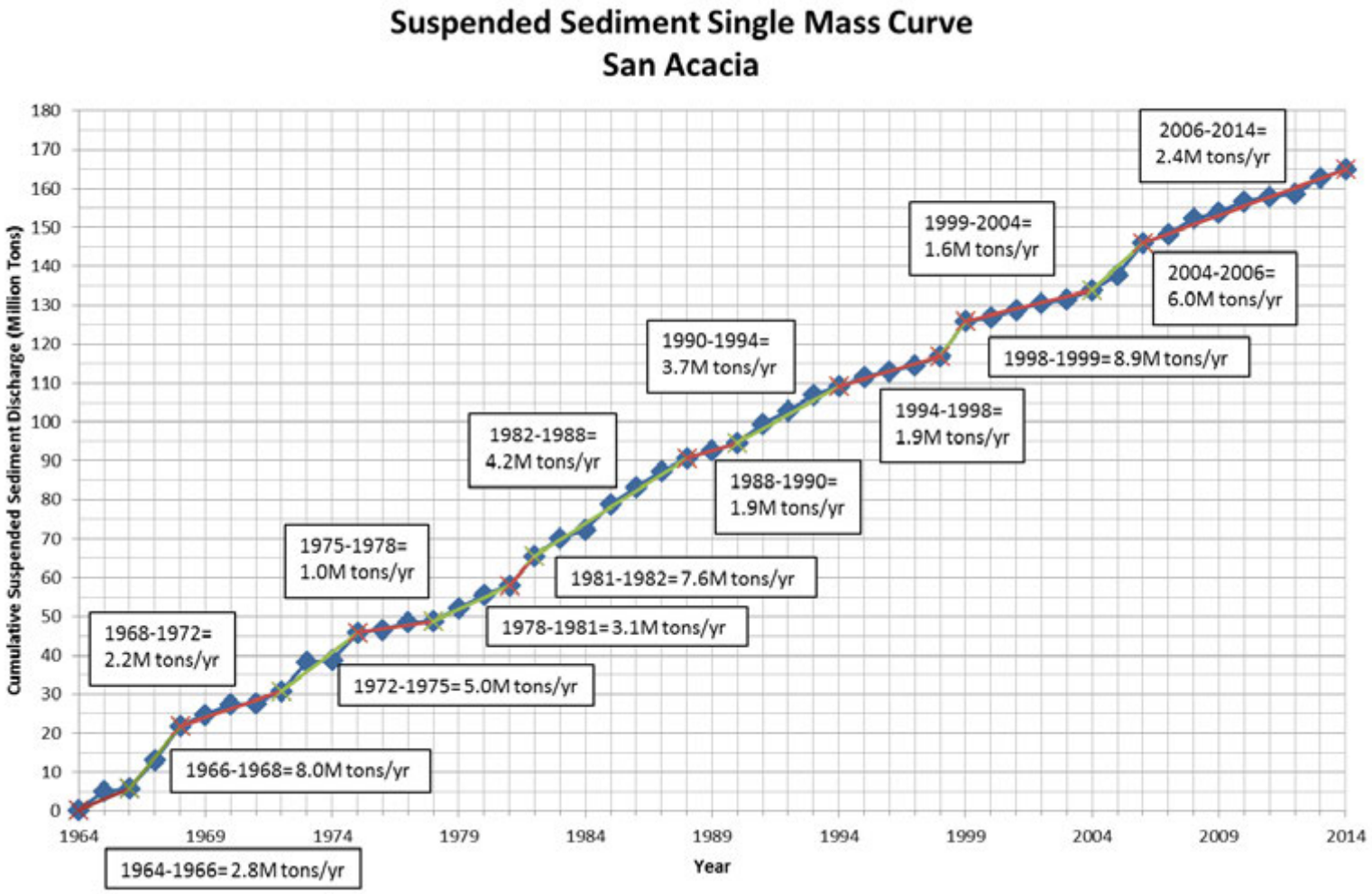

Figure 39: Rio Grande at San Acacia Single Mass Curve for Suspended Sediment

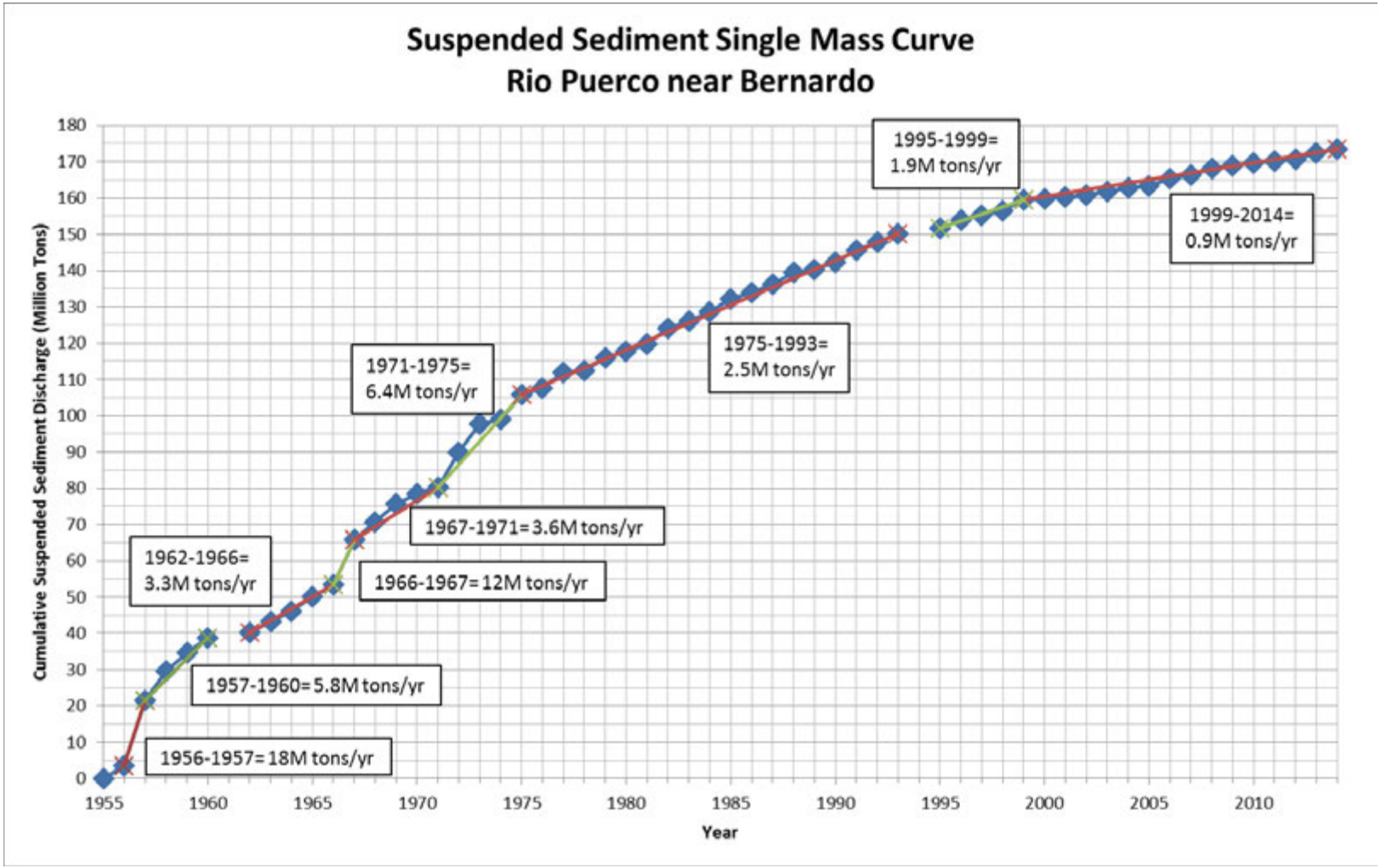

Figure 40: Rio Puerco near Bernardo Single Mass Curve for Suspended Sediment

3.2.1.2 Double Mass Curves

The double mass curve shows cumulative annual suspended sediment volumes paired with its concurrent cumulative annual discharge (water) volume. The slope of this curve reveals changes in the mean suspended sediment concentration over time. Double mass curves were created using available USGS gage data at the Albuquerque, Bernardo, and San Acacia gages on the Rio Grande and on the Rio Puerco gage near Bernardo. The suspended sediment data source is the same as described in the subsection 3.2.1.1. Single Mass Curves. The river discharge data source is the same as described in the subsection 3.1.1.1. Single Mass Curves.

In general, the mean annual suspended sediment concentration has decreased on the Rio Grande and the Rio Puerco since the 1960s for the analyzed USGS gages. Gellis (1991) also found a strong statistical trend of decreasing suspended sediment concentrations along the Rio Grande between the late 1940s and 1990.

The Albuquerque USGS gage (Figure 41) shows that the mean annual sediment concentration was highest prior to 1973, with a strong reduction between 1973 and 1978. The mean annual suspended sediment concentration decreased again between 1985 and 1993, followed by an increase in the following decade. A steeper slope on the Albuquerque USGS gage around 2012 suggests that the mean annual suspended sediment concentration has increased again. Between 1970 and 2014, a little over 57 million tons of suspended sediment have cumulatively passed by the gage at Albuquerque.

Table 8: Mean annual suspended sediment concentrations for various time periods at the Albuquerque gage based on slope of Double Mass Curve (Figure 41)

Period	Suspended Sediment Concentration (mg/L)
1970-1973	3,219
1974-1978	1,032
1979-1985	489
1986-1993	270
1994-1995	1,291
1996-2003	489
2004-2007	1,105
2008-2011	525
2012-2014	1,262

The Bernardo USGS gage (Figure 42) shows a similar trend, with the mean annual suspended sediment concentration decreasing between 1965 and 1975. This reduction in the mean annual suspended sediment concentration continued until around 1993. At this point the double mass curve steepens, suggesting an increase in the mean annual suspended sediment concentration that continues until the end of the analysis period (up to 2014). Between 1965 and 2014, a little over

42 million tons of suspended sediment have cumulatively passed by the gage at Bernardo. Culbertson and Dawdy (1964) measured suspended sediment concentrations about 13 miles upstream of the Bernardo USGS gage (near Casa Colorado, NM) in the late 1950s. They recorded suspended sediment concentrations between 1200 mg/L at 800 cfs and 13,700 mg/L at 8,300 cfs, indicating that prior to the time frame shown on the double mass curves the suspended sediment concentrations in the Rio Grande was considerably higher. Casa Colorado, NM is about 39 miles downstream of the Albuquerque USGS gaging station. It is interesting to note that the mean annual suspended sediment concentrations at the Bernardo USGS gage are lower than mean annual suspended sediment concentration at the Albuquerque USGS gage. This may be in part from sediment deposition in the reach or from discontinuity in the data.

Table 9: Mean annual suspended sediment concentrations for various time periods at the Bernardo gage

Period	Suspended Sediment Concentration (mg/L)
1966-1975	831
1976-1993	544
1994-2014*	825

*Note: Data is missing for July 2005 through September 2011

The double mass curves for the San Acacia USGS gage are shown in Figure 43. The mean annual suspended sediment concentrations derived from the slopes of the San Acacia curve shows that there is a decrease in the sediment concentration between 1967 and 1975. Another sediment concentration reduction occurs around 1985, but this is smaller than the earlier one and may be correlated with the cessation of the LFCC (Reclamation, 1985). An increase, however, in the mean annual suspended sediment concentration has occurred at San Acacia since the early 2000s. The rate of increase in suspended sediment concentration from 2000 to 2014 at the Albuquerque gage (about 700 mg/L) is similar to the rate of increase observed at the San Acacia gage (about 1,000 mg/L). The Bernardo USGS gage does not show any significant change during this period. Between 1965 and 2014, almost 165 million tons of suspended sediment have cumulatively passed by the gage at San Acacia.

The slope reduction in the double mass curves for the evaluated USGS gages on the Rio Grande is consistent with other research that has shown a reduction due to closure of upstream dams (Cochiti and Abiquiu) and the cessation of diversions on the LFCC (Gellis, 1991; Crawford et al., 1993; MEI, 2002; Albert, 2004; Bauer and Hilldale, 2006).

Table 10: Mean annual suspended sediment concentrations for various time periods at the San Acacia gage

Period	Suspended Sediment Concentration (mg/L)
1965-1967	5,576
1968-1975	3,615
1976-1985	4,215
1986-1998	2,332
1999	5,882
2000-2005	2,420
2006	5,037
2007-2014	3,554

The double mass curve for the USGS gage on the Rio Puerco (see Figure 44) suggests a relatively consistent mean annual suspended sediment concentration between the late 1950s through 1985. At this point there is a break in the double mass curve, with another consistent mean annual suspended sediment concentration from 1985 through 2014 (end of current analysis period). Between 1956 and 2014, a little over 173 million tons of suspended sediment have cumulatively passed by the Rio Puerco gage near Bernardo.

Estimates of the suspended sediment concentrations on the Rio Puerco near the Rio Grande confluence ranged from 150,000 to 165,000 mg/L in the 1940s/1950s, but had decreased to less than 74,000 mg/L by the early 1990s (Gellis, 1991; Gorbach, 1996; MEI, 2002). This is consistent with the single mass curves for the Rio Puerco that showed a reduction in the suspended sediment load. This and other research (Friedman et al., 2015) suggests that sediment deposition is occurring in the Lower Rio Puerco.

Table 11: Mean annual suspended sediment concentration for various time periods at the Rio Puerco gage

Period	Suspended Sediment Concentration (mg/L)
1956-1985	22,342
1986-2014	15,120

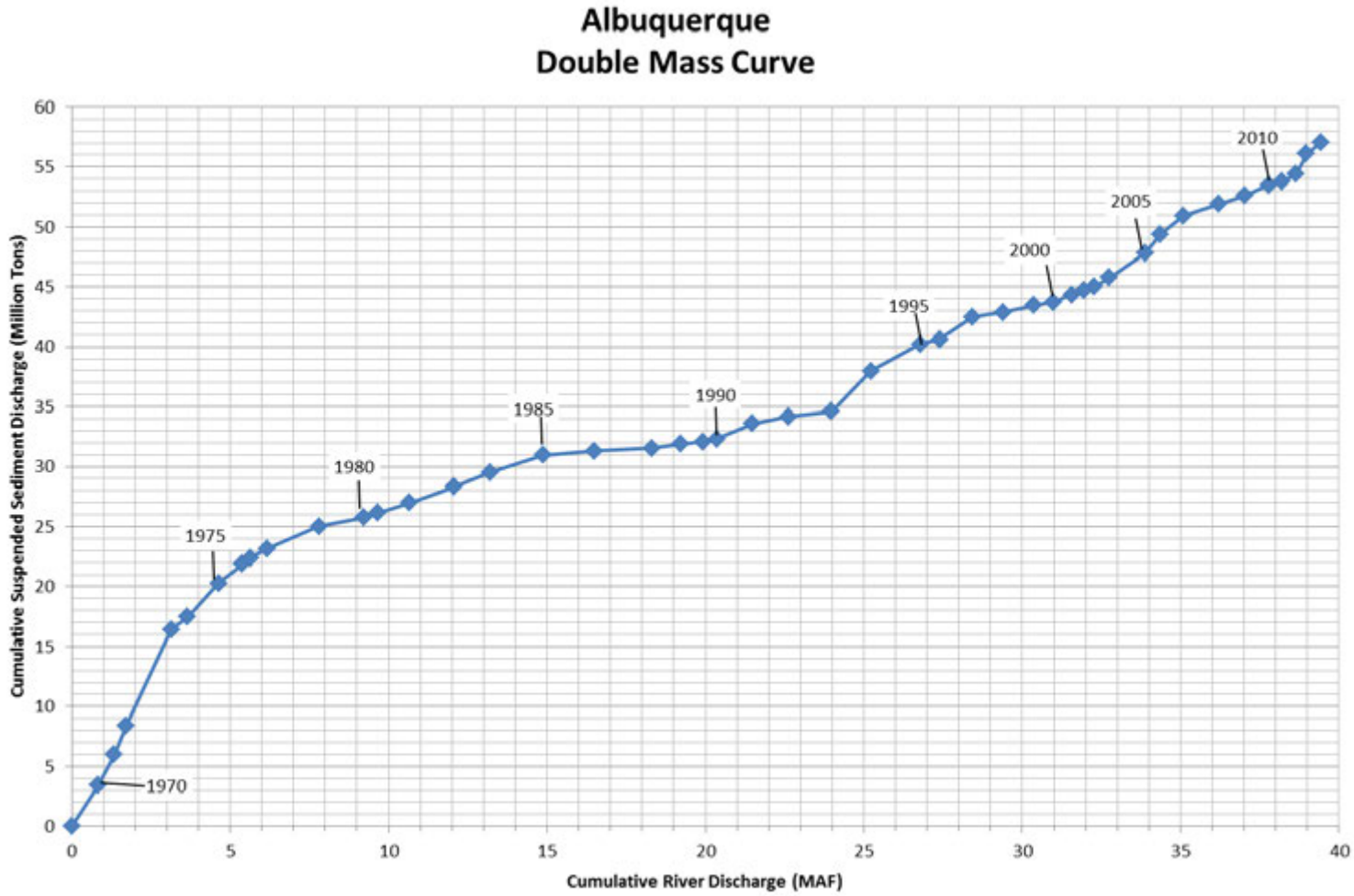

Figure 41: Albuquerque Double Mass Curve

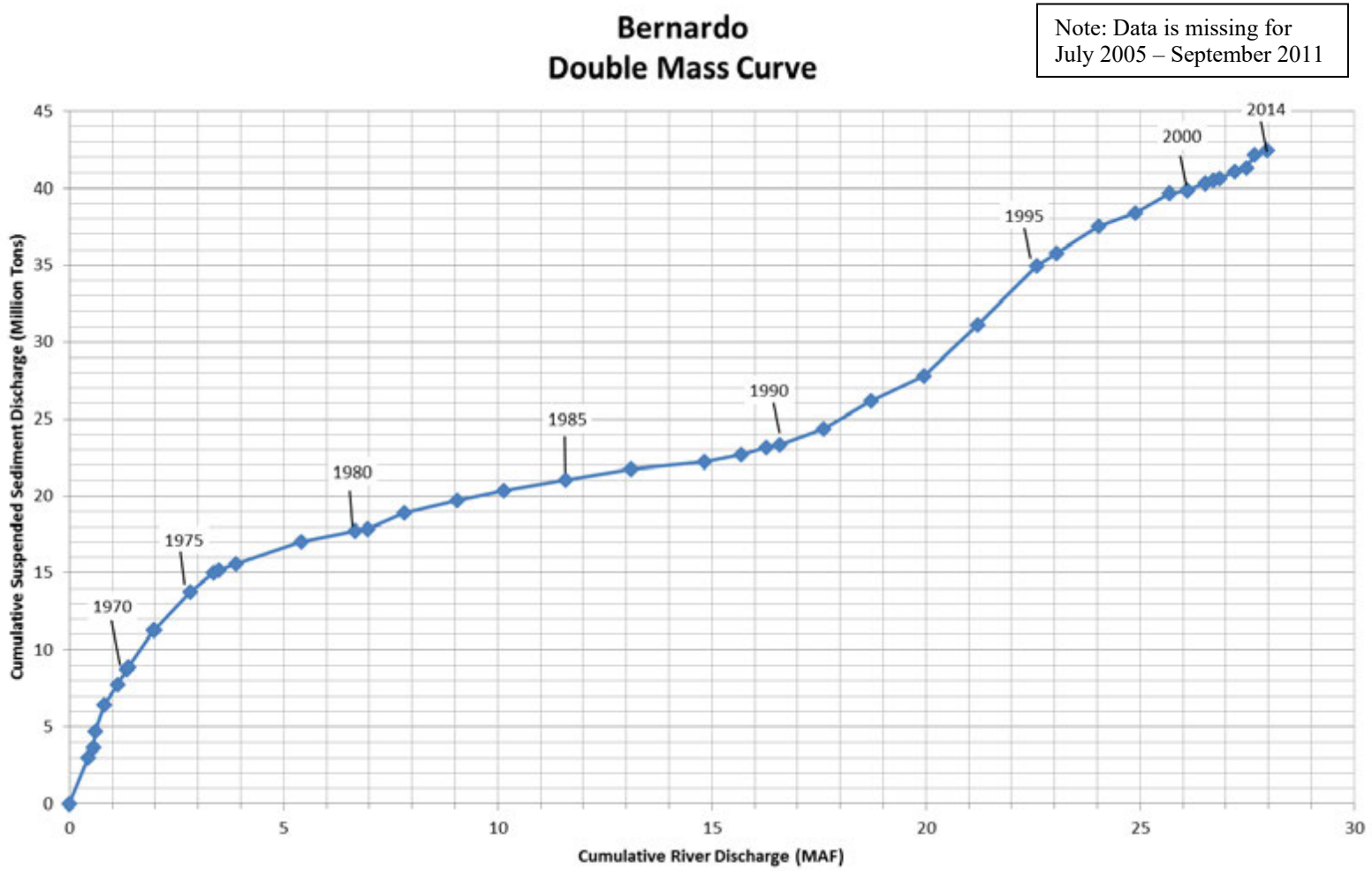

Figure 42: Bernardo Double Mass Curve

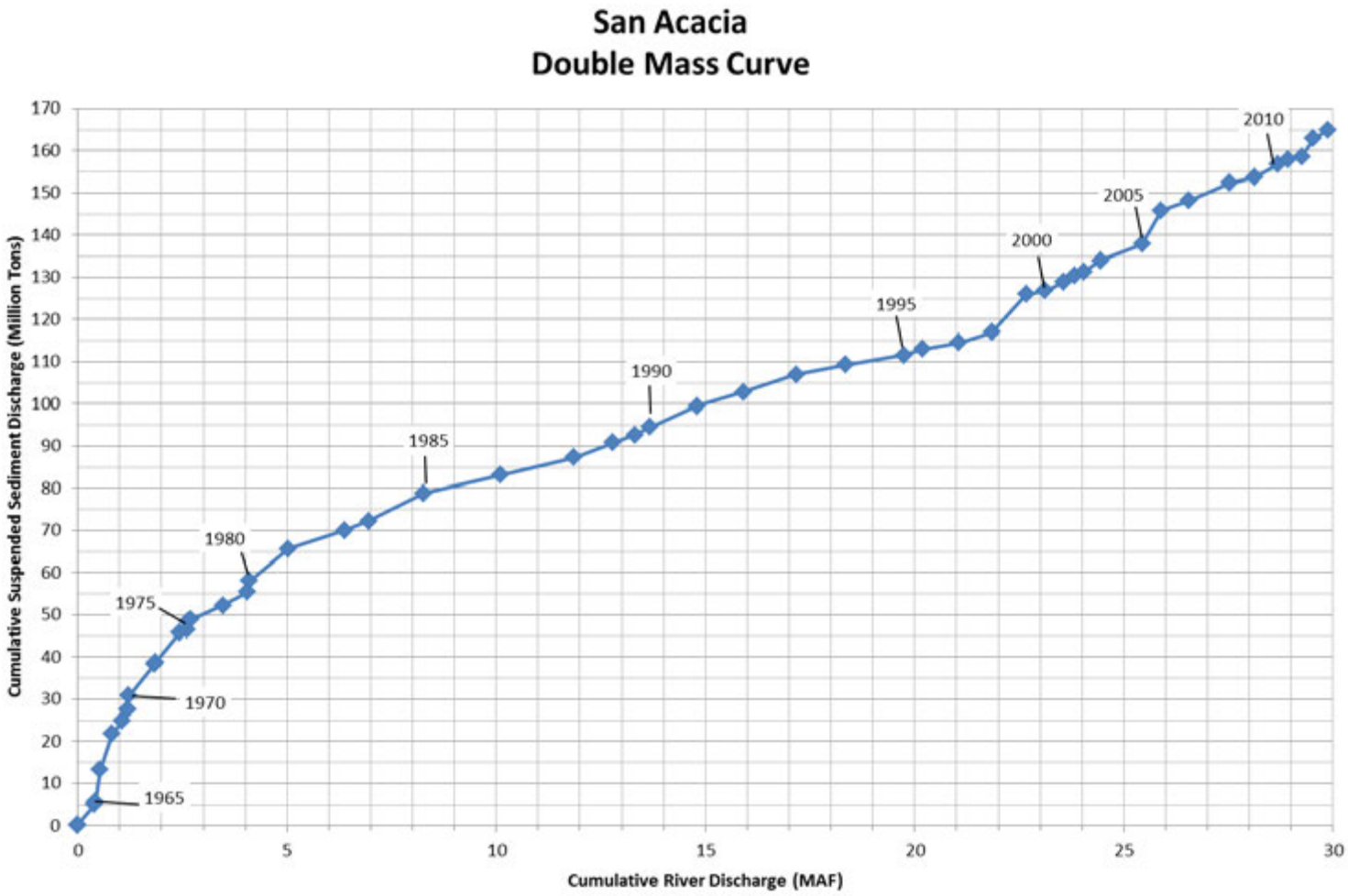

Figure 43: San Acacia Double Mass Curve

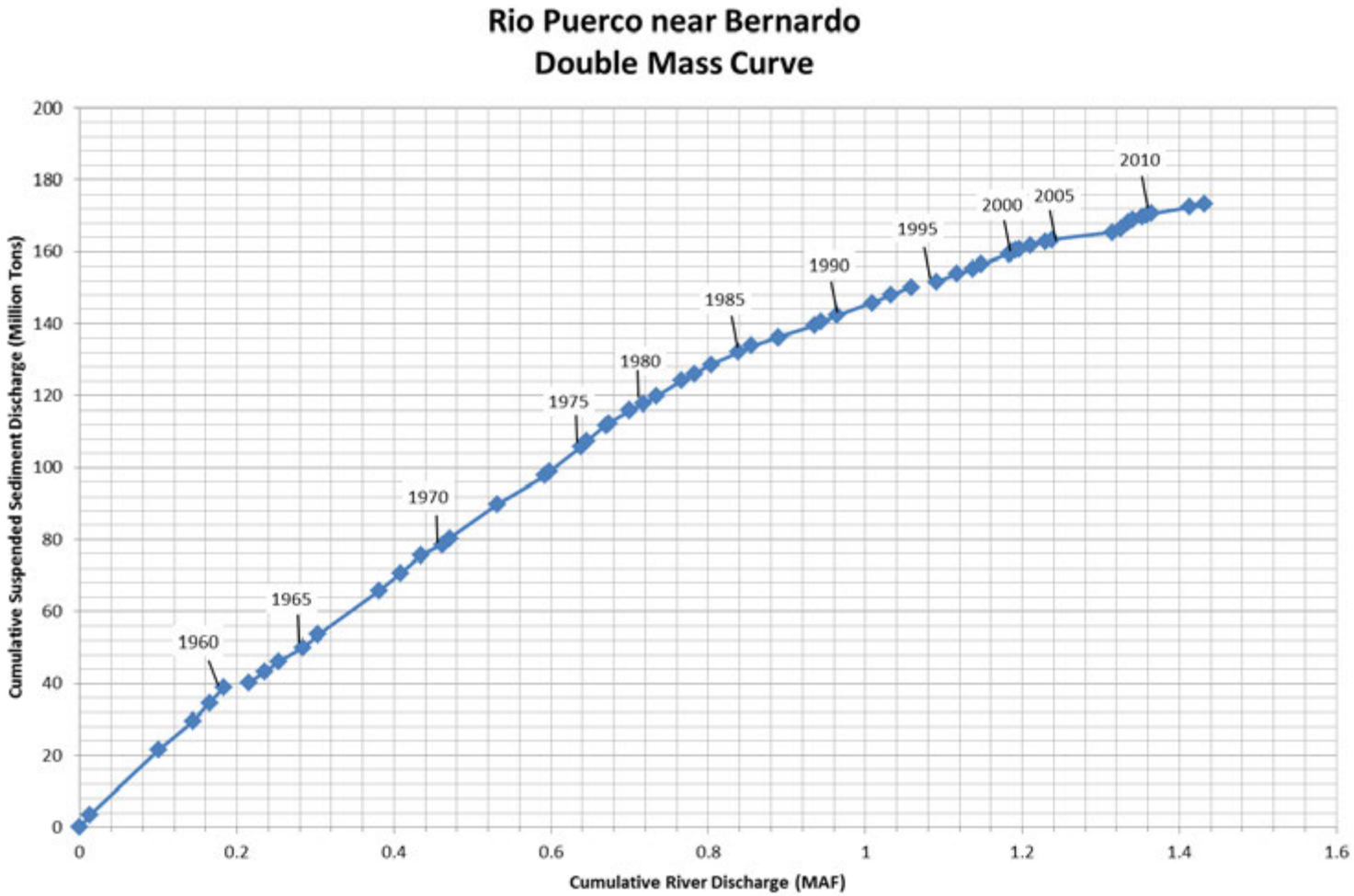

Figure 44: Rio Puerco near Bernardo Double Mass Curve

3.2.1.3 Average Monthly Histograms

Monthly histograms comparing the average monthly suspended sediment concentration, suspended sediment discharge load, and river discharge are shown in Figure 45 through Figure 48. The histograms use data averaged for each month between January 1995 and September 2014.

The data for Figure 45 was obtained from river gage "USGS 08330000 Rio Grande at Albuquerque, NM". The data for Figure 46 was obtained from river gage "USGS 08332010 Rio Grande Floodway near Bernardo, NM". The data for Figure 47 was obtained from river gage "USGS 08354900 Rio Grande Floodway at San Acacia, NM". The data for Figure 48 was obtained from river gage "USGS 08353000 Rio Puerco near Bernardo, NM".

The Albuquerque gage shows the highest daily suspended sediment discharge in May, which coincides with the largest river flows during the assessed time frame. Bernardo tells a similar story, but suspended sediment yield is equally as large in the month of July, which has the 9th largest water discharge. South of the Rio Puerco confluence, the largest sediment yields tend to occur during the late summer/early fall rainfall-runoff events. The San Acacia gage has a suspended sediment peak that occurs around August, which is the same time frame as the peak daily suspended sediment yield on the Rio Puerco. For all of the evaluated USGS gages the highest suspended sediment concentrations occur between July and September.

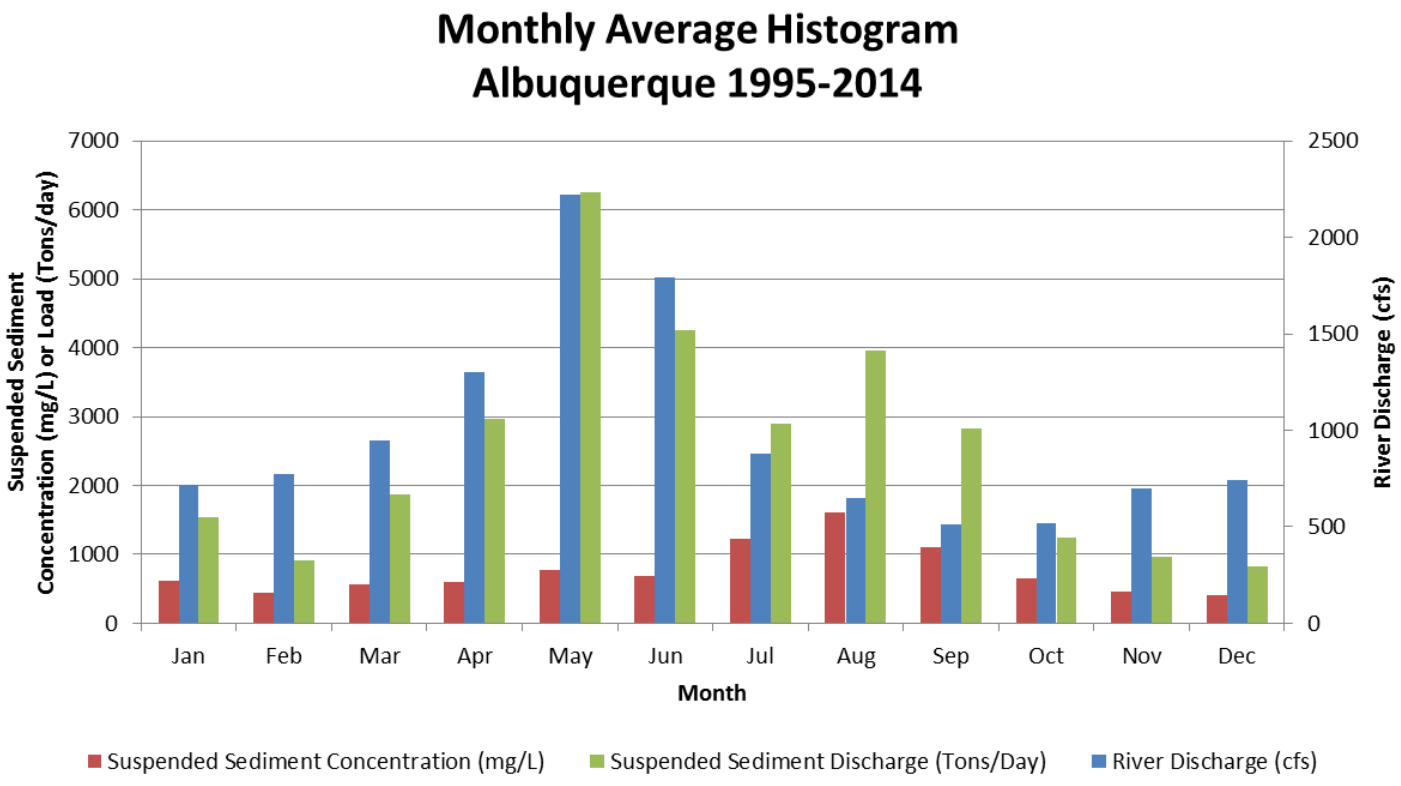

Figure 45: Monthly average histograms for the Albuquerque gage from 1995-2014. Values are the USGS reported mean monthly discharge, suspended sediment concentration, and suspended sediment discharge values derived from the approved mean daily flows.

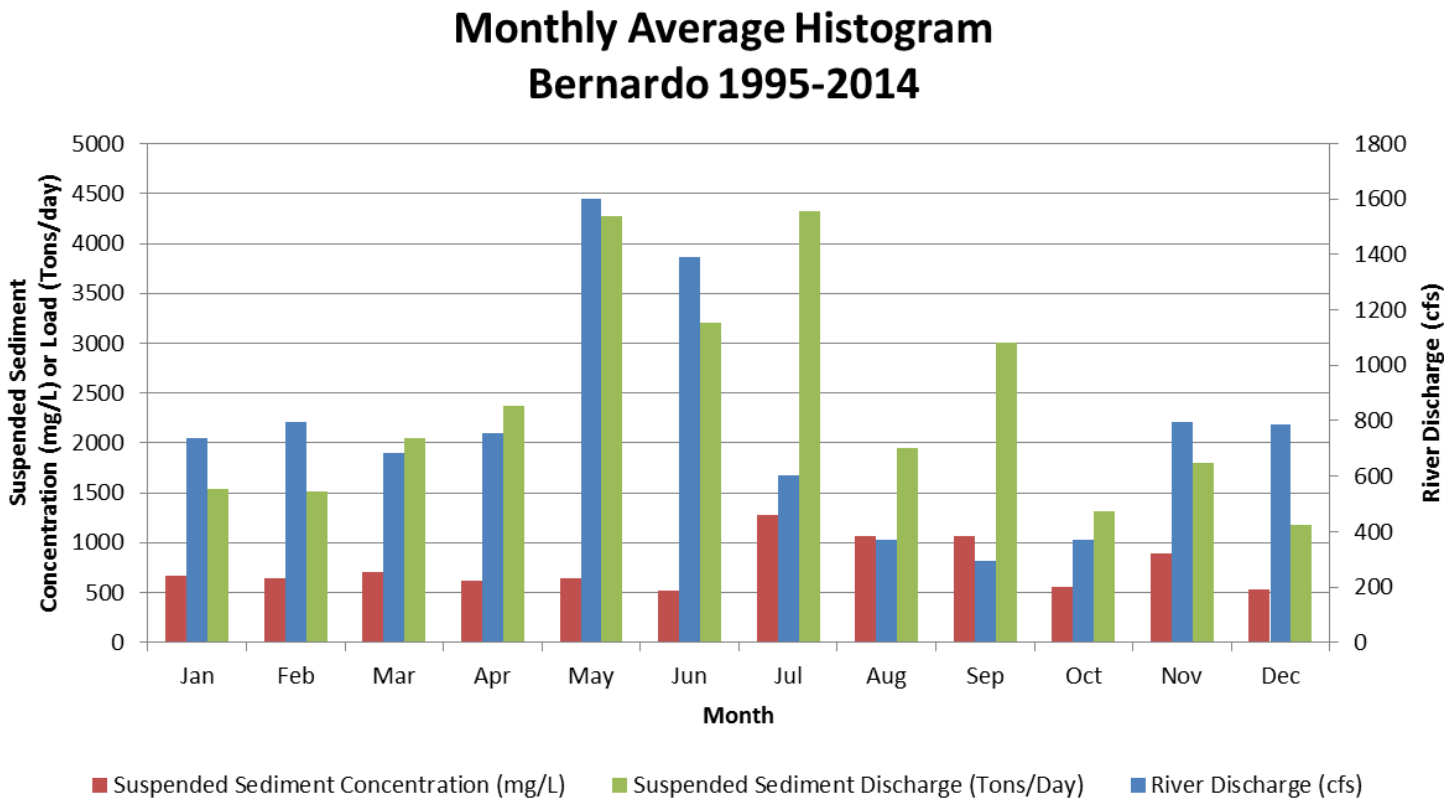

Figure 46: Monthly average histograms for the Bernardo gage from 1995-2014. Values are the USGS reported mean monthly discharge, suspended sediment concentration, and suspended sediment discharge values derived from the approved mean daily flows.

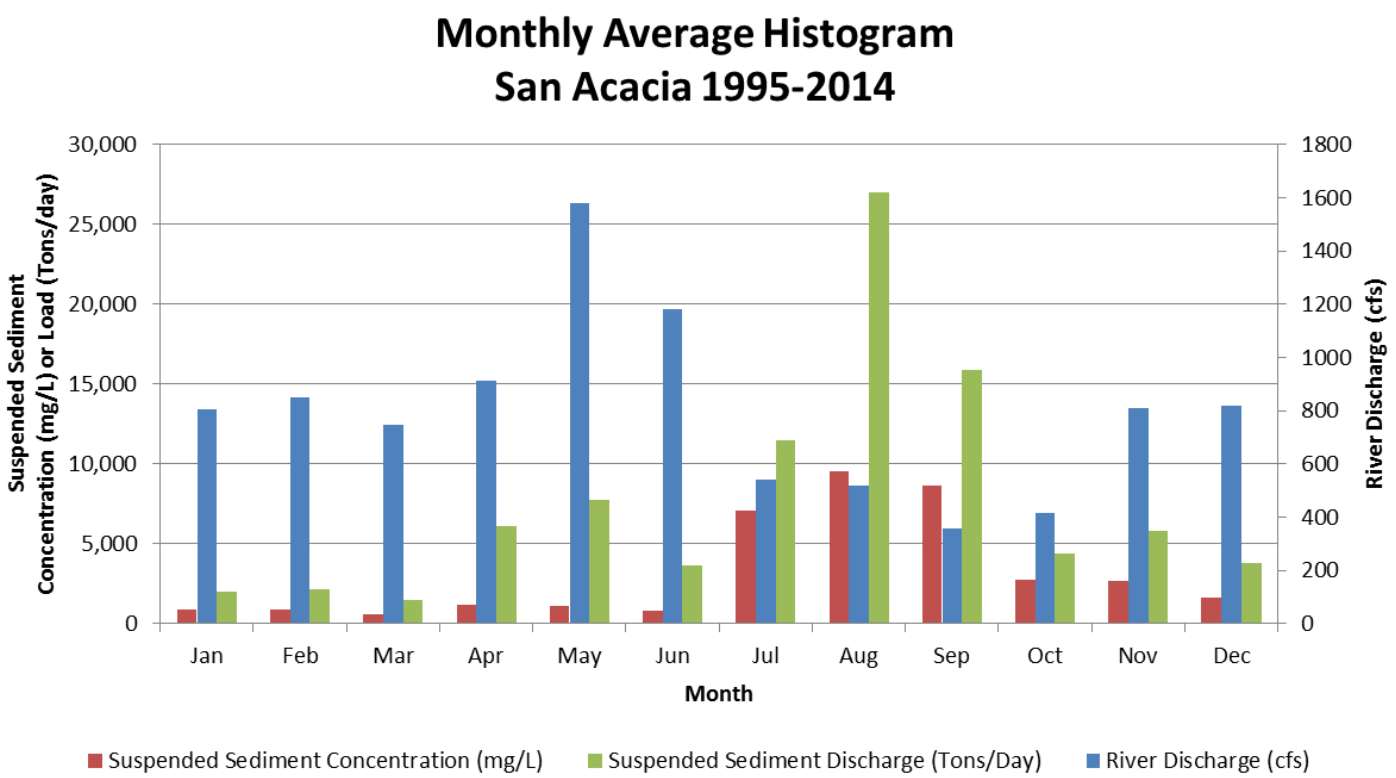

Figure 47: Monthly average histograms for the San Acacia gage from 1995-2014. Values are the USGS reported mean monthly discharge, suspended sediment concentration, and suspended sediment discharge values derived from the approved mean daily flows.

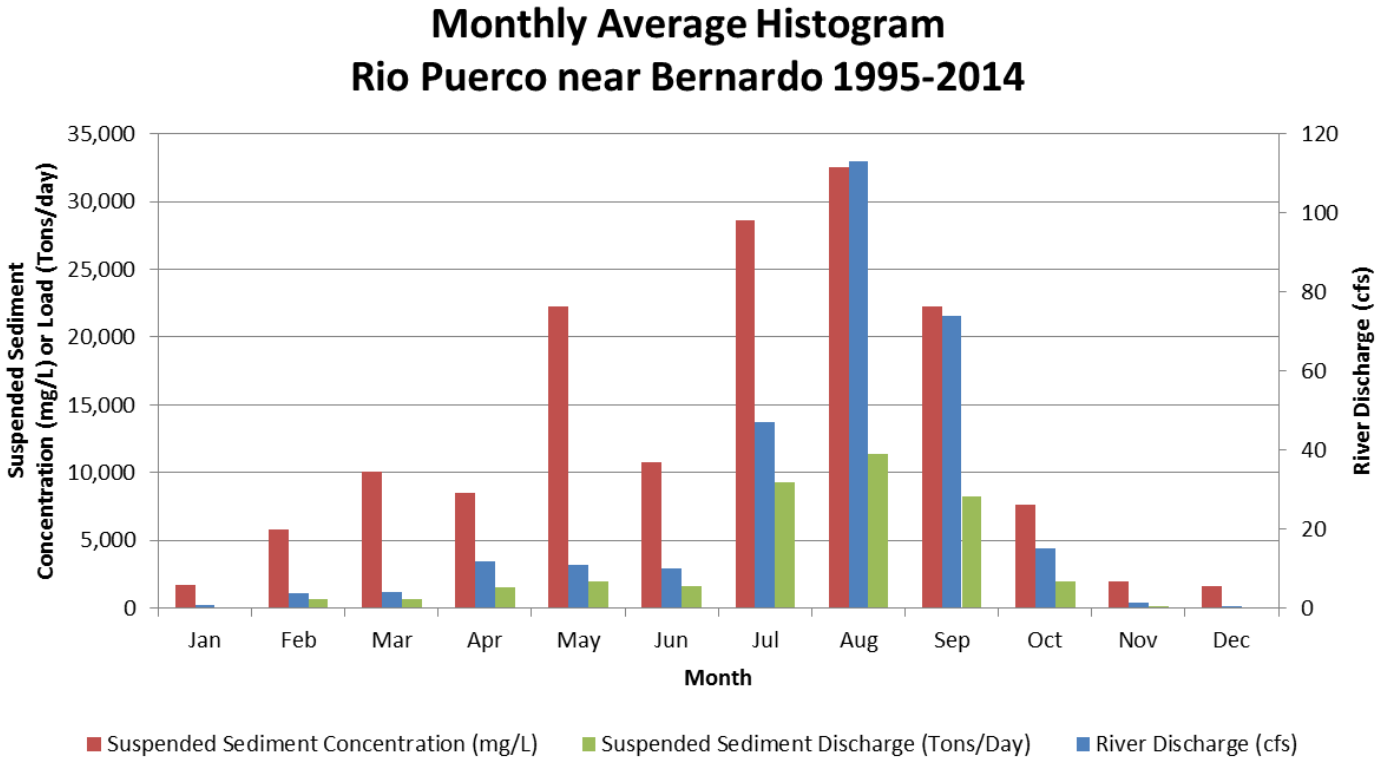

Figure 48: Monthly average histograms for the Rio Puerco gage near Bernardo from 1995-2014. Values are the USGS reported mean monthly discharge, suspended sediment concentration, and suspended sediment discharge values derived from the approved mean daily flows.

3.2.1.4 Difference Mass Curves

Difference Mass Curves are temporal representations of the increases and decreases in the suspended sediment volume present between two USGS gaging stations. Figure 49 compares the suspended sediment readings from USGS gages at Albuquerque (USGS 08330000) and San Acacia (USGS 08354900) on a daily time step (travel time and input/diversions from the system are not accounted for in the difference calculations). Positive slopes indicate times when San Acacia has more suspended sediment discharge than Albuquerque suggesting that the channel is degrading, widening, or receiving excess suspended sediment from inflowing tributaries between Albuquerque and San Acacia. Negative slopes indicate times when Albuquerque has more suspended sediment discharge than San Acacia implying that the channel is aggrading, storing sediment in the active channel or the floodplain, or losing sediment to irrigation diversions.

Figure 50 compares the suspended sediment readings from USGS gages at Albuquerque (USGS 08330000) and Bernardo (USGS 08332010) on a daily time step (travel time and input/diversions from the system are not accounted for in the difference calculations). Positive slopes indicate times when Bernardo has more suspended sediment discharge than Albuquerque suggesting that the channel is degrading, widening, or receiving excess suspended sediment from inflowing tributaries between Albuquerque and Bernardo. Negative slopes indicate times when Albuquerque has more suspended sediment discharge than Bernardo implying that the channel is aggrading, storing sediment in the active channel or the floodplain, or losing sediment to irrigation diversions.

The results show that in general the reach between Albuquerque and San Acacia is gaining suspended sediment. It is likely that this gain has more to do with the input of sediment from the large tributaries upstream, like the Rio Puerco and the Rio Salado, rather than sediment mass erosion from the beds and banks in the upstream reaches. Varyu and Fox (2014) estimated that the Rio Grande between the Rio Puerco and Rio Salado is gaining around 100,000 to 150,000 tons/year. Other studies (Richard et al., 2001; Bauer, 2009) have also indicated that the reach between Isleta and Bernardo is storing sediment. This is verified by Figure 50 which shows that sediment was stored between Isleta and Bernardo in years 1972-1985, and 2000-2014. Thus the large gain in suspended sediment at the San Acacia gage is likely from tributary contributions downstream of the Bernardo gage.

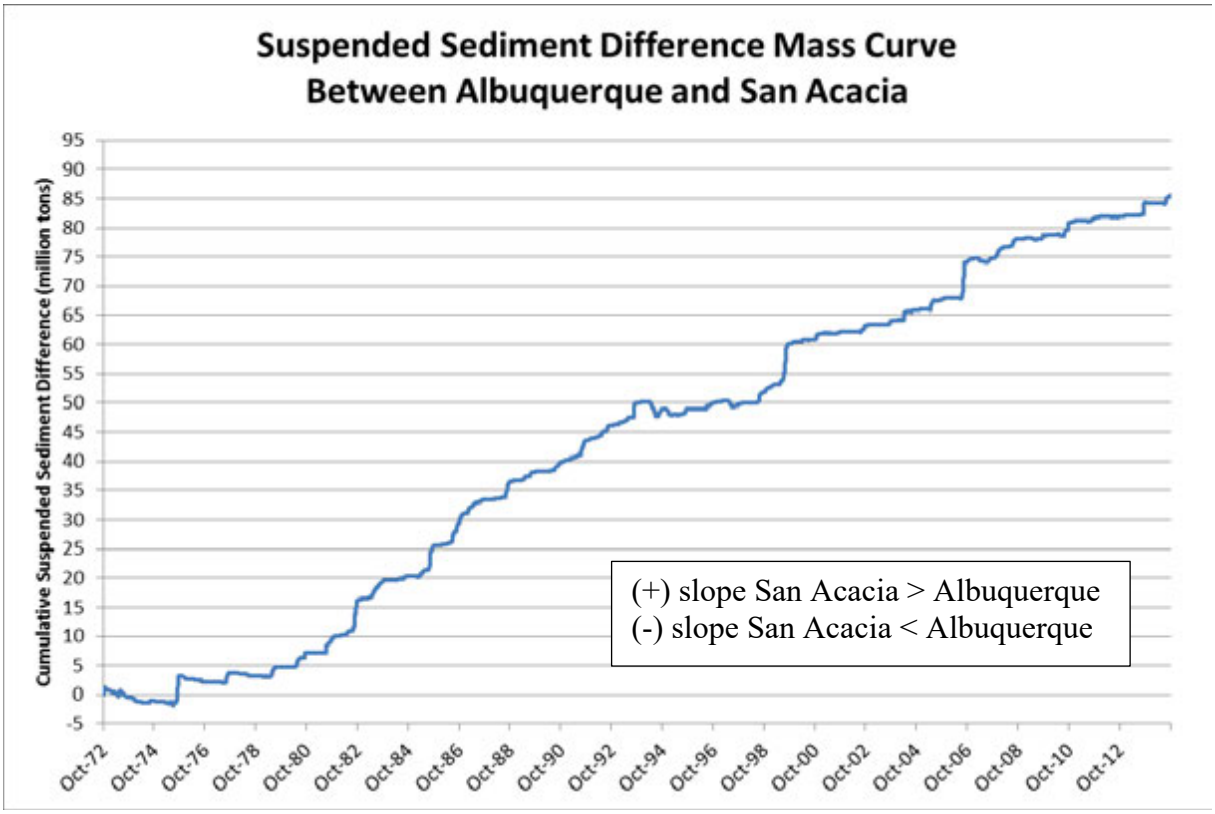

Figure 49. Suspended sediment difference mass curve between Albuquerque and San Acacia.

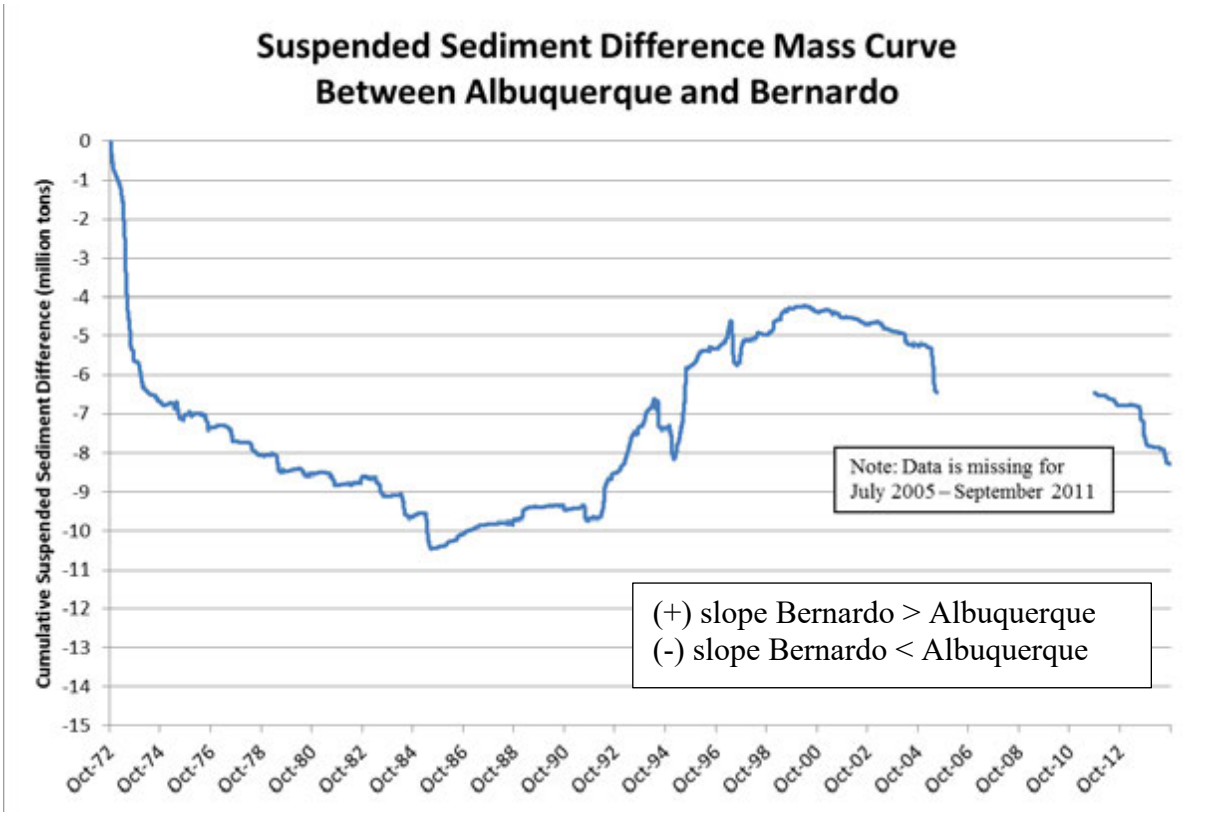

Figure 50. Suspended sediment difference mass curve between Albuquerque and Bernardo.

3.2.1.5 Seasonal effects on suspended sediment

Figure 51 through Figure 53 show the average daily suspended sediment concentration for various river flowrate bins based on data from water years 1995-2014. Figure 51 was built from data from the Albuquerque gage (USGS 08330000); Figure 52 was built with data from the Bernardo gage (USGS 08332010); and Figure 53 was built with data from the San Acacia gage (USGS 08354900).

For flows in July through October, the suspended sediment concentration tends to be higher than during others times of the year for the same flow. Also, March through June flows tend to have lower suspended sediment concentration than the rest of the year for the same flow.

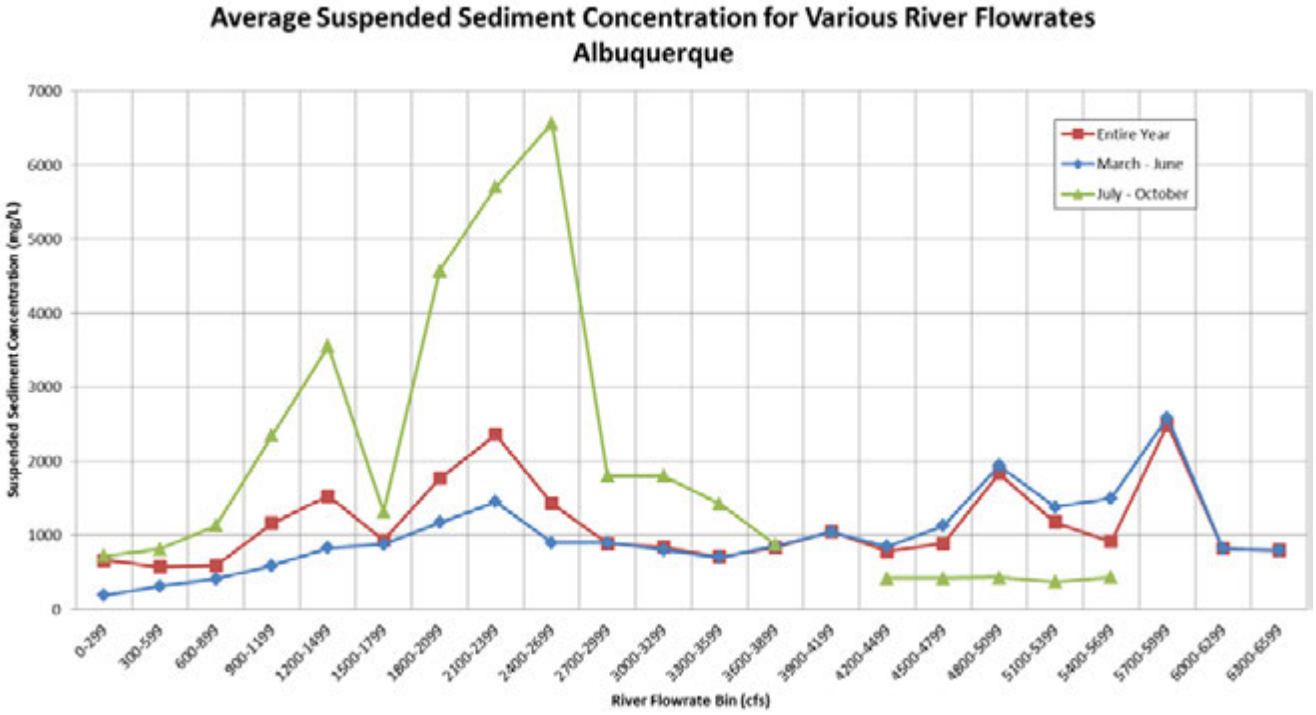

Figure 51: Average suspended sediment concentration for Albuquerque, 1995-2014

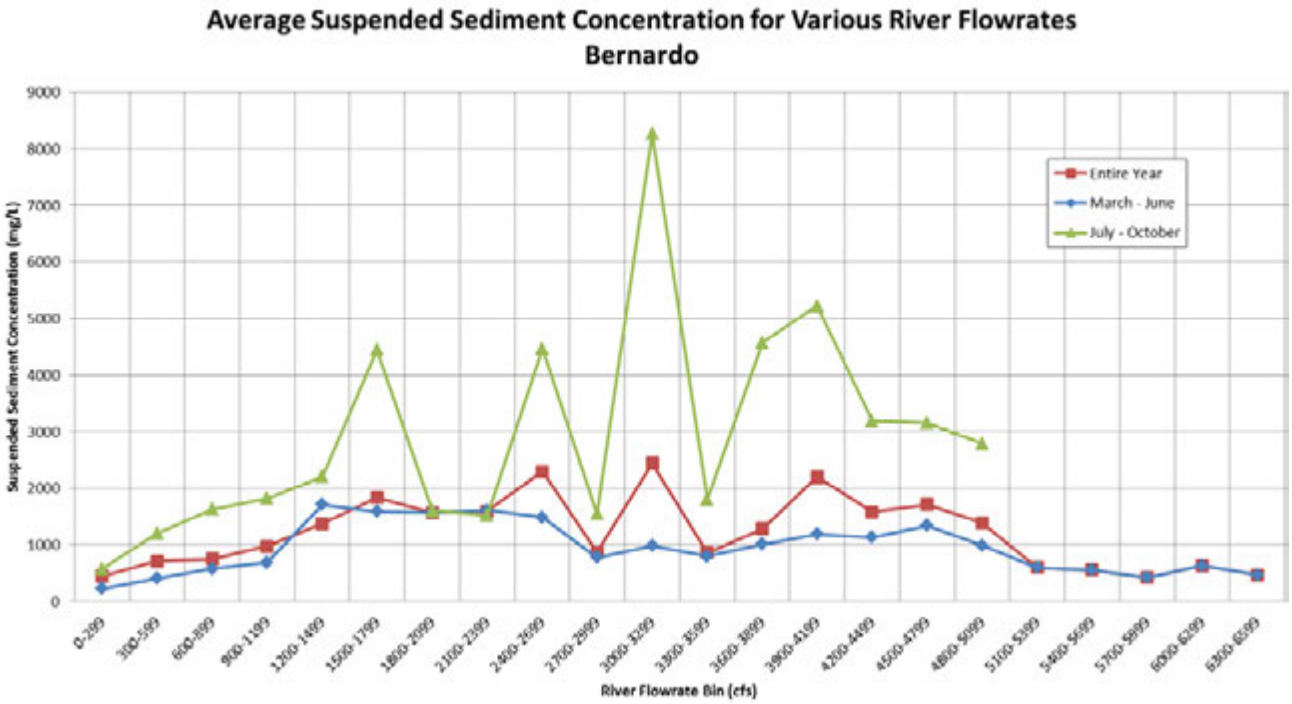

Figure 52: Average suspended sediment concentration for Bernardo, 1995-2014

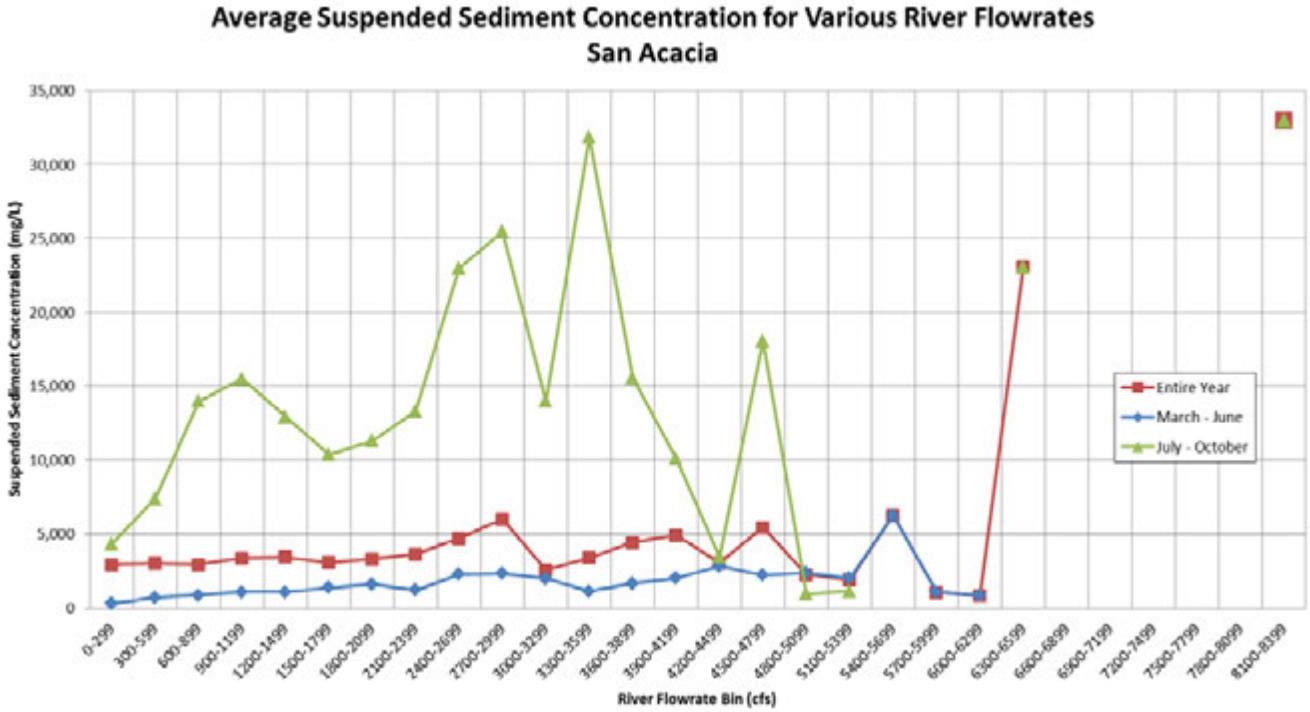

Figure 53: Average suspended sediment concentration for San Acacia, 1995-2014

3.2.1.6 Effective suspended sediment discharge

Figure 54 through Figure 56 show the suspended sediment rating curves at the USGS gages at Albuquerque (USGS 08330000), Bernardo (USGS 08332010) and

San Acacia (USGS 08354900) for water years 1995 through 2014. The Bernardo gage is missing data between July 2005 and October 2011.

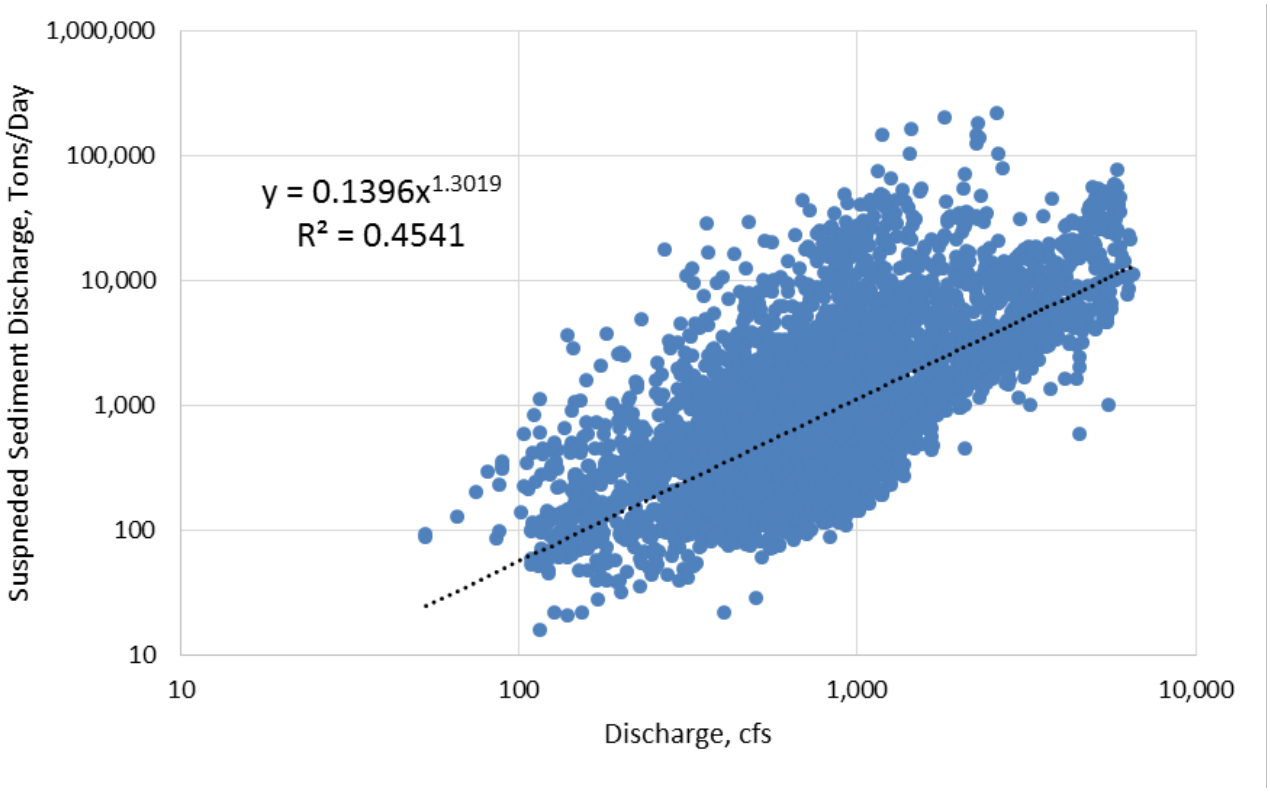

Figure 54: Suspended sediment rating curve at Albuquerque

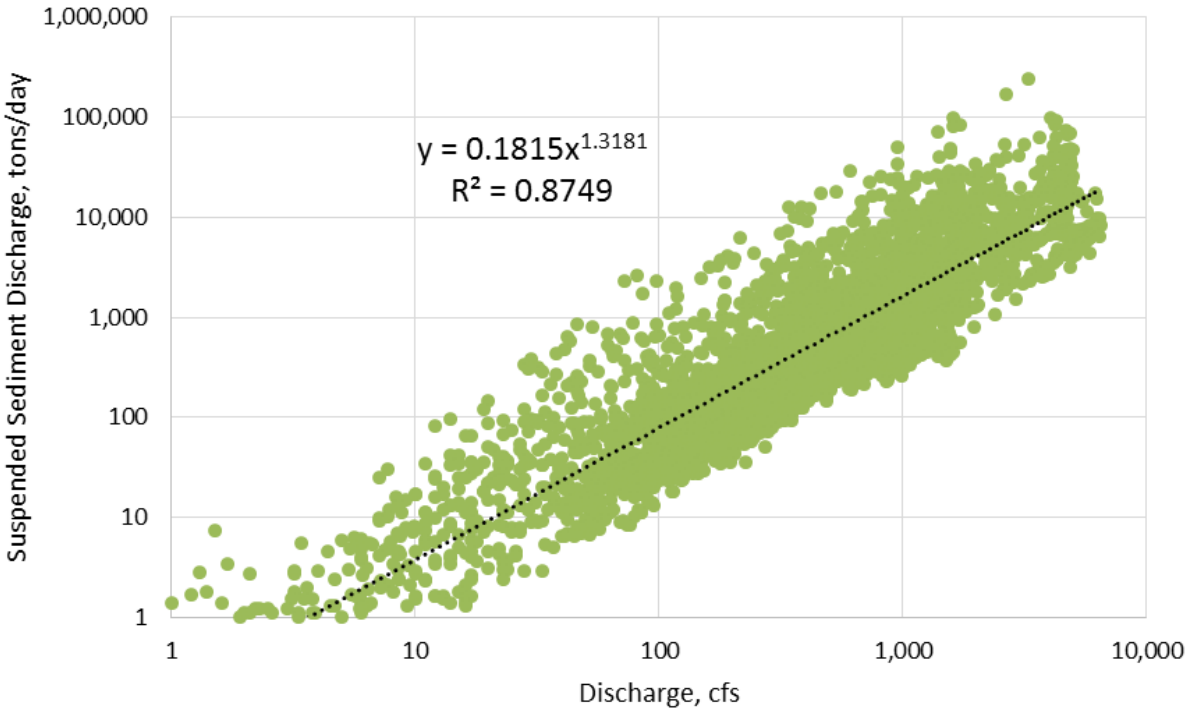

Figure 55: Suspended sediment rating curve at Bernardo

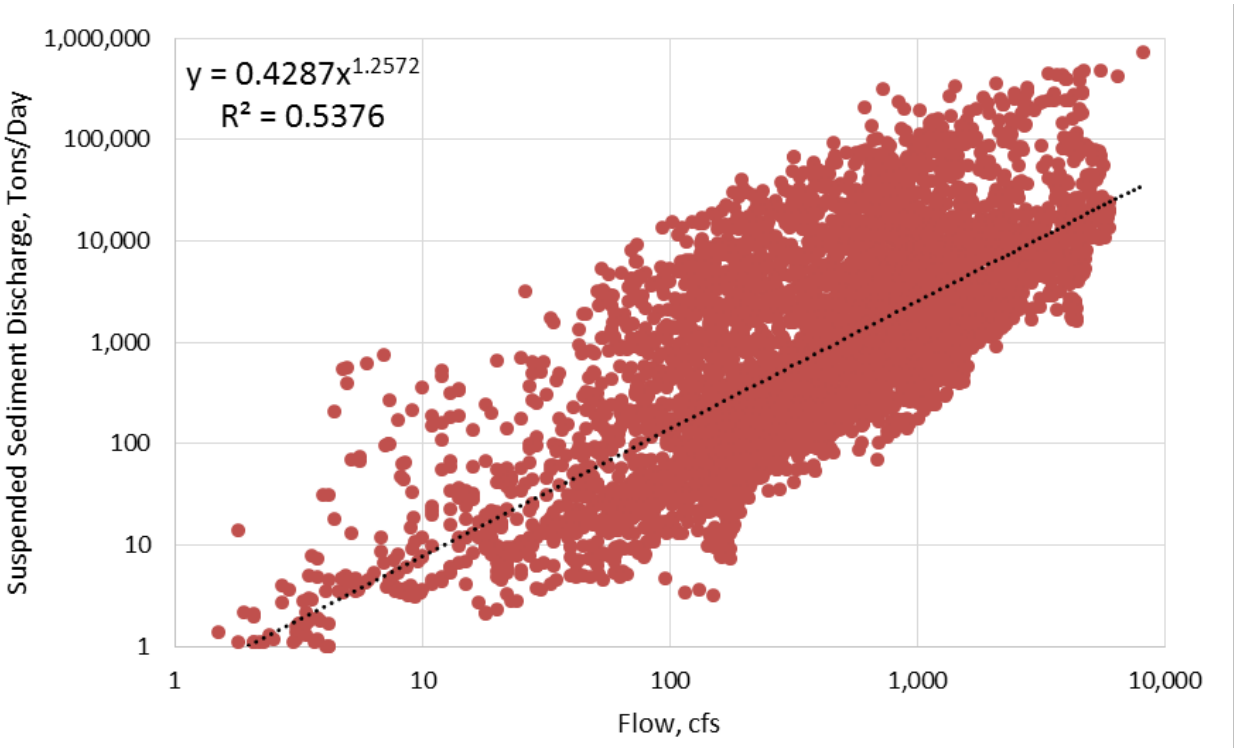

Figure 56: Suspended sediment rating curve at San Acacia

The typical procedure to develop effective discharge curves is to combine the flow-frequency distribution and the suspended sediment load rating curves to produce a suspended sediment load histogram which displays sediment load as a function of discharge for the period of record (Biedenharn, 2000). However, due to the poor trend between discharge and suspended sediment discharge in the three rating curves, direct measurements of the suspended sediment at specific discharges were used to develop the effective discharge relationships. Effective discharge curves were developed by totaling the tons of suspended sediment discharged at each gage between water years 1995 to 2014 for each river flowrate bin. These curves are shown in Figure 57 through Figure 59 for the Albuquerque through San Acacia gages. The effective discharge is the mean discharge value in the river flow rate bin that has moved the highest total amount of suspended sediment in the given time period.

The suspended sediment effective discharge values derived from this exercise are shown in Table 12. The table also includes values from an MEI analysis completed in 2002 which covered an analysis period of 1974 through 1998. It would be expected for the later analysis to have lower values since 1995-2014 covers a period of lower-than-average flows; however, this is not the case.

Table 12: Suspended Sediment Effective Discharge

USGS Gage	Suspended Sediment Effective Discharge (Q_{eff})	
	Current Analysis (1995-2014)	**MEI Analysis (1974-1998)**
Albuquerque	1,050 cfs	870 cfs
Bernardo	1,050 cfs	900 cfs
San Acacia	750 cfs	940 cfs

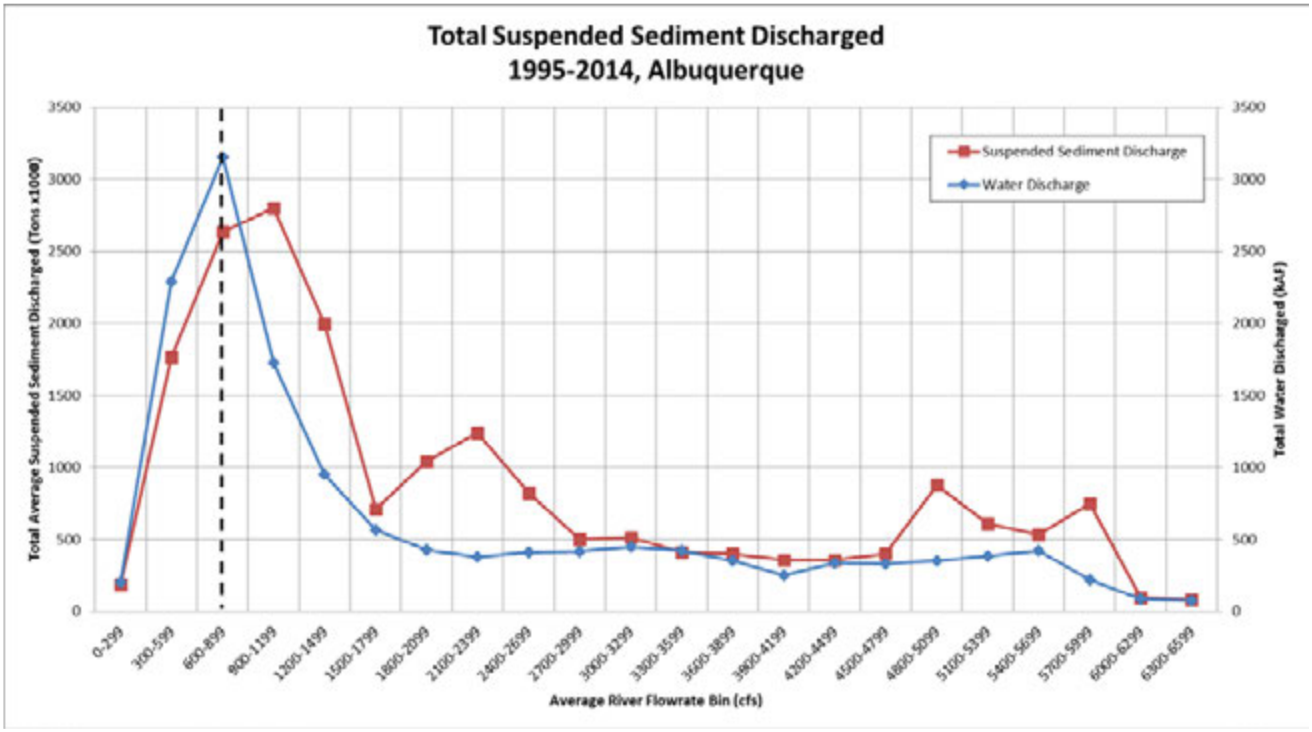

Figure 57: Total suspended sediment discharged between water years 1995 and 2014 for given river flow rates at the Albuquerque gage

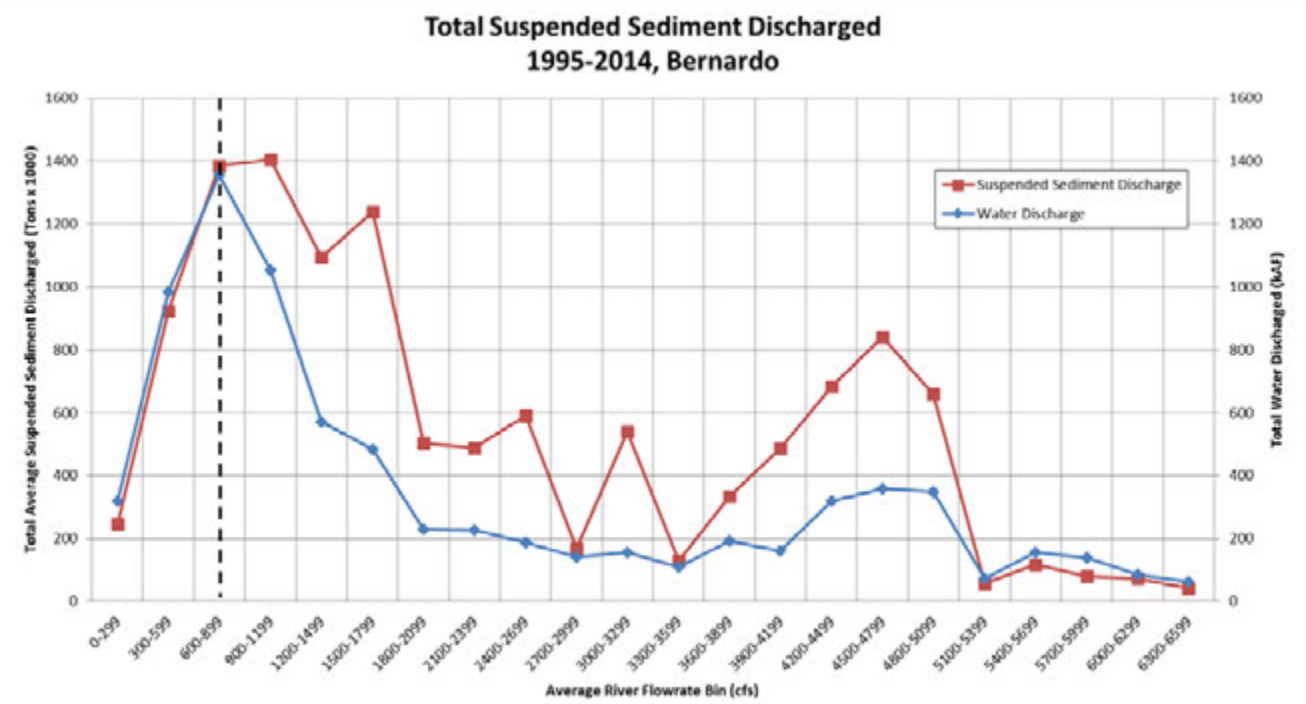

Figure 58: Total suspended Sediment discharged between water years 1995 and 2014 for given river flow rates at the gage near Bernardo

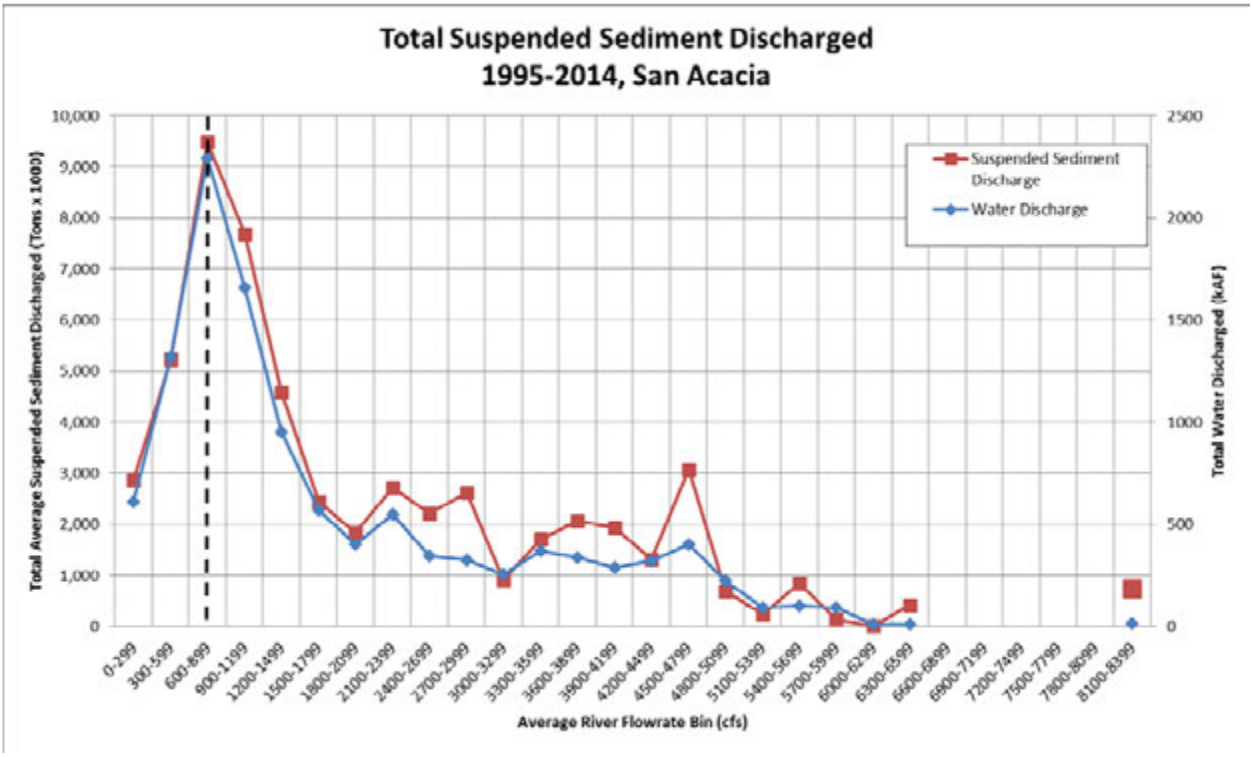

Figure 59: Total suspended sediment discharged between water years 1995 and 2014 for given river flow rates at the San Acacia gage

3.2.2 Total Load

3.2.2.1 Total Load Curves

Total load curves provide a contemporary estimate of the sediment load moved by various discharge levels at different seasons. Total load was calculated using the BORAMEP program, as described below, using sediment data from the USGS gage "USGS 08354900 Rio Grande Floodway at San Acacia, NM" for water years 1995 through 2014.

The suspended sediment data was downloaded from the section titled "Daily Data." The total load data was calculated with the BORAMEP program using data downloaded from the USGS gage section titled "Field/Lab Water-Quality Samples." It should be noted that the data downloaded from this section did not have readings spaced on regular intervals. The readings sometimes occurred multiple times per month and sometimes skipped months. Also, there were many instances (particularly common after 2005) where data was split between two or three samples taken on the same day or a few days apart. The data that was split was manually merged, given that the data was at most one day apart. Also, after March 11th, 2010, the USGS moved the average velocity data to a different column in the field report and the new location was not readable by the BORAMEP translation program. Thus the total load was not calculated after this date.

The USGS data file was downloaded in the format specified by Reclamation's BORAMEP report (Holmquist–Johnson, 2009), and then run through the program "Translate Raw USGS download 03-13-09.xls." The resulting output file was then used as input in the BORAMEP program, and that output file provided total sediment load in tons per day for the available dates.

The data for Figure 60 through Figure 66 comes from the BORAMEP output. The figures have been split by season and gradation type. Gravel was defined as being greater than 2 mm, sand was between 0.0625 mm and 2 mm, and silt/clay was less than 0.0625 mm (Wentworth, 1922). Total load calculations from the early 1990s through 2010 at the San Acacia USGS gage found that the predominant material transported by the river is sand (~68%). Finer material (silts and clays) constitutes around 32% of the total load at the San Acacia gage. The percentage of the total load moved by the Rio Grande past San Acacia that is sand has decreased from an average percentage of 73% in the 1990s to about 64% in the 2000s. The average percentage of finer material increased from about 27% in the 1990s to about 35%. The percentage of gravel moving also increased, but it is still had an average percent of the total load less than 1%. Sand loads were found to be 5 times greater during the summer/fall monsoonal period than the spring snow-melt runoff period up to a discharge of about 2,000 cfs. The primary sediment particles being mobilized in the Rio Grande past the San Acacia USGS gaging station therefore

are sand and finer material, being almost two orders of magnitude greater than the gravel movement.

Others (Nordin, 1963; Culbertson and Dawdy, 1964; Gorbach, 1996) have found that the movement of fine sediment (i.e. silts and clays) increases the transport of sand size particles. The Rio Puerco and Rio Salado are primarily driven by the summer rainfall-runoff period. The Rio Puerco carries a high silt load, along with sand (Nordin, 1963; Bryan and Post, 1972; Simons et al., 1981b)). The Rio Salado carries sand along with some gravel (Simons et al, 1981; MEI, 2002).

Figure 60 shows how gravel, sand, and silt/clay move for various river discharges, while Figure 61 shows the percentage of each sediment type relative to the total load. Trend lines were attempted to fit the data, but no strong correlations were found. This analysis revealed that data is better correlated when the sediment load is divided according to season as in Figure 62, Figure 63, and Figure 64 than when the load is not divided by season.

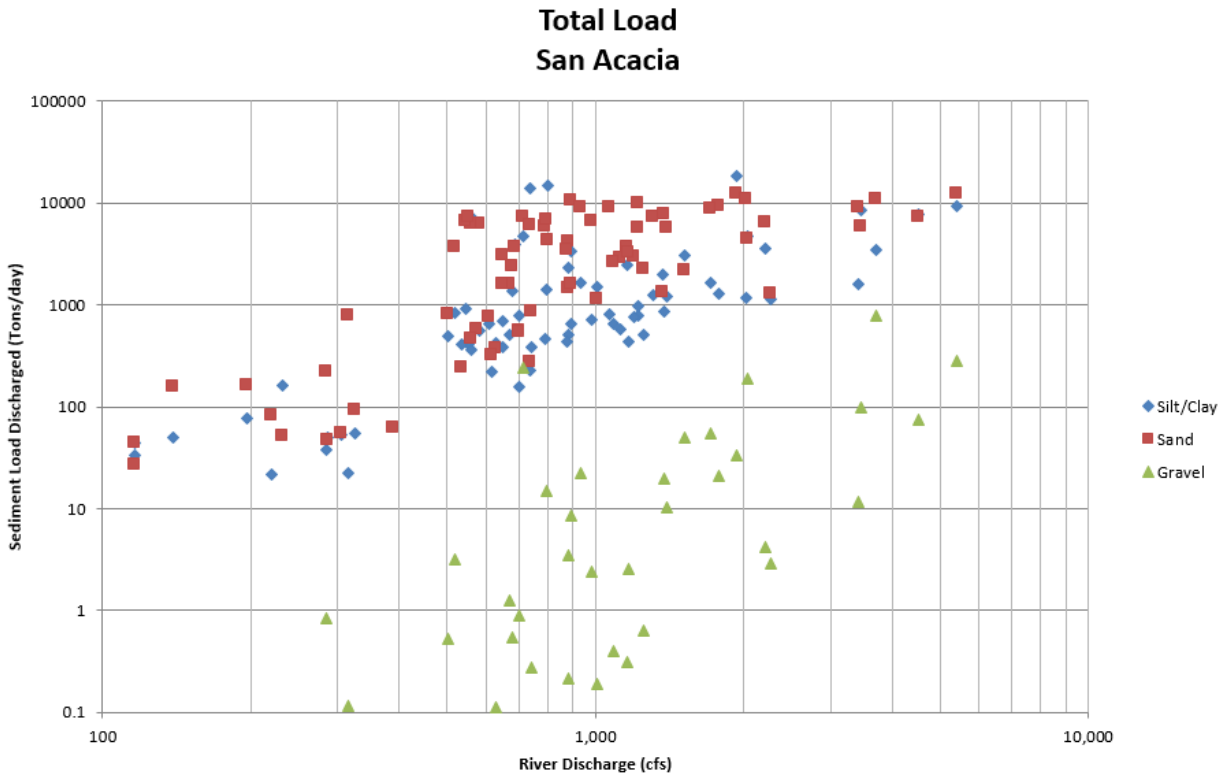

Figure 60: Sediment load graph comparing sediment type for various river discharges at San Acacia for water years 1995 through 2010 (gravel data points below 0.1 tons/day have been omitted)

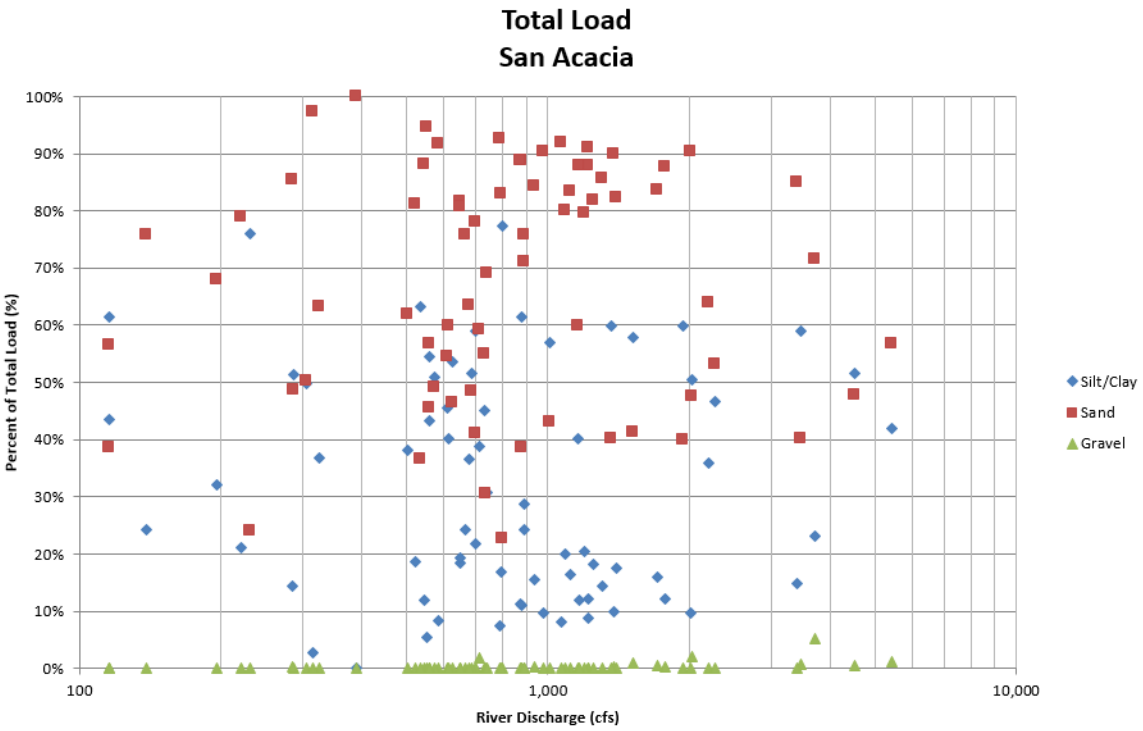

Figure 61: Percent of total load graph comparing sediment type for various river discharges at San Acacia for water years 1995 through 2010.

The movement of gravels on the Rio Grande is most noticeable during the spring snow-melt runoff time frame. Sand and smaller particles are transported during the spring snow-melt runoff period (March through June) and the summer rainfall-runoff period (July through October). Data for flows above 2,000 cfs is primarily from the spring snow-melt runoff period.

A trendline is shown in Figure 62 for the gravel discharged in spring runoff season, between March and June. However, the data points for the monsoon season's gravel discharge were scarce and often zero, and no trend could be found.

Trendlines showing expected sand discharge for various river flowrates are shown in Figure 63.

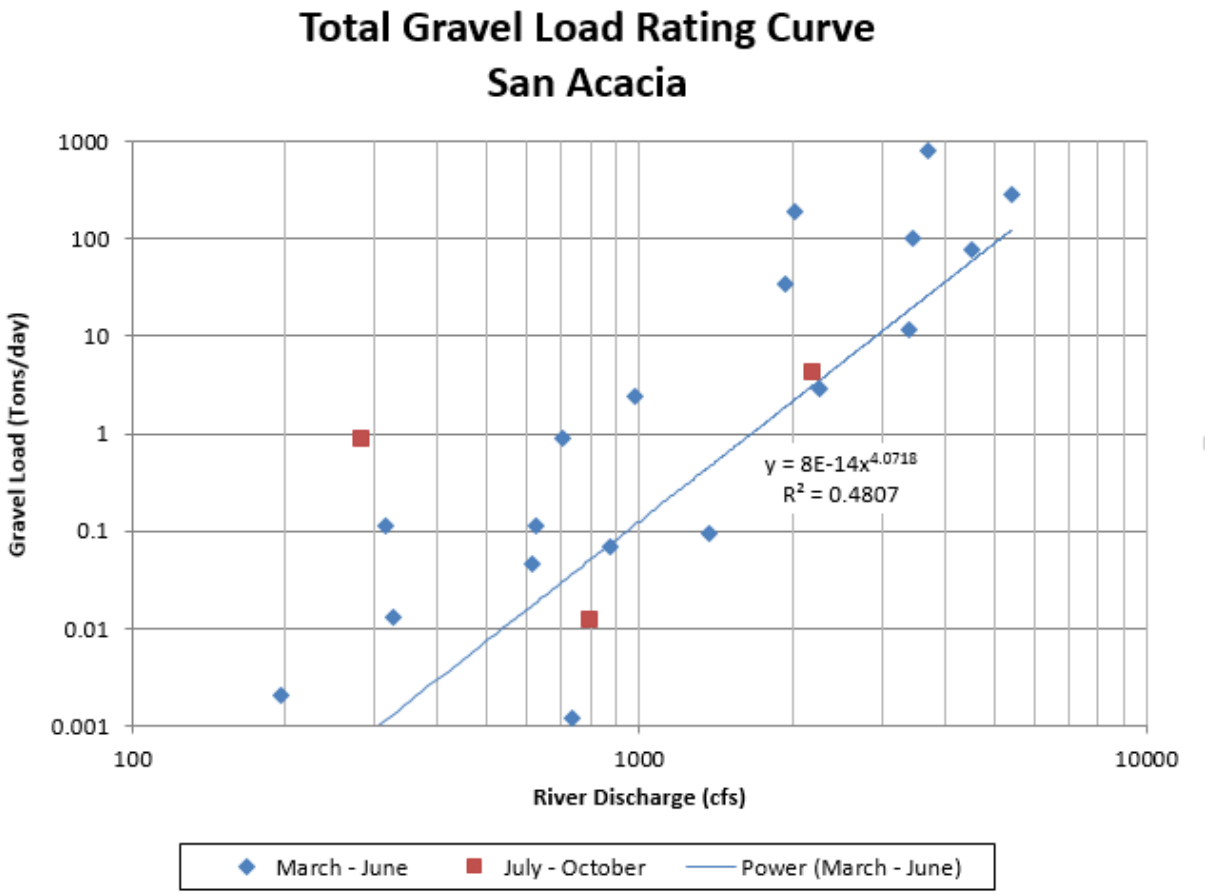

Figure 62: Total load rating curve for gravel at San Acacia for water years 1995 through 2010 (gravel data points below 0.001 tons/day have been omitted)

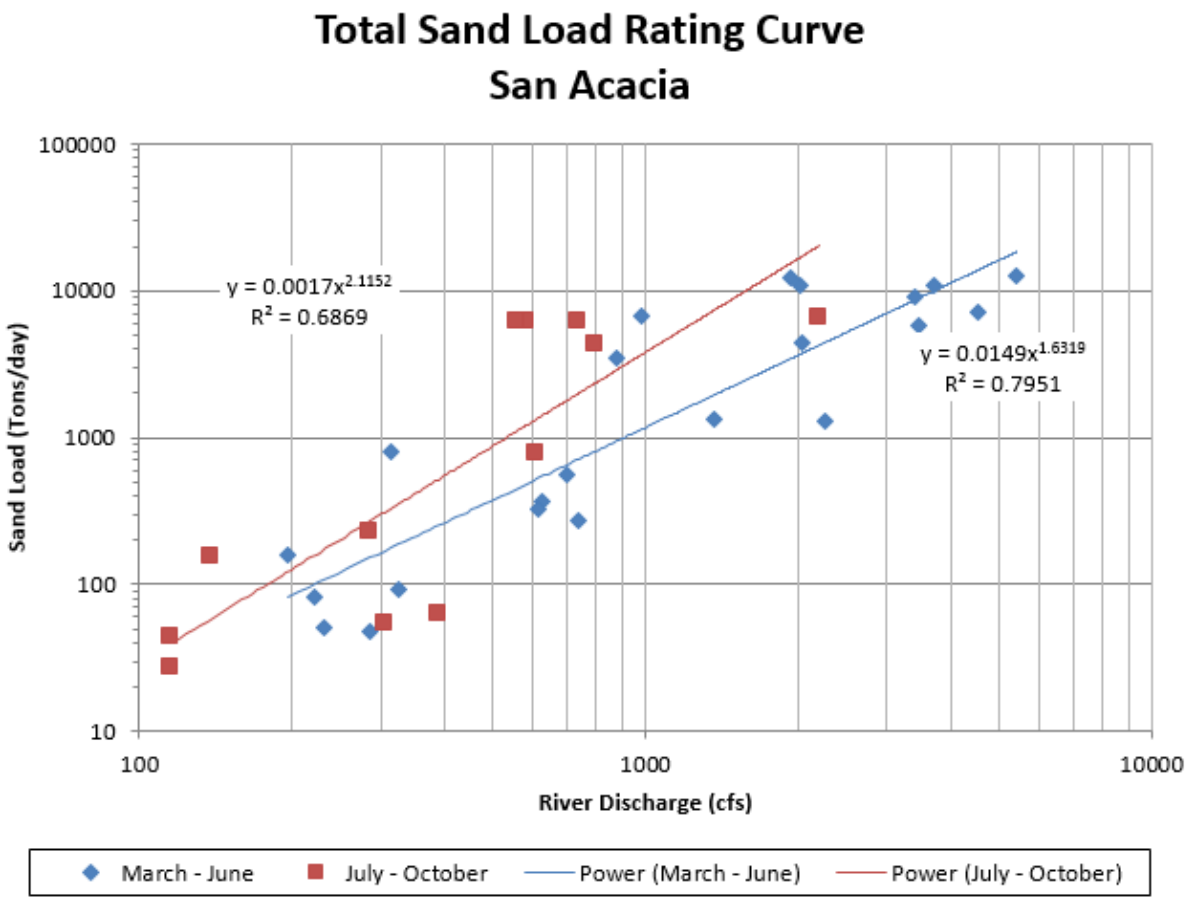

Figure 63: Total load rating curve for sand at San Acacia for water years 1995 through 2010

Figure 64 shows a trendline for the spring runoff season silt and clay load. However, the data for the monsoon season was sparse and widely varied, and no trend could be found.

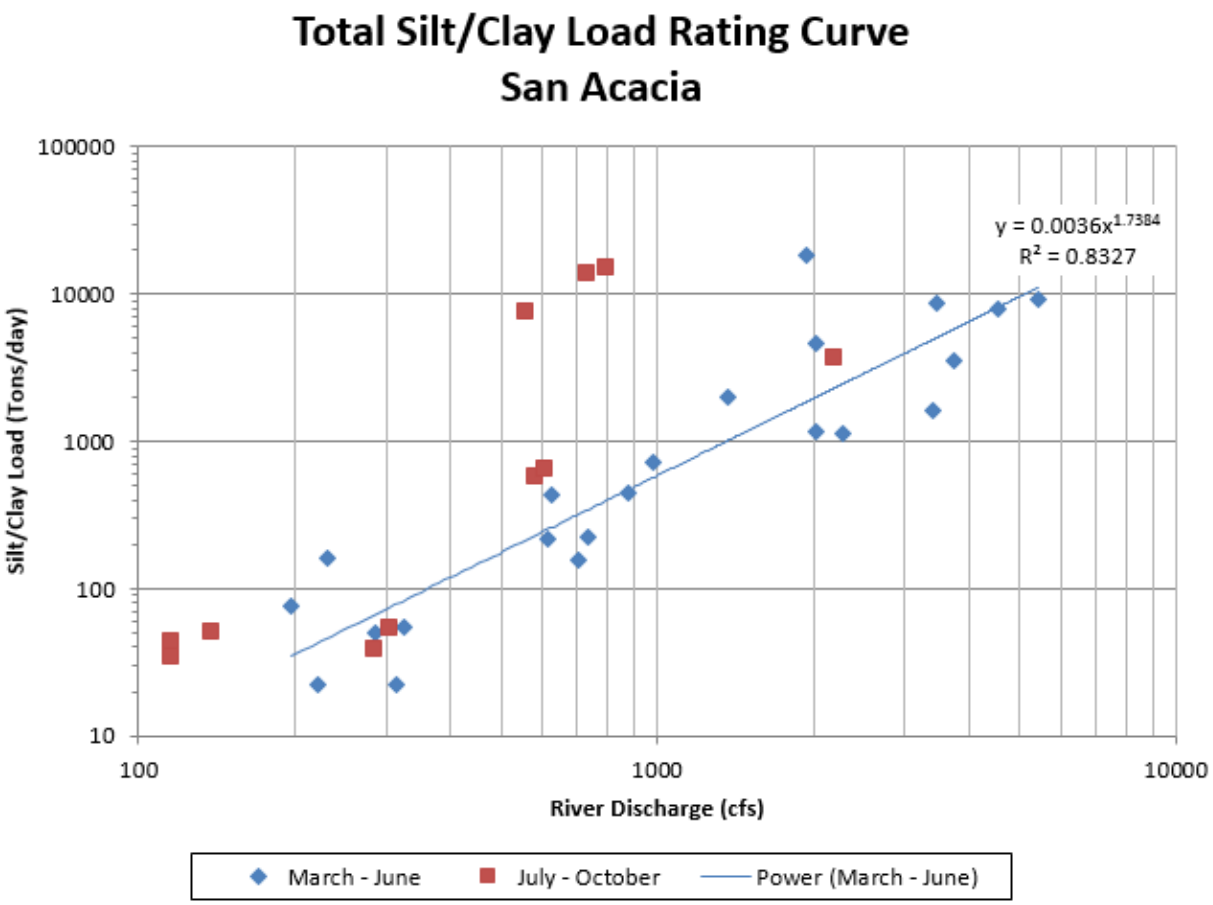

Figure 64: Total load rating curve for silt/clay at San Acacia for water years 1995 through 2010

Figure 65 shows the total load rating curve for all total load data points available between 1995 and 2010.

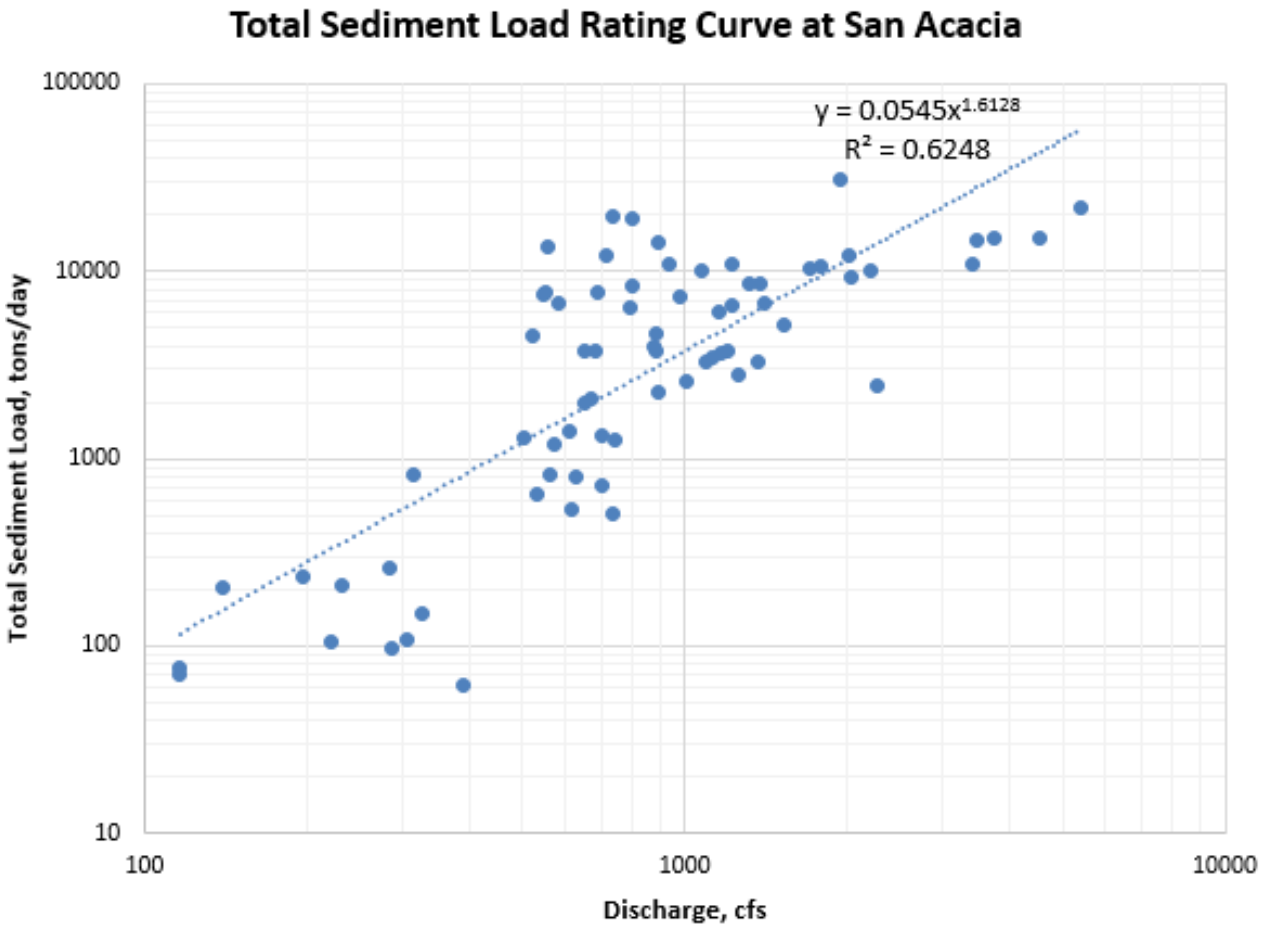

Figure 65: Total Load Rating Curve at San Acacia for water years 1995 through 2010

3.2.2.2 Total Load Effective Discharge Curves

Figure 66 shows the total load effective discharge curve for San Acacia. To create the effective discharge curve, the total load rating curve's trendline equation (Figure 65) was used to generate an expected total load for a given discharge bin. This value was then multiplied by the fraction of time that the daily average discharge fit in that bin out of all the days in the analysis period. Also, the median river discharge value for each bin was multiplied by the fraction of time that the daily average discharge fit into that bin out of all the days in the analysis period. The incremental water discharge volume is also displayed on the effective discharge curve.

The effective discharge curve shows that the highest incremental load for both sediment and water is at 750 cfs. In 2002, MEI found that the total load effective discharge at San Acacia was 940 cfs. Their period of analysis covered 1974 through 1998. It is expected that the current analysis would have a lower value than MEI since 1995-2010 covers a drought period.

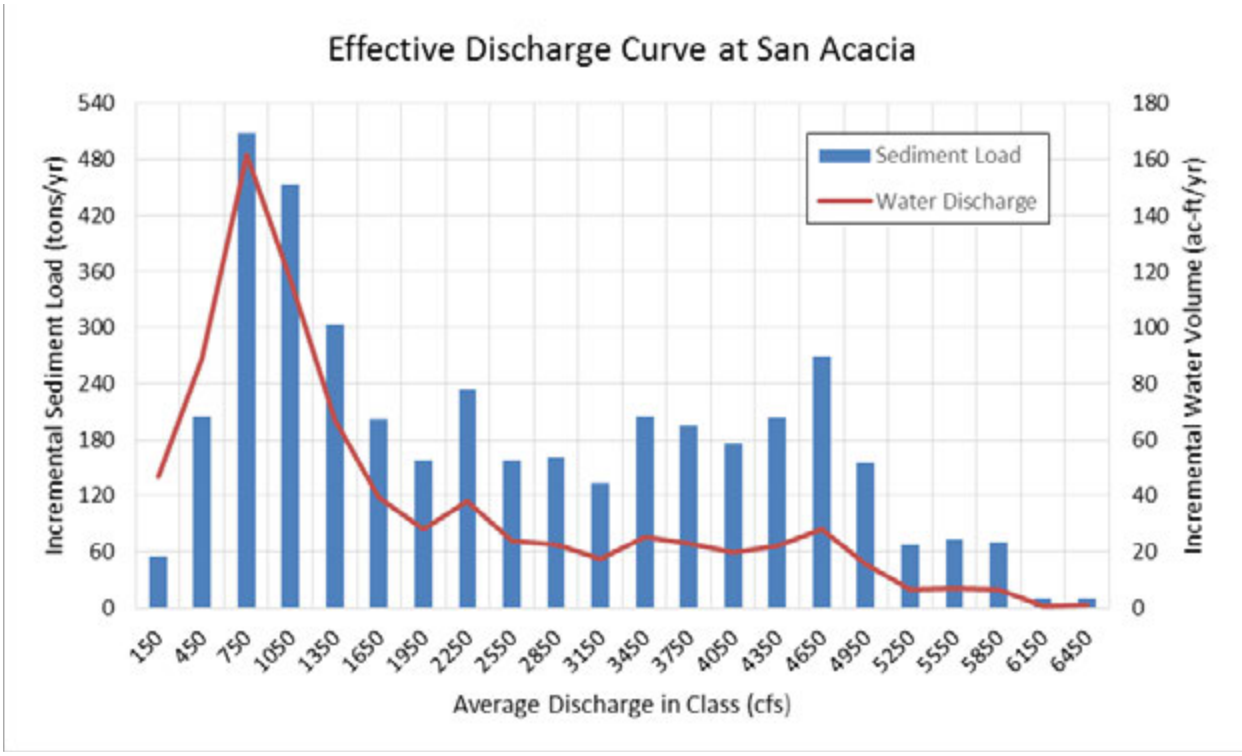

Figure 66: Total Load Effective Discharge Curve at San Acacia for water years 1995 through 2010

Figure 67 shows the average total load sediment discharge grouped into river flowrate bins for water years 1995 to 2010 at San Acacia by sediment type. This graph shows the predominance of sand and finer material over gravel at all evaluated discharge values.

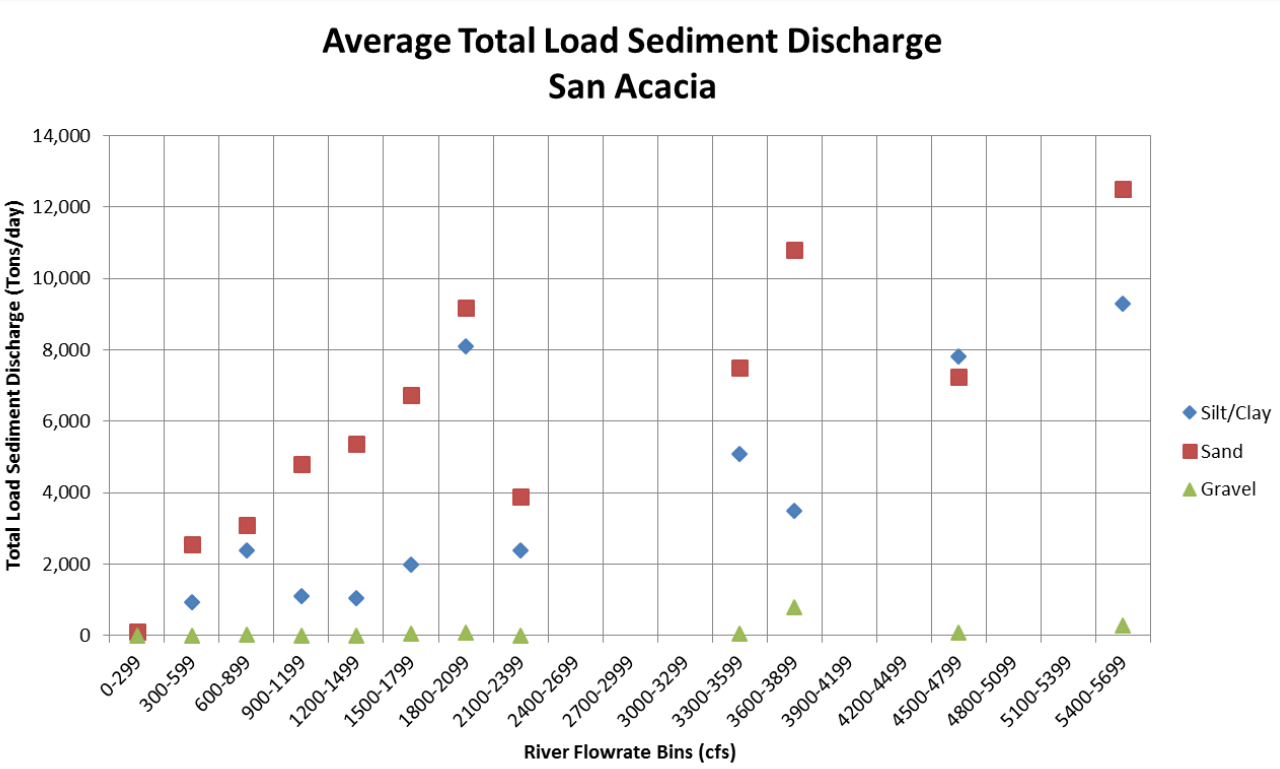

Figure 67: Average total load sediment discharge grouped into river flowrate bins for water years 1995 to 2010 at San Acacia

4.0 Assessment of Geomorphic Parameters

There are six geomorphology parameters used to assess and define changes occurring between Isleta and San Acacia Diversion Dams on the Middle Rio Grande, as defined by Makar and AuBuchon (2012). These include the following parameters: channel width, channel planform and location, channel slope, channel sinuosity, bed material size and type, and channel and floodway topography. An analysis of the data over time helps reveal patterns in these parameters, which coupled with trends observed in the drivers, help identify and elucidate observed geomorphic trends for this reach.

A summary of the major observations for the six analyzed geomorphic parameters are as follows:

- The average and range of the active channel width has decreased throughout the Isleta to San Acacia reach of the Rio Grande since the 1960s. The average active channel width in 2016 for the Isleta to Rio Puerco reach was just under 180 feet, while the Rio Puerco to San Acacia

reach was just over 150 feet (4.1 *Channel Width* p. 90 and 4.6 *Channel and Floodway Topography* p. 136).

- The constructed spoil levee widths have the same tendency as the valley width trends. The current active channel width only slightly reflects the valley width trends. (4.1.1 *Longitudinal Channel and Valley Width Schematic* p. 91).
- The Rio Grande planform between Isleta and San Acacia Diversion Dams has shifted from a multi-threaded channel to a primarily single thread channel between the 1990s and early 2010s (4.2.1 *Planform Classification on the Rio Grande* p. 95).
- Potential exists for the river to deepen and narrow, which may create a tendency for banks to laterally migrate. A higher terrace adjacent to the active channel in the Rio Puerco to San Acacia reach may also create a tendency for banks to laterally migrate (4.2.1 *Planform Classification on the Rio Grande* p. 95.)
- Vegetation has influenced the river planform since the early 1990s. Vegetation cover has increased as much as 20% on the Rio Grande since the 1990s, which has affected the local sinuosity and reach width (4.2.1 *Planform Classification on the Rio Grande* p. 95 and 4.2.3 *Vegetation Trends* p.111).
- Vegetation has influenced the Rio Puerco in the reach downstream of the railroad crossing, increasing the local sinuosity and narrowness (4.2.2 *Planform Classification on the Rio Puerco* p. 108).
- The number of mid-channel bars peaked in the reach between Isleta and San Acacia around the mid-1990s. The area encompassed by the mid-channel bars peaked in the early 2000s. The number and area of mid-channel bars has decreased since those peaks as mid-channel bars have become attached to the banklines (4.2.4 *Island Trends* p. 116).
- The slope of the Rio Grande through the Isleta to San Acacia reach has decreased from the 1980s to early 2010s. The slope of the Rio Grande from Isleta to the Rio Puerco has decreased from the 2000s to the early 2010s, while the slope of the Rio Grande from Rio Puerco to San Acacia has increased during the same time (4.3 *Channel Slope* p. 119).
- Temporal changes in the longitudinal mean channel bed profiles between Isleta and San Acacia Diversion Dam suggest a general degradational trend. The Isleta Diversion Dam to Los Lunas (NM 6 Bridge) has shown little net change, fluctuating between cycles of aggradation and degradation. Los Lunas to Abo Arroyo shows a slight degradational trend, while Abo Arroyo (and especially from around the U.S. 60 Bridge and downstream) there is a strong degradational trend, except around the Rio Salado. The mean bed elevations from the Rio Salado (both upstream and downstream) have generally tended towards an aggradational state (4.3 *Channel Slope* p. 119).
- The sinuosity of the Isleta to Rio Puerco geomorphic reach is currently increasing. A slight increase in the sinuosity occurred in this reach in the 1950s, but this is still lower than the sinuosity currently observed. The Rio

Puerco to San Acacia geomorphic reach is currently experiencing a slight increase, with a large peak in the early 1960s (around 1.17) and a moderate one in the late 2000s (around 1.11) (4.4 *Sinuosity* p. 126).

- Bed material tends to be coarsening between the Isleta and San Acacia diversion dams. Shear stress and particle stability analysis on the bed material particle shows that bed material is unstable except around the Rio Salado confluence (4.5 *Bed Material Size and Type* p. 127).
- An assessment of the channel and floodway topography between the mid-1990s and mid-2010s indicates that in some areas (between Los Lunas and Casa Colorado and upstream of San Acacia Diversion Dam) the river has incised. But there are other areas (Isleta Diversion Dam to Los Lunas and Casa Colorado to just upstream of San Acacia Diversion Dam) where the river has aggraded the same order of magnitude. The change in the bank height follows a similar trend. The increase in bank height is due to a combination of channel incision and vertical accretion of sediment on mid-channel bars and at the bankline (4.6 Channel and Floodway Topography p. 136).
- The Rio Grande between Isleta and San Acacia has various terrace surfaces. Between Isleta Diversion Dam and Tome, NM the active channel is slightly perched relative to the adjacent floodplain. From Abeytas, NM to San Acacia Diversion Dam a majority of the floodplain surfaces are high and elevated above the active channel. The area between Tome, NM and Abeytas, NM has a mix of these two characteristics (4.7 Terrace Mapping p. 150).

4.1 Channel Width

The Rio Grande flows through a geological feature called the Rio Grande rift, which separates the Great Plains region from the Colorado Plateau (Bauer, 2000; Berry and Lewis, 1997). The valley morphology has been relatively consistent over the last several thousand years, with a series of wide basins and narrow canyons. The Belen basin begins at the northern portion of this study reach where the valley narrows at the Isleta canyon. The Belen basin ends at the San Acacia canyon, which is at the downstream end of the study reach (Bauer, 2000; MEI, 2002). Both anthropogenic and natural climate changes have affected the width of the Rio Grande in the last couple of centuries. In the late 1800s through the early 1900s the loss of water to irrigation and the increased sediment loading from the tributaries caused the river to become wider and shallower (Crawford et al., 1993; MEI, 2002). The average channel width in 1918 was around 1300 feet on the upstream end of the reach and around 2100 feet on the downstream end. In 1918 the minimum channel width was around 800 feet and the maximum channel width was around 7500 feet, with a greater diversity in channel widths at the downstream end of the study reach (MEI, 2002). The channel has generally narrowed between the Isleta and San Acacia diversion dams since 1918 due to a combination of infrastructure building, channelization, reduction in peak flows,

upstream sediment reduction, and vegetation encroachment (Culbertson and Dawdy, 1964; Crawford et al., 1993; Berry and Lewis, 1997; Bauer, 2000; MEI, 2002; Bauer and Hilldale, 2006; Tashjian and Massong, 2006; Parametrix, 2008; Bauer, 2009; Makar, 2010; Makar and AuBuchon, 2012; Baird, 2014). This reduction in the channel width has also resulted in a more uniform distribution of channel widths (Crawford et al., 1993; Parametrix, 2008; Makar and AuBuchon, 2012).

4.1.1 Longitudinal Channel and Valley Width Schematic

Brierly and Fryirs (2005) outline a watershed geomorphic analysis approach that helps present a reach perspective. Figure 68 shows a graphical expression of the channel, spoil levee, and valley widths between Isleta Diversion Dam and San Acacia Diversion Dam for 2012. The canyon and basin morphology of the valley is evident in this schematic. The channel and spoil levee widths are on the same scale, but the valley widths are on a separate scale. The graphical expression of the widths is not centered on the river centerline, but rather symmetrically arranged along an imaginary line. This configuration then does not reflect the sinuosity around bends.

The channel, spoil levee, and valley widths were drawn using ESRI's ArcMap (version 10.4.1). A combination of aerial images, DEMs, and hillshade layers were used to delineate the centerlines and borders of the valley and the spoil levees. The hillshade and DEM files were produced by Intermap using Interferometric Synthetic Aperture Radar (IfSAR). The data was collected between 2007 and 2008 and was accurate to 2 meters RMSE horizontally and 1 meter RMSE vertically. Reclamation contractors developed channel centerlines and active channel borders from aerial imagery taken in 2012. The 2012 active channel was used to delineate the current channel width.

For this exercise the active channel was defined as that portion of the stream showing signs of actively being re-worked (no vegetation present). The spoil levee borders were roughly drawn to the spoil levee centerline. The valley was defined as the terrain area surrounding the active channel area that had a gentler topography than the adjacent mountainous regions. The valley width polygon included the area covering the active channel width polygon. Topography identification was qualitative and consisted of identifying definable geographic features that marked a significant slope change. For instance, the bottom of a steep mountain slope and the bottom edge of a rock wall are readily identifiable topographic areas that were used to delineate the edges of the valley. At tributary junctions the valley edge was defined by the confining valley edges on either side of the tributary.

These valley, spoil levee, and active channel borders were developed into polygons, split into segments, and each segment's area was determined. The valley, spoil levee, and active channel centerlines were also split into segments

and each segment's length was determined. The width for each segment was determined by dividing the segment's area by its length.

The x-axis distance on the figures corresponds to the length of the river (channel centerline) from Isleta Diversion Dam to San Acacia Diversion Dam.

From Figure 68 it can be seen that the constructed spoil levee widths have the same tendency as the valley width trends. It is also evident that south of the Rio Salado the valley width is the main lateral constraint on the river, as there is a spoil levee only on one side of the river. The current active channel width only slightly reflects the valley width trends, indicating that there are other influences beyond the placement of spoil levees that narrowed the active channel.

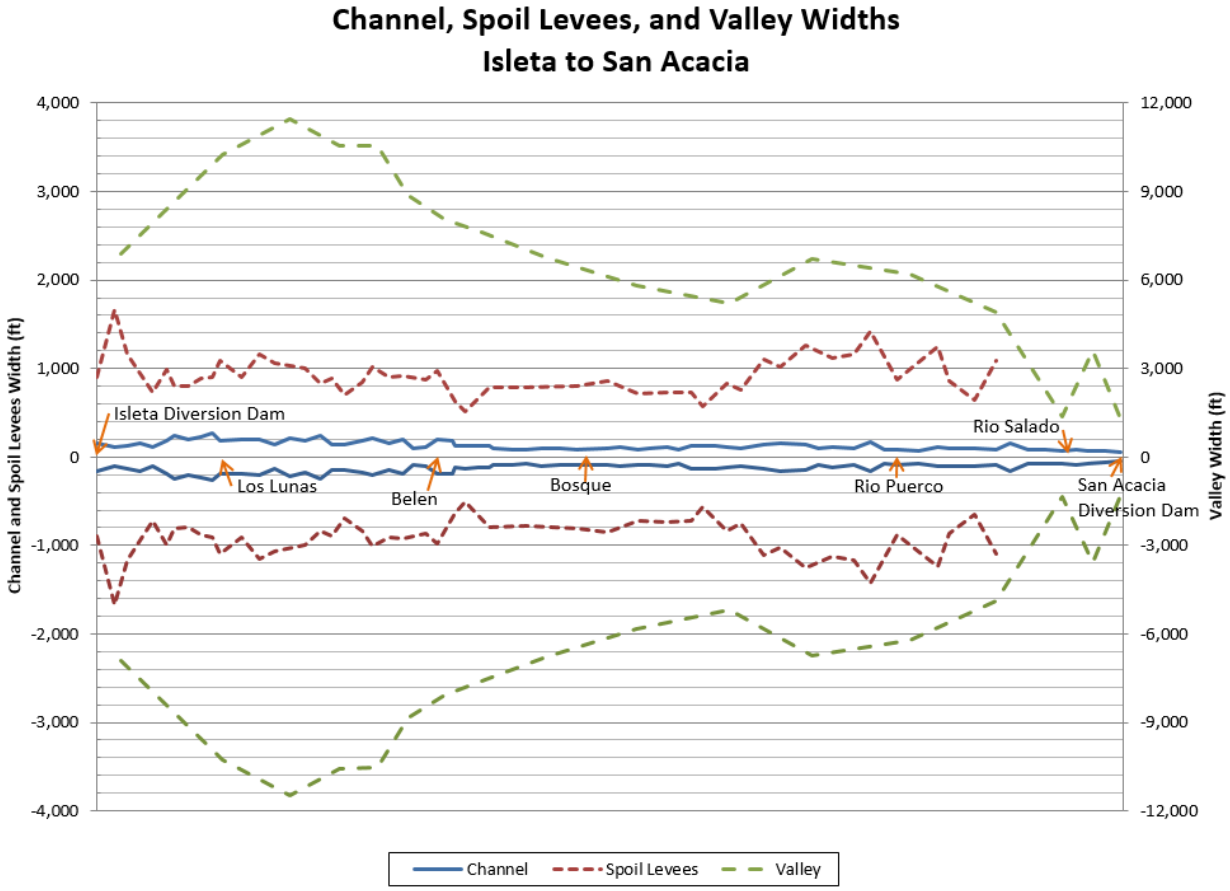

Figure 68: Longitudinal Channel (2012), Spoil Levee, and Valley Width Schematic. The spoil levee does not continue to San Acacia Dam on the east side and thus the width is not measurable.

4.1.2 Average reach width

Figure 69 and Figure 70 show the channel width over time for the study reach broken down into two geomorphic reaches: Isleta Diversion Dam to the Rio Puerco confluence and the Rio Puerco confluence to the San Acacia Diversion

Dam. The figures graphically show the active channel width, averaged along the aggradation-degradation lines within each geomorphic reach. The years analyzed were 1962, 1972, 1985, 1992, 2002, 2006, 2012, and 2016. For 1962 through 2012 the active channel widths were extracted along the established aggradation-degradation lines. The extracted width for the lines in each of the geomorphic reaches was then averaged to obtain the average reach width. The 2016 imagery was the only year that was not averaged along the aggradation-degradation lines; instead, one polygon was created for the entire active channel and the polygon's area was divided by the length of the channel centerline to obtain the average geomorphic width. Smaller polygons within each geomorphic reach were mapped in areas of similar width. The area of this polygon divided by the length of the channel centerline through that polygon gives an average channel width for that section. The range of widths for all of the mapped polygons in each geomorphic reach provides a range. The maximum and minimum from this range are shown in Figure 69 and Figure 70.

The minimum channel width has remained nearly the same from the 1960s until 2016, while the average and maximum channel widths have decreased. For the Isleta to Rio Puerco reach a decrease in the average active channel width occurred around 1992, while for the Rio Puerco to San Acacia reach this decrease occurred in the mid-1980s. The increase in channel width, observed in the Isleta to Rio Puerco reach in the 1980s, is believed to have been the results of a combination of a mechanical vegetation removal program (this program stopped around the mid-1980s) and large spring runoff flows that kept the active channel wider. (Bauer and Hilldale, 2006; Makar et al., 2006; Parametrix, 2008). The average active channel width is currently wider for the Isleta to Rio Puerco reach (~177 feet) than the Rio Puerco to San Acacia reach (~154 feet). The predicted future trend on the Rio Grande is continued narrowing (Vensel et al., 2006; Bauer. 2009). The 1961 Reclamation channel width equation, however, predicts a range of active channel widths between 150 and 190 feet for the Isleta to Rio Puerco reach (Baird, 2014), which is similar to the observed channel width in 2016.

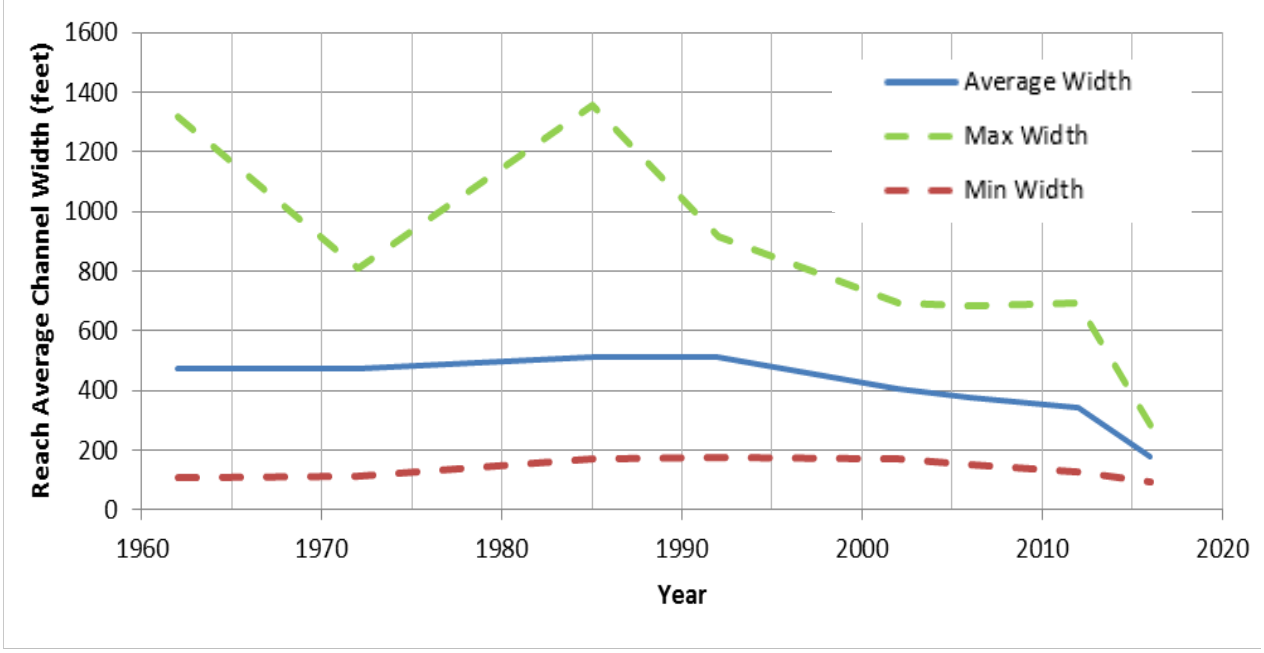

Figure 69. Average, Max, and Minimum Channel Widths for Isleta to Rio Puerco

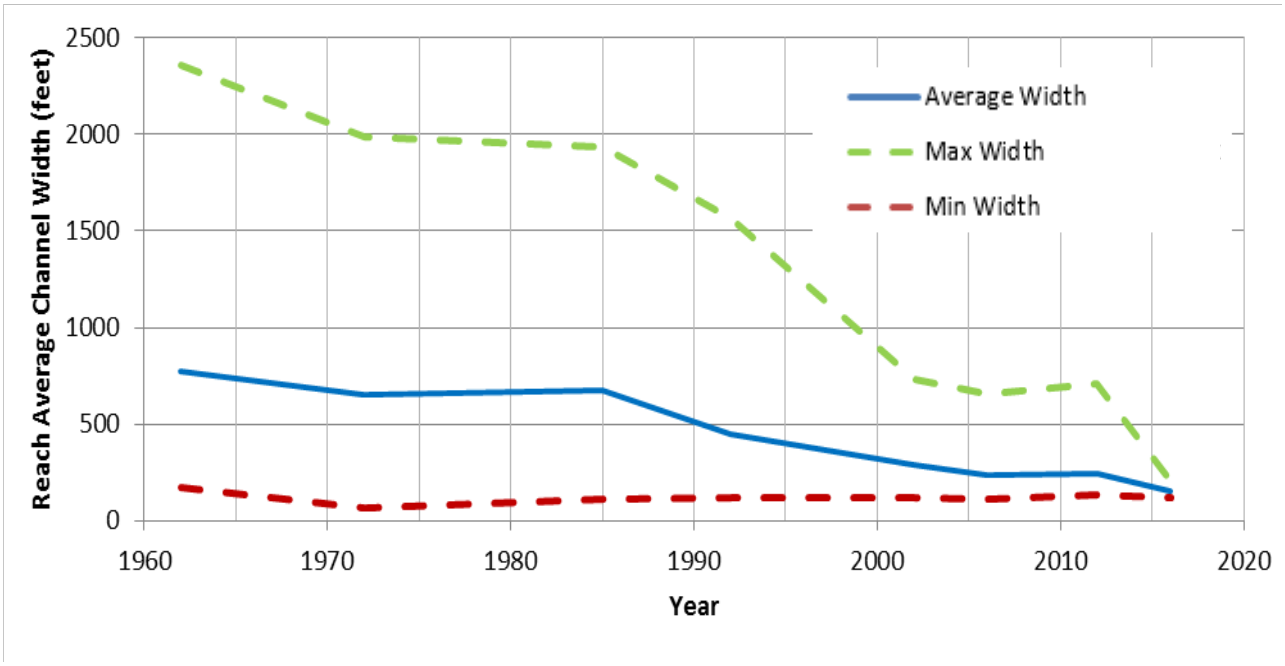

Figure 70: Average, Max, and Minimum Channel Widths for Rio Puerco to San Acacia

4.2 Channel location/planform

How the channel shape changes over time gives insight into the geomorphic trends. The channel shape is affected by the drivers (water and sediment supplied to the reach) and long term trends give insight into future channel movement. The Rio Grande in the 15th century was described as being a relatively deep waterway

with a low sediment load. The sediment load increased from the 16th to the mid-19th centuries creating a wider and shallower river system (Finch and Tainter, 1995; Scurlock; 1998). In recent decades the sediment load has decreased once again, along with a decrease in the flood frequency and flood peaks due to climatic and upstream flow regulations (Finch and Tainter, 1995; MEI, 2002). This has resulted in a planform termed "wandering" because changes are irregular and controlled by floods that occur episodically (MEI, 2002).

Between the Isleta and San Acacia reach the following analyses were pursued: planform classification, vegetation growth, and island development.

4.2.1 Planform Classification on the Rio Grande

The general shape of the channel was assessed for available snapshots in time between 1918 and 2016 using two classification schemes. The snapshots in time are summarized in Table 13. The two classification schemes are briefly described thereafter.

Table 13. Data used in planform classification between Isleta and San Acacia

Year	Collection timeframe	Format	Georeferenced	Area
1918	1917-1918	Linens	Yes	Isleta to San Acacia
1935	?	Film	Yes	Isleta to San Acacia
1949	?	Acetate	Yes	Isleta to San Acacia
1962	March	Mylar	Yes	Isleta to San Acacia
1972	April	Mylar	Yes	Isleta to San Acacia
1984	February	Mylar	No	Isleta to Belen
1985	March	Paper	No	Belen to San Acacia
1992	February	Mylar	Yes	Isleta to San Acacia
2002	Jan/Feb	Digital	Yes	Isleta to San Acacia
2012	February	Digital	Yes	Isleta to San Acacia
2016	October	Digital	Yes	Isleta to San Acacia

Schumm (1977; 1981) used a pattern classification scheme based on experience with fluvial rivers throughout the world, but primarily based on research observations of sand bed rivers in Canada and the Great Plains region of the western United States and mobile bed and bank flume studies. The classification is based on channel stability and the primary mode of sediment transport. Observations noted during the research of natural river systems and flume studies provided the opportunity to comment on the general conditions in which certain channel patterns develop and how channel pattern shifts may occur from changes in the sediment supply or through stabilizing effects such as vegetation. Schumm considered this a tentative pattern classification model until more data became available on the effects on the channel shape and pattern of the total sediment load and the predominant sediment size carried by the river. Schumm's classification scheme involved 14 patterns representing three dominant sediment load regimes: bed load (patterns 1-5), suspended load (patterns 11-15), and a mixed load for a

system that was not clearly bed load or suspended load dominated (patterns 6-10). Schumm's classification scheme is shown in Figure 71.

Massong et al. (2010) developed a planform evolution model based on information collected on the Middle Rio Grande, including empirical observations of channel planform changes, survey data, valley fill geologic data, historical photography, and available documented historical descriptions such as those in Scurlock (1998) and Bauer (2009). The model includes three stages of planform evolution, as shown in Figure 72. There is the initial stage (stage 1-3) followed by two branches of evolution. The two stages past the initial stage depend on whether the sediment supply is greater (aggrading stage: A4 –A6) or less than the transport capacity (migrating stage: M4-M8). Based on evidence of incision and bank erosion between Isleta and San Acacia (Bauer, 2000; Richard et al., 2001; MEI, 2002; Bauer and Hilldale, 2006; Vensel et al., 2006; Parametrix, 2008; Makar, 2010; Makar and AuBuchon, 2012; Varyu, 2013) it was assumed that the observed river planform within the assessed reaches is following the migrating stage.

Two geomorphic reaches have been identified between the Isleta and San Acacia Diversion Dams (Reclamation, 2012b). The planform classification was completed for each of these reaches, as shown in Table 14 and Table 15. The changes between the years are specifically described in subsequent paragraphs, however a brief explanation is provided herein of the planform changes described in Table 14 and Table 15.

The primary change since the late 1940s has been a transition to a narrower, slightly sinuous channel from a wide, braided channel. The Massong et al.'s (2010) M5 and M6 planform stages represent deeper and narrower river sections with channel bars that had been active, developed vegetation, and then became attached to the bank. These now function as river banks. The M6 planform stage occurs in the Rio Puerco to San Acacia reach, primarily below the Rio Salado planform and represents the set up and lateral migration of bends in the river. The movement to an M5 stage between Isleta to Rio Puerco is a possible prediction from Massong et al.'s planform model towards more lateral migration in the reach. This would especially be true if channel incision occurs below the established vegetative root zone. The Schumm (1977, 1981) channel pattern classification suggests a shift to a planform that has a higher relative stability, lower width to depth ratios, decreased channel gradient, increased channel sinuosity, and lower stream power for both the Isleta to Rio Puerco and the Rio Puerco to San Acacia geomorphic reaches. The Schumm classification scheme also suggests more of an influence of the suspended sediment load on the channel morphology than the sediment bed load.

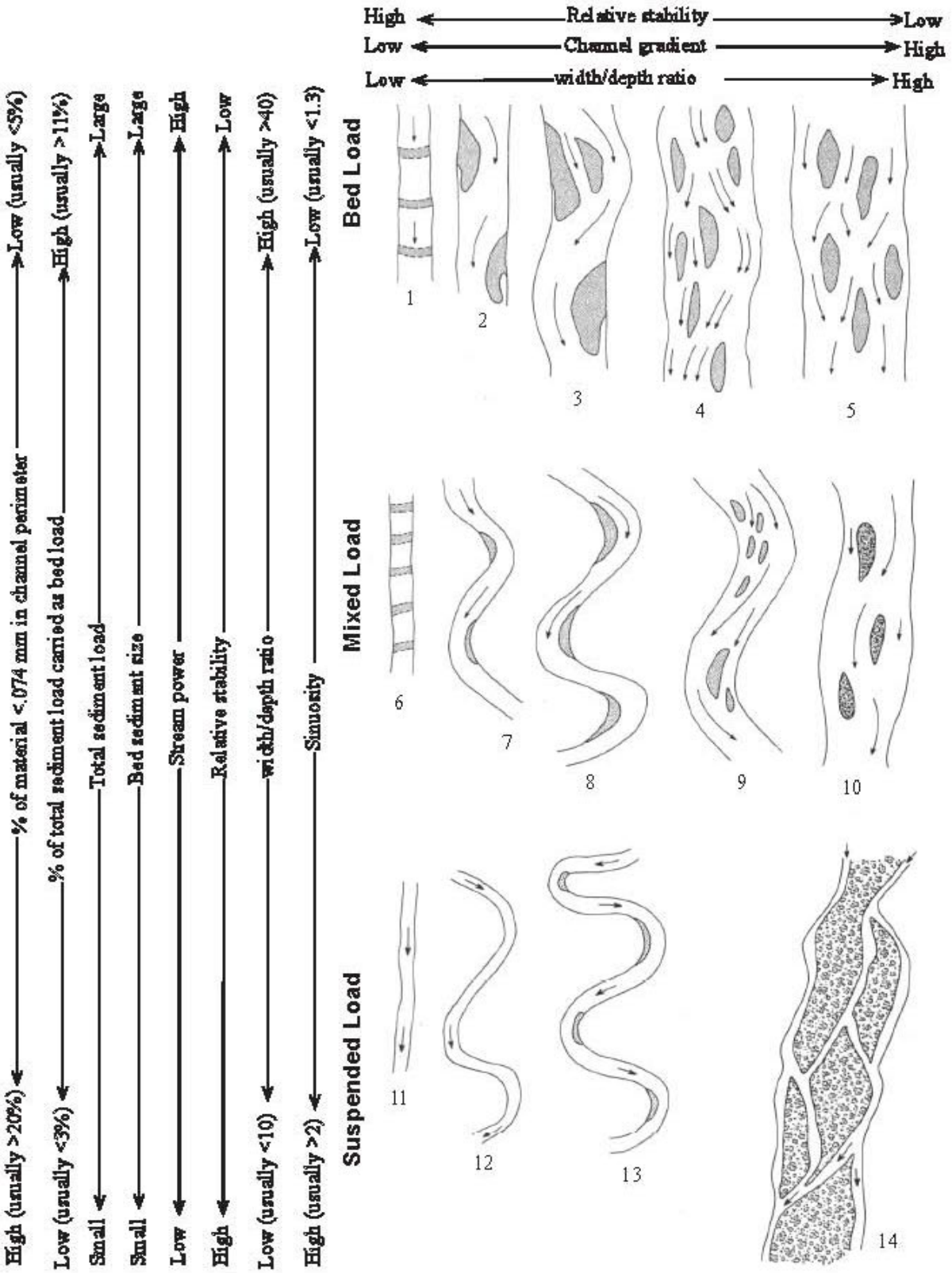

Figure 71. Classification of channel pattern (after Schumm 1977, 1981)

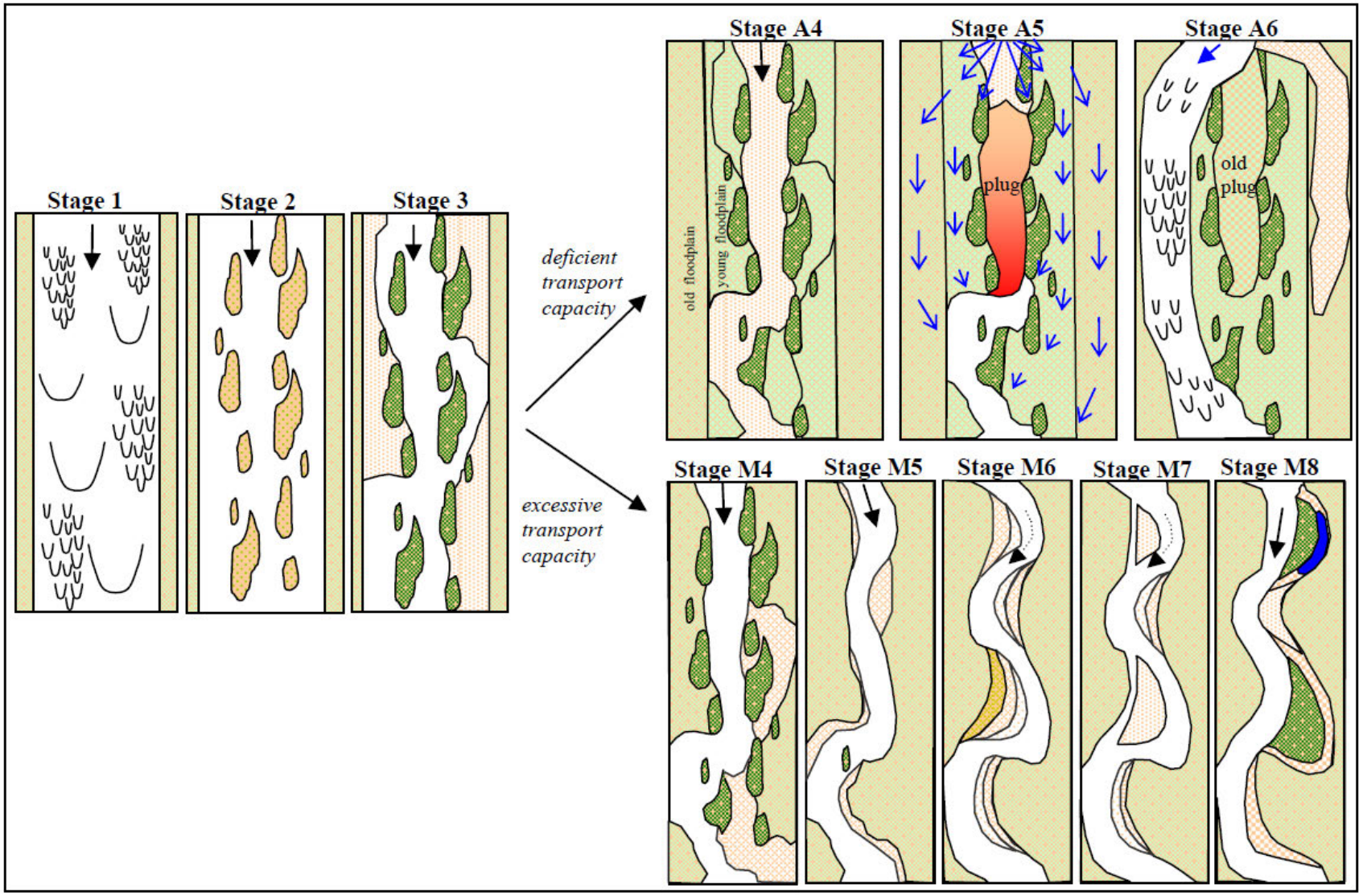

Figure 72. Massong et al. (2010) planform evolution model.

Table 14. Channel Classification for the Isleta to Rio Puerco geomorphic reach

Years	Massong et al. (2010)	Schumm (1977, 1981)
1918	2	3
1935	1	3
1949	2	3
1962	3	2
1972	3	2
1985	3	8/9
1992	3	8
2002	3	9
2012	M4	8
2016	M5	7

Table 15. Channel Classification for the Rio Puerco to San Acacia geomorphic reach

Years	Massong et al. (2010)	Schumm (1977, 1981)
1918	1	2
1935	1	4
1949	1	4
1962	2	3
1972	3/2	2/3
1985	3	2/3
1992	3	8
2002	M4	7
2012	M5/M6	7
2016	M5/M6	7/8

For most of the Isleta to Rio Puerco reach, the river's thalweg, according to the 1918 linens (maps hand drawn on linen sheets), is about 2-8 feet lower than the adjacent floodplain. The active channel is wide, with large sand bars. Sometimes the bars alternate sides on the channel and at other times the bars appear in the middle of the channel, acting as islands. A lot of the bars have secondary channels or chutes that dissect them. The sand bars are very low and for the most part have no vegetation on them. The few bars or islands that have vegetation may have been connected to the channel banks before the previous high flow event(s) changed the planform. There are significant stands of woody vegetation (or bosque) on both river banks. This is broken spatially by cultivated fields, alkali meadows, sand dunes, and sage fields. The 1918 linens for the Rio Puerco to San Acacia reach is similar to the upstream reach, but the bars are much larger. There is less area covered by vegetation, with areas demarcating salt grass meadows and sand flats. The adjacent floodplains are only about 1-4 feet higher than the river thalweg.

The 1935 aerial photography also shows a wide active channel with low sand bars that the low river flows braid across. In some stretches of the reach the river narrows and alternating sand bars appear. There are areas of woody vegetation,

some of which dissect areas denoted in the 1918 surveys. This would indicate that flow events occurred in the intervening years that were able to re work the channel morphology. There appears to be less agriculture occurring adjacent to the river and is difficult to discern salt grass or alkali meadows in the captured photography. Similar to the 1918 linens, the 1935 aerial photography shows a distinct planform difference downstream of the Rio Puerco. The number and extent of bars is more extensive, plus the low flow channel is significantly more braided through this reach. This may be indicative of a higher sediment load.

In 1949 the banks, and some of the bars, from 1935 are becoming vegetated. The result is a narrower channel than in 1935. The majority of bars within the active channel, however, still appear to be barren of vegetation. In some areas there has been extensive re-working of the channel as vegetated bars/islands in 1935 have been replaced by sand bars or river channel in the 1949 aerials. The channel planform is considerably wider downstream of the junction with the Rio Puerco, similar to the previous historical snapshots in time. The low flow channel is significantly more braided in this reach with more open bars. The planform narrows, similar to previous years, upstream of the junction with the Rio Salado and then widens out again downstream.

In 1962 the channel planform has narrowed. Lines of jetty jacks, both parallel and transverse to the flow, are visible. Areas of the 1949 active channel enclosed by the jetty jacks have become stabilized and colonized by vegetation. While the active channel has narrowed, there are still bars within the active channel that are not vegetated, especially in areas where the active channel is slightly wider. A primary flow path has developed and in many places this appears to have been constructed rather than having occurred naturally. As in previous years, the channel planform changes downstream of the Rio Puerco junction. While wider than the reach upstream, the Rio Puerco to San Acacia reach shows signs of bar stabilization and vegetation, although no jetty jacks are visible in the photographs. A meandering thalweg can now be identified through most of this reach

By 1972, the jetty jacks have definitely reshaped the river, as a significant portion of the river has either eroded or deposited sediment to the bankline jetty jack line (e.g. river banks are now parallel to the bankline jetty jacks through most of the reach). In the Isleta to Rio Puerco reach this has increased the width in many locations, but also resulted in a more uniform width. Within the active channel, the bars are primarily free of vegetation with a sinuous low flow channel. The Rio Grande narrows considerably upstream of the Rio Puerco, but in 1972 there isn't as large an increase in width of the active channel in the Rio Puerco to San Acacia reach until downstream of the Rio Salado. Up until the Rio Salado the planform of the Rio Puerco to San Acacia reach resembles the upstream planform from Isleta to Rio Puerco. The planform downstream of Rio Salado in 1972 is more similar to the 1962 planform for the entire Rio Puerco to San Acacia reach, albeit with some width reductions.

In 1984/1985 the floodplains appear to have well established vegetation. The majority of the bars within the active channel are predominantly non-vegetated, however there are some bars that have vegetation becoming established. Bars appear to be more stable as the river begins to meander back and forth between alternating point bars. This is especially noticeable between Isleta Diversion Dam and Abo Arroyo. Between Abo Arroyo and about one mile upstream of the Rio Puerco confluence with the Rio Grande the river has a much more braided look. In this section of the river there are point bars with multiple cut off chutes and more visible mid-channel bars. The Rio Grande still narrows upstream of the Rio Puerco, but the transition between the wider, braided upstream section and the narrower, meandering downstream section has moved downstream from 1972 (river mile 129.5 in 1972 and river mile 127.3 in 1985, 2012 river mile demarcations). Alternating bars in this section, however, still show indications (higher flow cutoffs, lack of vegetation, etc.) that the river is highly mobile in this area. Downstream of the Rio Puerco confluence and across from the Salas Arroyo confluence a cut-off berm is visible in the 1985 aerial photography. The cut-off berm is on river right and upstream of bank erosion along the Drain Unit 7 Extension drain. The bank erosion (about 4,000 feet in length) is also evident in the 1972 aerials, indicating that the cut-off berm was likely placed as protection for the drain. Below the Rio Puerco confluence the channel once again has a defined thalweg channel with alternating point bars. There are multiple cut off chutes in these bars. Between RM 122 (2012 demarcations) and the Rio Salado confluence the river narrows and there are no visible bars. Downstream of the Rio Salado confluence the Rio Grande once again widens with a defined thalweg alternating between point bars that appear to be stabilizing. Some cut off chutes are visible on these bars as well.

By 1992 the Rio Grande between Isleta and San Acacia Diversion Dams has a multiple thalweg channel that meanders back and forth between alternate bars that are becoming more well-defined and stabilized. The active channel widening observed in the 1985 aerials upstream of the Rio Puerco confluence has continued to move downstream to around river mile river mile 126.4 (2012 river mile demarcations). There are a few cut-off channels through the point bars and in some areas this gives a braided appearance. The only section of the river with no visible sediment bars is between RM 122 (2012 river mile demarcation) and the Rio Salado confluence. Below the Rio Salado the river narrows considerably and the large point bars that have formed show evidence of vegetation encroachment.

In 2002, the active channel between the Isleta Diversion Dam and the Rio Puerco confluence still has multiple thalweg channels that meander between alternate bars. A more discernible single thalweg channel is evident between the U.S. 60 Bridge and San Acacia Diversion Dam. There are still smaller side channels evident in the aerial photography that split off the main channel and cut through point bars, except in the section between RM 122 (2012 river mile demarcation) and the Rio Salado. There are more bars/islands than previous years within the Isleta Diversion Dam to Rio Puerco reach that show signs of vegetation. The

vegetated bars/islands add additional width constraints on the active channel, decreasing the active channel width compared to the 1992 aerials. The Rio Puerco confluence has jumped about 1200 feet upstream of its previous location near the Salas Arroyo confluence. This appears to have been a meander cut-off as a meander bend on the Rio Puerco (visible near the Rio Grande in the 1992 aerial photography) appears to have breached the bank of the Rio Grande, forming a new confluence location in 2002. The Rio Grande below the Rio Puerco is narrower with fewer bars. There are a few bars that have developed between RM 122 and the Rio Salado confluence, but the river is only slightly narrower here than upstream. The narrowness of the river continues downstream of the Rio Salado confluence as the bars through this section of the Rio Grande are becoming densely vegetated.

In the 2012 aerial photography, the vegetation has become more established within the active channel, with many of the bars in 2002 now connected to the banks. While there are still "bare-earth" bars, vegetated bars seem to be more predominant. This has both narrowed the channel and created fewer, but larger bars. A single thalweg channel has formed between Isleta and San Acacia Diversion Dam, with split flow conditions around the larger mid-channel bars. Between the Rio Puerco and San Acacia there are fewer mid-channel bars with some of the point bars in this reach beginning to grow, causing erosion on the opposite bank. This is especially noticeable just upstream of RM 117 where the river channel in 2012 is about 600 feet north of its location in 2002.

By 2016 the river appears to have narrowed more between Isleta Diversion Dam and the Rio Puerco confluence with the Rio Grande. The majority of the bars from the 2012 aerial photography are now connected to the banks, but additional non-vegetated sediment bars have developed within the active channel. There are a few larger cut-off chutes on these bars that become intermittent during lower flow periods. A distinct single thalweg channel is discernible from Isleta to San Acacia. The channel width between the Rio Puerco and the Rio Salado confluence has narrowed slightly through vegetation encroachment into the active channel. Between the Rio Salado confluence and San Acacia the active channel area has increased through channel migration or anthropogenic vegetation removal (noticeable just upstream of the San Acacia Diversion Dam).

The active channel planforms are shown in Figure 73 and Figure 74 for the Rio Grande between Isleta Diversion Dam and the San Acacia Diversion Dam. Three locations within this reach are also highlighted to show the specific variations that occurred through time. These snapshots are shown in Figure 75 through Figure 77.

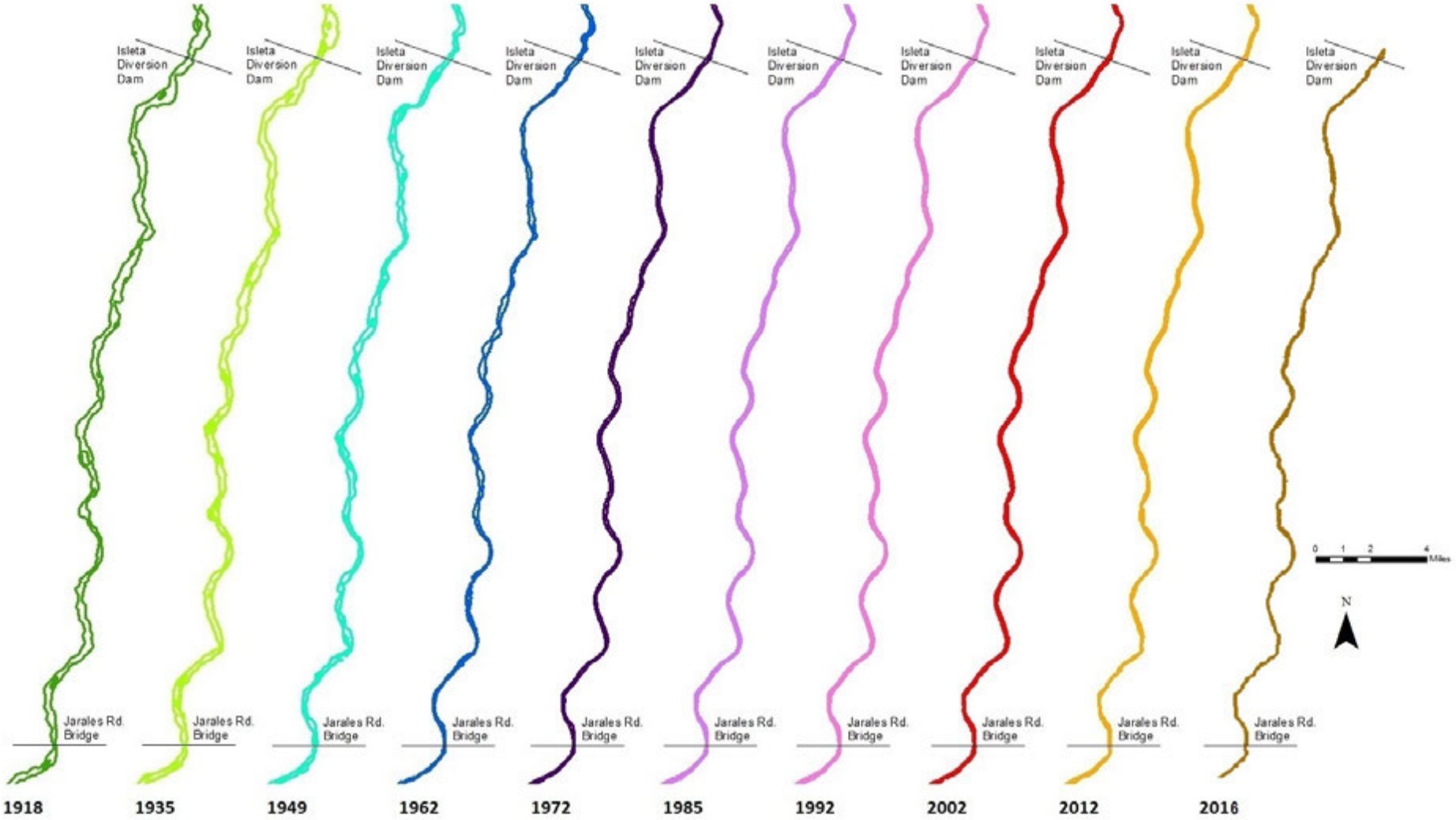

Figure 73: Rio Grande Planform from Isleta Diversion Dam to Jarales Bridge

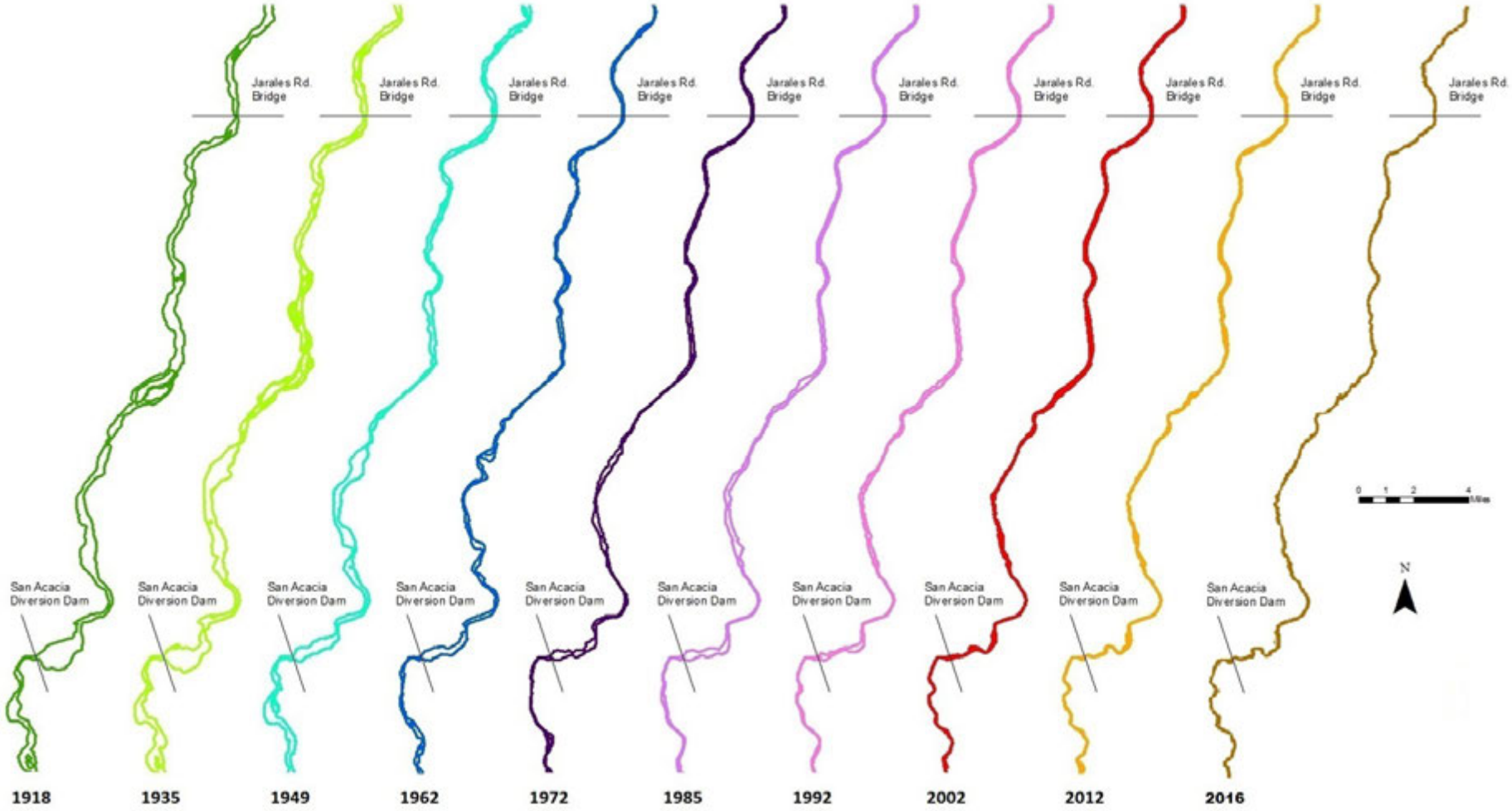

Figure 74: Rio Grande Planform from Jarales Bridge to San Acacia Diversion Dam

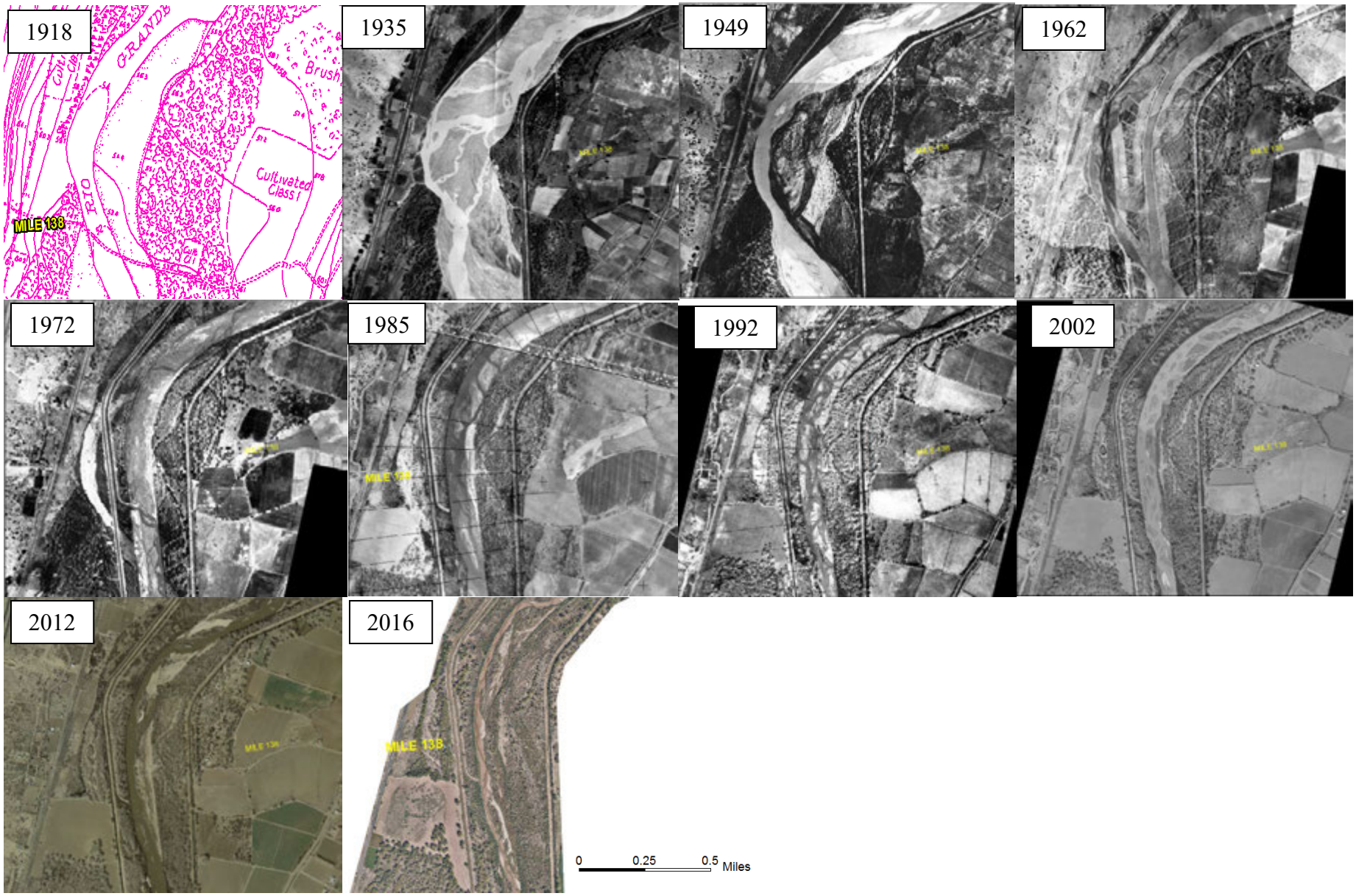

Figure 75: Aerial Photography and hand drawn linens around River Mile 138. The hand drawn linens are from 1918, while aerial photography ranges from 1935 through 2016. Aerial Photography is oriented north to south, with the Rio Grande flowing from top to bottom.

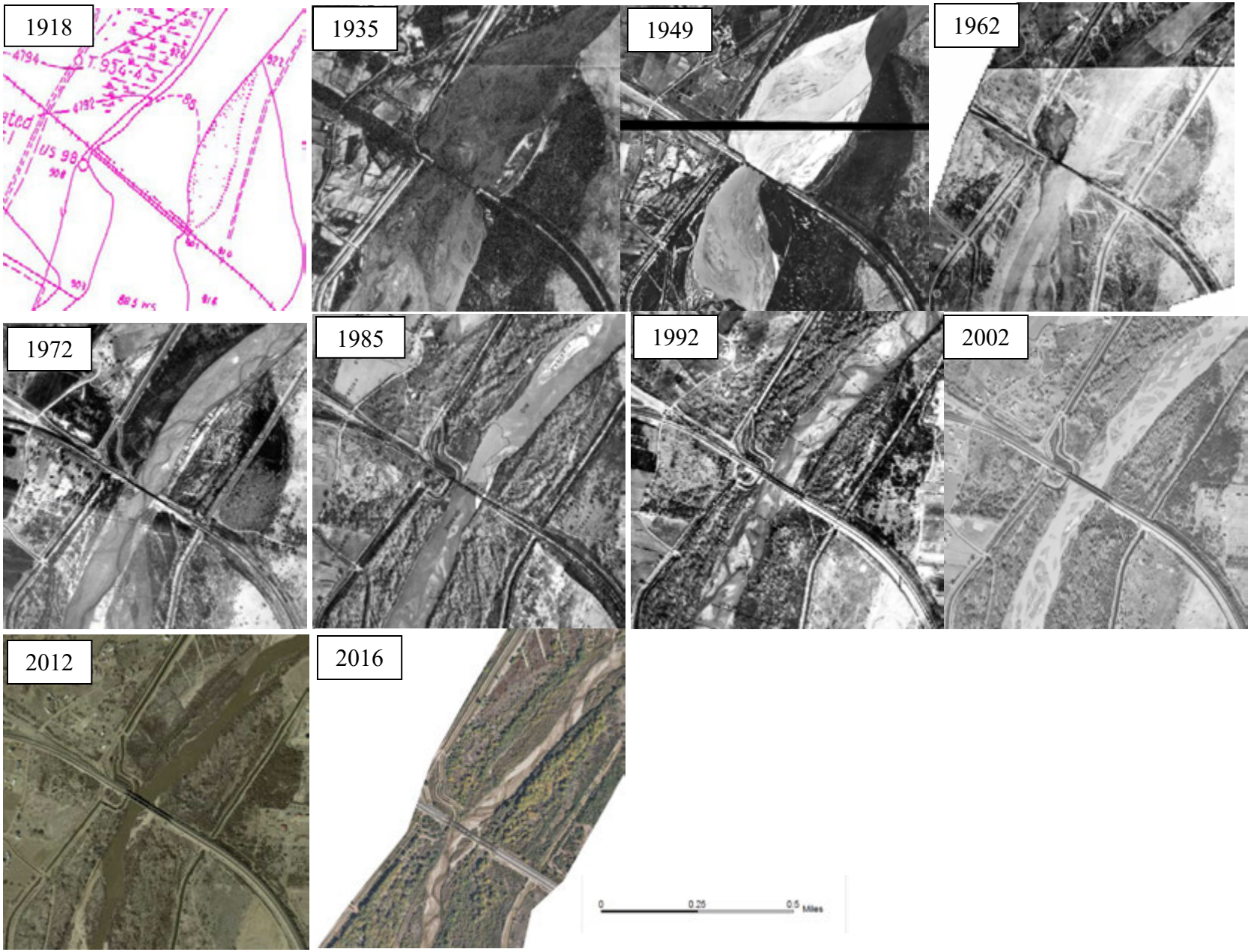

Figure 76: Aerial Photography and hand drawn linens around River Mile 148. The hand drawn linens are from 1918, while aerial photography ranges from 1935 through 2016. Snapshots are oriented north to south, with the Rio Grande flowing from top to bottom.

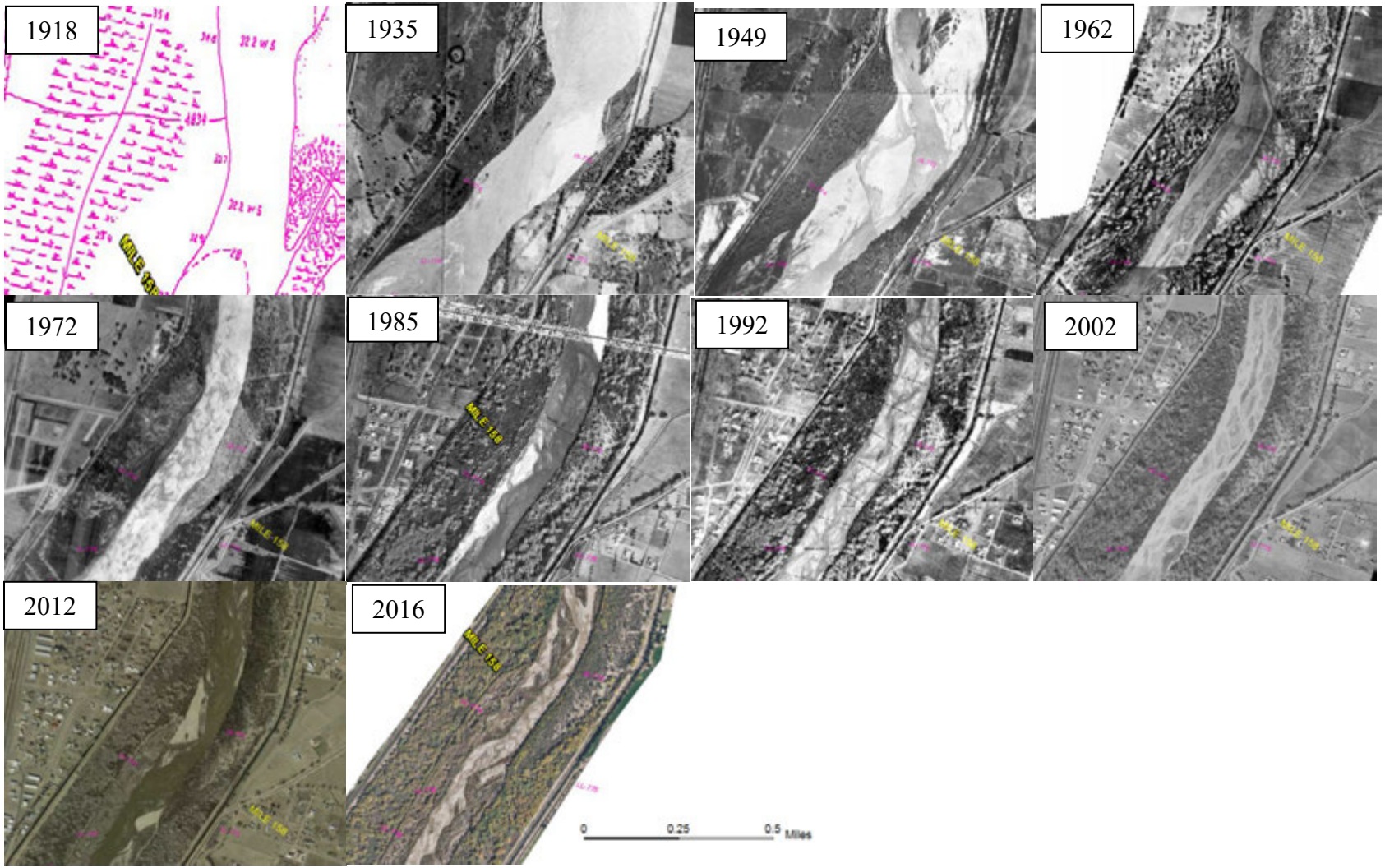

Figure 77: Aerial Photography and hand drawn linens around River Mile 158. The hand drawn linens are from 1918, while aerial photography ranges from 1935 through 2016. Aerial Photography is oriented north to south, with the Rio Grande flowing from top to bottom.

4.2.2 Planform Classification – Rio Puerco

The Rio Puerco's planform from the railroad bridge to the confluence with the Rio Grande (approximately 1.5 miles) was also classified according to Massong et al. (2010) and Schumm (1977, 1981) and the results are seen in Table 16. Figure 78 and Figure 79 show the active channel outline and aerial photographs of the Rio Puerco from the railroad bridge to the Rio Grande. This portion of the Rio Puerco narrows between 1918 and 2016. The channel is relatively straight for most of the years until 1992. There are some bends that develop by 1935, but by 1949 these have been mostly straightened. Then in 1992, the channel develops a meandering planform near the confluence. Between 1992 and 2002, one of the meander bends closest to the Rio Grande erodes the river right bankline on the Rio Grande. This results in a new confluence location for the Rio Puerco in 2002 that is about 1200 feet upstream of the confluence location in 1992. The meander bends further upstream also become more pronounced in 2002, and then in 2012 the largest meander bend in this downstream portion gets cut off. Channel classifications for the Rio Puerco following Massong et al.'s (2010) and Schumm's (1977; 1981) classification schemes are shown in Table 16.

Table 16. Channel Classification for the Rio Puerco

Years	Massong et al. (2010)	Schumm (1977, 1981)
1918	M5	11
1935	M6	12
1949	M6	12
1962	M5	11
1972	M5	11
1992	M6	13
2002	M6	13
2012	M8	12
2016	M8	12

Figure 78 shows the active channel planform on the Rio Puerco between the railroad bridge and the confluence with the Rio Grande between 1918 and 2016. Snapshots in time are shown in Figure 79. According to Schumm's classification, the changes over time are likely related to changes in the sediment load or discharge. Massong et al.'s (2010) classification schema suggests that the Rio Puerco's planform stage will be stable unless a large enough hydrologic event can reset the planform. These changes may indicate a decrease in the suspended sediment supply from the Rio Puerco. This stability and lowered sediment supply on the lower reach of the Rio Puerco is consistent with other analyses on the Rio Puerco (Elliot, 1979; Friedman et al., 2015).

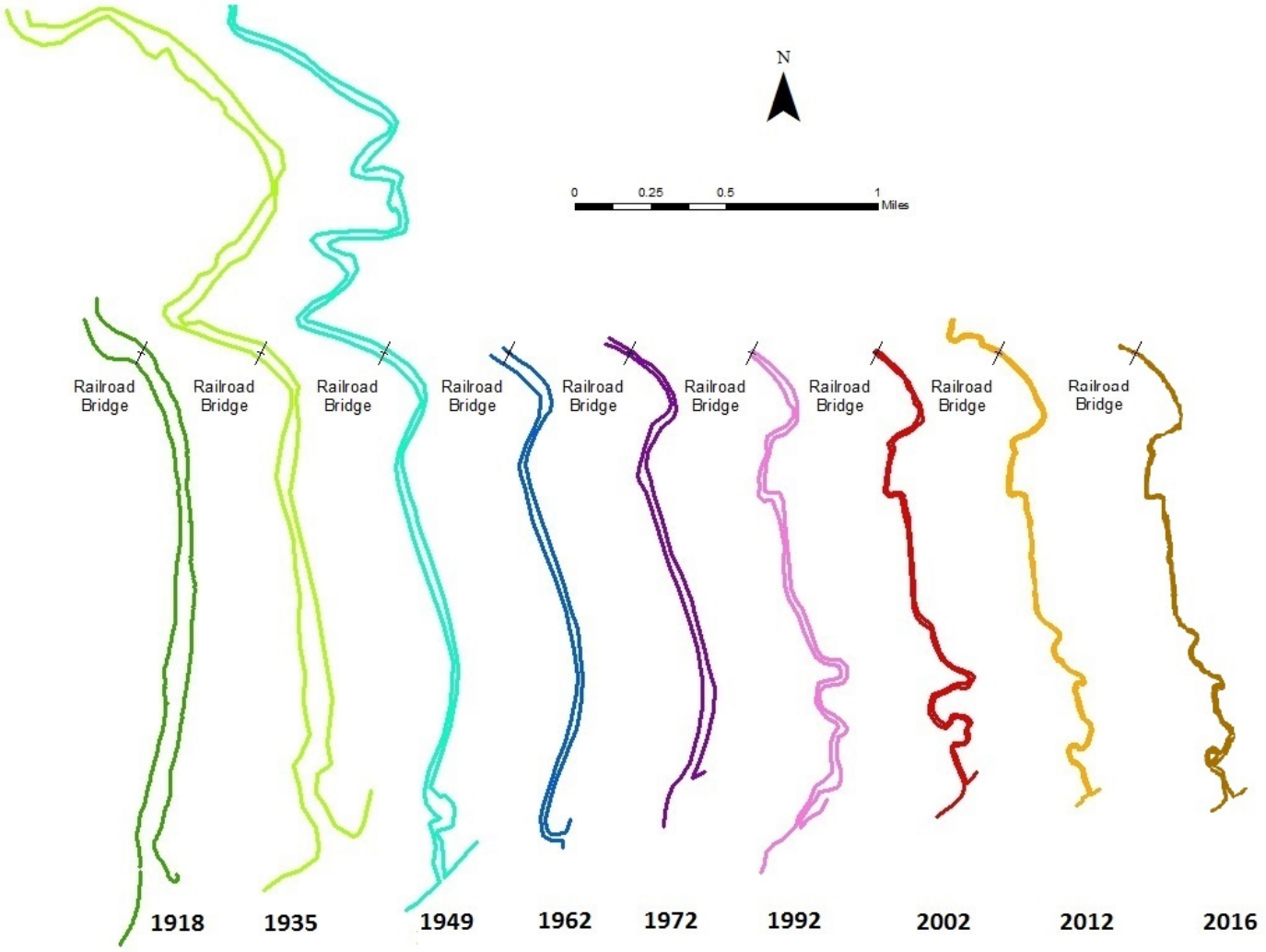

Figure 78: Rio Puerco planform from the railroad bridge to the confluence with the Rio Grande

Figure 79: Aerial Photography and hand drawn linens of the Rio Puerco from the railroad bridge to the confluence with the Rio Grande. The hand drawn linens are from 1918, while aerial photography ranges from 1935 through 2016. Aerial Photography is oriented north to south, with the Rio Puerco flowing from top left to bottom right.

4.2.3 Vegetation trends

One of the recent concerns along the Rio Grande between Isleta and San Acacia is the amount of vegetation encroachment that has occurred. Crawford et al. (1993) described the limitation of natural riverine processes on the Rio Grande that destroy and replenish native Bosque vegetation. The recruitment of new native Bosque stands requires a nearby water table and a bare earth substrate (MEI, 2002). The reduced variability in stream flows through the year and the reduction in peak flood flows that can remove established vegetation has influenced the vegetation growth in the Rio Grande through this reach and impacted the planform morphology (Crawford et al., 1993; Finch and Tainter, 1995; MEI, 2002; Parametrix, 2008; Bauer, 2009; Makar, 2010; Massong et al., 2010, Makar and AuBuchon, 2012).

Vegetation trends were assessed for the Rio Grande between Isleta and San Acacia diversion dams, by geomorphic reach, for periods of time in the last three decades using two different methods. Because annual vegetation is typically not observable in the aerial photography, it is assumed that the mapped vegetated areas reflect woody vegetation or dense annual vegetation. The first method looked at aerial photography between 1992 and 2016 and involved hand digitizing vegetation using GIS software. The second method used 4-band imagery captured in 2008, 2012, and 2016 to assess vegetation through a semi-automatic process based on differentiating objects from the captured pixel values for the multiple imagery bands. Both processes show an increase in the area being vegetated, although the hand digitization process shows this trend continuing through the last evaluated year (2016) while the semi-automatic method has leveled out recently. The results of these analyses are shown in Figure 80.

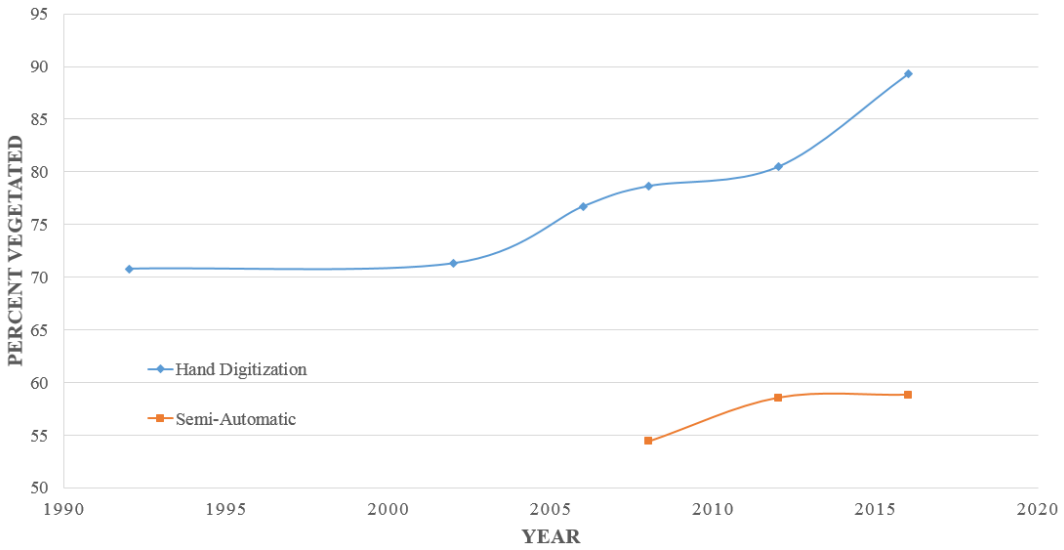

Figure 80. Percentage of woody vegetation within active channel area between Isleta Diversion Dam and San Acacia Diversion Dam. Analysis was completed using hand and semi-automatic digitization.

The process for hand digitization was performed at a scale of 1"=1000'. This resolution was chosen to best balance the need between visual identification of vegetative features and analysis time constraints. All digitization efforts were completed in the North American Datum of 1983 (NAD83), New Mexico State Plane, Central Zone (NMSP, zone 3002).

Years of aerial photography used in this analysis are shown in Table 17. All of the aerial photography was collected by Reclamation contractors and most are collected during leaf-off conditions. The two exceptions are the July 2008 and the October 2016 aerial photography that captured leaf-on conditions. While other aerial photography sets are available in 2008, the July captured a discharge more representative of the other evaluated years.

Table 17. Aerial Photography years used in the vegetation encroachment analysis.

Year	Month	Color	Bands
1992	February	Black & White	1
2002	January	Color	3
2006	January	Color	3
2008	July	Color	4
2012	February	Color	4
2016	October	Color	4

A distinct feature class representing the vegetated area was created for each aerial photography year. The digitized area in each year was compared against the assessment area. The assessment area included the river and riparian corridor from Isleta Diversion Dam to San Acacia Diversion Dam. The spoil levees and/or geological constraints formed the lateral extents of the assessment area. The total bounding area of the assessment area was 12,525 acres.

Features were digitized upstream to downstream. When vegetation was patchy, areas with at least 50% vegetation were counted as fully vegetated. A typical example of this vegetation digitization is shown in Figure 81. Tabular results from the hand digitization effort are shown in Table 18. Based on this table, the largest vegetation changes between Isleta and San Acacia diversion dams occurred from 2002 to 2006 and 2012 to 2016.

Table 18. Percent of woody vegetation cover (hand digitization) from 1992 to 2016 along the Rio Grande between Isleta and San Acacia Diversion Dams.

Year	Acres	Percent	Percent change
1992	8,865	70.8	—
2002	8,930	71.3	+0.5
2006	9,610	76.7	+5.4
2008	9,850	78.6	+1.9
2012	10,080	80.5	+1.8
2016	11,179	89.3	+8.8

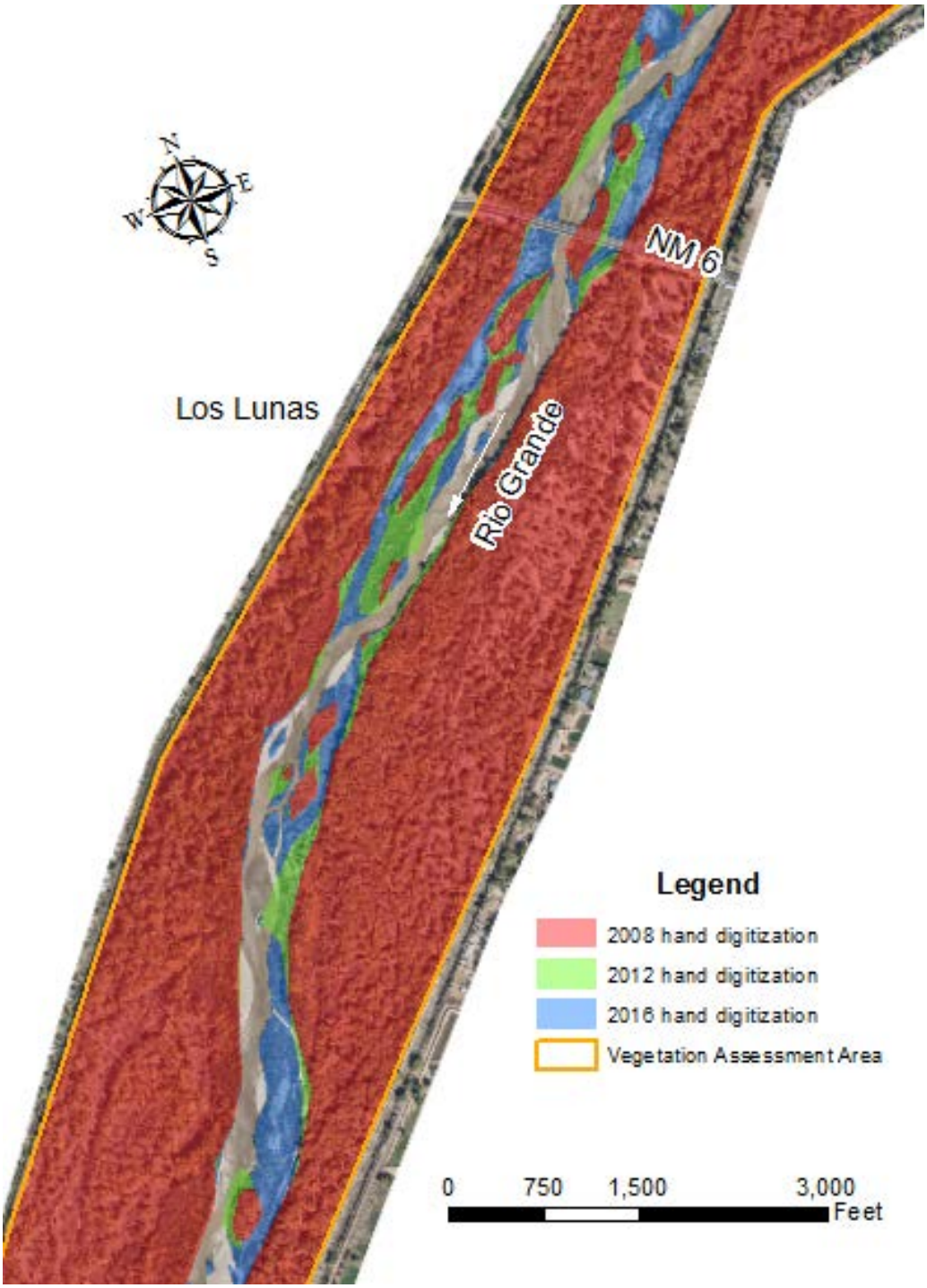

Figure 81. Woody vegetation hand digitization in the Los Lunas area. Shown are the 2008, 2012, and 2016 hand digitization efforts. The background imagery (2016) is from Reclamation.

A second method was also employed to evaluate vegetative changes on the Rio Grande between Isleta and San Acacia Diversion Dams. Since three of the collection years had 4-band imagery (red, green, blue, and near infrared bands) a

semi-automatic method was pursued to see if similar trends would be obtained. The following methodology was used to extract polygons delineating vegetation according to this second methodology:

- Classify imagery — each of the imagery tiles for a given year are visually reviewed to choose one that has the greatest variability of land surfaces. This image is classified using the Image Classification Toolbar within ESRI's ArcMap (version 10.2). This tool uses the multiple bands from aerial imagery to automatically cluster pixels with similar values. The "Iso Cluster Unsupervised Classification" tool is run from this toolbar until the number of chosen classes (20 were chosen for this analysis) is sufficient to distinguish between the different land surfaces in the imagery (e.g. water and trees). The tool is then run one more time to create a signature file. The signature file is used to batch the remaining imagery tiles using the same classification. ESRI's ArcMap "Maximum Likelihood Classification" tool within the Spatial Analyst Tools/Multivariate Toolbox is used to batch the files.
- Merge classified imagery — for subsequent classification analyses it is useful to have one image instead of separate imagery tiles. ESRI ArcToolbox's "Mosaic to New Raster" tool found within the Data Management Tools/Raster Tools/Raster Dataset Toolbox is used to merge all classified images into a single raster.
- Symbolize classification raster — it is useful to symbolize the mosaicked raster according to land types by class ranges. Use the ESRI ArcToolbox tool "Reclassify" within the Spatial Analyst Tools/Reclass Toolbox to assign a unique band for each of the symbology colors. Figure 82 shows a typical example of the final classification process. Each set of aerial photography has a slightly different arrangement of bands that correlate to water, bare earth, or vegetation. This must be checked and correlated with the true-color aerial photography from that year.
- Create an attribute table — this uses an ESRI ArcToolbox tool called "Build Raster Attribute Table" within the Data Management Tools/Raster Tools/Raster Properties Toolbox. This tool attributes the properties, like area for each of the classified polygons.
- Use the Attribute Table editor to calculate the number of pixels in the vegetation classified band. The number of pixels multiplied by the pixel area (cell size area from the underlying raster) provides the vegetated area.

Results of the semi-automatic digitization effort are shown in Table 19. While the results show a lower vegetated cover, the semi-automatic method also shows a measurable increase in vegetation between 2008 and 2012/2016, the largest change occurring between 2008 and 2012. The lower vegetation percentages is likely a result of classifying only vegetation areas (as opposed to manually digitizing areas predominantly composed of vegetation but interspersed with bare earth patches). There is also differences between the clustering of similar valued pixels into a vegetative band compared with the hand-digitizing effort.

Table 19. Percent of vegetation cover (semi-automatic digitization) of 4-band imagery from 2008, 2012, and 2016 along the Rio Grande between Isleta and San Acacia Diversion Dams.

Year	Acres	Percent	Percent Change
2008	6810	54.4	—
2012	7330	58.5	+4.1
2016	7364	58.8	+0.3

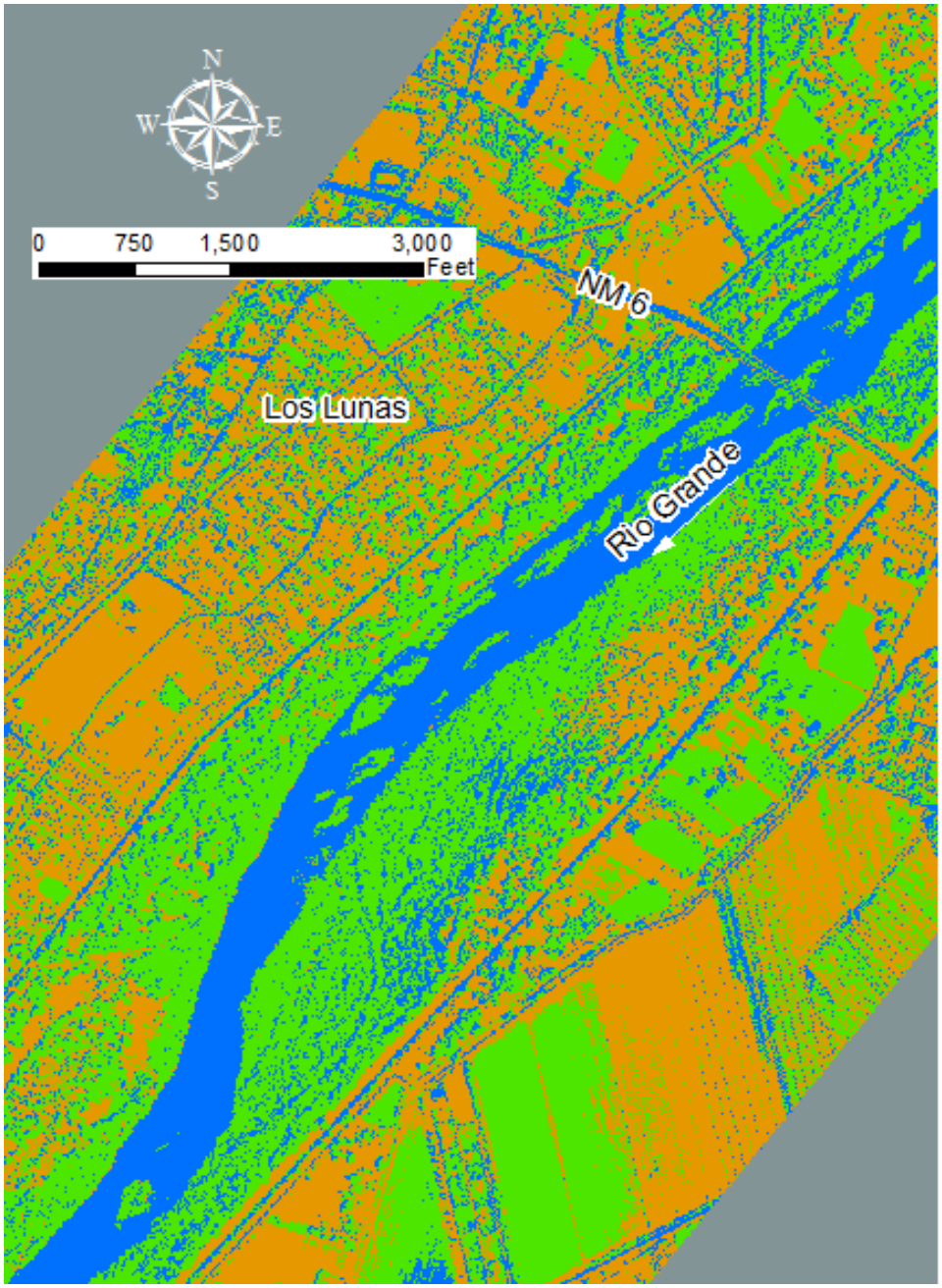

Figure 82. Classified 2008 4-band imagery showing delineation of land surfaces in the Los Lunas area. Water (color blue) – bands 1 and 3 [new band 1]; Vegetation (color green) – bands 2, 4, 5, and 8 [new band 2]; Bare earth (color orange) – bands 6, 7, and 9-19 [new band 3]

4.2.4 Island trends

Ortiz (2004) looked at vegetated islands along the Rio Grande in the Albuquerque Area, finding that the number and area of vegetated bars increased as the bed material coarsened. Meyer and Helper (2007) found a similar trend and found the area and number of vegetated islands increased downstream of the planform transition from a braided, multi-channel river to a meandering single thread river. These studies indicate that the area and/or number of islands may be related to potential planform changes. A similar analysis was performed along the Rio Grande between Isleta and San Acacia Diversion Dams using historical aerial photography to capture temporal snapshots in time. The results of this analysis are shown in Figure 83.

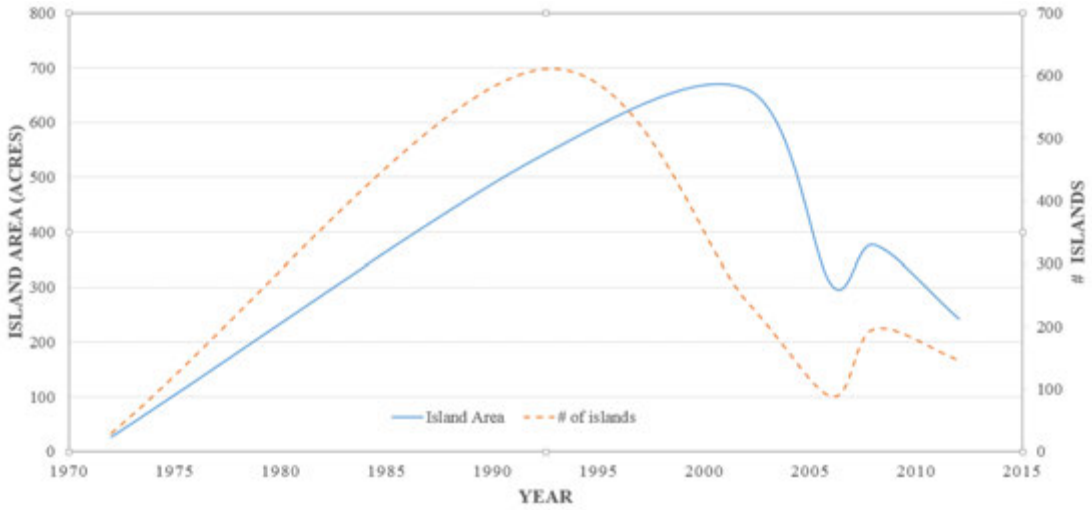

Figure 83. Island count and area within active channel area between Isleta Diversion Dam and San Acacia Diversion Dam. Analysis was completed using hand digitization.

The process for hand digitization was performed at a scale of 1"=1000'. This resolution was chosen to best balance the need between visual identification of islands and analysis time constraints. All digitization efforts were completed in the North American Datum of 1983 (NAD83), New Mexico State Plane, Central Zone (NMSP, zone 3002).

Years of aerial photography used in this analysis are shown in Table 20. All of the aerial photography was collected by Reclamation contractors and most are collected during leaf-off conditions. The exceptions are the April 1972, July 2008, and October 2016 aerial photography that captured leaf-on conditions. While other aerial photography sets are available in 2008, the July captured a discharge more representative of the other evaluated years. The April 1972 and October 2016 aerial photography sets are the only ones from those years.

Table 20. Aerial Photography years used in the bar hand digitization analysis.

Year	Month	Color	Bands	Approximate daily average discharge (cfs) at San Acacia USGS Gage (08354900)
1972	April	Black & White	1	5
1992	February	Black & White	1	650
2002	January	Color	3	600
2006	January	Color	3	580
2008	July	Color	4	1500
2012	February	Color	4	740
2016	October	Color	4	40

A distinct feature class of the vegetated bars was created for each aerial photography year. Features were digitized by hand upstream to downstream. Only bars not connected to the bank (islands) were digitized. Both vegetated and non-vegetated islands were captured. While most of the aerial photography was captured in the same range of flows, there was one year (2008) where the flow was higher and two (1972 and 2016) where the flow was lower. At the lower flows, islands were delineated if an area in the active channel (bare earth portion of the river channel) had vegetated or if an area of bare soil was dry or showed other signs (like sun glare or shadow) of being higher than the surrounding river bed. A typical example of the digitization effort is shown in Figure 84. Results from the digitization effort are shown in Table 21.

While the number and acreage of islands has increased temporally just looking at 1972 and 2016, the recent peak seems to have occurred between 1992 and 2002. It is interesting to note the lag in the island area from the number of islands. The number of islands peaks in 1992, while the acreage of islands peaks in 2002. This implies a consolidation of islands into larger features between 1992 and 2002. The decrease in number and acreage of islands from 2002 to 2006 and 2008 to 2016 may have to do with the bank attachment process, whereby sediment deposits on one side of an island, facilitating vegetation growth. Larger spring run-off flows in 2005, 2008, and 2010 may have also re-mobilized un-vegetated islands. Islands with vegetation or very narrow high flow channels may have encouraged deposition of suspended sediment, furthering the connection of islands to the adjacent banks.

Table 21. Island count and acreage (hand digitization) from 1972 to 2012 along the Rio Grande between Isleta and San Acacia Diversion Dams.

Year	Acres	Number
1972	26	29
1992	532	609
2002	660	240
2006	303	88
2008	376	196
2012	242	146
2016	247	55

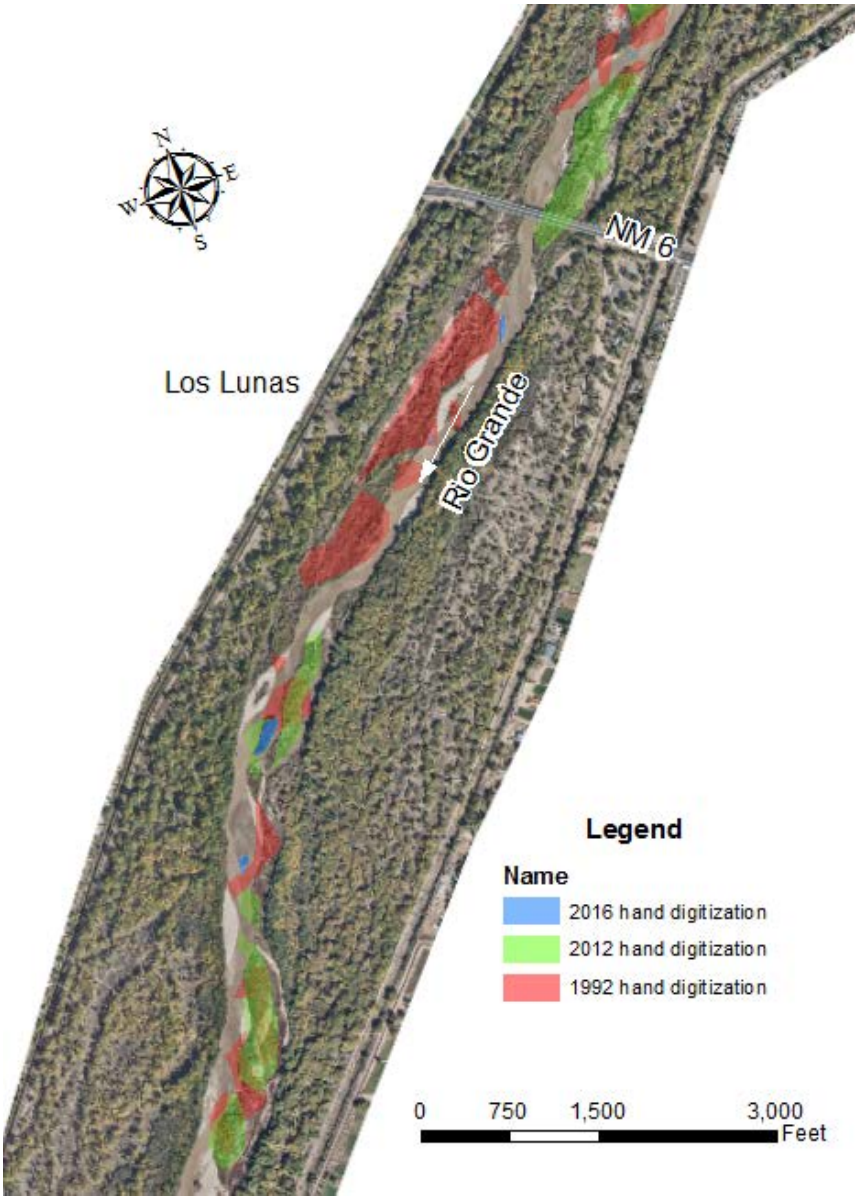

Figure 84. Island hand digitization in the Los Lunas area. Shown are the 1992, 2012, and 2016 hand digitization efforts. The background imagery (2016) is from Reclamation.

4.3 Channel Slope

The Rio Grande between Isleta and San Acacia tends to have a slope between 0.0007 ft/ft and 0.00085 ft/ft (Reclamation, 1961; Culbertson and Dawdy, 1964; Bauer, 2000; MEI, 2002; Makar, 2010; Makar and AuBuchon, 2012). Massong et al. (2010) had identified reaches prone to avulsions typically having slopes of less than 0.0007 ft/ft, while reaches prone to migrating bends typically have slopes greater than 0.0009 ft/ft. The Rio Grande between Isleta and San Acacia tends to oscillate between these two extremes, potentially indicating a tendency for both processes. A geologic uplift around the Rio Salado influences the local slope by causing an upstream slope reduction and a downstream slope increase (MEI, 2002; Parametrix, 2008). Slope changes can be used to understand geomorphic processes, for instance a decrease in the upstream sediment supply may cause the slope of the river to decrease since less energy is needed to now transport the available sediment. Both reach average bed and energy grade slopes are evaluated, along with a comparison of the mean channel bed elevations over time. The general trend for this reach indicates a slight decrease in the channel slope, which is consistent with modeling predictions (Vensel et al., 2006; Bauer, 2009; Reclamation, 2012b).

4.3.1 Reach Average Bed Slope

Reach average bed slopes have been previously calculated for various years between 1936 and 2007 and reported in the Makar (2010) report. Values reported in this study use the values from Makar (2010) extracted for the Isleta to Rio Puerco and the Rio Puerco to San Acacia reaches. This analysis also added in data from 2012 and 2016 data collections. The two additional reach average bed slope calculations were based off the 2012 Agg-Deg line data and the 2016 rangeline cross section survey data. The Makar (2010) data and the new 2012 and 2016 data are shown in Figure 85. This was accomplished by taking the measured channel thalweg elevation from the data at the furthest upstream river cross section in the sub-reach (IS-880 for Isleta to Rio Puerco sub-reach and RP-1100 for the Rio Puerco to San Acacia sub-reach) and subtracting the measured channel thalweg elevation at the furthest downstream cross section in the sub-reach (CO-1091 for Isleta to Rio Puerco and RP-1205.8 for Rio Puerco to San Acacia) to obtain an elevation difference. The river distance was measured between the upstream and downstream lines and the reach average bed slope obtained by dividing the difference of the thalweg elevations by the river distance for each evaluated reach.

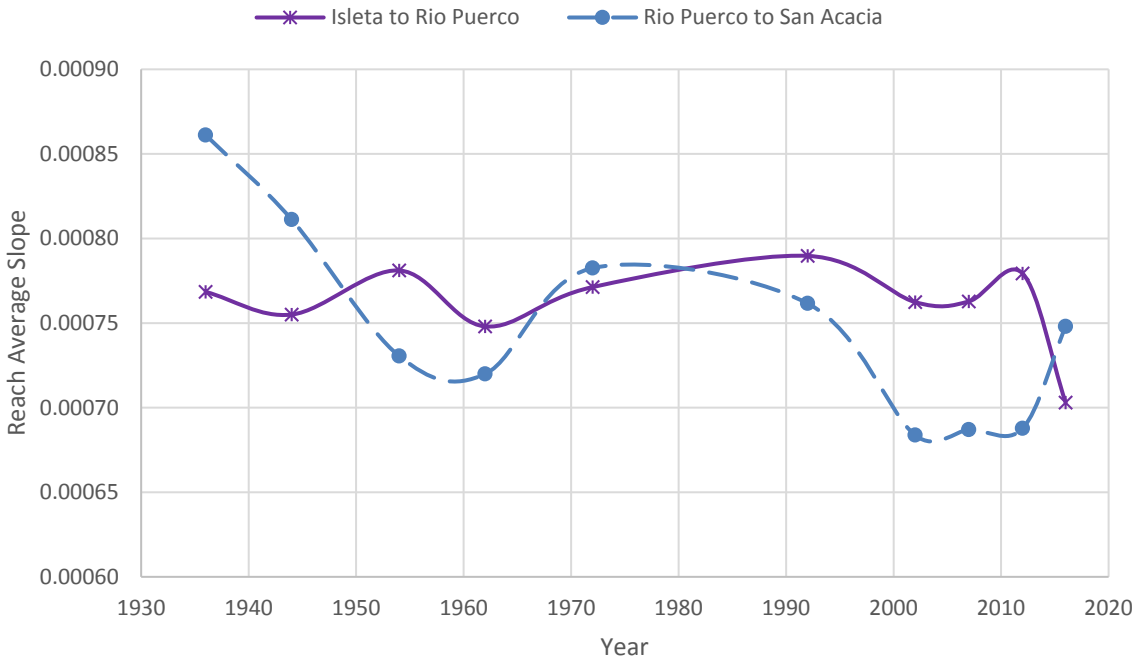

Figure 85. Reach average bed slopes since 1930 for the Isleta Reach (broken into two sections due to influence of the Rio Puerco).

The reach average bed slopes tend to oscillate between periods of steeper and flatter slopes. The Isleta to Rio Puerco reach has had more oscillations with less magnitude change than the Rio Puerco to San Acacia reach. In general, both reaches are experiencing a slight decrease in the bed slope over the decades. Currently (2012 to 2016) the Isleta to Rio Puerco reach is experiencing a slope flattening, while the Rio Puerco to San Acacia reach is experiencing a slope steepening.

4.3.2 Reach Average Energy Grade Slope

While the reach average bed and energy grade slopes should theoretically be similar for uniform flow conditions, these conditions are not typically found in fluvial systems. Typically, non-uniform flow conditions are expected in fluvial systems, such as occur on the Rio Grande with varying velocity and roughness values, and are likely to cause variations in calculated slope values. It is therefore useful to evaluate reach average energy grade slopes. Changes in the reach averaged energy grade line slope between 1962 and 2012 at a discharge of 5,000 cfs are shown in Figure 86. A discharge value of 5,000 cfs was used to provide a consistent reference point between the years. This value is close to the 2-year regulated peak flow values calculated by Wright (2010) for the USGS gage at Bernardo (4,900 cfs) and is of a similar magnitude to the USGS gages at Albuquerque (4,000 cfs) and San Acacia (7,800 cfs).

The average energy grade slope for the Isleta to Rio Puerco reach is 0.00083 ft/ft between 1962 and 2012, while the average slope for the Rio Puerco to San Acacia

reach is slightly steeper at 0.000851. These values are higher than the reach average bed slopes for the two reaches. This is likely due to a combination of numerical modeling that can capture steady, non-uniform flow conditions and methodologies for averaging reach slope values. The reach average bed slopes were determined by taking elevation difference from the upstream and downstream portions of the geomorphic reach and dividing by the measured channel distance between those points. The reach average energy grade slopes were determined by taking the calculated energy grade slope at aggradation-degradation lines within each geomorphic reach and distance-weighting the slope.

As shown in Figure 86, slope changes in the Isleta to Rio Puerco reach seem to lag behind the slope changes occurring in the Rio Puerco to San Acacia reach. The Rio Puerco to San Acacia reach appears to have gone through a period of slope steepening from 1962 to 1992, slope flattening between 1992 and 2002, and then a slight steepening of the slope again from 2002 to 2012. The Isleta to Rio Puerco reach has a period of slope flattening from 1962 to 1972, a period of slope steepening from 1972 to 2002, and then a period of slope flattening again from 2002 to 2012. Reclamation (2012a) performed 1-dimensional numerical sediment and hydraulic modeling, estimating the equilibrium slope for the Isleta to Rio Puerco and Rio Puerco to San Acacia reaches as 0.00077 ft/ft and 0.00076 ft/ft, respectively. This would indicate that the future slope trend would be one of flattening compared to the estimated energy grade slopes. The estimated bed slopes, however, are within this range, which would indicate future changes may dynamically fluctuate around the current bed condition barring no significant changes in the future sediment supply.

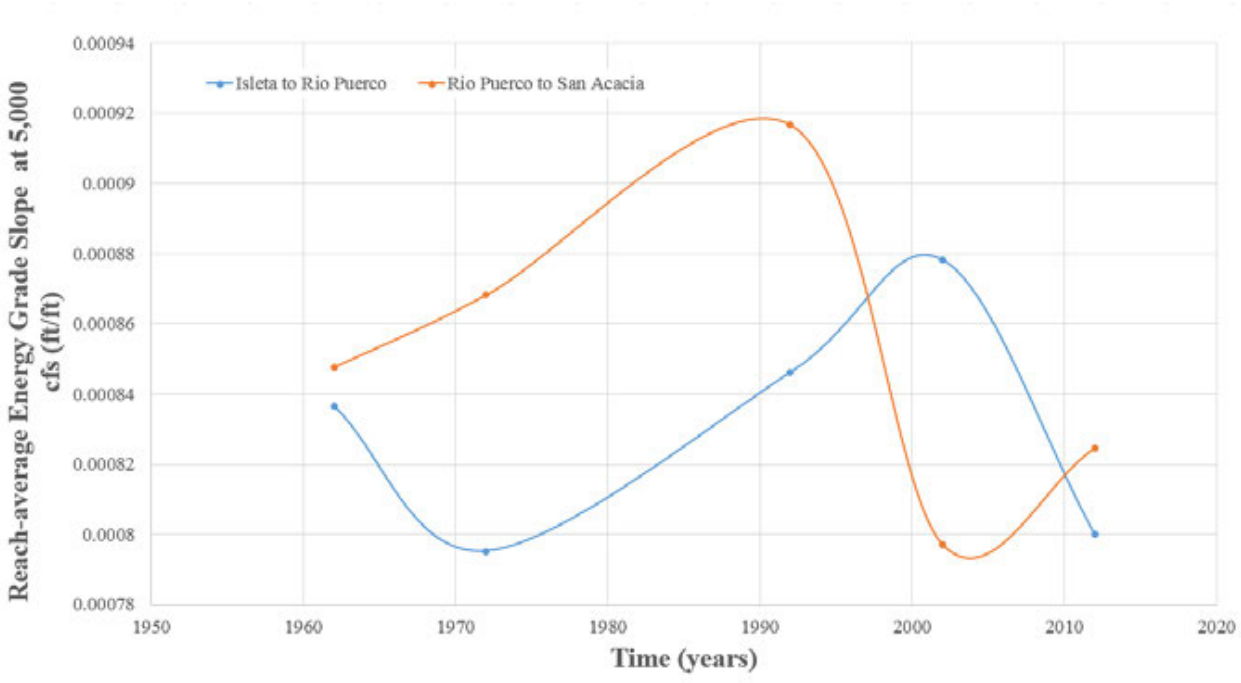

Figure 86. Reach Average Energy Grade Slope values for Isleta to Rio Puerco and Rio Puerco to San Acacia between 1962 and 2012.

4.3.3 Longitudinal River Profiles

Plotting river profiles over time is also a useful way to assess changes occurring in the longitudinal profile of the river. Longitudinal river profiles of the mean channel bed elevations from 1962 to 2014 are plotted from Isleta to San Acacia Diversion Dams. The longitudinal river profiles for the 1962 to 2012 data are obtained photogrammetrically through the decadal aggradation-degradation studies. These studies typically have a vertical accuracy of around +/- one foot. Because the elevation data is captured using photogrammetry techniques or directly through the use of LiDAR, the collected aggradation-degradation data does not capture the underwater prism. The Technical Services Center (TSC) in Denver, CO has developed an iterative process by which the active channel portion of the aggradation-degradation dataset is adjusted (bed is typically lowered) to obtain a best match for wetted channel widths (measured versus numerical model prediction). The underwater prism is assumed to be trapezoidal in shape with a constant bed elevation (Varyu, 2013).The adjusted aggradation-degradation geometry is then processed through an executable program called bedelevation.exe to extract the mean bed elevation between the established aggradation-degradation lines. Mean bed elevations estimated from 1962 to 2012 are shown in Figure 87.

Differences in the mean bed elevation between consecutive aggradation-degradation studies from 1962 and 2012 are shown in Figure 88. Negative differences indicate the mean bed elevation increased between measurements, suggesting a net aggradation condition for the river bed. Positive differences in the mean bed elevation indicate a decrease in the mean bed elevation, implying a net degradation condition for the river bed.

The 2014 cross section bathymetric survey data was obtained from on the ground surveys with an accuracy at a tenth of a foot or better. Because this information is a snapshot in time of the actual underwater bathymetry no further bed adjustments are made for developing a 1-dimensional hydraulic model. The mean depth was obtained by subtracting the hydraulic depth from the water surface elevation at each river cross section (hydraulic depth and water surface elevations are outputs from the hydraulic model at 500 cfs, however, mean bed elevation is not). This results in a slightly lower bed elevation for the 2014 dataset than the other years due to assumptions made in the development of the underwater profile for the aggradation-degradation data sets (Varyu, 2013). The 2014 survey data is plotted against the most recent aggradation-degradation data set (2012) in Figure 89 to provide a general comparison of changes in the mean bed. While the datasets are derived differently and therefore a direct comparison is not possible, it is useful to compare the two longitudinal profiles to see if the general trends are similar. The assumption being that the methodologies resulting in the two longitudinal profiles would produce a consistent difference, implying that the two lines should parallel each other in the absence of ongoing changes. Changes in how the lines track with each other may indicate ongoing changes since 2012.

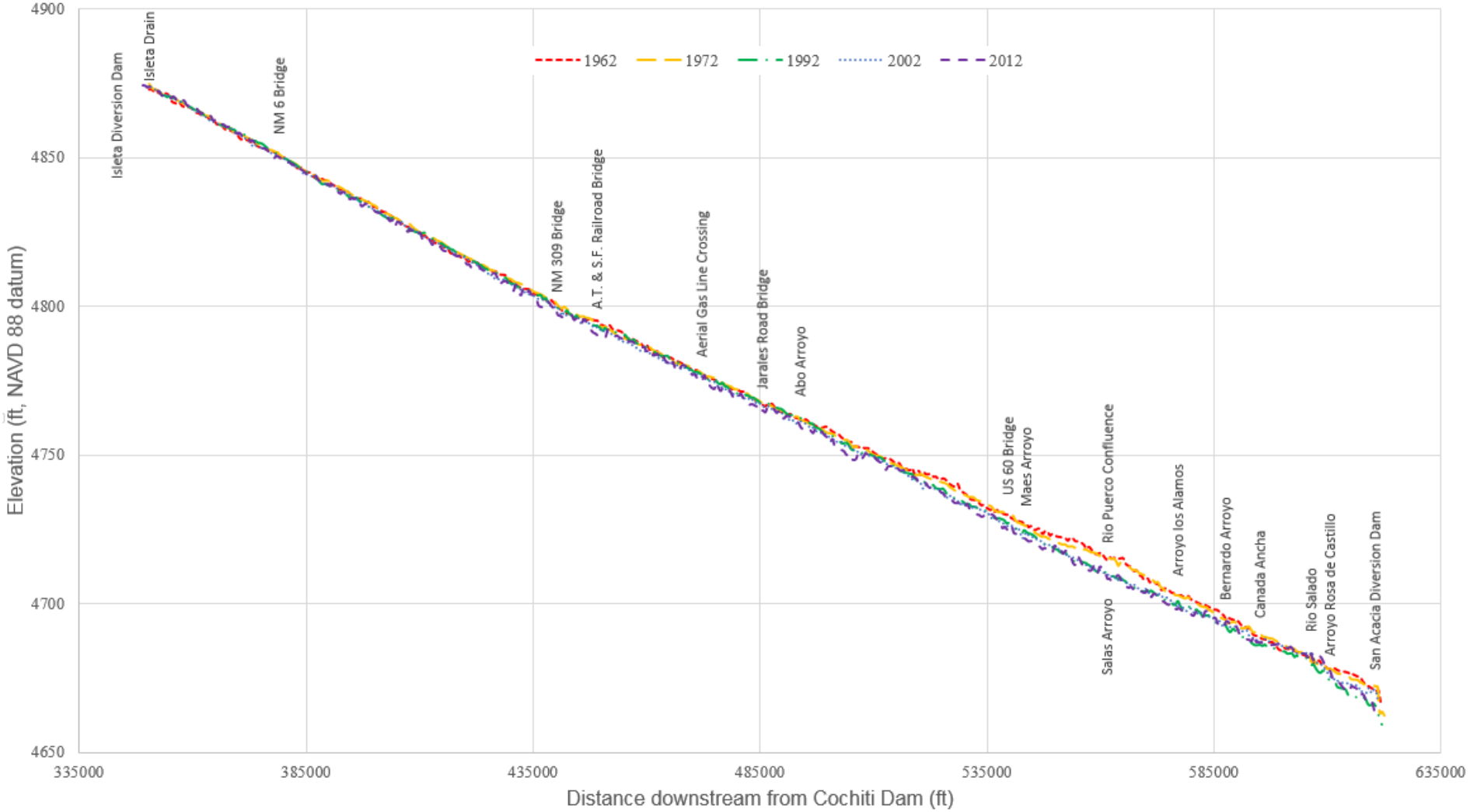

Figure 87. Channel mean bed elevations from 1962 to 2012.

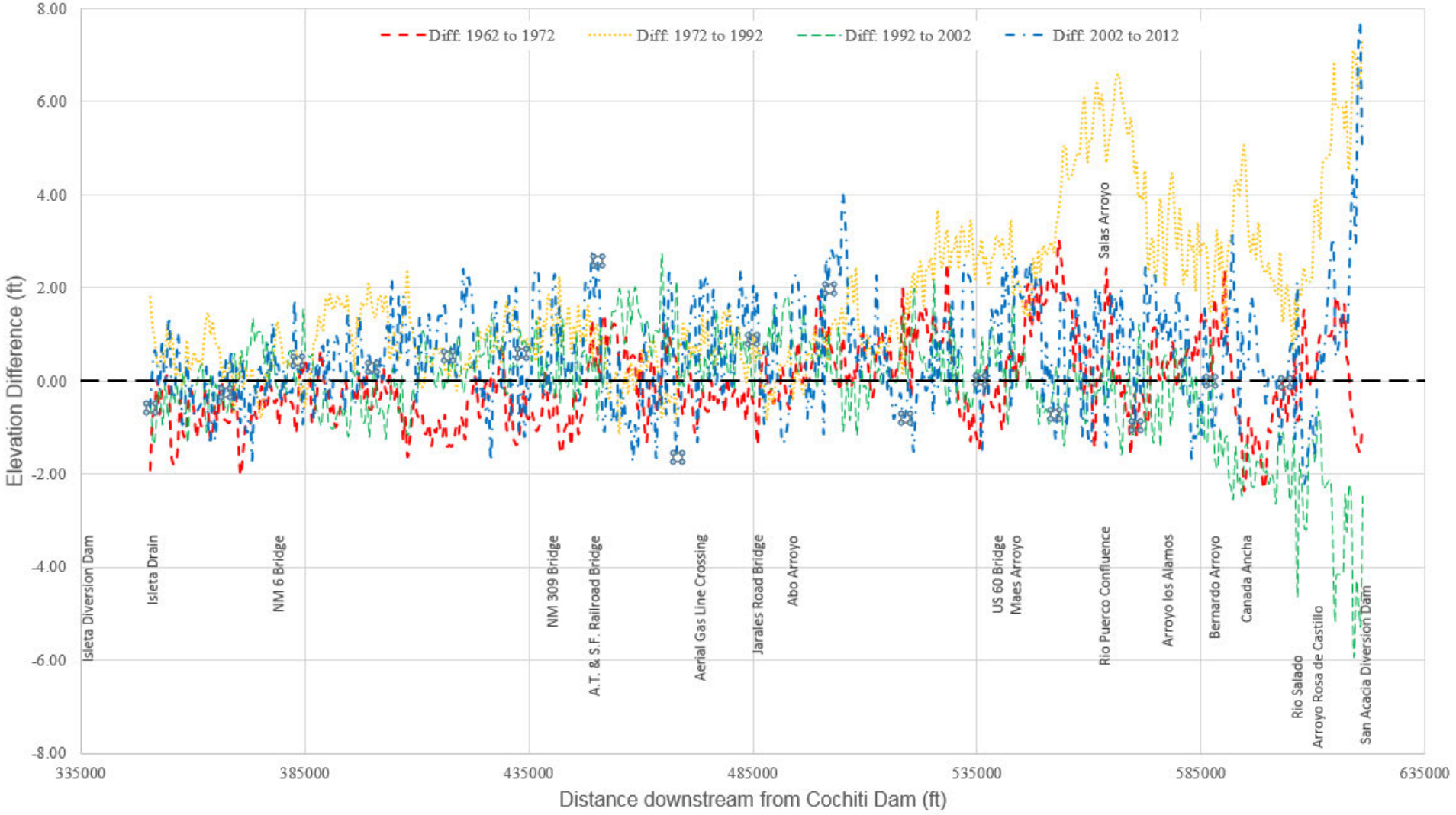

Figure 88. Difference in mean channel bed elevations from 1962 to 2012.

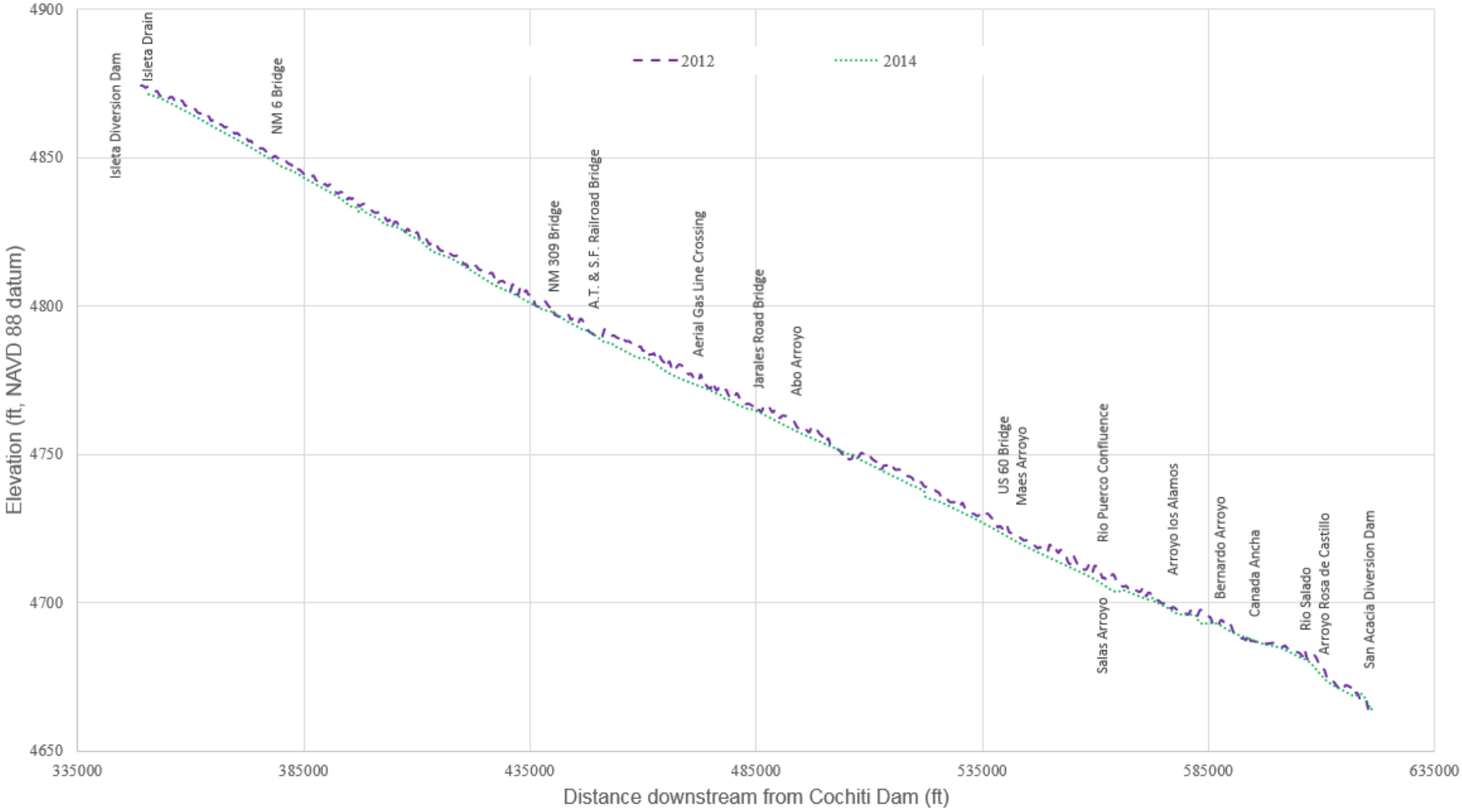

Figure 89. Channel mean bed elevations from 2012 and 2014.

The mean bed longitudinal profiles between Isleta Diversion Dam and the NM 6 Bridge, shown in Figure 87 and Figure 89, look very similar between 1962 and 2014. Figure 88 shows that there have been some slight changes between Isleta and the NM 6 Bridge in Los Lunas, going through periods of slight aggradation and degradation. Figure 89 indicates that the mean channel bed condition in 2014 is similar to that from 2012.

Between the NM 6 Bridge and Abo Arroyo, the mean bed longitudinal profiles shown in Figure 87 and Figure 89 indicate a slight degradational trend (around 0.5 to 1 foot), with a downward shift in the mean bed occurring between 1992 and 2002. Figure 88 indicates that the sub-reach between the NM 6 Bridge and Abo Arroyo tended to be aggradational between 1962 and 1972, but has tended towards a degradational trend since 1972, with some variations in these trends occurring between 1972 and 2012. Figure 89 indicates that the mean channel bed condition in 2014 is similar to that from 2012.

Figure 87 shows a larger downward shift in the mean bed (around one to six feet) occurred between 1972 and 1992 on the Rio Grande between Abo Arroyo and Canada Ancha. The largest degradation occurred around the Rio Puerco confluence. The mean bed is very similar, however, between Canada Ancho and the Rio Salado. Downstream of the Rio Salado, the mean bed degraded between 1972 and 1992, but has aggraded in recent years, likely as sediment has accumulated upstream of San Acacia Diversion Dam. The difference in the mean channel bed elevation, as shown in Figure 88, shows that the sub-reach between Abo Arroyo and San Acacia Diversion Dam was primarily degradational from 1962 to 1992. Then from 1992 to 2002 aggradation occurred, especially immediately upstream of San Acacia Diversion Dam. From 2002 to 2012 the general trend is also degradation, although there is an area around the Rio Salado (both upstream and downstream) that is aggrading. Changes in the longitudinal profile apparent in Figure 89 also suggest that between 2012 and 2014 aggradation may be continuing between the Rio Puerco and the San Acacia Diversion Dam.

4.4 Channel Sinuosity

The Rio Grande has a typical maximum sinuosity around 1.2, which is a relatively low sinuosity compared to other fluvial systems. The current sinuosity trend from the 1930s shows an increase in sinuosity over time.

Figure 90 shows the reach average channel sinuosity for the two geomorphic reaches within the study area. The sinuosity calculation for years 1935 through 2006 was described in Makar (2010) as the active channel centerline divided by the valley length. The sinuosity calculation for 2012 was based on the active channel centerline generated by Reclamation's contractor Woolpert from their 2012 aerial photography products. The sinuosity calculation for 2016 was based on the active channel centerline generated by Reclamation's contractor Atlantic

from their 2016 aerial photography products. The 2013 sinuosity calculation was created from google earth aerial imagery dated 1/17/2013. For years 2012-2016, the valley length was calculated as the centerline between confining geographical features.

The geomorphic reach between the Isleta Diversion Dam and the Rio Puerco had a small peak around 1950, with a continuing trend of increasing sinuosity since 1992. The Rio Puerco to San Acacia reach had a peak in its sinuosity around 1962, which may be a function of channel rectification work (Makar, 2010). A smaller peak occurred in the Rio Puerco to San Acacia reach around 2008. Since 2012 the sinuosity has been increasing in the Rio Puerco to San Acacia reach. This is consistent with the trend of the longitudinal profiles for the mean channel bed which indicate a degradational state except around the Rio Salado confluence. The recent trend of increasing bed and energy grade slope for the Rio Puerco to San Acacia reach seems to be contrary to an increase in the channel sinuosity. However, this slope increase was observed from 2002 to 2012 and the slope adjustment from 1962 to 2012 is still one of decreasing slope, indicating that the recent observations may imply a dynamic variation of the river's slope through this reach rather than a longer term trend.

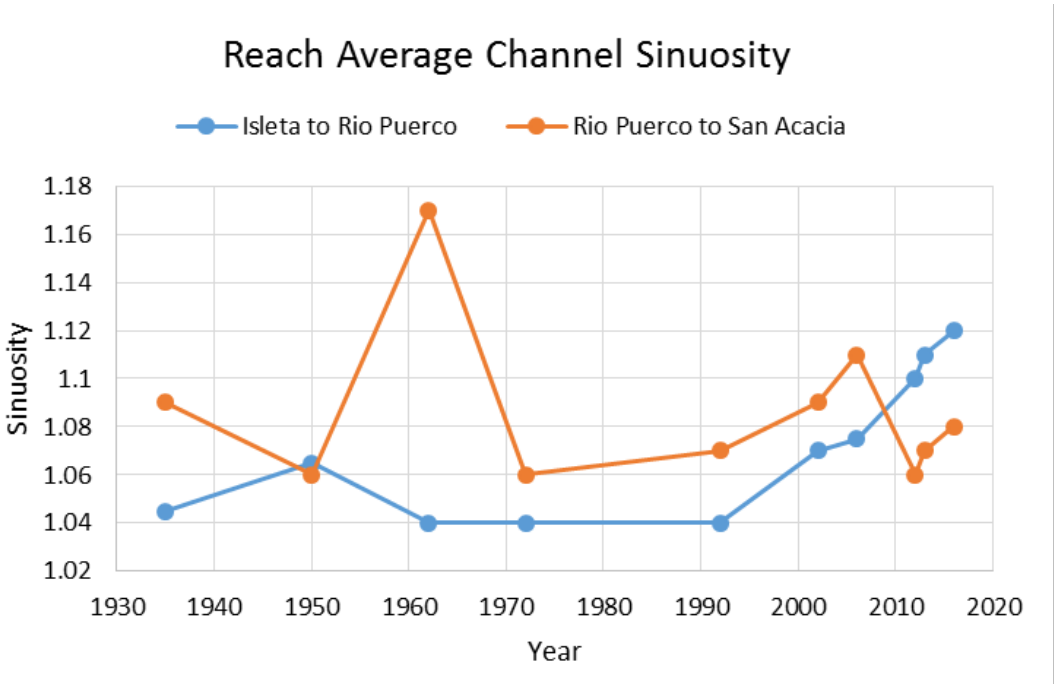

Figure 90. Reach Average Channel Sinuosity over time

4.5 Bed material size and type

The bed material between the Isleta and San Acacia Diversion Dams is primarily sand, with gravel becoming more dominant around the Rio Salado (Makar, 2010; Makar and AuBuchon, 2012; Varyu and Fox, 2014). In general, the bed material

has coarsened over time (Bauer, 2000; Richard et al., 2001; MEI, 2002; Vensel et al., 2006; Bauer, 2009; Reclamation, 2012b). Core samples show alternating layers in the bed, composed of sands, finer material (silts and clays), and gravels (Nordin, 1963; MEI, 2002; Hilldale and Bauer, 2003; Bauer, 2004; Bauer, 2007). Dynamic Cone Penetrometer testing indicated that there is the potential for bed control around the Rio Salado confluence of the Rio Grande (Bauer and Hilldale, 2006).

4.5.1 Median (D_{50}) and D_{84} bed material sizes

Bauer (2009) compiled a database of previously collected bed material samples from the Middle Rio Grande. Figure 91 and Figure 92 build upon his figures by including bed material collected in 2012, 2014, and 2016. The 2012 and 2014 bed material samples were collected by Reclamation contractors (TetraTech, 2012; Easterling Consultants LLC, 2014). The 2016 data collection was collected and processed by Reclamation personnel as described in Appendix A.

Samples in the 2000s (Bauer 2004; Bauer, 2007) were focused primarily on collecting coarser material within a reach and therefore not necessarily collected on an established rangeline. These samples were generally collected after a large spring snow-melt runoff and before the monsoon season. Since these samples were targeting coarser material, the samples are not directly comparable to the rangeline surface sampling of the 1990s and 2010s which collected a representative sample. The rangeline sampling timeframes varied throughout the year and did not always coincide with a collection after the spring snow-melt and before the summer monsoons.

The median bed material grain size was extracted from grain size analysis curves to plot the bed material change and variability over the last three decades (Figure 91). Recent data collections (2012 through 2016) are colored the same as they are from the same decade and provide a quick comparison to the ranges observed in the previous two decades. Each data collection in the 2010s though has a different symbol to help differentiate recent trends (most noticeable around the Rio Salado). In a similar fashion to the median bed material sizes, the one standard deviation (assuming a normal distribution) greater than the median bed material grain size (D_{84}) was extracted from grain size analysis curves to plot the bed material change and variability over the last three decades (Figure 92).

In general there has been a slight coarsening of the bed material between the 1990s and early 2010s. The 2016 samples (collected between spring runoff and monsoon season) show distinct coarsening between the Rio Salado and San Acacia Diversion Dam. The coarsening is more noticeable in the D_{84} graph than the D_{50} graph. Sampling in the 2000s indicated a wider range of bed material, but this may be attributed to temporal and method differences in the bed material sample collections.

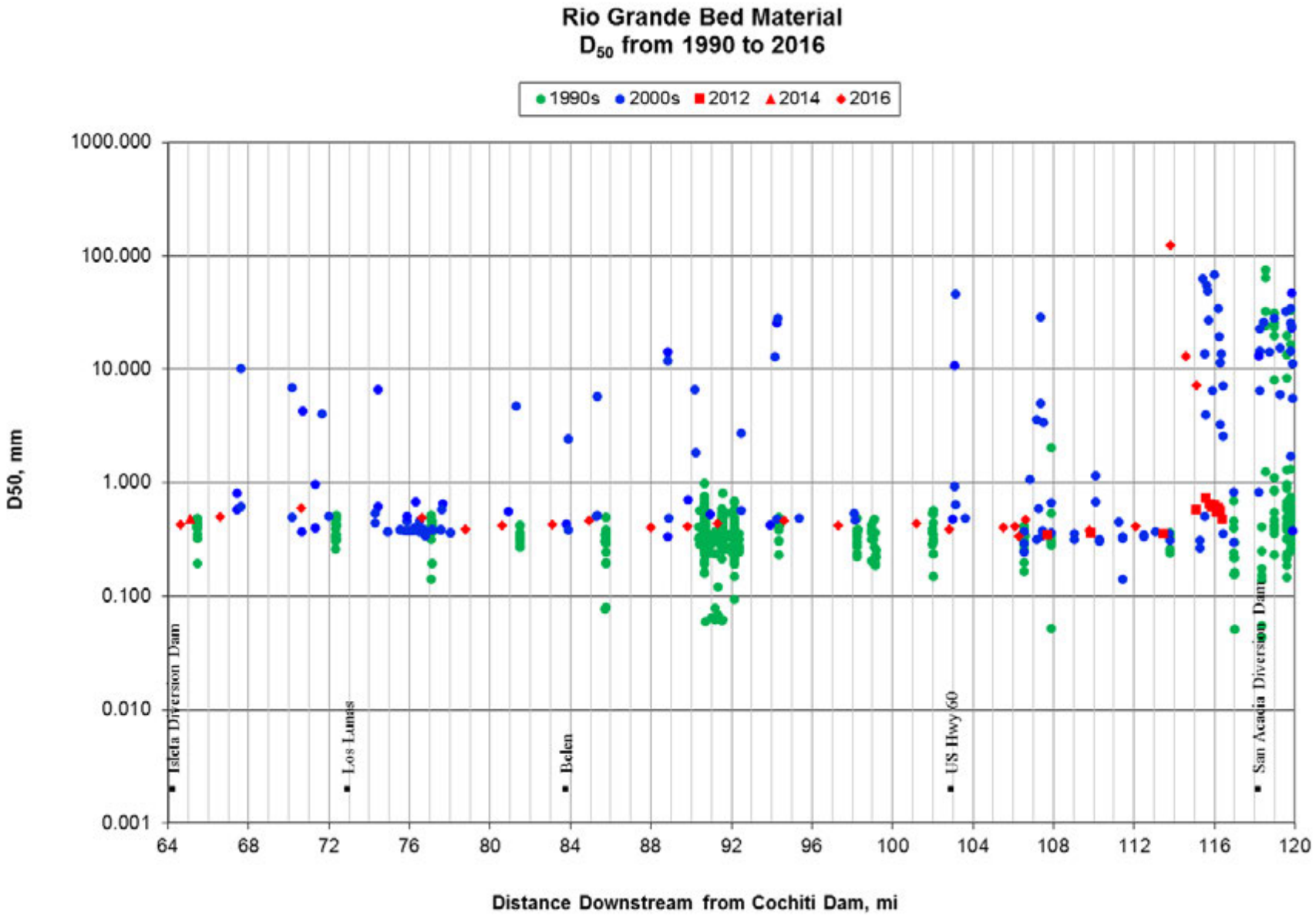

Figure 91. Median Bed Material Size on the Rio Grande from 1990 to 2016

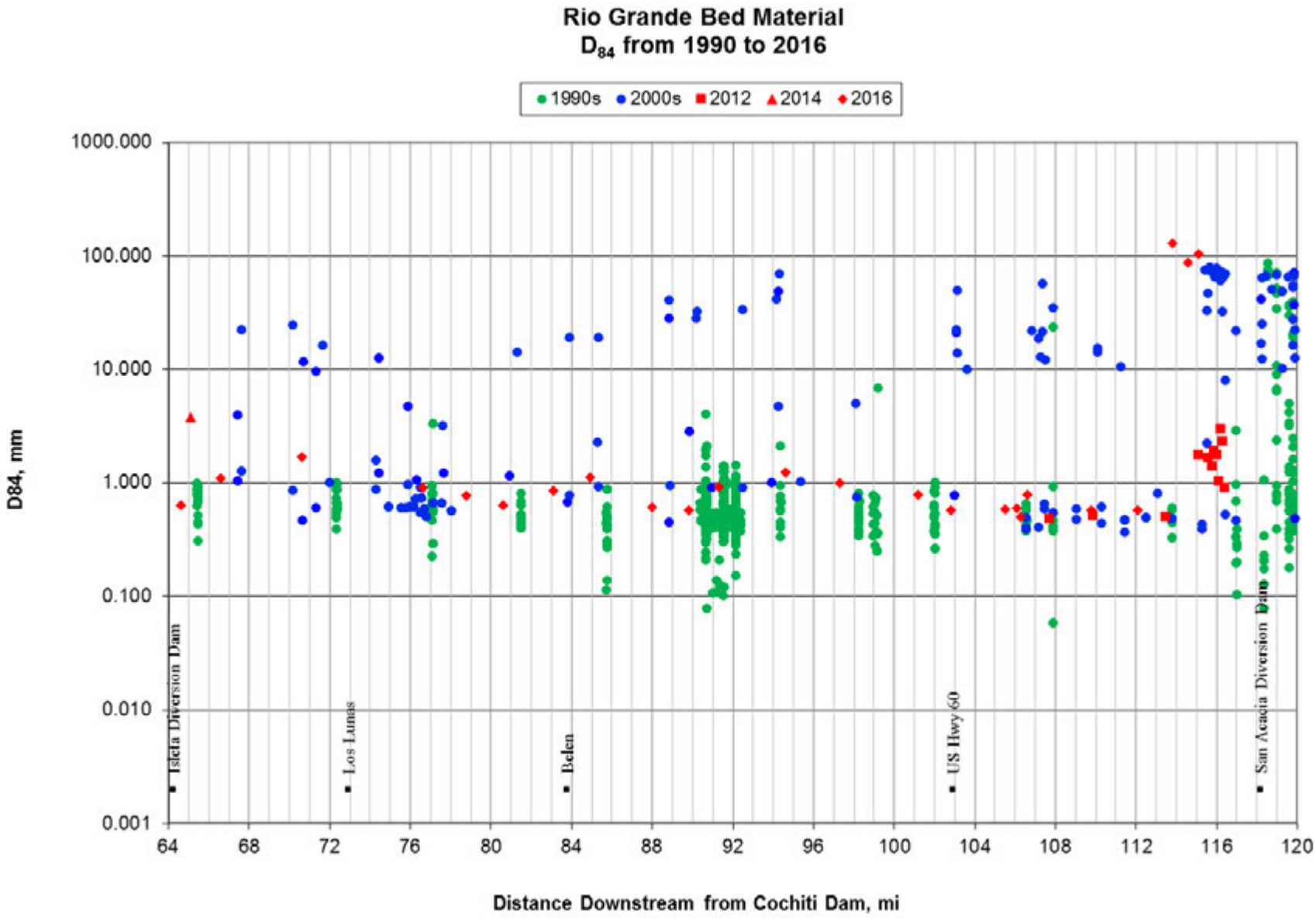

Figure 92. D_{84} Bed Material Size on the Rio Grande from 1990 to 2016

4.5.2 Bed particle stability

Bed stability was assessed at 26 cross sections in the study reach based on data collected between 2014 and 2016. The 2014 Montano to Isleta Dam Hydrographic Data Collection Report (Easterling Consultants LLC, 2014) provided bed material data on two Isleta cross sections. In the summer of 2016, Reclamation employees collected bed samples at 24 sites and processed these samples to determine the D_{50} and D_{84}, as described in Appendix A. Using data generated from a grain size analysis of the samples, the critical shear stress was calculated (see Table 22). Critical shear stress was calculated for the bed material (D_{50} and D_{84}). A 1-D numerical model was then used to provide estimates for average normal shear stress on the channel bed (see Table 23). The normal shear stress was then compared to the critical shear stress (Table 24 and Table 25) to assess the bed stability. If the critical shear stress was less than the expected cross section shear stress, then the bed material was expected to erode, but if the critical shear stress was greater than this threshold, the bed material was expected to remain stable. Bed particle stability results indicate that the surface bed material is unstable between Isleta and San Acacia Diversion Dams except around the Rio Salado confluence.

4.5.2.1 Critical Shear Stress

Critical shear stress is the minimum shear stress needed to initiate movement of the bed material particle (Lagasse et al., 2009). As the shear stress increases on the bed material particle with increasing energy in the fluvial system, eventually the driving forces will overcome the resisting forces and motion will occur. This initial motion is called incipient motion. Estimating the critical shear stresses provides an estimate of when incipient motion may occur. Critical shear stresses for this analysis were calculated using the Shield's equation (Yang, 1996). The critical shear stress was calculated for both the D_{50} and D_{84} particle size by using Equation 1 and Equation 2.

Equation 1. Critical Shear Stress for d_{50} (Yang, 1996) $$\tau_c = K_s*(\gamma_s - \gamma_w)*d_{50}$$

Equation 2. Critical Shear Stress for d_{84} (Yang, 1996) $$\tau_c = K_s*(\gamma_s - \gamma_w)*d_{84}$$

Where τ_c = critical shear stress [lb/ft^2],
K_s = Shields parameter [0.03]
γ_s = specific weight of sediment [165 lb/ft^3],
γ_w = specific weight of water [62.4 lb/ft^3],
d_{50} = median grain size [ft], and
d_{84} = one standard deviation greater than the median grain size [ft].

Shield's parameter was assumed to be 0.03 (Yang, 1996). The Shield's parameter can vary from 0.045 to 0.01 depending on the sand content of bed material (Wilcox et al., 2009). Larger Shield's parameter values might suggest that bed material was stable at certain flows when in reality the material may be transported, while smaller Shield's parameter values may suggest a more mobile

scenario. The majority of the collected samples are within the sand range, however there are gravels present (2 to 32 mm size range) and around the Rio Salado confluence even small cobbles (64 to 128 mm size range). Because of a mixed presence of sand and gravel a Shield's parameter value of 0.03 was used for this analysis. The specific weight of sediment was assumed to be 165 pounds per cubic foot (pcf). Table 22 provides the critical shear stress values calculated at 26 cross sections between Isleta and San Acacia Diversion Dams.

Table 22: Critical shear stress values for the D_{50} and D_{84} particle sizes.

Cross Section	D_{50} Critical Shear Stress (lb/ft^2)	D_{84} Critical Shear Stress (lb/ft^2)
IS-658	0.003	0.005
IS-675	0.005	0.039
IS-668	0.004	0.006
IS-690	0.005	0.011
732	0.006	0.017
LL-793	0.005	0.009
IS-815	0.004	0.008
CO-833	0.004	0.006
857	0.004	0.009
CO-877	0.005	0.011
IS-908	0.004	0.006
CC-927	0.004	0.006
CC-943	0.004	0.009
976	0.005	0.012
1004	0.004	0.010
CO-1044	0.004	0.008
1061	0.004	0.006
CO-1091	0.004	0.006
CO-1097	0.004	0.006
RP-1100	0.003	0.005
CO-1104	0.005	0.008
LJ-18	0.004	0.006
RP-1164	0.004	0.006
1183	1.253	1.317
RP-1190	0.133	0.892
CO-1194	0.073	1.064

4.5.2.2 Channel Shear Stress

Average channel shear stress values were estimated for a flow of 500 cfs and in 1,000 cfs intervals for flows between 1,000 cfs and 10,000 cfs. Most of the cross sections' shear stress was calculated using a 1-D numerical hydraulic model built from data gathered between 2012 and 2015. The model was run in HEC-RAS version 5.0.3, and average channel shear stress was a direct model output. The model was based on the 2015 channel geometry as described in The Isleta to San Acacia Hydraulic Modeling Report (Klein et al., 2018).

An additional numerical hydraulic model was used near the upstream end, since the 2015 model did not consist of rangelines near Isleta Diversion Dam. A different 1-D numerical hydraulic model was therefore built from the 2012 aggradation-degradation (agg-deg) data set. The 2012 model was used to generate data for the three upstream cross sections (IS-658, agg-deg line 668, and IS-675). The model was run in HEC-RAS version 5.0.3, and the model outputs of average energy grade slope and channel hydraulic radius were extracted. An average channel shear stress was calculated using Equation 3.

Equation 3. Average normal shear stress on the channel bed (Akan, 2006) $\tau_o = \gamma R S_f$

Where τ_o = channel shear stress [lb/ft^2],
γ = specific weight of water [62.4 lb/ft^3],
R = hydraulic radius [ft], and
S_f = channel slope [ft/ft].

The channel slope used for IS-658 through IS-675 was assumed to be represented by the average bed slope between IS-657 and IS-676. All other average normal shear stress calculation used the average energy grade slope at the specific cross section. Average normal shear stress value are shown in Table 23.

Table 23. Average normal shear stress values for the D_{50} and D_{84} particle sizes.

Cross Section	500 cfs	1,000 cfs	2,000 cfs	3,000 cfs	4,000 cfs	5,000 cfs	6,000 cfs	7,000 cfs	8,000 cfs	9,000 cfs	10,000 cfs
IS-658	0.07	0.11	0.15	0.19	0.21	0.23	0.23	0.24	0.25	0.26	0.27
668	0.08	0.13	0.19	0.23	0.27	0.27	0.29	0.24	0.25	0.26	0.29
IS-675	0.05	0.09	0.14	0.17	0.19	0.21	0.24	0.27	0.20	0.21	0.21
IS-690	0.08	0.12	0.18	0.24	0.25	0.25	0.3	0.33	0.35	0.37	0.39
732	0.05	0.07	0.1	0.12	0.15	0.14	0.16	0.17	0.19	0.2	0.21
LL-793	0.06	0.09	0.13	0.16	0.18	0.18	0.19	0.21	0.24	0.24	0.26
IS-815	0.07	0.1	0.14	0.18	0.2	0.2	0.22	0.23	0.25	0.26	0.28
CO-833	0.11	0.15	0.21	0.26	0.31	0.31	0.33	0.36	0.39	0.41	0.43
857	0.06	0.08	0.1	0.11	0.12	0.12	0.13	0.14	0.15	0.16	0.17
CO-877	0.1	0.12	0.15	0.16	0.17	0.16	0.17	0.2	0.22	0.23	0.25
IS-908	0.1	0.13	0.17	0.21	0.24	0.24	0.25	0.27	0.26	0.33	0.3
CC-927	0.07	0.1	0.16	0.18	0.22	0.22	0.24	0.27	0.29	0.3	0.32
CC-943	0.09	0.15	0.15	0.15	0.14	0.13	0.16	0.17	0.17	0.18	0.19
976	0.09	0.105	0.155	0.18	0.21	0.21	0.235	0.25	0.265	0.28	0.29
1004	0.07	0.12	0.19	0.25	0.28	0.28	0.32	0.35	0.38	0.42	0.43
CO-1044	0.09	0.13	0.18	0.23	0.25	0.25	0.27	0.29	0.31	0.33	0.33
1061	0.12	0.19	0.3	0.2	0.24	0.25	0.28	0.3	0.32	0.34	0.35
CO-1091	0.1	0.12	0.17	0.19	0.18	0.18	0.19	0.19	0.19	0.2	0.2
CO-1097	0.06	0.11	0.2	0.29	0.32	0.38	0.37	0.41	0.45	0.49	0.53
RP-1100	0.06	0.11	0.2	0.29	0.32	0.38	0.37	0.41	0.45	0.49	0.53
CO-1104	0.06	0.09	0.15	0.2	0.24	0.24	0.28	0.31	0.34	0.38	0.41
LJ-18	0.03	0.07	0.13	0.14	0.2	0.2	0.22	0.24	0.25	0.26	0.26
RP-1164	0.05	0.08	0.14	0.18	0.22	0.22	0.25	0.27	0.29	0.32	0.34
1183	0.13	0.19	0.3	0.39	0.48	0.47	0.54	0.59	0.51	0.62	0.69
RP-1190	0.08	0.1	0.13	0.15	0.16	0.15	0.16	0.19	0.21	0.2	0.2
CO-1194	0.12	0.16	0.23	0.29	0.36	0.35	0.41	0.34	0.35	0.36	0.37

Table 24: Predicted bed stability for D50 grain size.

Cross Section	D_{50} Grain Size (mm)	500 cfs	1,000 cfs	2,000 cfs	3,000 cfs	4,000 cfs	5,000 cfs	6,000 cfs	7,000 cfs	8,000 cfs	9,000 cfs	10,000 cfs
IS-658	0.34	Unstable	Unstable	Unstable	Unstable	Unstable	Unstable	Unstable	Unstable	Unstable	Unstable	Unstable
IS-668	0.43	Unstable	Unstable	Unstable	Unstable	Unstable	Unstable	Unstable	Unstable	Unstable	Unstable	Unstable
IS-675	0.48	Unstable	Unstable	Unstable	Unstable	Unstable	Unstable	Unstable	Unstable	Unstable	Unstable	Unstable
IS-690	0.50	Unstable	Unstable	Unstable	Unstable	Unstable	Unstable	Unstable	Unstable	Unstable	Unstable	Unstable
732	0.60	Unstable	Unstable	Unstable	Unstable	Unstable	Unstable	Unstable	Unstable	Unstable	Unstable	Unstable
LL-793	0.49	Unstable	Unstable	Unstable	Unstable	Unstable	Unstable	Unstable	Unstable	Unstable	Unstable	Unstable
IS-815	0.39	Unstable	Unstable	Unstable	Unstable	Unstable	Unstable	Unstable	Unstable	Unstable	Unstable	Unstable
CO-833	0.42	Unstable	Unstable	Unstable	Unstable	Unstable	Unstable	Unstable	Unstable	Unstable	Unstable	Unstable
857	0.43	Unstable	Unstable	Unstable	Unstable	Unstable	Unstable	Unstable	Unstable	Unstable	Unstable	Unstable
CO-877	0.46	Unstable	Unstable	Unstable	Unstable	Unstable	Unstable	Unstable	Unstable	Unstable	Unstable	Unstable
IS-908	0.40	Unstable	Unstable	Unstable	Unstable	Unstable	Unstable	Unstable	Unstable	Unstable	Unstable	Unstable
CC-927	0.41	Unstable	Unstable	Unstable	Unstable	Unstable	Unstable	Unstable	Unstable	Unstable	Unstable	Unstable
CC-943	0.44	Unstable	Unstable	Unstable	Unstable	Unstable	Unstable	Unstable	Unstable	Unstable	Unstable	Unstable
976	0.46	Unstable	Unstable	Unstable	Unstable	Unstable	Unstable	Unstable	Unstable	Unstable	Unstable	Unstable
1004	0.42	Unstable	Unstable	Unstable	Unstable	Unstable	Unstable	Unstable	Unstable	Unstable	Unstable	Unstable
CO-1044	0.44	Unstable	Unstable	Unstable	Unstable	Unstable	Unstable	Unstable	Unstable	Unstable	Unstable	Unstable
1061	0.39	Unstable	Unstable	Unstable	Unstable	Unstable	Unstable	Unstable	Unstable	Unstable	Unstable	Unstable
CO-1091	0.40	Unstable	Unstable	Unstable	Unstable	Unstable	Unstable	Unstable	Unstable	Unstable	Unstable	Unstable
CO-1097	0.41	Unstable	Unstable	Unstable	Unstable	Unstable	Unstable	Unstable	Unstable	Unstable	Unstable	Unstable
RP-1100	0.34	Unstable	Unstable	Unstable	Unstable	Unstable	Unstable	Unstable	Unstable	Unstable	Unstable	Unstable
CO-1104	0.47	Unstable	Unstable	Unstable	Unstable	Unstable	Unstable	Unstable	Unstable	Unstable	Unstable	Unstable
LJ-18	0.38	Unstable	Unstable	Unstable	Unstable	Unstable	Unstable	Unstable	Unstable	Unstable	Unstable	Unstable
RP-1164	0.41	Unstable	Unstable	Unstable	Unstable	Unstable	Unstable	Unstable	Unstable	Unstable	Unstable	Unstable
1183	123.68	Stable	Stable	Stable	Stable	Stable	Stable	Stable	Stable	Stable	Stable	Stable
RP-1190	13.08	Stable	Stable	Stable	Unstable	Unstable	Unstable	Unstable	Unstable	Unstable	Unstable	Unstable
CO-1194	7.21	Unstable	Unstable	Unstable	Unstable	Unstable	Unstable	Unstable	Unstable	Unstable	Unstable	Unstable

Table 25: Predicted bed stability for D_{84} grain size.

Cross Section	D_{84} Grain Size (mm)	500 cfs	1,000 cfs	2,000 cfs	3,000 cfs	4,000 cfs	5,000 cfs	6,000 cfs	7,000 cfs	8,000 cfs	9,000 cfs	10,000 cfs
IS-658	0.51	Unstable	Unstable	Unstable	Unstable	Unstable	Unstable	Unstable	Unstable	Unstable	Unstable	Unstable
IS-668	0.64	Unstable	Unstable	Unstable	Unstable	Unstable	Unstable	Unstable	Unstable	Unstable	Unstable	Unstable
IS-675	3.82	Unstable	Unstable	Unstable	Unstable	Unstable	Unstable	Unstable	Unstable	Unstable	Unstable	Unstable
IS-690	1.10	Unstable	Unstable	Unstable	Unstable	Unstable	Unstable	Unstable	Unstable	Unstable	Unstable	Unstable
732	1.68	Unstable	Unstable	Unstable	Unstable	Unstable	Unstable	Unstable	Unstable	Unstable	Unstable	Unstable
LL-793	0.90	Unstable	Unstable	Unstable	Unstable	Unstable	Unstable	Unstable	Unstable	Unstable	Unstable	Unstable
IS-815	0.77	Unstable	Unstable	Unstable	Unstable	Unstable	Unstable	Unstable	Unstable	Unstable	Unstable	Unstable
CO-833	0.63	Unstable	Unstable	Unstable	Unstable	Unstable	Unstable	Unstable	Unstable	Unstable	Unstable	Unstable
857	0.85	Unstable	Unstable	Unstable	Unstable	Unstable	Unstable	Unstable	Unstable	Unstable	Unstable	Unstable
CO-877	1.13	Unstable	Unstable	Unstable	Unstable	Unstable	Unstable	Unstable	Unstable	Unstable	Unstable	Unstable
IS-908	0.61	Unstable	Unstable	Unstable	Unstable	Unstable	Unstable	Unstable	Unstable	Unstable	Unstable	Unstable
CC-927	0.58	Unstable	Unstable	Unstable	Unstable	Unstable	Unstable	Unstable	Unstable	Unstable	Unstable	Unstable
CC-943	0.92	Unstable	Unstable	Unstable	Unstable	Unstable	Unstable	Unstable	Unstable	Unstable	Unstable	Unstable
976	1.23	Unstable	Unstable	Unstable	Unstable	Unstable	Unstable	Unstable	Unstable	Unstable	Unstable	Unstable
1004	1.00	Unstable	Unstable	Unstable	Unstable	Unstable	Unstable	Unstable	Unstable	Unstable	Unstable	Unstable
CO-1044	0.79	Unstable	Unstable	Unstable	Unstable	Unstable	Unstable	Unstable	Unstable	Unstable	Unstable	Unstable
1061	0.58	Unstable	Unstable	Unstable	Unstable	Unstable	Unstable	Unstable	Unstable	Unstable	Unstable	Unstable
CO-1091	0.59	Unstable	Unstable	Unstable	Unstable	Unstable	Unstable	Unstable	Unstable	Unstable	Unstable	Unstable
CO-1097	0.60	Unstable	Unstable	Unstable	Unstable	Unstable	Unstable	Unstable	Unstable	Unstable	Unstable	Unstable
RP-1100	0.50	Unstable	Unstable	Unstable	Unstable	Unstable	Unstable	Unstable	Unstable	Unstable	Unstable	Unstable
CO-1104	0.78	Unstable	Unstable	Unstable	Unstable	Unstable	Unstable	Unstable	Unstable	Unstable	Unstable	Unstable
LJ-18	0.57	Unstable	Unstable	Unstable	Unstable	Unstable	Unstable	Unstable	Unstable	Unstable	Unstable	Unstable
RP-1164	0.58	Unstable	Unstable	Unstable	Unstable	Unstable	Unstable	Unstable	Unstable	Unstable	Unstable	Unstable
1183	130.00	Stable	Stable	Stable	Stable	Stable	Stable	Stable	Stable	Stable	Stable	Stable
RP-1190	88.00	Stable	Stable	Stable	Stable	Stable	Stable	Stable	Stable	Stable	Stable	Stable
CO-1194	105.00	Stable	Stable	Stable	Stable	Stable	Stable	Stable	Stable	Stable	Stable	Stable

4.6 Channel and Floodway Topography

4.6.1 Hydrographic Cross Section Comparison

Hydrographic cross sections were compiled at 80 selected rangelines between the Isleta Diversion Dam and San Acacia Diversion Dam (distance of approximately 54 river miles). Elevation data within each of the profiles was obtained from cross sectional surveys conducted for Reclamation by independent contractors since 1995 (Flo, 1995; Flo, 1996; Flo, 1998a; Flo, 1998b; Flo, 1999a; Flo, 1999b; Tetra Tech, 2000; CSU, 2002; Tetra Tech, 2002; BIO, 2005a; BIO, 2005b; Tetra Tech, 2005; Tetra Tech, 2012; SSWD, 2014; Tetra Tech, 2015; Tetra Tech, 2016). The available years for each individual rangeline vary since not all rangelines are surveyed every year. The rangelines for which data post 1995 is available are listed in Table 26. Analysis was conducted on all rangelines with more than one temporal survey during the analysis period (1995 through 2016). Appendix B provides the specific rangeline comparisons and briefly describes the observable morphological changes over time.

Table 26. Rangelines between Isleta and San Acacia Diversion Dams used for cross section comparison between 1995 and 2016.

Rangeline	1995	1996	1998	1999	2000	2002	2004	2005	2006	2012	2013	2014	2015	2016
IS-691			X									X		
IS-705			X									X		
CO-713	X		X									X		
CO-738.1	X		X									X		
IS-741			X									X		
IS-748			X									X		
IS-752			X									X		
CO-765	X		X				X					X		
IS-772			X			X	X					X		
LL-774						X	X	X				X		
LL-775						X	X	X				X		
LL-776						X	X	X				X		
LL-778						X	X	X				X		
LL-779						X	X	X				X		
LL-781						X	X	X				X		
IS-782			X			X		X				X		
LL-783						X	X	X				X		
LL-784						X	X					X		
CO-787	X	X	X				X					X		
LL-792						X	X					X		
IS-797			X			X	X					X		

Rangeline	1995	1996	1998	1999	2000	2002	2004	2005	2006	2012	2013	2014	2015	2016
IS-801			X									X		
CO-806	X	X	X									X		
IS-815			X									X		
CO-833	X		X									X		
IS-841			X									X		
IS-849			X									X		
IS-854			**X**									X		
CO-858.1	X	X	X									X		
IS-864			X									X		
IS-872			X									X		
CO-877	X		X									X		
IS-880			X										X	X
IS-884			X										X	X
IS-885			X										X	X
IS-887			X										X	X
CO-895	X		X										**X**	X
IS-899			X										X	X
IS-908			X										X	X
CC-924	X	X											**X**	X
CC-927	X	X	X	X									X	X
CC-932	X	X											X	X
CC-936	X	X	X										X	X
CC-941	X	X											X	X
CC-945	X	X											X	X
CO-966	X		X										X	X
CO-986	X		X										X	X
CO-1006	X		X										X	X
AH-1													X	X
AH-3													X	X
AH-5													X	X
AH-7													X	X
CO-1026	X		X										X	X
CO-1044	X		X										X	X
CO-1064	X		X										X	X
CO-1091	X	X	X		X								X	X
RP-1100					**X**					X			**X**	**X**
CO-1104	X	X	X		**X**								X	
RP-1108					X					X			X	X
RP-1144					**X**					X			X	**X**
RP-1150					**X**					X			X	X

Rangeline	1995	1996	1998	1999	2000	2002	2004	2005	2006	2012	2013	2014	2015	2016
RP-1160					X					X			X	X
CO-1164	X	X	X		X								X	X
RP-1170					X					X			X	X
CO-1179	X		X							X			X	X
CO -1184					X					X			X	X
RP-1190					X					X			X	X
CO-1194	X		X		X					X			X	X
RP-1197.5									X	X			X	X
RP-1201					X				X	X			X	X
RP-1202.5									X	X			X	X
RP-1203.7									X	X			X	X
RP-1204.5									X	X			X	X
RP-1205					X				X	X			X	X
RP-1205.8									X	X			X	X

4.6.2 Rangeline Grouping and Typical Representatives

In order to summarize the cross section changes that have temporally occurred for cross section depth, width, and bank height, a single rangeline was chosen within each of eight delineated areas in Figure 93, each about seven miles in length. Reported measurements of depth, width and bank height were assessed for the oldest and most recent rangeline survey. Groupings of rangelines were arranged so that the selected rangline expressed the same general cross section trends as the other rangelines in the selected area. The one exception was image area #8 (Figure 101) where two rangelines were selected due to observed difference through this reach. The observed differences can spatially be separated by the Rio Salado and are likely due to the sediment load being delivered by the Rio Salado to the Rio Grande. The representative rangelines are summarized in Table 27. Each of the eight identified areas is shown in Figure 94 through Figure 101. Additional information about each cross section can also be found in Appendix B.

Figure 102 provides a typical cross section schematic to illustrate definitions for channel depth, width, and height. This schematic illustrates how they were measured in this analysis for use in Table 27. The focus for this illustration is on the decade between January 2004 and March 2014 (January 1998 and April 2002 surveys are not displayed on the graph for clarity). It should also be noted that the definitions used to extract width, depth, and channel bank were useful to make consistent comparisons between years for this analysis.

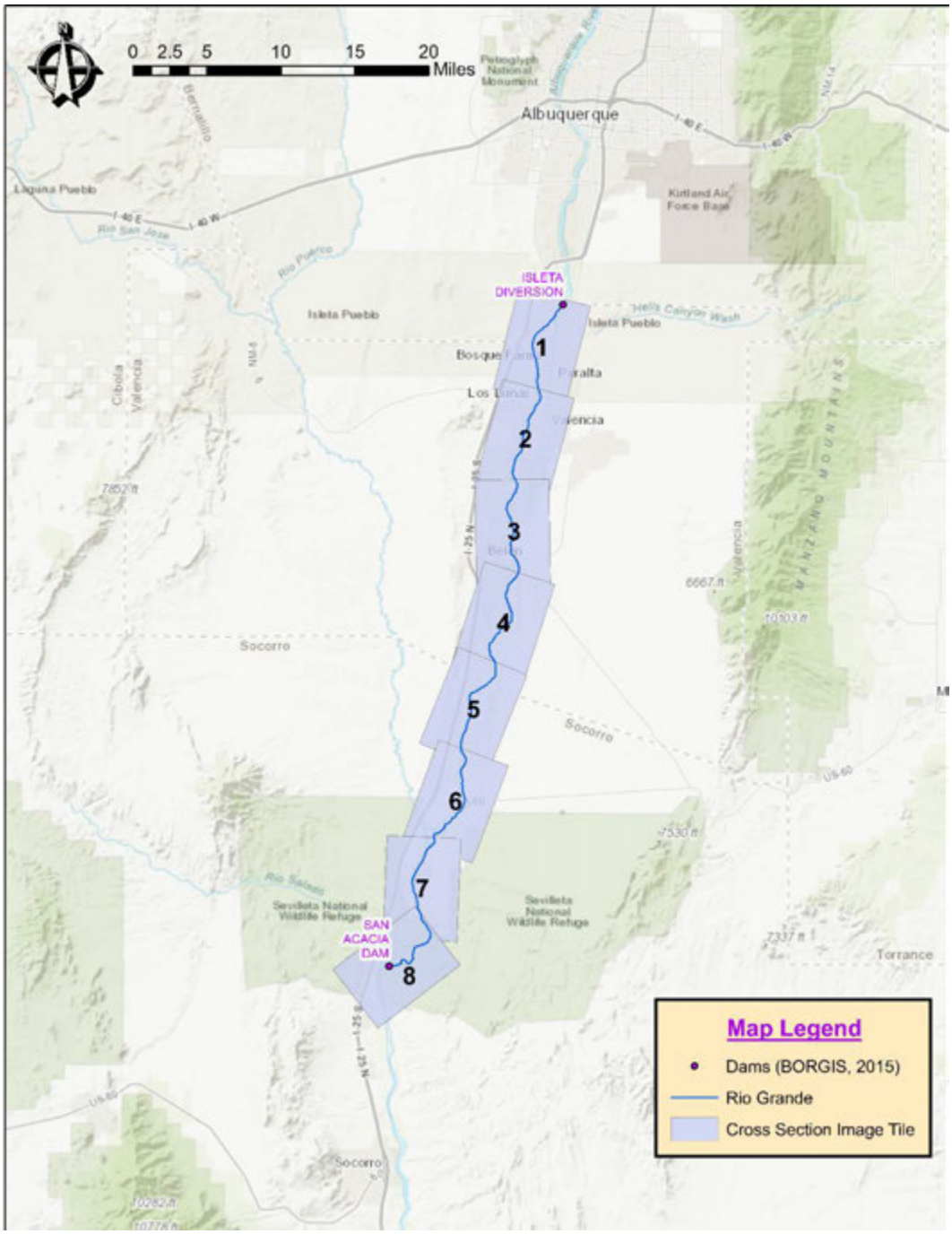

Figure 93. Identification of representative rangelines between Isleta and San Acacia Diversion Dams (basemap topographic layer from ESRI online, 2017).

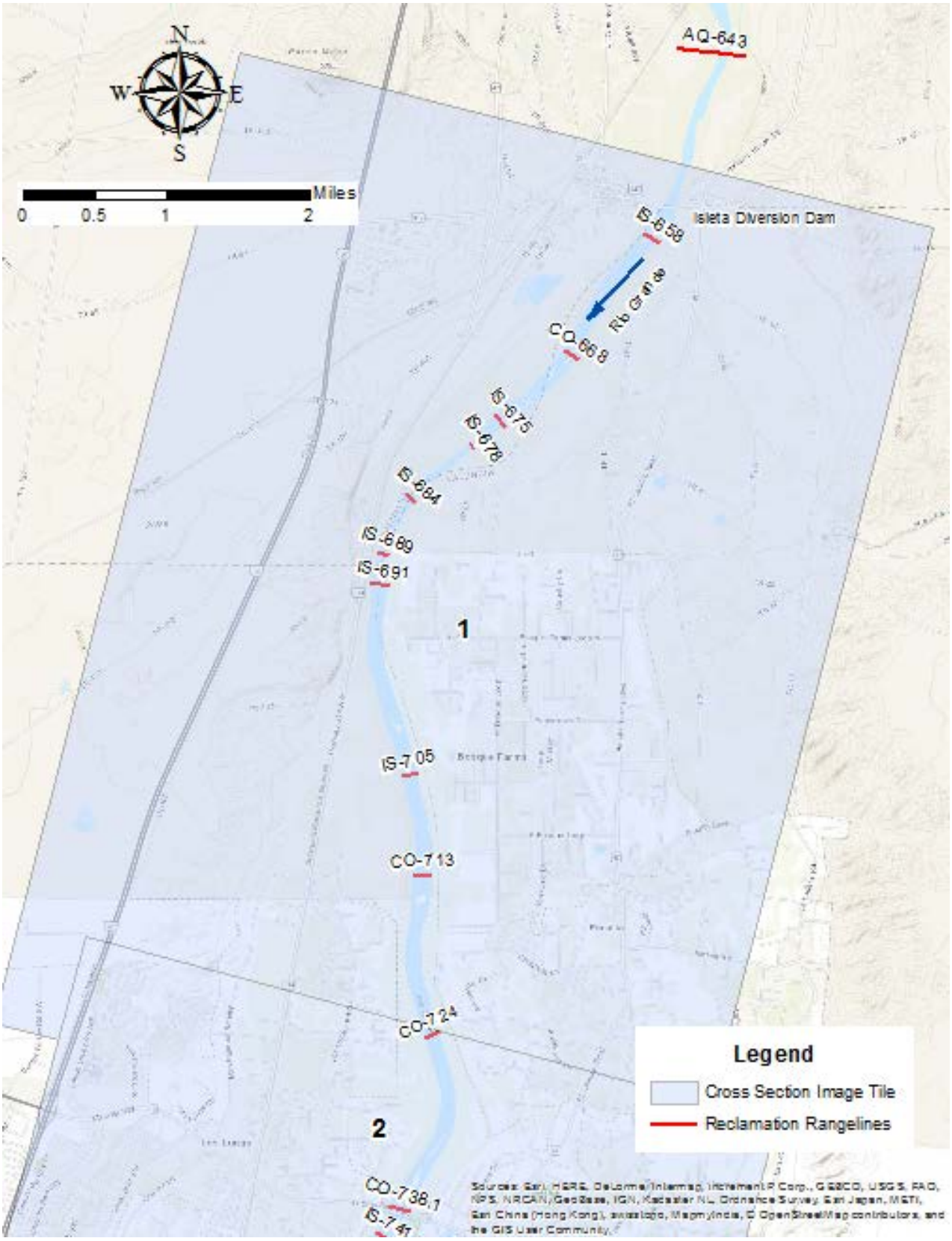

Figure 94. Delineated rangeline area #1 beginning at the Isleta Diversion Dam to Los Lunas, NM (basemap topographic layer from ESRI online, 2018).

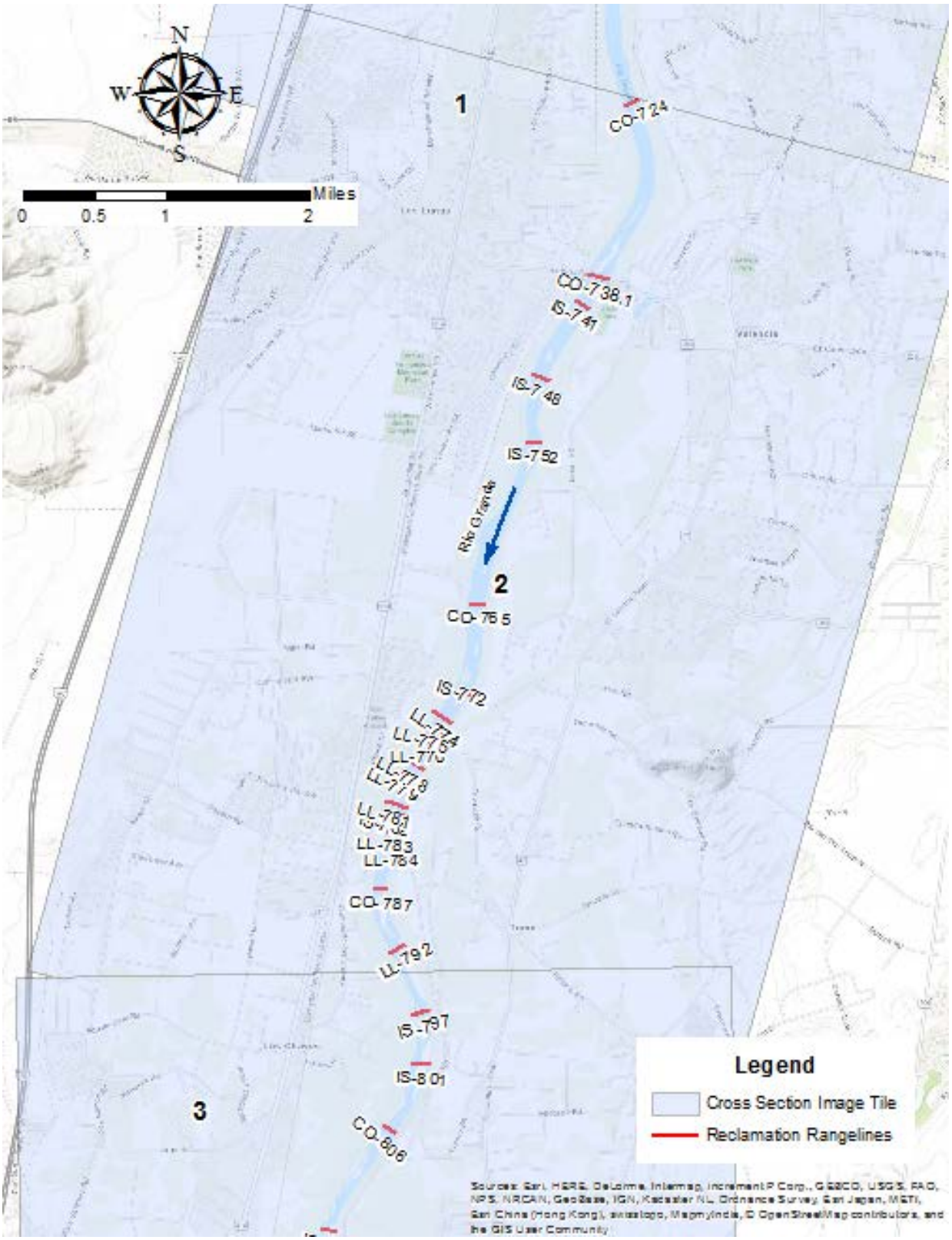

Figure 95. Delineated rangeline area #2 from Los Lunas to Tome, NM (basemap topographic layer from ESRI online, 2018).

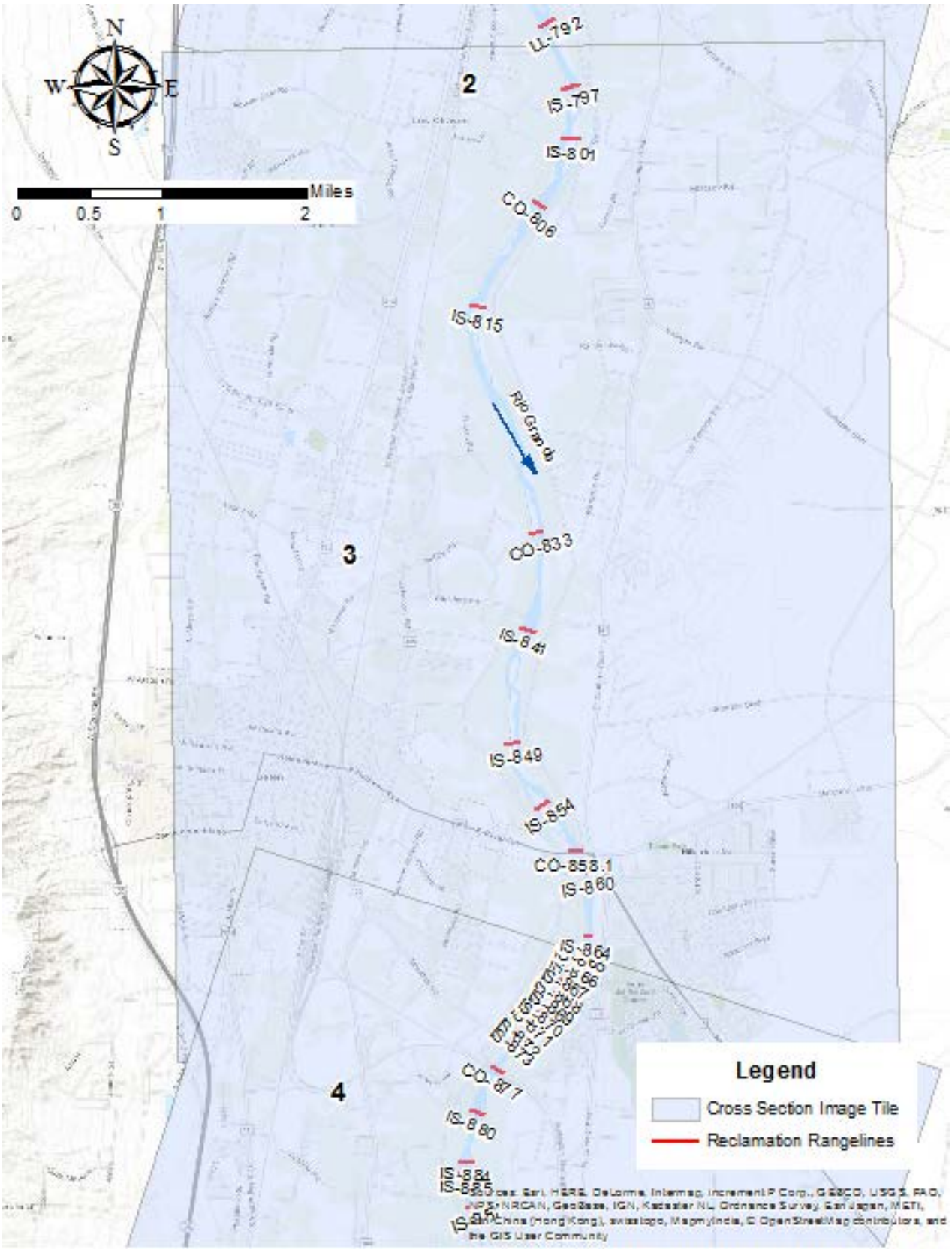

Figure 96. Delineated rangeline area #3 from Los Chavez to Belen, NM (basemap topographic layer from ESRI online, 2018).

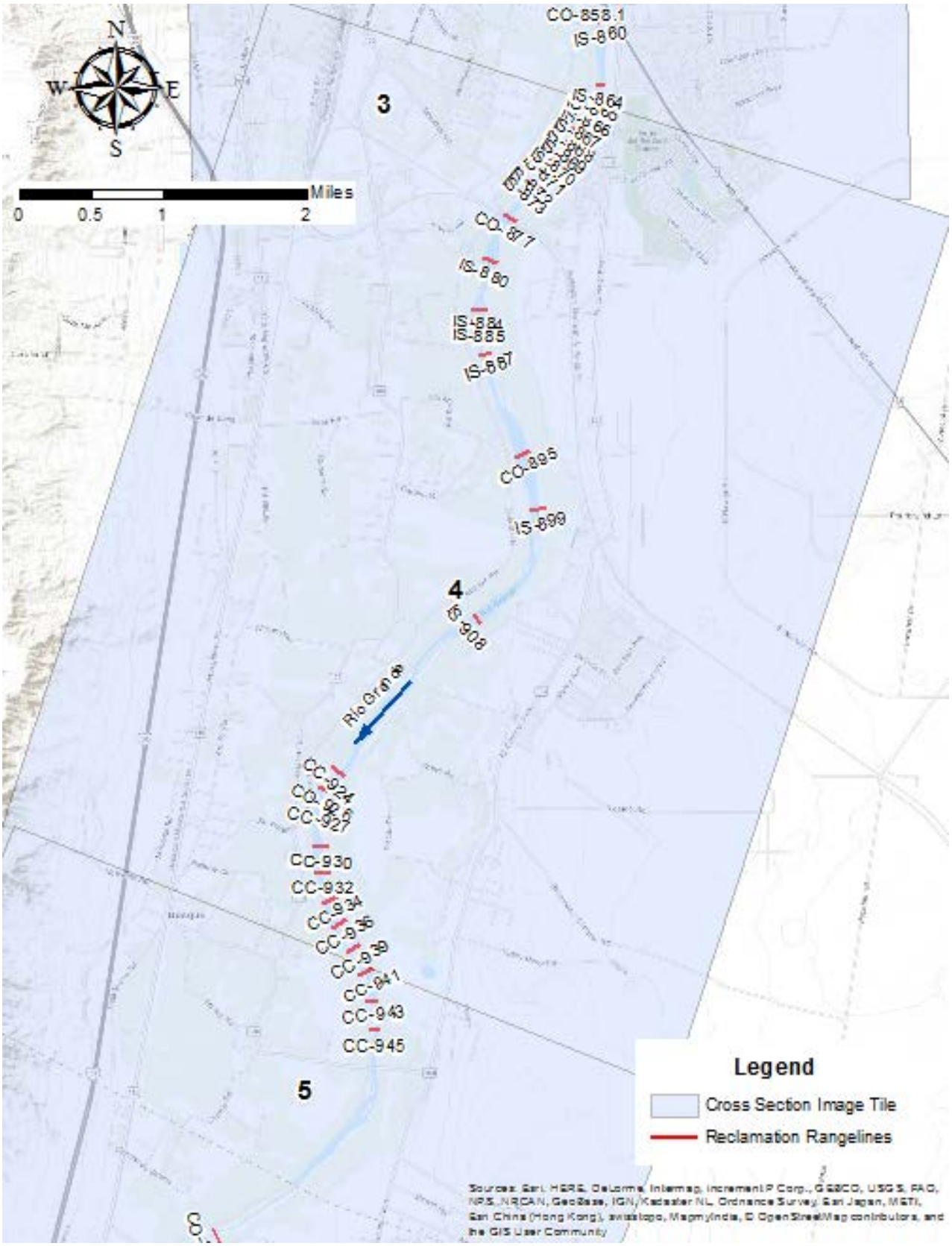

Figure 97. Delineated rangeline area #4 from Los Trujillos to Casa Colorado, NM (basemap topographic layer from ESRI online, 2018).

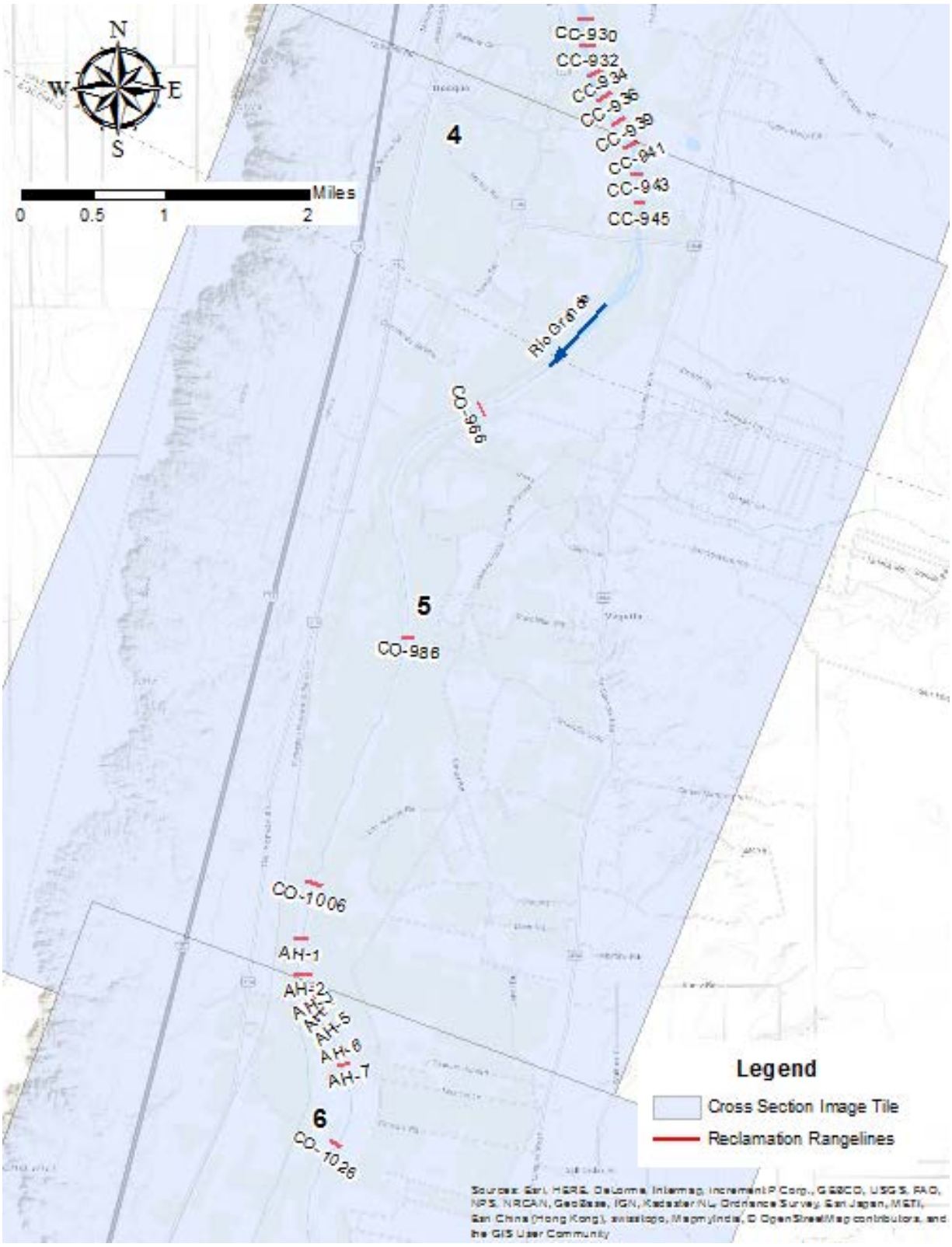

Figure 98. Delineated rangeline area #5 from Bosque to Las Nutrias, NM (basemap topographic layer from ESRI online, 2018).

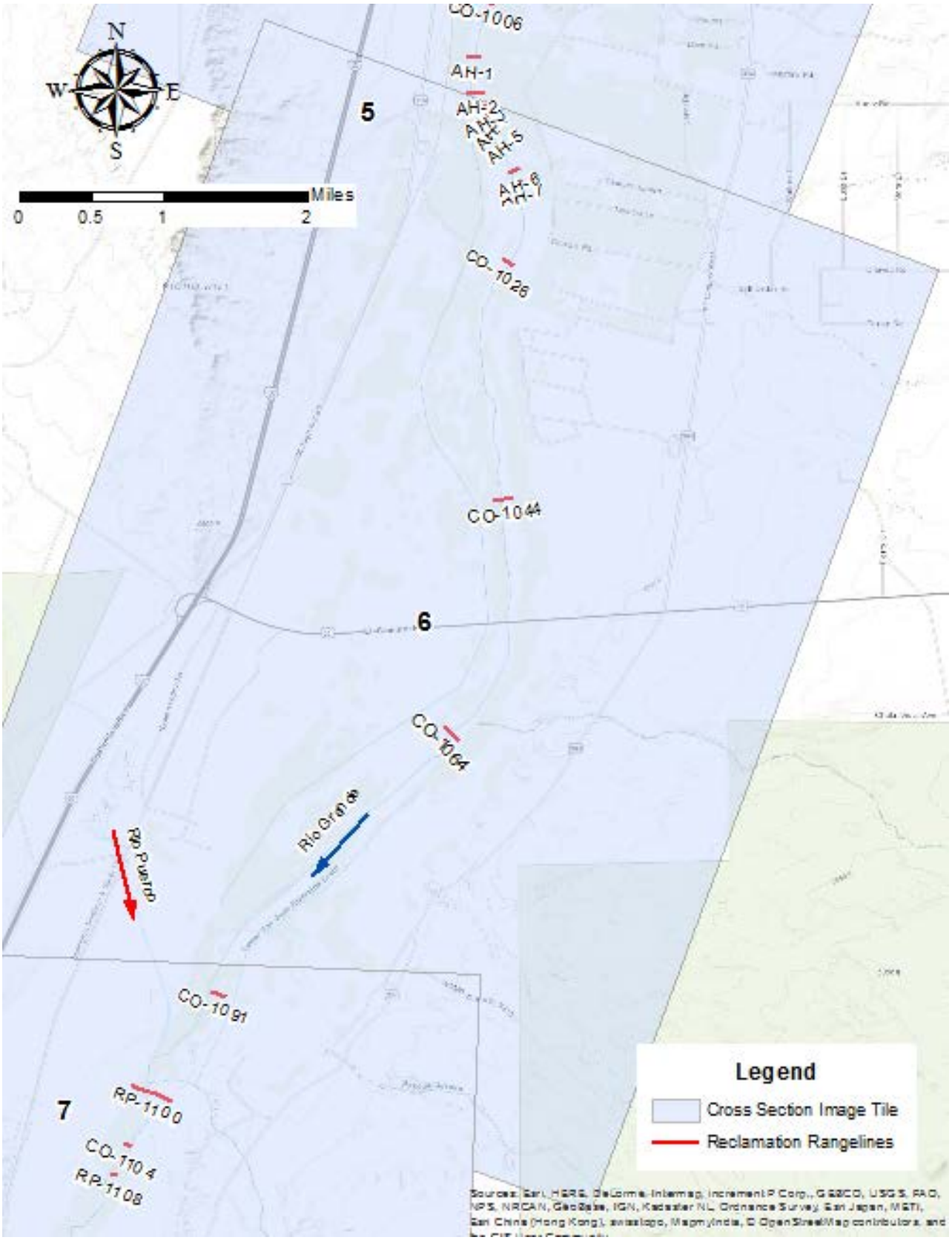

Figure 99. Delineated rangeline area tile #6 from Abeytas to Contreras, NM (basemap topographic layer from ESRI online, 2018).

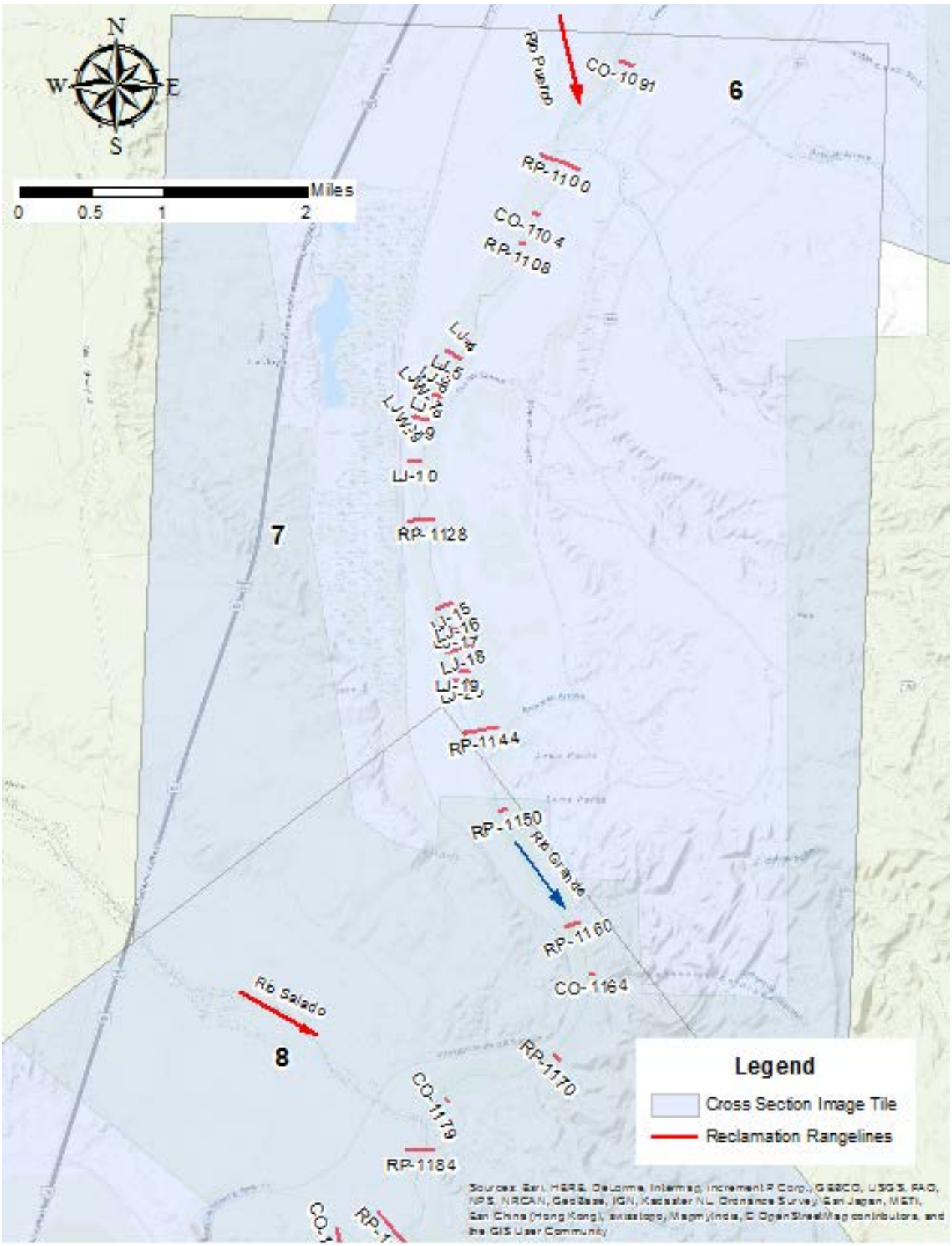

Figure 100 Delineated rangeline area #7 between the confluences of the Rio Puerco and the Rio Salado (basemap topographic layer from ESRI online, 2018).

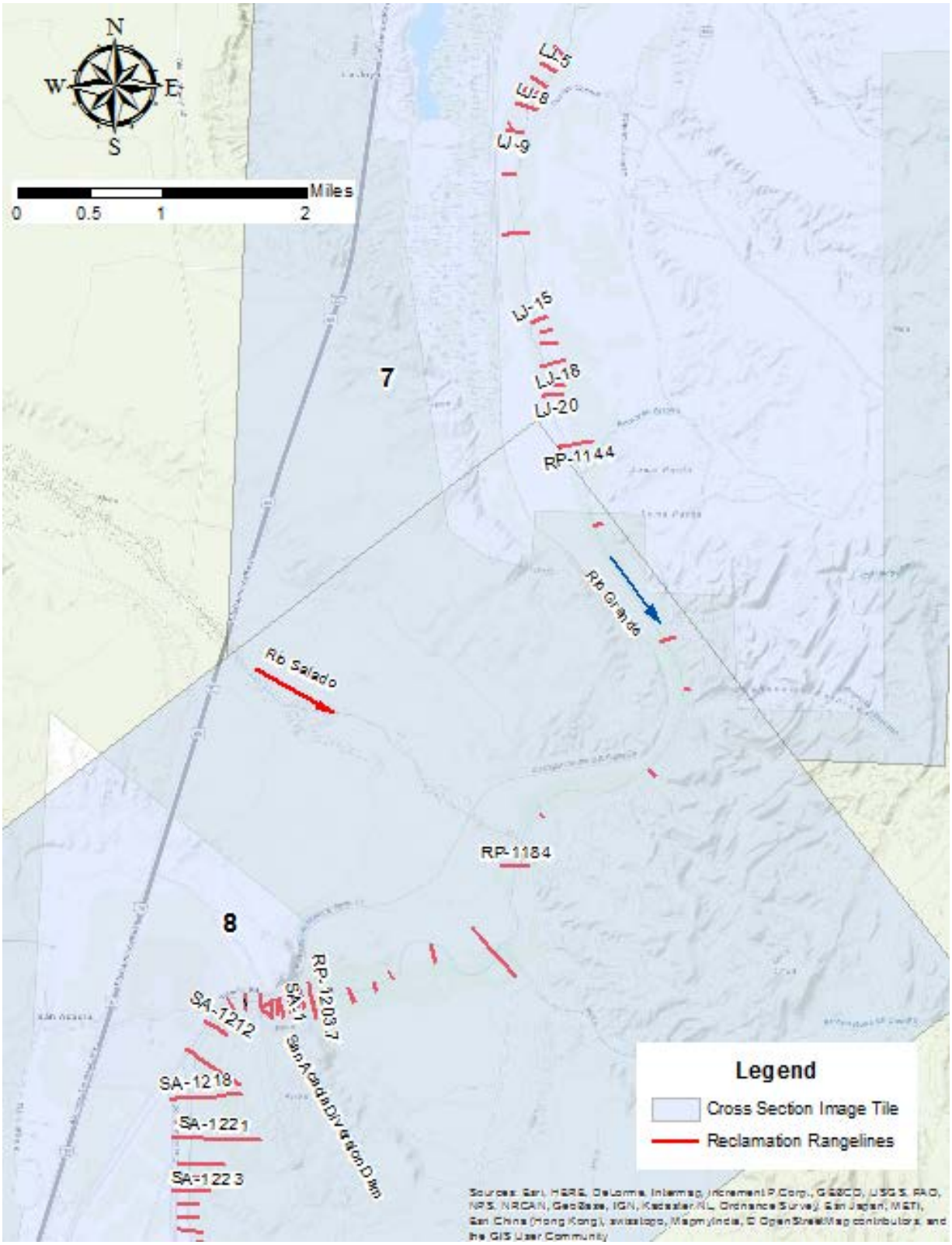

Figure 101. Delineated rangeline area #8 at San Acacia (southernmost extent of the study reach) (basemap topographic layer from ESRI online, 2018).

Table 27. Channel trend comparisons at selected river sections over the last decade or two.

Cross Section	*Image Tile*	*Depth*	*Delta Depth (ft)*	*Width*	*Delta Width (ft)*	*Bank Height*	*Delta Height (ft)*
CO-713	1	-	1.45	-	111	-	2.15
IS-782	2	+	0.57	-	121	+	1.47
IS-797	3	+	1.46	-	217	-	1.81
IS-885	4	+	1.42	-	221	+	0.92
CO-1006	5	-	1.22	-	156	-	2.19
CO-1044	6	-	1.41	-	195	-	2.48
RP-1100	7	-	0.42	-	243	-	0.58
CO-1179	8	-	1.78	-	54	-	3.01
RP-1203.7	8	+	3.05	-	69	+	4.70

Selected representative river cross sections and their attributes (depth, width, and height with "+" and "-" signs indicating increases or decreases, respectively).

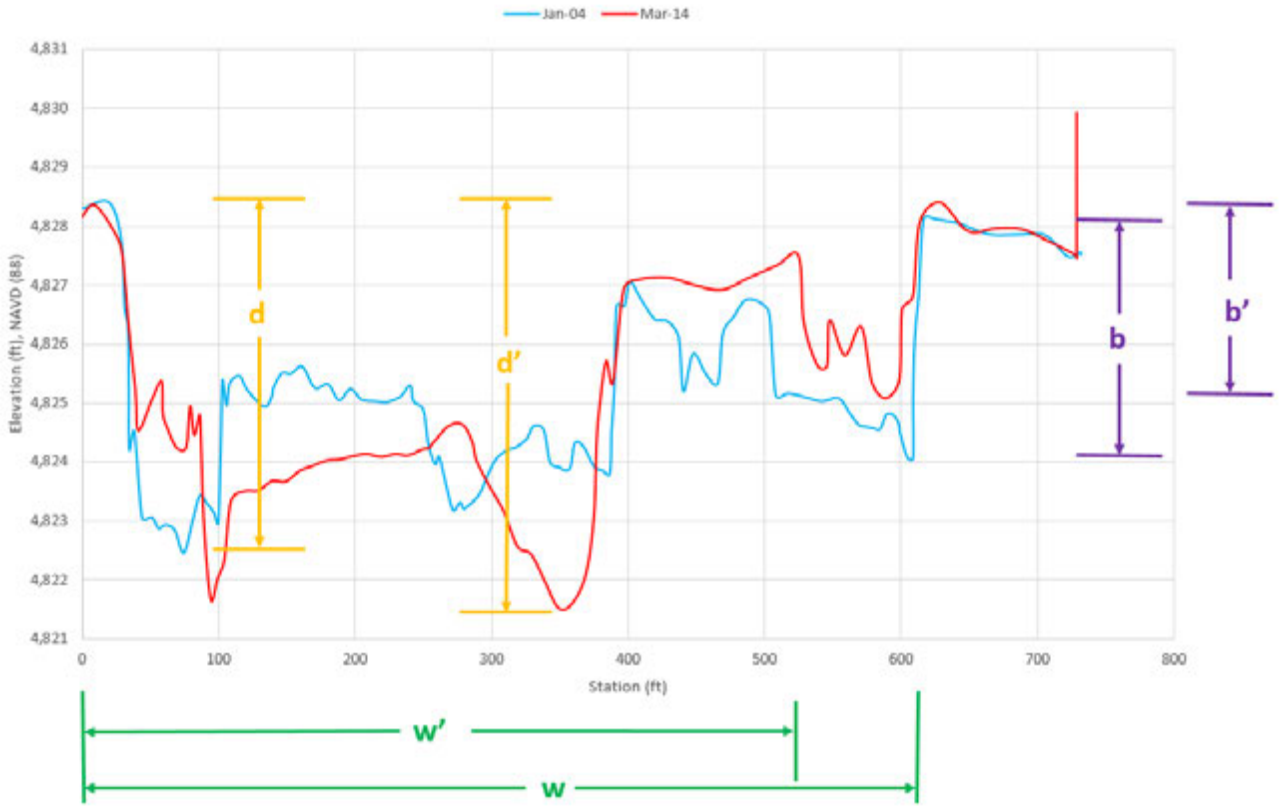

Figure 102. Channel width (w), channel depth (d), and channel bank height (b) are all shown on the figure for the January 2004 cross section survey at IS-797. The prime (w', d', and b') measurements reflect the March 2014 survey. Differences in these values represent changes summarized in Table 27.

A comparison of the rangelines between Isleta and San Acacia Diversion Dams, as illustrated in Table 27, shows that the channel width has been decreasing since the late 1990s to early 2010s. There are decreases and increases, however, in channel depth and bank height among the various sub-areas of this reach. While channel incision generally results in increased bank height, the channel data for the Isleta to San Acacia Diversion Dam reach also indicates there is deposition of material along the channel margins at many reach locations. This marginal, in-channel edge deposition of material results in channel bank heights decreasing, due to how bank heights were defined in Figure 102. Wherever channel incision is not dominate this can lead to decreasing bank heights.

Between Los Lunas and Casa Colorado the river has incised about 0.5 to 1.5 feet. The bank height has also increased between 1 to 1.5 feet in this area. The increase in bank height is likely due to a combination of channel incision and vertical accretion of sediment on mid-channel bars and at the bankline. The rangelines between Los Lunas and Casa Colorado indicate that in the late 1990s sediment stored in the active channel was easily moved around. The typical channel topography was a wider, shallow channel system that was often divided into two or three distinct flow paths. Between the 1990s and early 2010s the typical channel cross section show signs of sediment deposition in one or more of these flow paths. This has resulted in a higher floodplain surface and often resulted in a single, deep channel. There are still places with more than one channel, but in all cases the flow paths are narrower and deeper than in the 1990s. The deepest channel location in the 2010s is often located on river left or river right indicating a potential for lateral migration. Between Los Chavez, NM and Los Trujillos, NM this has resulted in a river section where the channel thalweg has incised, but aggradation in secondary channels has caused the bank height to decrease.

From Isleta Diversion Dam to Los Lunas, NM and between Casa Colorado, NM to just upstream of San Acacia Diversion Dam, the river has aggraded on the order of 0.5 to 2 feet. This has caused a decrease in the bank height ranging from 0.5 to 2.5 feet in these areas. The decrease in bank height is likely due to a combination of channel and floodplain aggradation. The rangelines between Isleta Diversion Dam and Los Lunas, NM indicate that there was some re-working of the sediment within the channel in the late 1990s. Between the late 1990s and early 2010s significant deposition occurred within the active channel, on the order of 2.5 to 6 feet. This deposition has primarily had the effect of creating deeper and narrower flow channels. There still appears to be a tendency for multiple flow paths, although there is a distinct thalweg location evident in the rangelines collected in 2014. Between Casa Colorado, NM and about a half a mile upstream of San Acacia Diversion Dam topography changes primarily reflect sediment deposition between the late 1990s/early 2000s and the early 2010s. There has been sediment deposition on the edges of the earlier active channel, creating a new floodplain terrace. This sediment deposition has often resulted in a single thread channel. There appears to be less re-working of the sediment in this sub-reach as the channel topography over time is more or less maintaining its shape.

Near San Acacia Diversion Dam the river has incised about 3 feet and the bank height has increased by over 4.5 feet. A review of the rangelines in this reach (RP-1201 to RP-1204.5) indicate that there is one primary flow path that has incised and narrowed over time.

4.7 Terrace Mapping

To evaluate general trends in the floodplain surface, relative elevation maps (REMs) were created along the Rio Grande between Isleta and San Acacia Diversion Dams (Slaughter and Hubert, 2014; Olson et al., 2014; Coe, 2016). REMs detrend a typical topographical elevation map to follow a river's water surface, allowing for greater discernment of fluvial features, such as river terraces. REMs, also known as height above river (HAR) rasters, show the elevation increases along a river corridor above a set water surface elevation.

The primary objective for pursuing an REM along the Rio Grande was to evaluate terrace heights adjacent to the active channel to help discern lower floodplain areas set back from the current banks of the Rio Grande. Terraces, for the purpose of this analysis, are relatively flat areas adjacent to the active river channel that are or were part of the Rio Grande's floodplain. Understanding the relative elevation heights of surfaces above a pre-determined water surface elevation (500 cfs was used for this analysis) provides insight into the degree of connectivity between the active river channel and the adjacent floodplain.

For the production of the REM surface, the reach between Isleta and San Acacia Diversion Dams was divided into approximately five mile stretches or "tiles" (see Figure 103 for the layout of the 12 terrace tiles). An REM was then generated for each "tile." The 2012 bare earth LiDAR dataset was used as the starting topographical surface. The water surface was created from a 1-dimensional HEC-RAS (version 5.0.3) numerical hydraulic model of the river at a discharge of 500 cfs. A discharge of 500 cfs was used since it was similar to the captured water surface at the time of the 2012 LiDAR collection.The 1-dimensional water surface was assumed to be constant across the assessment area (generally east to west). Variations in the downriver direction were based on the numerical model values for both surveyed and interpolated rangelines. The 500 cfs water surface elevation rasters were then subtracted from the 2012 LiDAR topographic surface to produce an REM raster. The REM was symbolized using 1-, 2-, 3-, 4-, and 5-foot plus elevations above the modeled water surface. The REMS for each of the 12 tiles are displayed in Figure 104 to Figure 115. There are some areas where there was not adequate 2012 LiDAR coverage and therefore the REM could not be produced in that area. These areas just show the underlying aerial photography.

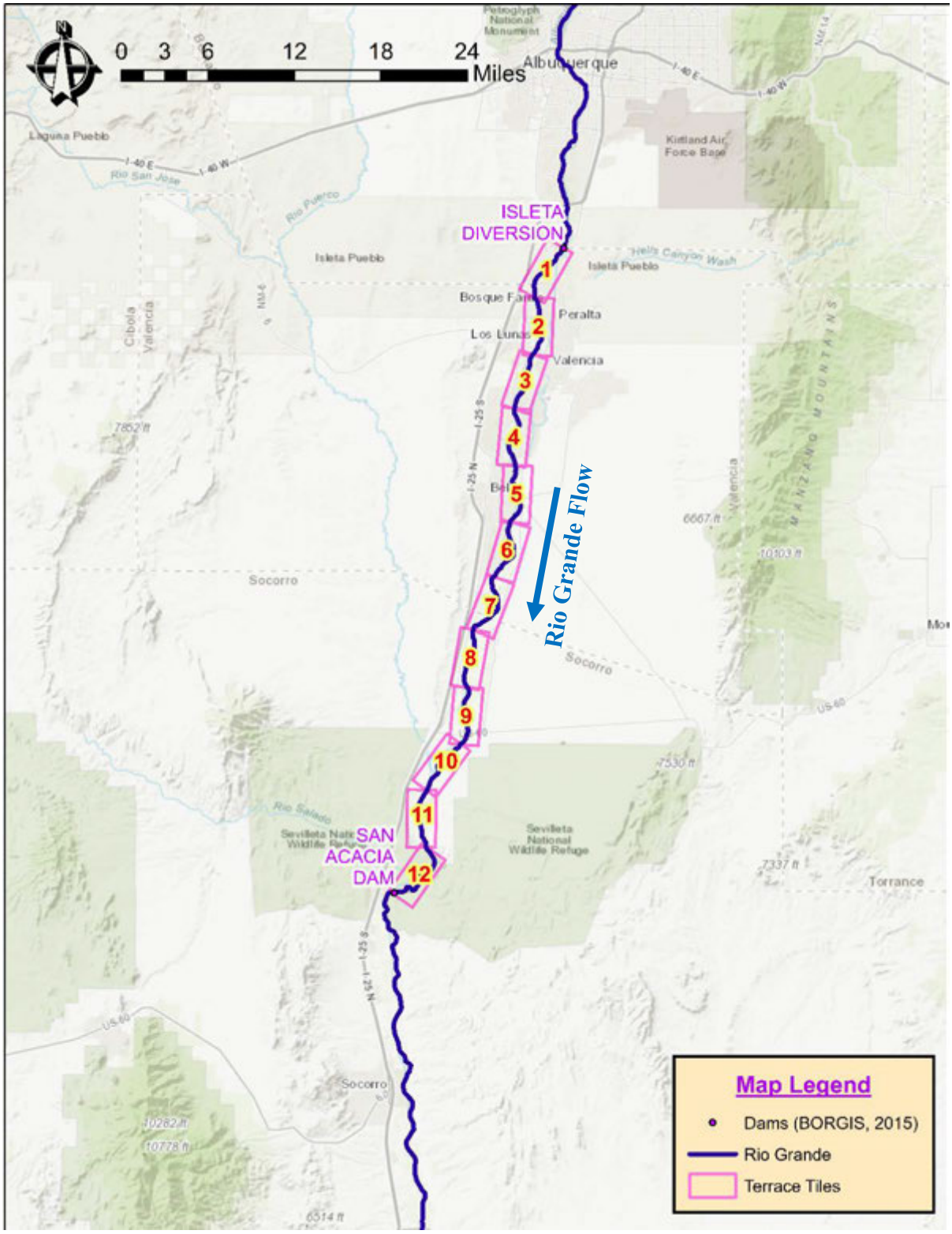

Figure 103. The Isleta Reach broken down into approximately 5 mile river lengths (terrace tiles) for detrended elevation analysis (topographic basemap layer from ESRI online, 2017).

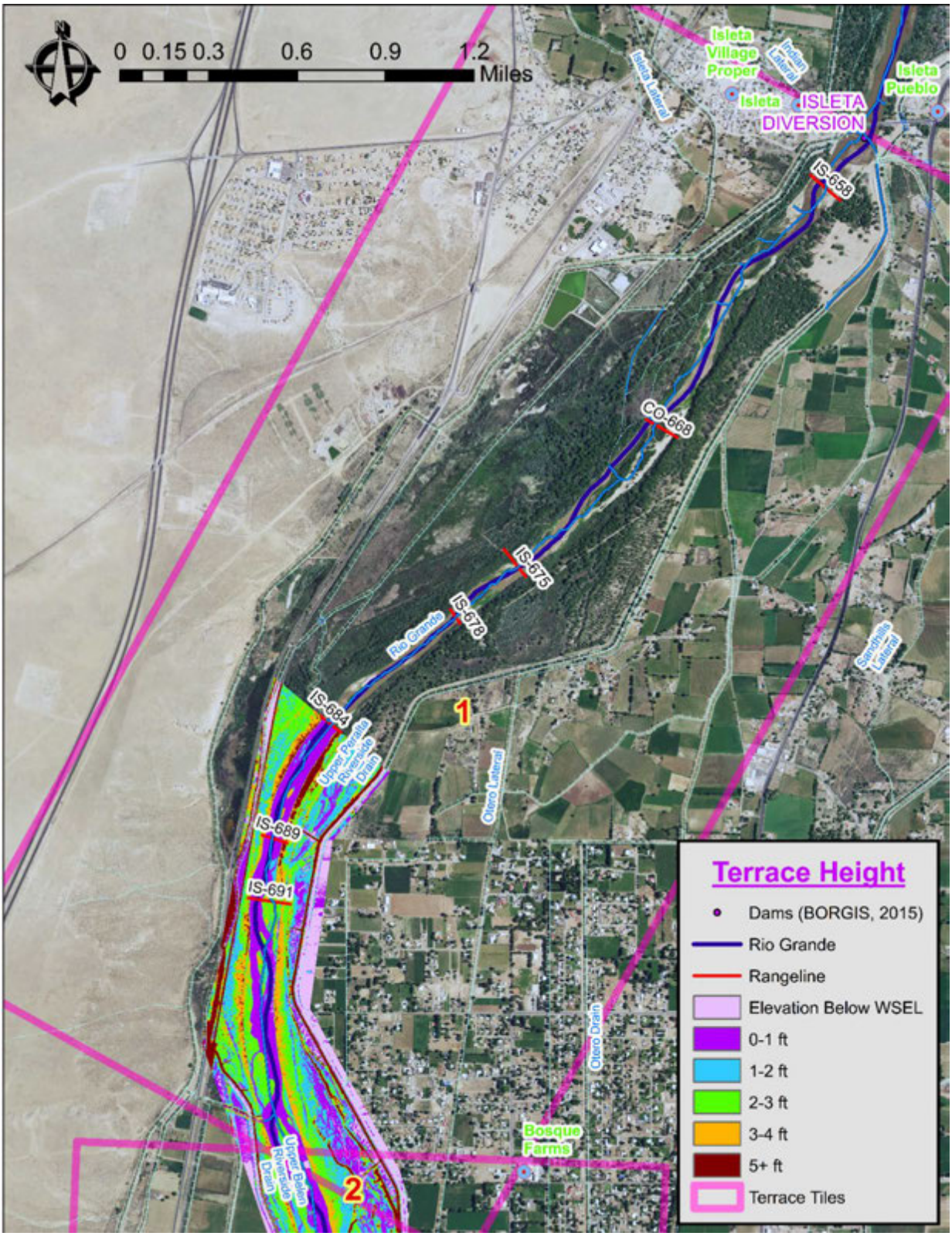

Figure 104. REM (or terrace heights above a 500 cfs water surface) between Isleta Diversion Dam and Bosque Farms (background imagery from NAIP, 2014 for all terracing figures; LiDAR data does not begin until the IS-684 rangeline).

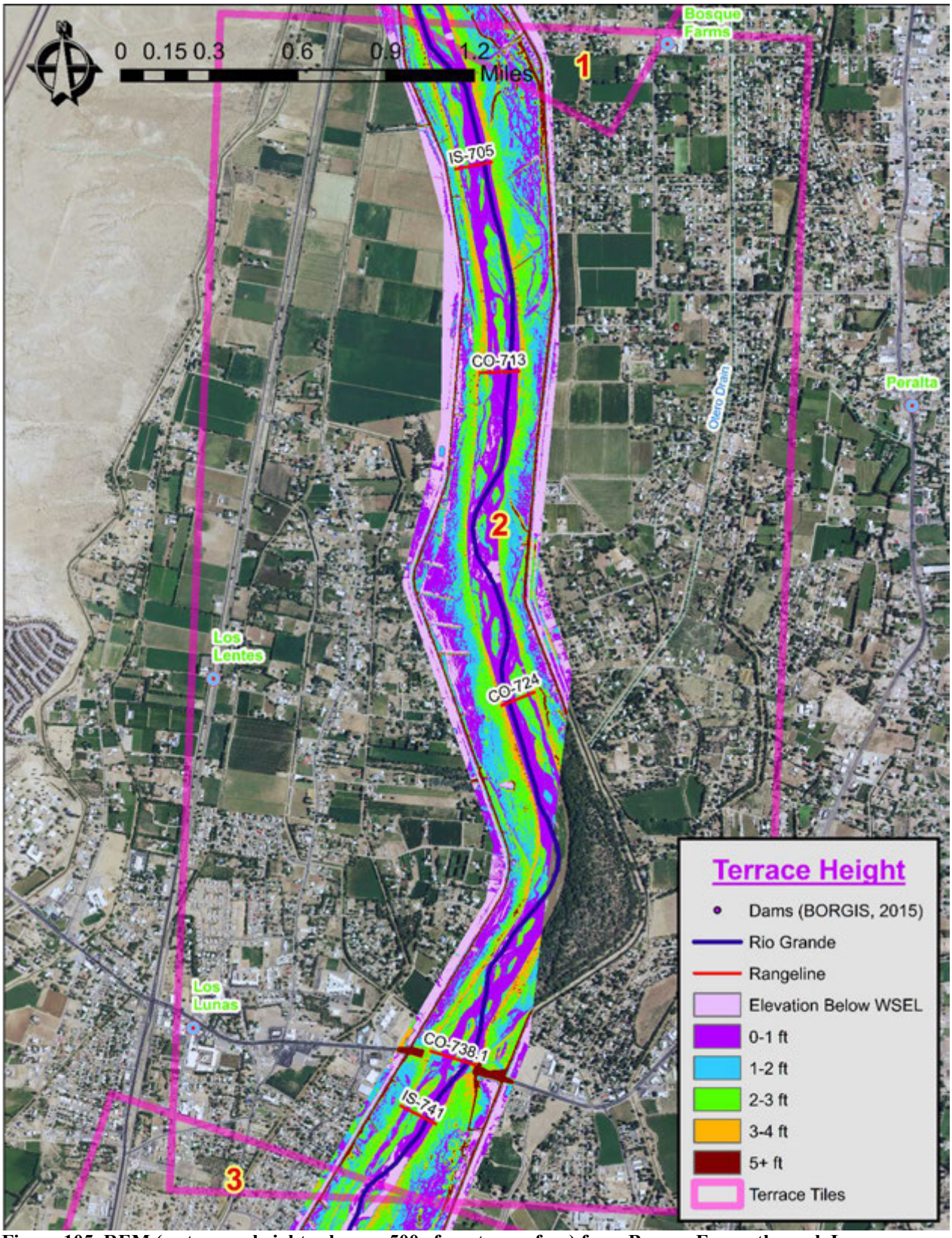

Figure 105. REM (or terrace heights above a 500 cfs water surface) from Bosque Farms through Los Lunas. LiDAR data was missing at the river bend downstream of CO-724 so this area was not analyzed.

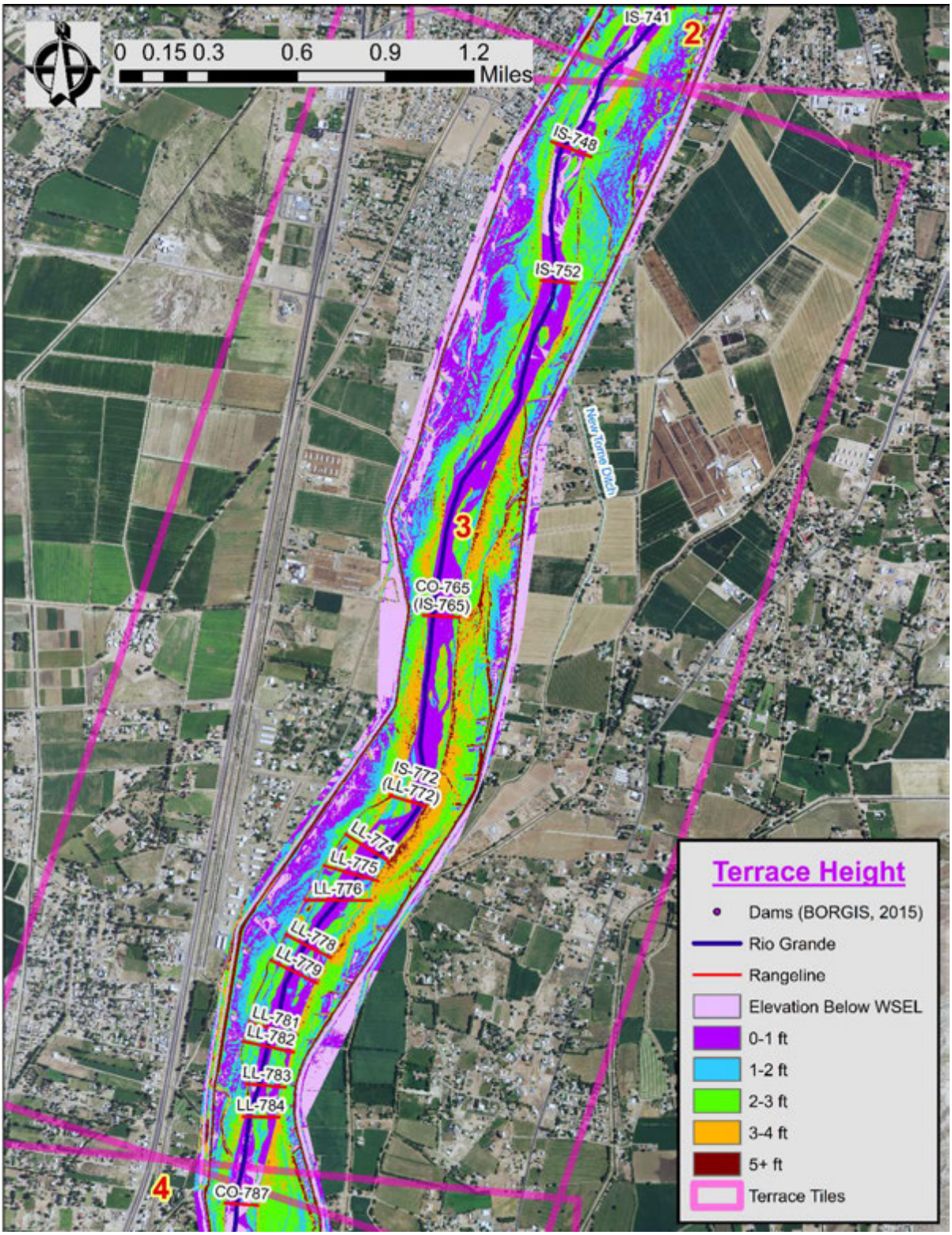

Figure 106. REM (or terrace heights above a 500 cfs water surface) from Valencia to Tome.

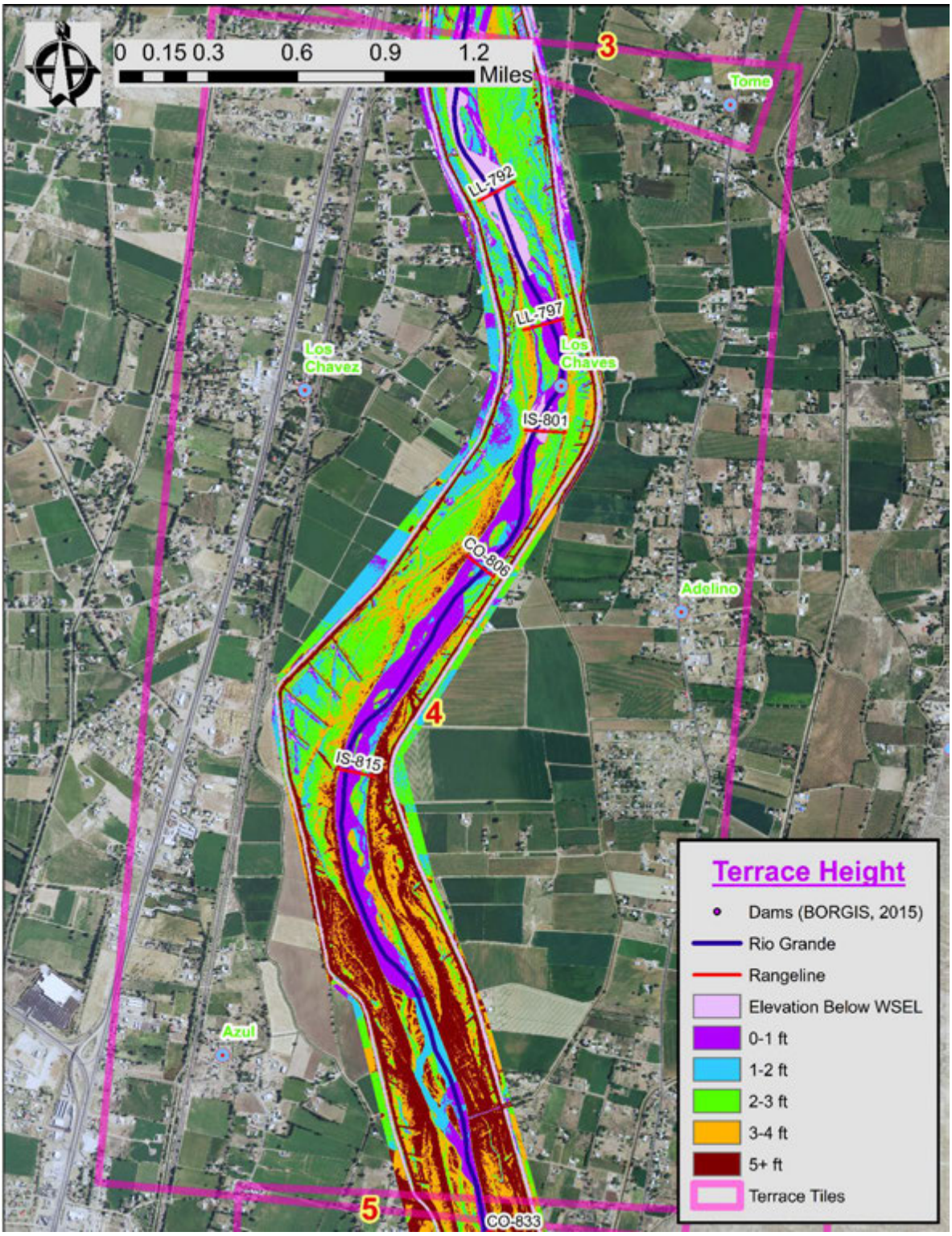

Figure 107. REM (or terrace heights above a 500 cfs water surface) from downstream of Tome to CO-833.

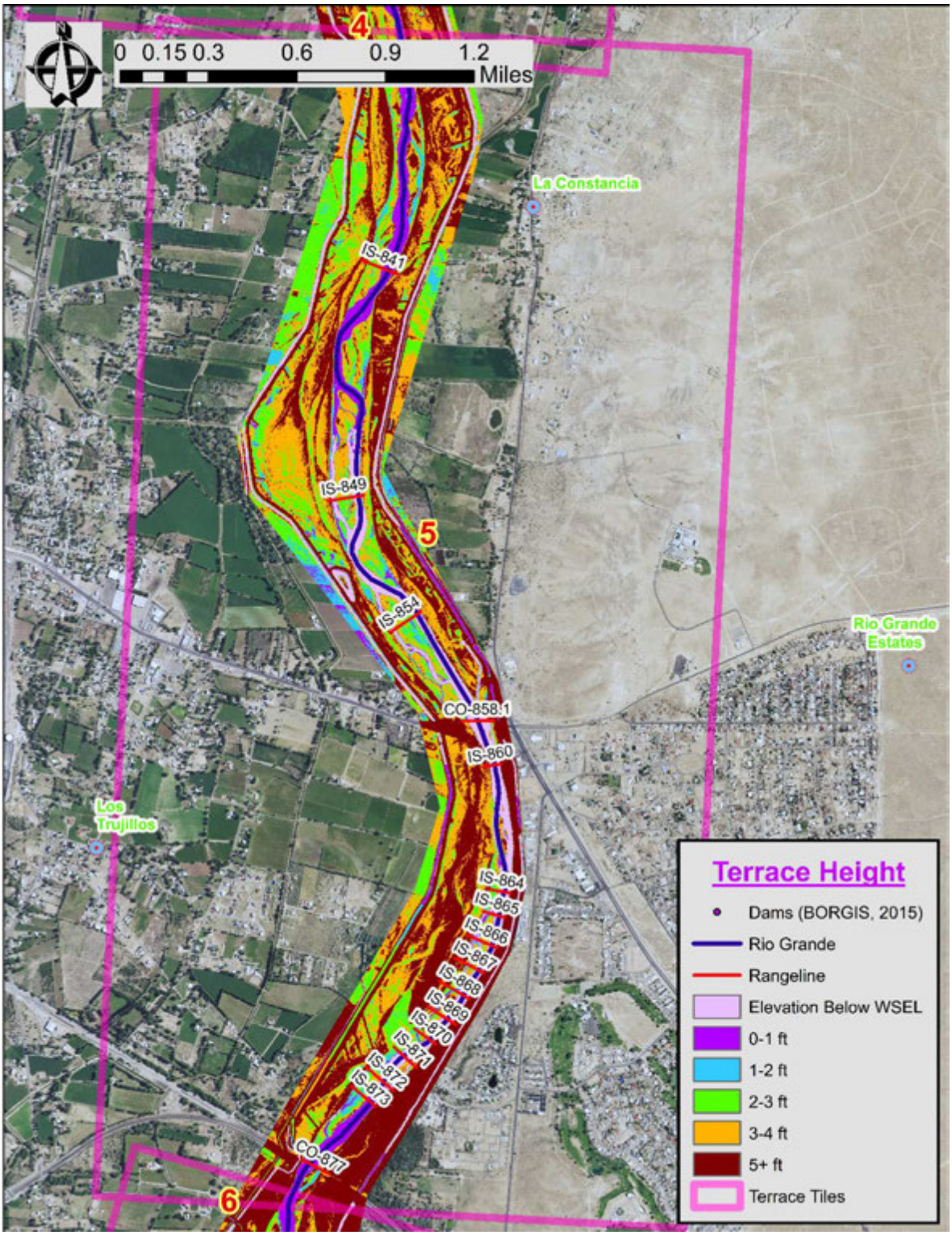

Figure 108. REM (or terrace heights above a 500 cfs water surface) through Belen from CO-833 to CO-877.

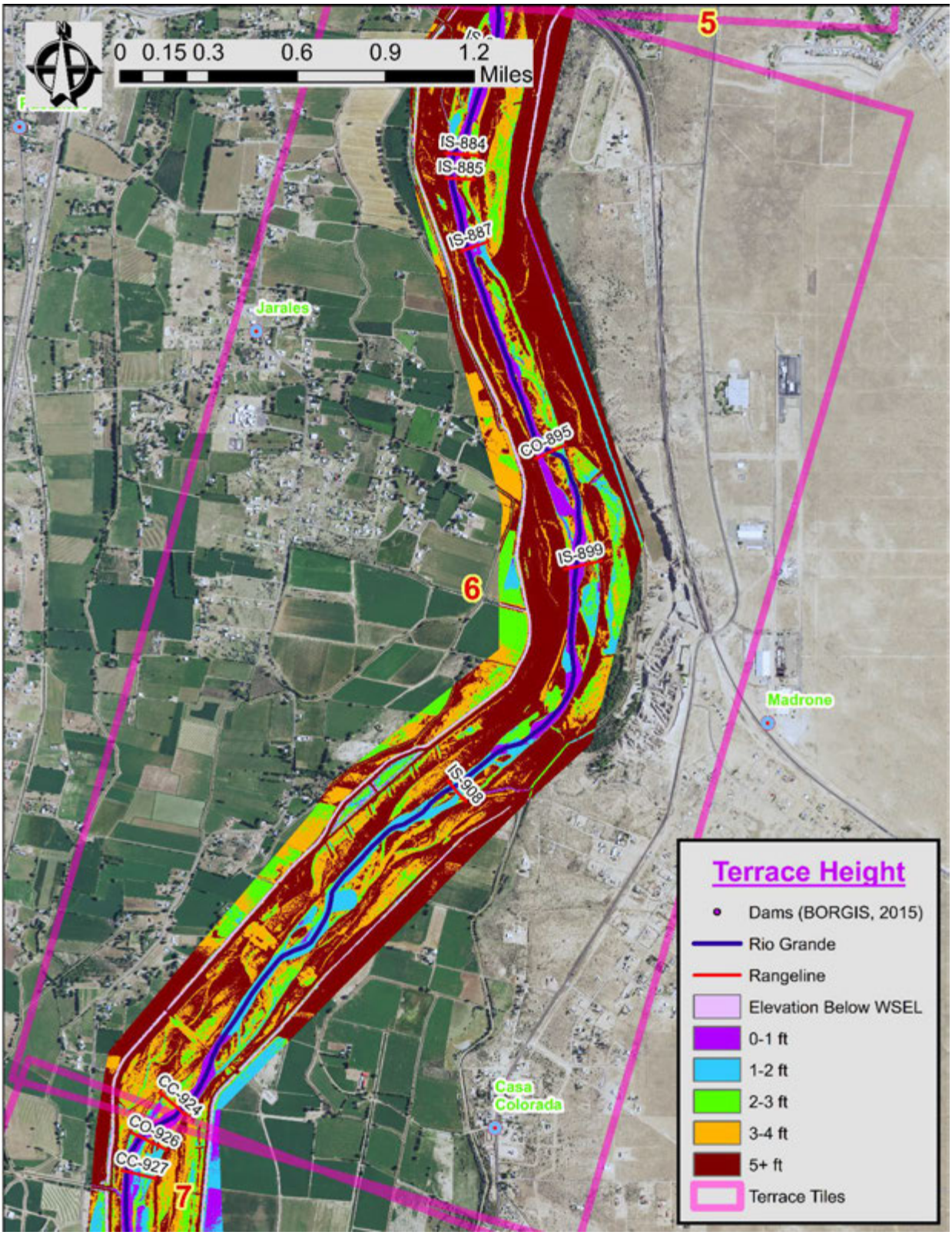

Figure 109. REM (or terrace heights above a 500 cfs water surface) from Pueblitos to Casa Colorado.

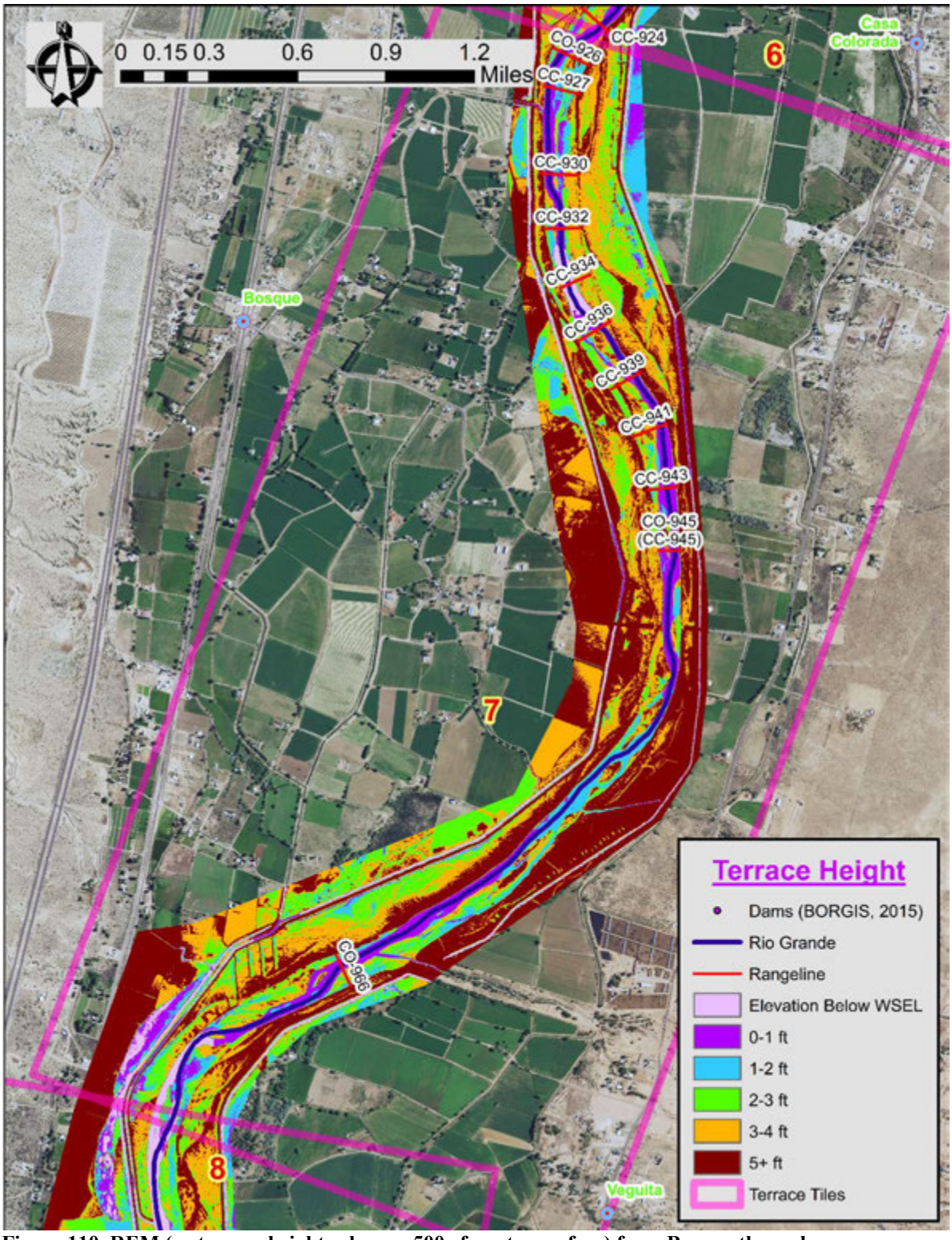

Figure 110. REM (or terrace heights above a 500 cfs water surface) from Bosque through Veguita.

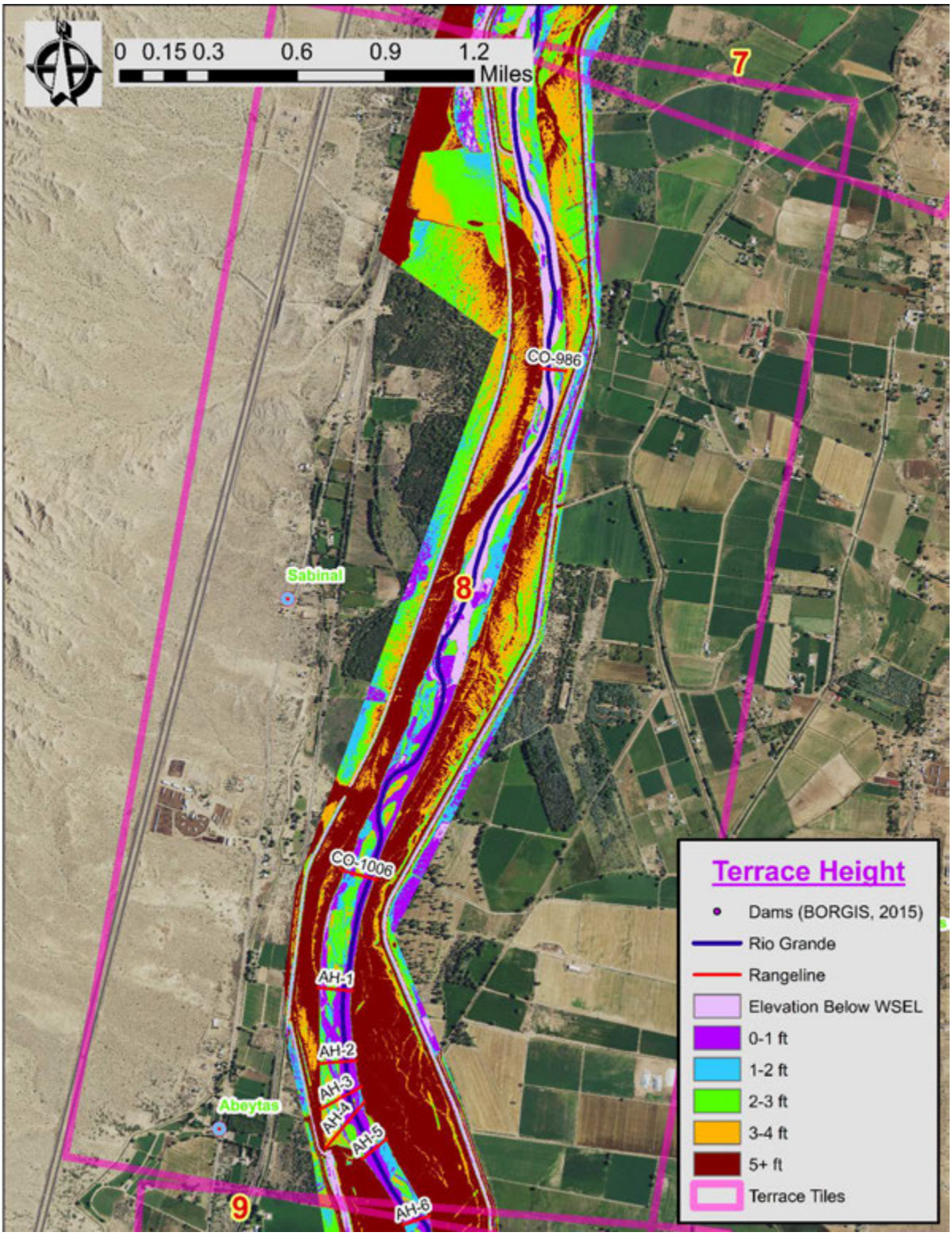

Figure 111. REM (or terrace heights above a 500 cfs water surface) from Sabinal to Abeytas.

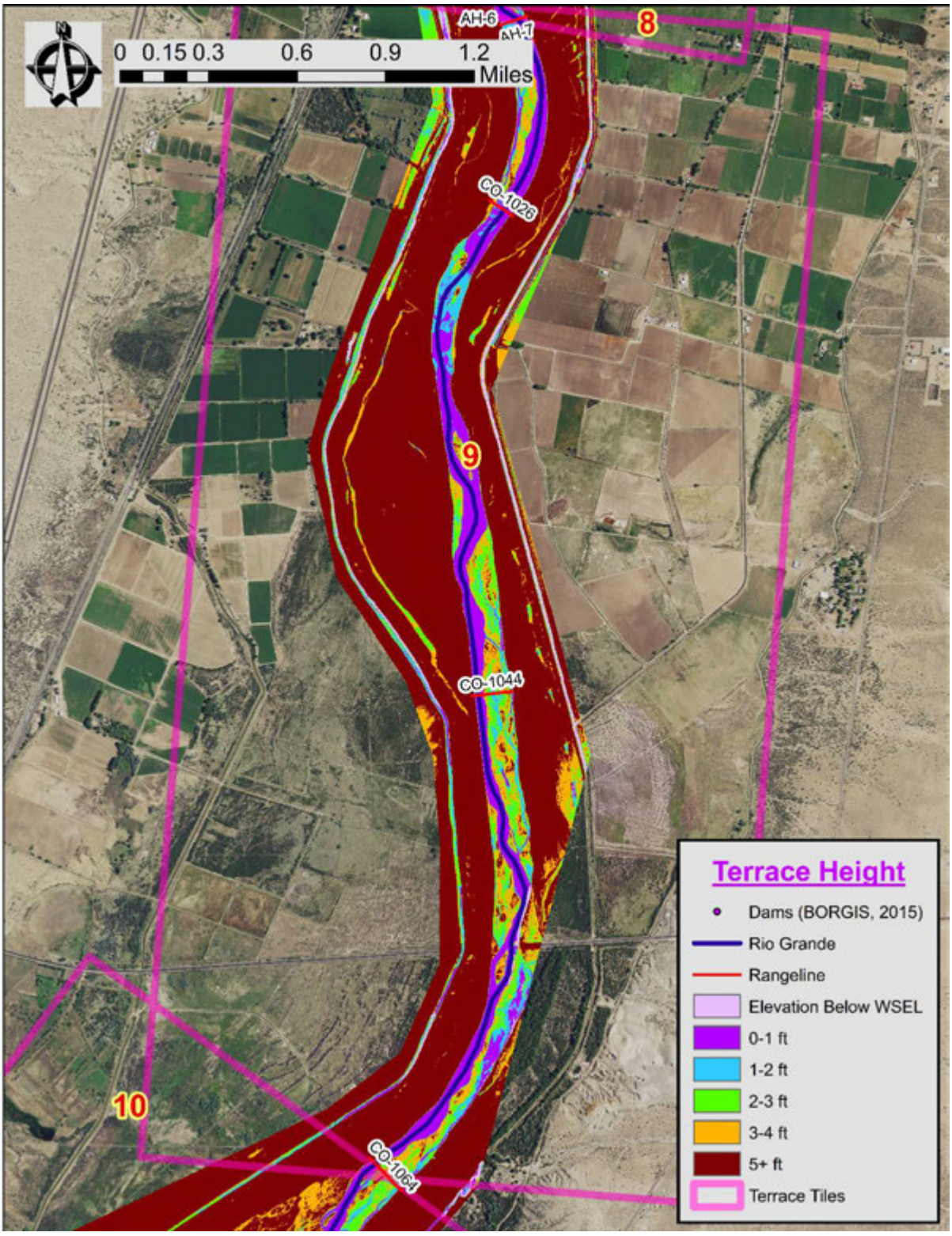

Figure 112. REM (or terrace heights above a 500 cfs water surface) between Abeytas and Bernardo. LiDAR data was missing for the river bend just downstream of CO-1044 and this floodplain area was not analyzed.

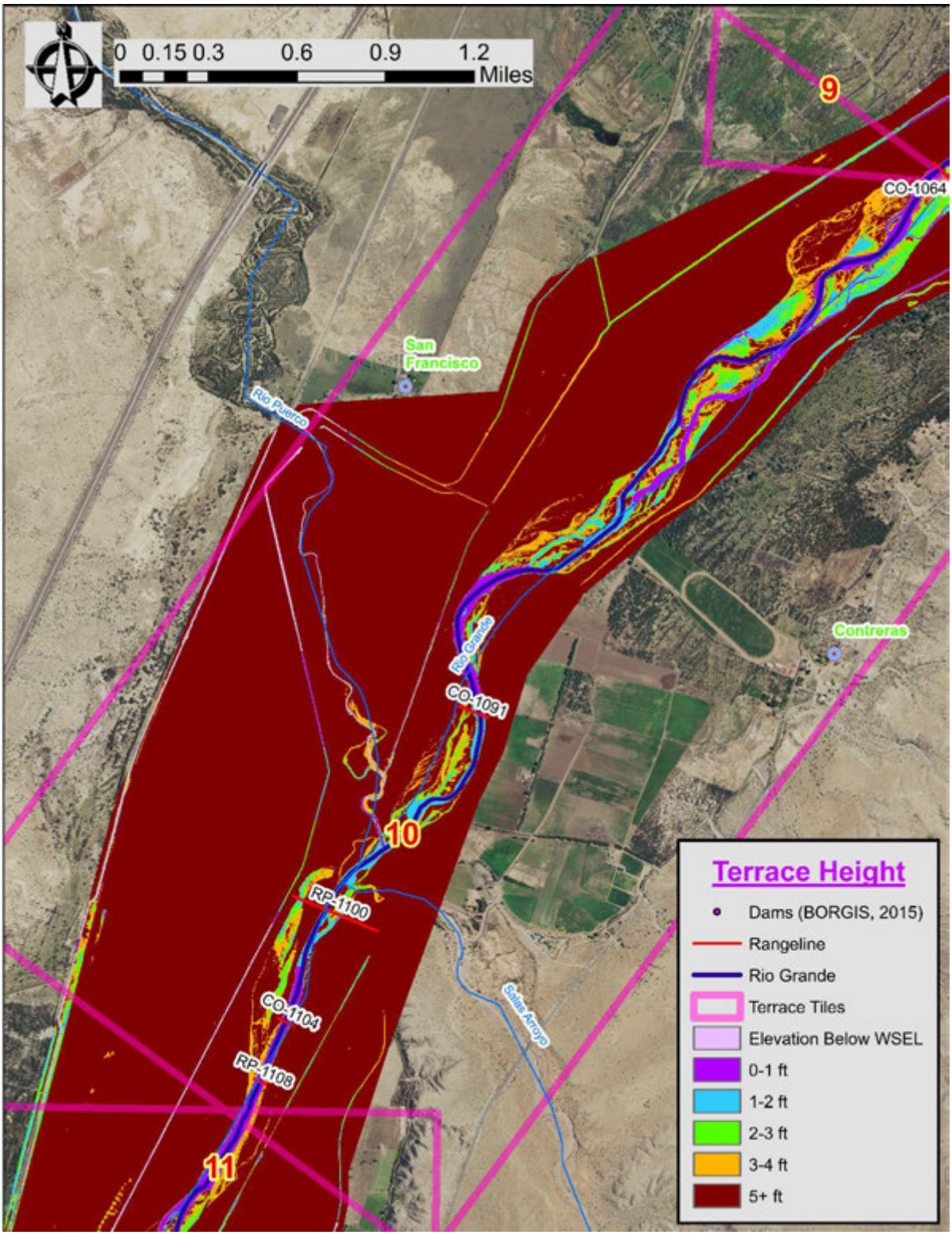

Figure 113. REM (or terrace heights above a 500 cfs water surface) near San Francisco, NM. This section contains the Rio Puerco confluence with the Rio Grande.

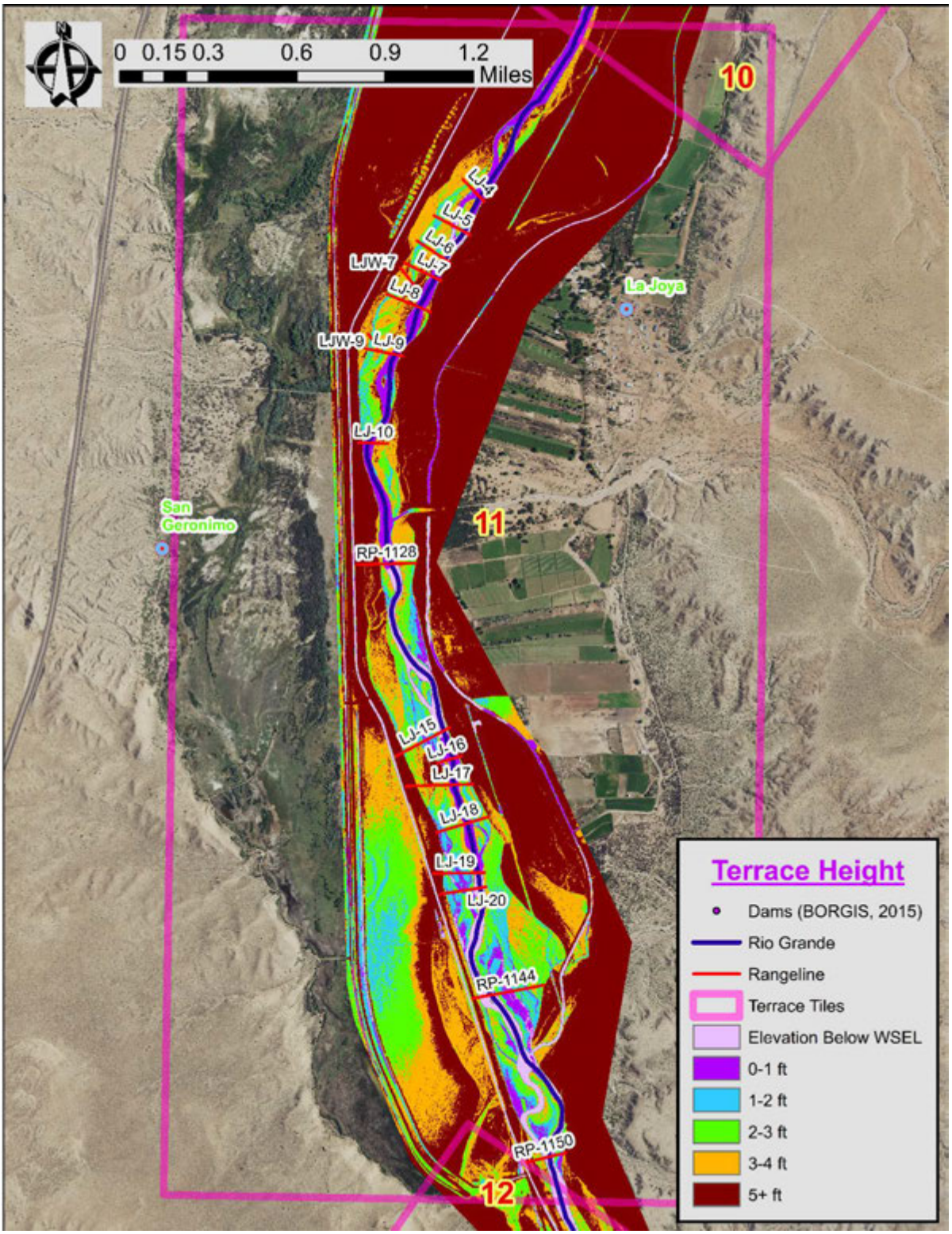

Figure 114. REM (or terrace heights above a 500 cfs water surface) near La Joya.

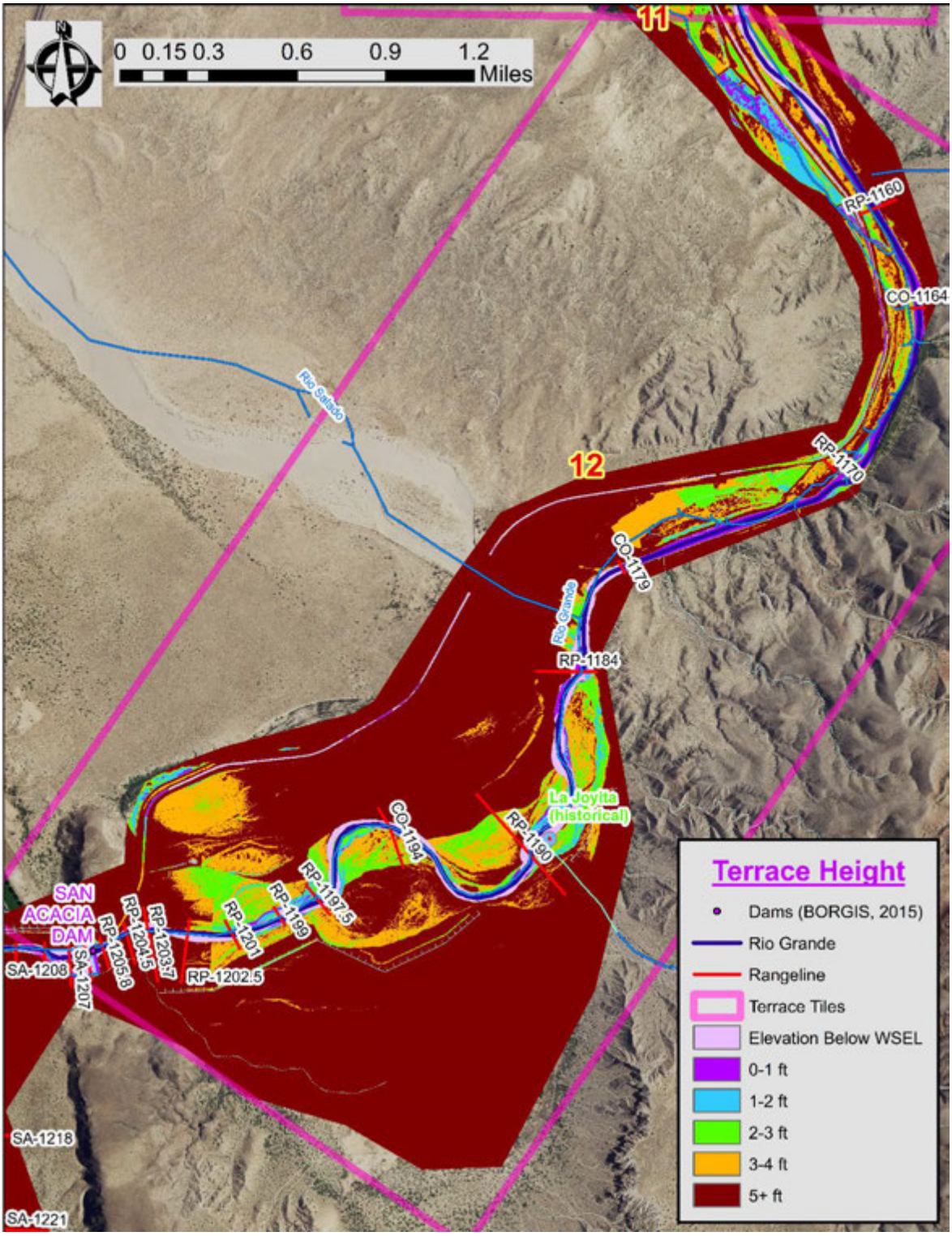

Figure 115. REM (or terrace heights above a 500 cfs water surface) at the southernmost terrace tile just upstream of San Acacia Diversion Dam. This tile also contains the confluence of the Rio Puerco and Rio Salado.

The REMs generated between Isleta and San Acacia Diversion Dam show the formation of multiple terrace surfaces between the existing infrastructure. From Isleta Diversion Dam downstream to around Los Chavez, NM (~ River Mile 154, 2012 river mile demarcations are used herein) there is a lower terrace adjacent to the active channel. Further away from the active channel there is a higher terrace (2-3 feet higher than the lower terrace) that often is a linear strip that parallels the active channel. This is likely a natural levee that has had formed through sediment deposition at the edges of what was once the banks of the active channel. Past this higher terrace the area within the infrastructure that bound either side of the Rio Grande, once again has lower elevations (about 1-3 feet lower than the higher terrace). This creates a channel condition within the infrastructure constraints where the active channel is at or slightly higher than the terrain adjacent to the infrastructure constraints. This creates a perched channel condition that would cause water to pool at the toes of the adjacent infrastructure.

Between Los Chavez, NM and Sabinal, NM (~ River Mile 135) the active channel continues to have an adjacent lower terrace. This lower terrace is bounded by a higher terrace (2 to 4+ feet higher than the lower terrace) that tends to extend to the infrastructure constraints. There are lower elevation surfaces (1 to 3 feet lower than the higher terrace) mixed within this higher terrace, such as on the river right upstream of the NM Highway 309 Bridge in Belen (~River Mile 151), river left at the aerial gas lines south of Belen (~ River Mile 144), the river right across from the confluence with Abo Arroyo (~ River Mile 140), and the river left around River Mile 138. These lower surfaces are often along the toe of the adjacent infrastructure, but not always, creating a patchwork of lower surfaces that often have linear extensions of the surface propagating from them. The latter are suggestive of a series of high flow channels, although these are not all interconnected.

From Sabinal, NM to San Acacia Diversion Dam the higher terrace encompasses the majority of the floodplain. This higher surface (often 2+ feet above the terrace adjacent to the active channel) has some patchwork of lower surfaces, but not as extensive as the preceding river reach. Most of these lower areas are linear in nature, suggesting higher flow paths or an abandoned historical active channel route. There is still the lower surface adjacent to the active channel, although this surface tends to be higher (1 to 4 feet) than in the upstream sections. Notable areas where the higher terrace separates the active channel from more extensive lower surfaces include the area on river left both upstream and downstream of the U.S. 60 Bridge (~River Mile 131), river left near the La Joya State Waterfowl Area (~River Mile 123), and a smaller area on river right near the southern boundary of Sevilleta National Wildlife Refuge (~River Mile 117).

5.0 Future Channel Response

The Rio Grande between Isleta and San Acacia Diversion Dams was identified as an area of river maintenance concern due to confinement by spoil levees on both sides and the increasing vegetation encroachment. An assessment of geomorphic drivers (water and sediment supply) and geomorphic parameters (width, planform, slope, sinuosity, bed material, and channel/floodplain topography) was conducted for this approximately 53 mile long reach of the Rio Grande to help identify current trends and predict potential future channel responses. This is a critical piece of understanding about the current fluvial system that helps with the development of viable future activities on the Rio Grande in this reach, both river maintenance and river rehabilitation (river restoration) work. A summary of the previously described assessments are presented in the following bullets:

- Water Supply
    - Annual water volume from Isleta to San Acacia has decreased from the 1990s to the early 2010s.
    - Most of the water volume is derived from the spring snow-melt runoff volumes in this reach, with a slight influence from the monsoonal discharges from tributary inputs.
    - The majority of the local precipitation occurs during the monsoonal season.
    - Peak discharges during the spring snow-melt from Isleta to San Acacia have decreased from the mid-1980s until the early 2010s. Peaks from the 1990s are similar to peaks in the 2000s.
    - Frequency of higher discharge events has decreased from the 1990s to the early 2010s.
    - Frequency of low flow events has increased at the Albuquerque USGS gage from the 1990s to the early 2010s, but decreased slightly for the Bernardo and San Acacia USGS gages.
    - Annual number of days with a discharge greater than or equal to 500 cfs has decreased between the mid-1990s and early 2010s.
    - Depth to shallow groundwater aquifer has increased from the 2000s to the early 2010s.
- Sediment Supply
    - Annual suspended sediment supply has decreased between the 1990s and early 2010s at the Albuquerque and Bernardo USGS gages. The annual suspended sediment supply at the San Acacia indicates a relatively constant trend between the 1990s and early 2010s.
    - Annual suspended sediment supply from the Rio Puerco has decreased from the 1990s to the early 2010s.
    - Highest suspended sediment concentrations at the Albuquerque, Bernardo, and San Acacia USGS gages occur during the monsoons. Suspended sediment concentrations at the San Acacia

USGS gage are about twice those measured at the Albuquerque USGS gage.
    - Largest suspended sediment discharge occurs during the spring snow-melt runoff at the Albuquerque USGS gage and during the monsoon season at the San Acacia USGS gage.
    - Effective discharge for suspended sediment and total load has decreased at the San Acacia USGS gage between the 1990s and early 2010s. The effective discharge for suspended sediment has increased at the Albuquerque USGS gage.
    - The sediment load at San Acacia tends to be primarily sands (~68%) with the remainder (~32%) consisting of finer material (silts and clays). Less than 1% of the sediment load at San Acacia consists of gravel material.
    - Between the 2000s and early 2010s the difference in the suspended sediment volume between the Albuquerque and Bernardo USGS gages indicates sediment is being stored in the reach.
    - Between the 2000s and early 2010s the difference in the suspended sediment volume between the Albuquerque and San Acacia USGS gages indicates sediment is being transported, stored, or mined in the reach.
- Width
    - Average and maximum active channel width between 1990s through early 2010s have continued to decrease.
- Slope
    - The slope of the Rio Grande from Isleta to the Rio Puerco has decreased from the 2000s to the early 2010s.
    - The slope of the Rio Grande from Rio Puerco to San Acacia has increased from the 2000s to the early 2010s.
    - The slope in both reaches decreased from the 1980s to the early 2010s.
- Sinuosity
    - The sinuosity of the Rio Grande from Isleta to Rio Puerco has increased from the 1990s to the early 2010s.
    - The sinuosity of the Rio Grande from the Rio Puerco to San Acacia has increased slightly from the 1990s to the early 2010s.
- Planform
    - Planform has shifted from a multi-threaded channel to a primarily single thread channel between the 1990s and early 2010s.
    - Potential exists for the river to deepen and narrow, which may create a tendency for banks to laterally migrate.
    - Vegetation has increased as much as 20% from the 1990s to the early 2010s.
    - Number and area of mid-channel bars (includes vegetated and un-vegetated bars) has decreased as these features have become attached to the banklines.
- Channel topography

    - From the mid-1990s to mid-2010s the river from Los Lunas, NM to Casa Colorado, NM and immediately upstream of San Acacia Diversion Dam has incised.
    - From the mid-1990s to mid-2010s the river from Isleta Diversion Dam to Los Lunas, NM and Casa Colorado, NM to just upstream of San Acacia Diversion Dam has aggraded.
    - Between Isleta Diversion Dam and Tome, NM the active channel is slightly perched relative to the adjacent floodplain.
    - Between Abeytas, NM to San Acacia Diversion Dam a majority of the floodplain surfaces are high and elevated above the active channel.
    - Between Tome, NM and Abeytas, NM the active channel and the adjacent floodplain surfaces have a mix of these two characteristics
- Bed material size
    - Bed material size has coarsened slightly between the 1990s and early 2010s between Isleta and San Acacia Diversion Dams.
    - The nominal bed material is primarily sand-sized between Isleta and San Acacia Diversion Dams. The notable exception is around the Rio Salado confluence where nominal bed material is gravel-sized.
    - Except around the Rio Salado confluence most of the bed material is unstable at discharges of 500 cfs and greater.

Based on these findings river projects (both river maintenance and river rehabilitation) can be better planned to work with the river channel in order to effectively transport water and sediment, protect riverside infrastructure, and promote ecosystem function. While the processes that form channel response may be inherently complex, changes in the geomorphic drivers and parameters can be used to understand current geomorphic trends and potential future channel responses. Qualitative fluvial relationships, such as those developed by Lane (1954) and Schumm (1977), and channel evolution models, like Massong et al.'s (2010) and Schumm's (1977; 1981), help provide insight into current geomorphic trends and potential future channel responses. Both qualitative fluvial relationships and channel evolution models are discussed in more detail in the sections below, followed by a future channel response section.

5.1 Qualitative Geomorphic Relationships

The current geomorphic trends observed on the Middle Rio Grande between the Isleta and San Acacia Diversion Dams are governed by climatic and anthropogenic forcings upon the fluvial system that affect the supply of water and sediment. The geomorphic drivers of flow and sediment are not constant and changes in their magnitude, duration, and frequency occur on seasonal (based on irrigation demand), annual (snowmelt or rainfall runoff), or inter-decadal (e.g. the El Niño Southern Oscillation rainfall pattern) timescales. The river channel adapts to these drivers by making adjustments observed in the geomorphic parameters.

Understanding the direction of these changes (e.g. is the river going to aggrade or degrade) is where the qualitative relationships developed by Lane (1954) and Schumm(1977) become useful. These need to be coupled with an understanding other system impacts that affect the observed channel response, such as bank control, bed control, floodplain lateral confinement, and floodplain connectivity.

Lane (1954) developed a qualitative relationship between the channel sediment bed load (Q_s) and the river discharge (Q) based on an assessment of data collected from a variety of western United States rivers. The Lane Balance, as it has become known, is shown below (see Equation 4: d_{50} term is measured in the laboratory by a sieve analysis and represents the particle size for which 50% of the sampled mass is smaller and S is the channel gradient):

Equation 4. $$Q_s d_{50} \propto QS$$

Another study conducted by Stanley Schumm (1977) developed relationships for channel discharge (Q) and channel bed load (Q_s) based on measures of channel width (b), depth (d), sinuosity (ρ), meander wavelength (λ), and channel gradient (S). These relationships are given in the two following equations (see Equation 5 and Equation 6 below):

Equation 5. $$Q \propto \frac{b,\lambda,d}{S}$$

Equation 6. $$Q_s \propto \frac{b,\lambda,S}{d,\rho}$$

The Lane and Schumm relationships help understand the current trends and provide for the analysis of future channel response by holding one or more parameters constant while assessing the direction of change for the related parameters (e.g. if channel discharge and d_{50} are constant, how does sinuosity vary with changes to sediment bed load?). Based on these relationships, theoretical fluvial responses for a reduction in sediment or water supply can be determined (see Table 28). Based on the analyses described previously, current geomorphic trends can be listed for the Isleta to Rio Puerco and Rio Puerco to San Acacia reaches (see Table 29). A comparison of the theoretical and currently observed geomorphic drivers and parameters helps provide insight into potential future geomorphic trends.

Table 28.Theoretical responses suggested from a reduction in water discharge or sediment supply based on Equations 4 through 6.

Theoretical Response	Q	Q_s	S	d_{50}	b	d	λ	ρ
Reduction in Q_s	No change	-	-	+	-	+	-	+
Reduction in Q	-	No change	+	-	-	-	-	?

Table 29. Current geomorphic trends (1990s to 2010s) on the Rio Grande between the Isleta and San Acacia Diversion Dams.

Geomorphic Reach	Q	Q_s	S	d_{50}	b	d	λ	ρ
Isleta to Rio Puerco— Los Lunas, NM to Casa Colorado, NM sub reach	-	-	-	+	-	+	-	+
Isleta to Rio Puerco — rest of reach	-	-	-	+	-	-	-	+
Rio Puerco to San Acacia	-	relatively constant	+	+	-	-	-	+

For the theoretical responses, reductions in the sediment supply and water discharge amplify each other with regard to decreasing width and meander wavelength, but oppose one another with regard to slope, bed material, and depth. If sediment supply or water discharge were increased the opposite trends would be expected.

In comparing the theoretical trends (Table 28) to observations on the Middle Rio Grande between Isleta and San Acacia Diversion Dams (Table 29) it is noted that observed geomorphic parameters reflect components of both a reduction in the sediment supply and the water discharge. Observations of changes in the geomorphic drivers of sediment and water supply indicate that for most of this reach the volume of each of these has seen a slight reduction from the 1990s through the early 2010s. The sediment supply, based on the San Acacia USGS gage, indicates some fluctuations, but still a relatively consistent annual sediment supply. This suggests that the expected channel response would follow theoretical responses for the geomorphic parameters listed in Table 28. The decreases in the channel width from the 1990s to the early 2010s within the Isleta to San Acacia Diversion Dam reaches support this suggestion, as do the decreases in the meander wavelength. But not all of the observed geomorphic parameters follow the expected theoretical responses. For these situations the qualitative relationships put forward by Lane (1954) and Schumm (1977) are still useful but must be coupled with other insight into local variations such as potential grade controls from gravel armoring or larger sediment loads at tributary confluences, or higher bank stability from vegetation encroachment and/or geological constraints. These system controls affect the observed geomorphic response and may help explain deviations from the theoretical expectations.

Geomorphic parameters, like depth and slope that have been observed to be both decreasing and increasing within this reach, suggest the need to utilize other insights gleaned from the observation of geomorphic parameters. The theoretical responses shown in Table 28 indicate that a reduction in the sediment supply would cause a temporal decrease in the channel slope, whereas a decrease in the water supply would cause a temporal increase in the channel slope. These theoretical responses assume that the other driver (sediment supply or water supply) is kept constant. As both of these drivers vary, an assumption is made that

the observed geomorphic response is from the strongest reduction in the drivers or affected by local controls.
For the Isleta to Rio Puerco reach this would suggest that recent slope reductions are influenced by the reduction in the sediment supply, whereas observed slope increases in the Rio Puerco to San Acacia reach are more strongly influenced by water supply reductions or local increases in the sediment supply. Observations of channel topography and bed material within this reach, suggest that perhaps the Rio Salado confluence is providing a local bed control, which affects the observed geomorphic parameter responses. The Rio Salado has significantly larger bed material than other areas of the Rio Grande, and from longitudinal profiles and topography changes it appears like the Rio Salado is acting as a grade control. In order for the Rio Grande to move the bed material at the Rio Salado more water has to be supplied (higher peak flows with longer duration) or other means of increasing the available energy to transport the sediment, such as slope increases, would need to occur. Thus while there appears to be an overall sediment supply reduction in the reach between the 1990s and early 2010s, the transport of material from a tributary to the Rio Grande in excess of what can be transported will cause adjustments in the observed geomorphic parameters that are inconsistent with a purely theoretical sediment supply reduction response.

Observations of depth are also inconsistent with the expected theoretical trends, with the Isleta to Rio Puerco reach having sub-reaches that follow the theoretical trends of a reduction in sediment supply and sub-reaches that mirror the theoretical channel response for a decrease in the water supply and/or an increase in the local sediment supply. This may be related to diversion at the Isleta Diversion Dam and seepage/transpiration losses through the reach that affect the specific geographical influence of the change in drivers. For instance, the loss of river discharge at Isleta Diversion Dam would be expected to, at least, cause a local downstream effect of decreasing the channel depth. This decreasing channel depth would be exacerbated if the downstream sediment supply was also locally increased because of sluicing sediment through the dam. The increased coverage of vegetation on the Rio Grande adds roughness at the channel edges and within the floodplain that encourage sediment deposition. So a local increase in the sediment supply may cause sediment deposition at the channel edges and/or floodplain that eventually may result in a portion of the downstream reach that experiences a decreasing sediment supply and causes the depth to increase. This adds local sediment, which may influence an additional reach further downstream. Further facilitates the deposition of sediment. Since this is what has been observed recently in the Isleta to Rio Puerco reach, the qualitative relationships help us to understand that there are likely local variations in the water and sediment supply that are influencing the sub-reach geomorphic parameters that are being observed.

Another example of coupling the qualitative relationships from Lane (1954) and Schumm (1977) with other insights to understand channel responses comes from an evaluation of the bed material within this reach. The bed material has been

observed to coarsen throughout the reach, which is a theoretical response observed as the sediment supply is reduced. The increase in the nominal bed material size between Isleta to San Acacia suggests that the effects of a sediment supply reduction are a considerably stronger trend than a decrease in the water discharge. The deviation of observed geomorphic parameters, like slope and depth, to the theoretical response for a sediment supply reduction suggests either the influence of water supply and/or the impact of local variations. Another potential explanation could be that the available sediment transport capacity for a given water discharge has increased. Sediment transport capacity is influenced by channel morphology changes that increase the observed stream velocity or shear stress for the same discharge. This too would also encourage the coarsening of bed material. Since the median bed material sizes (d_{50}), and even most of the d_{84} size class for the bed material, found in this reach are currently in the medium to coarse sand size range according to the Wentworth (1922) scale, it would seem plausible that bed material could be mobilized at even lower flows. Calculations showing a decrease in the effective discharge (San Acacia USGS gage) would indicate that lower flows are now responsible for moving more of the sediment supply through at least the lower portion of this reach. This is consistent with calculations MEI (2002) pursued that indicated a higher propensity of base flows to carry sand when comparing previous decades to the 1990s. Observations of the channel topography, also confirm that most surveyed rangelines have narrower and deeper flow paths in the early 2010s then they did in the 1990s. This is true even at those cross sections that have aggradation within the active channel. The qualitative relationships can thus be used to understand changes in the transport capacity of the river and how this further influences the geomorphic parameters.

5.2 Planform Evolution Models

Planform evolution models, such as the ones developed by Massong et al. (2010) for the Middle Rio Grande and by Schumm (1977; 1981) for alluvial rivers in general, also help interpret current observations and predict future channel responses. The general observation of the Rio Grande's channel planform through the Isleta to San Acacia reach is a shift from a braided to a more meandering planform. Schumm (1977; 1981) observed that for alluvial rivers this shift in planform represents a move towards greater stability. A shift that is typically associated in other fluvial systems with decreases in the width/depth ratio, slope, sediment supply, stream power, and flow velocity. As a more predominant meandering planform develops there is the potential for the suspended load to become more influential on the channel's morphology Schumm (1977; 1981).

Massong et al.'s (2010) planform model also suggests that the channel is becoming more stable. The current planform designation for the Massong et al. (2010) classification of the Isleta to Rio Puerco reach is Stage M5 and the Rio Puerco to San Acacia reach is between Stages M5 and M6. Stage M5 represents one of the initial stages in the planform evolution of a river reach that has

developed excess transport capacity (ability to transport sediment exceeds the sediment supply). Stage M5 can be a final stage depending upon ongoing slope adjustments and bank vegetation establishment. The M6 stage shows a continuation of the channel incision, coupled with lateral migration patterns. The Rio Grande downstream of the Rio Salado is in this stage with several migrating bends that have developed over the last decade. The very last stage on the track of an excess transport capacity for the Massong et al. (2010) planform model is the chute cutoff, where the channel cuts off an extended bar. At this point the river has created an inset floodplain, smaller than the historical floodplain, and the channel geometry begins again to be in dynamic equilibrium with its drivers.

5.3 Conclusions

Current trends for the geomorphic drivers on the Rio Grande between the Isleta and San Acacia Diversion Dams indicate a decrease in the water between the 1990s and early 2010s. The water supply has primarily been affected by decreases in the magnitude, frequency, and duration from the spring snow-melt runoff. Scientific studies have suggested that global temperatures will continue to rise (IPCC, 2007) which may further decrease the volume of water received from the spring snow-pack runoff (Smith and Finch, 2016; Lehner et al., 2017a; Lehner et al., 2017b) and increase the influence of the monsoonal events (Smith and Finch, 2016). Since there has been an observable trend of decreased peak snow-melt runoffs since the construction of the large main stem reservoirs on the Rio Grande (MEI, 2002; Makar and AuBuchon, 2012), it seems reasonable to expect a continuing decrease in the spring snow-melt runoff water supply (magnitude, frequency, and duration). While the high flow, long duration events that occurred in the 1980s may still occur, they are expected to be infrequent.

Lower flows on the Rio Grande may increase in frequency, evidenced at the Albuquerque USGS gage by higher discharges for “base flow” conditions (bottom 25^{th} percentile) experienced more frequently in the last two decades than the period between 1974 and 1999. An increase in the lower flows is likely, due to water stored during flood events in the main stem reservoirs being moved through the Rio Grande for irrigation needs and/or endangered species needs (U.S. Fish and Wildlife Service, 2016).

The sediment supply is currently (1990s through 2010s) observed to be decreasing at the Albuquerque and Bernardo USGS gages and remaining constant at the San Acacia USGS gage. The Rio Puerco, known to historically contribute significant sediment supply to the Rio Grande (Gorbach, 1996), has shown a decreasing sediment yield since the 1970s. This is likely due to observed aggradational trends in the lower portion of the Rio Puerco valley (Friedman et al., 2015). The relatively constant trend in sediment supply at the San Acacia USGS gage may indicate the increased importance of other tributaries between the Bernardo and San Acacia USGS gages or the increased influence of sediment mobilized from the bed and banks of the active channel. Coupling this with the

prediction of future influence of monsoonal events on the water supply for this reach, suggest that the suspended sediment load will become a larger component of the total sediment load.

It is uncertain, however, whether the future sediment supply for the Isleta to San Acacia reach will increase or decrease. Within the semi-arid southwest, vegetation influences the amount of sediment transported in tributaries to the Rio Grande and the transport efficiency within the Rio Grande by affecting the erodibility of the soil. Within the tributary watersheds and adjacent higher terraces to the active Rio Grande channel, drier conditions may exacerbate observed groundwater drops, causing vegetation desiccation. If predicted warming trends result in less precipitation and drier conditions prevail, this may eventually lead to a loss of vegetative ground cover. If significant dessication occurs in a reach (whether from drought or because of a fire) an increase in the sediment supply is likely, especially if monsoonal events, which tend to influence the local tributaries in the Isleta to San Acacia reach, increase in intensity and frequency. But reductions in the sediment supply of tributaries like the Rio Puerco may temporally cause a sediment supply reduction.

Drier conditions may also encourage vegetation encroachment on the Rio Grande through the Isleta to San Acacia reach. Groundwater drops were observed from the early 2000s to early 2010s on areas adjacent to the Rio Grande within this study reach, but a 20% increase in the vegetation was observed from the 1990s until the early 2010s within this study reach. Drier conditions tend to increase the irrigation demand, which as water moves along the Rio Grande, encourages vegetation growth. The lack of higher sustained peak flows to scour younger vegetation is likely one of the reasons for the observed vegetation encroachment. The increase in vegetation helps stabilize sediment features in the active channel, such as islands and point bars. The vegetation also influences the active channel hydraulics, increasing the roughness, lowering velocity, and encouraging sediment deposition. The observable impact on the Rio Grande between the Isleta and San Acacia Diversion Dams is a significant (> 1 foot) of sediment deposition in the floodplain observed at most rangelines. This indicates a potential sediment storage within the reach and may result in a reduction of the sediment supply further downstream. Massong et al.'s (2010) planform model, however, suggests that future channel changes may include additional lateral migration. If significant lateral migration occurs, this would likely increase the sediment supply downstream since the observed bank materials tend to be of similar gradation as the collected bed materials, except around the Rio Salado. Lateral migration is more likely between Los Lunas, NM and Casa Colorado, NM due to observed thalweg incision on rangeline profiles within this sub-reach of the Rio Grande between the mid-1990s and mid-2010s.

The near-future sediment supply for this reach is likely a continuation of the trend of a reduced sediment supply within the upstream portion of this reach (Isleta Diversion Dam to Rio Puerco) and a continuation of the sediment supply on the

downstream portion of the reach (Rio Puerco to San Acacia Diversion Dam). Vegetation encroachment is expected to increase, which would likely result in continued sediment deposition in the channel floodplain and active channel. Deposition in the active channel would also be expected to decrease the channel width.

The influence of sediment and water supply is expected to continue to affect the morphology of the Rio Grande into the future. Current trends in the channel morphology are described in Table 29. Future trends based on the qualitative relationships of Lane (1954) and Schumm (1977) and the future predictions of sediment and water supply described above are shown in Table 30. Local variations in the geomorphic parameter trends indicated in Table 30 would be expected as local water and sediment supply variations or controls influence the local observations.

Table 30. Future geomorphic trends on the Rio Grande between the Isleta and San Acacia Diversion Dams.

Geomorphic Reach	Q	Q_s	S	d_{50}	b	d	λ	ρ
Isleta to Rio Puerco	-	-	-	+	-	+	-	+
Rio Puerco to San Acacia	-	No change	+	-	-	-	-	+

The absence of higher snow-melt runoff peak flows and the continuation of extended low flow periods will likely promote the continued vegetation encroachment along river banks and upon inter-channel sand bars. This would facilitate natural levee building through sediment deposition at the vegetation edges (observed in the REMs for the Isleta Diversion Dam to Los Chavez, NM) or throughout the floodplain (observed in the REMs from Los Chavez, NM to the San Acacia Diversion Dam). A combination of continued channel incision and increases in the bank height through sediment deposition in the Isleta to Rio Puerco reach would further diminish floodplain connectivity. Separation of the active channel from the floodplain will tend to increase the channel uniformity, decreasing the channel diversity and complexity, which is an important aspect of riparian areas (Crawford et al., 1993; Tashjian and Massong, 2006; Parametrix, 2008; Tetra Tech, 2014).

Given the future predicted trends stated in Table 30 for the Isleta to Rio Puerco reach, potential river maintenance concerns within this reach include increased risk of infrastructure adjacent to the active channel and ineffective transport of sediment and water downstream. Areas between Los Lunas, NM and Casa Colorado, NM are currently the most at risk for lateral migration of the active channel. Isleta Diversion Dam to Tome, NM, and to a lesser extent Tome, NM to Abeytas, NM are the reaches most susceptible to ineffective transport of sediment and water as the floodplain adjacent to the active channel tends to be higher than terrain adjacent to the constraining infrastructure (e.g. perched channel conditions). Improving active channel-floodplain connection would likely be

beneficial, as would providing streambank protection paralleling the constraining infrastructure. This would help achieve river maintenance concerns while still providing the river some freedom to make adjustments. If maintenance was done to limit the influences of vegetation on bank stability, it is probable that channel uniformity would decrease.

Potential for increasing the channel diversity and floodplain connection within the Isleta to Rio Puerco reach would best be achieved through mechanical intervention. Mechanical intervention, through the removal of vegetation and re-connection of lower terraces or lowering of higher terrace adjacent to the active channel, may temporarily provide improved floodplain connection. If fluvial processes are able to continually remove newly established vegetation, sinuosity may increase, further improving the morphological diversity within the active channel. Depending on the magnitude of these changes, predicted trends for the downstream portion of the Isleta to Rio Puerco reach (see Table 30) may resemble the predicted trends for the Rio Puerco to San Acacia reach given enough sediment added to the system. These effects, however, would not be sustainable unless longer term changes in the sediment and water discharge loads were experienced.

A combination of continued channel aggradation through sediment deposition in the Rio Puerco to San Acacia reach may also help to increase floodplain connectivity. This would be controlled to a large extent by the influence of larger bed material around the Rio Salado acting like a grade control. Since this reach currently has high terraces adjacent to the active channel, the majority of the reach is currently susceptible to bank erosion on these surfaces through lateral migration. The future expectation would be for small aggradational changes within the active channel, with a tendency towards lateral migration and increased channel sinuosity. If the sediment supply increases or the grade control at the Rio Salado is more pronounced then floodplain connectivity to the high terrace may increase and reduce the lateral migration. This potential future lateral connection to the floodplain would tend to decrease the channel uniformity and increase the morphological channel complexity and diversity (Crawford et al., 1993; Tashjian and Massong, 2006; Parametrix, 2008; Tetra Tech, 2014).

Given the future predicted trends stated in Table 30 for the Rio Puerco to San Acacia reach, potential river maintenance concerns within this reach include increased risk of infrastructure adjacent to the active channel, especially where the valley is narrow downstream of the Rio Salado, ineffective transport of sediment and water downstream, and increased risk of flooding. Removal of vegetation near the bank may exacerbate the lateral migration and provide an opportunity for an inset floodplain to develop adjacent to the active channel. Vegetation growth, naturally or through bio-engineering methods, would tend to provide additional stability near infrastructure. The establishment of an inset floodplain, through encouraging lateral migration or by creating floodplain surfaces in the higher terrace, would help convey the effective transport of water and sediment

downstream. Methods that rehabilitate the active channel capacity and/or strengthen/raise the adjacent spoil levee are likely the most suitable options for addressing the risk of flooding.

Predicted future trends may result in local fining of sediment (although this is controlled to a large extent by tributary inputs, especially the Rio Salado) and a decrease in the sediment load further downstream (such as observed immediately upstream of the San Acacia Diversion Dam. The depth of the channel may also decrease within the Rio Puerco to San Acacia Diversion Dam reach, as the potential for the river to return to a braided planform increases. These effects, however, would not be sustainable unless longer term changes in the sediment and water discharge loads were experienced. Observations of the future morphological responses may provide opportunities for additional habitat rehabilitation efforts that augment the natural fluvial processes occurring within this reach.

6.0 References

Akan, A.O. 2006. Open Channel Hydraulics. Elsevier Ltd. Oxford, UK. 364 pp.

Albert, J.M. 2004. Thesis – Hydraulic Analysis and Double Mass Curves of the Middle Rio Grande from Cochiti to San Marcial New Mexico. Colorado State University, Fort Collins, CO. 224 pp.

AuBuchon, J. 1015. Isleta to San Acacia Reach Overview of Previous Work. U.S. Department of the Interior, Bureau of Reclamation, Upper Colorado Region, Albuquerque, NM. 34 pp.

Baird, D. 2014. Historical Rio Grande Channel Width Design Literature Review Summary. U.S. Department of the Interior, Bureau of Reclamation, Technical Services Center, Sedimentation and River Hydraulics Group. Denver, CO. 42 pp.

Bauer, T.R. 2000. Thesis – Morphology of the Middle Rio Grande from Bernalillo Bridge to the San Acacia Diversion Dam, New Mexico. Colorado State University, Fort Collins, CO. 331 pp.

Bauer, T.R. 2004. Bed Material Data Collection Trip Report Rio Grande, New Mexico July and August 2004. U.S. Department of the Interior, Bureau of Reclamation, Technical Services Center, Sedimentation and River Hydraulics Group. Denver, CO. 17 pp.

Bauer, T.R. 2007. 2006 Bed Material Sampling on the Middle Rio Grande, NM. U.S. Department of the Interior, Bureau of Reclamation, Technical Services Center, Sedimentation and River Hydraulics Group. Denver, CO. 87 pp.

Bauer, T.R. 2009. Sediment Evolution on the Middle Rio Grande, New Mexico. U.S. Department of the Interior, Bureau of Reclamation, Technical Services Center, Sedimentation and River Hydraulics Group. Denver, CO. 36 pp.

Bauer, T.R. and Hilldale, R. 2006. Sediment Model for the Middle Rio Grande – Phase 2: Isleta Diversion Dam to San Acacia Diversion Dam. U.S. Department of the Interior, Bureau of Reclamation, Technical Services Center, Sedimentation and River Hydraulics Group. Denver, CO. 295 pp.

Berry, K.L. and Lewis, K. 1997. Historical Documentation of Middle Rio Grande Flood Protection Projects: Corrales to San Marcial. Office of Contract Archaeology, the University of New Mexico, Albuquerque, NM. 62 pp.

Biedenharn, D.S. and Copeland, R.R. 2000. Effective Discharge Calculation. Technical Note, US Army Corps of Engineers Research and Development Center, Vicksburg, MS. 10 pp.

BIO. 2005a. Middle Rio Grande Hydrographic Data Collection, Cochiti Priority Site Line Surveys, December, 2004. Bio-West, Inc.

BIO. 2005b. Middle Rio Grande Hydrographic Data Collection, Field Data Collection Report, Supplemental Cross Section Surveys and Discharge Measurements, Cochiti Priority Site 3, June, 2005. Bio-West, Inc.

Brierly, G. and Fryirs, K. 2005. Geomorphology and River Management: Applications of the River Styles Framework. Blackwell Publishing, Oxford, United Kingdom. 398 pp.

Bryan, K. and Post, G.M. 1927. Erosion and Control of Silt on the Rio Puerco, New Mexico. Middle Rio Grande Conservancy District. Albuquerque, NM. 220 pp.

Bosque Ecosystem Monitoring Program. (2013, 12). *Data Sets & Forms.* Retrieved 11 18, 2015, from Bosque School: http://www.bosqueschool.org/Data_Sets__Forms.aspx

Bosque Ecosystem Monitoring Program. (2016). *Site Maps*. Retrieved Aug 7, 2017, from Bosque Ecosystem Monitoring Program Web Site: http://bemp.org/site-maps/

Brierly, G. and Fryirs, K. 2005. Geomorphology and River Management:Applications of the River Styles Framework. Blackwell Publishing, Oxford, United Kingdom. 398 pp.

Bui, C. 2014. Flow Duration Curve Analysis from Cochiti Dam to Elephant Butte Reservoir. U.S. Department of the Interior, Bureau of Reclamation, Upper Colorado Region, Albuquerque, NM. 51 pp.

Coe, D.E. 2016. Floodplain Visualization using lidar-derived relative elevation models. Washington State Department of Natural Resources, Division of Geology and Earth Resources, Olympia, WA. 3 pp.

Crawford, C.S., Cully, A.C., Leutheuser, R., Sifuentes, M.S., White, L.F., and Wilber, J.P. 1993. Middle Rio Grande Ecosystem: Bosque Biological Management Plan. Middle Rio Grande Biological Interagency team, Albuquerque, NM, 320 pp.

CSU. 2002. Rio Grande Monitoring at Santa Ana Pueblo, Data Collection Report, Cochiti to San Acacia (CO) Line Surveys, August, 2002. Colorado State University, Fort Collins, Colorado.

Culbertson, J.K. and Dawdy, D.R. 1964. A Study of Fluvial Characteristics and Hydraulic Variable Middle Rio Grande New Mexico. U.S. Geological Survey, Professional Paper 1498-F, Washington, D.C. 82 pp.

Easterling Consultants LLC. (2014). *Hydrographic Data Collection Report, Cross-Section and GPS Surveys, Montano Bridge to Isleta Dam, December 2013 - February 2014.*

Eichorst, K.D., Shaw, D.C., Dwyer, M.M., and Crawford, C.S. 2004. Bosque Ecosystem Monitoring Program (BEMP) Second Supplement: 2002-2003. University of New Mexico, Albuquerque, NM. 6 pp.

Eichorst, K.D., Shaw, D.C., Schuetz, J.F., Scheerer, K., Keithley, M., and Crawford, C.S. 2012. Bosque Ecosystem Monitoring Program "BEMP_ Comprehensive Report" 1997 – 2009. University of New Mexico, Albuquerque, NM. 76 pp.

Elliot, J.G. 1979. Thesis – Evolution of Large Arroyos: The Rio Puerco of New Mexico. Colorado State University, Fort Collins, CO. 70 pp.

Finch, D. and Tainter, J.A. ed. 1995. Ecology, Diversity, and Sustainability of the Middle Rio Grande Basin. U.S. Department of Agriculture, Rocky Mountain Research Station, Fort Collins, CO. 198 pp.

Flo. 1995. Middle Rio Grande Project Hydrographic Collection Cross Section Surveys Lower Socorro Lines. Flo Engineering, Inc.

Flo. 1996. Field Data Collection Report Elephant Butte Range Lines EB-10 through EB-26, August, 1996. Flo Engineering, Inc.
Flo. 1998(a). Middle Rio Grande Project Hydrographic Data Collection Volume II, Results of Data Collection Efforts, SO Lines March through July 1997. Flo Engineering, Inc.
Flo. 1998(b). Field Data Collection Report Elephant Butte Range Lines, EB-10 through EB-32 and Fort Craig Line, FC-1754, July, 1998. Flo Engineering, Inc.
Flo. 1999(a). Middle Rio Grande Hydrographic Data Collection Cross Section Surveys, Cochiti (CO) Lines Volume I: Report. Flo Engineering, Inc.
Flo. 1999(b). Middle Rio Grande Hydrographic Data Collection Cross Section Surveys, Cochiti (CO) Lines Volume II: Report. Flo Engineering, Inc.
Friedman, J.M., Vincent, K.R., Griffin, E.R., Scott, M.L., Shafroth, P.B., and Auble, G.T. 2015. Processes of arroyo filling in northern new Mexico, USA. Geological Society of America Bulletin, 127 (3/4) pp 621-640.
Gellis, A. 1991. Decreasing Trends of Suspended Sediment Concentrations at Selected Streamflow Stations in New Mexico. Agencies and Science Working for the Future: New Mexico Water Resources Research Institute, Albuquerque, NM, 17 pp.
Gorbach, C.A. 1996. Evaluation of Proposed Sediment Control Projects in the Rio Puerco Basin. Proceedings of the Sixth Federal Interagency Sedimentation Conference, Las Vegas, Nevada, 8 pp.
Harris, A. and AuBuchon, J. 2016. Arroyo de las Cañas Geomorphic, Hydraulic, and Sediment Transport Analysis. U.S. Department of the Interior, Bureau of Reclamation, Upper Colorado Region, Albuquerque, NM. 119 pp.
Hilldale. R. and Bauer, T. 2003. Trip Report on Bed Material and Substrate Composition using a Dynamic Cone Penetrometer on the Middle Rio Grande. U.S. Department of the Interior, Bureau of Reclamation, Technical Services Center, Denver, CO. 48 pp.
Holmquist–Johnson, C., Raff, D., and Russell, K. 2009. Bureau of Reclamation Automated Modified Einstein Procedure (BORAMEP) Program for Computing Total Sediment Discharge. U.S. Department of the Interior, Bureau of Reclamation, Technical Services Center, Flood Hydrology Group. Denver, CO. 52 pp.
IPCC. 2007. Memo on Report from Intergovernmental Panel on Climate Change. Intergovernmental Panel on Climate Change, Geneva, Switzerland. 19 pp.
Klein, M., AuBuchon, J., Lampert, T., and Herrington, C. 2018. Isleta to San Acacia Hydraulic Modeling Report. U.S. Department of the Interior, Bureau of Reclamation, Albuquerque Area Office, Albuquerque, NM. 92 pp.
Lagasse, P.F., Clopper, P.E., Pagán-Ortiz, J.E., Zevenbergen, L.W., Arneson, L.A., Schall, J.D., and Girard, L.G. 2009. Bridge Scour and Stream Stability Countermeasures: Experience, Selection and Design Guidance Volumes 1 and 2, third edition. Ayres Associates for U.S. Department of Transportation, Federal Highway Administration, Hydraulic Engineering Circular No. 23. Printed by National Technical Information Service. Springfield, VA. 376 pp.

Lane, E.W. 1954. The Importance of Fluvial Morphology in Hydraulic Engineering. Hydraulic Laboratory Report No. 372. Department of the Interior, Bureau of Reclamation, Engineering Laboratories, Denver, CO. 108 pp.

Lehner, F., Wood, A.W., Llewellyn, D., Blatchford, D.B., Goodbody, A.G., and Pappenberger, F. 2017a. Mitigating the Impacts of Climate Nonstationarity on Seasonal Streamflow Predictability in the U.S. Southwest. GeoPhysical Research Letters, Volume 44, Issue 24, AGU Publications, John Wiley and Sons, Inc., Hoboken, NJ. p. 12,208-12,217

Lehner, F., Wahl, E.R., Wood, A.W., Blatchford, D.B., and Llewellyn, D. 2017b. Assessing recent declines in Upper Rio Grande River runoff efficiency from a paleoclimate perspective. AGU Publications, John Wiley and Sons, Inc., Hoboken, NJ. https://onlinelibrary.wiley.com/doi/10.1002/2017GL073253

Maestas, J., Padilla, R., Nemeth, M., AuBuchon, J., Casuga, J., Makar, P., and Varyu, D. 2014. Determination of River Maintenance Need at Individual Sites and Reaches on the Middle Rio Grande, NM. U.S. Department of the Interior, Bureau of Reclamation, Upper Colorado Region, Albuquerque, NM. 32 pp.

Makar, P. 2010. Channel Characteristics of the Middle Rio Grande, New Mexico. U.S. Department of the Interior, Bureau of Reclamation, Technical Service Center, Denver, CO. 48 pp.

Makar, P. 2015. Lower Reach Conditions and Strategies, Report No. SRH-2015-30. Department of the Interior, Bureau of Reclamation, Technical Service Center, Denver, CO. 60 pp.

Makar, P. and AuBuchon, J. 2012. Channel Conditions and Dynamics of the Middle Rio Grande. U.S. Department of the Interior, Bureau of Reclamation, Upper Colorado Region, Albuquerque, NM. 108 pp.

Makar, P., Massong, T.M., and Bauer, T. 2006. Channel Widths Changes along the Middle Rio Grande, NM. 2006 Federal interagency Sedimentation Conference. 8 pp.

Massong, T.M., Makar, P.W., and Bauer, T.R. 2010. Planform Evolution Model for the Middle Rio Grande, NM. 2nd Joint Federal Interagency Conference, 12 pp.

MEI. 2002. Geomorphic and Sedimentologic Investigations of the Middle Rio Grande between Cochiti Dam and Elephant Butte Reservoir. Mussetter Engineering, Inc., Fort Collins, Co. 229 pp.

Meyer, G.A., and Hepler, C.W. 2007. Vegetated Island Formation and Change in the Middle Rio Grande near Albuquerque, New Mexico. The University of New Mexico, Albuquerque, NM. 47 pp.

Mosley, H. 2000. Peak Flow Frequency Analysis: Rio Puerco near Bernardo, NM and Rio Salado near Acacia, NM. U.S. Department of the Interior, Bureau of Reclamation, Upper Colorado Region, Albuquerque, NM. 17 pp.

Nordin, C.F. 1963. A Preliminary Study of Sediment Transport Parameters Rio Puerco near Bernardo, New Mexico. U.S. Geological Survey, Professional Paper 462-C, Washington, D.C. 26 pp.

Olson, P.L., Legg, N.T., Abbe, T.B., Reinhart, M.A., and Radloff, J.K. 2014. A Method for Delineating Planning-Level Channel Migration Zones. State of

Washington, Department of Ecology Publication no 14-06-025, Olympia, WA. 83 pp.
Ortiz, R.M. 2004. A River in Transition: Geomorphic and Bed Sediment Response to Cochiti Dam on the Middle Rio Grande, Bernalillo to Albuquerque, New Mexico. The University of New Mexico, Albuquerque, NM. 76 pp.
Parametrix. 2008. Restoration Analysis and recommendations for the Isleta Reach of the Middle Rio Grande, NM. Parametrix, Inc. Albuquerque, NM 292 pp.
Reclamation. 1961. Sediment Studies for Channelization of the Rio Grande between Cochiti and Mouth of Rio Puerco Middle Rio Grande Project, NM Vol I of IV. U.S. Department of the Interior, Bureau of Reclamation, Albuquerque Project Office. 89 pp.
Reclamation. 1985. *Volume XXXV Annual Project History: Calendar Year 1985*. Bureau of Reclamation, Upper Colorado Region, Albuquerque Area Office, Albuquerque, New Mexico. 161 pp.
Reclamation, 2000. *Rio Grande and Low Flow Conveyance Channel Modifications Draft Environmental Impact Statement*. Bureau of Reclamation, Albuquerque Area Office, Albuquerque, NM.
Reclamation. 2012a. Middle Rio Grande River Maintenance Program Comprehensive Plan and Guide: Appendix B: One-dimensional Modeling and Indicator Results for the Middle Rio Grande. U.S. Department of the Interior, Bureau of Reclamation, Upper Colorado Region, Albuquerque, NM. 135 pp.
Reclamation. 2012b. Middle Rio Grande River Maintenance Program Comprehensive Plan and Guide. U.S. Department of the Interior, Bureau of Reclamation, Upper Colorado Region, Albuquerque, NM. 210 pp.
Reclamation, 2014. Lab Standard Operating Procedure (SOP). U.S. Department of the Interior, Bureau of Reclamation, Upper Colorado Region, Albuquerque, NM. 32 pp.
Richard, G., Leon, C., and Julien, P. 2001. Hydraulic Modeling on the Middle Rio Grande, New Mexico: Rio Puerco Reach. Colorado State University, Fort Collins, CO. 102 pp.
Schumm, S.A. 1977. The Fluvial System. John Wiley and Sons, New York, NY. 338 pp.
Schumm, S.A. 1981. Evolution and Response of the Fluvial System, Sedimentologic Implications. Society of Economic Paleontologists and Mineralogists, Special Publication No. 31, Tulsa, OK. p. 19-29.
Scurlock, D. 1998. From the Rio to the Sierra: An Environmental History of the Middle Rio Grande Basin. U.S. Department of Agriculture, Rocky Mountain Research Station, Fort Collins, CO. 60 pp.
Simons, D.B., Li, R., Li, L., and Ballantine, M.J. 1981. Erosion and Sedimentation Analysis of Rio Puerco and Rio Salado Watersheds. Simons, Li, and Associates, Inc. 189 pp.
Slaughter, S.L. and Hubert, I.J. 2014. Geomorphic Mapping of the Chehalis River Floodplain, Cosmopolis To Pe Ell, Grays Harbor, Thurston, and Lewis Counties, Washington. Washington State Department of Natural Resources,

Divisino of Geology and Earth Resources, Information Circular 118, Olympia, WA. 63 pp.
Smith, D.M. and Finch, Deborah M. 2016. Riparian trees and aridland streams of the southwestern United States: An assessment of the past, present, and future. Journal of Arid Environments, volume 13, Elsevier Ltd., Devon, United Kingdom. p. 120-131
SSWD. 2014. Middle Rio Grande Project Hydrographic Data Collection, Final Report, Cross Section Surveys, Isleta to Belen Range Lines, March, 2014. Southwest Water Design, LLC. Albuquerque, NM.
Tashjian, P. and Massong, T. 2006. The Implications of Recent Floodplain Evolution on Habitat within the Middle Rio Grande, NM. 2006 Federal interagency Sedimentation Conference, 9 pp.
Tetra Tech. 2000. Middle Rio Grande Hydrographic Data Collection, Floodplain Extension, Cross Section Surveys Cochiti (CO) Lines, November, 2000. Tetra Tech, Inc.
Tetra Tech. 2002. Middle Rio Grande Hydrographic Data Collection, Cochiti (CO) Line Surveys, April, 2002. Tetra Tech, Inc.
Tetra Tech. 2005. Middle Rio Grande Project Hydrographic Data Collection, Field Data Collection Report, Cross Section Surveys and Plots, Cochiti (CO) Line Surveys, March, 2005. Tetra Tech, Inc.
Tetra Tech. 2012. Field Data Collection Report, Cross-Section Surveys and River Profile Survey, Rio Puerco (RP) Line Surveys, La Joya (LJ) Line Surveys, & Cochiti (CO) Line Surveys, February - April 2012. Tetra Tech, Inc.
Tetra Tech. 2014. Final Report: Ecohydrological Relationships along the Middle Rio Grande of New Mexico for the Endangered Rio Grande Silvery Minnow. Tetra Tech, Inc.115 pp.
Tetra Tech. 2015. Field Data Collection Report, Cross Section Surveys, 2015 Belen RR Bridge to San Acacia Rangeline Surveys. Tetra Tech, Inc., Albuquerque, NM, 32 pp.
Tetra Tech. 2016. Field Data Collection Report, Cross Section Surveys, Belen RR Bridge to San Acacia Lines Surveys. Tetra Tech, Inc., Albuquerque, NM, 22 pp.
U.S. Fish and Wildlife Service. 2016. Biological and Conference Opinion for Bureau of Reclamation, Bureau of Indian Affairs, and Non-federal Water Management and Maintenance Activities on the Middle Rio Grande, New Mexico. U.S. Department of the Interior, Fish and Wildlife Service, Albuquerque, NM. 266 pp.
Varyu, D. 2013. Aggradation/Degradation Volume Calculations: 2002-2012. U.S. Department of the Interior, Bureau of Reclamation, Technical Service Center, Denver, CO. 455 pp.
Varyu, D. and Fox, B. 2014. Middle Rio Grande Sediment Budget: Cochiti Dam to Delta Channel (AggDeg 17-1800). U.S. Department of the Interior, Bureau of Reclamation, Technical Service Center, Denver, CO. 38 pp.
Vensel, C, Richard, G., Leon, C., and Julien, P. 2006. Hydraulic Modeling on the Middle Rio Grande, New Mexico Rio Puerco Reach. Colorado State University, Ft. Collins, CO. 112 pp.

Wentworth, C.K. 1922. A scale of grade and class terms for clastic sediments. Journal of Geology, volume 30. Chicago, Il. pp 377-392

Wilcox, P., Pitlick, J., and Cui, Y. 2009. Sediment Transport Primer Estimating Bed-Material Transport in Gravel-bed Rivers. U.S. Department of Agriculture, Forest Service, Rocky Mountain Research Station, General Technical Report RMRS-GTR-226, Ft. Collins, CO. 78 pp.

Wright, J.M. 2010. Middle Rio Grande Peak Discharge Frequency Study. U.S. Department of the Interior, Bureau of Reclamation, Technical Service Center, Denver, CO. 151 pp.

Yang, C.T. 1996. Sediment Transport Theory and Practice. The McGraw-Hill Companies, Inc. New York, NY. 396 pp.

Appendix A: 2016 Bed Material Collections

Bed and bank material samples were collected between July 1st and 28th, 2016. The bed samples were collected with a sediment scoop, as seen in Figure 96. Samples were taken from across the active channel width. The samples were composited, unless significant grain size variations were apparent in the field.

The bank samples were collected with a standard shovel since the samples were all taken above water. See Figure 52 for an example of a bank sample and standard shovel. Only a single sample was taken for each location as the bank material was fairly uniform. The material sample collection crew varied by sample and included: Jonathan Aubuchon, Suzanne Devergie, Michelle Klein, Tony Lampert, and Bryan Lawlis.

The samples were processed in Reclamation's Albuquerque lab. The sieve process is governed by Reclamation's Lab Standard Operating Procedure (Reclamation, 2014). The samples were oven dried, weighed, and sieved to determine each sample's gradation. Bank samples were often clay clumps that were caught on sieve sizes much larger than the individual clay particles. These were broken down as much as possible, but cohesive particles were not fully broken down and so were caught on sieves representative of the intact particle.

Table 1 shows the names of the sample sites, whether the sample was a bed or bank sample, the date collected, and the sample locations. Figure 1 shows the locations of the samples graphically.

Table 2 provides the river flow rates for the data collection period. The flow rates come from the USGS gages on the Rio Grande at Isleta (USGS 08330875), at Bosque (USGS 08331510), and at San Acacia (USGS 08354900). Also, data is provided for the Rio Puerco (USGS 08353000).

Table 3 provides a summary of the sample gradation information including the D_{50} and D_{84} for the bed material samples, and Table 4 provides the same data but for the bank material samples.

Table 1: 2016 Bed and Bank Material Samples

Agg-deg Line or Rangeline	Type	Date Collected	Easting, NM State Plane NAD83 datum	Northing, NM State Plane, NAD 83 datum
668	bed	7/6/2016	1,506,068	1,416,047
IS-690	bed	7/6/2016	1,499,233	1,408,182
731	bank	7/6/2016	1,501,865	1,387,438
732	bed	7/6/2016	1,501,865	1,387,438
LL-793	bed	7/14/2016	1,492,505	1,359,464
IS-815	bed	7/14/2016	1,489,875	1,349,607
CO-833	bed	7/14/2016	1,492,328	1,341,166
857	bed	7/14/2016	1,493,436	1,329,697
863	bank	7/14/2016	1,494,222	1,327,393
CO-877	bed	7/14/2016	1,490,689	1,321,471
IS-908	bed	7/14/2016	1,489,605	1,306,806
CC-927	bed	7/14/2016	1,483,640	1,299,823
CC-943	bed	7/14/2016	1,485,753	1,292,694
974	bank	7/28/2016	1,476,648	1,281,664
976	bed	7/28/2016	1,476,471	1,280,598
1004	bed	7/28/2016	1,474,051	1,267,131
CO-1044	bed	7/28/2016	1,474,135	1,248,192
1061	bank	7/7/2016	1,472,800	1,240,336
1061	bed	7/7/2016	1,472,897	1,240,333
1086	bank	7/28/2016	1,465,120	1,232,652
1088	bank	7/7/2016	1,463,596	1,231,666
CO-1091	bed	7/28/2016	1,463,907	1,230,126
1094	bank	7/28/2016	1,463,892	1,229,078
1097	bed	7/7/2016	1,462,247	1,227,659
RP-1100	bed	7/7/2016	1,461,264	1,226,584
CO-1104	bed	7/1/2016	1,460,508	1,224,592
LJ-10	bank	7/1/2016	1,455,929	1,215,318
LJ-18	bed	7/1/2016	1,457,746	1,208,653
CO-1164	bed	7/7/2016	1,462,638	1,196,693
RP-1170	bank	7/7/2016	1,461,415	1,193,549
1183	bed	7/19/2016	1,456,532	1,190,886
RP-1190	bed	7/19/2016	1,455,630	1,186,803
CO-1194	bed	7/19/2016	1,453,678	1,187,272
RP-1202.5	bank	7/19/2016	1,450,002	1,185,322

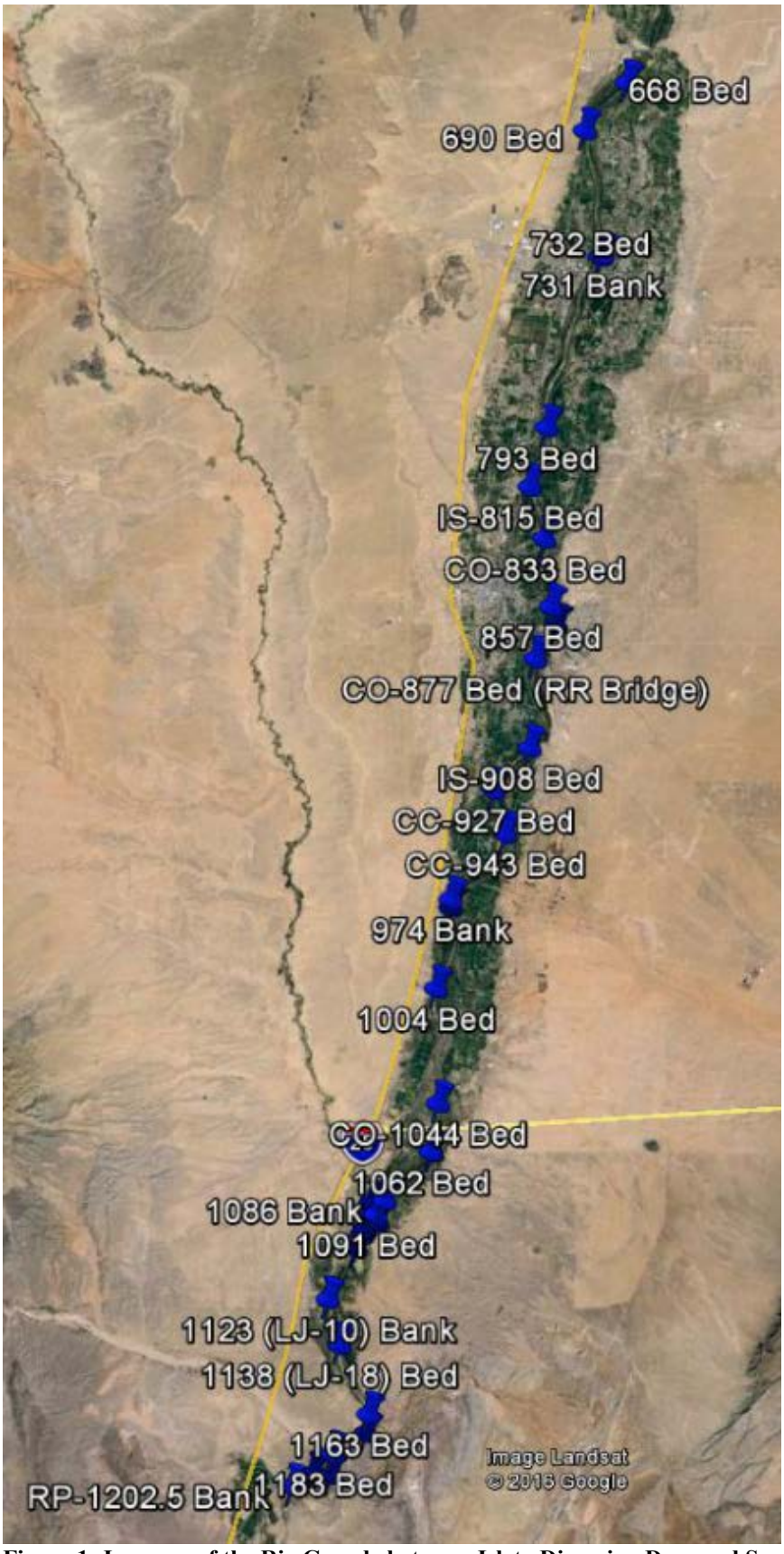

Figure 1: Imagery of the Rio Grande between Isleta Diversion Dam and San Acacia Diversion Dam. Bed and bank material sample locations are shown as blue pins labeled with their agg-deg or range line names and followed by a bed or bank sample type designation.

Table 2: Flow rates on the Rio Grande and the Rio Puerco during the period of bed material sample collection

Date	Isleta Gage Flow (cfs)	Bosque Gage Flow (cfs)	Rio Puerco Gage Flow (cfs)	San Acacia Gage Flow (cfs)
6/20/2016	1720	1250	0	1490
6/21/2016	1490	1040	0	1200
6/22/2016	1260	960	0	974
6/23/2016	1120	893	0	956
6/24/2016	912	604	0	895
6/25/2016	838	367	0	551
6/26/2016	895	317	0	458
6/27/2016	928	347	0	426
6/28/2016	933	365	0	402
6/29/2016	889	345	0	373
6/30/2016	830	297	0	345
7/1/2016	730	251	0	296
7/2/2016	740	220	0	305
7/3/2016	739	217	0	296
7/4/2016	737	251	0	305
7/5/2016	740	221	0	339
7/6/2016	733	209	0	311
7/7/2016	666	228	0	283
7/8/2016	618	177	0	269
7/9/2016	620	166	0	245
7/10/2016	614	141	0	221
7/11/2016	587	136	0	196
7/12/2016	556	123	0	173
7/13/2016	575	119	0	154
7/14/2016	618	106	0	143
7/15/2016	623	83	0	124
7/16/2016	658	74	0	104
7/17/2016	676	82.8	0	95.7
7/18/2016	683	86.3	0	87
7/19/2016	670	93	0	81.1
7/20/2016	640	91.6	0	80.6
7/21/2016	583	79.9	0	95.9
7/22/2016	594	58.8	0	65.2
7/23/2016	566	59.8	0	71.6
7/24/2016	589	50.6	0	74.3
7/25/2016	591	51.3	0	74.1
7/26/2016	624	46.3	0	68
7/27/2016	560	54.8	0	67.3
7/28/2016	523	34.3	0	67.4
7/29/2016	518	28.9	0	65.5
7/30/2016	726	29.2	0	61.9
7/31/2016	1220	172	0	60.7

Table 3: Bed material sample gradation data

Location	D_{50}	D_{84}
668	0.43	0.64
690	0.50	1.10
732	0.60	1.68
LL-792	0.49	0.90
IS-815	0.39	0.77
CO-833	0.42	0.63
857	0.43	0.85
CO-877	0.46	1.13
IS-908	0.40	0.61
CC-927	0.41	0.58
CC-943	0.44	0.92
976	0.46	1.23
1004	0.42	1.00
CO-1044	0.44	0.79
1062	0.39	0.58
CO-1091	0.40	0.59
1097	0.41	0.60
RP-1100	0.34	0.50
CO-1104	0.47	0.78
LJ-18	0.38	0.57
CO-1164	0.41	0.58
1183a	123.68	130.00
1183b	78.71	120.00
RP-1190	13.08	88.00
CO-1194	7.21	105.00

Table 4: Bank material sample gradation data

Location	D_{50}	D_{84}
731	0.29	0.61
863	0.34	0.55
974	0.17	0.25
1061	0.15	26.09
1086	0.14	6.31
1088	0.19	0.26
1094	4.81	8.84
LJ-10	0.12	1.56
RP-1170	22.96	39.83
RP-1202.5	0.22	0.48

The following pages of Appendix A provide photographs of the site at the time of sample collection. At the end of the photographs, lab sample sheets are provided which are hand-written records of the material sample information including weight retained on each sieve. Excel gradation sheets are also provided (following the lab sample sheets) which give the sample gradation information and gradation curves.

Sample: 668

Figure 2: Sample 668 looking downstream

Figure 3: Sample 668 looking right

Figure 4: Sample 668 looking upstream

Figure 5: Sample 668 looking left

Figure 6: Sample 668 looking left

Sample: IS-690

Figure 7: Sample IS-690 looking upstream right

Figure 8: Sample IS-690 looking right

Figure 9: Sample IS-690 looking downstream right

Figure 10: Sample IS-690 looking downstream

Figure 11: Sample IS-690 looking downstream left

Figure 12: Sample IS-690 looking left

Figure 13: Sample IS-690 looking left

Figure 14: Sample IS-690 looking upstream

Sample: 731 / 732

Figure 15: Sample 731 / 732 looking downstream

Figure 16: Sample 731 / 732 looking downstream right

Figure 17: Sample 731 / 732 looking right

Figure 18: Sample 731 / 732 looking upstream right

Figure 19: Sample 731 / 732 looking upstream

Figure 20: Sample 731 / 732 looking upstream

Figure 21: Sample 731 / 732 looking upstream left

Figure 22: Sample 731 / 732 looking left

Sample: LL-792

Figure 23: Sample LL-792 bed sample

Figure 24: Sample LL-792 bed sample

Figure 25: Sample LL-792 looking upstream

Figure 26: Sample LL-792 looking left

Figure 27: Sample LL-792 looking downstream

Figure 28: Sample LL-792 looking right

Sample: IS-815

Figure 29: Sample IS-815 looking upstream

Figure 30: Sample IS-815 looking left

Figure 31: Sample IS-815 looking downstream

Figure 32: Sample IS-815 looking right

Figure 33: Sample IS-815 bed sample

Figure 34: Sample IS-815 bed sample

Sample: CO-833

Figure 35: Sample CO-833 looking upstream

Figure 36: Sample CO-833 looking left

Figure 37: Sample CO-833 looking downstream

Figure 38: Sample CO-833 looking right

Figure 39: Sample CO-833 bed sample

Figure 40: Sample CO-833 bed sample

Sample: 857

Figure 41: Sample 857 looking upstream

Figure 42: Sample 857 looking left

Figure 43: Sample 857 looking downstream

Figure 44: Sample 857 looking right

Figure 45: Sample 857 bed sample

Figure 46: Sample 857 bed sample

Sample: 863

Figure 47: Sample 863 looking upstream

Figure 48: Sample 863 looking left

Figure 49: Sample 863 looking left

Figure 50: Sample 863 looking downstream

Figure 51: Sample 863 looking right

Figure 52: Sample 863 bank sample

Sample: CO-877

Figure 53: Sample CO-877 looking upstream

Figure 54: Sample CO-877 looking left

Figure 55: Sample CO-877 looking downstream

Figure 56: Sample CO-877 looking right

Figure 57: Sample CO-877 bed sample

Figure 58: Sample CO-877 bed sample

Sample: IS-908

Figure 59: Sample IS-908 looking upstream

Figure 60: Sample IS-908 looking left

Figure 61: Sample IS-908 looking downstream

Figure 62: Sample IS-908 looking right

Figure 63: Sample IS-908 bed sample

Figure 64: Sample IS-908 bed sample

Sample: CC-927

Figure 65: Sample CC-927 looking upstream

Figure 66: Sample CC-927 looking left

Figure 67: Sample CC-927 looking downstream

Figure 68: Sample CC-927 looking right

Figure 69: Sample CC-927 bed sample

Figure 70: Sample CC-927 bed sample

Sample: CC-943

Figure 71: Sample CC-943 looking upstream

Figure 72: Sample CC-943 looking left

Figure 73: Sample CC-943 looking downstream

Figure 74: Sample CC-943 looking right

Figure 75: Sample CC-943 bed sample

Figure 76: Sample CC-943 bed sample

Sample: 974

Figure 77: Sample 974 looking upstream

Figure 78: Sample 974 looking left

Figure 79: Sample 974 looking downstream

Figure 80: Sample 974 looking right

Figure 81: Sample 974 bank sample

Figure 82: Sample 974 bank sample

Figure 83: Sample 974 bank sample

Figure 84: Sample 974 bank sample

Figure 85: Sample 974 bank sample

Figure 86: Sample 974 bank sample

Sample: 976

Figure 87: Sample 976 looking upstream

Figure 88: Sample 976 looking left

Figure 89: Sample 976 looking downstream

Figure 90: Sample 976 looking right

Figure 91: Sample 976 bed sample

Sample: 1004

Figure 92: Sample 1004 looking upstream

Figure 93: Sample 1004 looking left

Figure 94: Sample 1004 looking downstream

Figure 95: Sample 1004 looking right

Figure 96: Sample 1004 bed sample

Figure 97: Sample 1004 bed sample

Sample: CO-1044

Figure 98: Sample CO-1044 looking upstream

Figure 99: Sample CO-1044 looking left

Figure 100: Sample CO-1044 looking downstream

Figure 101: Sample CO-1044 looking right

Figure 102: Sample CO-1044 bed sample

Sample: 1061 / 1062

Figure 103: Sample 1061 / 1062 looking upstream

Figure 104: Sample 1061 / 1062 looking left

Figure 105: Sample 1061 / 1062 looking downstream

Figure 106: Sample 1061 / 1062 looking right

Sample: 1086

Figure 107: Sample 1086 looking upstream

Figure 108: Sample 1086 looking left

Figure 109: Sample 1086 looking downstream

Figure 110: Sample 1086 looking right

Figure 111: Sample 1086 bank sample

Sample: 1088

Figure 112: Sample 1088 looking upstream

Figure 113: Sample 1088 looking left

Figure 114: Sample 1088 looking downstream

Figure 115: Sample 1088 looking right

Figure 116: Sample 1088 bank sample

Figure 117: Sample 1088 bed sample

Sample: CO-1091

Figure 118: Sample CO-1091 bed sample

Figure 119: Sample CO-1091 looking upstream

Figure 120: Sample CO-1091 looking left

Figure 121: Sample CO-1091 looking downstream

Figure 122: Sample CO-1091 looking right

Sample: 1094

Figure 123: Sample CO-1094 bank sample

Sample: 1097

Figure 124: Sample 1097 looking downstream at the Rio Puerco confluence on the right side of the Rio Grande

Figure 125: Sample 1097 looking upstream

Figure 126: Sample 1097 looking left

Figure 127: Sample 1097 looking downstream

Figure 128: Sample 1097 looking right

Sample: RP-1100

Figure 129: Sample RP-1100 looking upstream

Figure 130: Sample RP-1100 looking left

Figure 131: Sample RP-1100 looking left

Figure 132: Sample RP-1100 looking downstream

Figure 133: Sample RP-1100 looking right

Sample: CO-1104

Figure 134: Sample CO-1104 looking left

Figure 135: Sample CO-1104 looking right

Figure 136: Sample CO-1104 looking upstream

Figure 137: Sample CO-1104 looking downstream

Figure 138: Sample CO-1104 bed sample

Sample: LJ-10

Figure 139: Sample LJ-10 looking downstream

Figure 140: Sample LJ-10 looking downstream right

Figure 141: Sample LJ-10 looking upstream

Figure 142: Sample LJ-10 looking right

Figure 143: Sample LJ-10 looking right

Figure 144: Sample LJ-10 looking upstream

Figure 145: Sample LJ-10 looking left

Figure 146: Sample LJ-10 looking left

Figure 147: Sample LJ-10 looking right

Sample: LJ-18

Figure 148: Sample LJ-18 looking downstream

Figure 149: Sample LJ-18 looking upstream

Figure 150: Sample LJ-18 looking right

Figure 151: Sample LJ-18 looking left

Sample: CO-1164

Figure 152: Sample CO-1164 looking upstream

Figure 153: Sample CO-1164 looking left

Figure 154: Sample CO-1164 looking downstream

Figure 155: Sample CO-1164 looking downstream right

Figure 156: Sample CO-1164 looking right

Figure 157: Sample CO-1164 looking downstream

Sample: RP-1170

Figure 158: Sample RP-1170 island

Figure 159: Sample RP-1170 looking upstream

Figure 160: Sample RP-1170 left bank sample

Figure 161: Sample RP-1170 looking left

Figure 162: Sample RP-1170 looking downstream

Figure 163: Sample RP-1170 looking downstream right

Figure 164: Sample RP-1170 looking right

Figure 165: Sample RP-1170 looking right

Sample: 1183

Figure 166: Sample 1183 looking left

Figure 167: Sample 1183 looking downstream

Figure 168: Sample 1183 looking upstream

Figure 169: Sample 1183 looking upstream

Figure 170: Sample 1183 looking right

Figure 171: Sample 1183 looking right

Figure 172: Sample 1183 looking downstream

Sample: RP-1190

Figure 173: Sample RP-1190 looking upstream

Figure 174: Sample RP-1190 looking left

Figure 175: Sample RP-1190 looking downstream

Figure 176: Sample RP-1190 looking upstream

Figure 177: Sample RP-1190 looking right

Figure 178: Sample RP-1190 looking downstream right

Sample: CO-1194

Figure 179: Sample CO-1194 looking upstream

Figure 180: Sample CO-1194 looking right

Figure 181: Sample CO-1194 looking right

Figure 182: Sample CO-1194 looking downstream

Figure 183: Sample CO-1194 looking downstream

Figure 184: Sample CO-1194 looking left

Figure 185: Sample CO-1194 looking left

Figure 186: Sample CO-1194 looking upstream

Sample: RP-1202.5

Figure 187: Sample RP-1202.5 looking right

Figure 188: Sample RP-1202.5 looking upstream right

Figure 189: Sample RP-1202.5 looking downstream right

Figure 190: Sample RP-1202.5 left bank sample

Figure 191: Sample RP-1202.5 looking left

Lab Sample Report

Lab Number: IS668070616

Sample Information:

Sample Location: locations on bed across cross section

Station: IS-668

Sample Number: IS-668

Date & Time Sampled: 7/6/2016

Date Received: 7/6/16

Sample Testing:

Composite: Y (N)

Dry Weight: 3813.0

Sieve:	Weight Retained:
2" (50 mm)	—
1" (25 mm)	—
3/4" (19 mm)	—
1/2" (12.5 mm)	—
3/8" (9.5 mm)	—
No. 4 (4.75 mm)	12.9
No. 8 (2.36 mm)	23.9
No. 10 (2 mm)	10.2
No. 16 (1.18 mm)	68.9
No. 30 (0.6 mm)	544.7
No. 40 (0.425 mm)	1327.8
No. 50 (0.3 mm)	1360.1
No. 100 (0.15 mm)	444.4
No. 200 (0.075 mm)	24.4
No. 230 (0.063 mm)	0.6
Pan	0.5
Total Retained:	3818.4

if sample is composited Sample numbers and Station:	

Additional Remarks:

In the shaker 7/12/16

7:28am.

processed 8:54am by JA 7/12/16

Lab Sample Report Lab Number: IS690070616

Sample Information:
Sample Location: IS-8A 690- locations on bed at cross section Station: _____ Sample Number: IS-690
Date & Time Sampled: 7/6/16 Date Received: 7/7/16

Sample Testing:

Composite: Y N

Dry Weight: 4045.7

Sieve:	Weight Retained:
2" (50 mm)	—
1" (25 mm)	—
3/4" (19 mm)	—
1/2" (12.5 mm)	—
3/8" (9.5 mm)	2.7
No. 4 (4.75 mm)	24.8
No. 8 (2.36 mm)	122.4
No. 10 (2 mm)	57.0
No. 16 (1.18 mm)	327.7
No. 30 (0.6 mm)	1045.1
No. 40 (0.425 mm)	852.6
No. 50 (0.3 mm)	770.5
No. 100 (0.15 mm)	531.7
No. 200 (0.075 mm)	208.9
No. 230 (0.063 mm)	35.6
Pan	63.5
Total Retained:	4042.5

if sample is composited Sample numbers and Station:	

Additional Remarks:

IN the shaker 7/12/16 9:20 Am
processed 9:40 Am 7/12/16 by JA

Lab Sample Report Lab Number: 731070616

Sample Information:					
Sample Location:	IS to SA bad Creek collection	Station:	Bank	Sample Number:	731
Date & Time Sampled:	7/6/16	Date Received:	7/6/16		

Sample Testing:

Composite: Y (N)

Dry Weight: 3776.0

Sieve:	Weight Retained:
2" (50 mm)	
1" (25 mm)	
3/4" (19 mm)	116.0
1/2" (12.5 mm)	35.4
3/8" (9.5 mm)	7.1
No. 4 (4.75 mm)	72.2
No. 8 (2.36 mm)	69.1
No. 10 (2 mm)	26.5
No. 16 (1.18 mm)	97.9
No. 30 (0.6 mm)	286.7
No. 40 (0.425 mm)	494.6
No. 50 (0.3 mm)	748.5
No. 100 (0.15 mm)	722.1
No. 200 (0.075 mm)	779.4
No. 230 (0.063 mm)	167.6
Pan	253.0
sticks	0.2
Total Retained:	3776.4

if sample is composited Sample numbers and Station:	

Additional Remarks:

information on bank written on bag
willow grasses, juvenile cottonwood

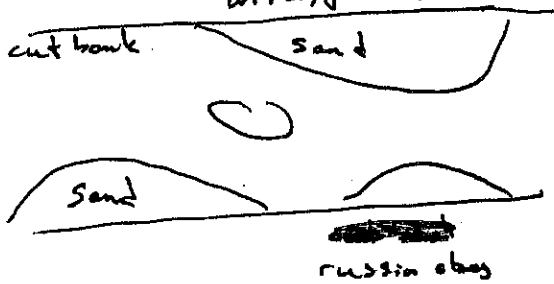

sep attached

set out to air dry 7/13/16

placed in oven 7/15/16 - bottom shelf

set in sieve 9:26 7/18/16

appears to be clay particles in large gravel sized clumps.

Lab Sample Report Lab Number: 732070616

Sample Information:
Sample Location: I5 to SA bed/bank collection Station: bed Sample Number: 732
Date & Time Sampled: 7/6/16 Date Received: 7/6/16

Sample Testing:

Composite: Y (N)

Dry Weight: 3803.8

Sieve:	Weight Retained:
2" (50 mm)	
1" (25 mm)	
3/4" (19 mm)	28.8
1/2" (12.5 mm)	83.5
3/8" (9.5 mm)	41.8
No. 4 (4.75 mm)	142.7
No. 8 (2.36 mm)	148.0
No. 10 (2 mm)	54.3
No. 16 (1.18 mm)	328.2
No. 30 (0.6 mm)	1059.6
No. 40 (0.425 mm)	770.1
No. 50 (0.3 mm)	708.6
No. 100 (0.15 mm)	390.5
No. 200 (0.075 mm)	39.9
No. 230 (0.063 mm)	2.5
Pan	3.0
Total Retained:	3801.5

if sample is composited Sample numbers and Station:	

Additional Remarks:

set out to air dry 7/13/16

placed in shaker 7/22/16 @ 9:30 AM

Entered in xls @ 10:55 AM

Lab Sample Report

Lab Number: LL~~97~~793 071416

Sample Information:

Sample Location: 1S to SA data collection Station: Bed Sample Number: LL-793

Date & Time Sampled: 7/14/16

Date Received: 7/14/16

Sample Testing:

Composite: Y (N)

Dry Weight: 6596.2

Sieve:	Weight Retained:
2" (50 mm)	
1" (25 mm)	
3/4" (19 mm)	
1/2" (12.5 mm)	
3/8" (9.5 mm)	2.7
No. 4 (4.75 mm)	16.6
No. 8 (2.36 mm)	74.3
No. 10 (2 mm)	39.8
No. 16 (1.18 mm)	240.7
No. 30 (0.6 mm)	1675.5
No. 40 (0.425 mm)	2153.0
No. 50 (0.3 mm)	1764.3
No. 100 (0.15 mm)	533.2
No. 200 (0.075 mm)	77.2
No. 230 (0.063 mm)	7.2
Pan	9.2
Total Retained:	6593.7

if sample is composited Sample numbers and Station:	

Additional Remarks:

Placed in shaker @ 11:15 AM 7/25/16

Entered in xls @ 12:45 PM 7/25/16

Lab Sample Report

Lab Number: 1881507M416

Sample Information:

Sample Location: 1S to SA data collection Station: Bed Sample Number: 15-815

Date & Time Sampled: 07/14/16

Date Received: 07/14/16

Sample Testing:

Composite: Y (N)

Dry Weight: 4540.7

Sieve:	Weight Retained:
2" (50 mm)	—
1" (25 mm)	—
3/4" (19 mm)	—
1/2" (12.5 mm)	—
3/8" (9.5 mm)	2.0
No. 4 (4.75 mm)	17.5
No. 8 (2.36 mm)	81.7
No. 10 (2 mm)	30.4
No. 16 (1.18 mm)	167.2
No. 30 (0.6 mm)	685.9
No. 40 (0.425 mm)	843.8
No. 50 (0.3 mm)	1724.3
No. 100 (0.15 mm)	932.5
No. 200 (0.075 mm)	51.3
No. 230 (0.063 mm)	2.6
Pan	3.0
Total Retained:	4542.2

if sample is composited Sample numbers and Station:	

Additional Remarks:

Pan drying 7/19/16

In oven 7/25

put in shaker 7/26/16

Lab Sample Report

Lab Number: CO 833071416

Sample Information:

Sample Location: IS to SA data collection Station: Bed Sample Number: CO-833

Date & Time Sampled: 07/14/16

Date Received: 07/14/16

Sample Testing:

Composite: Y (N)

Dry Weight: 4265.6

Sieve:	Weight Retained:
2" (50 mm)	
1" (25 mm)	
3/4" (19 mm)	
1/2" (12.5 mm)	3.9
3/8" (9.5 mm)	1.1
No. 4 (4.75 mm)	8.3
No. 8 (2.36 mm)	29.1
No. 10 (2 mm)	15.3
No. 16 (1.18 mm)	89.7
No. 30 (0.6 mm)	580.2
No. 40 (0.425 mm)	1344.6
No. 50 (0.3 mm)	1518.5
No. 100 (0.15 mm)	588.7
No. 200 (0.075 mm)	66.0
No. 230 (0.063 mm)	6.7
Pan	10.2
Total Retained:	4262.8

if sample is composited Sample numbers and Station:	

Additional Remarks:

Removed from oven 7/22/16

Placed in shaker @ 8:33AM

entered into x/s @ 9:40 AM 7/25/16

Lab Sample Report

Lab Number: 857071416

Sample Information:

Sample Location: 15-SA data collection Station: Bed Sample Number: 857

Date & Time Sampled: 07/14/16

Date Received: 07/14/16

Sample Testing:

Composite: Y (N)

Dry Weight: 4282.8

Sieve:	Weight Retained:
2" (50 mm)	
1" (25 mm)	
3/4" (19 mm)	
1/2" (12.5 mm)	2.1
3/8" (9.5 mm)	2.6
No. 4 (4.75 mm)	15.0
No. 8 (2.36 mm)	64.3
No. 10 (2 mm)	29.9
No. 16 (1.18 mm)	180.0
No. 30 (0.6 mm)	796.4
No. 40 (0.425 mm)	1050.3
No. 50 (0.3 mm)	1391.7
No. 100 (0.15 mm)	698.2
No. 200 (0.075 mm)	32.4
No. 230 (0.063 mm)	3.5
Pan	11.2
organics	0.2
Total Retained:	4277.6

if sample is composited Sample numbers and Station:	

Additional Remarks:

Removed from oven 7/22/16

Entered into XLS 8:30AM 7/25/16

Lab Sample Report Lab Number: 863071416

Sample Information:
Sample Location: IS to SA data collection Station: Bank Sample Number: 863
Date & Time Sampled: 7/26/16 Date Received: 7/26/16

Sample Testing:

Composite: Y (N)

Dry Weight: 6571.1

Sieve:	Weight Retained:	
2" (50 mm)	—	
1" (25 mm)	—	
3/4" (19 mm)	38.1	clay clods
1/2" (12.5 mm)	73.7	" "
3/8" (9.5 mm)	31.5	" "
No. 4 (4.75 mm)	154.0	clay clods + twig
No. 8 (2.36 mm)	107.7	clay clods + twigs
No. 10 (2 mm)	30.5	" "
No. 16 (1.18 mm)	90.5	" "
No. 30 (0.6 mm)	267.8	" "
No. 40 (0.425 mm)	1085.0	some small twigs
No. 50 (0.3 mm)	2268.4	" "
No. 100 (0.15 mm)	804.7	
No. 200 (0.075 mm)	1077.1	
No. 230 (0.063 mm)	243.5	
Pan	300.2	
Total Retained:	6572.7	

if sample is composited Sample numbers and Station:	

Additional Remarks:

placed in oven on 7/26/16 Bottom rock
processed 7/27/16

largest particle
mass - 9.3 g
a axis — 32mm
b axis — 29mm
c axis — 17mm

Lab Sample Report

Lab Number: (0877071416

Sample Information:

Sample Location: IS to SA data collection Station: Bed Sample Number: CO-877

Date & Time Sampled: 7/14/16

Date Received: 7/14/16

Sample Testing:

Composite: Y N

Dry Weight: 5337.1

Sieve:	Weight Retained:
2" (50 mm)	
1" (25 mm)	
3/4" (19 mm)	17.6
1/2" (12.5 mm)	90.2
3/8" (9.5 mm)	43.8
No. 4 (4.75 mm)	126.3
No. 8 (2.36 mm)	182.1
No. 10 (2 mm)	52.6
No. 16 (1.18 mm)	279.6
No. 30 (0.6 mm)	997.6
No. 40 (0.425 mm)	1166.7
No. 50 (0.3 mm)	1449.0
No. 100 (0.15 mm)	800.8
No. 200 (0.075 mm)	108.5
No. 230 (0.063 mm)	7.7
Pan	13.8
organics	0.5
Total Retained:	5336.3

if sample is composited Sample numbers and Station:	

Additional Remarks:

Placed in shaker @ 9:45 7/25/16

Entered in XLS @ 11:10 AM 7/25/16

Lab Sample Report Lab Number: 18908071416

Sample Information:

Sample Location: 18 to 8A data collection Station: Bed Sample Number: 15-908

Date & Time Sampled: 07/14/16 Date Received: 07/14/16

Sample Testing:

Composite: Y (N)

Dry Weight: 3938.9

Sieve:	Weight Retained:
2" (50 mm)	
1" (25 mm)	
3/4" (19 mm)	
1/2" (12.5 mm)	5.3
3/8" (9.5 mm)	6.1
No. 4 (4.75 mm)	22.3
No. 8 (2.36 mm)	45.2
No. 10 (2 mm)	18.4
No. 16 (1.18 mm)	93.8
No. 30 (0.6 mm)	448.5
No. 40 (0.425 mm)	1038.4
No. 50 (0.3 mm)	1542.5
No. 100 (0.15 mm)	663.6
No. 200 (0.075 mm)	46.1
No. 230 (0.063 mm)	4.1
Pan	13.1
Total Retained:	3947.4

if sample is composited Sample numbers and Station:	

Additional Remarks:

Entered in xls @ 1:55 PM 7/25/16

Lab Sample Report

Lab Number: CC927 071416

Sample Information:

Sample Location: IS to SA data collection Station: bed Sample Number: CC-927

Date & Time Sampled: 7/14/16

Date Received: 7/14/16

Sample Testing:

Composite: Y (N)

Dry Weight: 5230.2

Sieve:	Weight Retained:
2" (50 mm)	
1" (25 mm)	
3/4" (19 mm)	
1/2" (12.5 mm)	9.4
3/8" (9.5 mm)	0.7
No. 4 (4.75 mm)	3.0
No. 8 (2.36 mm)	11.9
No. 10 (2 mm)	7.2
No. 16 (1.18 mm)	56.0
No. 30 (0.6 mm)	595.1
No. 40 (0.425 mm)	1675.4
No. 50 (0.3 mm)	2019.6
No. 100 (0.15 mm)	803.4
No. 200 (0.075 mm)	35.9
No. 230 (0.063 mm)	0.1
Pan	7.3
Total Retained:	5227.0

if sample is composited Sample numbers and Station:	

Additional Remarks:

put in pan to begin air drying on 7/15/16

placed in shaker @ 2:20 PM 7/22/16

Entered into xls @ 4:40 PM 7/22/16

Lab Sample Report Lab Number: CC943071416

Sample Information:
Sample Location: 18-SA data collection Station: Bed Sample Number: CC-943
Date & Time Sampled: 07/14/16 Date Received: 07/14/16

Sample Testing:

Composite: Y (N)

Dry Weight: 5051.5

Sieve:	Weight Retained:	
2" (50 mm)	—	
1" (25 mm)	—	
3/4" (19 mm)	—	
1/2" (12.5 mm)	2.4	some wood pieces
3/8" (9.5 mm)	12.0	some wood pieces
No. 4 (4.75 mm)	21.2	some organics (branches)
No. 8 (2.36 mm)	90.7	"
No. 10 (2 mm)	43.1	"
No. 16 (1.18 mm)	253.7	
No. 30 (0.6 mm)	1026.8	
No. 40 (0.425 mm)	1200.8	
No. 50 (0.3 mm)	1450.0	
No. 100 (0.15 mm)	836.3	
No. 200 (0.075 mm)	90.1	
No. 230 (0.063 mm)	10.65	
Pan	14.8	
Total Retained:	5052.4	

if sample is composited Sample numbers and Station:	

Additional Remarks:

air drying 7/22/16
In oven 7/25
put in shaker 7/26/16

Lab Sample Report Lab Number: 974072816

Sample Information:
Sample Location: IS to SA data collection Station: bank Sample Number: 974
Date & Time Sampled: 7/28/16 Date Received: 7/28/16

Sample Testing:

Composite: Y (N)

Dry Weight: 4437.4

Sieve:	Weight Retained:
2" (50 mm)	
1" (25 mm)	
3/4" (19 mm)	
1/2" (12.5 mm)	1.3
3/8" (9.5 mm)	8.1
No. 4 (4.75 mm)	7.3
No. 8 (2.36 mm)	12.2
No. 10 (2 mm)	5.0
No. 16 (1.18 mm)	19.4
No. 30 (0.6 mm)	18.6
No. 40 (0.425 mm)	17.7
No. 50 (0.3 mm)	25.4
No. 100 (0.15 mm)	2479.2
No. 200 (0.075 mm)	1236.5
No. 230 (0.063 mm)	248.4
Pan	360.9
Total Retained:	4440.0

clay clod
" "
clay clod + gravel

if sample is composited
Sample numbers and Station:

Additional Remarks:

plowed out to air dry 7/29/16
Placed in shaker at 11:50 AM
Entered into xls @ 1:12 PM 8/12/16

Lab Sample Report Lab Number: 976072816

Sample Information:
Sample Location: IS to SA data collection Station: bed Sample Number: 976
Date & Time Sampled: 7/28/16 Date Received: 7/28/16

Sample Testing:

~~Composite:~~ Y (N)

Dry Weight: 4029.0

Sieve:	Weight Retained:
2" (50 mm)	
1" (25 mm)	48.6
3/4" (19 mm)	
1/2" (12.5 mm)	29.8
3/8" (9.5 mm)	32.9
No. 4 (4.75 mm)	124.3
No. 8 (2.36 mm)	167.4
No. 10 (2 mm)	50.6
No. 16 (1.18 mm)	205.8
No. 30 (0.6 mm)	618.5
No. 40 (0.425 mm)	942.1
No. 50 (0.3 mm)	978.9
No. 100 (0.15 mm)	685.1
No. 200 (0.075 mm)	75.0
No. 230 (0.063 mm)	14.8
Pan	52.0
Total Retained:	4025.8

if sample is composited Sample numbers and Station:	

Additional Remarks:

placed out to air dry 7/29/16
placed in Shaker @ 8:35 AM
entered in xls @ 9:45 AM 8/9/16

Lab Sample Report Lab Number: 1004072816

Sample Information:
Sample Location: IS to SA data collection Station: bed Sample Number: 1004
Date & Time Sampled: 7/28/16 Date Received: 7/28/16

Sample Testing: 6933.0 Composite: Y N

Dry Weight: ~~6929.1~~

Sieve:	Weight Retained:
2" (50 mm)	
1" (25 mm)	
3/4" (19 mm)	121.9
1/2" (12.5 mm)	87.9
3/8" (9.5 mm)	48.3
No. 4 (4.75 mm)	110.6
No. 8 (2.36 mm)	156.1
No. 10 (2 mm)	50.3
No. 16 (1.18 mm)	267.1
No. 30 (0.6 mm)	1064.8
No. 40 (0.425 mm)	1421.6
No. 50 (0.3 mm)	2184.9
No. 100 (0.15 mm)	1188.0
No. 200 (0.075 mm)	166.1
No. 230 (0.063 mm)	22.2
Pan	43.1
Total Retained:	6932.9

if sample is composited Sample numbers and Station:	

Additional Remarks:

placed out to air dry 7/29/16
placed in shaker at 2:50 PM
entered in LS at 4 PM 8/11/16

Lab Sample Report Lab Number: CO 1044 07 2816

Sample Information:
Sample Location: Is to SA data collection Station: bed Sample Number: CO-1044
Date & Time Sampled: 7/28/16 Date Received: 7/28/16

Sample Testing:

~~Composite:~~ Y (N)

Dry Weight: 6172.2

Sieve:	Weight Retained:
2" (50 mm)	
1" (25 mm)	
3/4" (19 mm)	9.2
1/2" (12.5 mm)	13.9
3/8" (9.5 mm)	20.1
No. 4 (4.75 mm)	42.0
No. 8 (2.36 mm)	31.0
No. 10 (2 mm)	12.3
No. 16 (1.18 mm)	105.9
No. 30 (0.6 mm)	1283.9
No. 40 (0.425 mm)	1792.2
No. 50 (0.3 mm)	1949.3
No. 100 (0.15 mm)	850.6
No. 200 (0.075 mm)	54.9
No. 230 (0.063 mm)	2.2
Pan	3.9
Total Retained:	6177.4

if sample is composited Sample numbers and Station:	

Additional Remarks:

placed out to air dry 7/29/16
placed in shaker at 12 PM
Entered in XLS 2:40 PM on 8/10/16

Lab Sample Report Lab Number: CO106107016

Sample Information:
Sample Location: IS-SA Station: Bank sample Sample Number: 1061 Bank
Date & Time Sampled: 7/7/16 Date Received: 7/7/16

Sample Testing:

Composite: Y (N)

Dry Weight: 2614.1

Sieve:	Weight Retained:	
2" (50 mm)	—	
1" (25 mm)	445.3	clay clods
3/4" (19 mm)	121.3	clay clods
1/2" (12.5 mm)	114.5	clay clods
3/8" (9.5 mm)	29.7	clay clods
No. 4 (4.75 mm)	168.4	clay clods
No. 8 (2.36 mm)	86.9	clay clods
No. 10 (2 mm)	19.9	clay balls
No. 16 (1.18 mm)	46.8	clay balls w/ organics (plant stems)
No. 30 (0.6 mm)	32.1	
No. 40 (0.425 mm)	30.8	
No. 50 (0.3 mm)	37.2	some organics
No. 100 (0.15 mm)	160.5	
No. 200 (0.075 mm)	657.5	
No. 230 (0.063 mm)	246.4	
Pan	418.9	
Total Retained:	2616.2	

if sample is composited Sample numbers and Station:	

Additional Remarks:

put in sieve on 7/13/16 @ 9:20 AM

processed 7/13/16 @ 10:15 AM

Largest particle mass - 57.0 g
axis a — 65 mm
axis b — 57 mm
axis c — 20 mm

Lab Sample Report

Lab Number: 1061070716

Sample Information:

Sample Location: 15-SA Station: bed samples Sample Number: 1061 Bed

Date & Time Sampled: 7/7/16

Date Received: 7/7/16

Sample Testing:

Dry Weight: 3243.5

Composite: Y (N)

Sieve:	Weight Retained:
2" (50 mm)	—
1" (25 mm)	—
3/4" (19 mm)	—
1/2" (12.5 mm)	—
3/8" (9.5 mm)	—
No. 4 (4.75 mm)	2.0
No. 8 (2.36 mm)	7.4
No. 10 (2 mm)	3.9
No. 16 (1.18 mm)	36.4
No. 30 (0.6 mm)	376.5
No. 40 (0.425 mm)	885.4
No. 50 (0.3 mm)	1236.8
No. 100 (0.15 mm)	672.5
No. 200 (0.075 mm)	16.4
No. 230 (0.063 mm)	0.3
Pan	0.5
Total Retained:	3238.1

some organics (wood)

if sample is composited Sample numbers and Station:	

Additional Remarks:

placed in oven 7/13/16 → middle shelf

↳ taken out of oven 7/14/16

put in shaker 7/15/16 @ 8:55 am

15-690 1061 Bed 1061 Bank cat 1164

Lab Sample Report Lab Number: 1086072816

Sample Information:
Sample Location: IStoSA data collection Station: bank Sample Number: 1086
Date & Time Sampled: 7/28/16 Date Received: 7/28/16

Sample Testing:

~~Composite:~~ Y N

Dry Weight: 4544.8

Sieve:	Weight Retained:
2" (50 mm)	
1" (25 mm)	350.5
3/4" (19 mm)	91.9
1/2" (12.5 mm)	62.7
3/8" (9.5 mm)	30.8
No. 4 (4.75 mm)	324.6
No. 8 (2.36 mm)	160.0
No. 10 (2 mm)	46.4
No. 16 (1.18 mm)	93.1
No. 30 (0.6 mm)	50.7
No. 40 (0.425 mm)	51.5
No. 50 (0.3 mm)	59.9
No. 100 (0.15 mm)	708.2
No. 200 (0.075 mm)	1738.0
No. 230 (0.063 mm)	288.9
Pan	1389.5 - pan 901.3
Total Retained:	4545.4

clayclods

if sample is composited Sample numbers and Station:	

Additional Remarks:

placed out to air dry 7/29/16
placed in shaker at 1:35 PM
entered in XLS @ 2:55 PM 8/12/16

Lab Sample Report Lab Number: 1088070716

Sample Information:					
ample Location:	near agg-dep 1088	Station:	last sample	Sample Number:	1088
ıte & Time sampled:	7/7/16	Date Received:	7/7/16		

Sample Testing:

Composite: Y (N)

Dry Weight: 3822.8

Sieve:	Weight Retained:	
2" (50 mm)	—	
1" (25 mm)	—	
3/4" (19 mm)	—	
1/2" (12.5 mm)	—	
3/8" (9.5 mm)	0.8	sand conglomerate
No. 4 (4.75 mm)	10.6	" "
No. 8 (2.36 mm)	19.5	" "
No. 10 (2 mm)	8.2	" "
No. 16 (1.18 mm)	15.0	
No. 30 (0.6 mm)	11.5	→ some organics (twigs)
No. 40 (0.425 mm)	11.2	→
No. 50 (0.3 mm)	26.9	
No. 100 (0.15 mm)	2833.4	
No. 200 (0.075 mm)	599.8	
No. 230 (0.063 mm)	102.7	
Pan	183.3	
Total Retained:	3822.9	

if sample is composited Sample numbers and Station:	

Additional Remarks:

placed in oven 7/14/16 ⇒ bottom shelf

put in shaker 7/15/16 @ 10:15 AM

processed @ 11:00 AM

Lab Sample Report Lab Number: 1091072816

Sample Information:
Sample Location: Is to SA data collection Station: bed Sample Number: 1091
Date & Time Sampled: 7/28/16 Date Received: 7/28/16

Sample Testing:

Composite: Y (N)

Dry Weight: 5064.1

Sieve:	Weight Retained:
2" (50 mm)	
1" (25 mm)	
3/4" (19 mm)	
1/2" (12.5 mm)	
3/8" (9.5 mm)	
No. 4 (4.75 mm)	3.1
No. 8 (2.36 mm)	10.0
No. 10 (2 mm)	5.2
No. 16 (1.18 mm)	50.4
No. 30 (0.6 mm)	632.1
No. 40 (0.425 mm)	1498.8
No. 50 (0.3 mm)	1843.9
No. 100 (0.15 mm)	924.4
No. 200 (0.075 mm)	63.3
No. 230 (0.063 mm)	8.1
Pan	18.1
Total Retained:	5057.4

if sample is composited Sample numbers and Station:	

Additional Remarks:

placed out to air dry 7/29/16
Placed in shaker at 7:28AM
entered into xls 8/9/16 at 8:20AM

Lab Sample Report Lab Number: 1094 072816

Sample Information:
Sample Location: IS to SH data collection Station: bank Sample Number: 1094
Date & Time Sampled: 7/28/16 Date Received: 7/28/16

Sample Testing:

~~Composite:~~ ~~Y~~ ~~N~~

Dry Weight: 2402.7

Sieve:	Weight Retained:
2" (50 mm)	
1" (25 mm)	681.4
3/4" (19 mm)	58.8
1/2" (12.5 mm)	145.4
3/8" (9.5 mm)	48.7
No. 4 (4.75 mm)	274.2
No. 8 (2.36 mm)	133.4
No. 10 (2 mm)	33.2
No. 16 (1.18 mm)	67.3
No. 30 (0.6 mm)	51.0
No. 40 (0.425 mm)	40.0
No. 50 (0.3 mm)	35.8
No. 100 (0.15 mm)	230.4
No. 200 (0.075 mm)	285.4
No. 230 (0.063 mm)	93.7
Pan	617.1 - container 388.7
organics	3.2
Total Retained:	2407.1 (organics not counted)

clay clods

if sample is composited Sample numbers and Station:	

Additional Remarks:

placed out to air dry 7/29/16
placed in shaker @ 9:55
Entered in x15 @ 11:20AM 8/12/16

Lab Sample Report Lab Number: CO1097070716

Sample Information:					
ıple Location:	various locations on bed along ravgeline	Station: CO-1097		Sample Number:	1097
ıte & Time Sampled:	7/7/16	Date Received:	7/7/16		

Sample Testing:

Composite: Y (N)

Dry Weight: 4520.2

Sieve:	Weight Retained:
2" (50 mm)	—
1" (25 mm)	—
3/4" (19 mm)	—
1/2" (12.5 mm)	—
3/8" (9.5 mm)	2.2
No. 4 (4.75 mm)	9.7
No. 8 (2.36 mm)	31.3
No. 10 (2 mm)	14.0
No. 16 (1.18 mm)	84.7
No. 30 (0.6 mm)	559.7
No. 40 (0.425 mm)	1344.3
No. 50 (0.3 mm)	1599.2
No. 100 (0.15 mm)	829.6
No. 200 (0.075 mm)	39.4
No. 230 (0.063 mm)	1.4
Pan	1.4
Total Retained:	4516.9

if sample is composited Sample numbers and Station:	

Additional Remarks:

put in sieve on 7/12/16 @ 12:27pm
proceed @ 1:00pm JA

Lab Sample Report

Lab Number: RP1100070716

Sample Information:
Sample Location: Sampled at locations of bed
Station: RP-1100
Sample Number: RP-1100
Date & Time Sampled: 7/7/16
Date Received: 7/7/16

Sample Testing:

Composite: Y (N)

Dry Weight: 2931.8

Sieve:	Weight Retained:
2" (50 mm)	—
1" (25 mm)	—
3/4" (19 mm)	—
1/2" (12.5 mm)	—
3/8" (9.5 mm)	5.5
No. 4 (4.75 mm)	5.7
No. 8 (2.36 mm)	11.1
No. 10 (2 mm)	4.5
No. 16 (1.18 mm)	24.1
No. 30 (0.6 mm)	156.4
No. 40 (0.425 mm)	472.5
No. 50 (0.3 mm)	1259.4
No. 100 (0.15 mm)	942.4
No. 200 (0.075 mm)	48.0
No. 230 (0.063 mm)	1.9
Pan	1.9
Total Retained:	2933.4

if sample is composited Sample numbers and Station:	

Additional Remarks:

put in sieve on 7/12/16 @ 11:35 Am
processed at 12:00 by OA

Lab Sample Report

Lab Number:

Sample Information:
Sample Location: Isleta - San Acacia
Station:
Sample Number: 1104
Date & Time Sampled: 7-1-2016
Date Received: 7-5-2016

Sample Testing:

Composite: Y N

Dry Weight: 5464.1

Sieve:	Weight Retained:
2" (50 mm)	
1" (25 mm)	
3/4" (19 mm)	
1/2" (12.5 mm)	1.1
3/8" (9.5 mm)	1.0
No. 4 (4.75 mm)	12.3
No. 8 (2.36 mm)	28.8
No. 10 (2 mm)	13.8
No. 16 (1.18 mm)	110.3
No. 30 (0.6 mm)	1156.1
No. 40 (0.425 mm)	1965.9
No. 50 (0.3 mm)	1511.1
No. 100 (0.15 mm)	596.3
No. 200 (0.075 mm)	37.1
No. 230 (0.063 mm)	6.7
Pan	20.4
organics	0.6
Total Retained:	

~~if sample is composited~~
~~Sample numbers and Station:~~

sieve weight	total weight

Additional Remarks:

Placed in oven 7/6/2016, 10:12 AM
middle shelf
weight at 11:05am 7/7/2016
6398.5 g

Entered into xls 7/8/16 @ 7:30AM

Lab Sample Report Lab Number: LJ10070116

Sample Information:
Sample Location: Isleta San Acacia Station: Bank sample Sample Number: LJ-10
Date & Time Sampled: 7-1-2016 Date Received: 7-5-2016

Sample Testing:

Composite: Y N

Dry Weight: 2185.9

Sieve:	Weight Retained:	
2" (50 mm)	—	clay clods and organics (wood)
1" (25 mm)	41.1	
3/4" (19 mm)	83.2	
1/2" (12.5 mm)	91.2	
3/8" (9.5 mm)	21.6	
No. 4 (4.75 mm)	39.2	clay clumps
No. 8 (2.36 mm)	16.0	clay clumps + organics (wood)
No. 10 (2 mm)	2.5	primarily small clay balls
No. 16 (1.18 mm)	115.6	small clay balls
No. 30 (0.6 mm)	75.3	
No. 40 (0.425 mm)	43.9	
No. 50 (0.3 mm)	42.0	
No. 100 (0.15 mm)	251.7	
No. 200 (0.075 mm)	732.7	
No. 230 (0.063 mm)	263.8	
Pan	366.2	
Total Retained:	2186.0	

if sample is composited
Sample numbers and Station:

Additional Remarks:

Put in oven 7/6/2016, 9:56AM
Top Shelf

Weight at 11:05 am 7/7/2016
3096.2 g

proceed in sieve on 7/12/16
↳ hand broke clay clods - proceed rest since river may transport them as such

largest particle (24.8 g)
a axis - 35mm
b axis - 32mm
c axis - 22mm

Lab Sample Report

Lab Number:

Sample Information:
Sample Location: Isleta - San Acacia Station: Sample Number: LJ-18
Date & Time Sampled: 7-1-2016 Date Received: 7-5-2016

Sample Testing:

Composite: Y N

Dry Weight: 3902.2

Sieve:	Weight Retained:
2" (50 mm)	
1" (25 mm)	
3/4" (19 mm)	
1/2" (12.5 mm)	
3/8" (9.5 mm)	3.4
No. 4 (4.75 mm)	~~27.6 - 8.9~~ ~~21.1~~ 17.7
No. 8 (2.36 mm)	~~48.9~~ 25.3
No. 10 (2 mm)	8.9
No. 16 (1.18 mm)	61.9
No. 30 (0.6 mm)	397.8
No. 40 (0.425 mm)	862.3
No. 50 (0.3 mm)	1644.7
No. 100 (0.15 mm)	851.6
No. 200 (0.075 mm)	21.1
No. 230 (0.063 mm)	2.9
Pan	3.1
organics	1.4
Total Retained:	3902.1

if sample is composited Sample numbers and Station:	

Additional Remarks:

Placed in oven 7/6/2016 10:13 AM
bottom shelf

weight at 11:05 am, 7/7/2016
4751.8

Entered into xls 7/7/16 @ 4:30 PM.

Lab Sample Report Lab Number: CO1164070716

Sample Information:
Sample Location: IS-SA Station: sampled at 3 locations on bed Sample Number: CO-1164
Date & Time Sampled: 7/7/16 Date Received: 7/7/16

Sample Testing:

Composite: Y (N)

Dry Weight: 3061.0

Sieve:	Weight Retained:
2" (50 mm)	—
1" (25 mm)	—
3/4" (19 mm)	—
1/2" (12.5 mm)	—
3/8" (9.5 mm)	—
No. 4 (4.75 mm)	2.5
No. 8 (2.36 mm)	7.1
No. 10 (2 mm)	3.6
No. 16 (1.18 mm)	23.4
No. 30 (0.6 mm)	333.3
No. 40 (0.425 mm)	1022.6
No. 50 (0.3 mm)	1170.8
No. 100 (0.15 mm)	458.3
No. 200 (0.075 mm)	31.9
No. 230 (0.063 mm)	3.8
Pan	4.7
Total Retained:	3062

if sample is composited Sample numbers and Station:	

Additional Remarks:

put in shaker 10:09 AM 7/12/16
processed 7/12/16 @ 11:00 AM by DA

Lab Sample Report Lab Number: RP1170 070716

Sample Information:
Sample Location: IS to SA bed/bank collection Station: bed bank Sample Number: RP-1170
Date & Time Sampled: 7/7/16 Date Received: 7/7/16

Sample Testing:

Composite: Y (N)

Dry Weight: 2904.3

Sieve:	Weight Retained:	
2" (50 mm)		
1" (25 mm)	1357.4	clayclods
3/4" (19 mm)	318.0	clayclods
1/2" (12.5 mm)	286.0	" "
3/8" (9.5 mm)	75.8	" "
No. 4 (4.75 mm)	136.3	" "
No. 8 (2.36 mm)	166.9	" "
No. 10 (2 mm)	32.1	" "
No. 16 (1.18 mm)	74.9	" " + organics
No. 30 (0.6 mm)	54.6	" " "
No. 40 (0.425 mm)	30.3	" "
No. 50 (0.3 mm)	29.0	" "
No. 100 (0.15 mm)	143.6	
No. 200 (0.075 mm)	73.8	
No. 230 (0.063 mm)	24.9	
Pan	108.2	
organics	0.5	
Total Retained:	2911.8	

if sample is composited Sample numbers and Station:	

Additional Remarks:

set out to air dry 7/13/16

placed in shaker @ 11:35AM 7/22/16

entered into x|s 7/22/16 @ 1:45AM

Lab Sample Report Lab Number: 118307 1916a

Sample Information:
Sample Location: IS to SA data collection Station: bad sample a Sample Number: 1183
Date & Time Sampled: 7/19/16 Date Received: 7/19/16

Sample Testing:

Composite: Y (N)

Dry Weight: 9710.9

Sieve:	Weight Retained:	
2" (50 mm)	8124.3	10 rocks
1" (25 mm)	1432.5	
3/4" (19 mm)	109.1	
1/2" (12.5 mm)	30.3	
3/8" (9.5 mm)	12.9	
No. 4 (4.75 mm)	6.6	1 wood piece
No. 8 (2.36 mm)	3.1	some stems
No. 10 (2 mm)	0.6	" "
No. 16 (1.18 mm)	1.3	" "
No. 30 (0.6 mm)	0.9	some woody matl
No. 40 (0.425 mm)	0.9	" "
No. 50 (0.3 mm)	1.4	
No. 100 (0.15 mm)	1.8	
No. 200 (0.075 mm)	1.3	
No. 230 (0.063 mm)	0.4	
Pan	0.8	
Total Retained:	9728.2	

if sample is composited Sample numbers and Station:	

Additional Remarks:

placed in oven 7/26/16 (top rack)
processed 7/27/16

sample is representative of armor layer on bed

rocks in largest bin

#	mass (g)	axis a (mm)	axis b (mm)	axis c (mm)
1	4718.7	195 mm	175	139
2	467.3	108	64	57
3	515.5	95	83	75
4	576.0	132	64	47
5	461.9	99	68	56
6	346.7	94	74	35
7	282.1	94	58	39

#	mass (g)	axis a (mm)	axis b (mm)	axis c (mm)
8	317.3	94	75	46
9	241.8	87	79	22
10	196.3	82	63	38

Lab Sample Report Lab Number: 11830719Lb

Sample Information:
Sample Location: IS to SA data collection Station: bed sample b Sample Number: 1183
Date & Time Sampled: 7/19/16 Date Received: 7/19/16

Sample Testing:

Composite: Y (N)

Dry Weight: 6691.1

Sieve:	Weight Retained:	
2" (50 mm)	3789.8	
1" (25 mm)	798.6	
3/4" (19 mm)	62.7	
1/2" (12.5 mm)	—	
3/8" (9.5 mm)	7.2	
No. 4 (4.75 mm)	11.7	
No. 8 (2.36 mm)	31.5	some woody matl
No. 10 (2 mm)	16.7	" "
No. 16 (1.18 mm)	56.9	" "
No. 30 (0.6 mm)	117.3	some small twigs
No. 40 (0.425 mm)	178.8	
No. 50 (0.3 mm)	470.8	
No. 100 (0.15 mm)	995.3	
No. 200 (0.075 mm)	128.4	
No. 230 (0.063 mm)	7.6	
Pan	21.2	
Total Retained:	6694.5	

if sample is composited Sample numbers and Station:	

Additional Remarks:

Air drying - set out 7/25/16

Placed in oven 7/27/16

sample is representative of subsurface + bars (out of water at time of collection)

large rocks on #2" sieve

#	mass (g)	axis a (mm)	axis b (mm)	axis c (mm)
1	1574.9	168	132	104
2	783.9	139	116	61
3	701.4	124	109	62
4	210.8	79	67	34
5	259.1	88	78	43
6	~~259~~ 260.1	84	64	46

Lab Sample Report Lab Number: RPW190071916

Sample Information:
Sample Location: IS to SA data collection Station: Bed Sample Number: RP-1190
Date & Time Sampled: 7/19/16 Date Received: 7/19/16

Sample Testing:

Composite: Y (N)

Dry Weight: 7682.2

Sieve:	Weight Retained:	
2" (50 mm)	2190.9	
1" (25 mm)	998.3	
3/4" (19 mm)	218.8	
1/2" (12.5 mm)	469.1	
3/8" (9.5 mm)	153.7	
No. 4 (4.75 mm)	447.5	some wood pieces
No. 8 (2.36 mm)	330.6	" "
No. 10 (2 mm)	59.0	" "
No. 16 (1.18 mm)	157.5	some twigs
No. 30 (0.6 mm)	284.3	" "
No. 40 (0.425 mm)	424.5	" "
No. 50 (0.3 mm)	790.9	
No. 100 (0.15 mm)	943.6	
No. 200 (0.075 mm)	150.9	
No. 230 (0.063 mm)	13.8	
Pan	53.0	
Total Retained:	7686.4	

if sample is composited Sample numbers and Station:	

Additional Remarks:

dried in oven 7/25/16
put in shaker 7/26/16

largest particle
mass - 1406.3 g
a axis - 172 mm
b axis - 122 mm
c axis - 82 mm

Lab Sample Report Lab Number: CO11940719 LL

Sample Information:
Sample Location: IS to SA data collection Station: Bed Sample Number: CO-11941
Date & Time Sampled: 7/19/16 Date Received: 7/19/16

Sample Testing:

Composite: Y (N)

Dry Weight: 9368.7

Sieve:	Weight Retained:
2" (50 mm)	3281.5
1" (25 mm)	805.5
3/4" (19 mm)	233.0
1/2" (12.5 mm)	168.1
3/8" (9.5 mm)	76.6
No. 4 (4.75 mm)	300.7
No. 8 (2.36 mm)	193.9
No. 10 (2 mm)	77.7
No. 16 (1.18 mm)	197.4
No. 30 (0.6 mm)	385.3
No. 40 (0.425 mm)	847.7
No. 50 (0.3 mm)	1269.9
No. 100 (0.15 mm)	881.8
No. 200 (0.075 mm)	419.5
No. 230 (0.063 mm)	67.0
Pan	163.4
Total Retained:	9369.0

some woody matl & dirt clods
" "
" "
" "

if sample is composited
Sample numbers and Station:

Additional Remarks:

set out to air dry 7/22/16

placed in oven 7/27/16

rocks that didn't pass 2" sieve

#	mass (g)	axis a (mm)	axis b (mm)	axis c (mm)
1	1438.4	146	126	81
2	983.0	104	104	84
3	529.2	91	89	62
4	331.1	71	68	48

Lab Sample Report Lab Number: RP1202_5071916

Sample Information:
Sample Location: IS to SA data collection Station: Bank Sample Number: RP-1202.5
Date & Time Sampled: 7/19/16 Date Received: 7/19/16

Sample Testing:

Composite: Y (N)

Dry Weight: 2663.6

Sieve:	Weight Retained:	
2" (50 mm)	—	
1" (25 mm)	—	
3/4" (19 mm)	—	
1/2" (12.5 mm)	6.4	clay clods
3/8" (9.5 mm)	2.8	clay clods
No. 4 (4.75 mm)	44.4	clay clods w/ organics (woody mat'l)
No. 8 (2.36 mm)	60.2	" "
No. 10 (2 mm)	28.0	" "
No. 16 (1.18 mm)	85.1	" "
No. 30 (0.6 mm)	119.4	some organics (woody mat'l)
No. 40 (0.425 mm)	123.6	
No. 50 (0.3 mm)	310.0	
No. 100 (0.15 mm)	1180.7	
No. 200 (0.075 mm)	390.4	
No. 230 (0.063 mm)	111.9	
Pan	208.4	
Total Retained:	2671.3	

if sample is composited
Sample numbers and Station:

Additional Remarks:

placed in oven 7/26/16 (middle rack)

processed in shaker 7/27/16

largest particle (clay clod)
mass - 3.9g
axis a — 30mm
axis b — 22mm
axis c — 13mm

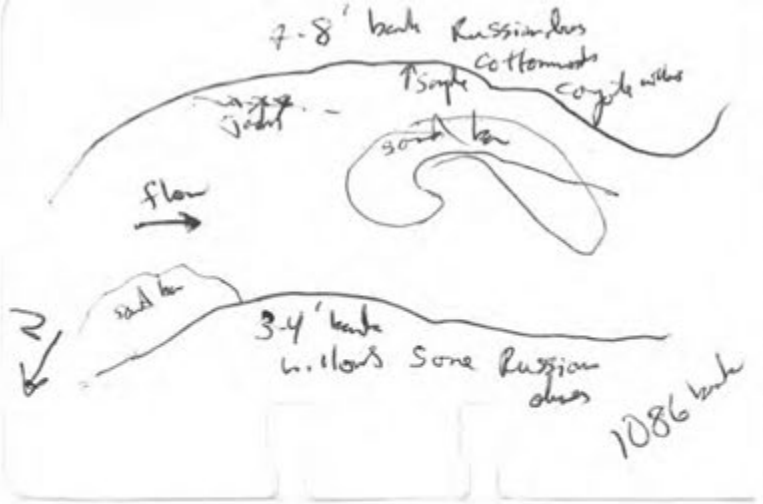
7-8' bank
Russian dies
Cottonwoods
Coyote willows
Jetty
sand bar
flow
sand bar
3-4' bank
willows some Russian olives
1086 bank

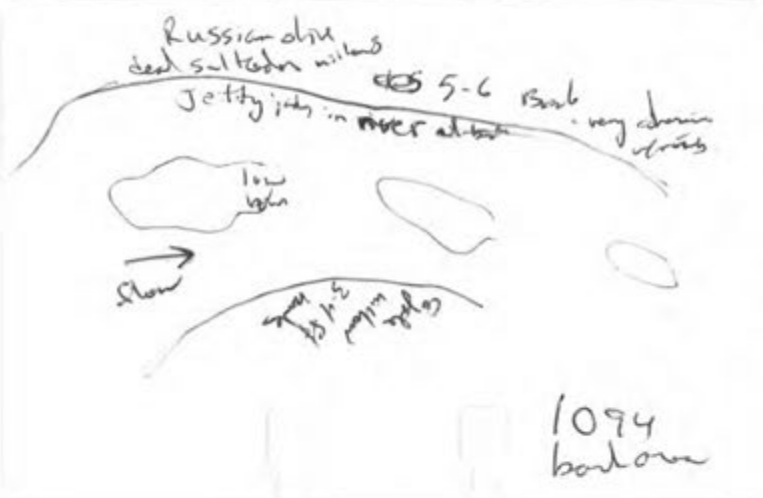
Russian olive
dead salt cedar willows
Jetty jetty in river at bank
5-6 Bank
very dense trees
low bank
flow
1094
bank low

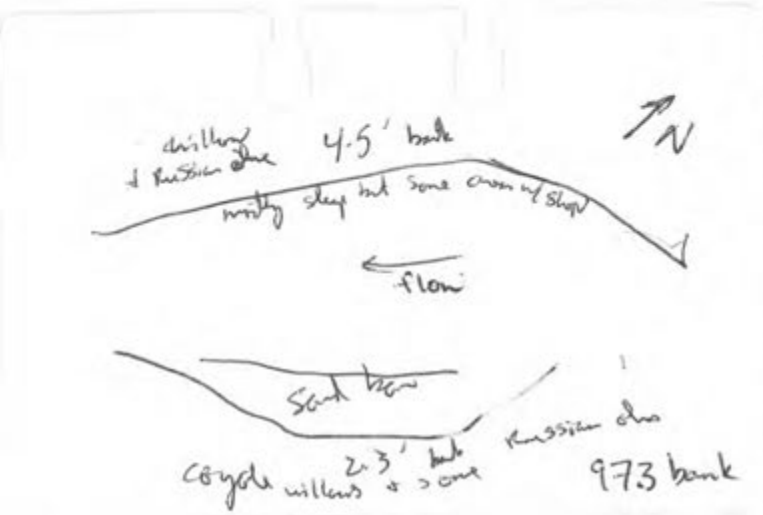
drift log
& Russian olive
4-5' bank
N
mostly steep but some areas of slope
flow
sand bar
Russian olive
Coyote willows
2-3' bank
& some
973 bank

Lab Number IS668070616 Sample # IS-668 Station:

Sieve Size and Percent passing for Soil Samples

Sample Size = 3813 grams

Sieve		Mass of soil		* based on Minitial					
No. (US std)	size (mm)	with pan (g)	w/o pan (g)	% retained	sum(% retained)	% passing			
2"	50.80			0.00%	0.00%	100.00%	D_{100}		
1"	25.00			0.00%	0.00%	100.00%	D_{84}	0.64	1 std deviation greater than median
3/4"	19.00			0.00%	0.00%	100.00%	D_{75}	0.56	
1/2"	12.70			0.00%	0.00%	100.00%	D_{60}	0.48	Median size
3/8"	9.50			0.00%	0.00%	100.00%	D_{50}	0.43	
#4	4.75		12.9	0.34%	0.34%	99.66%	D_{30}	0.36	1 std deviation less than median
#8	2.36		23.9	0.63%	0.96%	99.04%	D_{16}	0.31	Effective Size
#10	2.00		10.2	0.27%	1.23%	98.77%	D_{10}	0.26	Uniformity coefficient
#16	1.18		68.9	1.80%	3.04%	96.96%	C_u	1.83	Coefficient of gradation
#30	0.60		544.7	14.27%	17.30%	82.70%	C_c	1.02	
#40	0.425		1327.8	34.77%	52.07%	47.93%	poorly graded		Particle size distribution curve
#50	0.30		1360.1	35.62%	87.69%	12.31%			
#100	0.150		444.4	11.64%	99.33%	0.67%			
#200	0.075		24.4	0.64%	99.97%	0.03%			
#230	0.063		0.6	0.02%	99.99%	0.01%			
pan	--		0.5	0.01%	100.00%	0.00%			
	Totals	0	3818.4	--	--	--			

Total weight % Difference = 0.1 %

Notes

Sample location

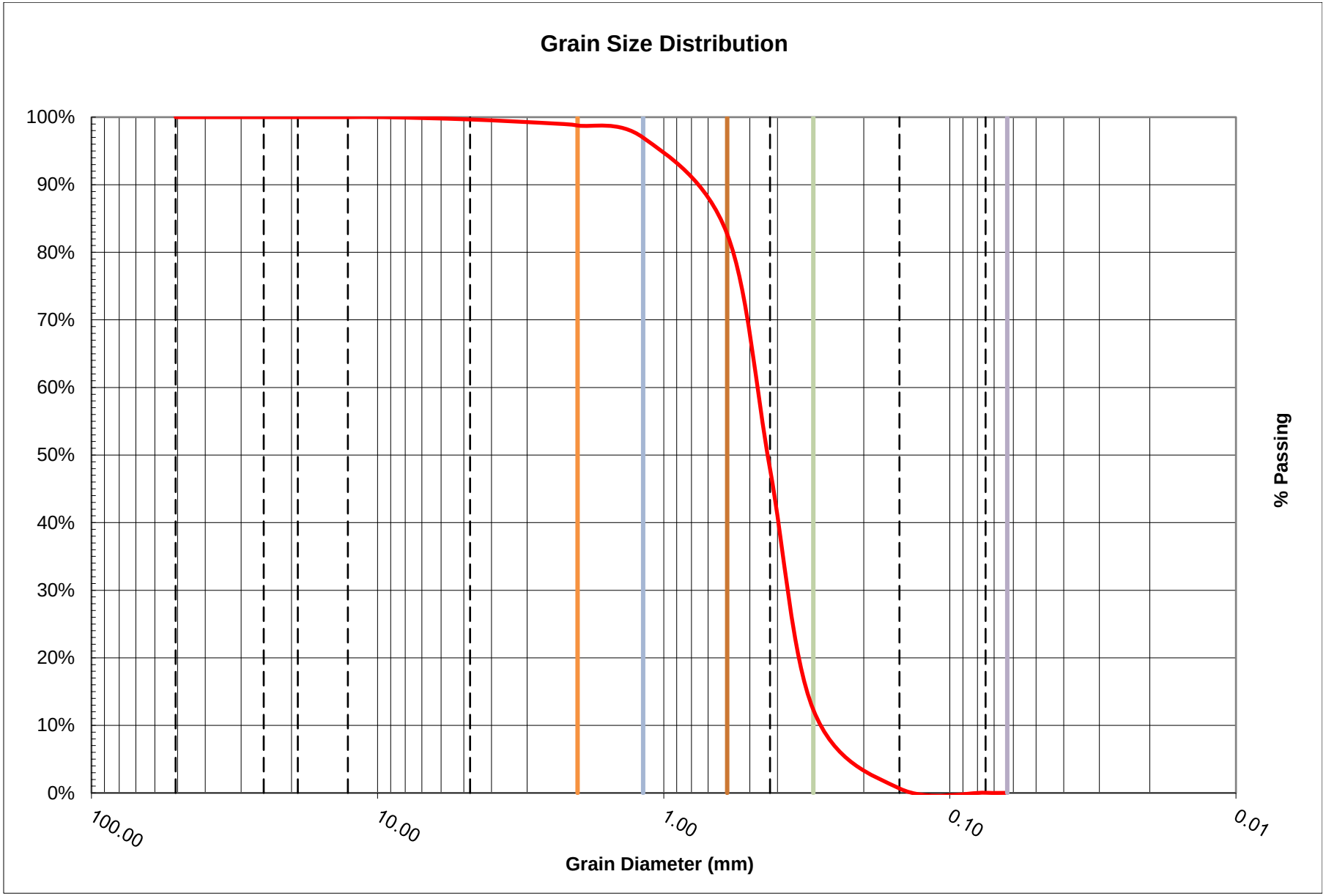
Grain Size Distribution
100%
90%
80%
70%
60%
50%
40%
30%
20%
10%
0%
% Passing
100.00
10.00
1.00
0.10
0.01
Grain Diameter (mm)

Lab Number IS690070616 Sample # IS-690 Station:

Sieve Size and Percent passing for Soil Samples

Sample Size = 4045.7 grams

Sieve		Mass of soil		* based on Minitial					
No. (US std)	size (mm)	with pan (g)	w/o pan (g)	% retained	sum(% retained)	% passing			
2"	50.80			0.00%	0.00%	100.00%	D_{100}		
1"	25.00			0.00%	0.00%	100.00%	D_{84}	1.10	1 std deviation greater than median
3/4"	19.00			0.00%	0.00%	100.00%	D_{75}	0.87	
1/2"	12.70			0.00%	0.00%	100.00%	D_{60}	0.59	Median size
3/8"	9.50		2.7	0.07%	0.07%	99.93%	D_{50}	0.50	
#4	4.75		24.8	0.61%	0.68%	99.32%	D_{30}	0.36	1 std deviation less than median
#8	2.36		122.4	3.03%	3.71%	96.29%	D_{16}	0.23	Effective Size
#10	2.00		57.0	1.41%	5.12%	94.88%	D_{10}	0.17	Uniformity coefficient
#16	1.18		327.7	8.11%	13.22%	86.78%	C_u	3.48	Coefficient of gradation
#30	0.60		1045.1	25.85%	39.08%	60.92%	C_c	1.25	
#40	0.425		852.6	21.09%	60.17%	39.83%	poorly graded		Particle size distribution curve
#50	0.30		770.5	19.06%	79.23%	20.77%			
#100	0.150		531.7	13.15%	92.38%	7.62%			
#200	0.075		208.9	5.17%	97.55%	2.45%			
#230	0.063		35.6	0.88%	98.43%	1.57%			
pan	--		63.5	1.57%	100.00%	0.00%			
	Totals	0	4042.5	--	--	--			

Total weight % Difference = 0.1 %

Notes

Sample location

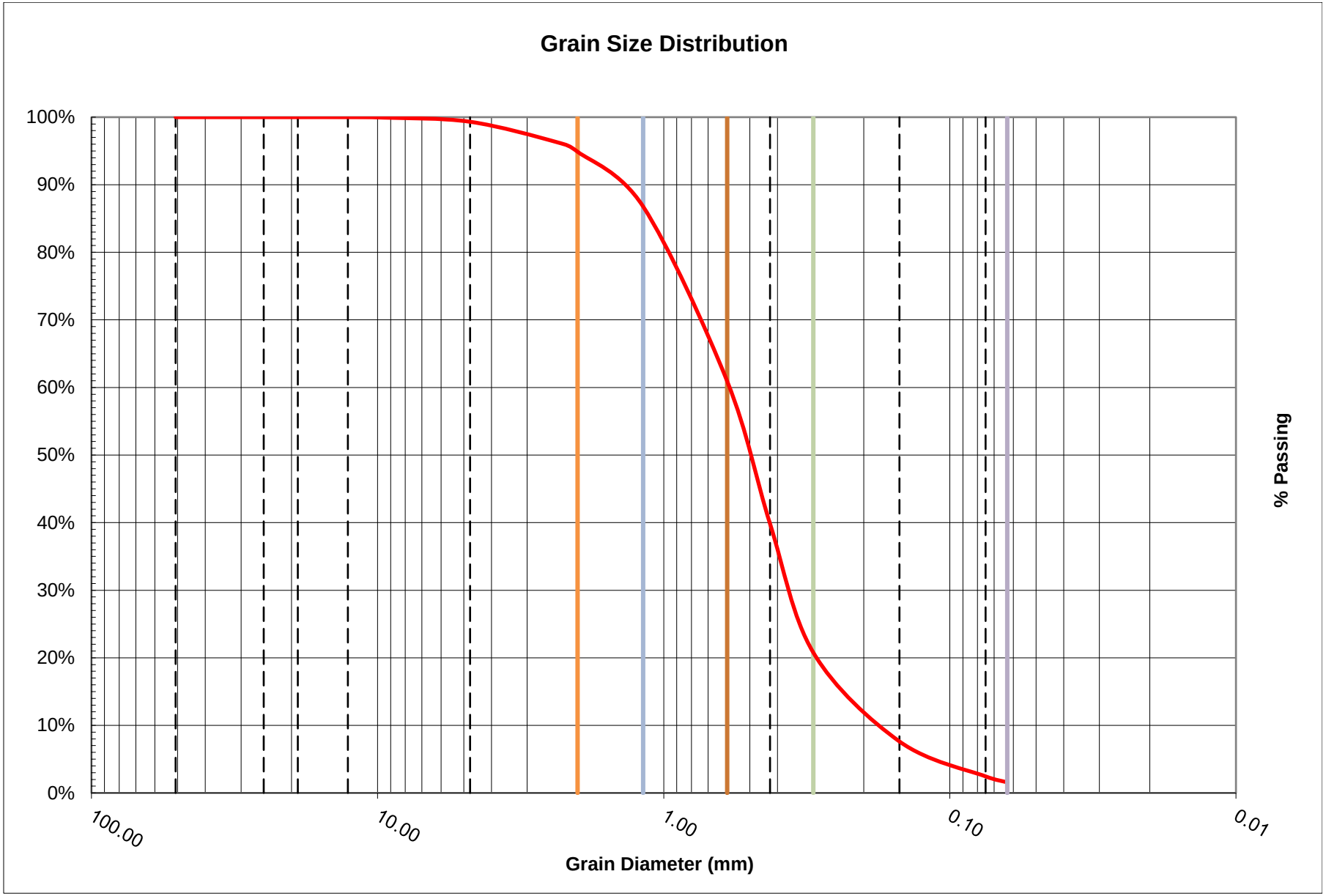
Grain Size Distribution
100%
90%
80%
70%
60%
50%
40%
30%
20%
10%
0%
% Passing
100.00
10.00
1.00
0.10
0.01
Grain Diameter (mm)

Lab Number IS731070616 Sample # bank Station:

Sieve Size and Percent passing for Soil Samples

Sample Size = 3775.8 grams **0.2 grams were sticks or stems, removed.**

Sieve		Mass of soil		* based on Minitial					
No. (US std)	size (mm)	with pan (g)	w/o pan (g)	% retained	sum(% retained)	% passing			
2"	50.80			0.00%	0.00%	100.00%	D_{100}		
1"	25.00			0.00%	0.00%	100.00%	D_{84}	0.61	1 std deviation greater than median
3/4"	19.00		16	0.42%	0.42%	99.58%	D_{60}	0.35	
1/2"	12.70		35.4	0.94%	1.36%	98.64%	D_{50}	0.29	Median size
3/8"	9.50		7.1	0.19%	1.55%	98.45%	D_{30}	0.14	
#4	4.75		72.2	1.91%	3.46%	96.54%	D_{16}	0.09	1 std deviation less than median
#8	2.36		69.1	1.83%	5.29%	94.71%	D_{10}	0.07	Effective Size
#10	2.00		26.8	0.71%	6.00%	94.00%	C_u	4.91	Uniformity coefficient
#16	1.18		97.9	2.59%	8.59%	91.41%	C_c	0.79	Coefficient of gradation
#30	0.60		286.7	7.59%	16.18%	83.82%			
#40	0.425		494.6	13.10%	29.28%	70.72%	gap graded		Particle size distribution curve
#50	0.30		748.5	19.82%	49.10%	50.90%			
#100	0.150		722.1	19.12%	68.22%	31.78%			
#200	0.075		779.4	20.64%	88.86%	11.14%			
#230	0.063		167.6	4.44%	93.30%	6.70%			
pan	--		253.0	6.70%	100.00%	0.00%			
	Totals	0	3776.4	--	--	--			

Total weight % Difference = 0.0 %

Notes

Sample location

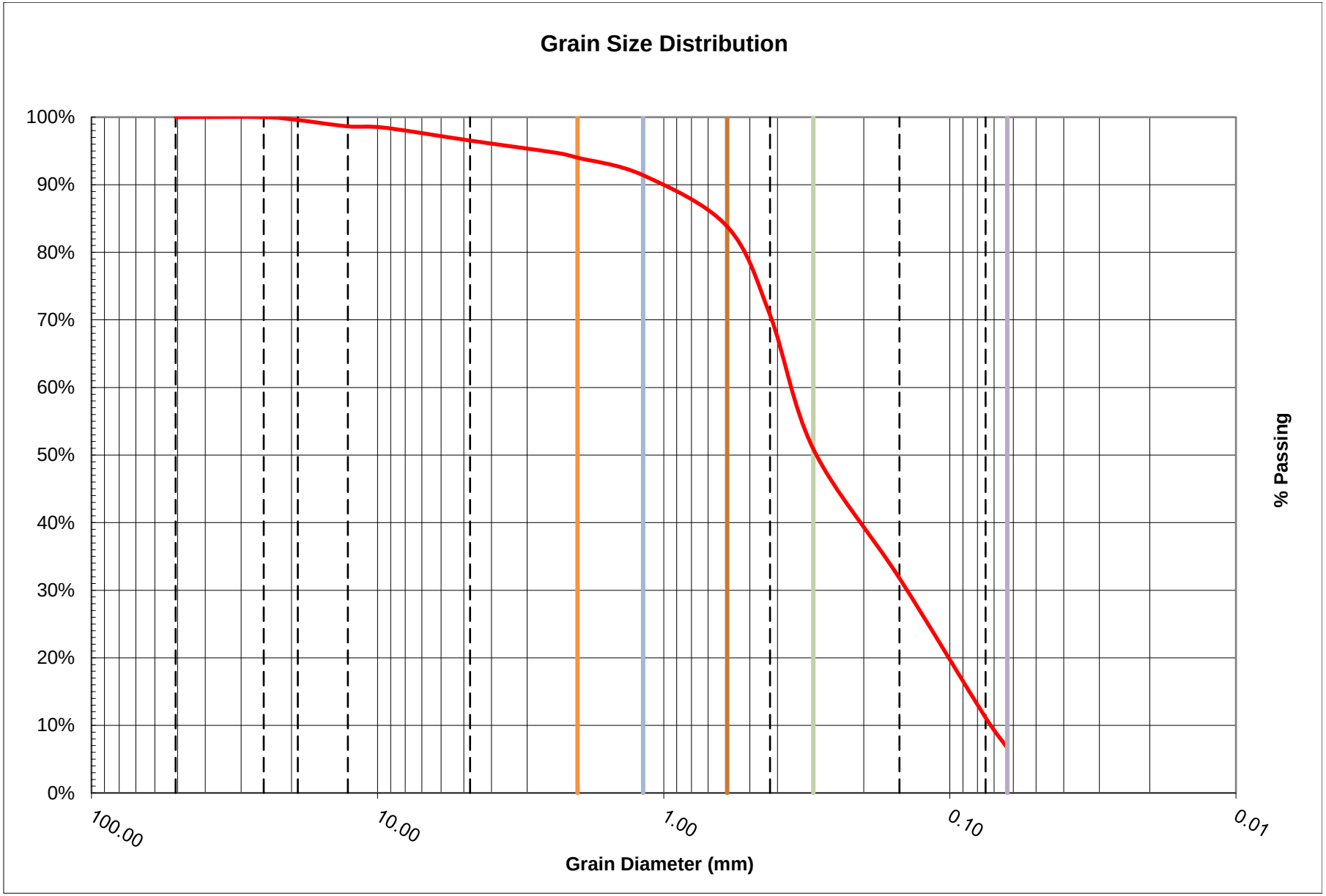
Grain Size Distribution
100%
90%
80%
70%
60%
50%
40%
30%
20%
10%
0%
% Passing
100.00
10.00
1.00
0.10
0.01
Grain Diameter (mm)

Lab Number 732070616 Sample # 1 Station:

Sieve Size and Percent passing for Soil Samples

Sample Size = 3803.8 grams

Sieve		Mass of soil		* based on Minitial					
No. (US std)	size (mm)	with pan (g)	w/o pan (g)	% retained	sum(% retained)	% passing			
2"	50.80			0.00%	0.00%	100.00%	D_{100}		
1"	25.00			0.00%	0.00%	100.00%	D_{84}	1.68	1 std deviation greater than median
3/4"	19.00		28.8	0.76%	0.76%	99.24%	D_{75}	1.09	
1/2"	12.70		83.5	2.20%	2.95%	97.05%	D_{60}	0.76	Median size
3/8"	9.50		41.8	1.10%	4.05%	95.95%	D_{50}	0.60	
#4	4.75		142.7	3.75%	7.81%	92.19%	D_{30}	0.42	1 std deviation less than median
#8	2.36		148	3.89%	11.70%	88.30%	D_{16}	0.33	Effective Size
#10	2.00		54.3	1.43%	13.13%	86.87%	D_{10}	0.27	Uniformity coefficient
#16	1.18		328.2	8.63%	21.76%	78.24%	C_u	2.79	Coefficient of gradation
#30	0.60		1059.6	27.87%	49.64%	50.36%	C_c	0.87	
#40	0.425		770.1	20.26%	69.89%	30.11%	gap graded		Particle size distribution curve
#50	0.30		708.6	18.64%	88.53%	11.47%			
#100	0.150		390.5	10.27%	98.81%	1.19%			
#200	0.075		39.9	1.05%	99.86%	0.14%			
#230	0.063		2.5	0.07%	99.92%	0.08%			
pan	--		3.0	0.08%	100.00%	0.00%			
	Totals	0	3801.5	--	--	--			

Total weight % Difference = 0.1 %

Notes

Sample location

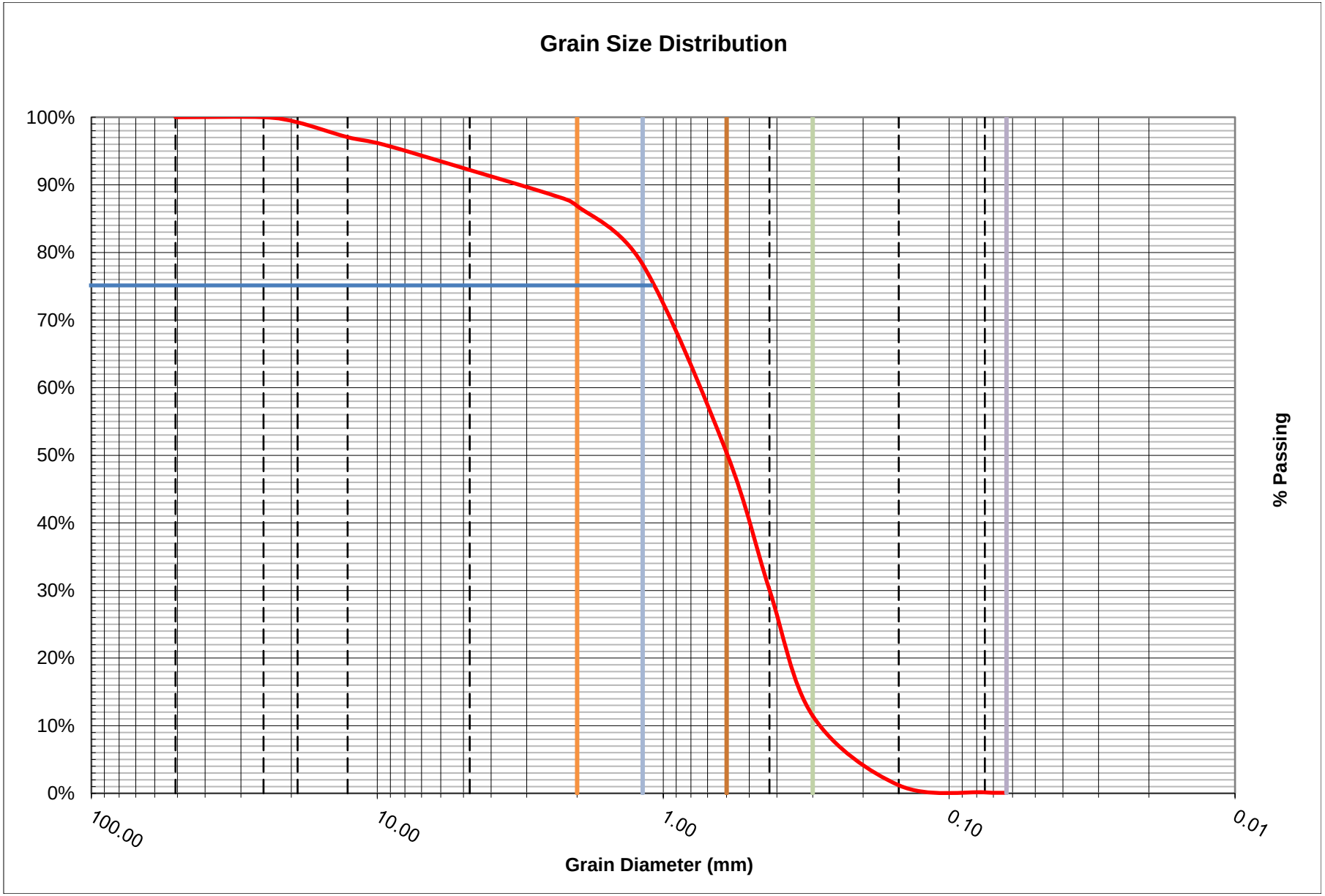
Grain Size Distribution
100%
90%
80%
70%
60%
50%
40%
30%
20%
10%
0%
100.00
10.00
1.00
0.10
0.01
Grain Diameter (mm)
% Passing

Lab Number LL793071614 Sample # 1 Station:

Sieve Size and Percent passing for Soil Samples

Sample Size = 6596.2 grams

Sieve		Mass of soil		* based on Minitial					
No. (US std)	size (mm)	with pan (g)	w/o pan (g)	% retained	sum(% retained)	% passing			
2"	50.80			0.00%	0.00%	100.00%	D_{100}		
1"	25.00			0.00%	0.00%	100.00%	D_{84}	0.90	1 std deviation greater than median
3/4"	19.00			0.00%	0.00%	100.00%	D_{75}	0.71	
1/2"	12.70			0.00%	0.00%	100.00%	D_{60}	0.55	Median size
3/8"	9.50		2.7	0.04%	0.04%	99.96%	D_{50}	0.49	
#4	4.75		16.6	0.25%	0.29%	99.71%	D_{30}	0.39	1 std deviation less than median
#8	2.36		74.3	1.13%	1.42%	98.58%	D_{16}	0.33	Effective Size
#10	2.00		39.8	0.60%	2.02%	97.98%	D_{10}	0.30	Uniformity coefficient
#16	1.18		240.7	3.65%	5.67%	94.33%	C_u	1.81	Coefficient of gradation
#30	0.60		1675.5	25.41%	31.08%	68.92%	C_c	0.93	
#40	0.425		2153.0	32.65%	63.74%	36.26%	gap graded		Particle size distribution curve
#50	0.30		1764.3	26.76%	90.49%	9.51%			
#100	0.150		533.2	8.09%	98.58%	1.42%			
#200	0.075		77.2	1.17%	99.75%	0.25%			
#230	0.063		7.2	0.11%	99.86%	0.14%			
pan	--		9.2	0.14%	100.00%	0.00%			
	Totals	0	6593.7	--	--	--			

Total weight % Difference = 0.0 %

Notes

Sample location

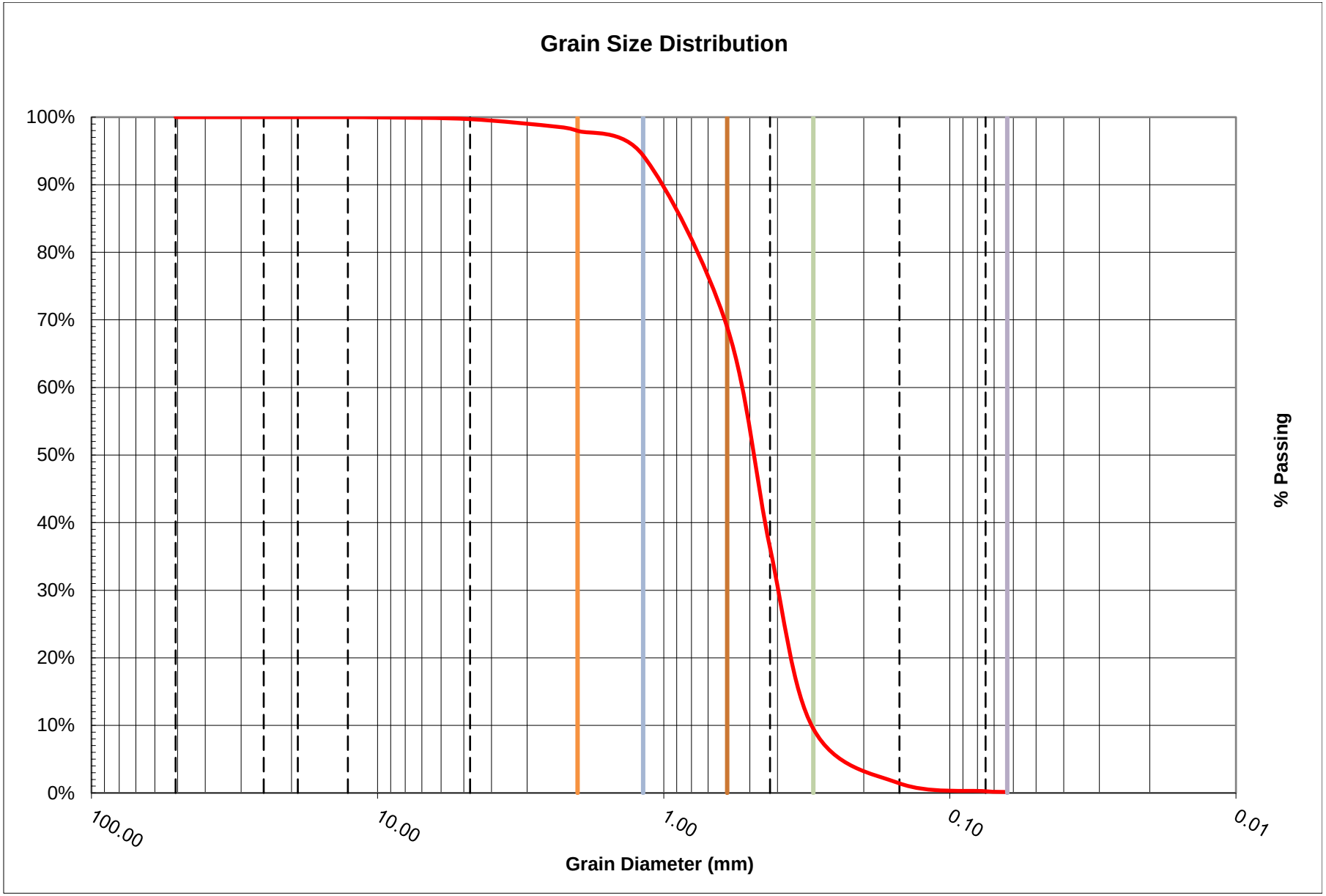
Grain Size Distribution
100%
90%
80%
70%
60%
50%
40%
30%
20%
10%
0%
% Passing
100.00
10.00
1.00
0.10
0.01
Grain Diameter (mm)

Lab Number IS815071416 Sample # bed Station:

Sieve Size and Percent passing for Soil Samples

Sample Size = 4540.7 grams

Sieve		Mass of soil		* based on Minitial					
No. (US std)	size (mm)	with pan (g)	w/o pan (g)	% retained	sum(% retained)	% passing			
2"	50.80			0.00%	0.00%	100.00%	D_{100}		
1"	25.00			0.00%	0.00%	100.00%	D_{84}	0.77	1 std deviation greater than median
3/4"	19.00			0.00%	0.00%	100.00%	D_{75}	0.56	
1/2"	12.70			0.00%	0.00%	100.00%	D_{60}	0.43	Median size
3/8"	9.50		2.0	0.04%	0.04%	99.96%	D_{50}	0.39	
#4	4.75		17.5	0.39%	0.43%	99.57%	D_{30}	0.32	1 std deviation less than median
#8	2.36		81.7	1.80%	2.23%	97.77%	D_{16}	0.25	Effective Size
#10	2.00		30.4	0.67%	2.90%	97.10%	D_{10}	0.20	Uniformity coefficient
#16	1.18		167.2	3.68%	6.58%	93.42%	C_u	2.12	Coefficient of gradation
#30	0.60		685.9	15.10%	21.68%	78.32%	C_c	1.22	
#40	0.425		843.8	18.58%	40.26%	59.74%	poorly graded		Particle size distribution curve
#50	0.30		1724.3	37.96%	78.22%	21.78%			
#100	0.150		932.5	20.53%	98.75%	1.25%			
#200	0.075		51.3	1.13%	99.88%	0.12%			
#230	0.063		2.6	0.06%	99.93%	0.07%			
pan	--		3.0	0.07%	100.00%	0.00%			
	Totals	0	4542.2	--	--	--			

Total weight % Difference = 0.0 %

Notes

Sample location

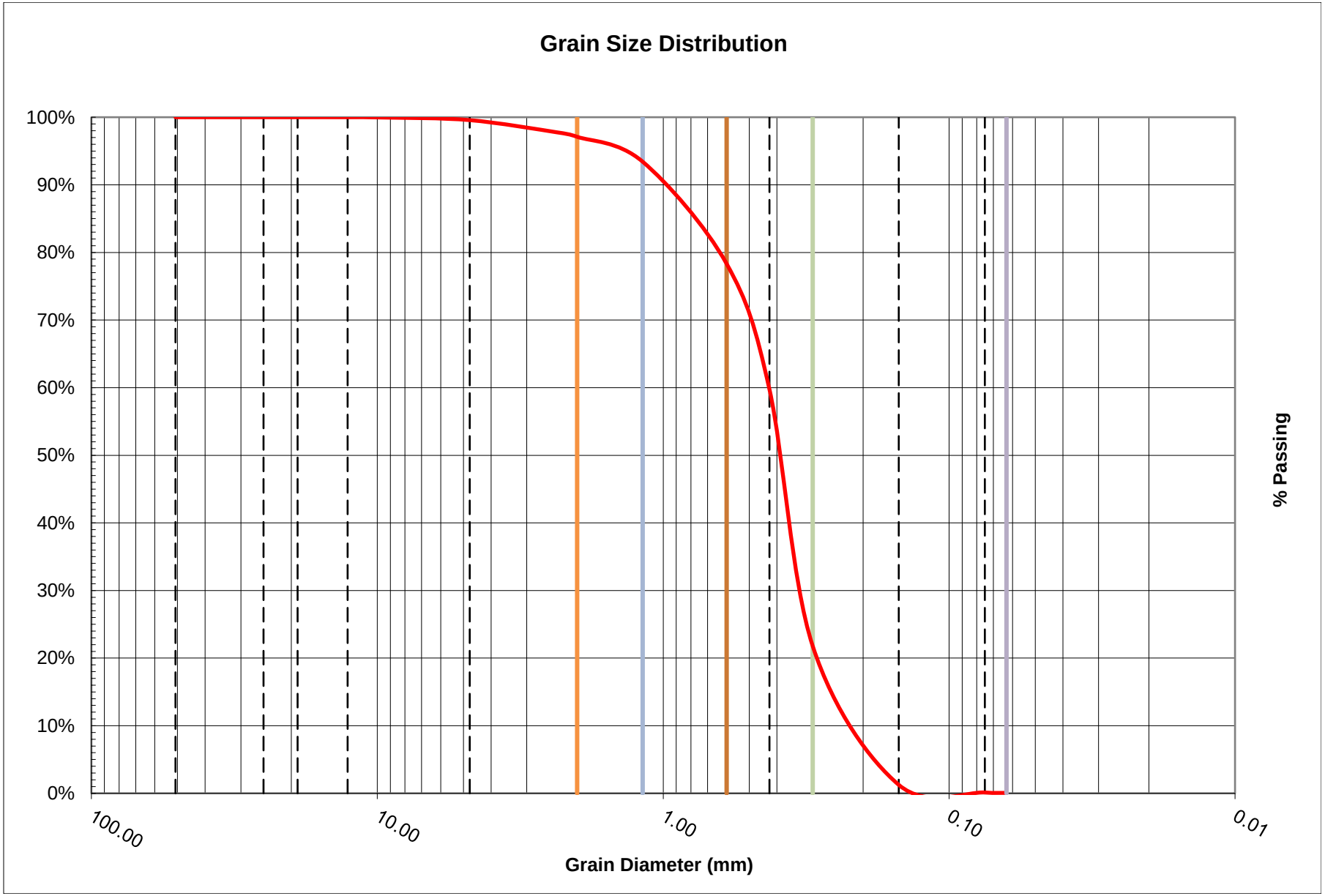
Grain Size Distribution
100%
90%
80%
70%
60%
50%
40%
30%
20%
10%
0%
% Passing
100.00
10.00
1.00
0.10
0.01
Grain Diameter (mm)

Lab Number CO833071416 Sample # 1 Station:

Sieve Size and Percent passing for Soil Samples

Sample Size = 4265.6 grams

Sieve		Mass of soil		* based on Minitial					
No. (US std)	size (mm)	with pan (g)	w/o pan (g)	% retained	sum(% retained)	% passing			
2"	50.80			0.00%	0.00%	100.00%	D_{100}		
1"	25.00			0.00%	0.00%	100.00%	D_{84}	0.63	1 std deviation greater than median
3/4"	19.00			0.00%	0.00%	100.00%	D_{75}	0.55	
1/2"	12.70		3.9	0.09%	0.09%	99.91%	D_{60}	0.47	Median size
3/8"	9.50		1.1	0.03%	0.12%	99.88%	D_{50}	0.42	
#4	4.75		8.3	0.19%	0.31%	99.69%	D_{30}	0.34	1 std deviation less than median
#8	2.36		29.1	0.68%	0.99%	99.01%	D_{16}	0.30	Effective Size
#10	2.00		15.3	0.36%	1.35%	98.65%	D_{10}	0.22	Uniformity coefficient
#16	1.18		89.7	2.10%	3.46%	96.54%	C_u	2.08	Coefficient of gradation
#30	0.60		580.7	13.62%	17.08%	82.92%	C_c	1.13	
#40	0.425		1344.6	31.54%	48.62%	51.38%	gap graded		Particle size distribution curve
#50	0.30		1518.5	35.62%	84.25%	15.75%			
#100	0.150		588.7	13.81%	98.06%	1.94%			
#200	0.075		66.0	1.55%	99.60%	0.40%			
#230	0.063		6.7	0.16%	99.76%	0.24%			
pan	--		10.2	0.24%	100.00%	0.00%			
	Totals	0	4262.8	--	--	--			

Total weight % Difference = 0.1 %

Notes

Sample location

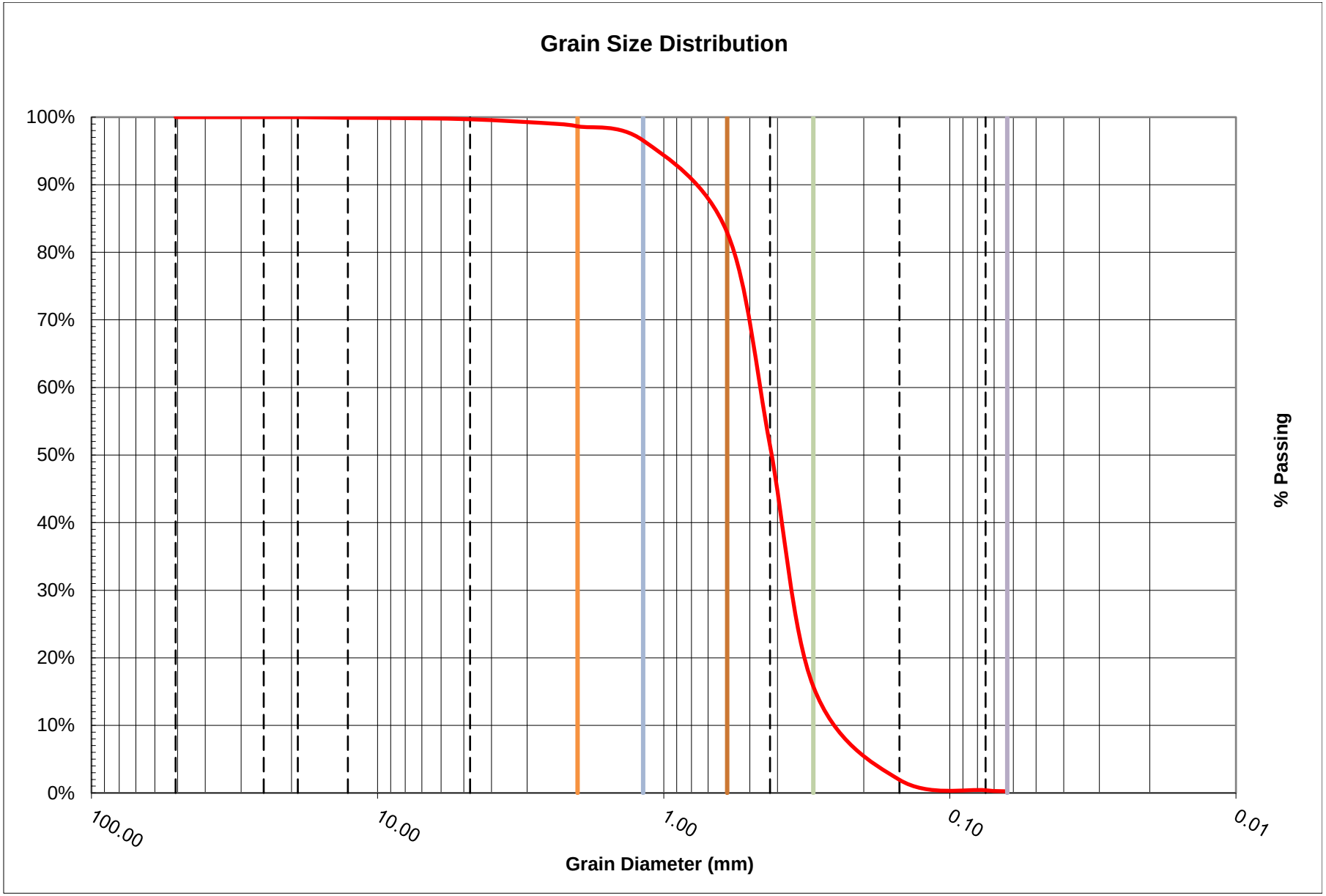
Grain Size Distribution
100%
90%
80%
70%
60%
50%
40%
30%
20%
10%
0%
% Passing
100.00
10.00
1.00
0.10
0.01
Grain Diameter (mm)

Lab Number 857071416 Sample # 1 Station:

Sieve Size and Percent passing for Soil Samples

Sample Size = 4282.8 grams

Sieve		Mass of soil		* based on Minitial					
No. (US std)	size (mm)	with pan (g)	w/o pan (g)	% retained	sum(% retained)	% passing			
2"	50.80			0.00%	0.00%	100.00%	D_{100}		
1"	25.00			0.00%	0.00%	100.00%	D_{84}	0.85	1 std deviation greater than median
3/4"	19.00			0.00%	0.00%	100.00%	D_{75}	0.61	
1/2"	12.70		2.1	0.05%	0.05%	99.95%	D_{60}	0.49	Median size
3/8"	9.50		2.6	0.06%	0.11%	99.89%	D_{50}	0.43	
#4	4.75		15.0	0.35%	0.46%	99.54%	D_{30}	0.34	1 std deviation less than median
#8	2.36		64.3	1.50%	1.96%	98.04%	D_{16}	0.28	Effective Size
#10	2.00		29.9	0.70%	2.66%	97.34%	D_{10}	0.22	Uniformity coefficient
#16	1.18		180	4.21%	6.87%	93.13%	C_u	2.24	Coefficient of gradation
#30	0.60		796.4	18.62%	25.49%	74.51%	C_c	1.10	
#40	0.425		1050.3	24.55%	50.04%	49.96%	gap graded		Particle size distribution curve
#50	0.30		1391.7	32.53%	82.58%	17.42%			
#100	0.150		698.2	16.32%	98.90%	1.10%			
#200	0.075		32.4	0.76%	99.66%	0.34%			
#230	0.063		3.5	0.08%	99.74%	0.26%			
pan	--		11.2	0.26%	100.00%	0.00%			
	Totals	0	4277.6	--	--	--			

Total weight % Difference = 0.1 %

Notes

Sample location

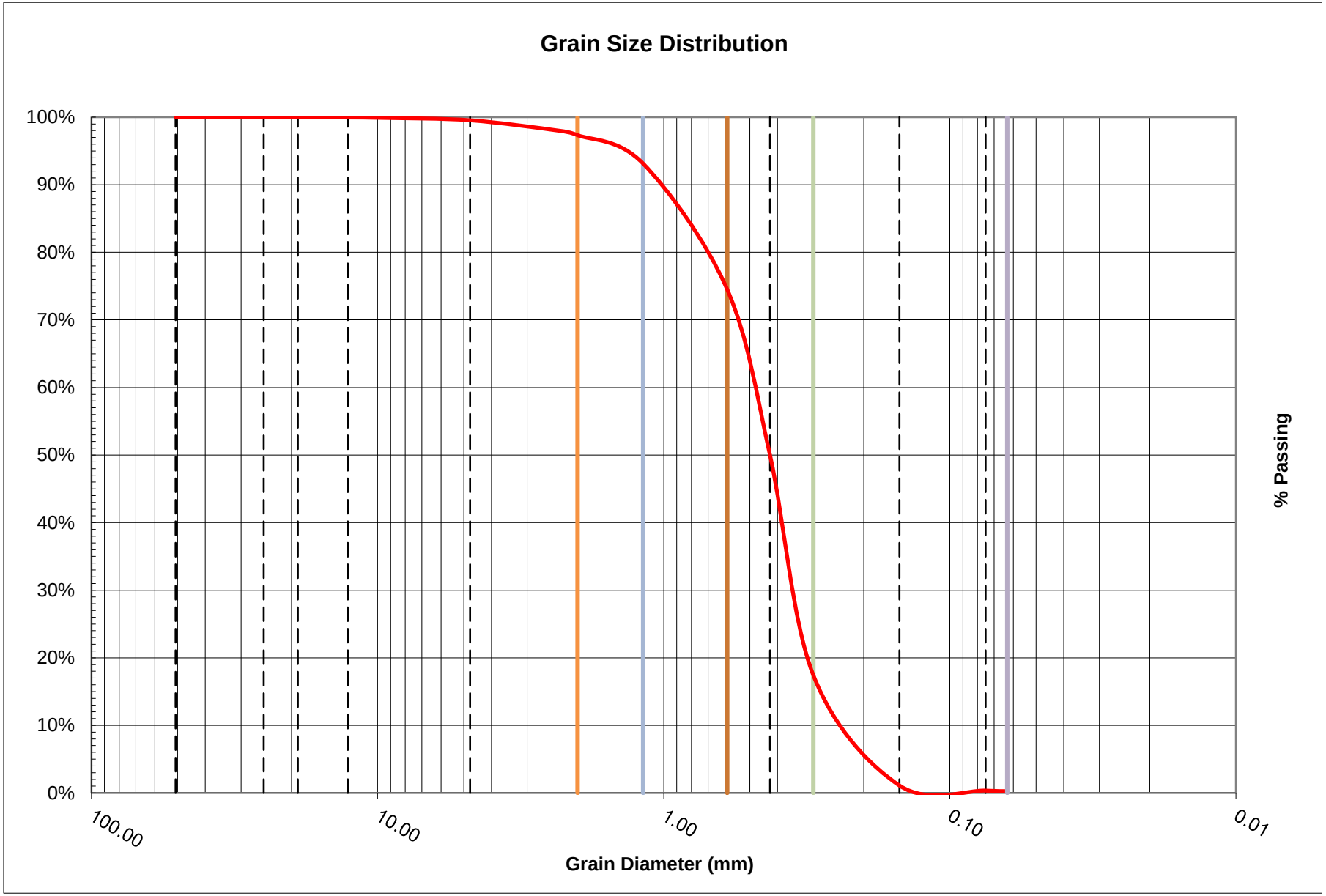
Grain Size Distribution
100%
90%
80%
70%
60%
50%
40%
30%
20%
10%
0%
% Passing
100.00
10.00
1.00
0.10
0.01
Grain Diameter (mm)

Lab Number 863071416 Sample # bank Station:

Sieve Size and Percent passing for Soil Samples

Sample Size = 6571.1 grams

Sieve		Mass of soil		* based on Minitial					
No. (US std)	size (mm)	with pan (g)	w/o pan (g)	% retained	sum(% retained)	% passing			
2"	50.80			0.00%	0.00%	100.00%	D_{100}	29.00	
1"	25.00			0.00%	0.00%	100.00%	D_{84}	0.55	1 std deviation greater than median
3/4"	19.00		38.1	0.58%	0.58%	99.42%	D_{60}	0.38	
1/2"	12.70		73.7	1.12%	1.70%	98.30%	D_{50}	0.34	Median size
3/8"	9.50		31.5	0.48%	2.18%	97.82%	D_{30}	0.20	
#4	4.75		154.0	2.34%	4.52%	95.48%	D_{16}	0.10	1 std deviation less than median
#8	2.36		107.7	1.64%	6.16%	93.84%	D_{10}	0.08	Effective Size
#10	2.00		30.5	0.46%	6.63%	93.37%	C_u	4.69	Uniformity coefficient
#16	1.18		90.5	1.38%	8.00%	92.00%	C_c	1.35	Coefficient of gradation
#30	0.60		267.8	4.07%	12.08%	87.92%			
#40	0.425		1085.0	16.51%	28.58%	71.42%	gap graded		Particle size distribution curve
#50	0.30		2268.4	34.51%	63.10%	36.90%			
#100	0.150		804.7	12.24%	75.34%	24.66%			
#200	0.075		1077.1	16.39%	91.73%	8.27%			
#230	0.063		243.5	3.70%	95.43%	4.57%			
pan	--		300.2	4.57%	100.00%	0.00%			
	Totals	0	6572.7	--	--	--			

Total weight % Difference = 0.0 %

Notes
The largest particle (clay clod) has a mass of 9.3 g
a axis 32 mm
b axis 29 mm
c axis 17 mm

Sample location

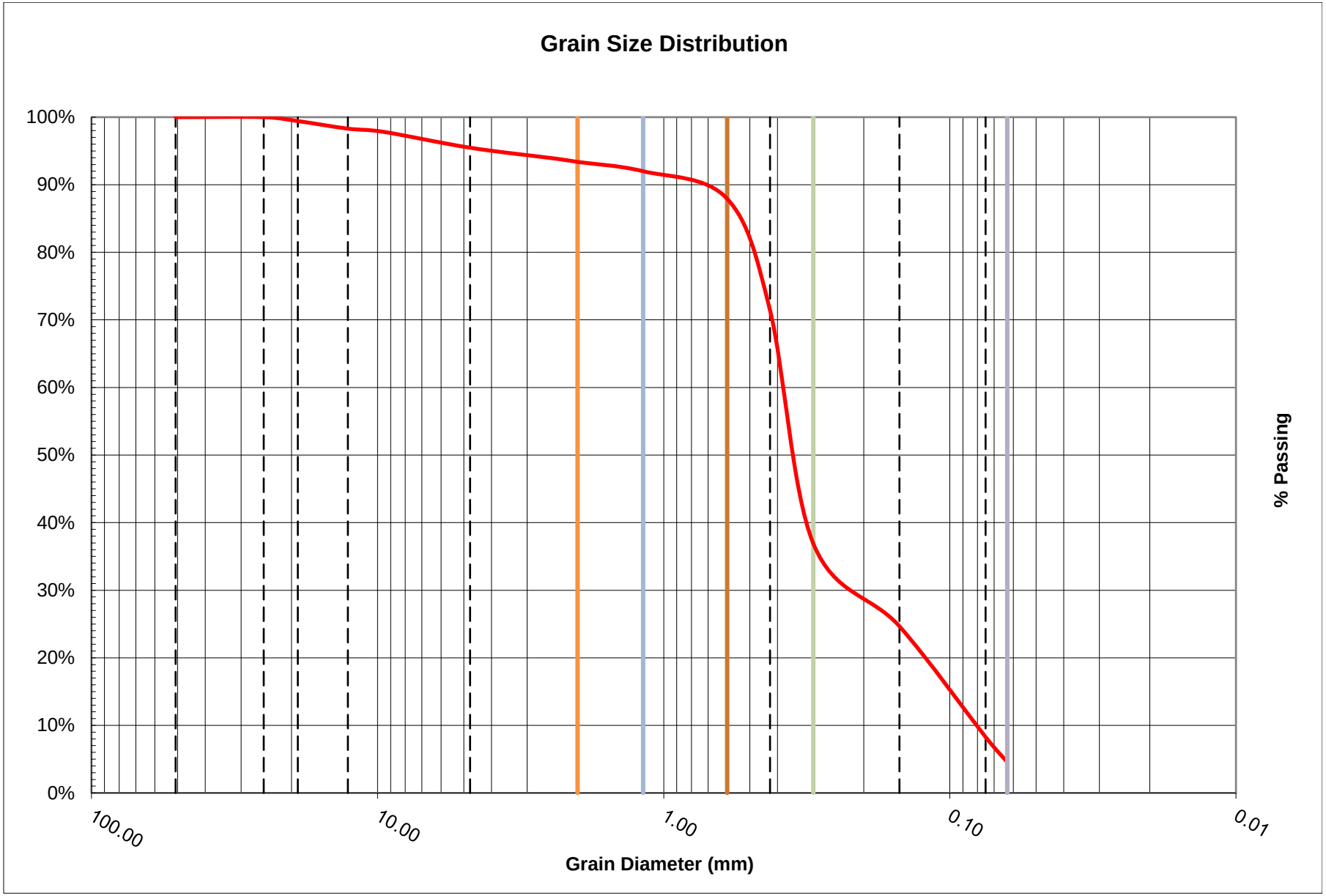
Grain Size Distribution
100%
90%
80%
70%
60%
50%
40%
30%
20%
10%
0%
% Passing
100.00
10.00
1.00
0.10
0.01
Grain Diameter (mm)

Lab Number CO877071416 Sample # 1 Station:

Sieve Size and Percent passing for Soil Samples

Sample Size = 5337.1 grams

Sieve		Mass of soil		* based on Minitial					
No. (US std)	size (mm)	with pan (g)	w/o pan (g)	% retained	sum(% retained)	% passing			
2"	50.80			0.00%	0.00%	100.00%	D_{100}		
1"	25.00			0.00%	0.00%	100.00%	D_{84}	1.13	1 std deviation greater than median
3/4"	19.00		17.6	0.33%	0.33%	99.67%	D_{75}	0.82	
1/2"	12.70		90.2	1.69%	2.02%	97.98%	D_{60}	0.54	Median size
3/8"	9.50		43.8	0.82%	2.84%	97.16%	D_{50}	0.46	
#4	4.75		126.3	2.37%	5.21%	94.79%	D_{30}	0.35	1 std deviation less than median
#8	2.36		182.1	3.41%	8.62%	91.38%	D_{16}	0.28	Effective Size
#10	2.00		52.6	0.99%	9.61%	90.39%	D_{10}	0.21	Uniformity coefficient
#16	1.18		279.6	5.24%	14.85%	85.15%	C_u	2.55	Coefficient of gradation
#30	0.60		997.6	18.69%	33.54%	66.46%	C_c	1.08	
#40	0.425		1166.7	21.86%	55.40%	44.60%	gap graded		Particle size distribution curve
#50	0.30		1449	27.15%	82.56%	17.44%			
#100	0.150		800.8	15.01%	97.56%	2.44%			
#200	0.075		108.5	2.03%	99.60%	0.40%			
#230	0.063		7.7	0.14%	99.74%	0.26%			
pan	--		13.8	0.26%	100.00%	0.00%			
	Totals	0	5336.3	--	--	--			

Total weight % Difference = 0.0 %

Notes

Sample location

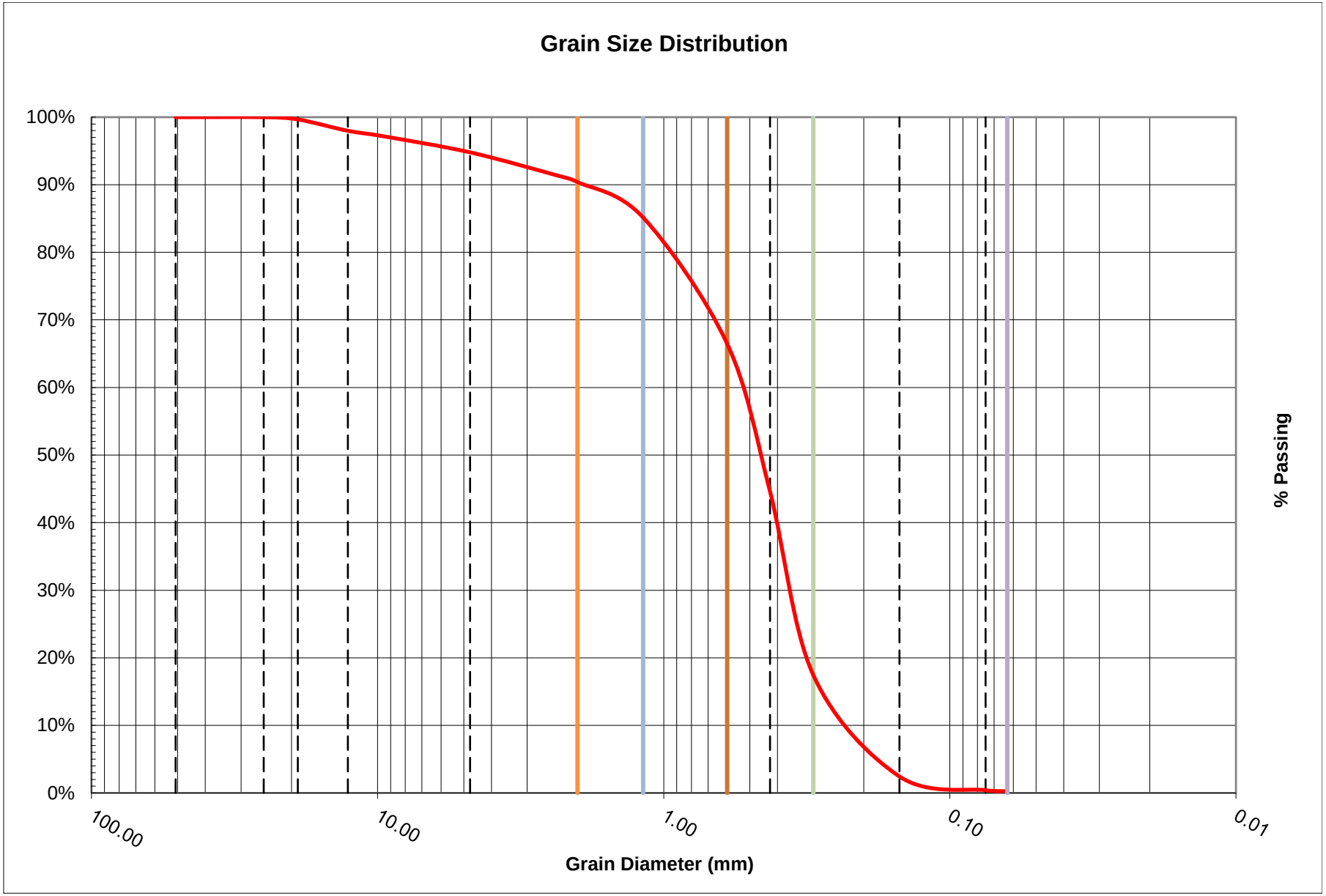
Grain Size Distribution
100%
90%
80%
70%
60%
50%
40%
30%
20%
10%
0%
% Passing
100.00
10.00
1.00
0.10
0.01
Grain Diameter (mm)

Lab Number IS908071416 Sample # 1 Station:

Sieve Size and Percent passing for Soil Samples

Sample Size = 3938.9 grams

Sieve		Mass of soil		* based on Minitial					
No. (US std)	size (mm)	with pan (g)	w/o pan (g)	% retained	sum(% retained)	% passing			
2"	50.80			0.00%	0.00%	100.00%	D_{100}		
1"	25.00			0.00%	0.00%	100.00%	D_{84}	0.61	1 std deviation greater than median
3/4"	19.00			0.00%	0.00%	100.00%	D_{75}	0.53	
1/2"	12.70		5.3	0.13%	0.13%	99.87%	D_{60}	0.44	Median size
3/8"	9.50		6.1	0.15%	0.29%	99.71%	D_{50}	0.40	
#4	4.75		22.3	0.56%	0.85%	99.15%	D_{30}	0.33	1 std deviation less than median
#8	2.36		45.2	1.15%	2.00%	98.00%	D_{16}	0.27	Effective Size
#10	2.00		18.4	0.47%	2.46%	97.54%	D_{10}	0.21	Uniformity coefficient
#16	1.18		93.8	2.38%	4.84%	95.16%	C_u	2.07	Coefficient of gradation
#30	0.60		448.5	11.36%	16.20%	83.80%	C_c	1.19	
#40	0.425		1038.4	26.31%	42.51%	57.49%	gap graded		Particle size distribution curve
#50	0.30		1542.5	39.08%	81.59%	18.41%			
#100	0.150		663.6	16.81%	98.40%	1.60%			
#200	0.075		46.1	1.17%	99.56%	0.44%			
#230	0.063		4.1	0.10%	99.67%	0.33%			
pan	--		13.1	0.33%	100.00%	0.00%			
	Totals	0	3947.4	--	--	--			

Total weight % Difference = 0.2 %

Notes

Sample location

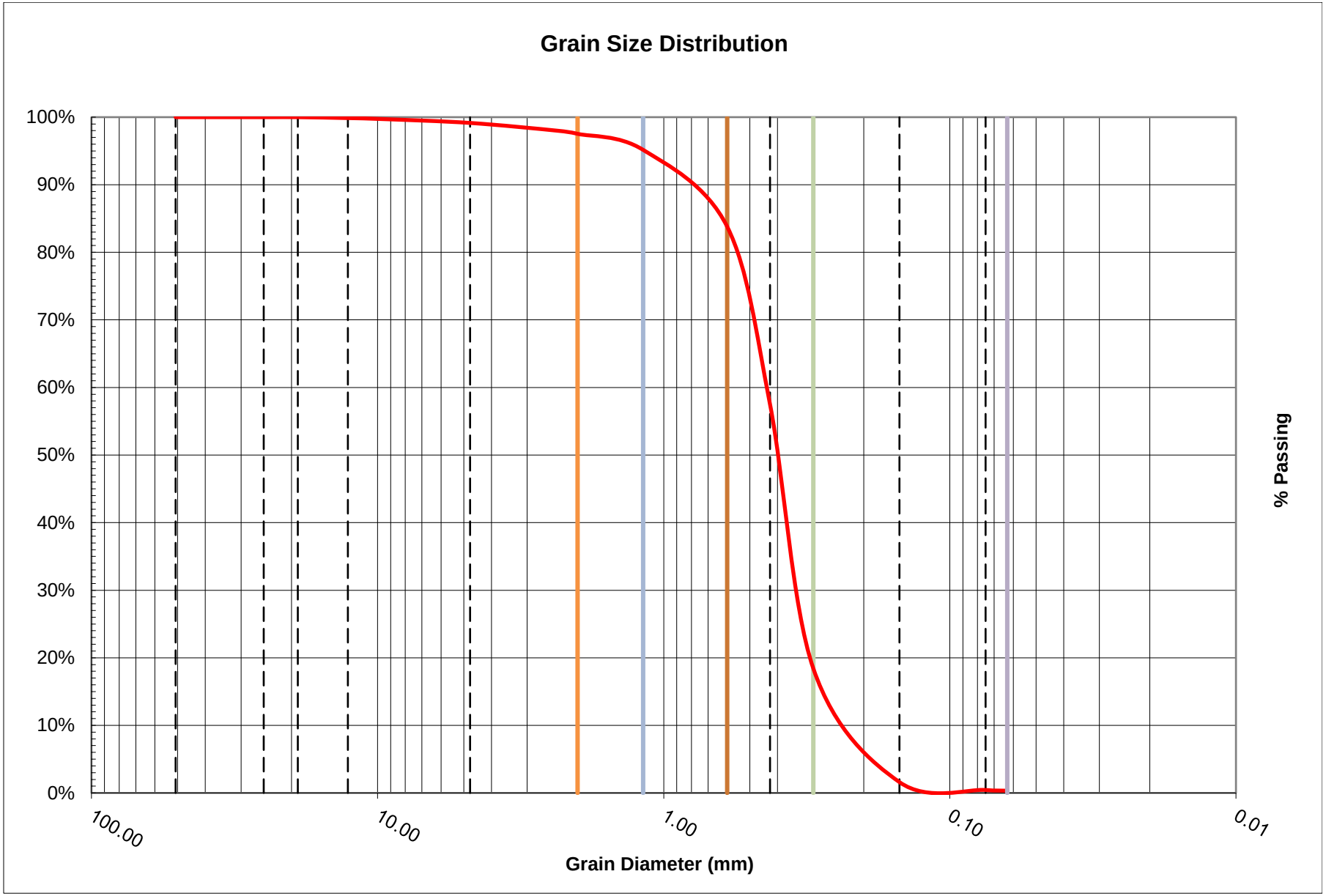
Grain Size Distribution
100%
90%
80%
70%
60%
50%
40%
30%
20%
10%
0%
% Passing
100.00
10.00
1.00
0.10
0.01
Grain Diameter (mm)

Lab Number CC927071416 Sample # 1 Station:

Sieve Size and Percent passing for Soil Samples

Sample Size = 5230.2 grams

Sieve		Mass of soil		* based on Minitial					
No. (US std)	size (mm)	with pan (g)	w/o pan (g)	% retained	sum(% retained)	% passing			
2"	50.80			0.00%	0.00%	100.00%	D_{100}		
1"	25.00			0.00%	0.00%	100.00%	D_{84}	0.58	1 std deviation greater than median
3/4"	19.00			0.00%	0.00%	100.00%	D_{75}	0.53	
1/2"	12.70		9.4	0.18%	0.18%	99.82%	D_{60}	0.45	Median size
3/8"	9.50		0.7	0.01%	0.19%	99.81%	D_{50}	0.41	
#4	4.75		3.0	0.06%	0.25%	99.75%	D_{30}	0.34	1 std deviation less than median
#8	2.36		11.9	0.23%	0.48%	99.52%	D_{16}	0.30	Effective Size
#10	2.00		7.2	0.14%	0.62%	99.38%	D_{10}	0.23	Uniformity coefficient
#16	1.18		56	1.07%	1.69%	98.31%	C_u	1.98	Coefficient of gradation
#30	0.60		595.1	11.39%	13.07%	86.93%	C_c	1.13	
#40	0.425		1675.4	32.05%	45.13%	54.87%	gap graded		Particle size distribution curve
#50	0.30		2019.6	38.64%	83.76%	16.24%			
#100	0.150		803.4	15.37%	99.13%	0.87%			
#200	0.075		35.9	0.69%	99.82%	0.18%			
#230	0.063		2.1	0.04%	99.86%	0.14%			
pan	--		7.3	0.14%	100.00%	0.00%			
	Totals	0	5227	--	--	--			

Total weight % Difference = 0.1 %

Notes

Sample location

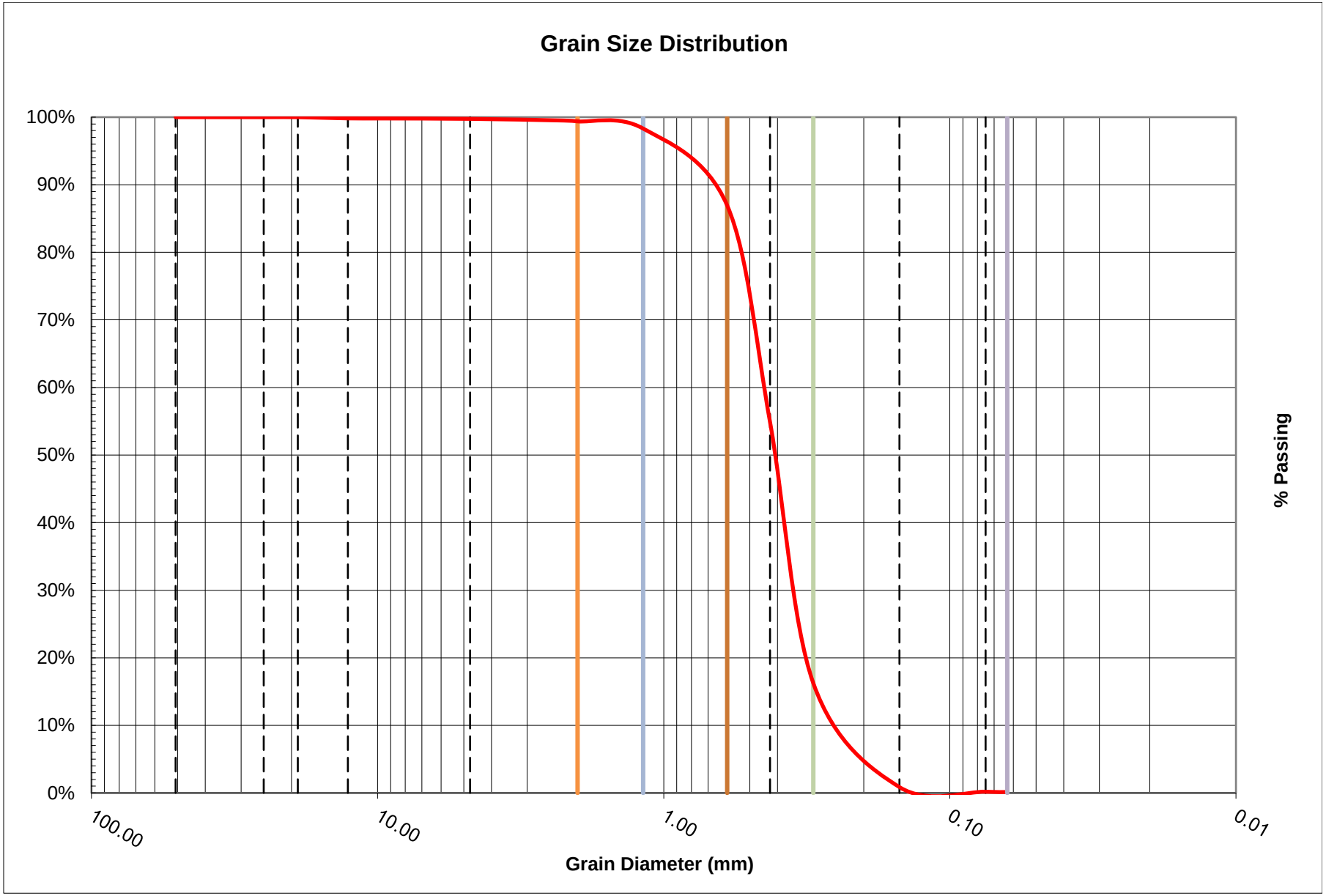
Grain Size Distribution
100%
90%
80%
70%
60%
50%
40%
30%
20%
10%
0%
% Passing
100.00
10.00
1.00
0.10
0.01
Grain Diameter (mm)

Lab Number CC943071416 Sample # 1 Station:

Sieve Size and Percent passing for Soil Samples

Sample Size = 5051.5 grams

Sieve		Mass of soil		* based on Minitial					
No. (US std)	size (mm)	with pan (g)	w/o pan (g)	% retained	sum(% retained)	% passing			
2"	50.80			0.00%	0.00%	100.00%	D_{100}		
1"	25.00			0.00%	0.00%	100.00%	D_{84}	0.92	1 std deviation greater than median
3/4"	19.00			0.00%	0.00%	100.00%	D_{75}	0.68	
1/2"	12.70		2.4	0.05%	0.05%	99.95%	D_{60}	0.51	Median size
3/8"	9.50		12.0	0.24%	0.29%	99.71%	D_{50}	0.44	
#4	4.75		21.2	0.42%	0.70%	99.30%	D_{30}	0.34	1 std deviation less than median
#8	2.36		90.7	1.80%	2.50%	97.50%	D_{16}	0.27	Effective Size
#10	2.00		43.1	0.85%	3.35%	96.65%	D_{10}	0.21	Uniformity coefficient
#16	1.18		253.7	5.02%	8.37%	91.63%	C_u	2.46	Coefficient of gradation
#30	0.60		1026.8	20.32%	28.70%	71.30%	C_c	1.12	
#40	0.425		1200.8	23.77%	52.46%	47.54%	poorly graded		Particle size distribution curve
#50	0.30		1450	28.70%	81.16%	18.84%			
#100	0.150		836.3	16.55%	97.72%	2.28%			
#200	0.075		90.1	1.78%	99.50%	0.50%			
#230	0.063		10.5	0.21%	99.71%	0.29%			
pan	--		14.8	0.29%	100.00%	0.00%			
	Totals	0	5052.4	--	--	--			

Total weight % Difference = 0.0 %

Notes

Sample location

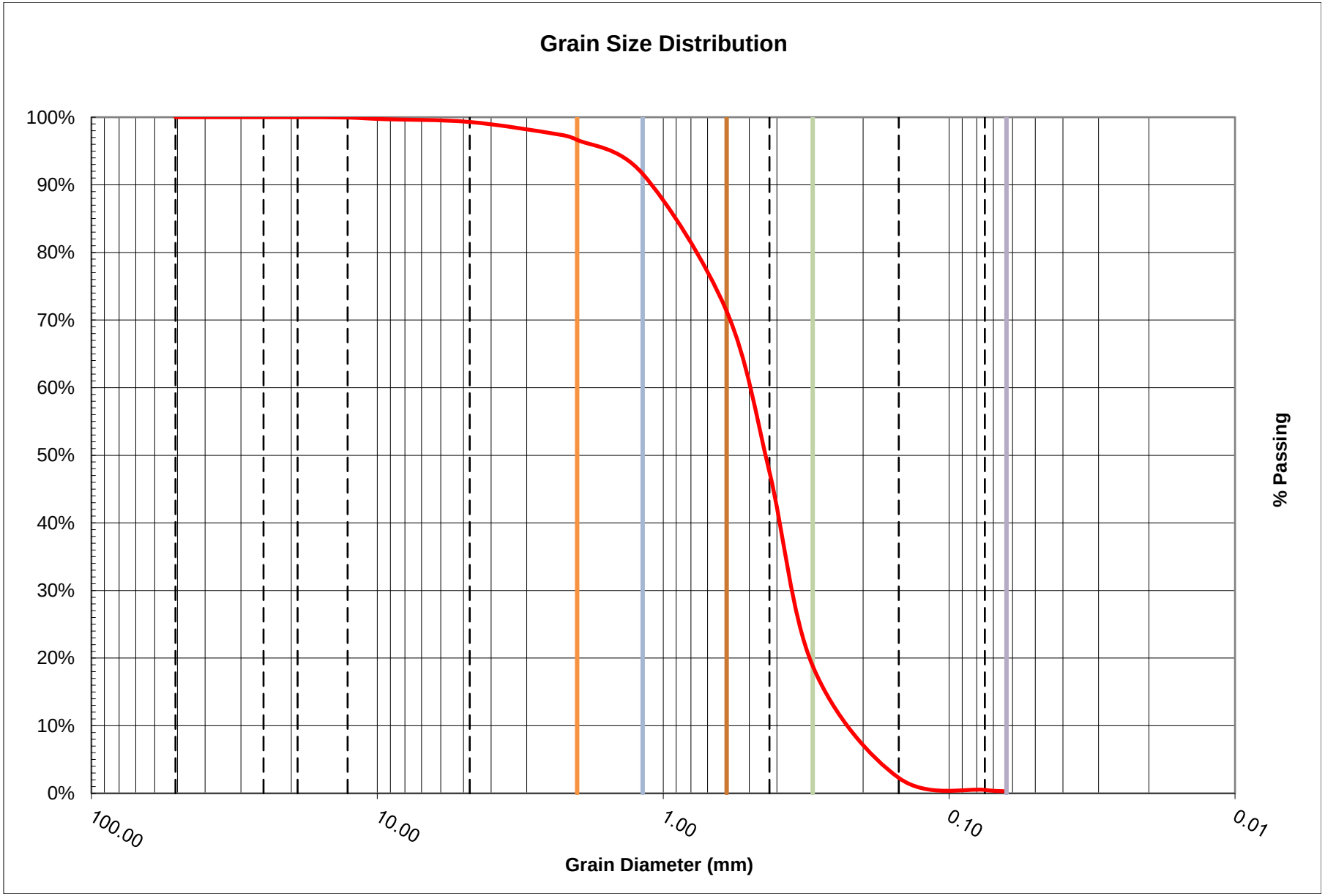
Grain Size Distribution
100%
90%
80%
70%
60%
50%
40%
30%
20%
10%
0%
% Passing
100.00
10.00
1.00
0.10
0.01
Grain Diameter (mm)

Lab Number 974072816 Sample # Station:

Sieve Size and Percent passing for Soil Samples

Sample Size = 4437.4 grams

Sieve		Mass of soil		* based on Minitial					
No. (US std)	size (mm)	with pan (g)	w/o pan (g)	% retained	sum(% retained)	% passing			
2"	50.80			0.00%	0.00%	100.00%	D_{100}		
1"	25.00			0.00%	0.00%	100.00%	D_{84}	0.25	1 std deviation greater than median
3/4"	19.00			0.00%	0.00%	100.00%	D_{60}	0.19	
1/2"	12.70		1.3	0.03%	0.03%	99.97%	D_{50}	0.17	Median size
3/8"	9.50		8.1	0.18%	0.21%	99.79%	D_{30}	0.11	
#4	4.75		7.3	0.16%	0.38%	99.62%	D_{16}	0.08	1 std deviation less than median
#8	2.36		12.2	0.27%	0.65%	99.35%	D_{10}	0.07	Effective Size
#10	2.00		5.0	0.11%	0.76%	99.24%	C_u	2.82	Uniformity coefficient
#16	1.18		19.4	0.44%	1.20%	98.80%	C_c	1.00	Coefficient of gradation
#30	0.60		18.6	0.42%	1.62%	98.38%			
#40	0.425		17.7	0.40%	2.02%	97.98%	gap graded		Particle size distribution curve
#50	0.30		25.4	0.57%	2.59%	97.41%			
#100	0.150		2479.2	55.84%	58.43%	41.57%			
#200	0.075		1236.5	27.85%	86.28%	13.72%			
#230	0.063		248.4	5.59%	91.87%	8.13%			
pan	--		360.9	8.13%	100.00%	0.00%			
	Totals	0	4440	--	--	--			

Total weight % Difference = 0.1 %

Notes
Clay clod for the 1/2" and 3/8" sieve sizes. Below that the clay clods continue but there are some grains that size too.

Sample location

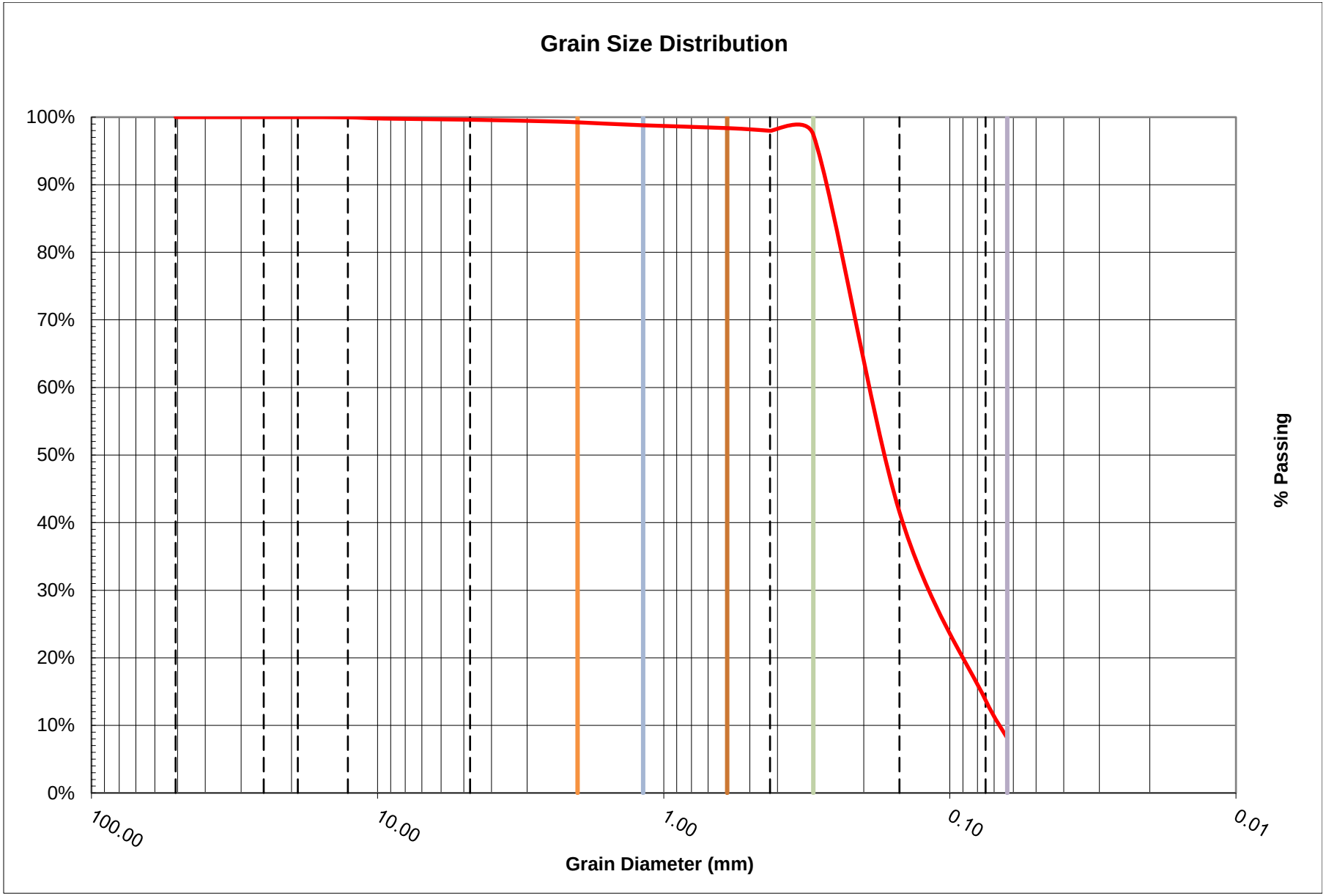
Grain Size Distribution
100%
90%
80%
70%
60%
50%
40%
30%
20%
10%
0%
% Passing
100.00
10.00
1.00
0.10
0.01
Grain Diameter (mm)

Lab Number 976072816 Sample # Station:

Sieve Size and Percent passing for Soil Samples

Sample Size = 4029 grams

Sieve		Mass of soil		* based on Minitial					
No. (US std)	size (mm)	with pan (g)	w/o pan (g)	% retained	sum(% retained)	% passing			
2"	50.80			0.00%	0.00%	100.00%	D_{100}		
1"	25.00		48.6	1.21%	1.21%	98.79%	D_{84}	1.23	1 std deviation greater than median
3/4"	19.00			0.00%	1.21%	98.79%	D_{75}	0.81	
1/2"	12.70		29.8	0.74%	1.95%	98.05%	D_{60}	0.53	Median size
3/8"	9.50		32.9	0.82%	2.76%	97.24%	D_{50}	0.46	
#4	4.75		124.3	3.09%	5.85%	94.15%	D_{30}	0.34	1 std deviation less than median
#8	2.36		167.4	4.16%	10.01%	89.99%	D_{16}	0.25	Effective Size
#10	2.00		50.6	1.26%	11.27%	88.73%	D_{10}	0.20	Uniformity coefficient
#16	1.18		205.8	5.11%	16.38%	83.62%	C_u	2.72	Coefficient of gradation
#30	0.60		618.5	15.36%	31.74%	68.26%	C_c	1.14	
#40	0.425		942.1	23.40%	55.14%	44.86%	gap graded		Particle size distribution curve
#50	0.30		978.9	24.32%	79.46%	20.54%			
#100	0.150		685.1	17.02%	96.48%	3.52%			
#200	0.075		75.0	1.86%	98.34%	1.66%			
#230	0.063		14.8	0.37%	98.71%	1.29%			
pan	--		52.0	1.29%	100.00%	0.00%			
	Totals	0	4025.8	--	--	--			

Total weight % Difference = 0.1 %

Notes

Sample location

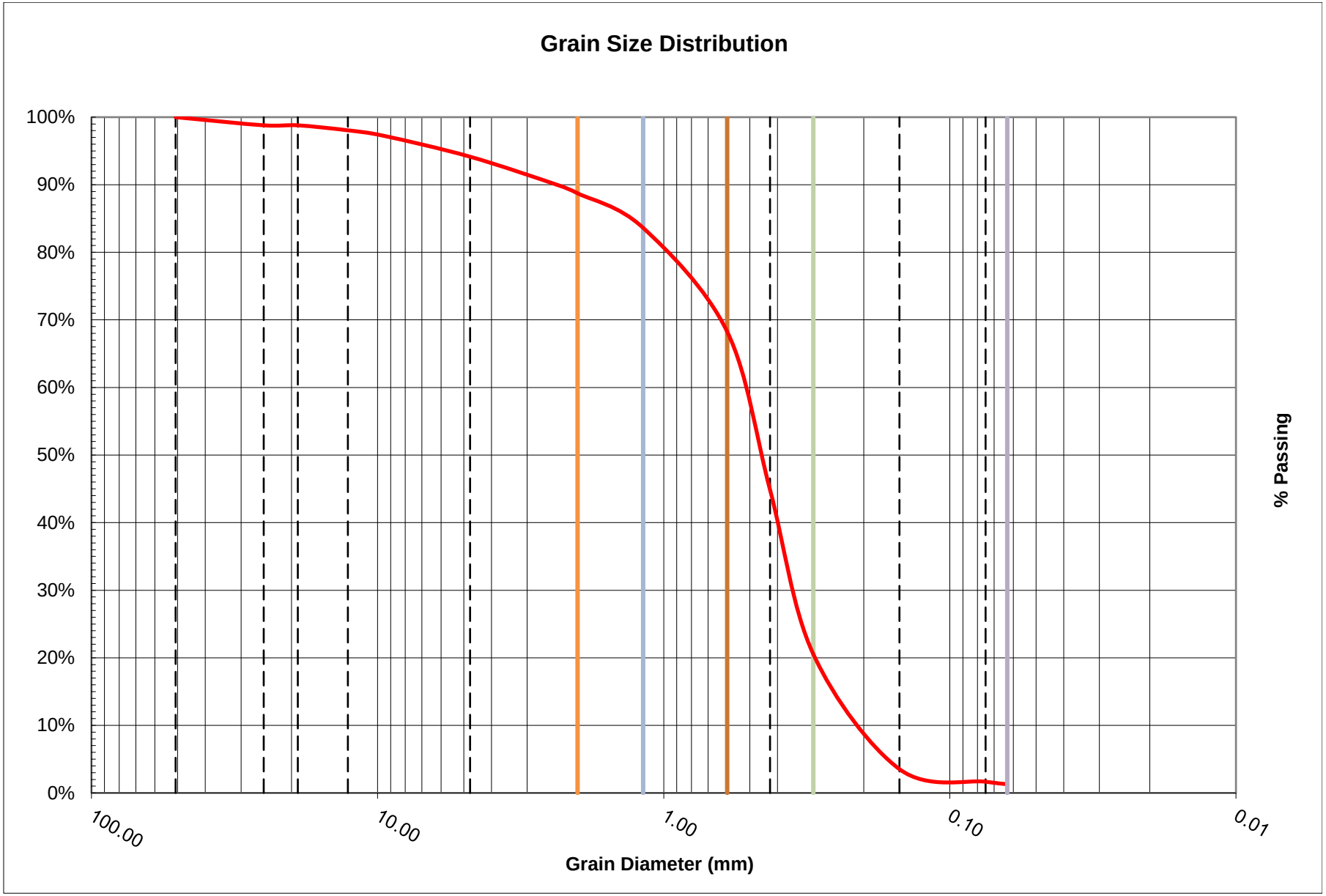
Grain Size Distribution
100%
90%
80%
70%
60%
50%
40%
30%
20%
10%
0%
% Passing
100.00
10.00
1.00
0.10
0.01
Grain Diameter (mm)

Lab Number 1004072816 Sample # Station:

Sieve Size and Percent passing for Soil Samples

Sample Size = 6933 grams

Sieve		Mass of soil		* based on Minitial					
No. (US std)	size (mm)	with pan (g)	w/o pan (g)	% retained	sum(% retained)	% passing			
2"	50.80			0.00%	0.00%	100.00%	D_{100}		
1"	25.00			0.00%	0.00%	100.00%	D_{84}	1.00	1 std deviation greater than median
3/4"	19.00		121.9	1.76%	1.76%	98.24%	D_{75}	0.67	
1/2"	12.70		87.9	1.27%	3.03%	96.97%	D_{60}	0.49	Median size
3/8"	9.50		48.3	0.70%	3.72%	96.28%	D_{50}	0.42	
#4	4.75		110.6	1.60%	5.32%	94.68%	D_{30}	0.33	1 std deviation less than median
#8	2.36		156.1	2.25%	7.57%	92.43%	D_{16}	0.25	Effective Size
#10	2.00		50.3	0.73%	8.30%	91.70%	D_{10}	0.20	Uniformity coefficient
#16	1.18		267.1	3.85%	12.15%	87.85%	C_u	2.48	Coefficient of gradation
#30	0.60		1064.8	15.36%	27.51%	72.49%	C_c	1.16	
#40	0.425		1421.6	20.51%	48.01%	51.99%	gap graded		Particle size distribution curve
#50	0.30		2184.9	31.51%	79.53%	20.47%			
#100	0.150		1188.0	17.14%	96.66%	3.34%			
#200	0.075		166.1	2.40%	99.06%	0.94%			
#230	0.063		22.2	0.32%	99.38%	0.62%			
pan	--		43.1	0.62%	100.00%	0.00%			
	Totals	0	6932.9	--	--	--			

Total weight % Difference = 0.0 %

Notes

Sample location

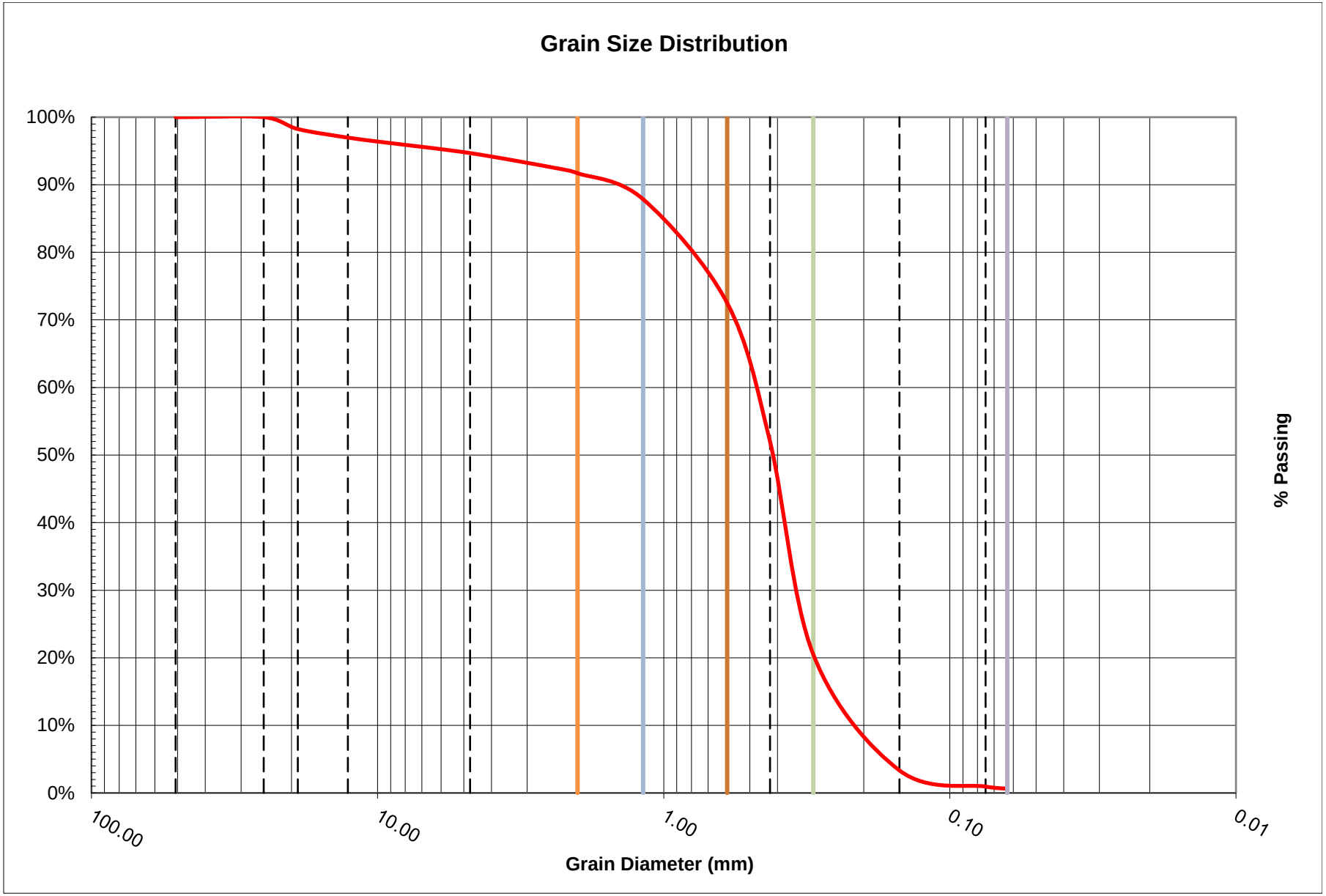
Grain Size Distribution
100%
90%
80%
70%
60%
50%
40%
30%
20%
10%
0%
% Passing
100.00
10.00
1.00
0.10
0.01
Grain Diameter (mm)

Lab Number CO1044072816 Sample # Station:

Sieve Size and Percent passing for Soil Samples

Sample Size = 6172.2 grams

Sieve		Mass of soil		* based on Minitial					
No. (US std)	size (mm)	with pan (g)	w/o pan (g)	% retained	sum(% retained)	% passing			
2"	50.80			0.00%	0.00%	100.00%	D_{100}		
1"	25.00			0.00%	0.00%	100.00%	D_{84}	0.79	1 std deviation greater than median
3/4"	19.00		9.2	0.15%	0.15%	99.85%	D_{75}	0.60	
1/2"	12.70		13.9	0.23%	0.37%	99.63%	D_{60}	0.50	Median size
3/8"	9.50		20.1	0.33%	0.70%	99.30%	D_{50}	0.44	
#4	4.75		42.0	0.68%	1.38%	98.62%	D_{30}	0.35	1 std deviation less than median
#8	2.36		31	0.50%	1.88%	98.12%	D_{16}	0.30	Effective Size
#10	2.00		12.3	0.20%	2.08%	97.92%	D_{10}	0.24	Uniformity coefficient
#16	1.18		105.9	1.72%	3.80%	96.20%	C_u	2.12	Coefficient of gradation
#30	0.60		1283.9	20.80%	24.60%	75.40%	C_c	1.07	
#40	0.425		1792.2	29.04%	53.64%	46.36%	gap graded		Particle size distribution curve
#50	0.30		1949.3	31.59%	85.23%	14.77%			
#100	0.150		850.6	13.78%	99.01%	0.99%			
#200	0.075		54.9	0.89%	99.90%	0.10%			
#230	0.063		2.2	0.04%	99.94%	0.06%			
pan	--		3.9	0.06%	100.00%	0.00%			
	Totals	0	6171.4	--	--	--			

Total weight % Difference = 0.0 %

Notes

Sample location

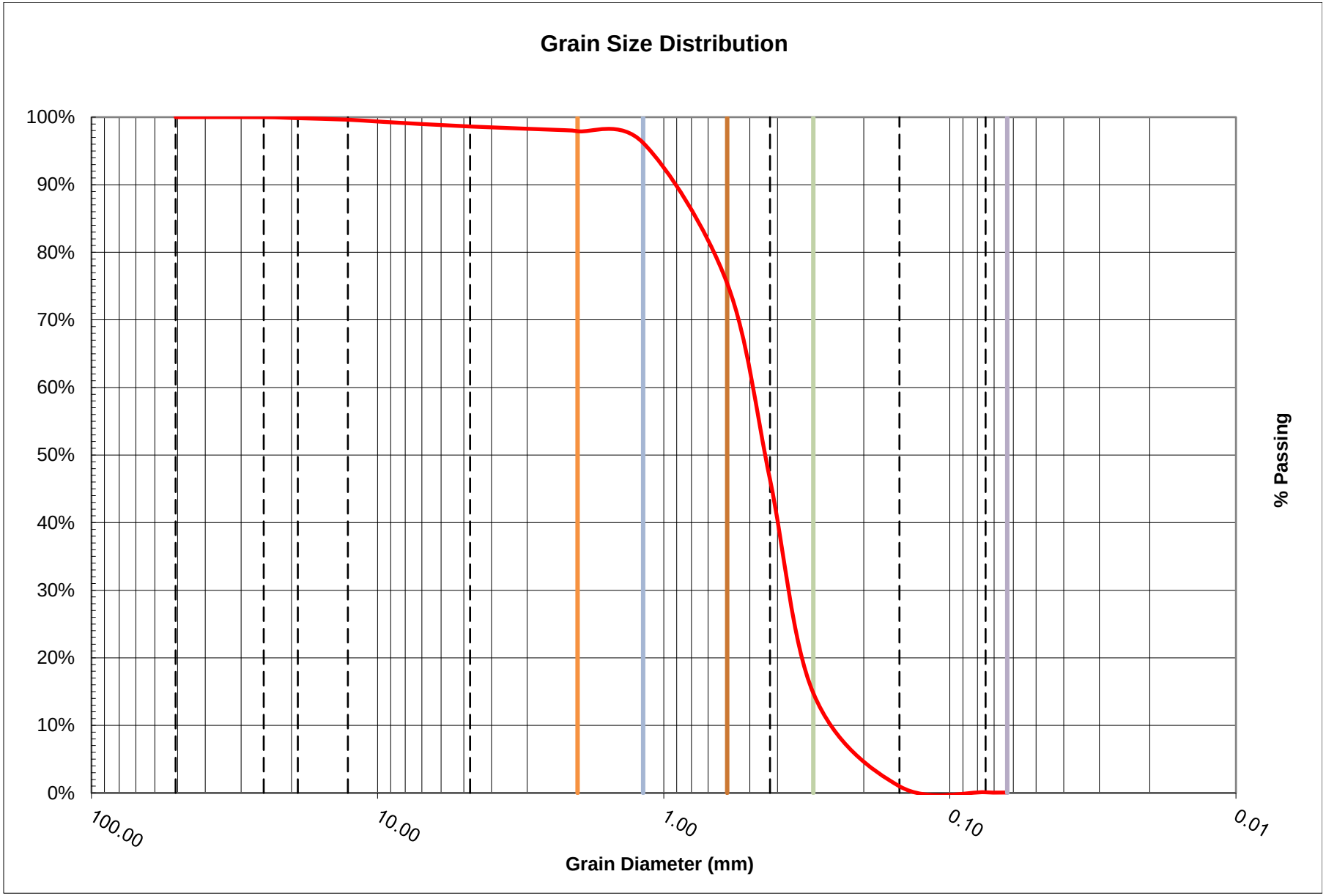
Grain Size Distribution
100%
90%
80%
70%
60%
50%
40%
30%
20%
10%
0%
% Passing
100.00
10.00
1.00
0.10
0.01
Grain Diameter (mm)

Lab Number CO1061070716 Bank Sample # 1061 Station:

Sieve Size and Percent passing for Soil Samples

Sample Size = 2614.1 grams

Sieve		Mass of soil		* based on Minitial					
No. (US std)	size (mm)	with pan (g)	w/o pan (g)	% retained	sum(% retained)	% passing			
2"	50.80			0.00%	0.00%	100.00%	D_{100}	57.00	
1"	25.00		445.3	17.02%	17.02%	82.98%	D_{84}	26.09	1 std deviation greater than median
3/4"	19.00		121.3	4.64%	21.66%	78.34%	D_{60}	0.88	
1/2"	12.70		114.5	4.38%	26.03%	73.97%	D_{50}	0.15	Median size
3/8"	9.50		29.7	1.14%	27.17%	72.83%	D_{30}	0.09	
#4	4.75		168.4	6.44%	33.61%	66.39%	D_{16}	0.06	1 std deviation less than median
#8	2.36		86.9	3.32%	36.93%	63.07%	D_{10}	0.18	Effective Size
#10	2.00		19.9	0.76%	37.69%	62.31%	C_u	4.97	Uniformity coefficient
#16	1.18		46.8	1.79%	39.48%	60.52%	C_c	0.05	Coefficient of gradation
#30	0.60		32.1	1.23%	40.70%	59.30%			
#40	0.425		30.8	1.18%	41.88%	58.12%	gap graded		Particle size distribution curve
#50	0.30		37.2	1.42%	43.30%	56.70%			
#100	0.150		160.5	6.13%	49.44%	50.56%			
#200	0.075		657.5	25.13%	74.57%	25.43%			
#230	0.063		246.4	9.42%	83.99%	16.01%			
pan	--		418.9	16.01%	100.00%	0.00%			
	Totals	0	2616.2	--	--	--			

Total weight % Difference = 0.1 %

Notes
largest particle (clay clod) has a weight of 57.0 g
a axis 65 mm
b axis 57 mm
c axis 20 mm

Sample location

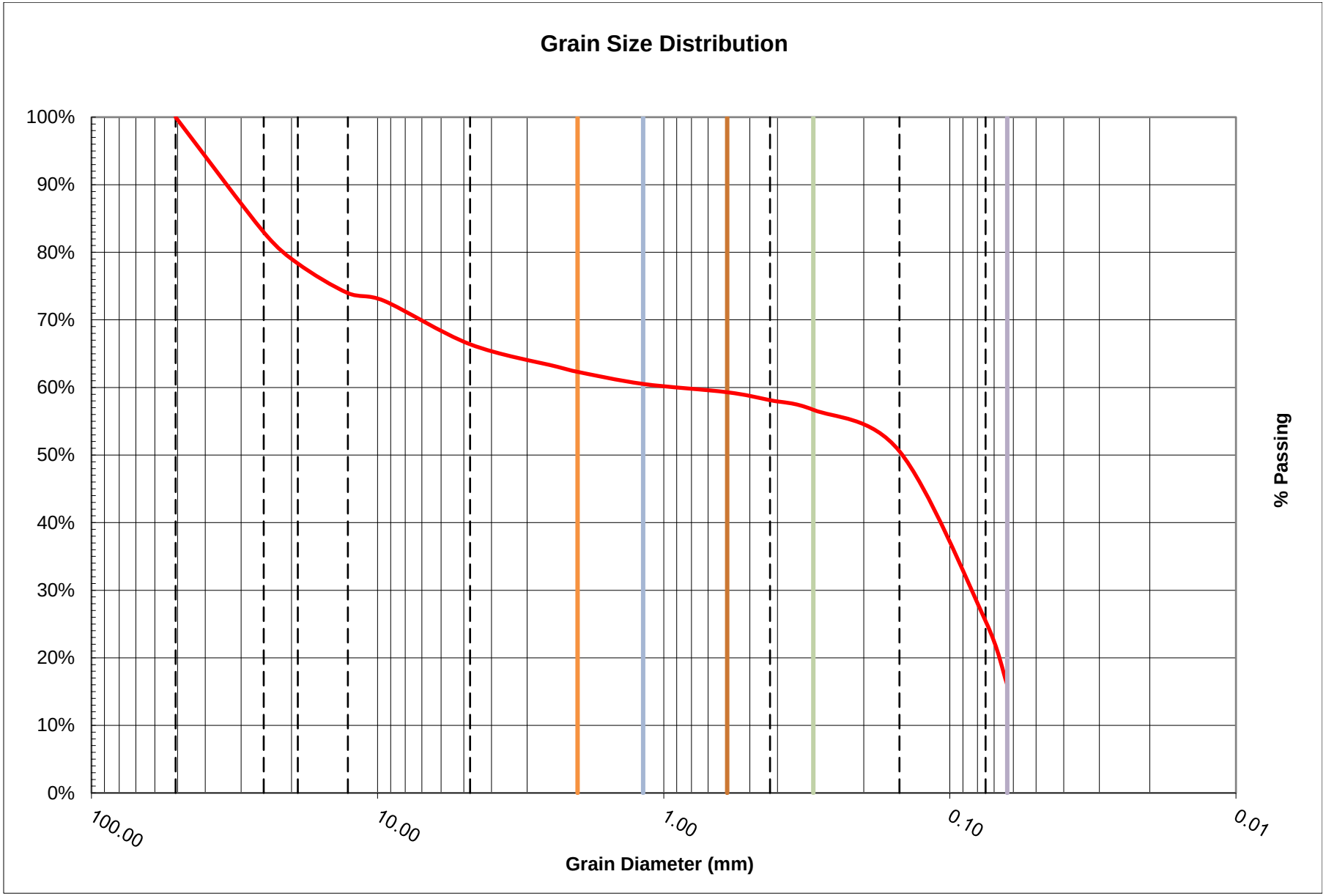
Grain Size Distribution
100%
90%
80%
70%
60%
50%
40%
30%
20%
10%
0%
% Passing
100.00
10.00
1.00
0.10
0.01
Grain Diameter (mm)

Lab Number 1062070716 Bed Sample # 1062 Station:

Sieve Size and Percent passing for Soil Samples

Sample Size = 3243.5 grams

Sieve		Mass of soil		* based on Minitial		
No. (US std)	size (mm)	with pan (g)	w/o pan (g)	% retained	sum(% retained)	% passing
2"	50.80			0.00%	0.00%	100.00%
1"	25.00			0.00%	0.00%	100.00%
3/4"	19.00			0.00%	0.00%	100.00%
1/2"	12.70			0.00%	0.00%	100.00%
3/8"	9.50			0.00%	0.00%	100.00%
#4	4.75		2.0	0.06%	0.06%	99.94%
#8	2.36		7.4	0.23%	0.29%	99.71%
#10	2.00		3.9	0.12%	0.41%	99.59%
#16	1.18		36.4	1.12%	1.53%	98.47%
#30	0.60		376.5	11.63%	13.16%	86.84%
#40	0.425		885.4	27.34%	40.51%	59.49%
#50	0.30		1236.8	38.20%	78.70%	21.30%
#100	0.150		672.5	20.77%	99.47%	0.53%
#200	0.075		16.4	0.51%	99.98%	0.02%
#230	0.063		0.3	0.01%	99.98%	0.02%
pan	--		0.5	0.02%	100.00%	0.00%
	Totals	0	3238.1	--	--	--

D_{100}		
D_{84}	0.58	1 std deviation greater than median
D_{75}	0.52	
D_{60}	0.43	Median size
D_{50}	0.39	
D_{30}	0.32	1 std deviation less than median
D_{16}	0.25	Effective Size
D_{10}	0.21	Uniformity coefficient
C_u	2.08	Coefficient of gradation
C_c	1.20	
poorly graded		Particle size distribution curve

Total weight % Difference = 0.2 %

Notes

Sample location

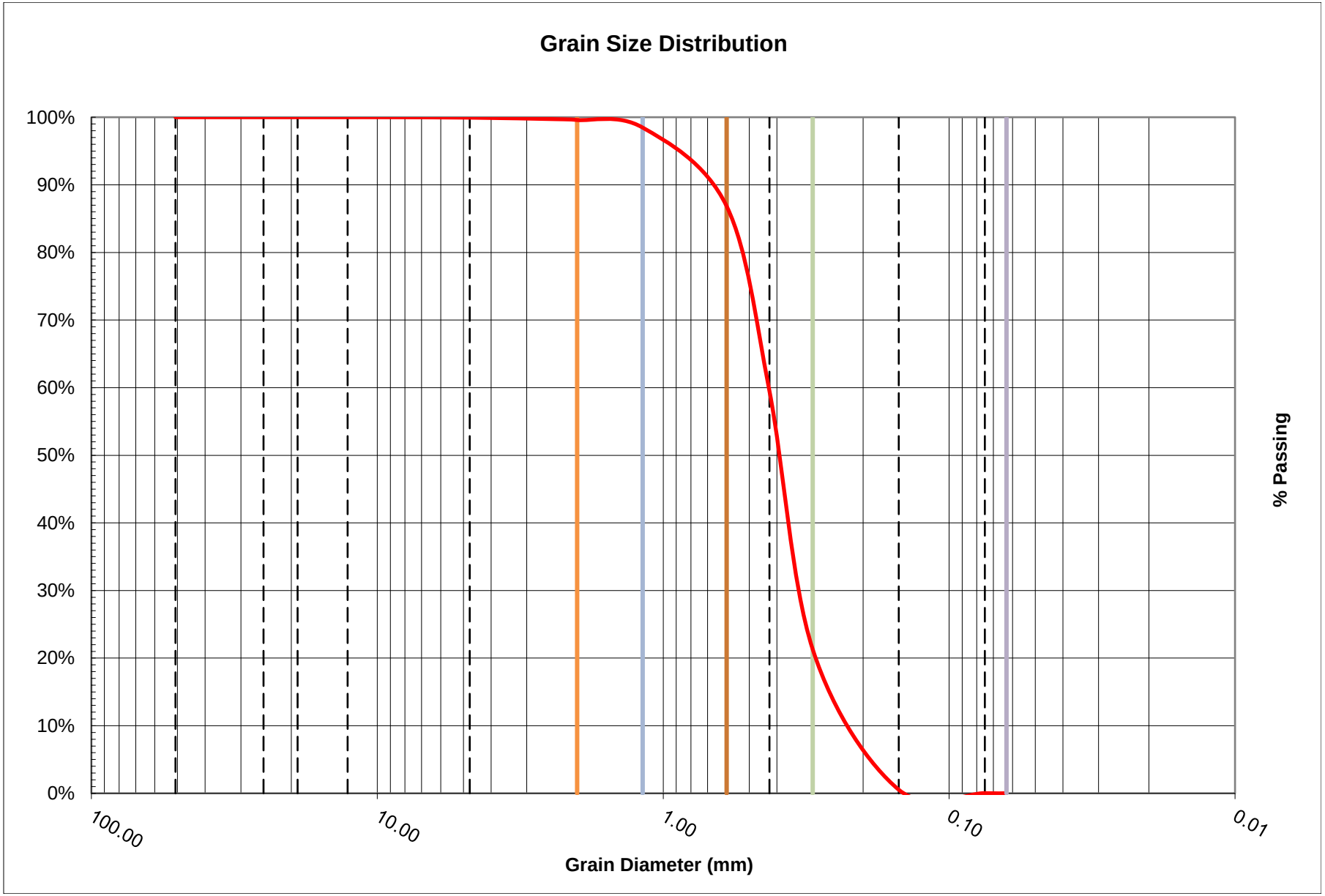
Grain Size Distribution
100%
90%
80%
70%
60%
50%
40%
30%
20%
10%
0%
% Passing
100.00
10.00
1.00
0.10
0.01
Grain Diameter (mm)

Lab Number 1086072816 Sample # Station:

Sieve Size and Percent passing for Soil Samples

Sample Size = 4544.8 grams

Sieve		Mass of soil		* based on Minitial					
No. (US std)	size (mm)	with pan (g)	w/o pan (g)	% retained	sum(% retained)	% passing			
2"	50.80			0.00%	0.00%	100.00%	D_{100}		
1"	25.00		350.5	7.71%	7.71%	92.29%	D_{84}	6.31	1 std deviation greater than median
3/4"	19.00		91.9	2.02%	9.73%	90.27%	D_{60}	0.18	
1/2"	12.70		62.7	1.38%	11.11%	88.89%	D_{50}	0.14	Median size
3/8"	9.50		30.8	0.68%	11.79%	88.21%	D_{30}	0.09	
#4	4.75		324.6	7.14%	18.93%	81.07%	D_{16}	0.07	1 std deviation less than median
#8	2.36		160	3.52%	22.45%	77.55%	D_{10}	0.08	Effective Size
#10	2.00		46.4	1.02%	23.47%	76.53%	C_u	2.42	Uniformity coefficient
#16	1.18		93.1	2.05%	25.52%	74.48%	C_c	0.64	Coefficient of gradation
#30	0.60		50.7	1.12%	26.64%	73.36%			
#40	0.425		51.5	1.13%	27.77%	72.23%	gap graded		Particle size distribution curve
#50	0.30		59.9	1.32%	29.09%	70.91%			
#100	0.150		708.2	15.58%	44.67%	55.33%			
#200	0.075		1738.0	38.24%	82.90%	17.10%			
#230	0.063		288.9	6.36%	89.26%	10.74%			
pan	--		488.2	10.74%	100.00%	0.00%			
	Totals	0	4545.4	--	--	--			

Total weight % Difference = 0.0 %

Notes
Clay clods made up virtually all of the sand and gravel grain sizes.

Sample location

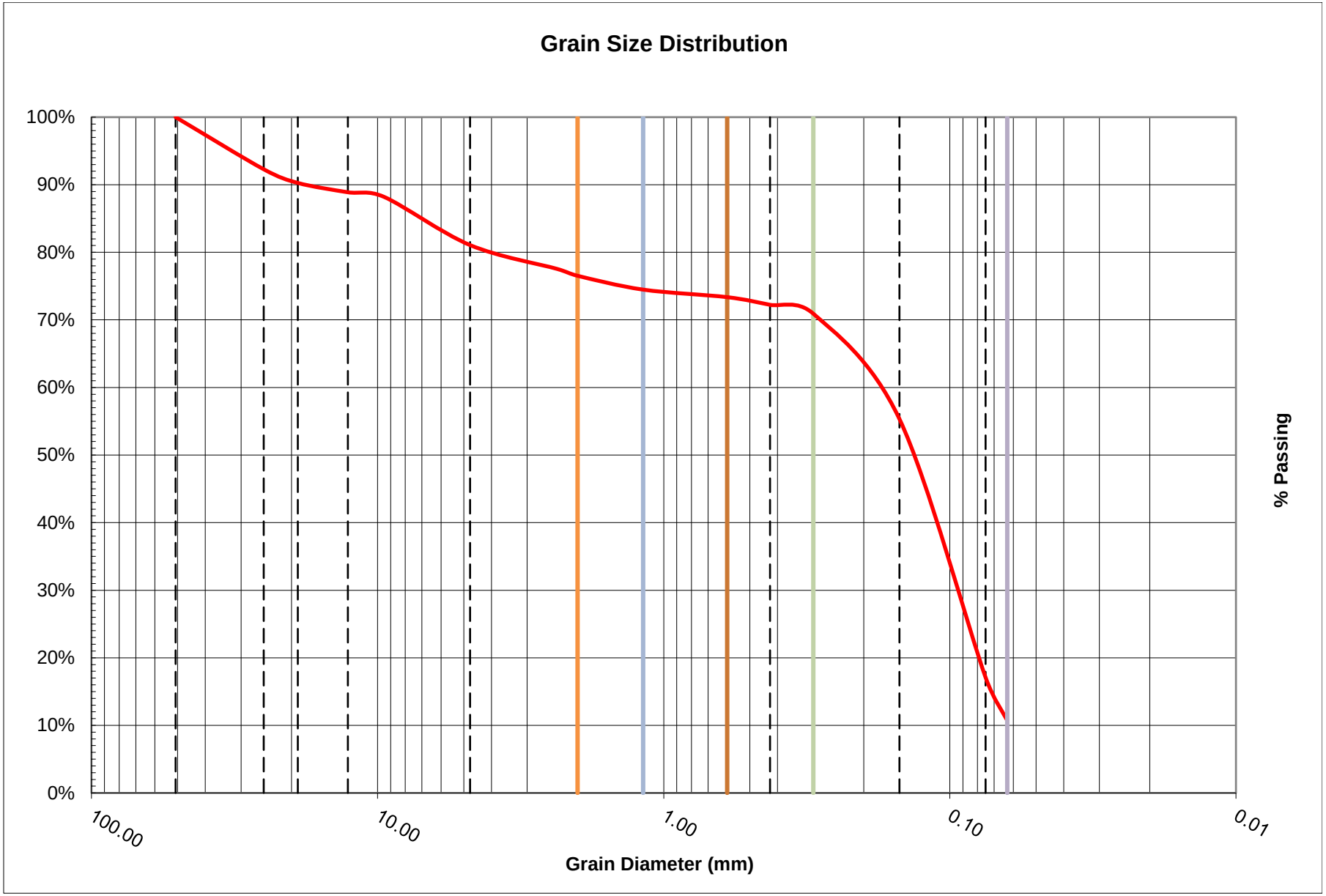
Grain Size Distribution
100%
90%
80%
70%
60%
50%
40%
30%
20%
10%
0%
% Passing
100.00
10.00
1.00
0.10
0.01
Grain Diameter (mm)

Lab Number 1088070716 Sample # bank Station:

Sieve Size and Percent passing for Soil Samples

Sample Size = 3822.8 grams

Sieve		Mass of soil		* based on Minitial					
No. (US std)	size (mm)	with pan (g)	w/o pan (g)	% retained	sum(% retained)	% passing			
2"	50.80			0.00%	0.00%	100.00%	D_{100}		
1"	25.00			0.00%	0.00%	100.00%	D_{84}	0.26	1 std deviation greater than median
3/4"	19.00			0.00%	0.00%	100.00%	D_{60}	0.21	
1/2"	12.70			0.00%	0.00%	100.00%	D_{50}	0.19	Median size
3/8"	9.50		0.8	0.02%	0.02%	99.98%	D_{30}	0.16	
#4	4.75		10.6	0.28%	0.30%	99.70%	D_{16}	0.11	1 std deviation less than median
#8	2.36		19.5	0.51%	0.81%	99.19%	D_{10}	0.08	Effective Size
#10	2.00		8.2	0.21%	1.02%	98.98%	C_u	2.53	Uniformity coefficient
#16	1.18		15	0.39%	1.42%	98.58%	C_c	1.44	Coefficient of gradation
#30	0.60		11.5	0.30%	1.72%	98.28%			
#40	0.425		11.2	0.29%	2.01%	97.99%	poorly graded		Particle size distribution curve
#50	0.30		26.9	0.70%	2.71%	97.29%			
#100	0.150		2833.4	74.12%	76.83%	23.17%			
#200	0.075		599.8	15.69%	92.52%	7.48%			
#230	0.063		102.7	2.69%	95.21%	4.79%			
pan	--		183.3	4.79%	100.00%	0.00%			
	Totals	0	3822.9	--	--	--			

Total weight % Difference = 0.0 %

Notes

Sample location

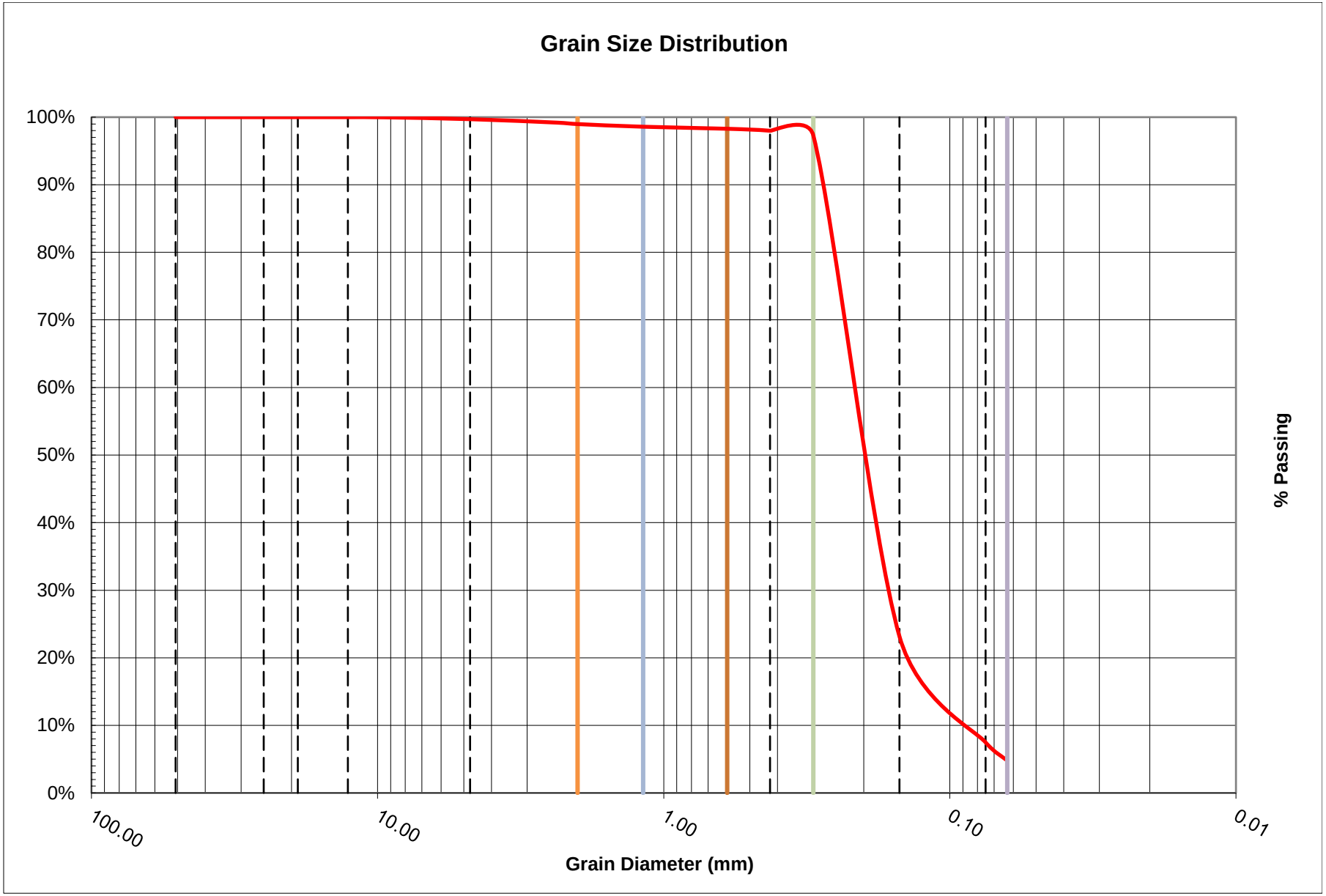
Grain Size Distribution
100%
90%
80%
70%
60%
50%
40%
30%
20%
10%
0%
% Passing
100.00
10.00
1.00
0.10
0.01
Grain Diameter (mm)

Lab Number 1091072816 Sample # Station:

Sieve Size and Percent passing for Soil Samples

Sample Size = 5064.1 grams

Sieve		Mass of soil		* based on Minitial					
No. (US std)	size (mm)	with pan (g)	w/o pan (g)	% retained	sum(% retained)	% passing			
2"	50.80			0.00%	0.00%	100.00%	D_{100}		
1"	25.00			0.00%	0.00%	100.00%	D_{84}	0.59	1 std deviation greater than median
3/4"	19.00			0.00%	0.00%	100.00%	D_{75}	0.53	
1/2"	12.70			0.00%	0.00%	100.00%	D_{60}	0.44	Median size
3/8"	9.50			0.00%	0.00%	100.00%	D_{50}	0.40	
#4	4.75		3.1	0.06%	0.06%	99.94%	D_{30}	0.33	1 std deviation less than median
#8	2.36		10	0.20%	0.26%	99.74%	D_{16}	0.26	Effective Size
#10	2.00		5.2	0.10%	0.36%	99.64%	D_{10}	0.20	Uniformity coefficient
#16	1.18		50.4	1.00%	1.36%	98.64%	C_u	2.16	Coefficient of gradation
#30	0.60		632.1	12.50%	13.86%	86.14%	C_c	1.20	
#40	0.425		1498.8	29.64%	43.49%	56.51%	gap graded		Particle size distribution curve
#50	0.30		1843.9	36.46%	79.95%	20.05%			
#100	0.150		924.4	18.28%	98.23%	1.77%			
#200	0.075		63.3	1.25%	99.48%	0.52%			
#230	0.063		8.1	0.16%	99.64%	0.36%			
pan	--		18.1	0.36%	100.00%	0.00%			
	Totals	0	5057.4	--	--	--			

Total weight % Difference = 0.1 %

Notes

Sample location

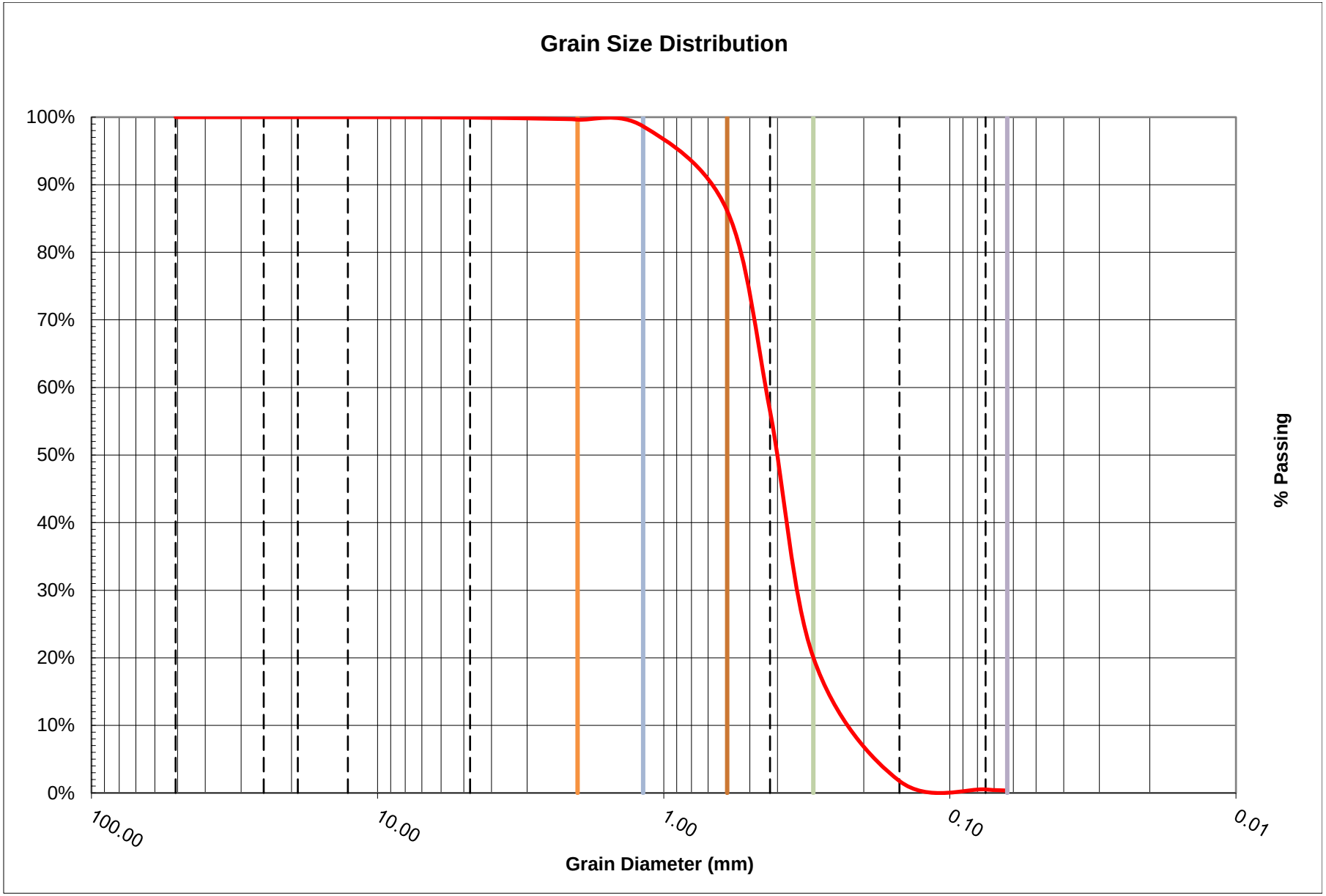
Grain Size Distribution
100%
90%
80%
70%
60%
50%
40%
30%
20%
10%
0%
% Passing
100.00
10.00
1.00
0.10
0.01
Grain Diameter (mm)

Lab Number 1094072816 Sample # Station:

Sieve Size and Percent passing for Soil Samples

Sample Size = 2399.5 grams

Sieve		Mass of soil		* based on Minitial					
No. (US std)	size (mm)	with pan (g)	w/o pan (g)	% retained	sum(% retained)	% passing			
2"	50.80			0.00%	0.00%	100.00%	D_{100}		
1"	25.00		681.4	28.31%	28.31%	71.69%	D_{84}	34.03	1 std deviation greater than median
3/4"	19.00		58.8	2.44%	30.75%	69.25%	D_{60}	8.84	
1/2"	12.70		145.4	6.04%	36.79%	63.21%	D_{50}	4.81	Median size
3/8"	9.50		48.7	2.02%	38.81%	61.19%	D_{30}	0.21	
#4	4.75		274.2	11.39%	50.21%	49.79%	D_{16}	0.09	1 std deviation less than median
#8	2.36		133.4	5.54%	55.75%	44.25%	D_{10}	0.06	Effective Size
#10	2.00		33.2	1.38%	57.13%	42.87%	C_u	137.12	Uniformity coefficient
#16	1.18		67.3	2.80%	59.92%	40.08%	C_c	0.08	Coefficient of gradation
#30	0.60		51.0	2.12%	62.04%	37.96%			
#40	0.425		40.0	1.66%	63.70%	36.30%	gap graded		Particle size distribution curve
#50	0.30		35.8	1.49%	65.19%	34.81%			
#100	0.150		230.4	9.57%	74.76%	25.24%			
#200	0.075		285.4	11.86%	86.62%	13.38%			
#230	0.063		93.7	3.89%	90.51%	9.49%			
pan	--		228.4	9.49%	100.00%	0.00%			
	Totals	0	2407.1	--	--	--			

Total weight % Difference = 0.3 %

Notes
Weight of organics subtracted out of sample size cell
Weight of pan subtracted out of pan cell
All samples above the #50 seive consisted of sediment clods

Sample location

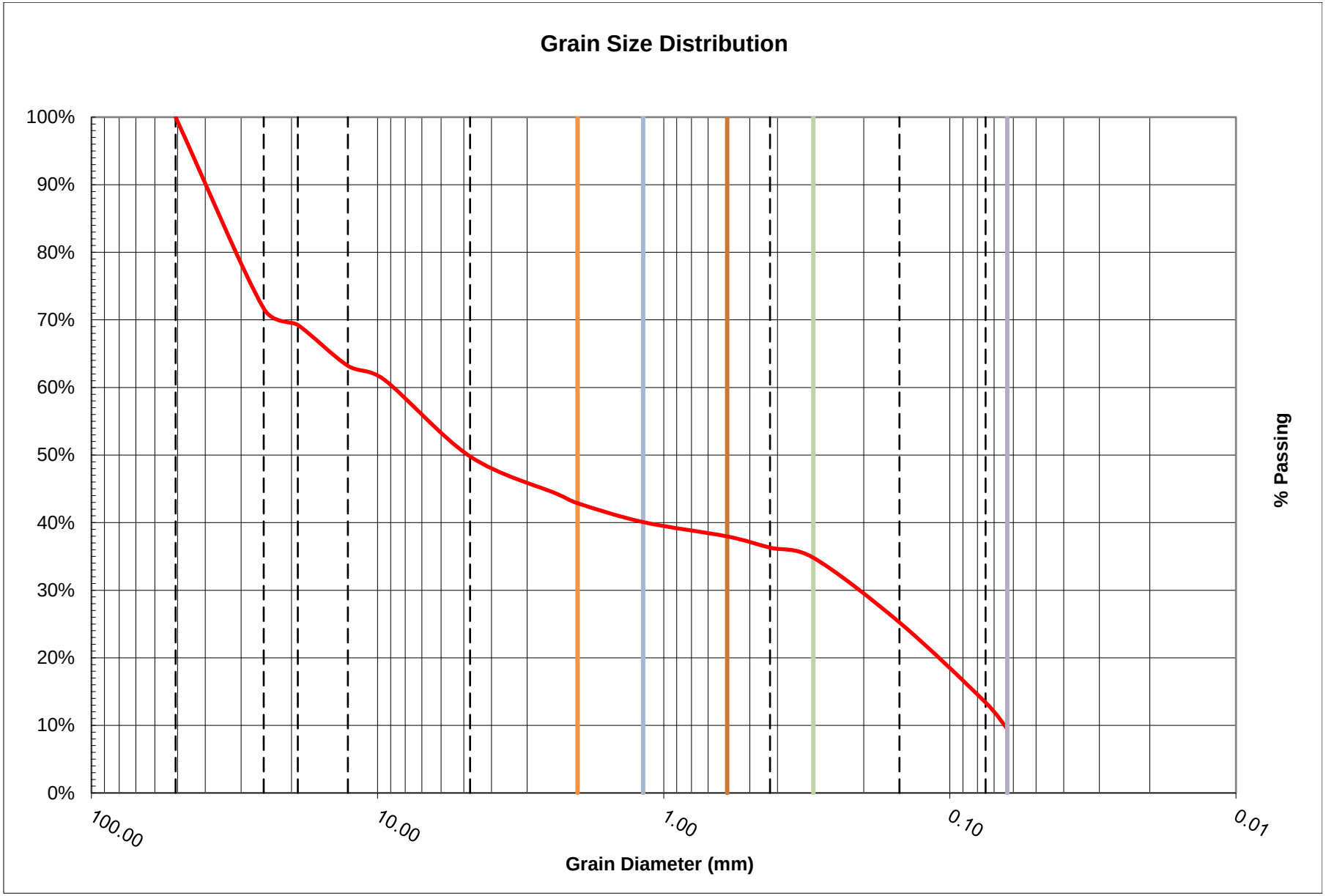
Grain Size Distribution
100%
90%
80%
70%
60%
50%
40%
30%
20%
10%
0%
% Passing
100.00
10.00
1.00
0.10
0.01
Grain Diameter (mm)

Lab Number CO1097070716 Sample # CO-1097 Station:

Sieve Size and Percent passing for Soil Samples

Sample Size = 4520.2 grams

Sieve		Mass of soil		* based on Minitial					
No. (US std)	size (mm)	with pan (g)	w/o pan (g)	% retained	sum(% retained)	% passing			
2"	50.80			0.00%	0.00%	100.00%	D_{100}		
1"	25.00			0.00%	0.00%	100.00%	D_{84}	0.60	1 std deviation greater than median
3/4"	19.00			0.00%	0.00%	100.00%	D_{75}	0.54	
1/2"	12.70			0.00%	0.00%	100.00%	D_{60}	0.45	Median size
3/8"	9.50		2.2	0.05%	0.05%	99.95%	D_{50}	0.41	
#4	4.75		9.7	0.21%	0.26%	99.74%	D_{30}	0.33	1 std deviation less than median
#8	2.36		31.3	0.69%	0.96%	99.04%	D_{16}	0.26	Effective Size
#10	2.00		14.0	0.31%	1.27%	98.73%	D_{10}	0.21	Uniformity coefficient
#16	1.18		84.7	1.88%	3.14%	96.86%	C_u	2.14	Coefficient of gradation
#30	0.60		559.7	12.39%	15.53%	84.47%	C_c	1.16	
#40	0.425		1344.3	29.76%	45.29%	54.71%	poorly graded		Particle size distribution curve
#50	0.30		1599.2	35.40%	80.70%	19.30%			
#100	0.150		829.6	18.37%	99.07%	0.93%			
#200	0.075		39.4	0.87%	99.94%	0.06%			
#230	0.063		1.4	0.03%	99.97%	0.03%			
pan	--		1.4	0.03%	100.00%	0.00%			
	Totals	0	4516.9	--	--	--			

Total weight % Difference = 0.1 %

Notes

Sample location

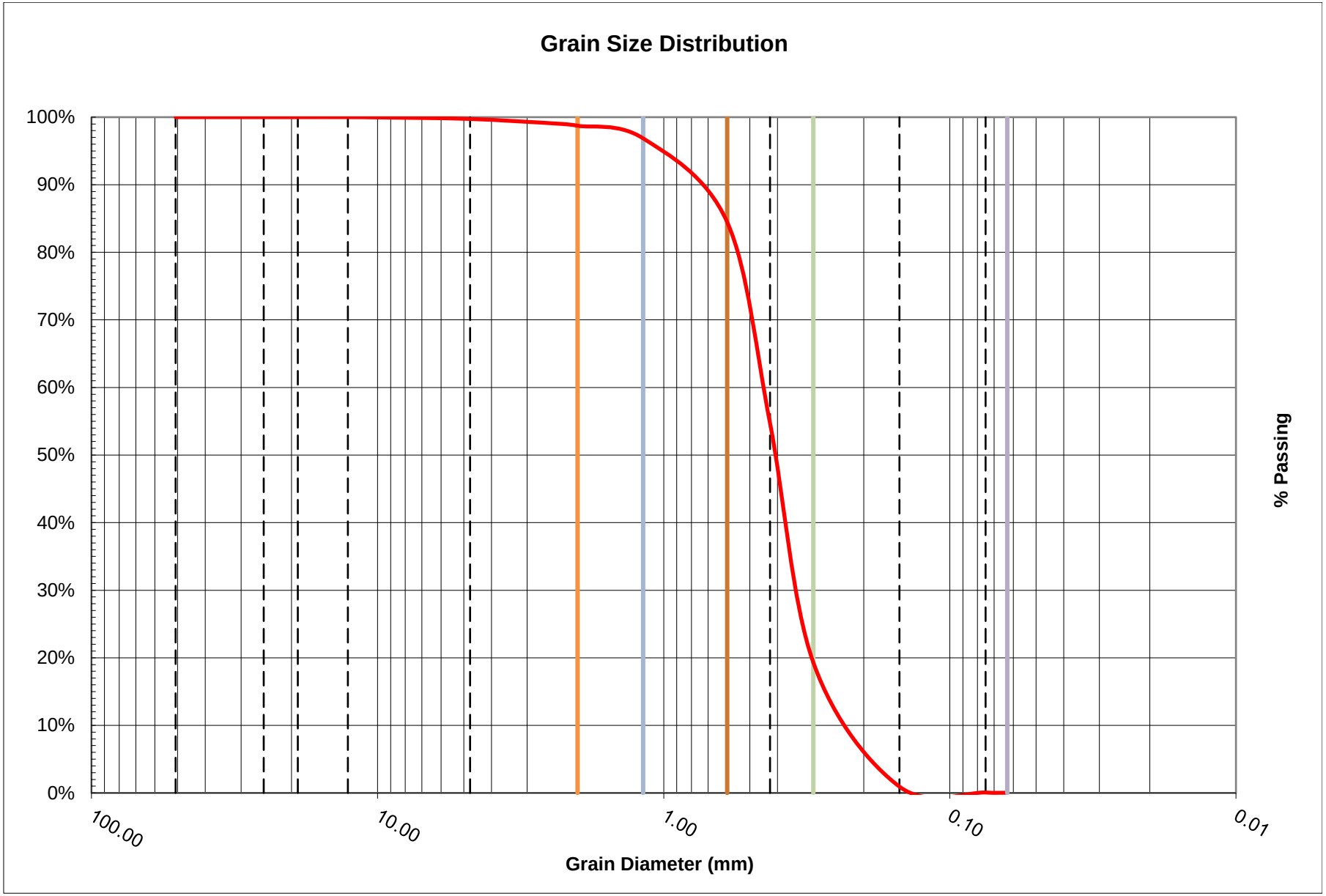
Grain Size Distribution
100%
90%
80%
70%
60%
50%
40%
30%
20%
10%
0%
% Passing
100.00
10.00
1.00
0.10
0.01
Grain Diameter (mm)

Lab Number RP1100070716 Sample # RP-1100 Station:

Sieve Size and Percent passing for Soil Samples

Sample Size = 2931.8 grams

Sieve		Mass of soil		* based on Minitial					
No. (US std)	size (mm)	with pan (g)	w/o pan (g)	% retained	sum(% retained)	% passing			
2"	50.80			0.00%	0.00%	100.00%	D_{100}		
1"	25.00			0.00%	0.00%	100.00%	D_{84}	0.50	1 std deviation greater than median
3/4"	19.00			0.00%	0.00%	100.00%	D_{75}	0.42	
1/2"	12.70			0.00%	0.00%	100.00%	D_{60}	0.37	Median size
3/8"	9.50		5.5	0.19%	0.19%	99.81%	D_{50}	0.34	
#4	4.75		5.7	0.19%	0.38%	99.62%	D_{30}	0.28	1 std deviation less than median
#8	2.36		11.1	0.38%	0.76%	99.24%	D_{16}	0.20	Effective Size
#10	2.00		4.5	0.15%	0.91%	99.09%	D_{10}	0.18	Uniformity coefficient
#16	1.18		24.1	0.82%	1.74%	98.26%	C_u	2.07	Coefficient of gradation
#30	0.60		156.4	5.33%	7.07%	92.93%	C_c	1.15	
#40	0.425		472.5	16.11%	23.17%	76.83%	poorly graded		Particle size distribution curve
#50	0.30		1259.4	42.93%	66.11%	33.89%			
#100	0.150		942.4	32.13%	98.23%	1.77%			
#200	0.075		48.0	1.64%	99.87%	0.13%			
#230	0.063		1.9	0.06%	99.94%	0.06%			
pan	--		1.9	0.06%	100.00%	0.00%			
	Totals	0	2933.4	--	--	--			

Total weight % Difference = 0.1 %

Notes

Sample location

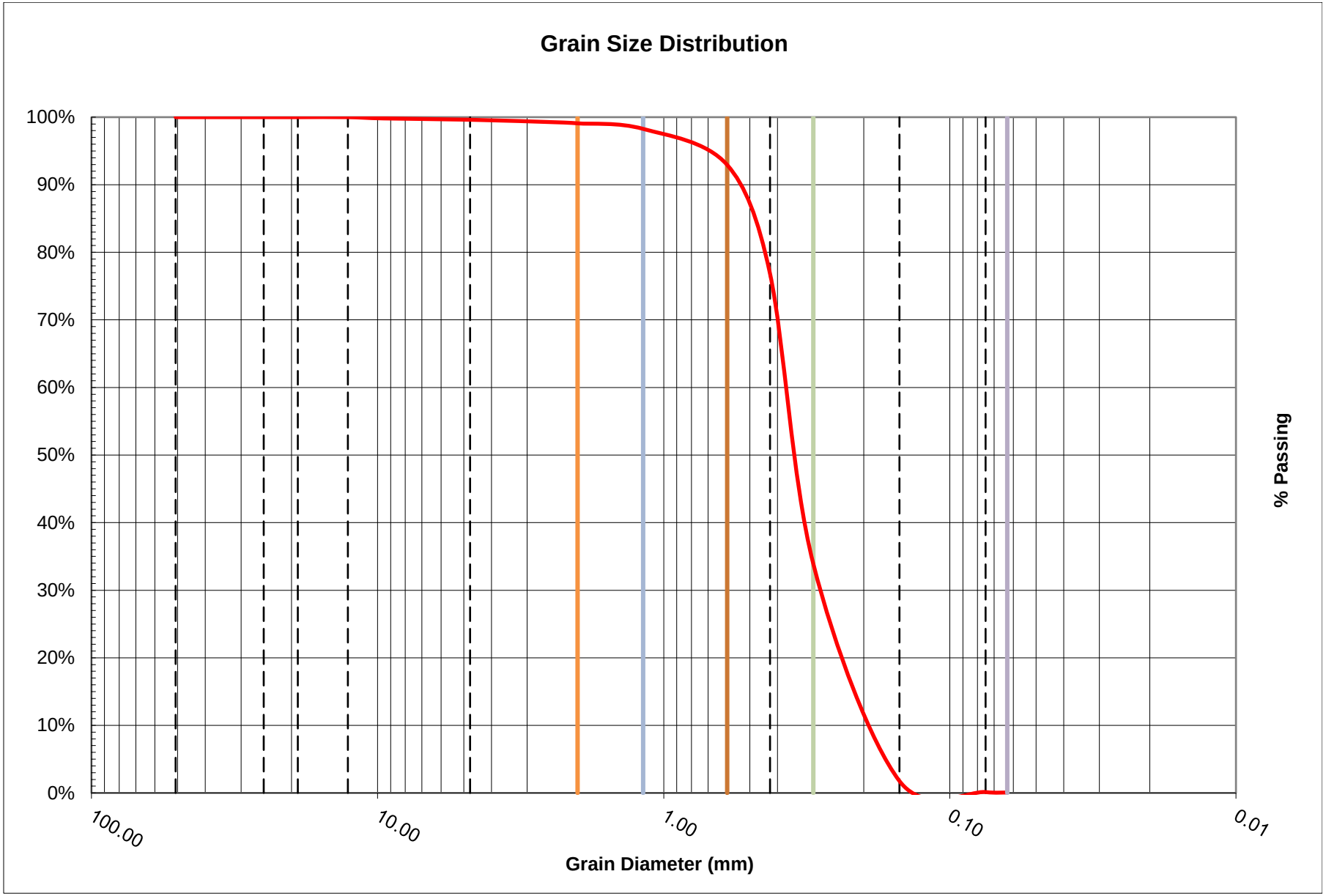
Grain Size Distribution
100%
90%
80%
70%
60%
50%
40%
30%
20%
10%
0%
% Passing
100.00
10.00
1.00
0.10
0.01
Grain Diameter (mm)

Lab Number 110401070116 Sample # 1 Station:

Sieve Size and Percent passing for Soil Samples

Sample Size = 5464.1 grams

Sieve		Mass of soil		* based on Minitial					
No. (US std)	size (mm)	with pan (g)	w/o pan (g)	% retained	sum(% retained)	% passing			
2"	50.80			0.00%	0.00%	100.00%	D_{100}		
1"	25.00			0.00%	0.00%	100.00%	D_{84}	0.78	1 std deviation greater than median
3/4"	19.00			0.00%	0.00%	100.00%	D_{75}	0.60	
1/2"	12.70		1.1	0.02%	0.02%	99.98%	D_{60}	0.52	Median size
3/8"	9.50		1.0	0.02%	0.04%	99.96%	D_{50}	0.47	
#4	4.75		12.3	0.23%	0.26%	99.74%	D_{30}	0.38	1 std deviation less than median
#8	2.36		28.8	0.53%	0.79%	99.21%	D_{16}	0.32	Effective Size
#10	2.00		13.8	0.25%	1.04%	98.96%	D_{10}	0.26	Uniformity coefficient
#16	1.18		110.3	2.02%	3.06%	96.94%	C_u	1.96	Coefficient of gradation
#30	0.60		1156.1	21.17%	24.23%	75.77%	C_c	1.04	
#40	0.425		1965.9	36.00%	60.23%	39.77%	gap graded		Particle size distribution curve
#50	0.30		1511.1	27.67%	87.90%	12.10%			
#100	0.150		596.3	10.92%	98.82%	1.18%			
#200	0.075		37.1	0.68%	99.50%	0.50%			
#230	0.063		6.7	0.12%	99.63%	0.37%			
pan	--		20.4	0.37%	100.00%	0.00%			
	Totals	0	5460.9	--	--	--			
organics			0.6						

Total weight % Difference = 0.1 %

Notes

Sample location

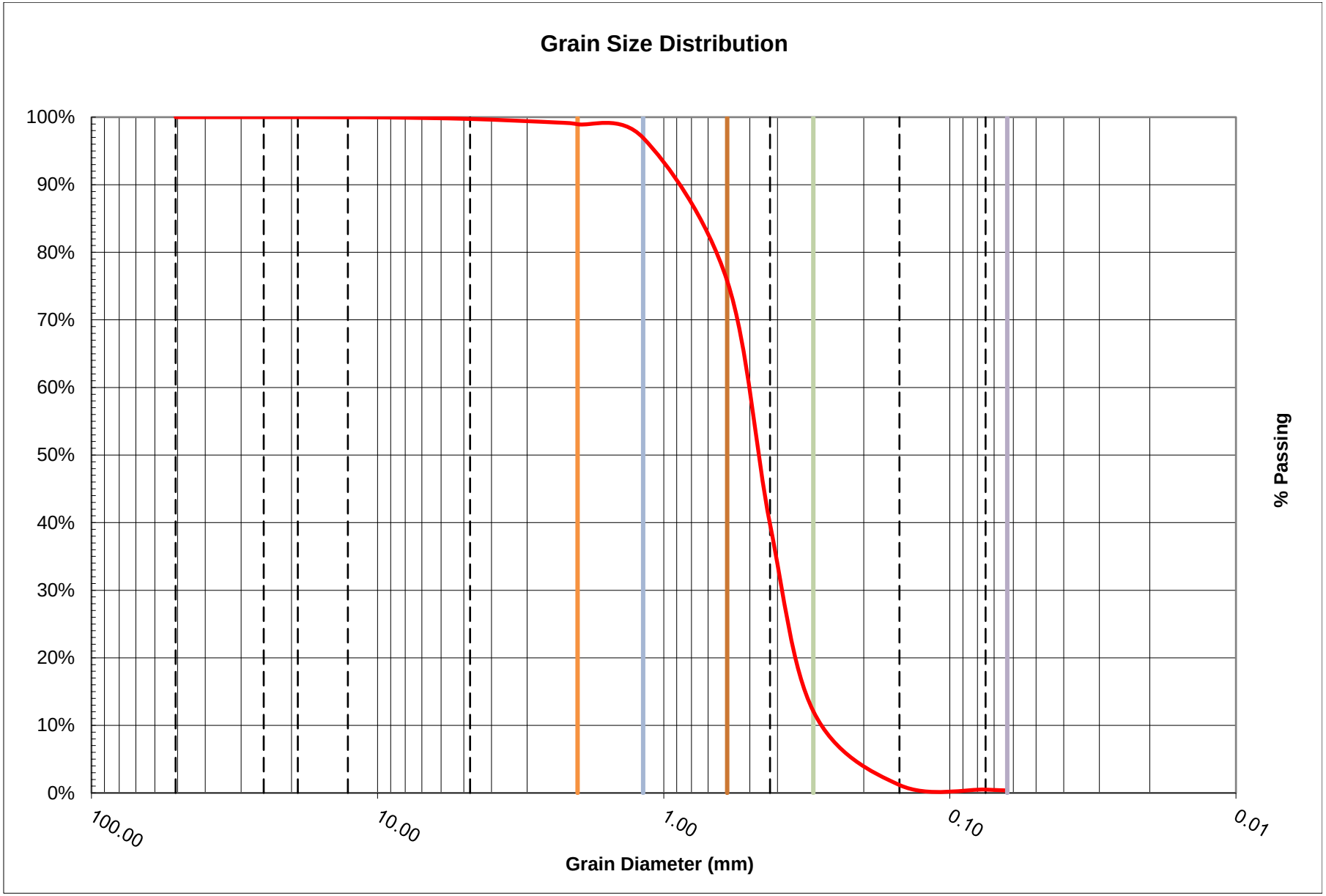
Grain Size Distribution
100%
90%
80%
70%
60%
50%
40%
30%
20%
10%
0%
% Passing
100.00
10.00
1.00
0.10
0.01
Grain Diameter (mm)

Lab Number LJ10070116 Sample # LJ-10 Station:

Sieve Size and Percent passing for Soil Samples

Sample Size = 2185.9 grams

Sieve		Mass of soil		* based on Minitial					
No. (US std)	size (mm)	with pan (g)	w/o pan (g)	% retained	sum(% retained)	% passing			
2"	50.80			0.00%	0.00%	100.00%	D_{100}	32.00	
1"	25.00		41.1	1.88%	1.88%	98.12%	D_{84}	1.56	1 std deviation greater than median
3/4"	19.00		83.2	3.81%	5.69%	94.31%	D_{60}	0.14	
1/2"	12.70		91.2	4.17%	9.86%	90.14%	D_{50}	0.12	Median size
3/8"	9.50		21.6	0.99%	10.85%	89.15%	D_{30}	0.08	
#4	4.75		39.2	1.79%	12.64%	87.36%	D_{16}	0.07	1 std deviation less than median
#8	2.36		16	0.73%	13.37%	86.63%	D_{10}	0.19	Effective Size
#10	2.00		2.5	0.11%	13.49%	86.51%	C_u	0.74	Uniformity coefficient
#16	1.18		115.6	5.29%	18.77%	81.23%	C_c	0.22	Coefficient of gradation
#30	0.60		75.3	3.44%	22.22%	77.78%			
#40	0.425		43.9	2.01%	24.23%	75.77%	poorly graded		Particle size distribution curve
#50	0.30		42	1.92%	26.15%	73.85%			
#100	0.150		251.7	11.51%	37.66%	62.34%			
#200	0.075		732.7	33.52%	71.18%	28.82%			
#230	0.063		263.8	12.07%	83.25%	16.75%			
pan	--		366.2	16.75%	100.00%	0.00%			
	Totals	0	2186	--	--	--			

Total weight % Difference = 0.0 %

Notes
largest particle (clay clod) has a weight of 24.8 g
a axis 35 mm
b axis 32 mm
c axis 22 mm

Sample location

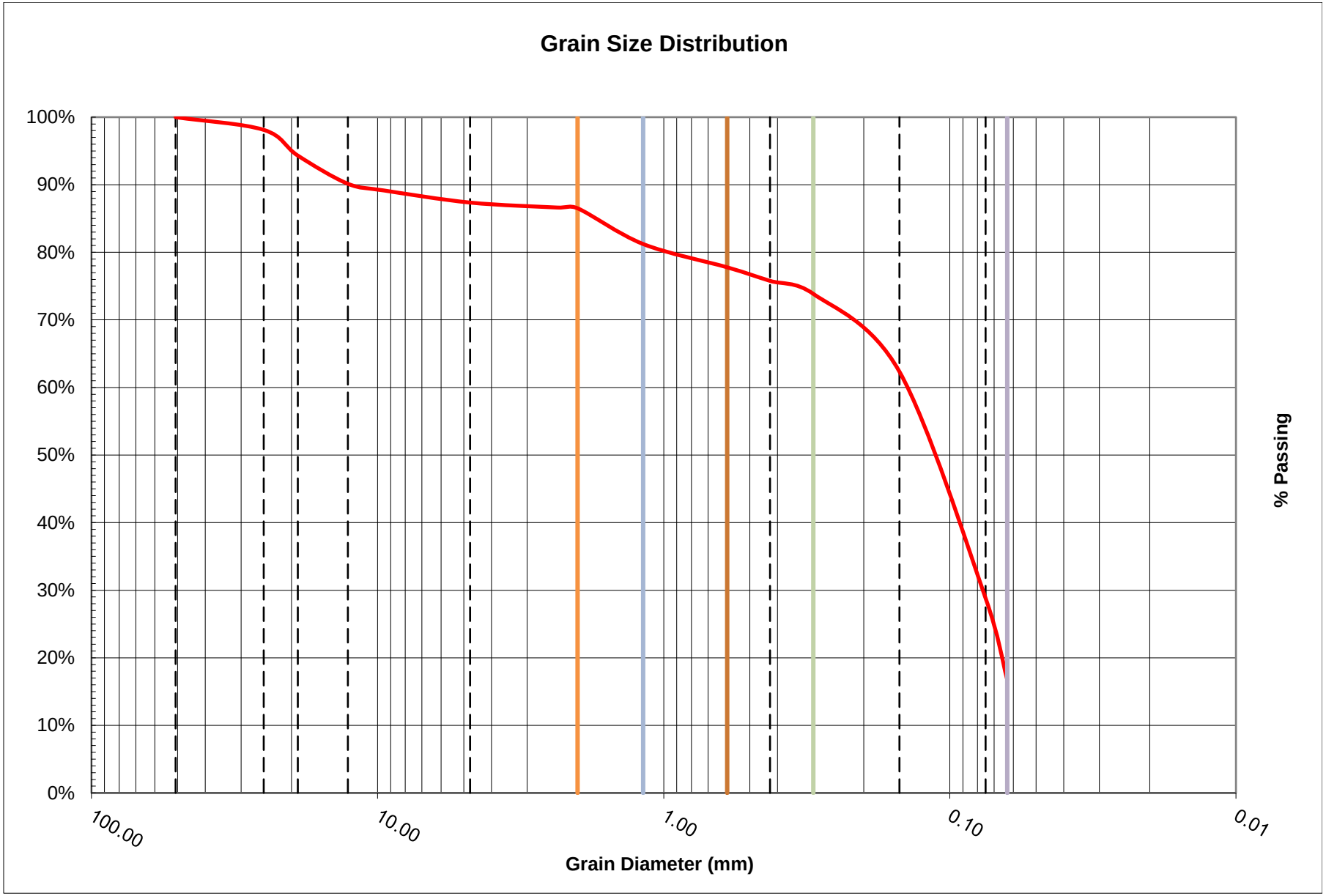
Grain Size Distribution
100%
90%
80%
70%
60%
50%
40%
30%
20%
10%
0%
% Passing
100.00
10.00
1.00
0.10
0.01
Grain Diameter (mm)

Lab Number LJ1801070116 Sample # 1 Station:

Sieve Size and Percent passing for Soil Samples

Sample Size = 3902.2 grams

Sieve		Mass of soil		* based on Minitial					
No. (US std)	size (mm)	with pan (g)	w/o pan (g)	% retained	sum(% retained)	% passing			
2"	50.80			0.00%	0.00%	100.00%	D_{100}		
1"	25.00			0.00%	0.00%	100.00%	D_{84}	0.57	1 std deviation greater than median
3/4"	19.00			0.00%	0.00%	100.00%	$D7_5$	0.50	
1/2"	12.70			0.00%	0.00%	100.00%	D_{60}	0.41	Median size
3/8"	9.50		3.4	0.09%	0.09%	99.91%	D_{50}	0.38	
#4	4.75		17.7	0.45%	0.54%	99.46%	D_{30}	0.32	1 std deviation less than median
#8	2.36		25.3	0.65%	1.19%	98.81%	D_{16}	0.24	Effective Size
#10	2.00		8.9	0.23%	1.42%	98.58%	D_{10}	0.20	Uniformity coefficient
#16	1.18		61.9	1.59%	3.00%	97.00%	C_u	2.03	Coefficient of gradation
#30	0.60		397.8	10.20%	13.20%	86.80%	C_c	1.24	
#40	0.425		862.3	22.11%	35.31%	64.69%	gap graded		Particle size distribution curve
#50	0.30		1644.7	42.16%	77.47%	22.53%			
#100	0.150		851.6	21.83%	99.31%	0.69%			
#200	0.075		21.1	0.54%	99.85%	0.15%			
#230	0.063		2.9	0.07%	99.92%	0.08%			
pan	--		3.1	0.08%	100.00%	0.00%			
	Totals	0	3900.7	--	--	--			
organics			1.4						

Total weight % Difference = 0.0 %

Notes

Sample location

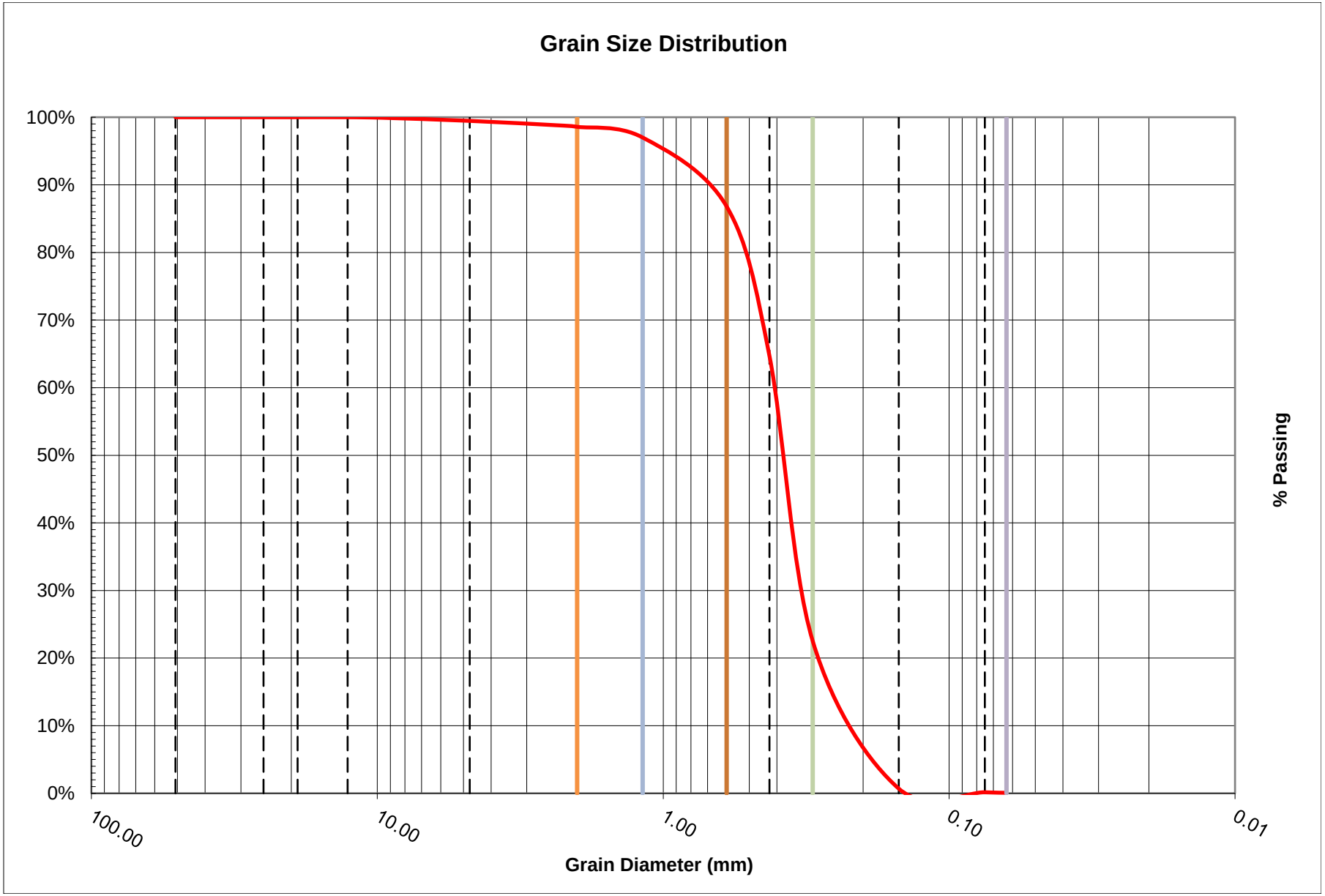
Grain Size Distribution
100%
90%
80%
70%
60%
50%
40%
30%
20%
10%
0%
% Passing
100.00
10.00
1.00
0.10
0.01
Grain Diameter (mm)

Lab Number CO1164070716 Sample # CO-1164 Station:

Sieve Size and Percent passing for Soil Samples

Sample Size = 3061 grams

Sieve		Mass of soil		* based on Minitial					
No. (US std)	size (mm)	with pan (g)	w/o pan (g)	% retained	sum(% retained)	% passing			
2"	50.80			0.00%	0.00%	100.00%	D_{100}		
1"	25.00			0.00%	0.00%	100.00%	D_{84}	0.58	1 std deviation greater than median
3/4"	19.00			0.00%	0.00%	100.00%	D_{75}	0.53	
1/2"	12.70			0.00%	0.00%	100.00%	D_{60}	0.45	Median size
3/8"	9.50			0.00%	0.00%	100.00%	D_{50}	0.41	
#4	4.75		2.5	0.08%	0.08%	99.92%	D_{30}	0.34	1 std deviation less than median
#8	2.36		7.1	0.23%	0.31%	99.69%	D_{16}	0.30	Effective Size
#10	2.00		3.6	0.12%	0.43%	99.57%	D_{10}	0.22	Uniformity coefficient
#16	1.18		23.4	0.76%	1.20%	98.80%	C_u	2.01	Coefficient of gradation
#30	0.60		333.3	10.89%	12.08%	87.92%	C_c	1.15	
#40	0.425		1022.6	33.40%	45.48%	54.52%	poorly graded		Particle size distribution curve
#50	0.30		1170.8	38.24%	83.71%	16.29%			
#100	0.150		458.3	14.97%	98.68%	1.32%			
#200	0.075		31.9	1.04%	99.72%	0.28%			
#230	0.063		3.8	0.12%	99.85%	0.15%			
pan	--		4.7	0.15%	100.00%	0.00%			
	Totals	0	3062	--	--	--			

Total weight % Difference = 0.0 %

Notes

Sample location

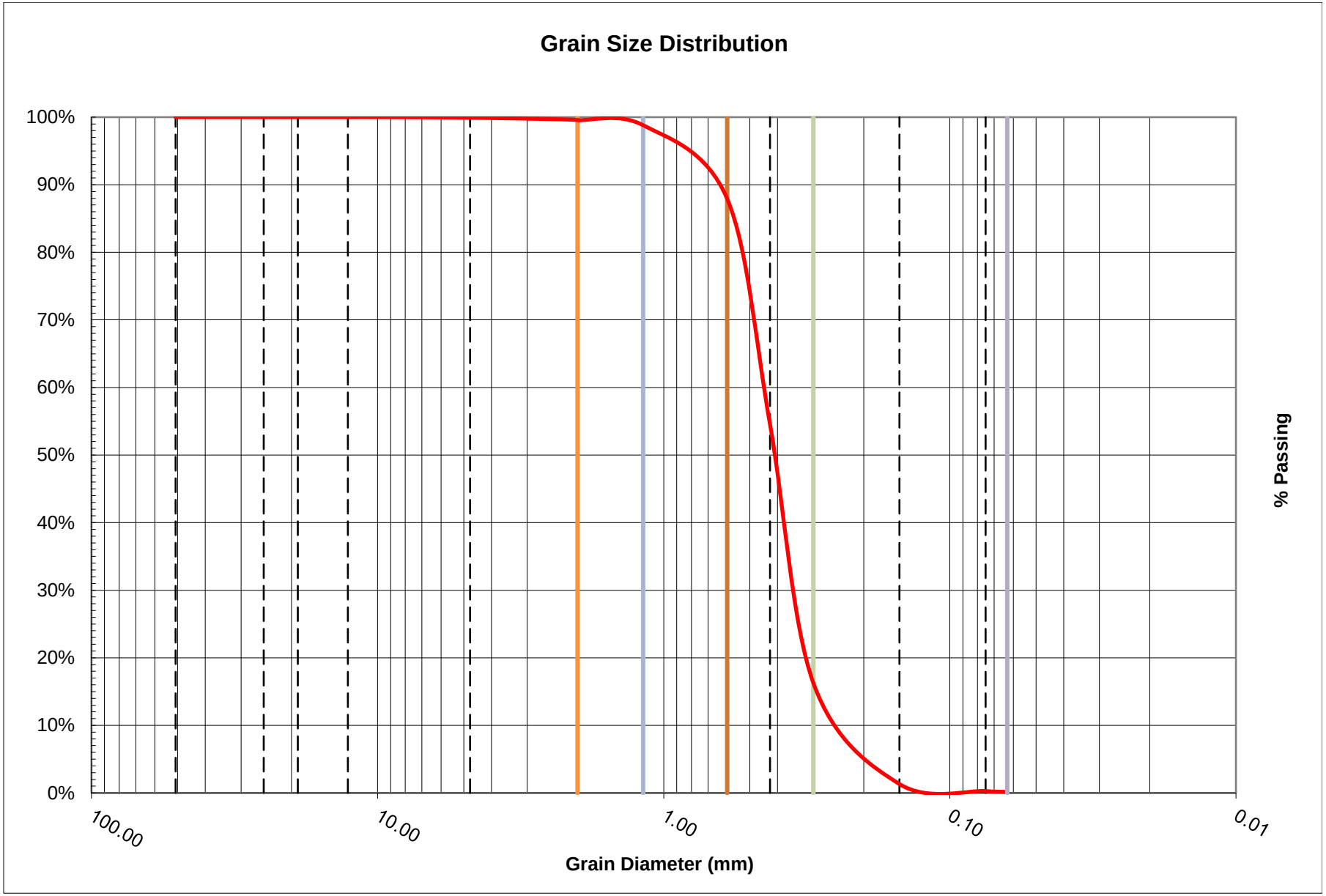
Grain Size Distribution
100%
90%
80%
70%
60%
50%
40%
30%
20%
10%
0%
% Passing
100.00
10.00
1.00
0.10
0.01
Grain Diameter (mm)

Lab Number RP1170070716 Sample # 1 Station:

Sieve Size and Percent passing for Soil Samples

Sample Size = 2904.3 grams

Sieve		Mass of soil		* based on Minitial					
No. (US std)	size (mm)	with pan (g)	w/o pan (g)	% retained	sum(% retained)	% passing			
2"	50.80			0.00%	0.00%	100.00%	D_{100}		
1"	25.00		1357.4	46.62%	46.62%	53.38%	D_{84}	39.83	1 std deviation greater than median
3/4"	19.00		318	10.92%	57.54%	42.46%	D_{60}	27.65	
1/2"	12.70		286.0	9.82%	67.36%	32.64%	D_{50}	22.96	Median size
3/8"	9.50		75.8	2.60%	69.96%	30.04%	D_{30}	9.45	
#4	4.75		136.3	4.68%	74.64%	25.36%	D_{16}	1.19	1 std deviation less than median
#8	2.36		166.9	5.73%	80.38%	19.62%	D_{10}	0.23	Effective Size
#10	2.00		32.1	1.10%	81.48%	18.52%	C_u	122.71	Uniformity coefficient
#16	1.18		74.9	2.57%	84.05%	15.95%	C_c	14.33	Coefficient of gradation
#30	0.60		54.6	1.88%	85.93%	14.07%			
#40	0.425		30.3	1.04%	86.97%	13.03%	gap graded		Particle size distribution curve
#50	0.30		29	1.00%	87.96%	12.04%			
#100	0.150		143.6	4.93%	92.89%	7.11%			
#200	0.075		73.8	2.53%	95.43%	4.57%			
#230	0.063		24.9	0.86%	96.28%	3.72%			
pan	--		108.2	3.72%	100.00%	0.00%			
	Totals	0	2911.8	--	--	--			

Total weight % Difference = 0.3 %

Notes
organics 0.5 g
The entirety of this sample was clay and silt, but the sample was retained as clay clods on the sieves.
The sieves retained a large amount of organics (grasses and twigs) which were removed until the No. 10 sieve, and then they became too numerous to remove them all.

Sample location

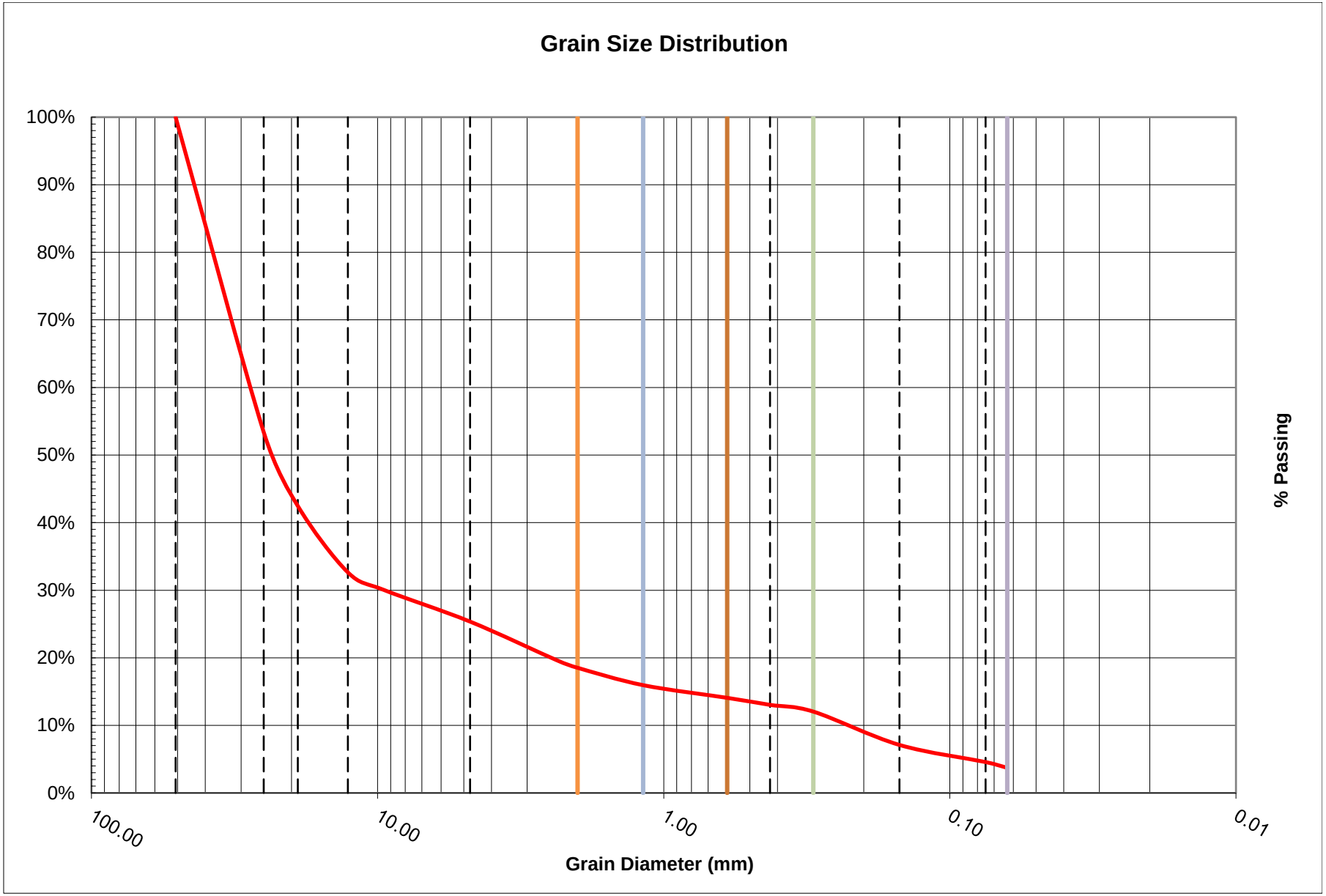
Grain Size Distribution
100%
90%
80%
70%
60%
50%
40%
30%
20%
10%
0%
% Passing
100.00
10.00
1.00
0.10
0.01
Grain Diameter (mm)

Lab Number 1183071916a Sample # bed Station:

Sieve Size and Percent passing for Soil Samples

Sample Size = 9710.9 grams

Sieve		Mass of soil		* based on Minitial								
No. (US std)	size (mm)	with pan (g)	w/o pan (g)	% retained	sum(% retained)	% passing						
	175					100.00%						
	128					51.49%						
	64					21.41%						
	50.8					16.49%						
2"	50.80		8124.3	83.51%	83.51%	16.49%	D_{100}	175.00		1.00	16 NA	2.24
1"	25.00		1432.5	14.73%	98.24%	1.76%	D_{84}	130.00	1 std deviation greater than median	0.84	18 19.00	2.11
3/4"	19.00		109.1	1.12%	99.36%	0.64%	D_{60}	120.00		0.60	18 19.00	2.08
1/2"	12.70		30.3	0.31%	99.67%	0.33%	D_{50}	123.68	Median size	0.50	17 18.00	2.09
3/8"	9.50		12.9	0.13%	99.80%	0.20%	D_{30}	78.01		0.30	17 18.00	1.89
#4	4.75		6.6	0.07%	99.87%	0.13%	D_{16}	49.61	1 std deviation less than median	0.16	15 16.00	1.70
#8	2.36		3.1	0.03%	99.90%	0.10%	D_{10}	37.16	Effective Size	0.10	15 16.00	1.57
#10	2.00		0.6	0.01%	99.91%	0.09%	C_u	3.23	Uniformity coefficient			
#16	1.18		1.3	0.01%	99.92%	0.08%	C_c	1.36	Coefficient of gradation			
#30	0.60		0.9	0.01%	99.93%	0.07%						
#40	0.425		0.9	0.01%	99.94%	0.06%	poorly graded		Particle size distribution curve			
#50	0.30		1.4	0.01%	99.96%	0.04%						
#100	0.150		1.8	0.02%	99.97%	0.03%						
#200	0.075		1.3	0.01%	99.99%	0.01%						
#230	0.063		0.4	0.00%	99.99%	0.01%						
pan	--		0.8	0.01%	100.00%	0.00%						
	Totals	0	9728.2	--	--	--						

Total weight % Difference = 0.2 %

Notes
sample is representative of armor layer on the river bed in this area
Ten rocks comprised the volume of material that did not pass through the #2 sieve
Information on these rocks is listed below

#	mass (g)	axis a (mm)	axis b (mm)	axis c (mm)	Desc
1	4718.7	195	175	139	large cobble
2	467.3	108	64	57	small cobble
3	515.5	95	83	75	small cobble
4	576	132	64	47	small cobble
5	461.9	99	68	56	small cobble
6	346.7	94	74	35	small cobble
7	282.1	94	58	39	very coarse gravel
8	317.3	94	75	46	small cobble
9	241.8	87	79	22	small cobble
10	196.3	82	63	38	very coarse gravel

Taking the ten largest rocks and sorting them by scale for pebble count template

#	mass	axis b	FISP US SA-97 scale category		Total mass	% retained	SUM (% re	% passing
			175	128				
1	4719		175	128	4718.7	48.51%	48.51%	51.49%
3	515.5		83	64	2926.5	30.08%	78.59%	21.41%
5	461.9		68	64				
6	346.7		74	64				
8	317.3		75	64				
9	241.8		79	64				
4	576		64	64				
2	467.3		64	64				
7	282.1		58	45	478.4	4.92%	83.51%	16.49%
10	196.3		63	45				

For gradation plot

Size (mm)	% passing
175	100.00%
128	51.49%
64	21.41%
50.8	16.49%
25.00	1.76%
19.00	0.64%
12.70	0.33%
9.50	0.20%
4.75	0.13%
2.36	0.10%
2.00	0.09%
1.18	0.08%
0.60	0.07%
0.425	0.06%
0.30	0.04%
0.150	0.03%
0.075	0.01%
0.063	0.01%

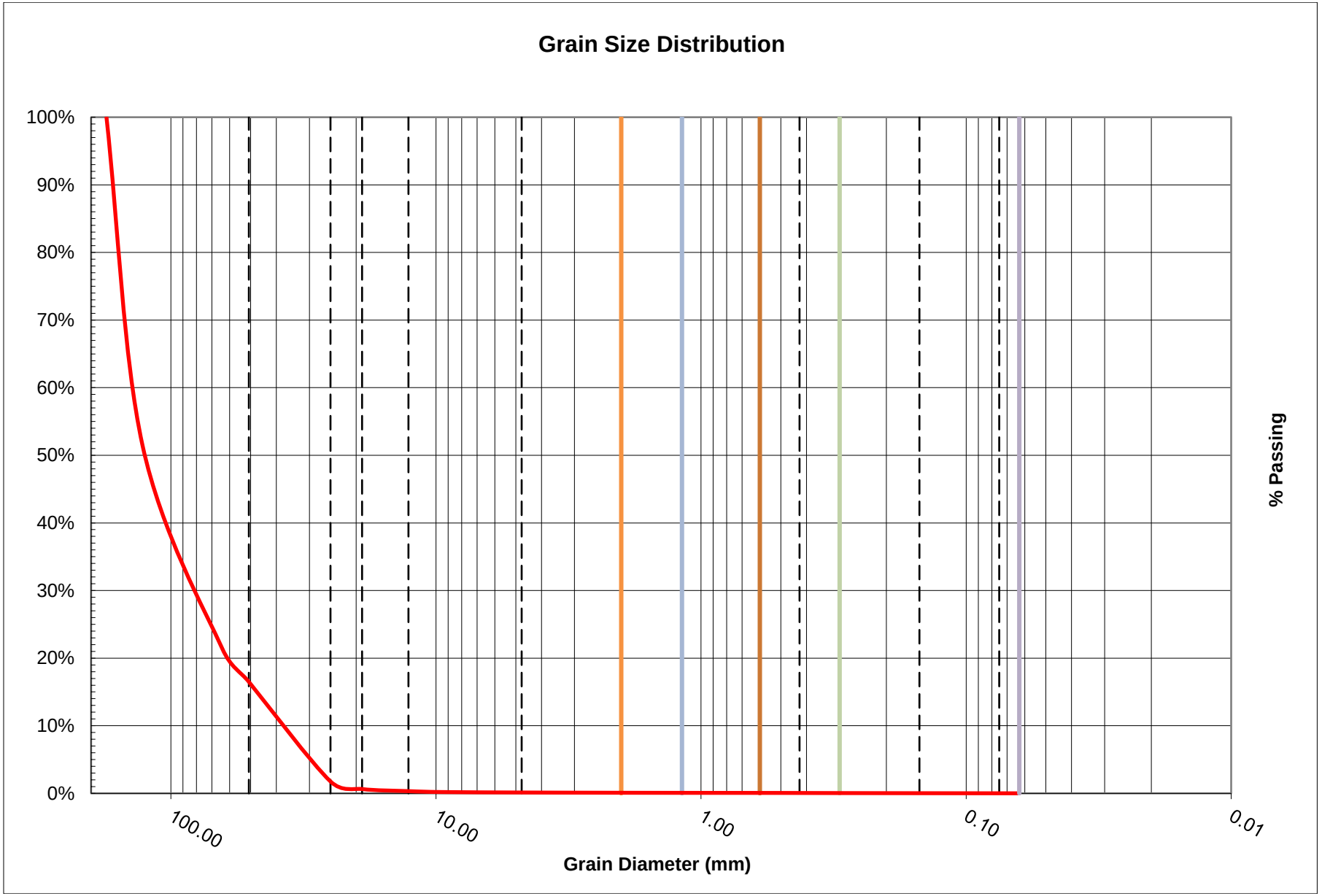
Grain Size Distribution
100%
90%
80%
70%
60%
50%
40%
30%
20%
10%
0%
% Passing
100.00
10.00
1.00
0.10
0.01
Grain Diameter (mm)

Lab Number 1183071916b Sample # bed Station:

Sieve Size and Percent passing for Soil Samples

Sample Size = 6691.1 grams

Sieve		Mass of soil		* based on Minitial								
No. (US std)	size (mm)	with pan (g)	w/o pan (g)	% retained	sum(% retained)	% passing						
	132					100.00%						
	128					76.47%						
	90					54.29%						
	64					43.38%						
2"	50.80		3789.8	56.61%	56.61%	43.39%	D_{100}	132.00		1.00	16	19.00	2.12
1"	25.00		798.6	11.93%	68.54%	31.46%	D_{84}	120.00	1 std deviation greater than median	0.84	18	19.00	2.08
3/4"	19.00		62.7	0.94%	69.48%	30.52%	D_{60}	98.54		0.60	17	18.00	1.99
1/2"	12.70		0.0	0.00%	69.48%	30.52%	D_{50}	78.71	Median size	0.50	16	17.00	1.90
3/8"	9.50		7.2	0.11%	69.58%	30.42%	D_{30}	3.32		0.30	10	11.00	0.52
#4	4.75		11.7	0.17%	69.76%	30.24%	D_{16}	0.28	1 std deviation less than median	0.16	4	5.00	-0.55
#8	2.36		31.5	0.47%	70.23%	29.77%	D_{10}	0.21	Effective Size	0.10	4	5.00	-0.67
#10	2.00		16.7	0.25%	70.48%	29.52%	C_u	459.84	Uniformity coefficient				
#16	1.18		56.9	0.85%	71.33%	28.67%	C_c	0.52	Coefficient of gradation				
#30	0.60		117.3	1.75%	73.08%	26.92%							
#40	0.425		178.8	2.67%	75.75%	24.25%	gap graded		Particle size distribution curve				
#50	0.30		470.8	7.03%	82.78%	17.22%							
#100	0.150		995.3	14.87%	97.65%	2.35%							
#200	0.075		128.4	1.92%	99.57%	0.43%							
#230	0.063		7.6	0.11%	99.68%	0.32%							
pan	--		21.2	0.32%	100.00%	0.00%							
	Totals	0	6694.5	--	--	--							

Total weight % Difference = 0.1 %

Notes
sample is representative of armor layer on the river bed in this area
Six rocks comprised the volume of material that did not pass through the #2 sieve
Information on these rocks is listed below

#	mass (g)	axis a (mm)	axis b (mm)	axis c (mm)	Desc
1	1574.9	168	132	104	large cobble
2	783.9	139	116	61	small cobble
3	701.4	124	109	62	small cobble
4	210.8	79	67	34	small cobble
5	259.1	88	78	43	small cobble
6	260.1	84	64	46	small cobble

Taking the six largest rocks and sorting them by scale for pebble count template

#	mass	axis b	FISP US SA-97 scale category		Total mass	% retained	SUM (% re	% passing
1	1575		132	128	1574.9	23.53%	23.53%	76.47%
2	783.9		116	90	1485.3	22.19%	45.71%	54.29%
3	701.4		109	90				
6	260.1		64	64	730	10.90%	56.62%	43.38%
5	259.1		78	64				
4	210.8		67	64				

For gradation plot

Size (mm)	% passing
132	100.00%
128	76.47%
90	54.29%
64	43.38%
25.00	31.46%
19.00	30.52%
12.70	30.52%
9.50	30.42%
4.75	30.24%
2.36	29.77%
2.00	29.52%
1.18	28.67%
0.60	26.92%
0.425	24.25%
0.30	17.22%
0.150	2.35%
0.075	0.43%
0.063	0.32%

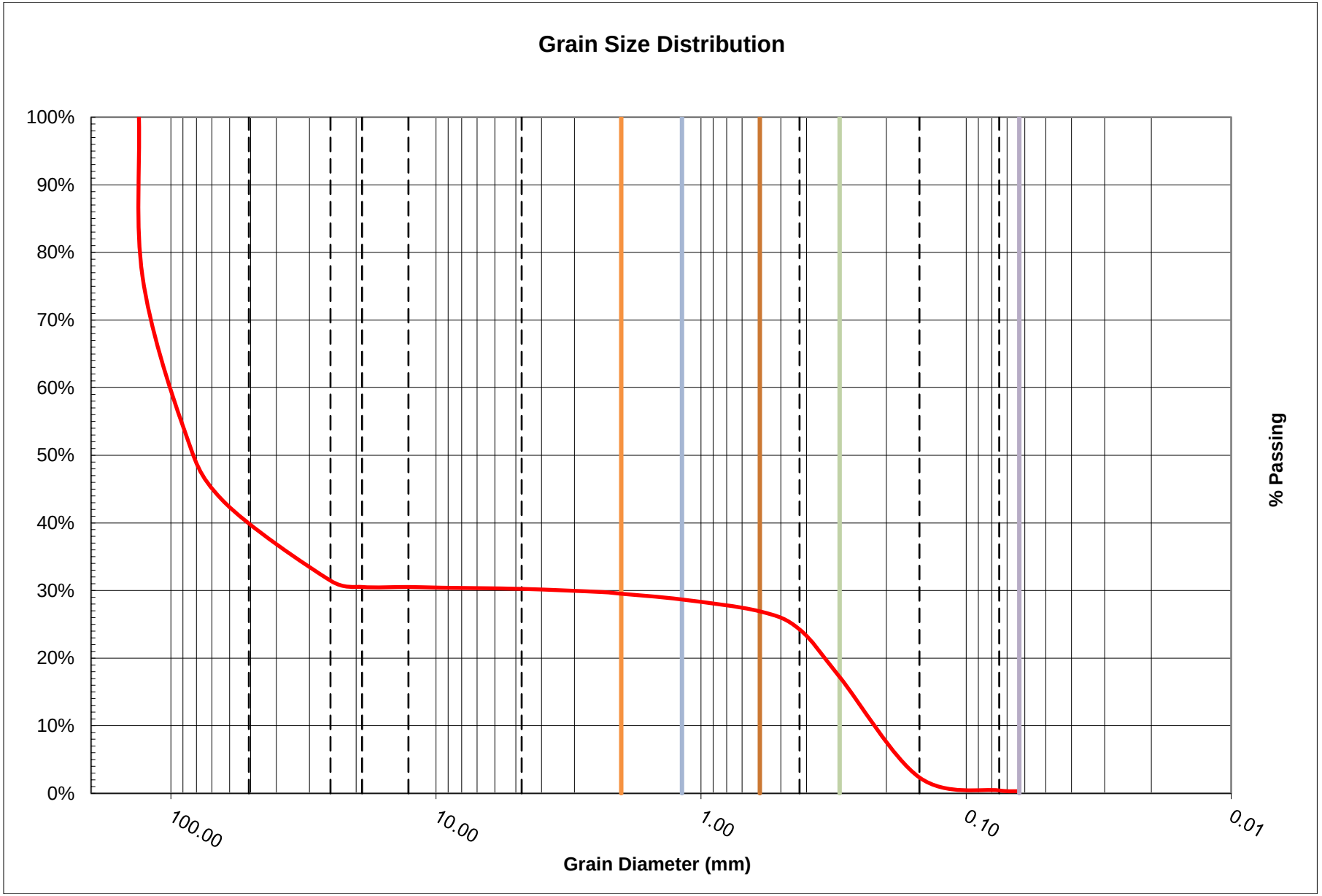
Grain Size Distribution
100%
90%
80%
70%
60%
50%
40%
30%
20%
10%
0%
% Passing
100.00
10.00
1.00
0.10
0.01
Grain Diameter (mm)

Lab Number RP1190071916 Sample # bed Station:

Sieve Size and Percent passing for Soil Samples

Sample Size = 7682.2 grams

Sieve		Mass of soil		* based on Minitial					
No. (US std)	size (mm)	with pan (g)	w/o pan (g)	% retained	sum(% retained)	% passing			
	172					100.00%			
2"	50.80		2190.9	28.50%	28.50%	71.50%	D_{100}	172.00	
1"	25.00		998.3	12.99%	41.49%	58.51%	D_{84}	88.00	1 std deviation greater than median
3/4"	19.00		218.8	2.85%	44.34%	55.66%	D_{60}	27.12	
1/2"	12.70		469.1	6.10%	50.44%	49.56%	D_{50}	13.08	Median size
3/8"	9.50		153.7	2.00%	52.44%	47.56%	D_{30}	0.57	
#4	4.75		447.5	5.82%	58.26%	41.74%	D_{16}	0.31	1 std deviation less than median
#8	2.36		330.6	4.30%	62.56%	37.44%	D_{10}	0.22	Effective Size
#10	2.00		59.0	0.77%	63.33%	36.67%	C_u	120.63	Uniformity coefficient
#16	1.18		157.5	2.05%	65.38%	34.62%	C_c	0.05	Coefficient of gradation
#30	0.60		284.3	3.70%	69.08%	30.92%			
#40	0.425		424.5	5.52%	74.60%	25.40%	gap graded		Particle size distribution curve
#50	0.30		790.9	10.29%	84.89%	15.11%			
#100	0.150		943.6	12.28%	97.17%	2.83%			
#200	0.075		150.9	1.96%	99.13%	0.87%			
#230	0.063		13.8	0.18%	99.31%	0.69%			
pan	--		53.0	0.69%	100.00%	0.00%			
	Totals	0	7686.4	--	--	--			

Total weight % Difference = 0.1 %

Notes
largest particle had a mass of 1406.3 g and the following dimensions
a-axis 172 mm
b-axis 122 mm
c-axis 82 mm

Sample location

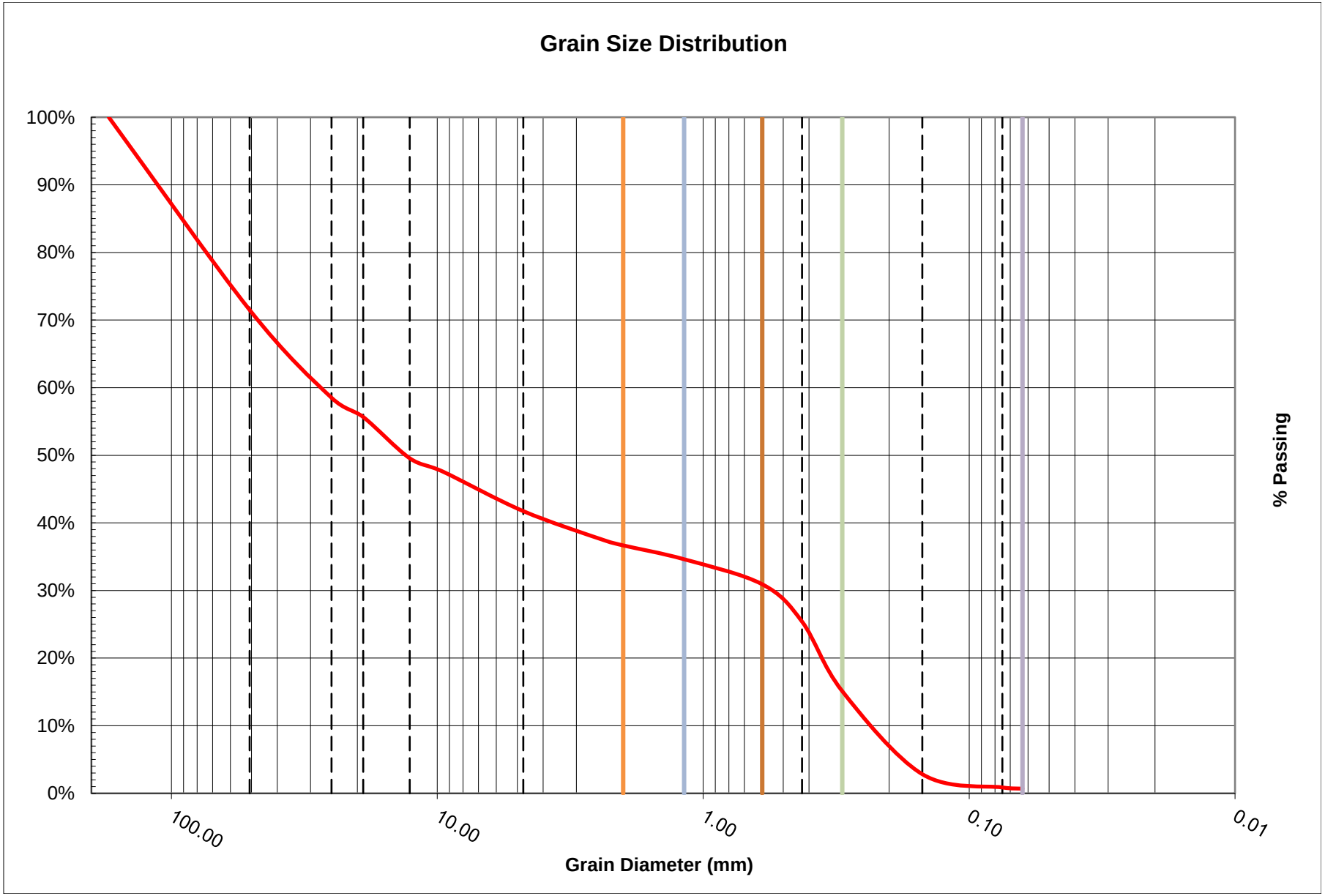
Grain Size Distribution
100%
90%
80%
70%
60%
50%
40%
30%
20%
10%
0%
% Passing
100.00
10.00
1.00
0.10
0.01
Grain Diameter (mm)

Lab Number CO1194071916 Sample # bed Station:

Sieve Size and Percent passing for Soil Samples

Sample Size = 9368.7 grams

Sieve No. (US std)	Sieve size (mm)	Mass of soil with pan (g)	Mass of soil w/o pan (g)	* based on Minitial % retained	* based on Minitial sum(% retained)	* based on Minitial % passing
	126					100.00%
	90					74.16%
	64					64.97%
2"	50.80		3281.5	35.03%	35.03%	64.97%
1"	25.00		805.5	8.60%	43.62%	56.38%
3/4"	19.00		233	2.49%	46.11%	53.89%
1/2"	12.70		168.1	1.79%	47.90%	52.10%
3/8"	9.50		76.6	0.82%	48.72%	51.28%
#4	4.75		300.7	3.21%	51.93%	48.07%
#8	2.36		193.9	2.07%	54.00%	46.00%
#10	2.00		77.7	0.83%	54.83%	45.17%
#16	1.18		197.4	2.11%	56.94%	43.06%
#30	0.60		385.3	4.11%	61.05%	38.95%
#40	0.425		847.7	9.05%	70.10%	29.90%
#50	0.30		1269.9	13.55%	83.65%	16.35%
#100	0.150		881.8	9.41%	93.06%	6.94%
#200	0.075		419.5	4.48%	97.54%	2.46%
#230	0.063		67	0.72%	98.26%	1.74%
pan	--		163.4	1.74%	100.00%	0.00%
	Totals	0	9369	--	--	--

D_{100}	126.00		1.00	15	18.00	2.10
D_{84}	105.00	1 std deviation greater than median	0.84	17	18.00	2.02
D_{60}	37.15		0.60	15	16.00	1.57
D_{50}	7.21	Median size	0.50	11	12.00	0.86
D_{30}	0.43		0.30	6	7.00	-0.37
D_{16}	0.29	1 std deviation less than median	0.16	4	5.00	-0.53
D_{10}	0.19	Effective Size	0.10	4	5.00	-0.73
C_u	197.66	Uniformity coefficient				
C_c	0.03	Coefficient of gradation				
gap graded		Particle size distribution curve				

Total weight % Difference = 0.0 %

Taking the six largest rocks and sorting them by scale for pebble count template

#	mass	axis b	FISP US SA-97 scale	category	Total mass	% retained	SUM (% re	% passing
1	1438		126	90	2421.4	25.84%	25.84%	74.16%
2	983		104	90				
3	529.2		89	64	860.3	9.18%	35.03%	64.97%
4	331.1		68	64				

Notes

sample is representative of armor layer on the river bed in this area

Four rocks comprised the volume of material that did not pass through the #2 sieve

Information on these rocks is listed below

#	mass (g)	axis a (mm)	axis b (mm)	axis c (mm)	Desc
1	1438.4	146	126	81	large cobble
2	983	104	104	84	small cobble
3	529.2	91	89	62	small cobble
4	331.1	71	68	48	small cobble

For gradation plot

Size (mm)	% passing
126	100.00%
90	74.16%
64	64.97%
25.00	56.38%
19.00	53.89%
12.70	52.10%
9.50	51.28%
4.75	48.07%
2.36	46.00%
2.00	45.17%
1.18	43.06%
0.60	38.95%
0.425	29.90%
0.30	16.35%
0.150	6.94%
0.075	2.46%
0.063	1.74%

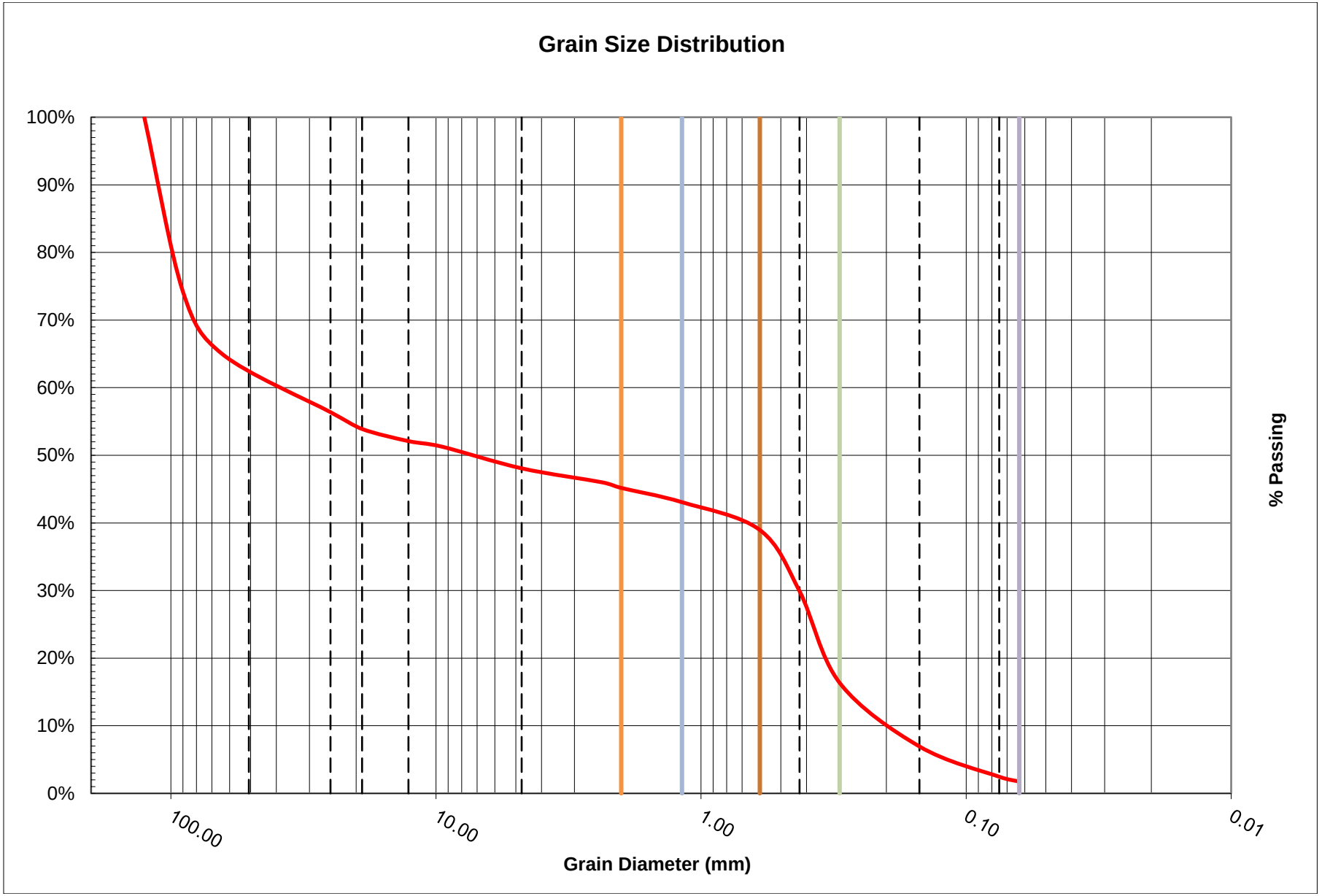
Grain Size Distribution
100%
90%
80%
70%
60%
50%
40%
30%
20%
10%
0%
% Passing
100.00
10.00
1.00
0.10
0.01
Grain Diameter (mm)

Lab Number RP1202_5071916 Sample # bank Station:

Sieve Size and Percent passing for Soil Samples

Sample Size = 2663.6 grams

Sieve		Mass of soil		* based on Minitial					
No. (US std)	size (mm)	with pan (g)	w/o pan (g)	% retained	sum(% retained)	% passing			
2"	50.80			0.00%	0.00%	100.00%	D_{100}	22.00	
1"	25.00			0.00%	0.00%	100.00%	D_{84}	0.48	1 std deviation greater than median
3/4"	19.00			0.00%	0.00%	100.00%	D_{60}	0.25	
1/2"	12.70		6.4	0.24%	0.24%	99.76%	D_{50}	0.22	Median size
3/8"	9.50		2.8	0.10%	0.34%	99.66%	D_{30}	0.16	
#4	4.75		44.4	1.66%	2.01%	97.99%	D_{16}	0.09	1 std deviation less than median
#8	2.36		60.2	2.25%	4.26%	95.74%	D_{10}	0.07	Effective Size
#10	2.00		28.0	1.05%	5.31%	94.69%	C_u	3.67	Uniformity coefficient
#16	1.18		85.1	3.19%	8.49%	91.51%	C_c	1.43	Coefficient of gradation
#30	0.60		119.4	4.47%	12.96%	87.04%			
#40	0.425		123.6	4.63%	17.59%	82.41%	poorly graded		Particle size distribution curve
#50	0.30		310	11.60%	29.20%	70.80%			
#100	0.150		1180.7	44.20%	73.39%	26.61%			
#200	0.075		390.4	14.61%	88.01%	11.99%			
#230	0.063		111.9	4.19%	92.20%	7.80%			
pan	--		208.4	7.80%	100.00%	0.00%			
	Totals	0	2671.3	--	--	--			

Total weight % Difference = 0.3 %

Notes
largest particle (clay clod) has a weight of 3.9g
a axis 30 mm
b axis 22 mm
c axis 13 mm

Sample location

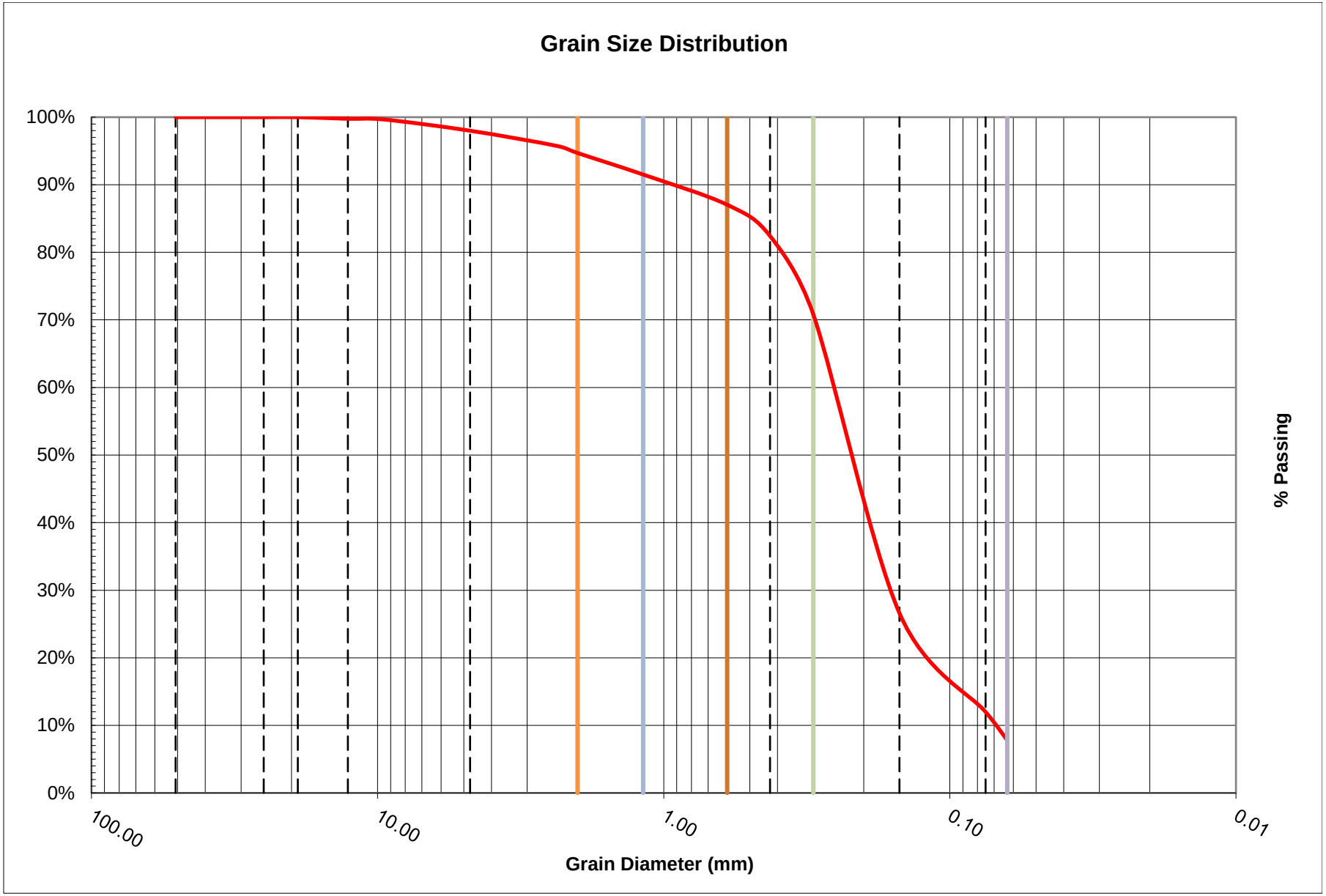
Grain Size Distribution
100%
90%
80%
70%
60%
50%
40%
30%
20%
10%
0%
% Passing
100.00
10.00
1.00
0.10
0.01
Grain Diameter (mm)

Appendix B: Channel Trend Comparisons for Isleta to San Acacia

Channel Trend Comparisons for Isleta to San Acacia

IS-691

This river section is located approximately 3.25 miles downstream of Isleta Pueblo near the town of Chical. Between June of 1998 and March 2014 this river section has become further confined to river right where it has incised 2 feet. The main channel narrowed from a width of 600 feet in 1998 to only 220 feet by 2014. Sediment has deposited on river left between 2.5 and 4 feet. Primary concerns with channel migration of the river towards the river right bank include the possibility of the river encroaching onto the nearby riverside drain and NM Hwy 314.

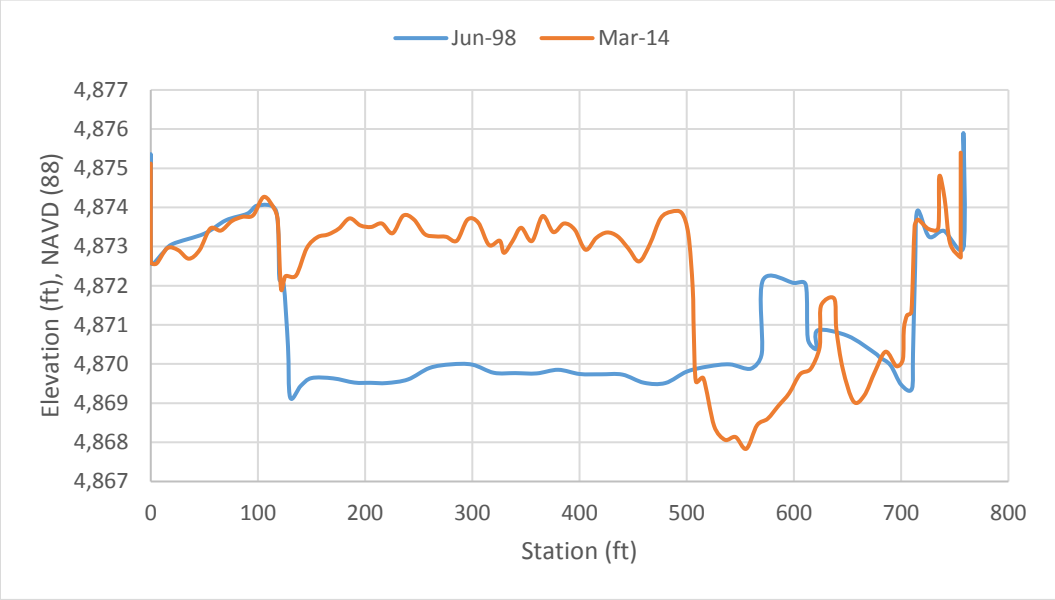

Figure 1. Isleta (IS-691) cross section survey comparison.

IS-705

The channel has shifted inwards from two dominate bankline channels and reduced the extent of the central island formation in this section. It appears that deposition has filled in the riverbed from 4 to 6 feet on the left and right banks since 1998. This has brought the bed elevation at these locations close to level with the 1998 floodplain. The deepest portion of the channel in 2014 is about a foot higher than in 1998. There also appears to be three primary channels in 2014, compared with two in 1998. The bank elevations along the channel edges in 2014 are about 1-2 feet higher than the island bank edges in 1998.

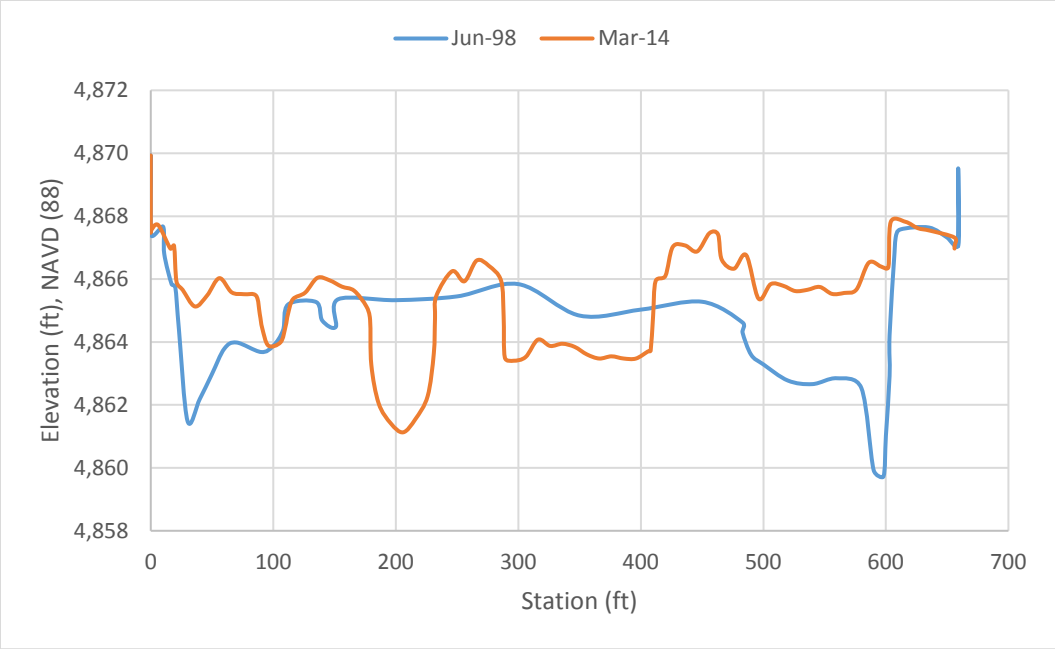

Figure 2. Isleta (IS-705) cross section survey comparison.

CO-713

The river section lies at the northern boundary of Los Lunas just to the west of Bosque Farms. Deposition between 1995 and 1998 raised the channel thalweg almost 4 feet and shifted it to river right by about 300 feet. Between 1998 and 2014 the channel thalweg shifted back to river left about 200 feet, deepening about 2 feet. The portion of the channel on river right was fairly stable between 1995 and 1998, but has seen about 3 feet of deposition between 1998 and 2014. Channel locations have adjusted back and forth between 1995 and 1998, with the current configuration having two primary channels. Channel widths have decreased with time as well.

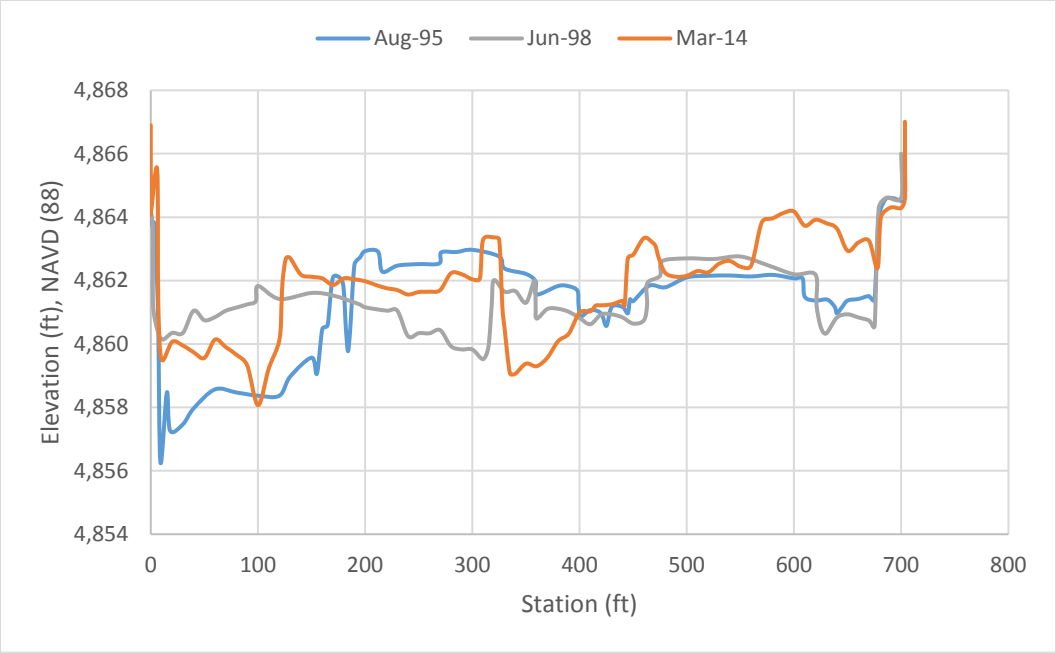

Figure 3. Cochiti (CO-713) cross section survey comparison.

CO-738.1

This rangeline is situated at the upstream face of the NM-6 (Main Street) bridge in Los Lunas. Between 1995 and 1998 two primary channel locations are evident in the cross section surveys. These channels were more defined in 1995 than in 1998. The survey data indicates a re-working of the sediment between 1995 and 1998 that lowered the center terrace about 2 feet, raising the river right channel invert by about the same amount and lowering the river left channel invert by about a foot. Between 1998 and 2014 further fluvial adjustments have created a single channel location at this cross section that has a thalweg elevation about 1 foot deeper than either 1995 or 1998. The previous channel locations in 1998 have been filled in with sediment between 1 and 4 feet, with about a 7 foot terrace on either side from the 2014 channel thalweg invert. Channel width between 1995 and 2014 has decreased, but it did increase between 1995 and 1998.

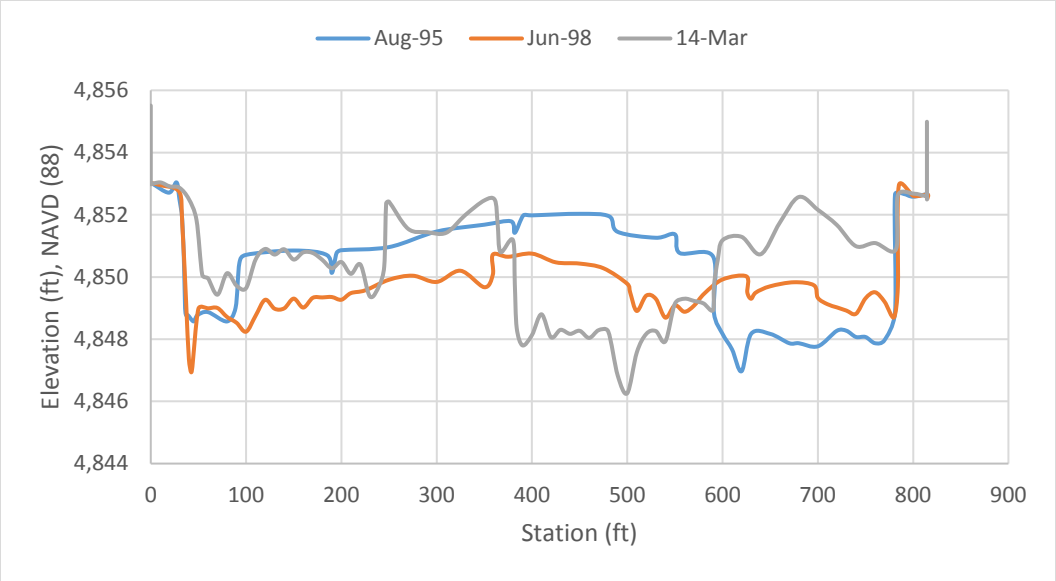

Figure 4. Cochiti (CO-738.1) cross section survey comparison.

IS-741

Cross section survey for IS-741 indicates that the river channel is narrowing below the NM-6 Bridge and continuing to incise. River right bed elevations have increased from 1998 to 2014 by as much as 3 feet in some locations. Current imagery shows that vegetation has become denser on the river right bank and suggests that river flows have not inundated this area for some time. In 1998 three primary flow paths are evident in the collected topography. Only one primary channel path is evident in the 2014 data. The thalweg elevation has decreased by about 1.5 feet and shifted to the river left,

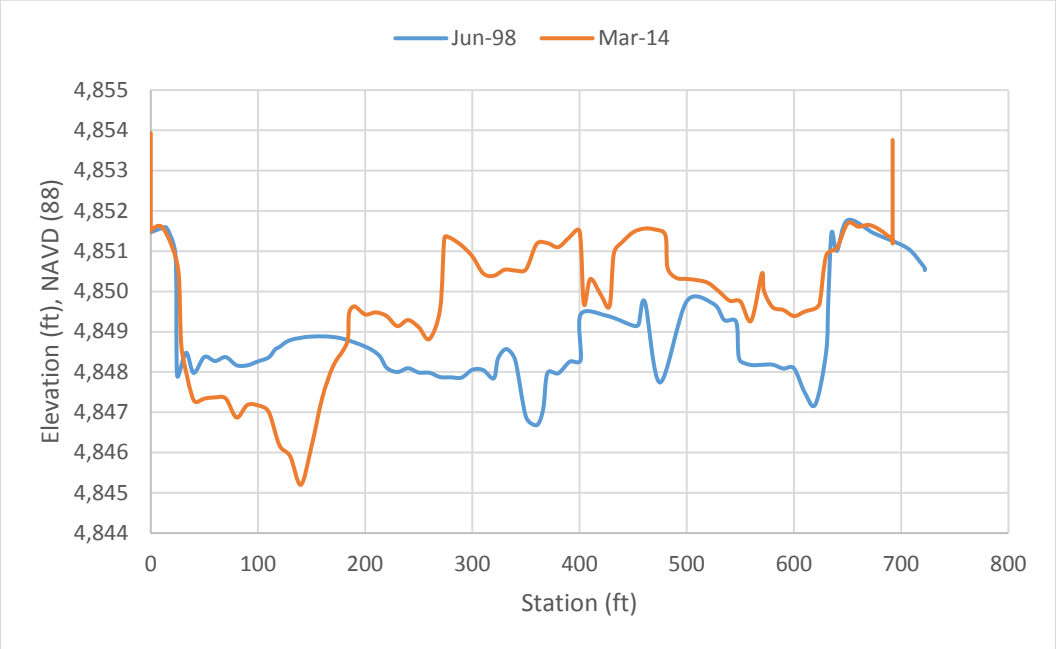

Figure 5. Isleta (IS-741) cross section survey comparison.

IS-748

Slight adjustments have occurred at this cross section location between 1998 and 2014. The thalweg elevation has increased by about a foot and shifted more to the channel center. One primary flow path is evident in the 1998 data, while two are evident in 2014. The two primary channels seen in the 2014 data are relatively deep and narrow compared to the 1998 data. For instance in 1995 the bank height was about 4.5 feet above the thalweg invert, with a terrain that allowed variable inundation levels over a width of about 300 feet. In 2014, the two channels have a bank height relative to the channel invert of 4-5 feet, but limited terrain variability over the 150 feet of channel width until overbanking occurs. Imagery from 2014 does show that the bar islands are becoming vegetated. It is expected that the islands would remain as permanent channel features under the current flow regime (lower river flows for extended periods and reductions in peak flows).

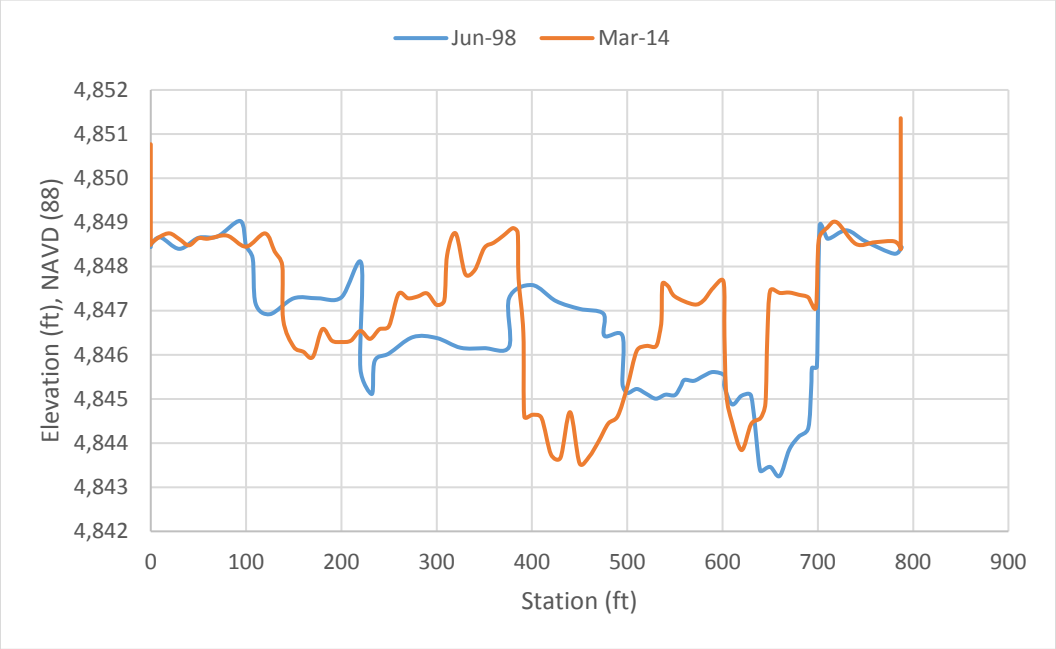

Figure 6. Isleta (IS-748) cross section survey comparison.

IS-752

Cross section survey data from June 1998 shows two main river channels flowing near each bank line of the river. Since this time these channels have both widened and become more prominent with the river right thalweg deepening by about one foot and the river left thalweg remaining at relatively the same elevation as before. 2014 imagery confirms that the terracing in the center of the river channel has now produced a vegetated island that is forcing river flow towards the left and right bank lines. Direction of flow to the river left bank has an increased risk of compromising the Lower Peralta Riverside Drain and Otero Lateral that are situated approximately six hundred feet away.

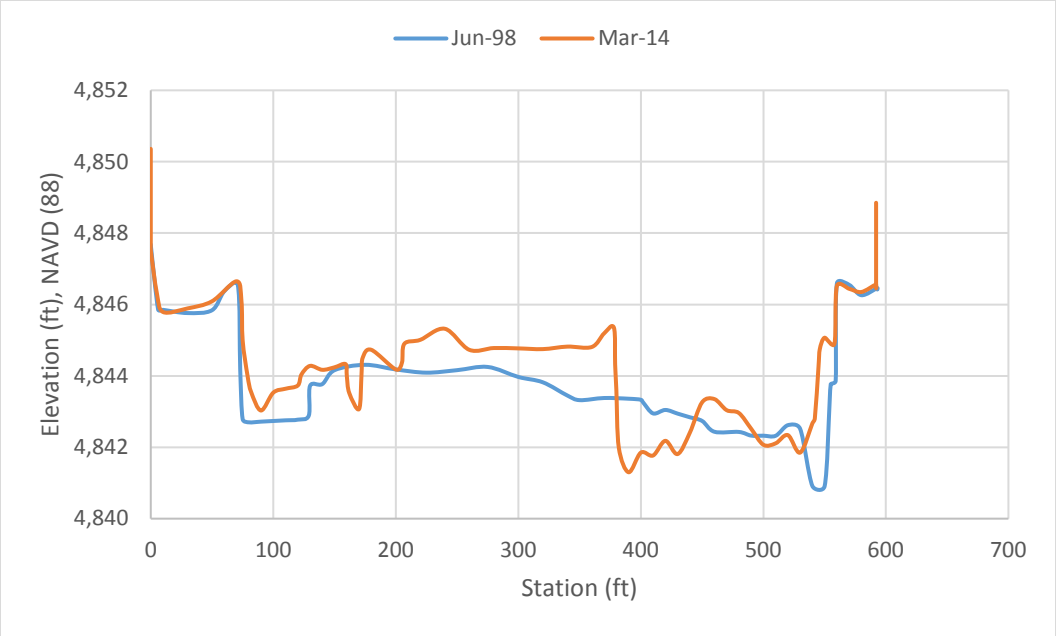

Figure 7. Isleta (IS-752) cross section survey comparison.

CO-765

From 1995 to 2014 the channel cross section has experienced a transition from two primary flow paths to three. The invert of the right channel thalweg has increased in elevation by over two feet (become shallower than before) and the river left channel has both deepened by about two feet and deposited around three feet of sediment along the left bank, raising the bed elevation here to an elevation of 4,841 feet.

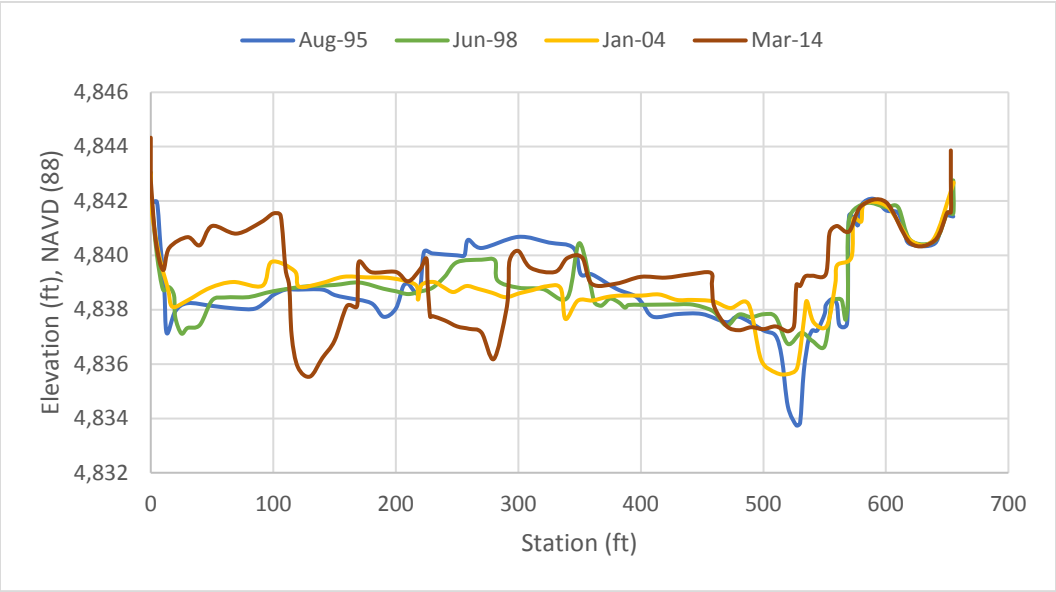

Figure 8. Cochiti (CO-765) cross section survey comparison.

IS-772

Significant deposition within the right river channel occurred between 2004 and 2014, forcing the main channel thalweg to completely fill in and shift the river channel all the way to its left. Current imagery suggests that the river left channel will continue to migrate by cutting into the river left bank and could impact the Lower Peralta Riverside Drain if left unabated.

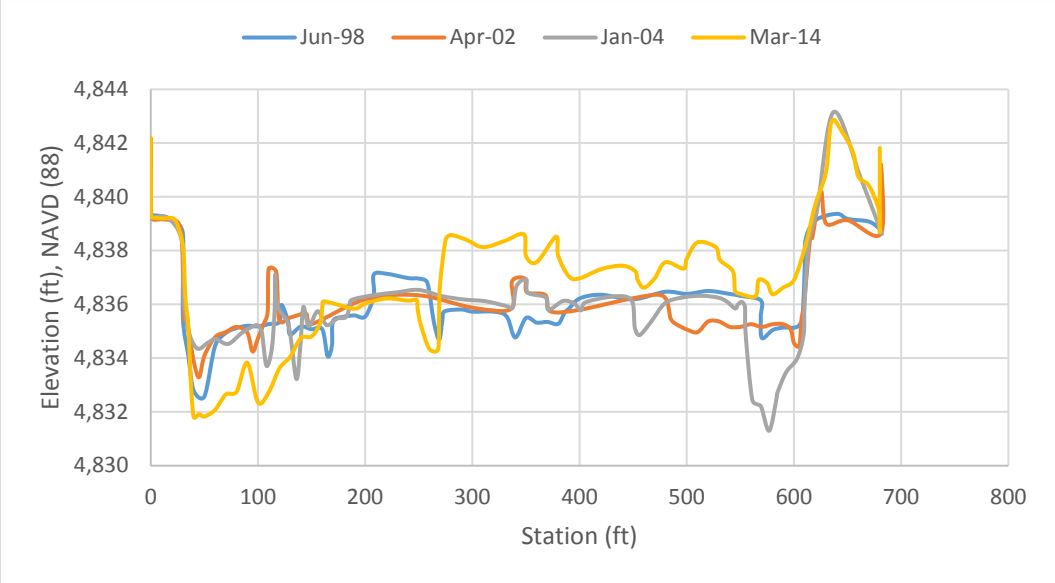

Figure 9. Isleta (IS-772) cross section survey comparison.

LL-774

Deepening of the river left thalweg by three feet at this location between January, 2004 and March, 2014 echoes the channel response in the upstream IS-772 cross section. The left channel thalweg experienced minor deposition from April, 2002 to January, 2004 and then started to incise after this point. Survey trends suggest that the river will continue to favor the left bank and could eventually impact the Lower Peralta Riverside Drain at this location.

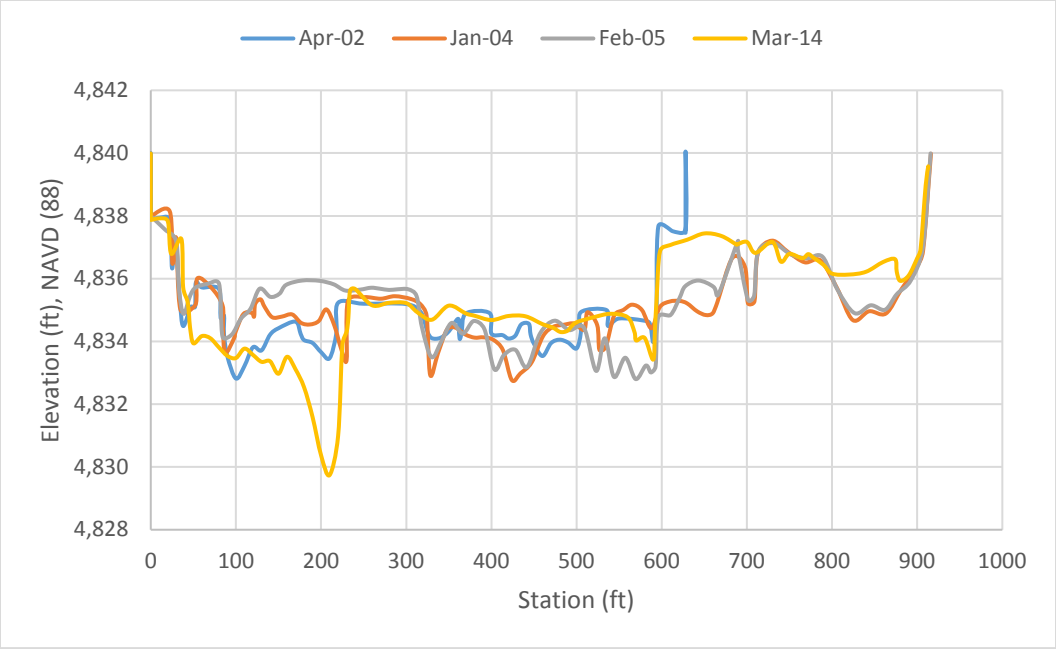

Figure 10. Los Lunas (LL-774) cross section survey comparison.

LL-775

Historical trends in bed topography at this location suggest a centralized shift of main channel flow from the left channel directly upstream of the cross section. Deposition within the river left channel since 2004 has mostly eliminated the left flow path and the main channel thalweg in the center of the river has incised by two to three feet, creating a singular primary flow path.

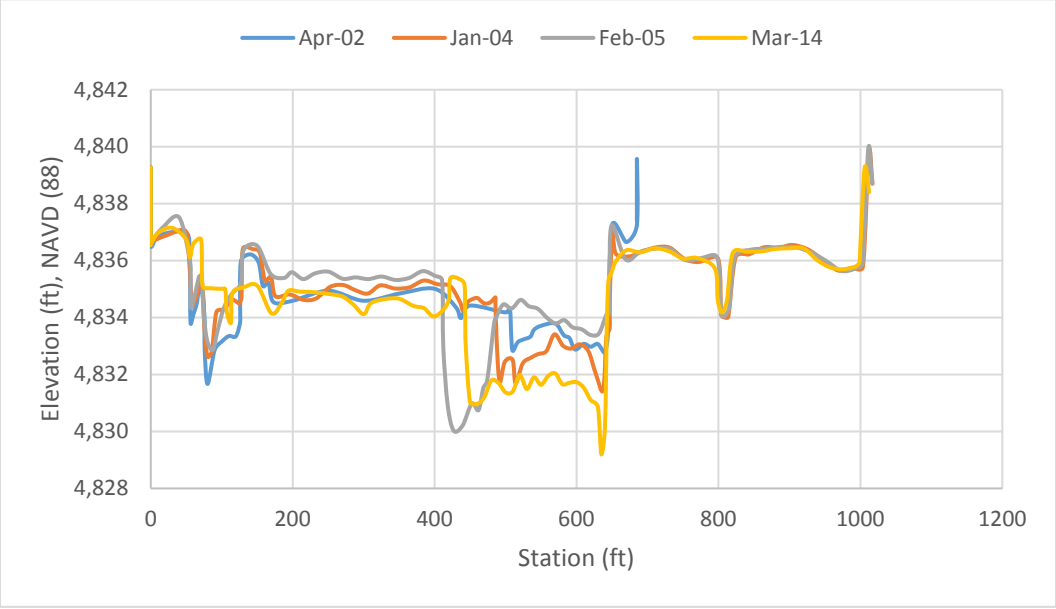

Figure 11. Los Lunas (LL 775) cross section survey comparison.

LL-776

This river cross section has seen a reduction from three primary flow paths in 2004 to two flow paths in 2014. Both the right and left riverbeds have risen two to three feet. Both of the more

recent channel flow paths are concentrated in the center of the channel and separated by a small, un-vegetated island bar formation.

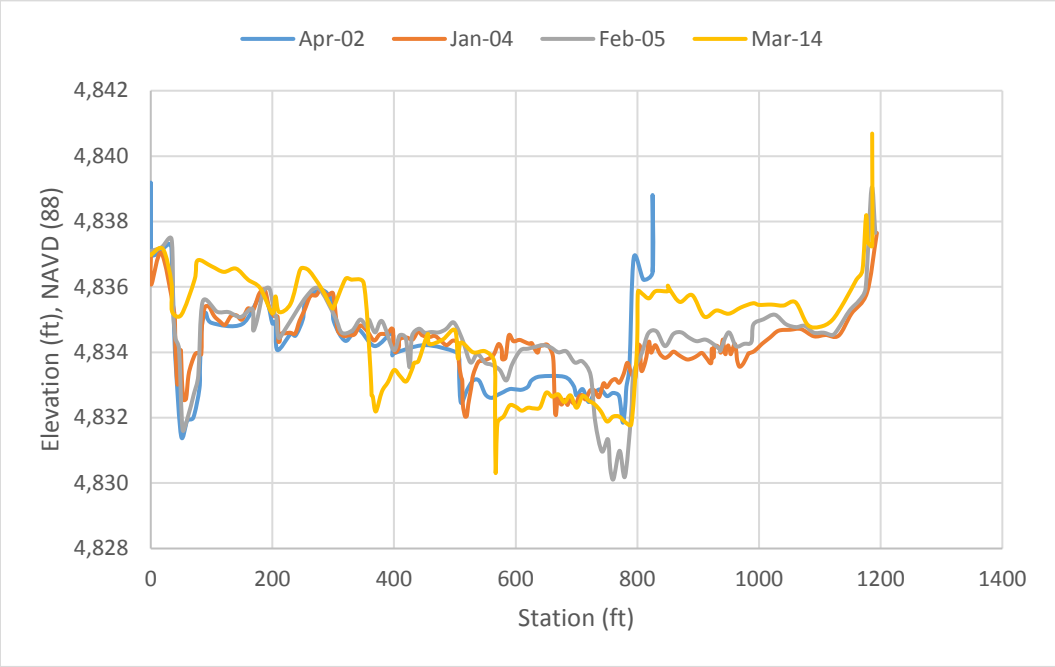

Figure 12. Los Lunas (LL-776) cross section survey comparison.

LL-778

Channel thalweg elevation has lowered in the section from 4,832 to 4829.5 feet between April, 2002 and March, 2014. Deposition on the river left bed has increased the bed elevation by two feet over the same time period and the channel has transitioned from being characterized by multiple flow paths to a single central path with some filling in of the river right channel also by sediment deposition.

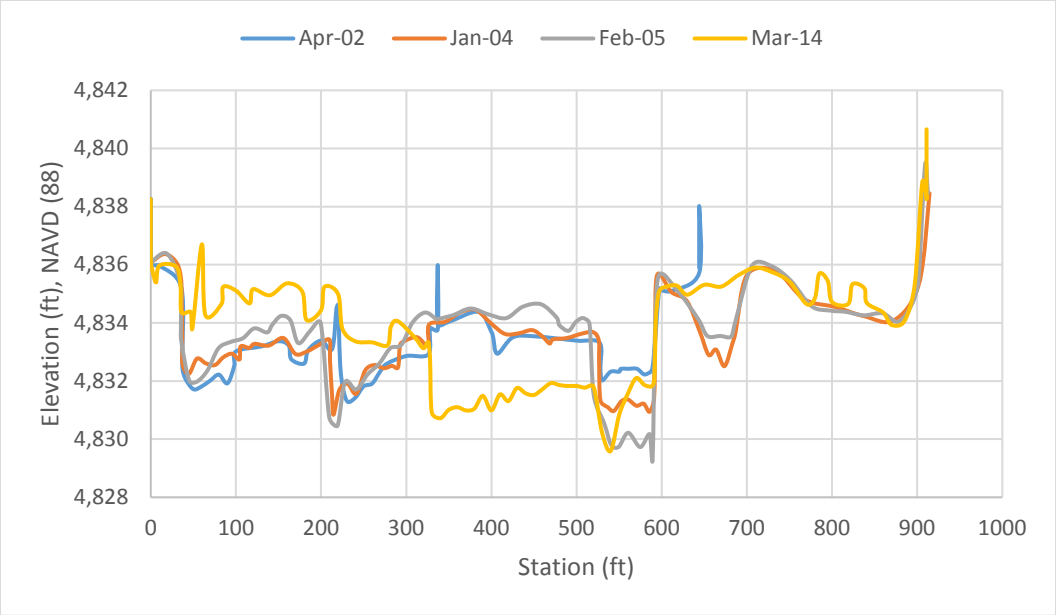

Figure 13. Los Lunas (LL-778) cross section survey comparison.

LL-779

The channel thalweg increased in width by 140 feet from 2004 to 2014 while its depth remained the same. Sediment deposition can be seen on both the right and left channel beds, however, defined flow paths are still evident on each side. Flows along the river left bank have begun to flank the island bar formation here and it appears they are becoming ever more prominent.

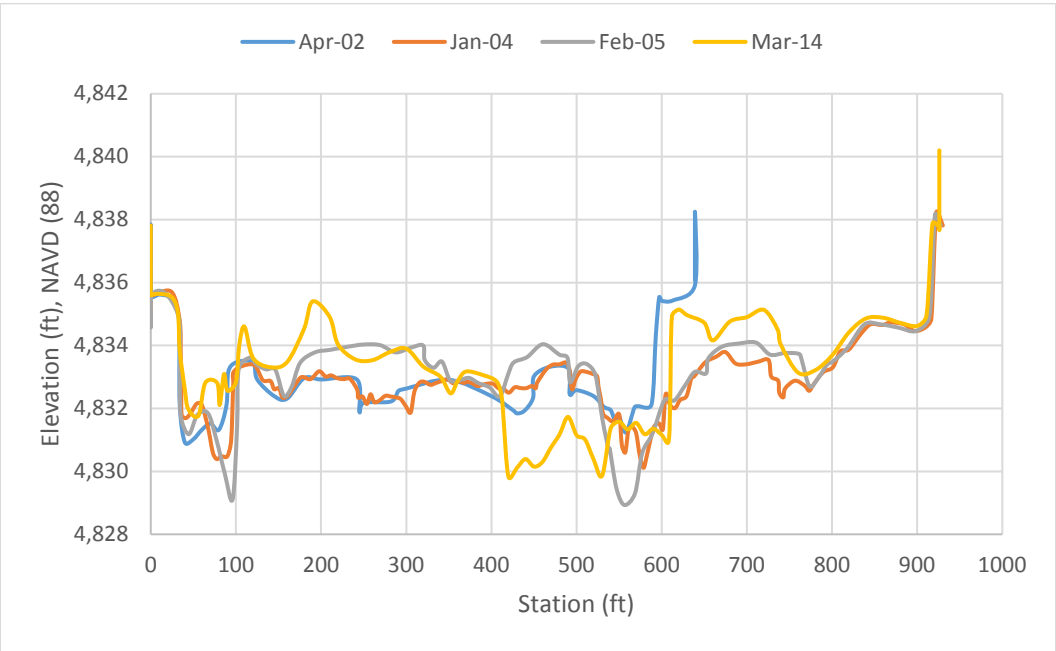

Figure 14. Los Lunas (LL-779) cross section survey comparison.

LL-781

River flow becomes increasingly restricted by lateral constraints provided by a berm on the west side of the channel (extends downstream to cross section LL-783) and the levee for the Lower

Peralta Riverside Drain to the east. The western berm appears to have been constructed to protect the Upper Belen Riverside Drain and the Los Chavez Wasteway that has its outfall just below the LL-784 section. The channel thalweg dropped two and a half feet in elevation between April, 2004 and March, 2014. The western berm (right side of river section) appears to exert an influence on the river by forcing flows towards the left bank. An island formation here has encouraged sediment deposition providing some resistance to channel migration towards the left bank, however, the left flow path is still relatively prominent here and appears to operate even at moderate to moderately low flows.

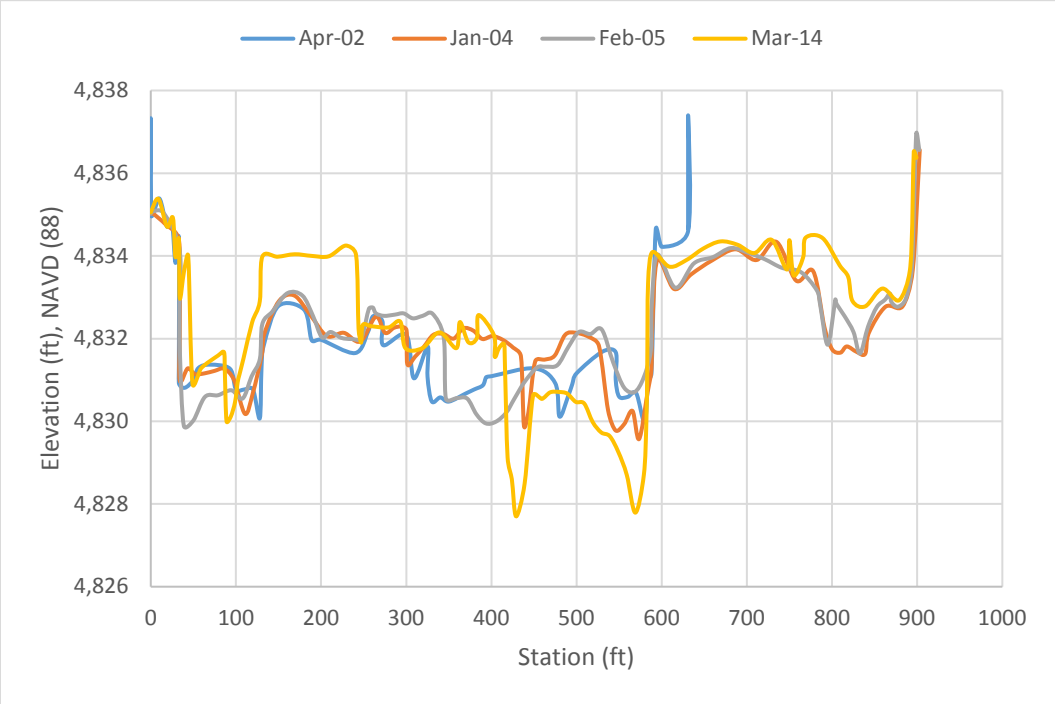

Figure 15. Los Lunas (LL-781) cross section survey comparison.

IS 782

The location of the thalweg has adjusted slightly over the years from 1998 to 2014, however, its invert elevation remains fairly constant through this section. The major change within the section over the sixteen year period depicted here was the formation of a significant sand bar on the left riverbed that has grown in height and breadth over time and the deposition that can be seen on the right bed of approximately one foot from February, 2005 to March of 2014. Any lateral migration of the river channel towards the left bank would be a significant threat to the adjacent Lower Peralta Riverside Drain as the geometry of the drainage canal bends eastwards at this location with a distance of only 285 feet between it and the river left bank.

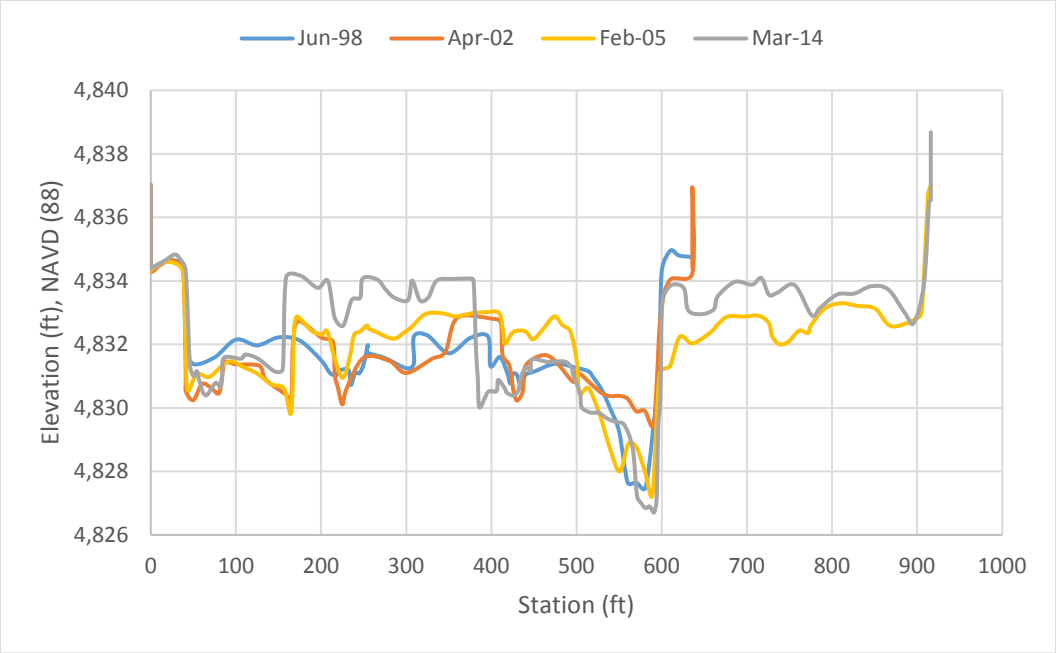

Figure 16. Isleta (IS-782) cross section survey comparison.

LL-783

The main river channel is extremely constricted by the right and left bank berms at this section. The two berms are only separated by a distance of 865 feet while the 2014 river channel spanned a distance of 500 feet according to its survey. The thalweg is both widening and gaining in elevation (approximately one foot) at this point since 2004 after incising between 2002 and 2004. The island formation continues through this section from upstream and lateral channel migration towards either bank would threaten river infrastructure.

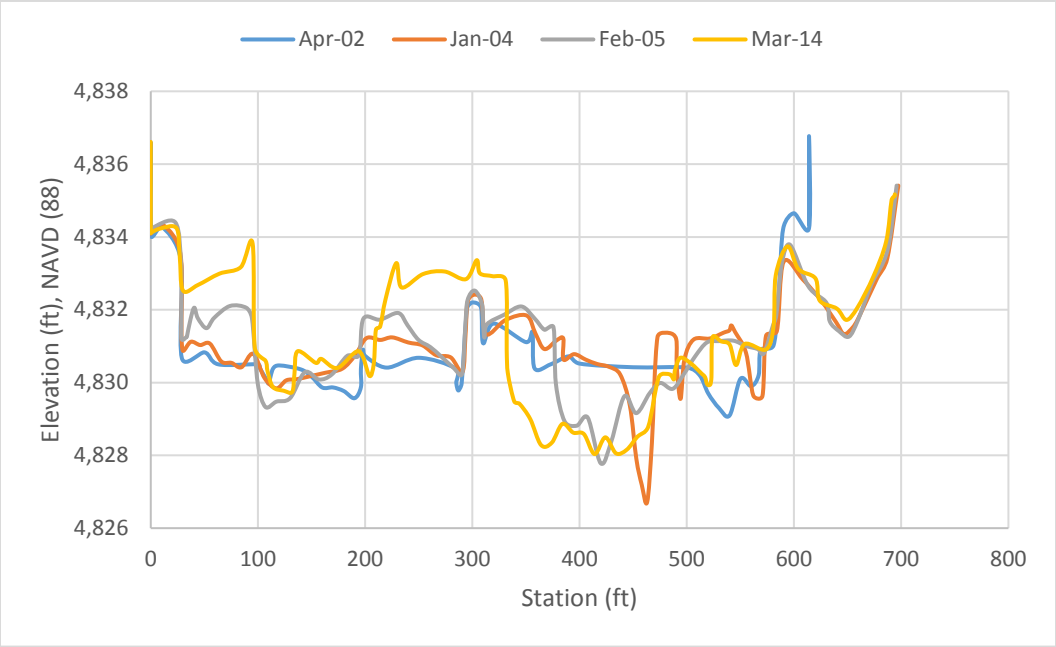

Figure 17. Los Lunas (LL-783) cross section survey comparison.

LL-784

In similar pattern to its upstream sections this location has experienced island bar formation in the central channel that has directed flows to either side of the bar. The thalweg that is located within the left river has incised almost five feet between 2002 and 2014, and the river right invert has also lowered by one and a half feet since 2004.

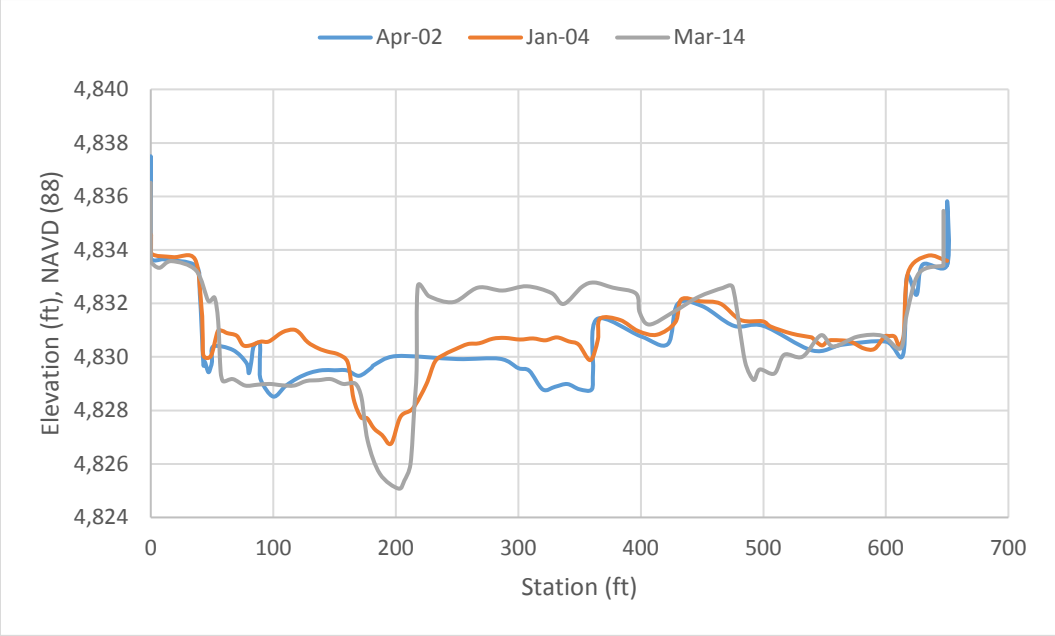

Figure 18. Los Lunas (LL-784) cross section survey comparison.

CO-787

River flow below this cross section has traditionally aligned itself towards the Lower Belen Riverside Drain berm on the west side of the river (e.g. the right river). From 1996 to 2014 the river right has filled up with sediment and the bed elevation has increased nearly ten feet, shifting the thalweg three-hundred feet towards the channel center. Continued shifting of the thalweg towards the river left is preferable in order to prevent it from impacting the Belen Drain.

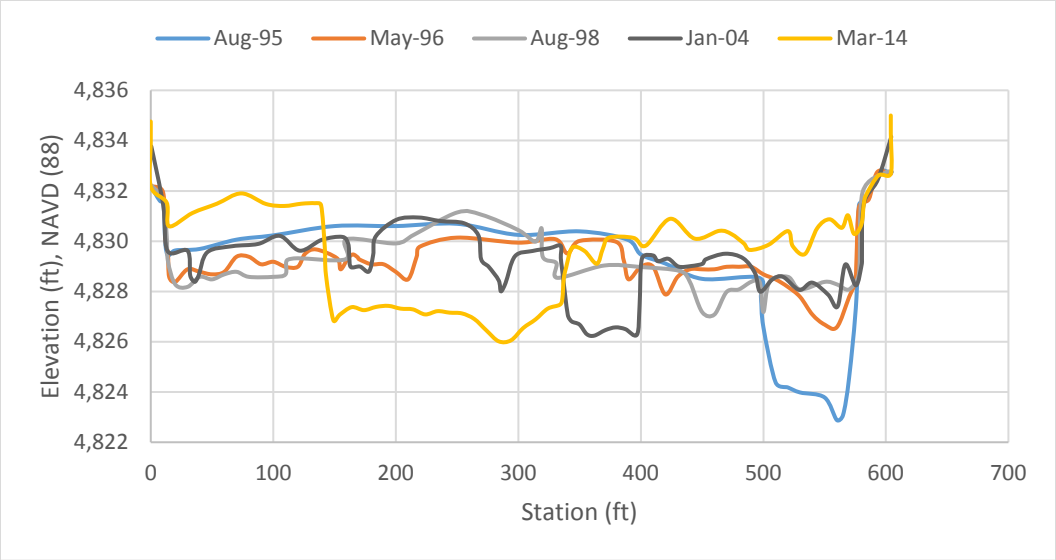

Figure 19. Cochiti (CO-787) cross section survey comparison.

LL-792

The river left bed has filled in with about two feet of sediment since 2002 while the thalweg within the river right as incised two feet and begun to widen. The 2002 cross section supported four primary flow paths and this number has been reduced to two as of the most recent survey.

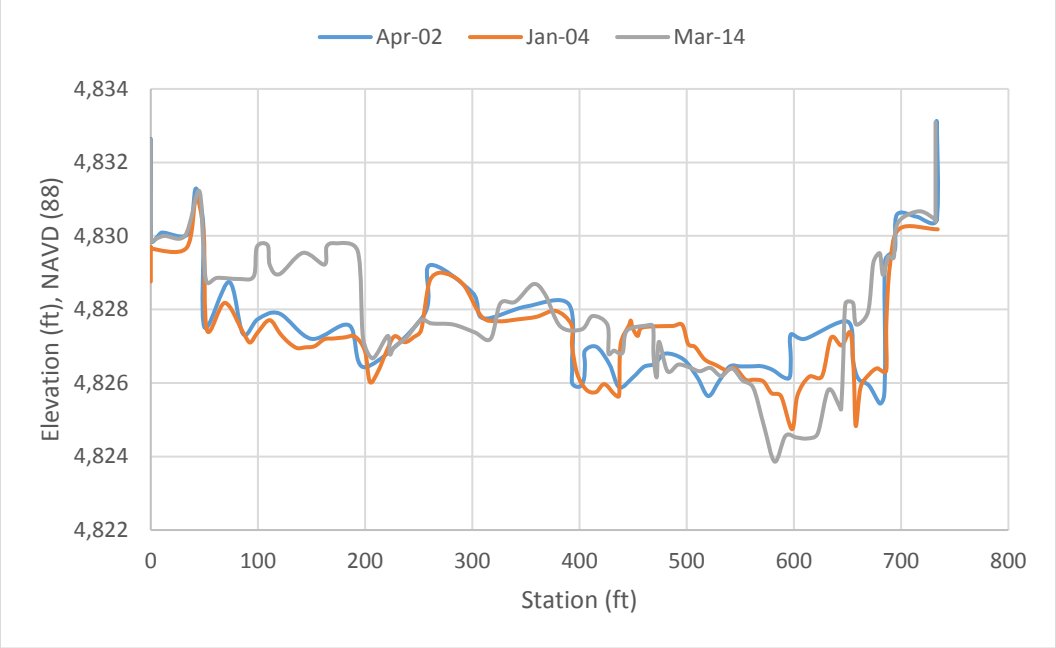

Figure 20. Los Lunas (LL-792) cross section survey comparison.

IS-797

The channel thalweg has shifted more towards the cross section center since 1998 and the river right channel has filled in with three feet of sediment and become perched above the central thalweg. The river left channel has incised two feet since 1998.

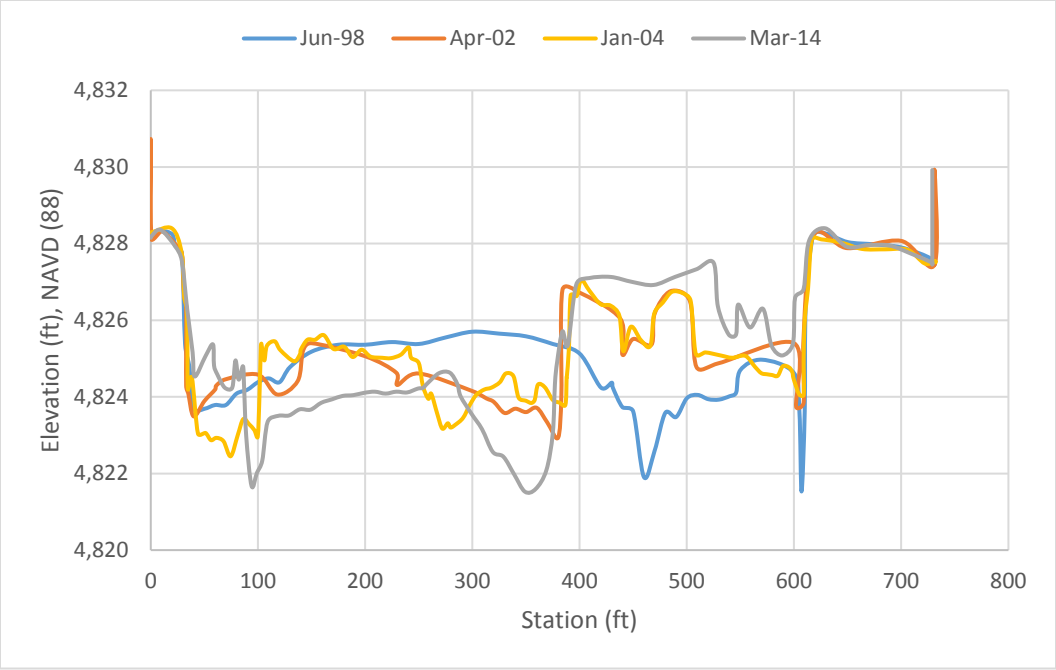

Figure 21. Isleta (IS-797) cross section survey comparison.

IS-801

Since 1998 a terrace has formed on the river left where the channel bed has risen nearly five feet in some areas. The thalweg has shifted away from the river left and located itself within the center of the channel cross section where it has maintained its invert elevation. Below this cross section the levee alignment forces the river to flow in a southwesterly direction, therefore it is preferable for the channel to shift away from the left bank as it has in order to protect the adjacent Lower Peralta Riverside Drain and Peralta Main Canal.

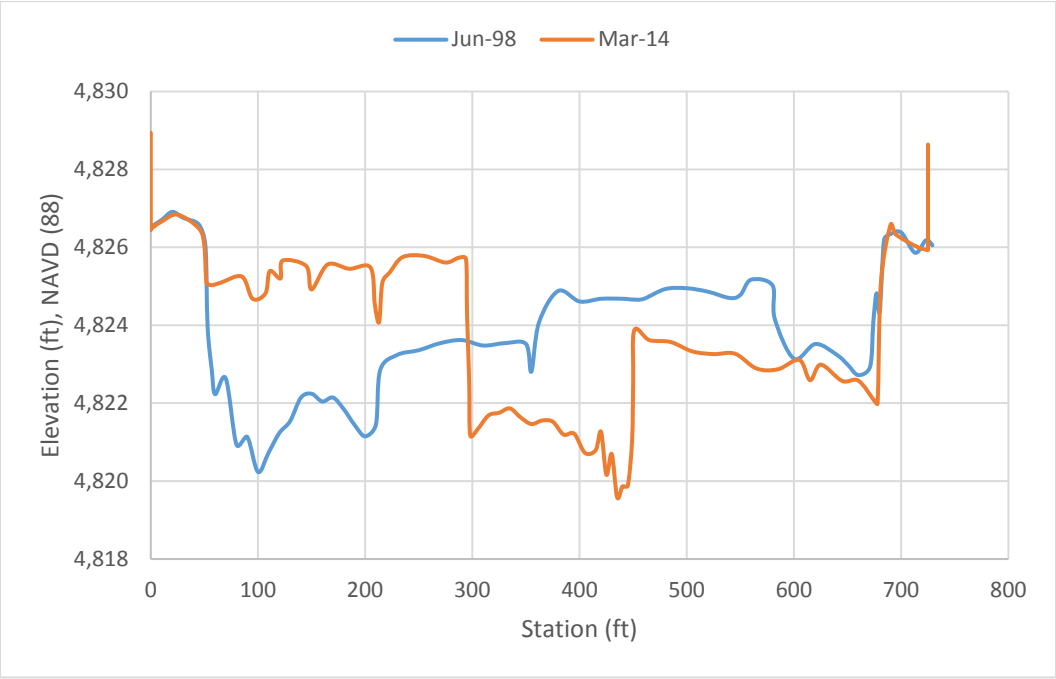

Figure 22. Isleta (IS-801) cross section survey comparison.

CO-806

Incision of the river left bed occurred from August, 1995 to May, 1996 (this trend was evident in cross section records from pre-1995 data that are not shown here) and then in 1998 the incision ceased and deposition was the dominant trend at this location with the river bed rising by six feet. This resulted in the thalweg shifting completely to the opposite side of the river channel where it lowered the bed elevation here equivalently. The shift of the thalweg to the river right is favorable as there is ample space for the river to adjust itself on the river right bank without endangering riverside infrastructure.

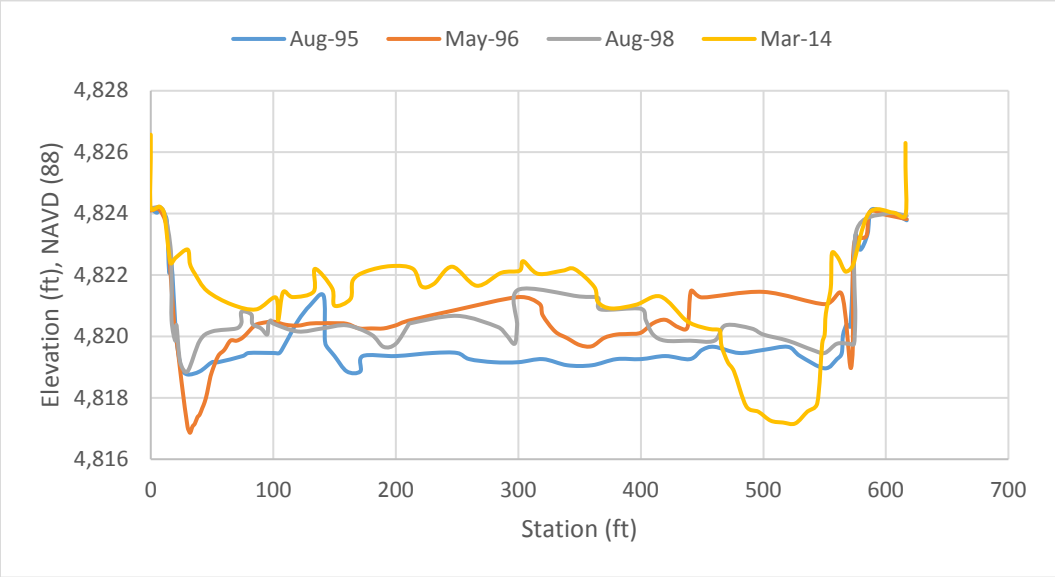

Figure 23. Cochiti (CO-806) cross section survey comparison.

IS-815

The 2014 cross section data suggests that the river is experiencing two feet of deposition on the river left and is incising from the center of the section to the river right by a foot at most locations. Movement of the river thalweg away from the left bank is preferable regarding the safety of infrastructure within this section.

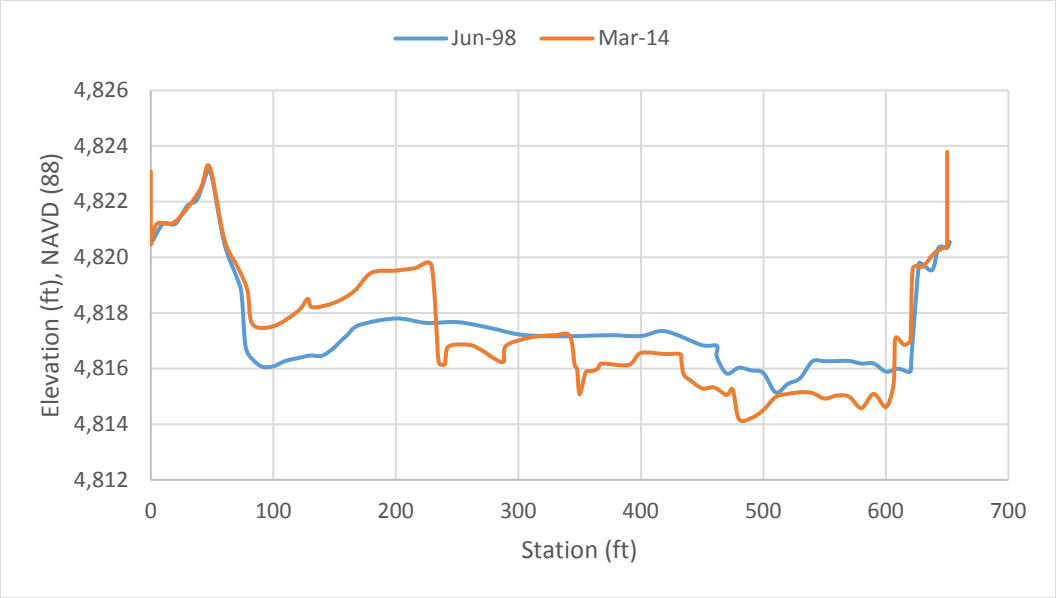

Figure 24. Isleta (IS-815) cross section survey comparison.

CO-833

From 1995 to 2014 the river's thalweg has fully shifted from the extreme right to river left section and the profiles are almost exact mirrors of each other. The river right has filled in with six feet of sediment and the river left has incised by about six feet. Continued channel incision on the river left and the subsequent destabilization of the river left bank could pose a threat to the Lower Belen Riverside Drain that is situated approximately 250 feet away from the left bank endpoint.

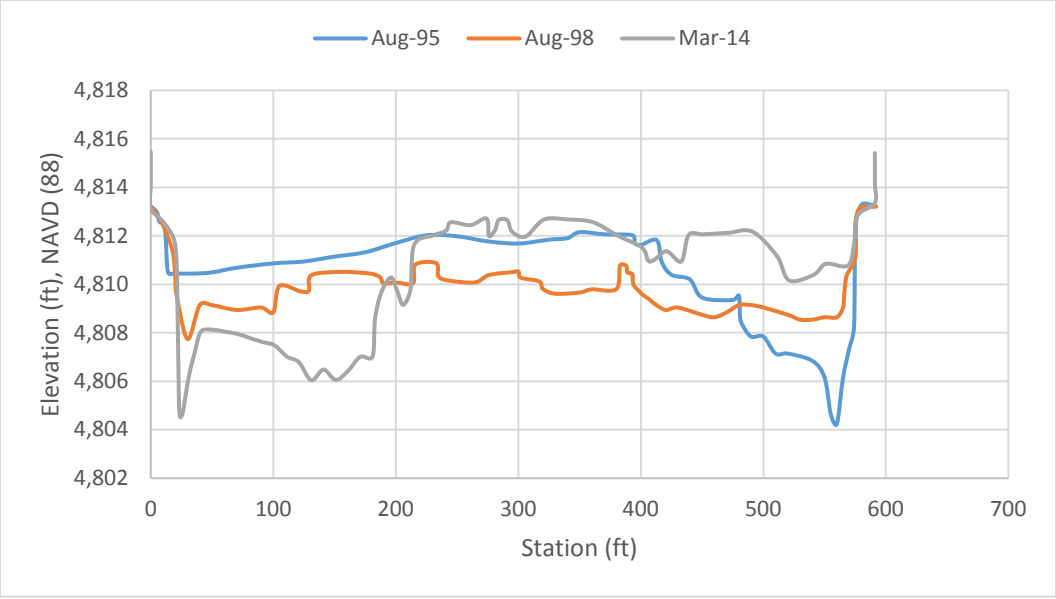

Figure 25. Cochiti (CO-833) cross section survey comparison.

IS-841

The channel thalweg has remained in the same location (river left) between 1998 and 2014, however, it has widened from 80 to 230 feet. Deposition within the river right has raised the bed

elevation by three feet. Current channel trends inferred from the cross sectional data suggest that the left river bank is stable and the thalweg is widening towards the center of the cross section which does not appear to endanger any bankline infrastructure.

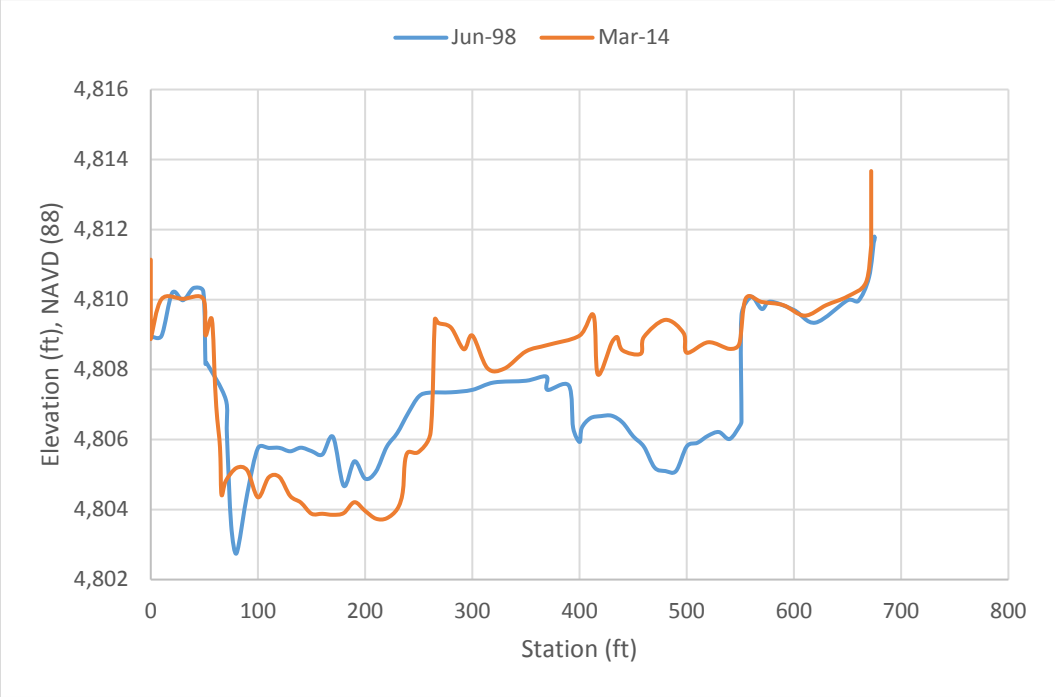

Figure 26. Isleta (IS-841) cross section survey comparison.

IS-849

A distance of only 180 feet separates the March, 2014 left endpoint from the levee of the Lower Peralta Riverside Drain. The thalweg has shifted from the center of the section in 1998 to the left river by a distance of about 300 feet. In this time the central bed raised five feet and has created a bar island with mature vegetation with two flow paths around it to the left and river right sections. River flow favors the river left flow path and continued incision at this location could impact the nearby levee.

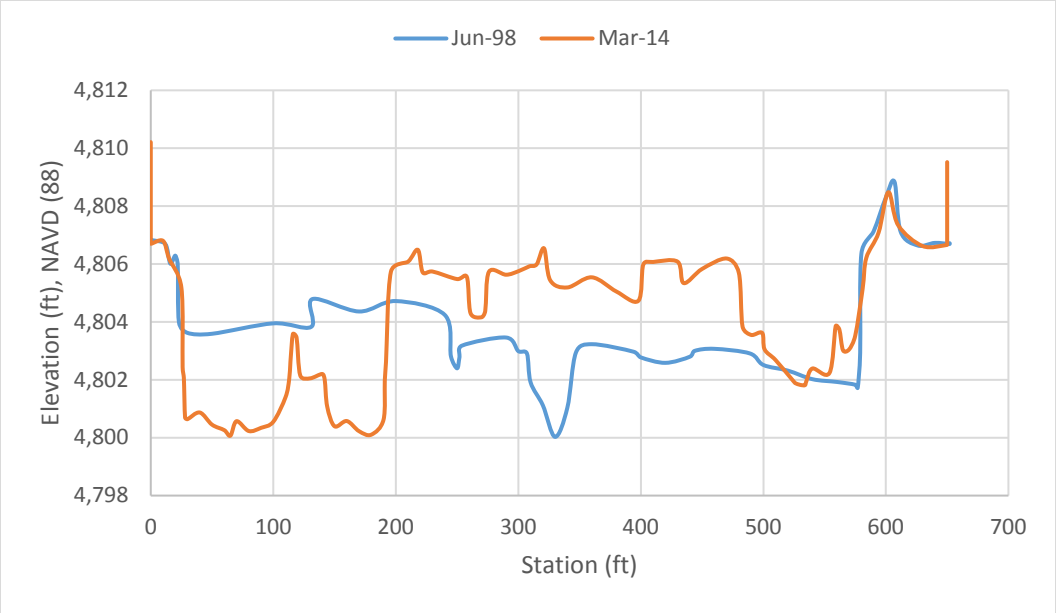

Figure 27. Isleta (IS-849) cross section survey comparison.

IS-854

A reduction from three to two channel flow paths has occurred in this river section since 1998. The central riverbed elevation rose by two feet as the thalweg at the river left section widened by 110 feet. The bed elevation rose in the river right channel by just under two feet during the same time period. There do not appear to be any hazards to riverside infrastructure by the channel changes at this location.

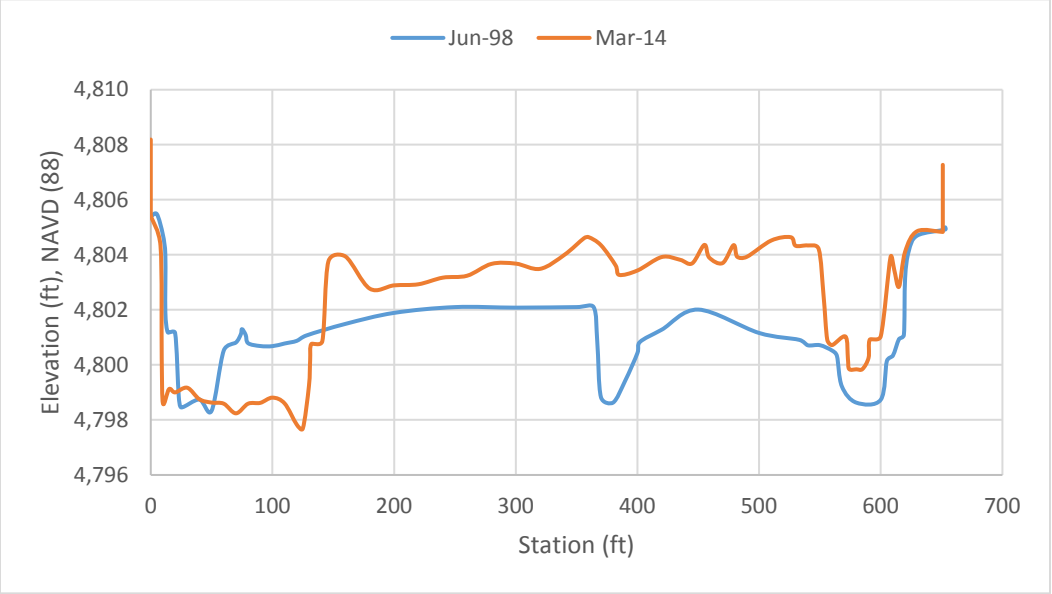

Figure 28. Isleta (IS-854) cross section survey comparison.

CO-858.1

This section lies just upstream of the Highway 309 Bridge crossing in Los Trujillos. The channel thalweg has adjusted from the river right section to the central section since 1995 and it has become both wider and shallower. Sediment deposition on the left and right channel banks has

begun to narrow the channel width at this location. Flow preference to avoid impacts to nearby infrastructure would be through the center of the cross section.

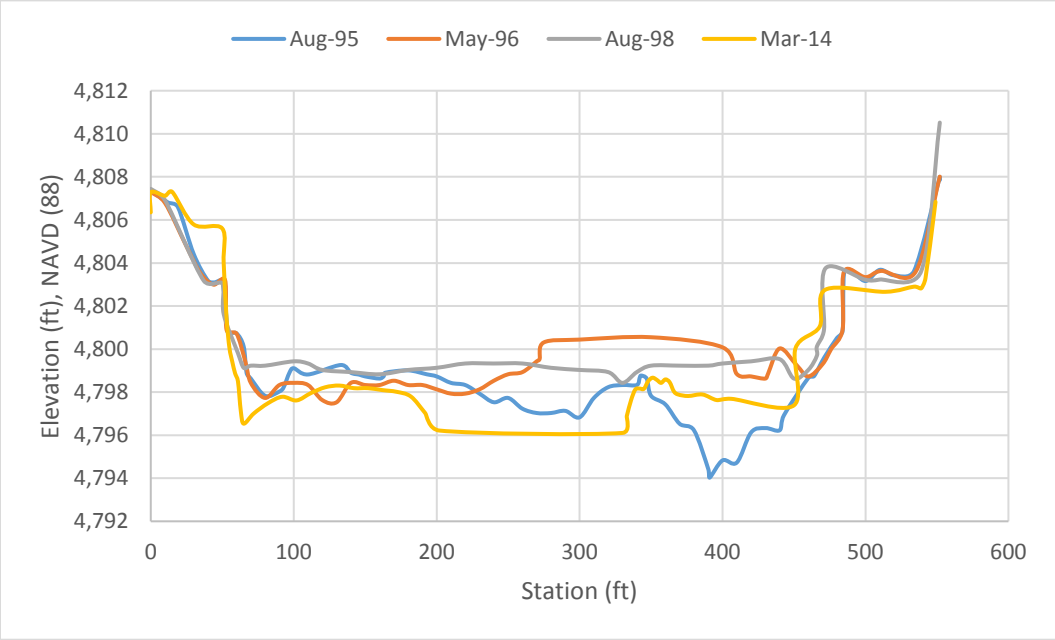

Figure 29. Cochiti (CO 858.1) cross section survey comparison.

IS-864

The left endpoint in this section sits just 95 feet from the levee berm to the San Juan Feeder Channel on the east side of the river. Since 1998 the thalweg has been positioned at the left river and has widened around 75 feet while the river right bed has risen up to four feet. Although the thalweg has widened the overall river channel has narrowed by over 150 feet and the deepest part of the river section is still situated at the river left bank. Any migration of the river thalweg away from the left bankline would be ideal to protect the integrity of the San Juan Channel.

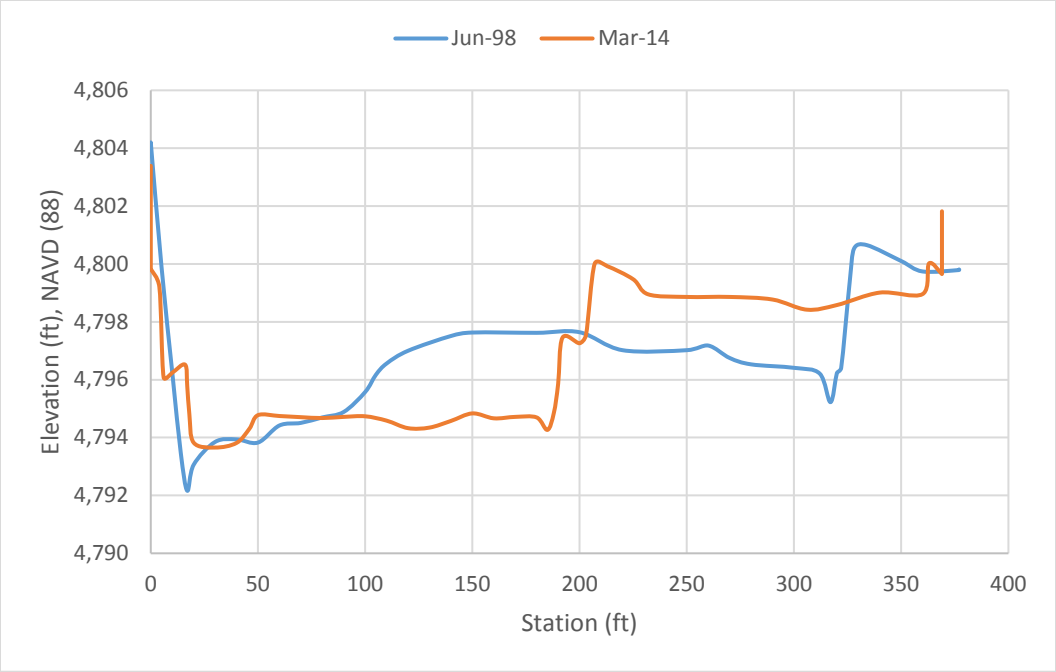

Figure 30. Isleta (IS-864) cross section survey comparison.

IS-872

Sediment deposition along the river left and right channels has increased the bed elevation in these sections by up to two feet. Sand bar formation has increased the number of flow paths from two to three and the center bed elevation has incised by four feet. As a result of the incision the thalweg has shifted to the center of the cross section.

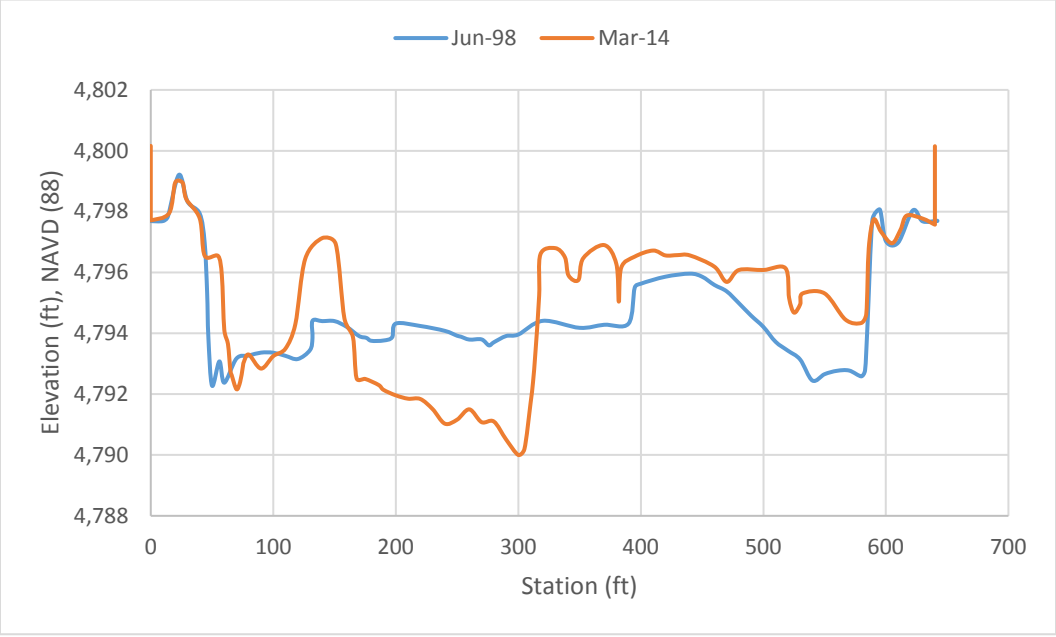

Figure 31. Isleta (IS-872) cross section survey comparison.

CO-877

This section is located just upstream of a railroad bridge crossing north of Jarales, NM. Deposition on the river left and incision from the central to river right have created a cross

section with multiple flow paths and the thalweg has widened on the river right by 90 feet. The Lower Belen Riverside Drain becomes the Upper Sabinal Riverside Drain at the railroad bridge and the channel thalweg is located immediately adjacent to the levee protecting the drain. Movement of the thalweg towards the left river section would be preferred.

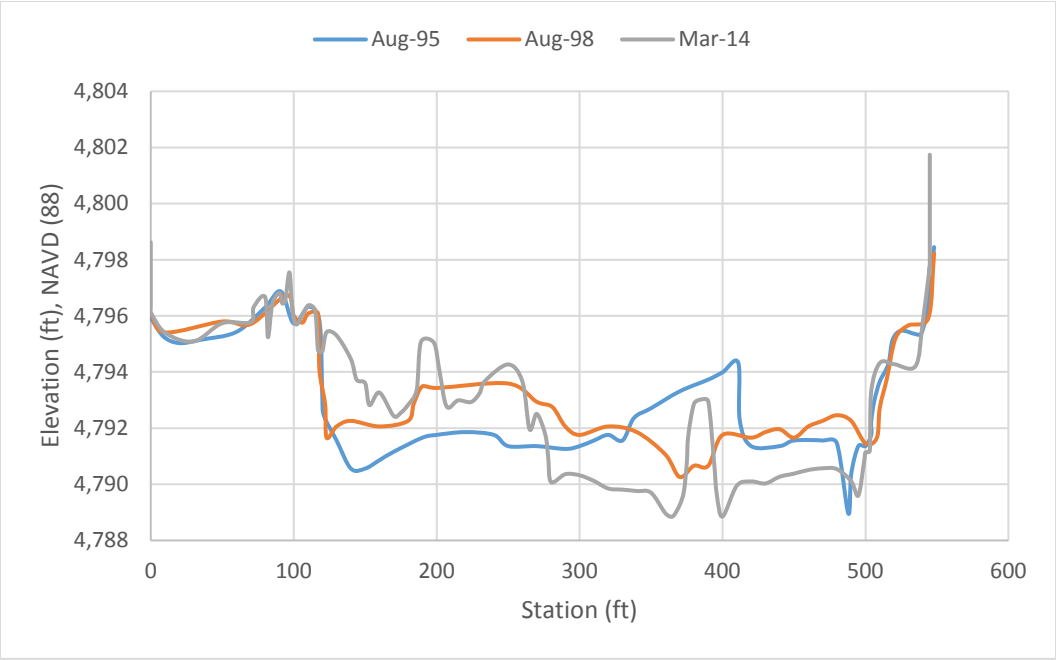

Figure 32. Cochiti (CO-877) cross section survey comparison.

IS-880

The channel thalweg has been deepening since 1998, however, this behavior was exacerbated between 2015 and 2016 where it increased in depth by two feet in only a year. Overall, the thalweg has incised by five feet since 1998 and the central to right river section has filled with sediment to a depth of three feet. The river in this section is not currently impacting any riverside infrastructure.

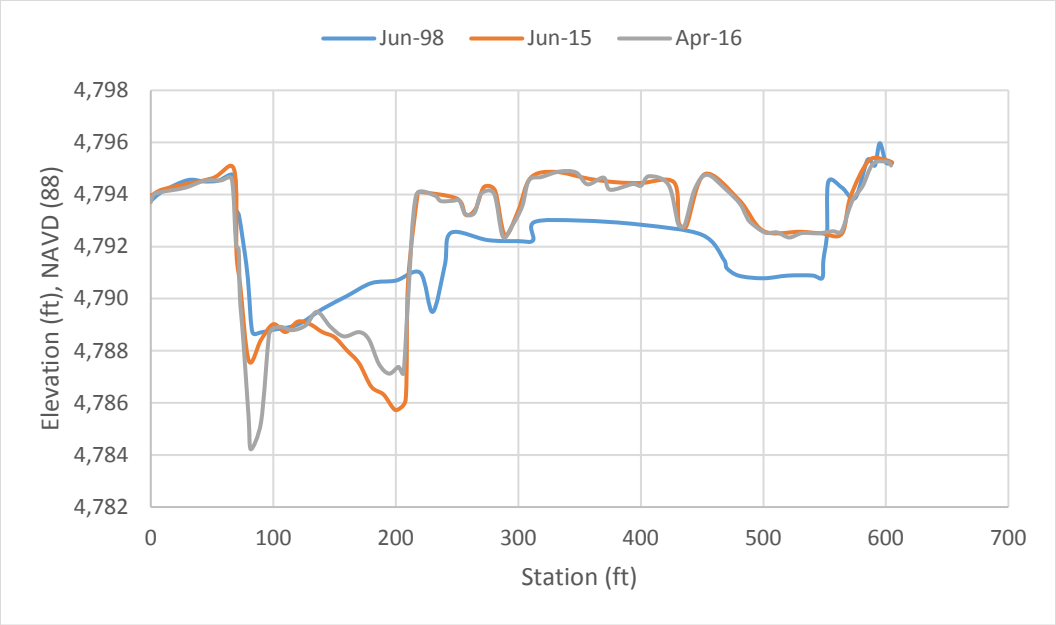

Figure 33. Isleta (IS-880) cross section survey comparison.

IS-884

Deposition on the river left has increased the bed elevation by approximately four feet since June, 1998. This has resulted in the thalweg shifting towards the river right a distance of 250 feet. Between 2015 and 2016 the channel thalweg has widened slightly and there appears to be deposition occurring along the river right bank.

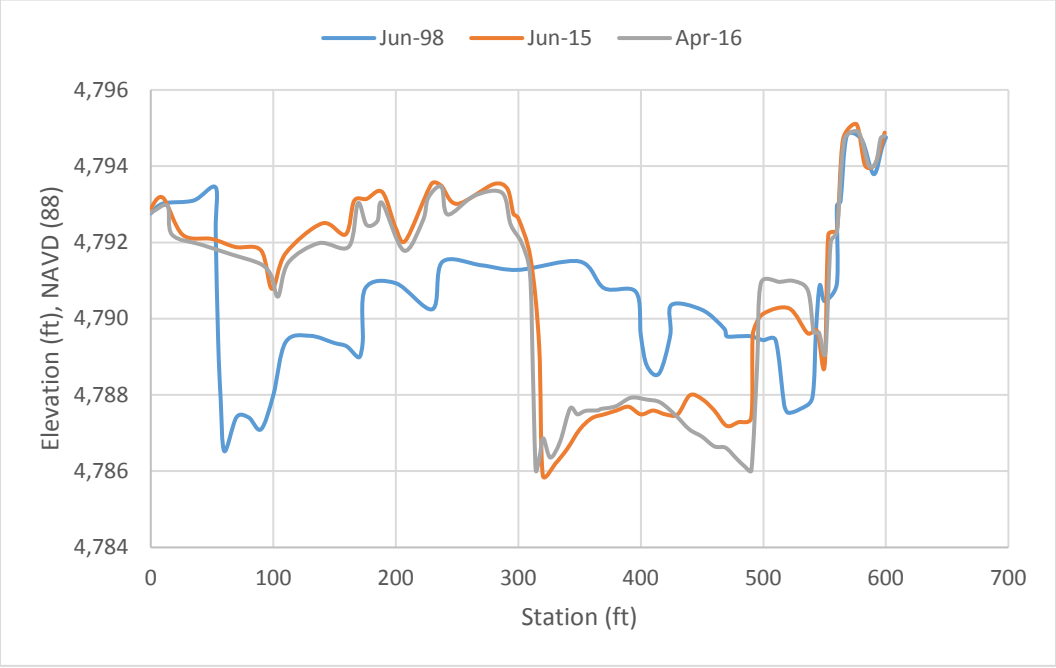

Figure 34. Isleta (IS-884) cross section survey comparison.

IS-885

Channel changes through this section resemble those upstream with significant deposition occurring within the river left and incision dominating the river right. Minor adjustments to bed

elevations within the thalweg took place from 2015 to 2016 and the river left section has incised four feet since 1998. Further movement of the river channel towards the right bank could result in it compromising the levee of the Upper Sabinal Riverside Drain and Sabinal Ditch.

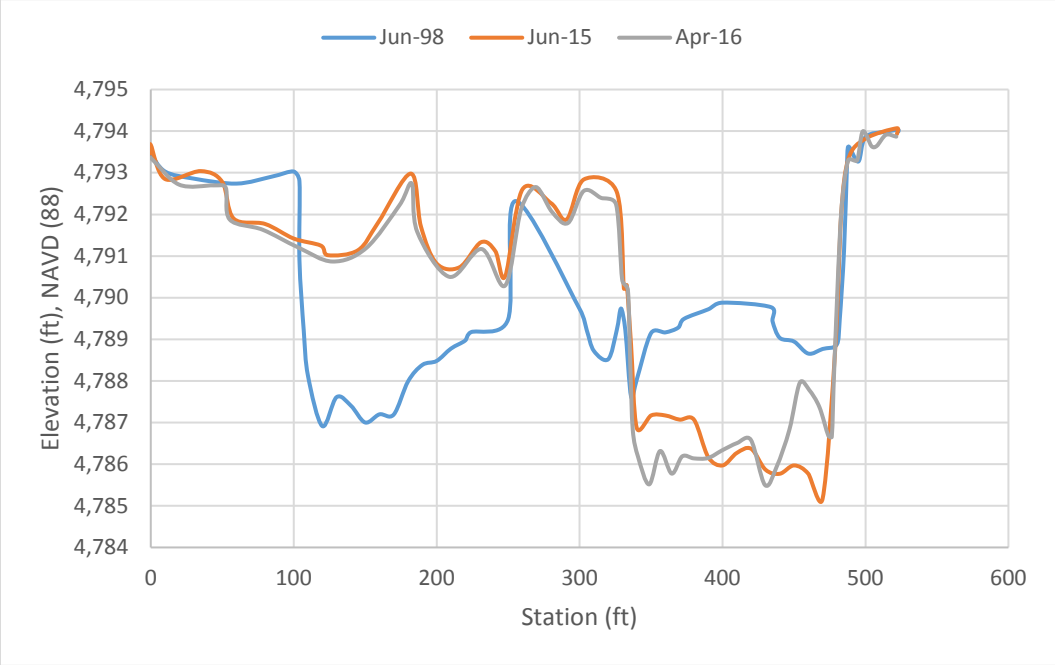

Figure 35. Isleta (IS-885) cross section survey comparison.

IS-887

Since 1998 the river's thalweg has moved from the river left to right channel and the section has transitioned from a system with multiple flow paths to one with a single, wider path. In the last year, the thalweg has moved further towards the right bank and incised by two feet at this location. Aerial photography from 2016 indicates that the right cross section end point sits 225 feet from the Upper Sabinal Riverside Drain levee and the continued incision by the thalweg on the right bank is unfavorable.

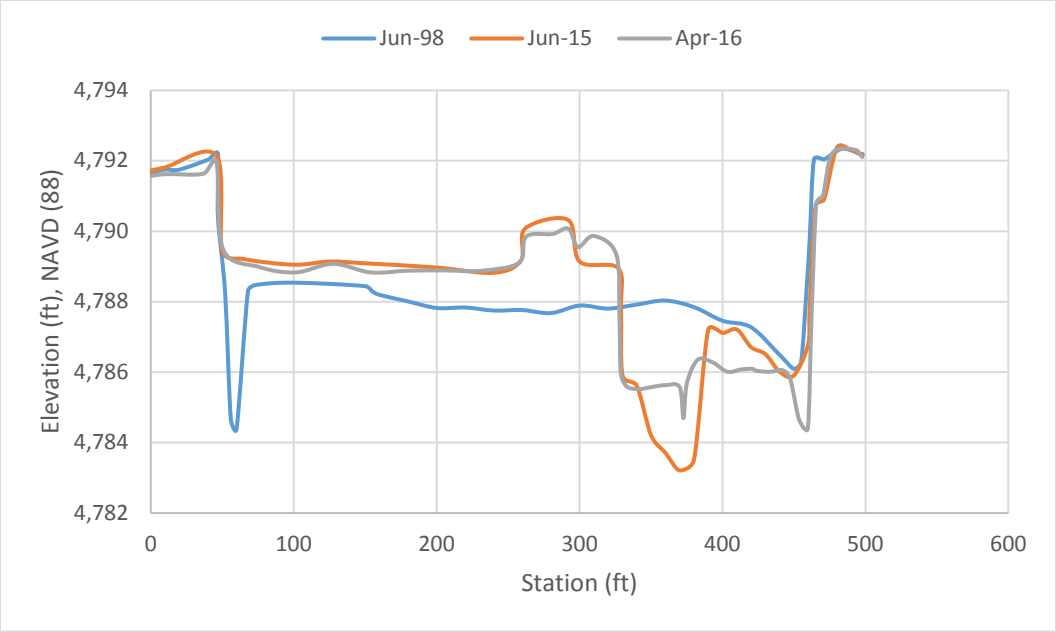

Figure 36. Isleta (IS-887) cross section survey comparison.

CO-895

The channel section has transitioned from two primary flow paths situated on each bank line to three since 1995. Since 1998 the thalweg has increasingly favored the river right section and has widened 80 feet. As is the case in the river sections immediately upstream, the movement of the thalweg to the river right is unfavorable due to its close proximity to the nearby riverside drain.

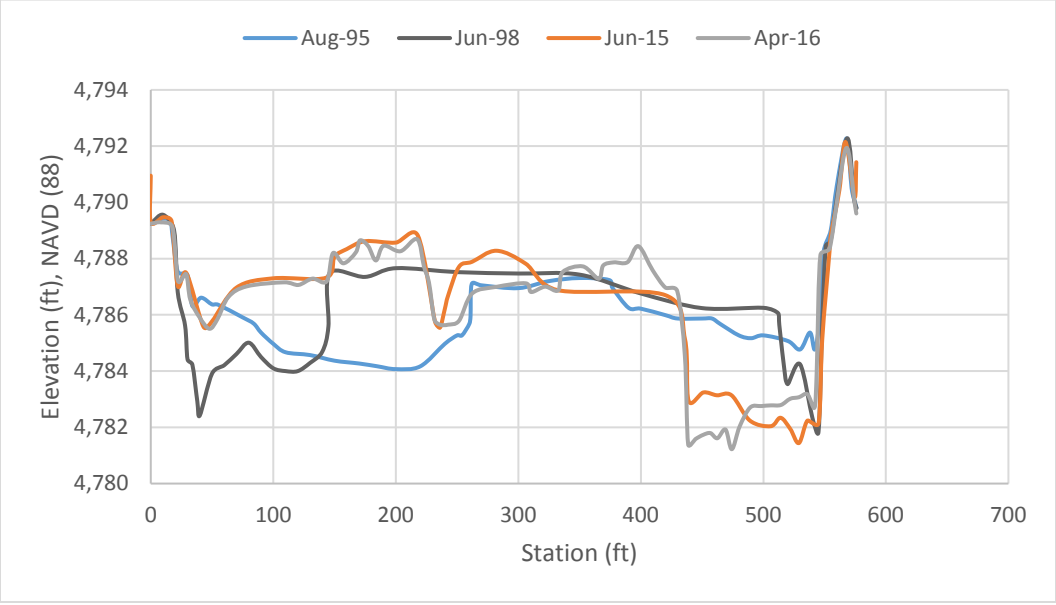

Figure 37. Cochiti (CO-895) cross section survey comparison.

IS-899

The river left channel elevation rose eight feet in some areas between 1998 and 2016 and has incised on the river right by four feet at the thalweg location. Channel topography indicates that incision on the river right increased between 2015 and 2016 while bed elevations on the river left remained relatively unchanged. Spoil levees on both banks confine the channel and prevent it

from impacted riverside infrastructure on either bankline, and it appears these levees are functioning as intended.

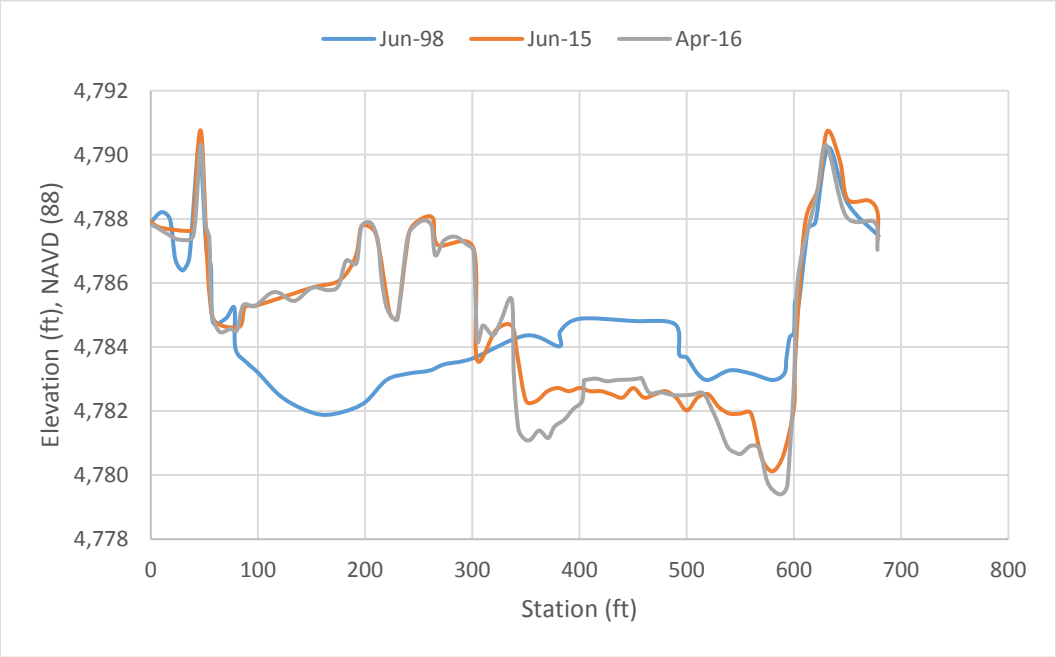

Figure 38. Isleta (IS-899) cross section survey comparison.

IS-908

Deposition has occurred on each river bank since 1998, with the depth of the river right increasing slightly while the river left bed elevation rose by six feet. Bankline sediment deposition has resulted in the river channel narrowing and has shifted the thalweg from the left river to the center of the cross section where it has incised nearly ten feet. The bed incision does appear to be quite rapid as the thalweg invert fell as additional two feet just last year. The main river channel is not currently threatening riverside infrastructure at this location.

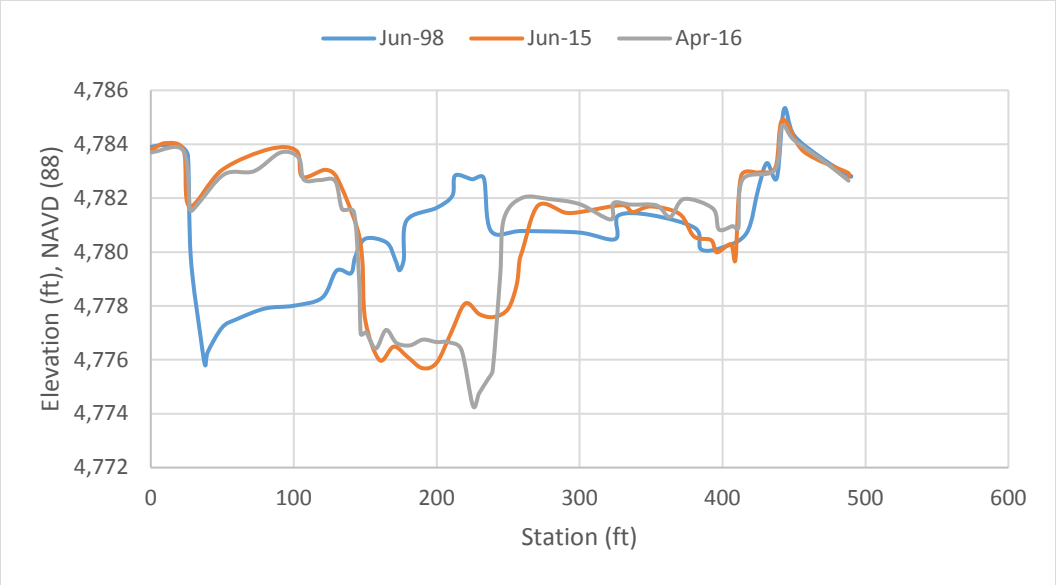

Figure 39. Isleta (IS-908) cross section survey comparison.

CC-924

The channel thalweg became shallower from 1995 to 1996 and the river section has since lowered by about a foot on the river left and experienced near a foot of deposition on the river right by March 2016. Channel width has also narrowed from 1996 with flow becoming more concentrated to the river left.

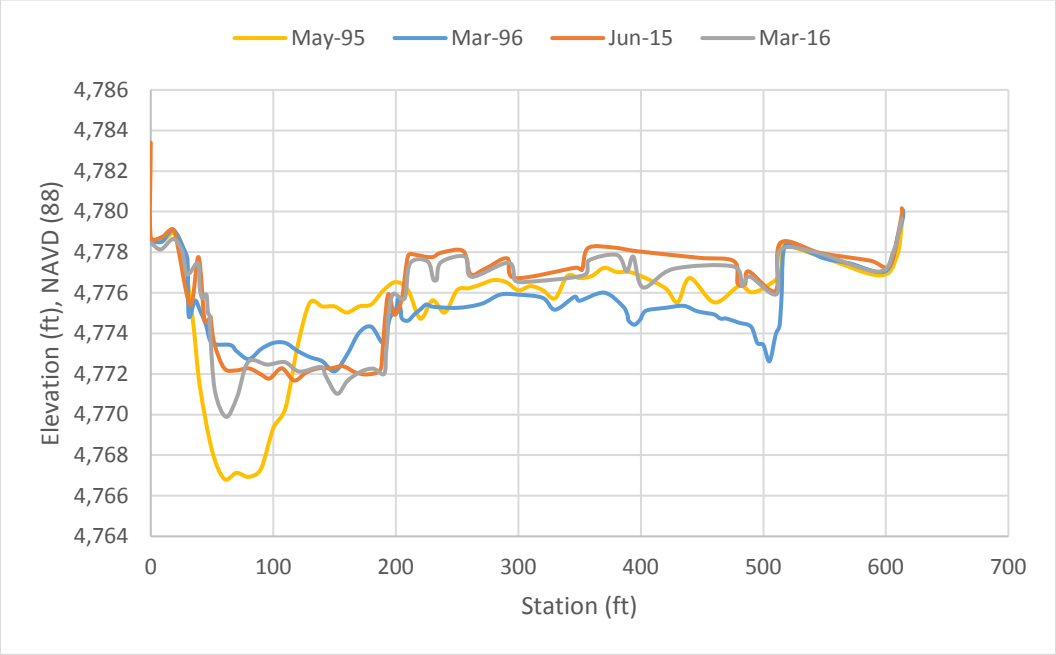

Figure 40. Casa Colorado (CC-924) cross section survey comparison.

CC-927

Over time the river left bed has filled in with five feet of sediment and the river channel has shifted towards the river right where it has incised approximately two feet. The thalweg in 1995 was located in the central cross section which has now filled in and been replaced by a bar island

that extends back to the left bank. The shift of the channel thalweg towards the right bank could impact the operations of Feeder Ditch #3 in Valencia County just south of Jarales.

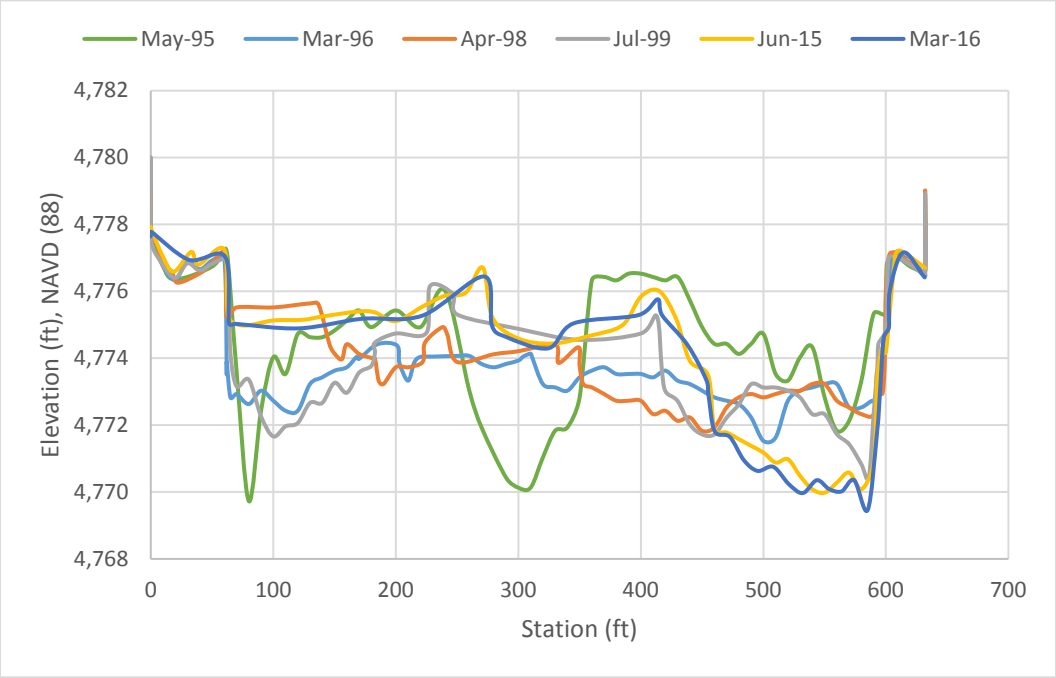

Figure 41. Casa Colorado (CC-927) cross section survey comparison.

CC-932

After the initial deposition within the thalweg from 1995 to 1996 the thalweg has again deepened to near its 1995 depth and has widened towards the river right section. From 1995 approximately four to six feet of sediment has been deposited on the river right which has reduced the number of primary flow paths through the section and confined flow largely to the section's center. The river has room to move further to the river left within this section without impacting infrastructure.

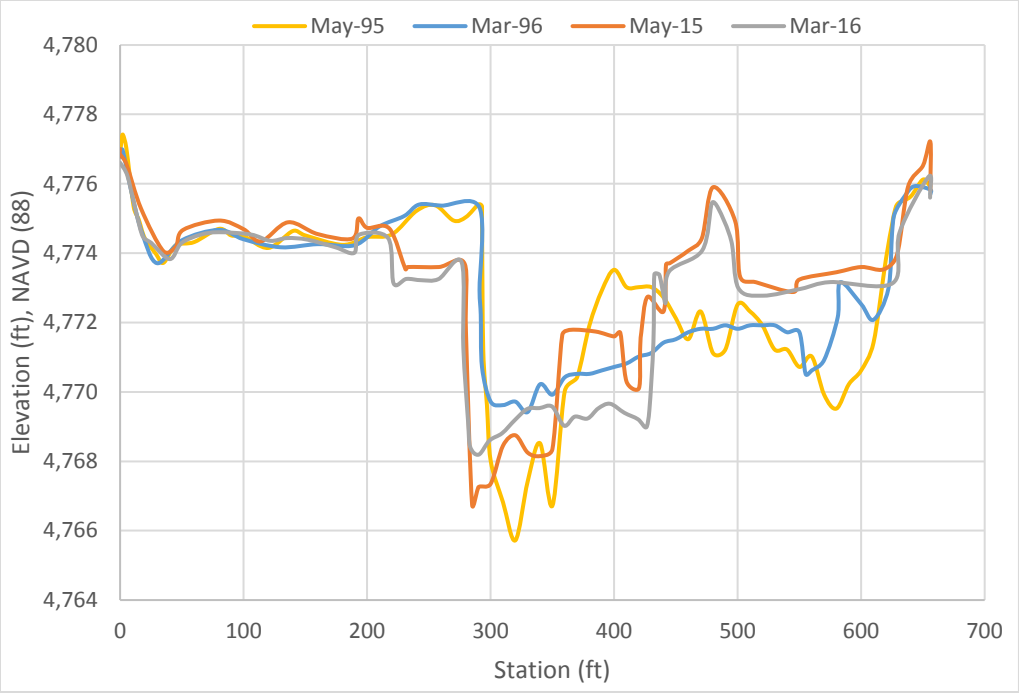

Figure 42. Casa Colorado (CC-932) cross section survey comparison.

CC-936

The thalweg within the river left section has deepened two feet and widened 120 feet since March, 1996. Additionally, the river right has risen in elevation by approximately two feet. This created a bar island in the cross section center that now has become directly connected to the river right bank which is beneficial to nearby lateral riverside drains.

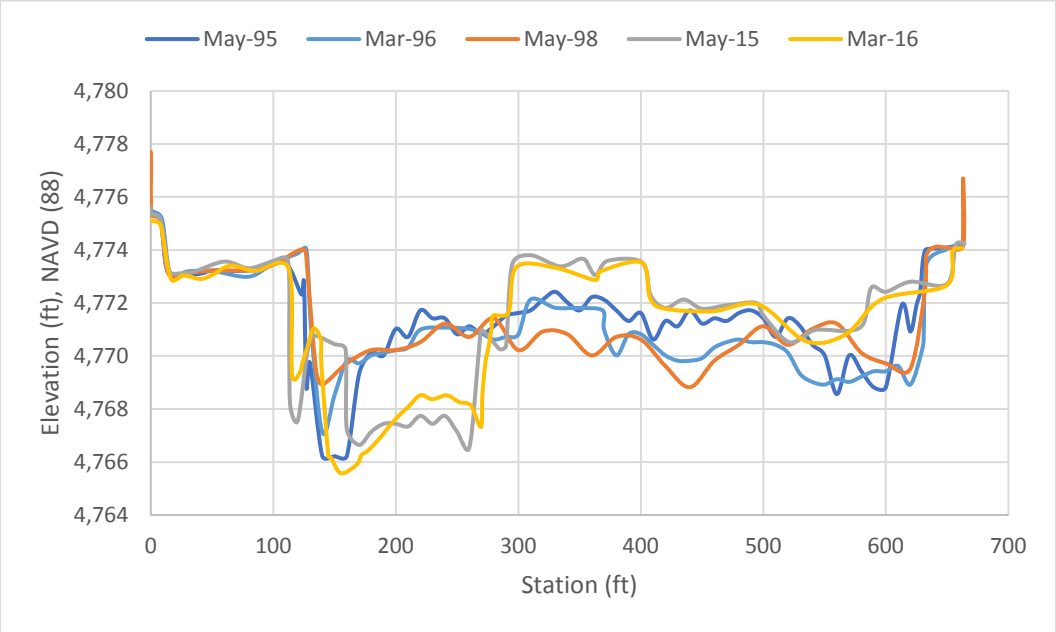

Figure 43. Casa Colorado (CC-936) cross section survey comparison.

CC-941

The river channel has long been confined to the river left through this section. Movement away from the river left towards the center is shown in the 2016 survey data and this shift is beneficial from the standpoint of securing riverside infrastructure. A net deposition of sediment across the entire section has occurred since 1995 and the thalweg invert has increased by two feet during this time period.

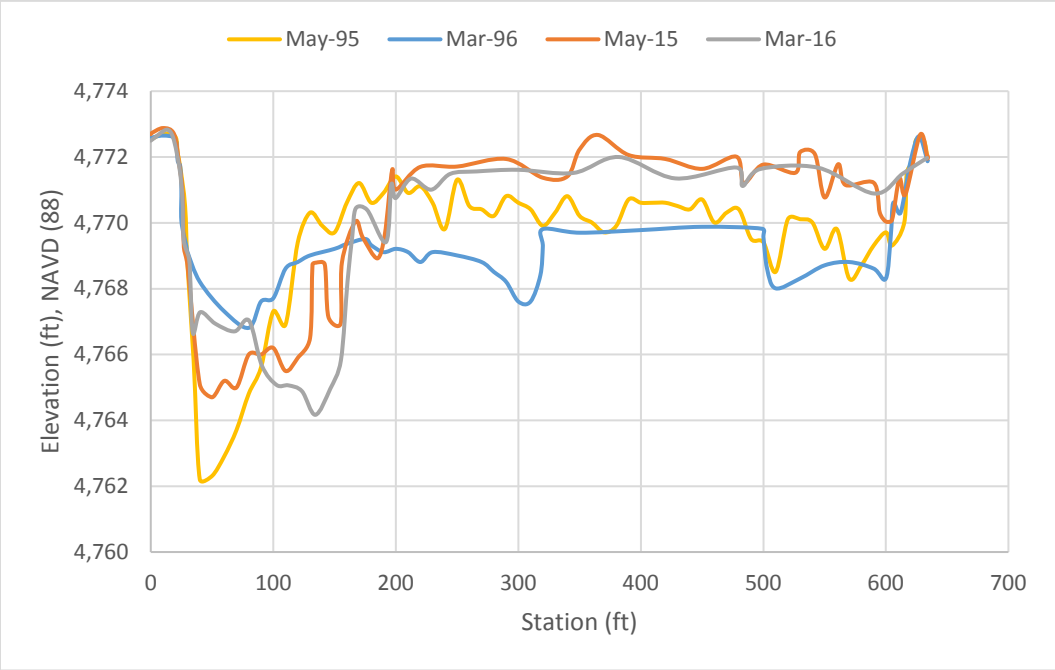

Figure 44. Casa Colorado (CC-941) cross section survey comparison.

CC-945

The 1995 thalweg in the river right has become perched over time, increasing in elevation by eight feet as of March, 2016. The deposition of sediment within the river right has forced flows to shift towards the left bank and the new river thalweg to be located at the section center.

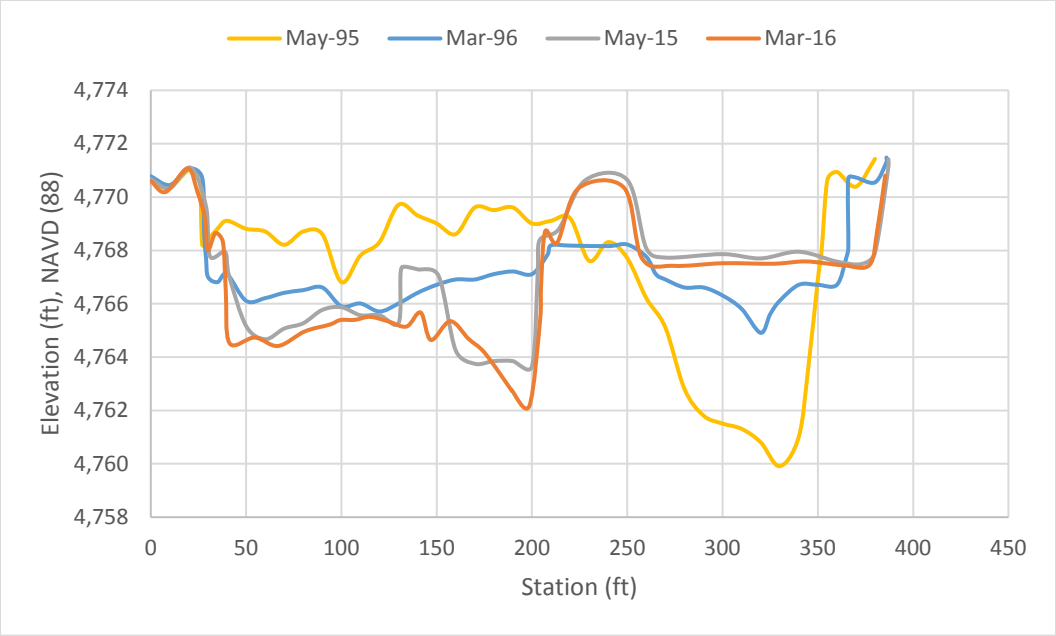

Figure 45. Casa Colorado (CC-945) cross section survey comparison.

CO-966

From 1995 to 1998 the river channel experienced considerable sediment deposition across the section, filling in the thalweg at the right river a depth of five feet. This produced a river section with many shallow, branched flow paths. Since that time the river has again incised the thalweg to its original depth but this time at the center of the cross section. Flow within the section is now largely confined to the channel thalweg.

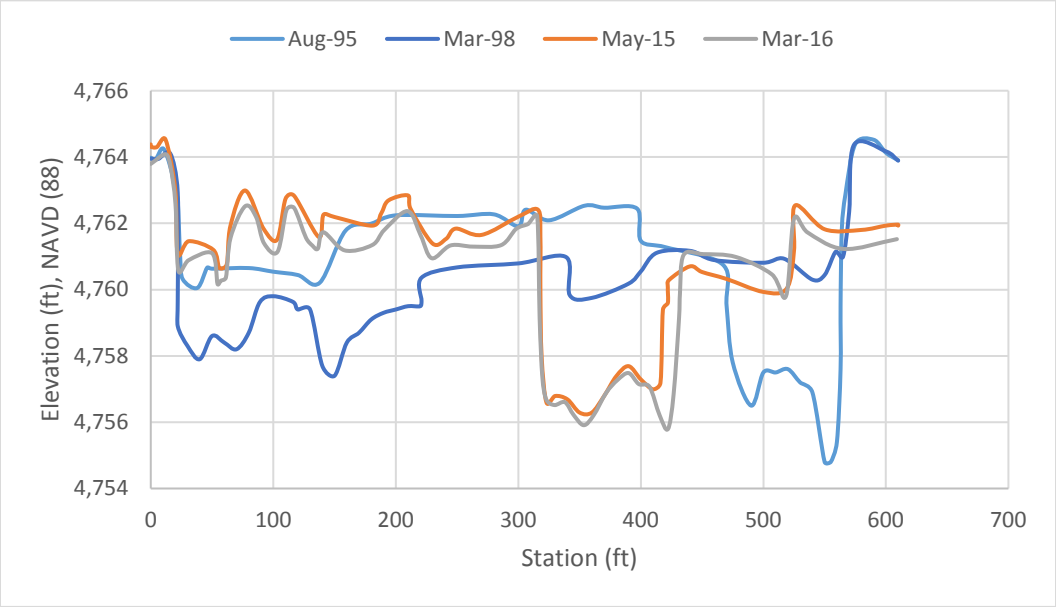

Figure 46. Cochiti (CO-966) cross section survey comparison.

CO-986

This section has largely increased in bed elevation since 1995 with the thalweg shifting inwards from the river right. A possible explanation for the raise in bed elevation rather than the

predominant incision from upstream cross sections is that the Abo Arroyo seems to deliver a significant sediment load to the river and it is located two river miles upstream from this section. At some point in time spoil levees were placed on each river bank just outside of these cross section endpoints, providing resistance to lateral movement of the river channel.

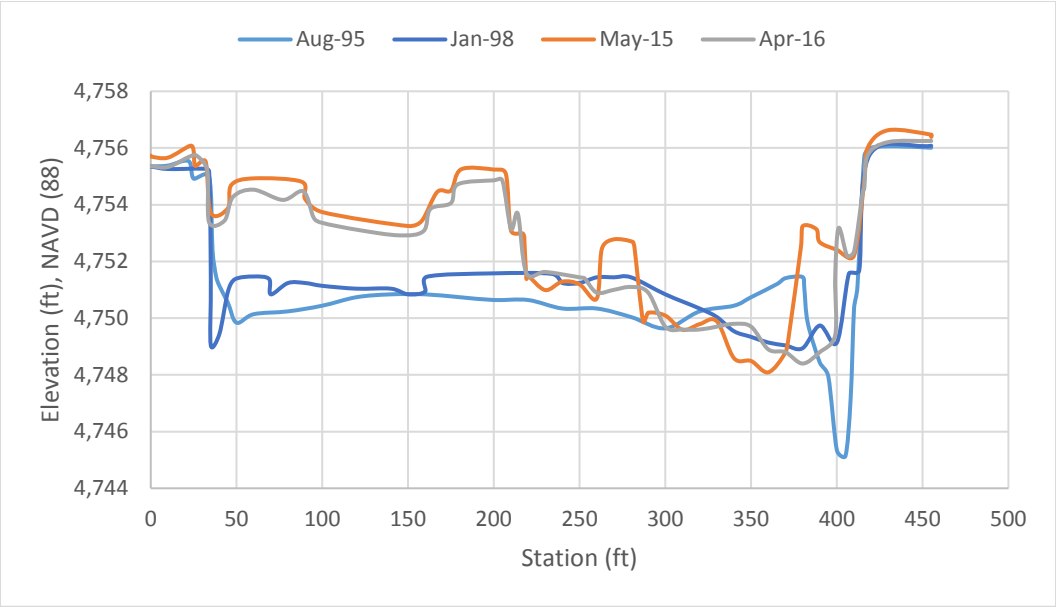

Figure 47. Cochiti (CO-986) cross section survey comparison.

CO-1006

The channel section experienced a considerable amount of sediment deposition between 1995 and 1998, raising the bed elevations and creating a channel cross section that was relatively flat across its entire width. After 1998 incision once again reduced the river left and right elevations as well as established a central bar island that has persisted through the 2016 survey.

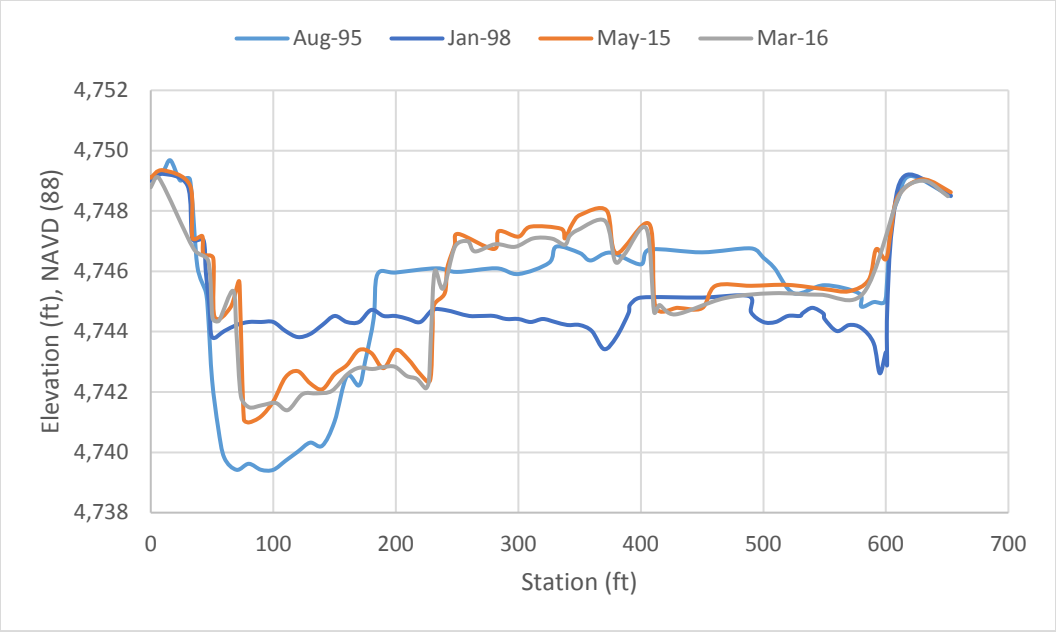

Figure 48. Cochiti (CO-1006) cross section survey comparison.

AH-1

The bar island from the upstream cross section carries through this section where it has separated the river flow into two primary flow paths at the river left and right edges. Channel topography was remained relatively stable between 2015 and 2016 at this location.

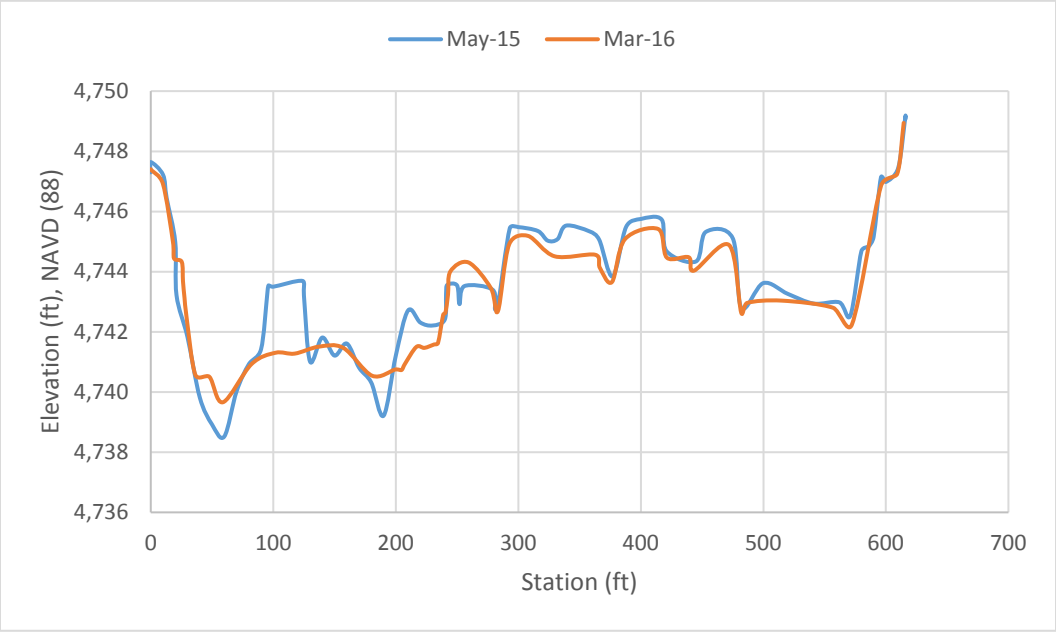

Figure 49. Abeyta's Heading (AH-1) cross section survey comparison.

AH-3

The channel profile again appears to be relatively stable in this cross section from 2015 to 2016. The most significant change through the year is the shift of the thalweg towards a more central location from the left bank.

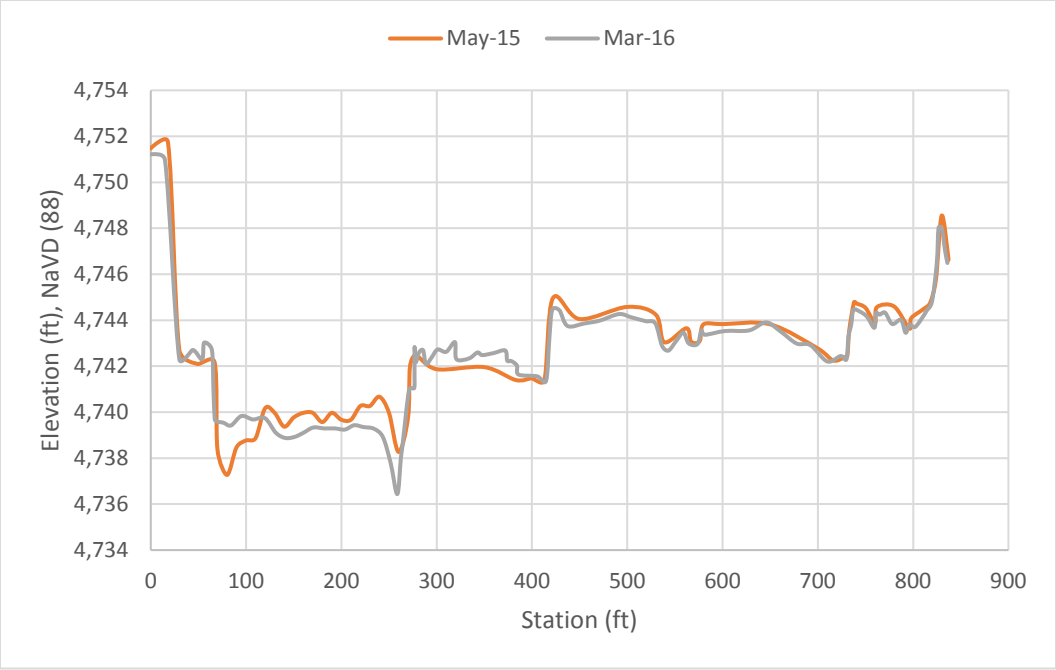

Figure 50. Abeyta's Heading (AH-3) cross section survey comparison.

AH-5

Minor bed lowering has occurred within the river right section since 2015, however, cross sectional bed elevation changes are minimal.

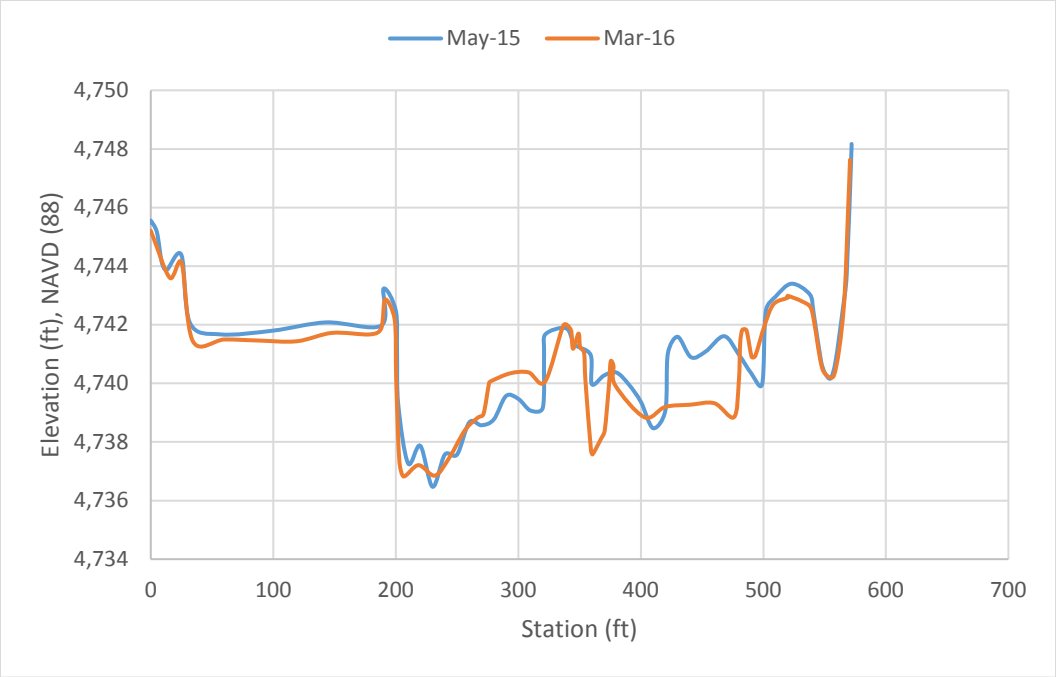

Figure 51. Abeyta's Heading (AH-5) cross section survey comparison.

AH-7

There has been a two foot increase in the channel thalweg through this section since 2015 and it has widened slightly in this period. Some deposition can be viewed in the river right section, although this is minimal.

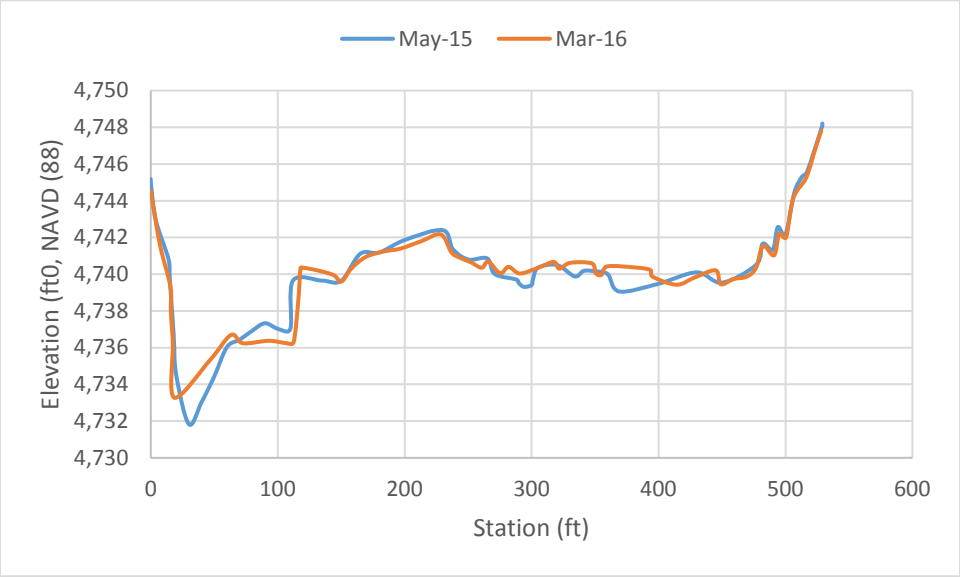

Figure 52. Abeyta's Heading (AH-7) cross section survey comparison.

CO-1026

Channel incision has dominated within the river left section since 1998 and sediment deposition has raised the river left bed by three feet at various locations. Current aerial imagery shows that the river right has become densely vegetated indicating that recent flows have not been high enough in the river to dislodge this growth from the channel bed.

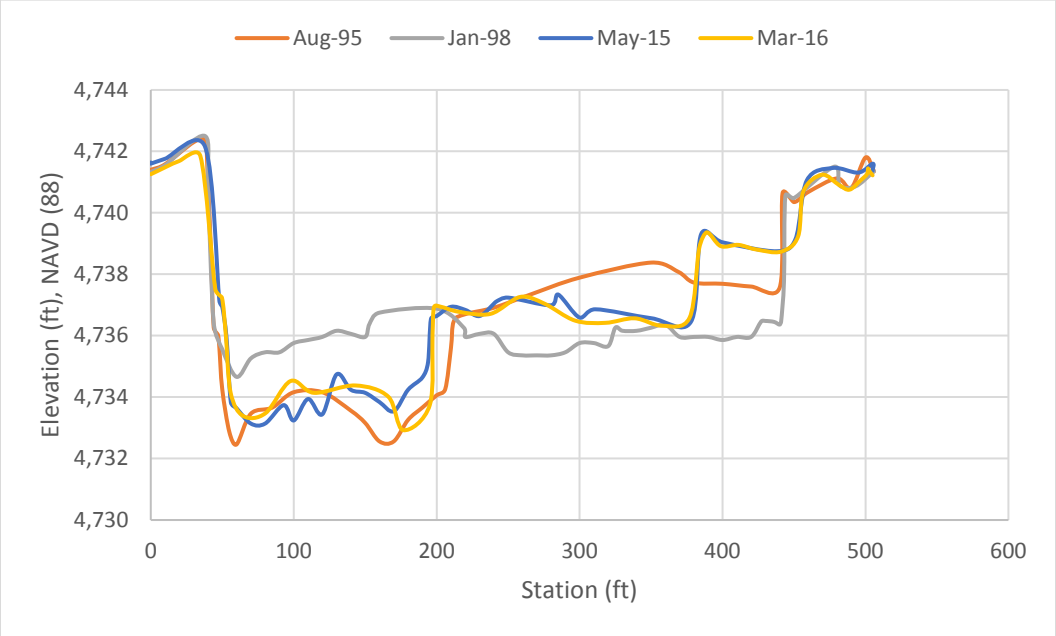

Figure 53. Cochiti (CO-1026) cross section survey comparison.

CO-1044

Since 1998 the river left has experienced deposition while the river right incised almost to its 1995 elevation of 4,724 feet (six feet of incision). The thalweg in the river right has increased in width since 2015 towards the river right bank.

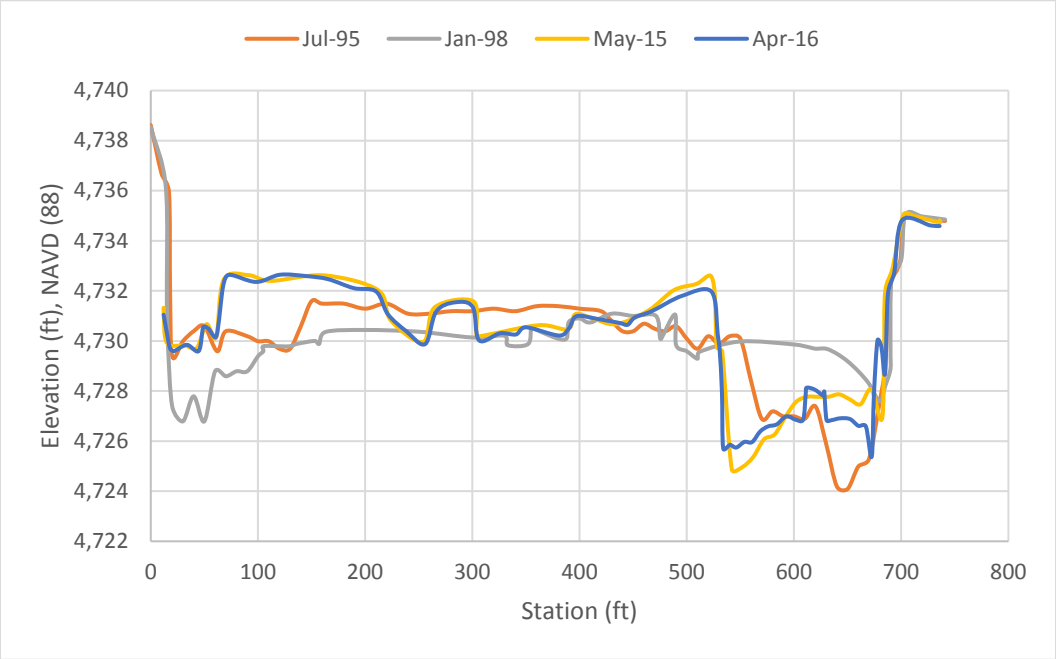

Figure 54. Cochiti (CO-1044) cross section survey comparison.

CO-1064

From 1995 to 2015 the river thalweg moved from the left bank to the right bank. Sediment deposited in the original 1995 thalweg increasing its bed elevation while the right bed has incised four feet in this time. A sand bar formation along the river left bank appears to be reinforced by sediment deposits emptying into the river from the Maes Arroyo to the east.

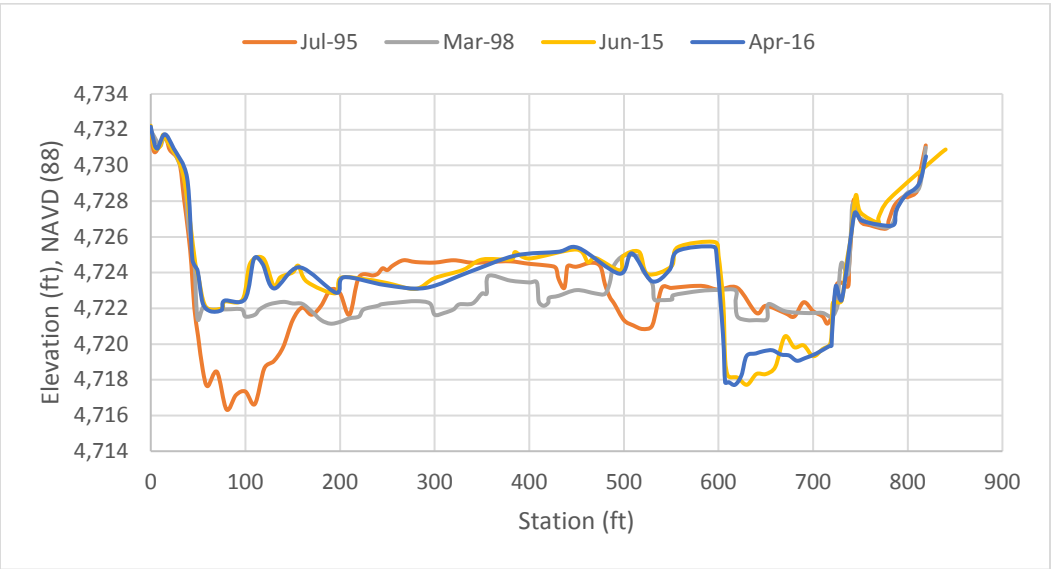

Figure 55. Cochiti (CO-1064) cross section survey comparison.

CO-1091

This cross section is situated just north of the confluence of the river with the Rio Puerco. Bed elevations across the entire channel have been increasing since 1995, with the exception of the period between November, 2000 and June, 2015 where the thalweg elevation had risen five feet in 2000 and then incised almost three feet by 2015. In 2016 the thalweg incision was reversed and the channel began to fill in again with sediment, increasing the thalweg elevation by up to two feet. It is preferred that the primary river flow path be directed away from the river left bank due to its proximity to the levee of the Lower San Juan Riverside Drain.

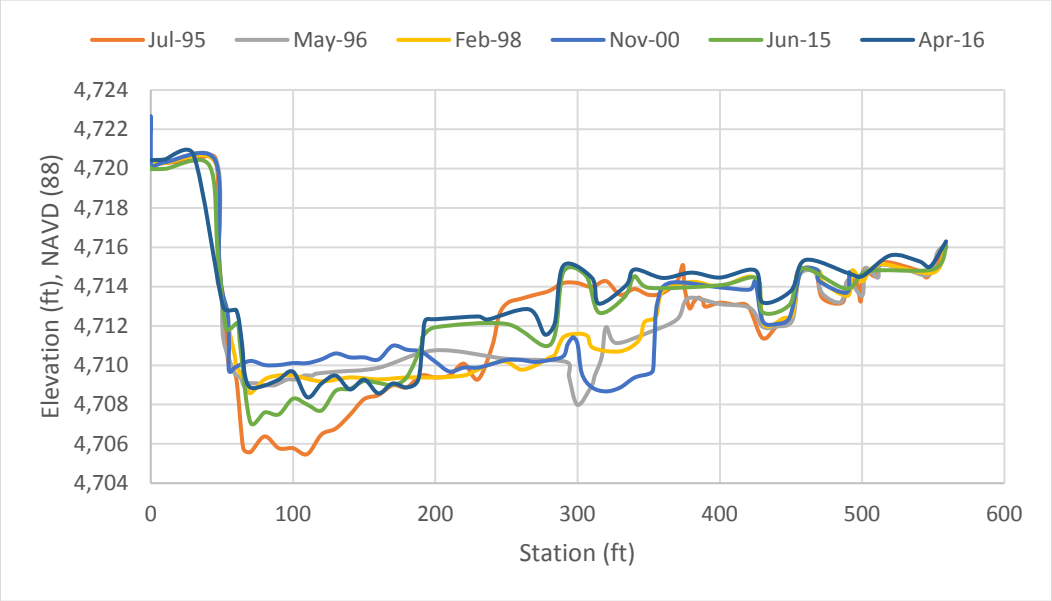

Figure 56. Cochiti (CO-1091) cross section survey comparison.

RP-1100

Endpoint locations have been altered multiple times through this section since 2000. This is due to the cross section being located immediately downstream of the confluence with the Rio Puerco which annually carries very high suspended sediment loads to the Rio Grande. Both the 2015 and 2016 cross section surveys were adjusted to capture a wider swath of the channel and as such a new right endpoint was established which becomes apparent in Figure 157 below. Four feet of deposition in the river left occurred between 2000 and 2012 and the river central section has been more dynamic with both deposition and incision taking place between 2000 and 2016. The more recent surveys have identified additional flow paths towards the river right section and bed elevations within this section have remained relatively stable between 2015 and 2016.

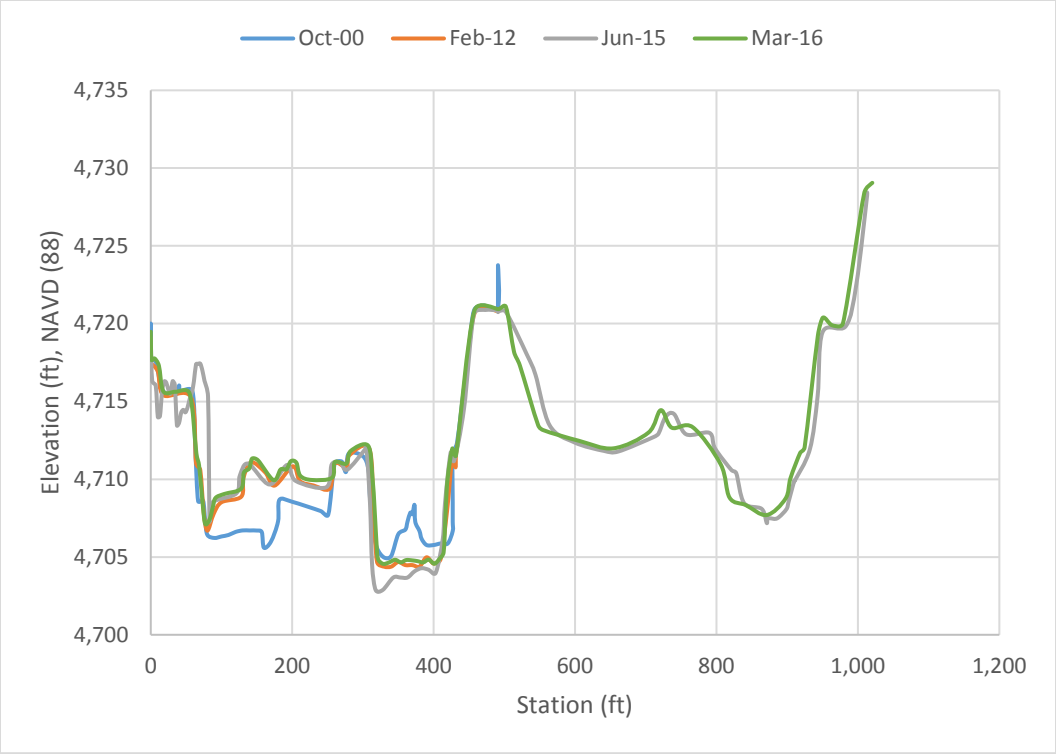

Figure 57. Rio Puerco (RP-1100) cross section survey comparison.

CO-1104

Bed elevations rose in the channel from 1995 to 1996 by two feet. Incision then occurred in the river left in 1998 and the thalweg elevation lowered by three feet while sediment accumulated within the river central section. Sedimentation in the channel then completely filled in the left channel thalweg, leaving behind a river bed that was fairly uniform in elevation across a width of 165 feet. After 2000, incision began again in the river left and the channel width narrowed to 90 feet by 2015. The effects of lateral inputs of water and sediment by the Rio Puerco and Salas Arroyo upstream of the section have resulted in a very dynamic channel at this location, with both sedimentation and channel incision taking place on any given year.

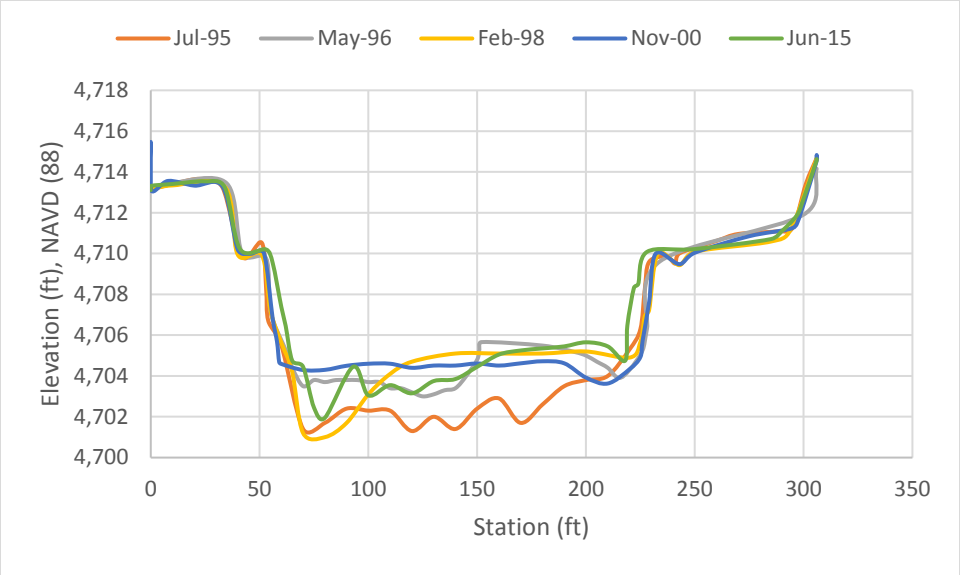

Figure 58. Cochiti (CO-1104) cross section survey comparison.

RP-1108

The location of the channel thalweg at this cross section has remained fairly stable over the last two decades. Thalweg depth and width have also been relatively stable, however, there is some aggradation present along the channel bottom from the top of the thalweg slope to the right channel bank toe (approximately one foot deep).

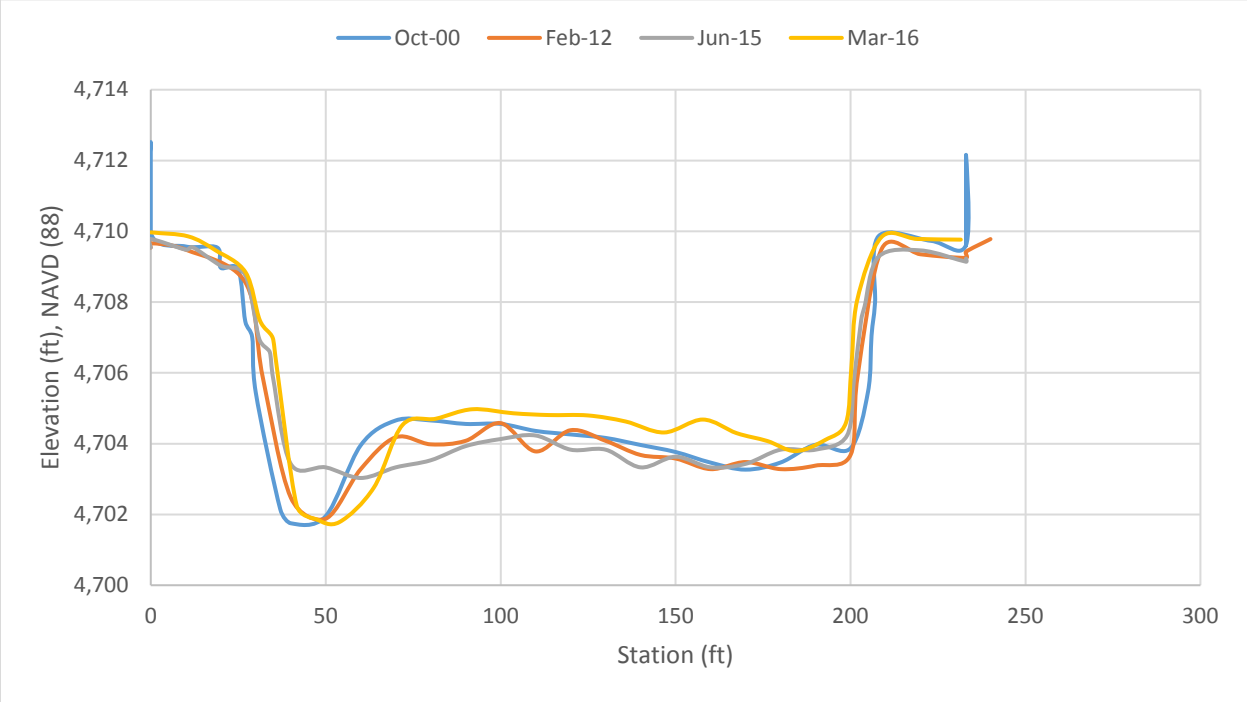

Figure 59. Rio Puerco (RP-1108) cross section survey comparison.

RP-1144

The right endpoint of this cross section survey was reestablished in 2012 to a point further to the east. Considerable sediment accumulation in the river center channel has taken place since 2000 which has forced the channel thalweg to migrate towards the river right. The thalweg narrowed between 2012 and 2016 by 90 feet. Movement of the thalweg towards the river right does have the possibility of impacting the Drain Unit 7 Extension that runs from Contreras to San Acacia.

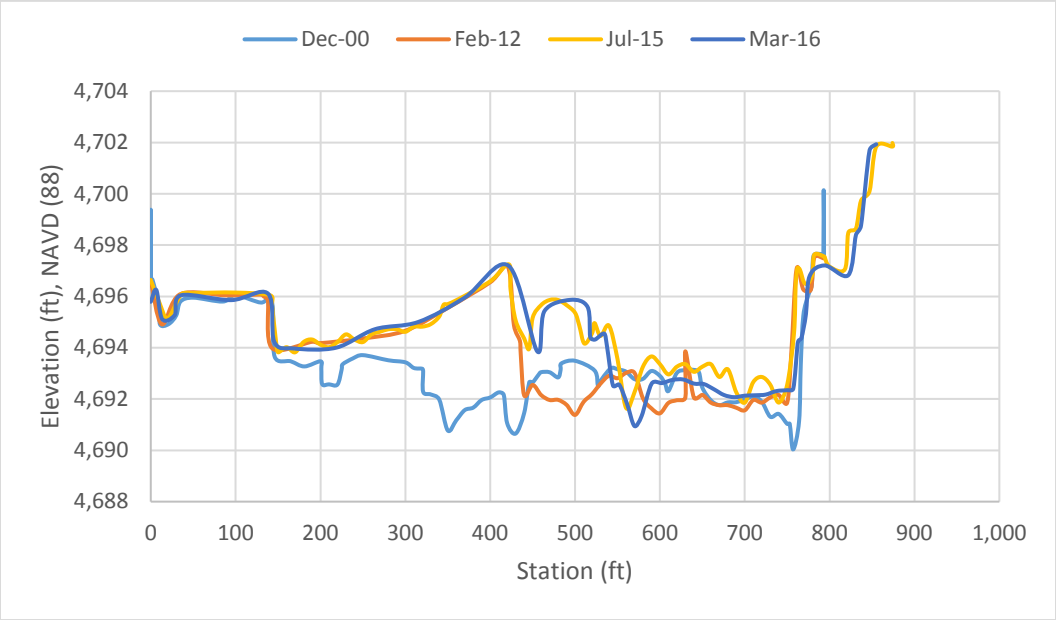

Figure 60. Rio Puerco (RP-1144) cross section survey comparison.

RP-1150

Since October 2000 this section has experienced considerable deposition along the river left and right to a depth of five feet at some locations. The thalweg has been adjusting laterally slightly on the right bank and has become shallower in depth. Just below this section flow becomes increasingly confined as the river is squeezed between the levee berm of the Drain Unit 7 Extension to the west and a high bluff wall to the east. The only concern to riverside infrastructure would be with the western drain if the thalweg expanded or realigned itself towards the river left bank. The left endpoint of the cross section was reassigned with the 2016 survey, thus extending the profile another 280 feet to the west.

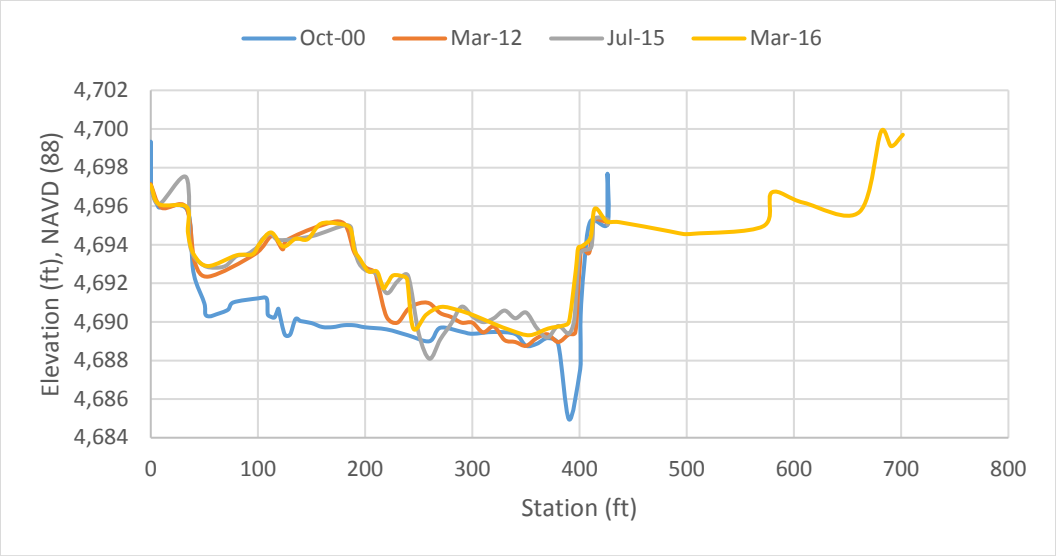

Figure 61. Rio Puerco (RP-1150) cross section survey comparison.

RP-1160

Flows remain heavily confined through this section with the Drain Unit 7 Extension on the right bank and high bluffs bordering the left. A lateral input by an intermittent stream (the Cañada Ancha) occasionally delivers additional sediment load to the left bank just above the cross section. The section profile has been mostly stable since 2000, with a two foot incision at the thalweg between 2000 and 2012 that had recovered (filled back in with sediment) by the 2015 survey.

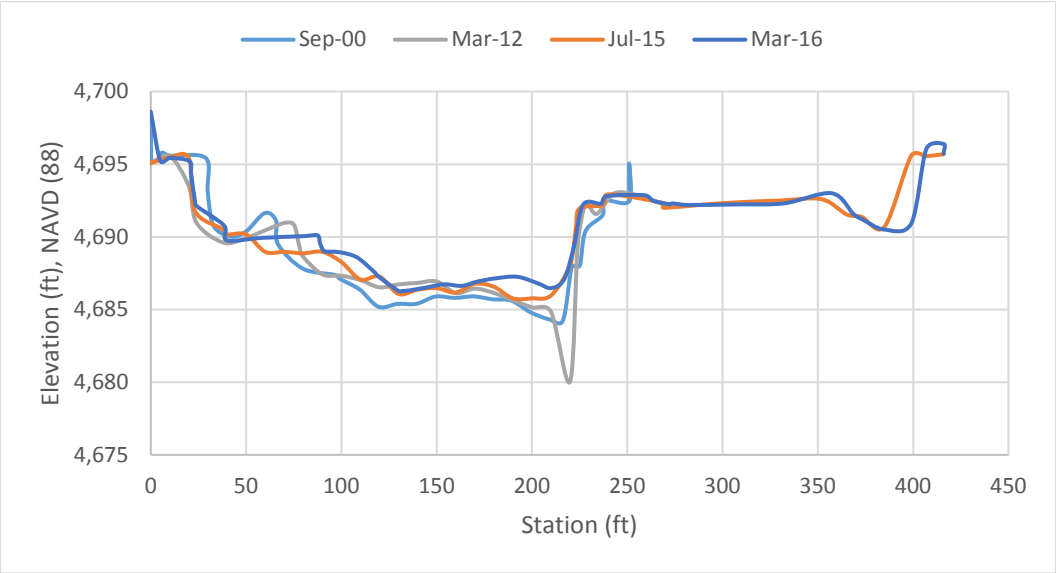

Figure 62. Rio Puerco (RP-1160) cross section survey comparison.

CO-1164

The channel bed has been increasing in elevation since the 1995 survey until March, 2016 where the river left bed elevation incised three feet. The thalweg has shifted from its central location in 1995 to the right channel in 2000, and then finally to the river left by 2016. Flows are still

confined by high bluffs to the east and the Drain Unit 7 Extension to the west until they empty from RP-1170 downstream of this section.

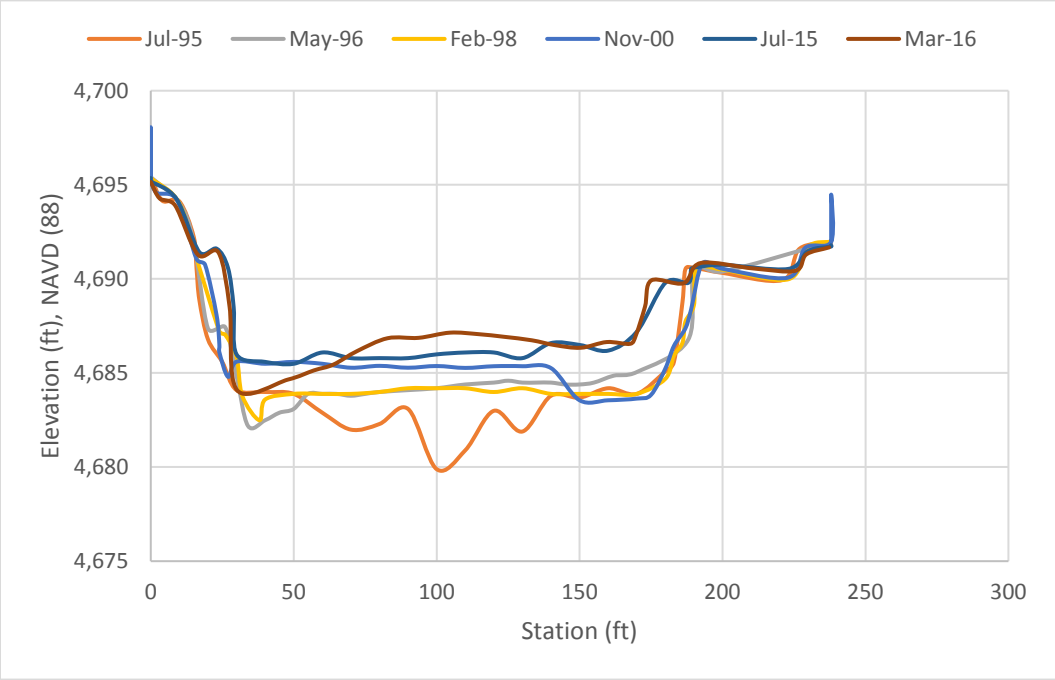

Figure 63. Cochiti (CO-1164) cross section survey comparison.

RP-1170

The relocation of the right endpoint to the levee berm of the Drain Unit 7 Extension in 2016 now extends the channel profile to fit within the entire active river channel. Sometime after the September 2000 survey a central island formed in the cross section and was established by March, 2012. In 2016, this bed elevation had risen six feet since 2000. The bar island has now separated the main channel flow into two pathways directed towards the river left and right banks. The 2015 survey found that there was incision occurring on the river left while the river right bed elevations rose, however, opposing processes took place in each section during the next year. Riverbed profiles in this section are highly variable.

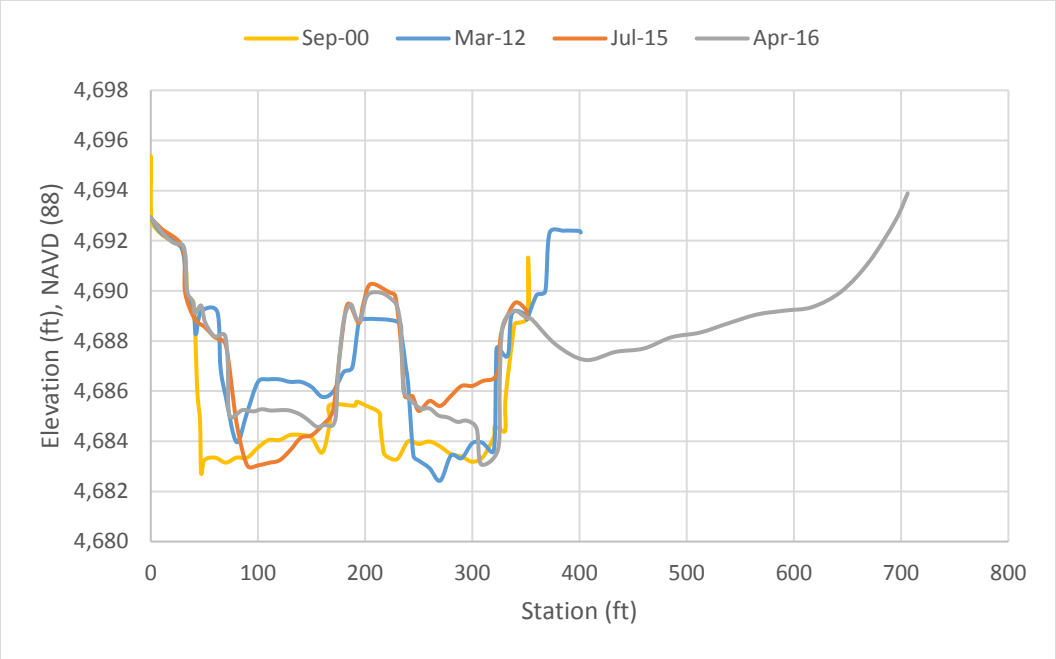

Figure 64. Rio Puerco (RP-1170) cross section survey comparison.

CO-1179

This cross section lies immediately upstream of the confluence with the Rio Salado and has seen bed elevations steadily rising with the exception of 2015 where some channel incision took place on the river left (1-2 feet of elevation drop). Overall the bed had risen approximately four feet since July 1995. The right endpoint was reestablished during the March, 2012 survey and bank elevation at this point had increased around four feet since the 1998 survey. The channel width has narrowed to 130 feet from its maximum width of 170 feet in 1995.

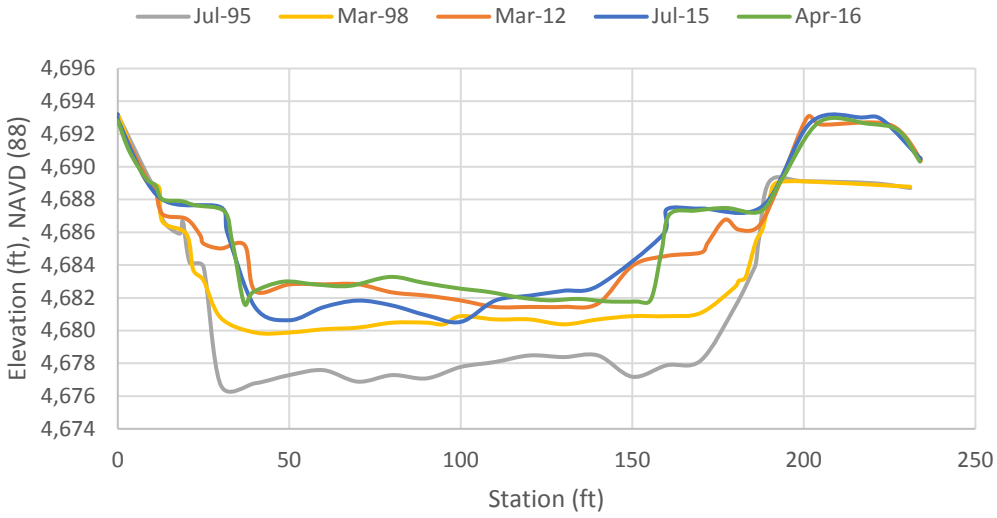

Figure 65. Cochiti (CO-1179) cross section survey comparison.

RP-1184

The confluence with the Rio Salado is directly upstream of this section and as such the cross section profile at this location is highly dynamic. The overall trend within this section has been

sediment deposition raising the bed elevation, however, the 2016 survey data shows a 213 foot wide by three foot deep portion of the river right being removed from the section and the channel widening back to the 2012 extent.

.

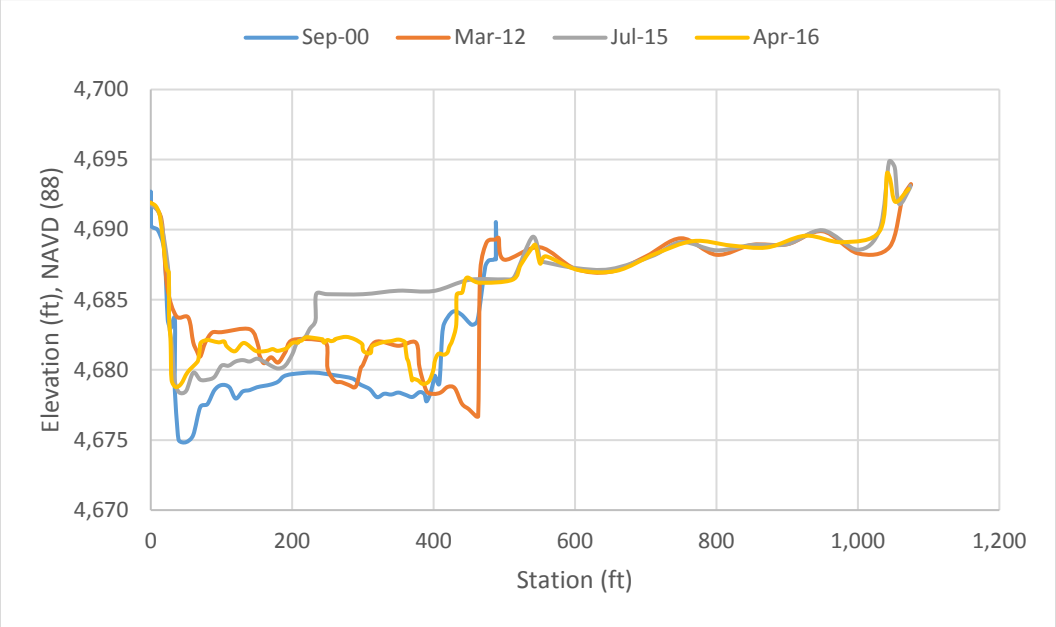

Figure 66. Rio Puerco (RP-1184) cross section survey comparison.

RP-1190

The main channel and river thalweg are very active in this section most likely as a result of its location downstream of the Rio Salado confluence. General trends in sediment deposition and channel incision are not clear for the section. Additionally, both the LEP and REP have been relocated multiple times for the cross section further complicating any analysis.

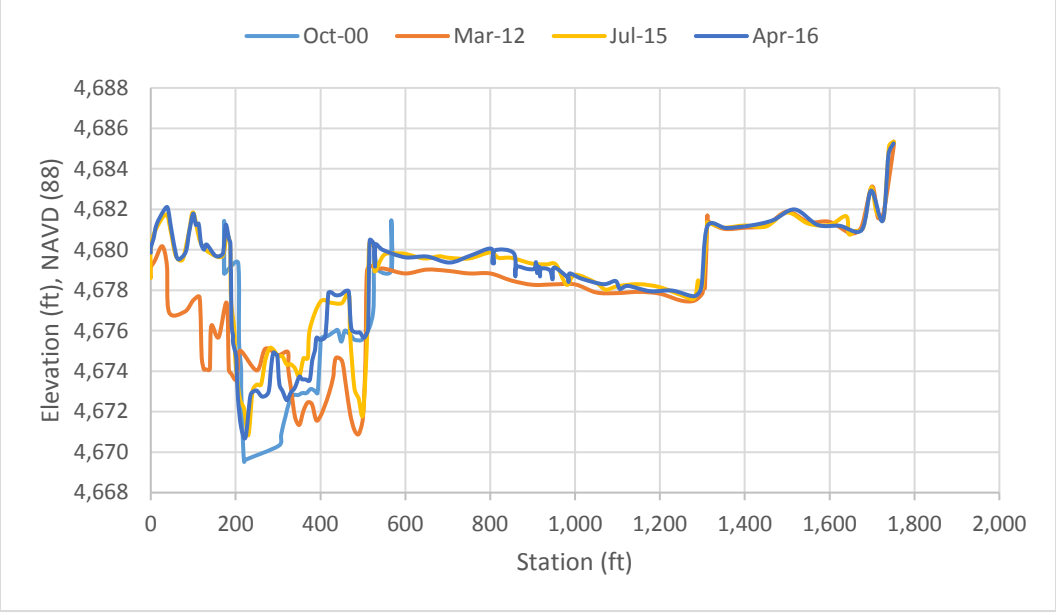

Figure 67. Rio Puerco (RP-1190) cross section survey comparison.

CO-1194

The river channel width has been fairly constant since the early 2000s. The river right bank has migrated laterally to the west close to 260 feet between 1995 and 2016. Between 1995 and 2000 thought the thalweg shifted to the east. Since 2000 sediment has been accreting on the river left floodplain on the order of four to five feet. The thalweg has also incised about 3.5 feet between 1995 and 2016. This river section continues to be heavily impacted by sediment transport from the Rio Salado and remains very dynamic.

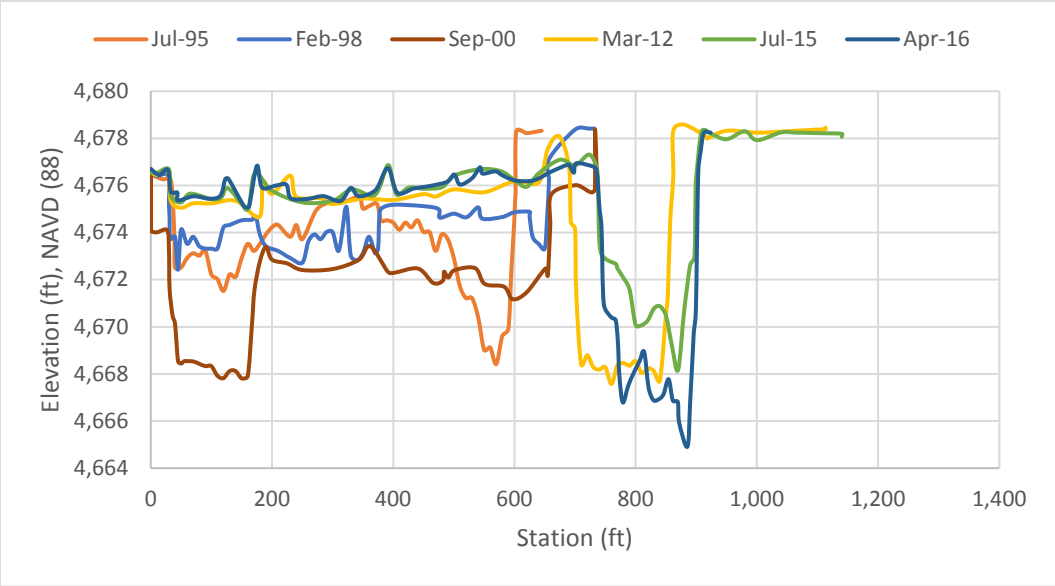

Figure 68. Cochiti (CO-1194) cross section survey comparison.

RP-1197.5

The river channel has been widening at this location since 2012 and the REP of the cross section has been shifted twice to account for this. The thalweg incised slightly between 2006 and 2012, became filled with sediment to a depth of four feet by 2015, and then incised three feet by April, 2016. This river section continues to be heavily impacted by sediment transport from the Rio Salado and remains very dynamic.

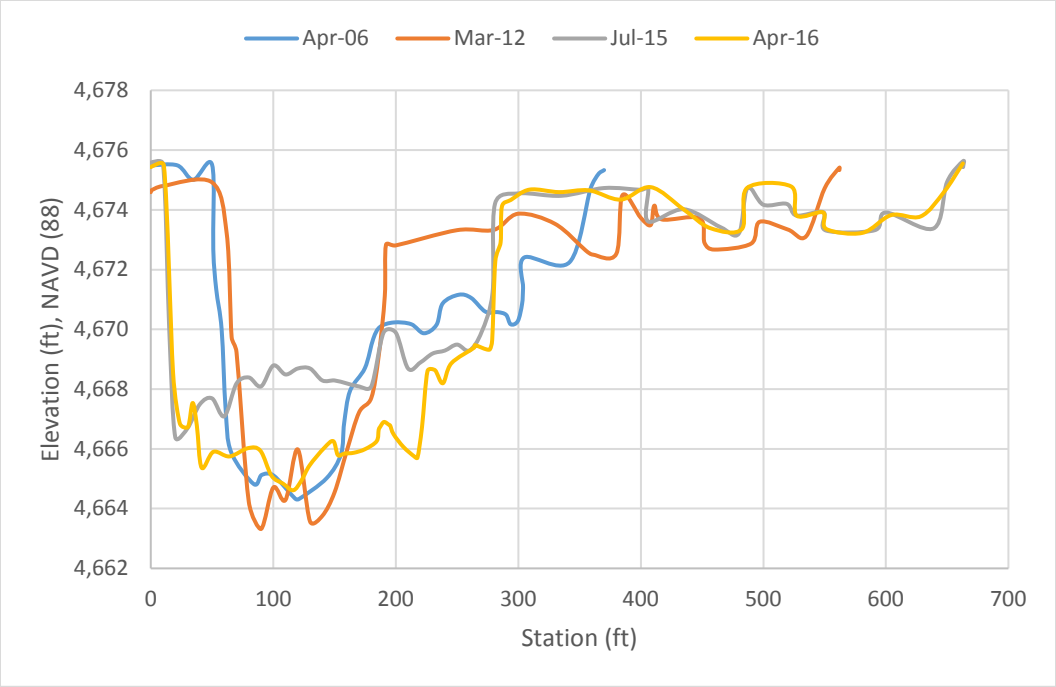

Figure 69. Rio Puerco (RP-1197.5) cross section survey comparison.

RP-1201

A cycle of deposition followed by incision has been repeated with each new survey of the cross section. Recently the channel has narrowed and has incised six feet back to its September 2000 elevation. There is no drainage infrastructure immediately adjacent to the channel at this location.

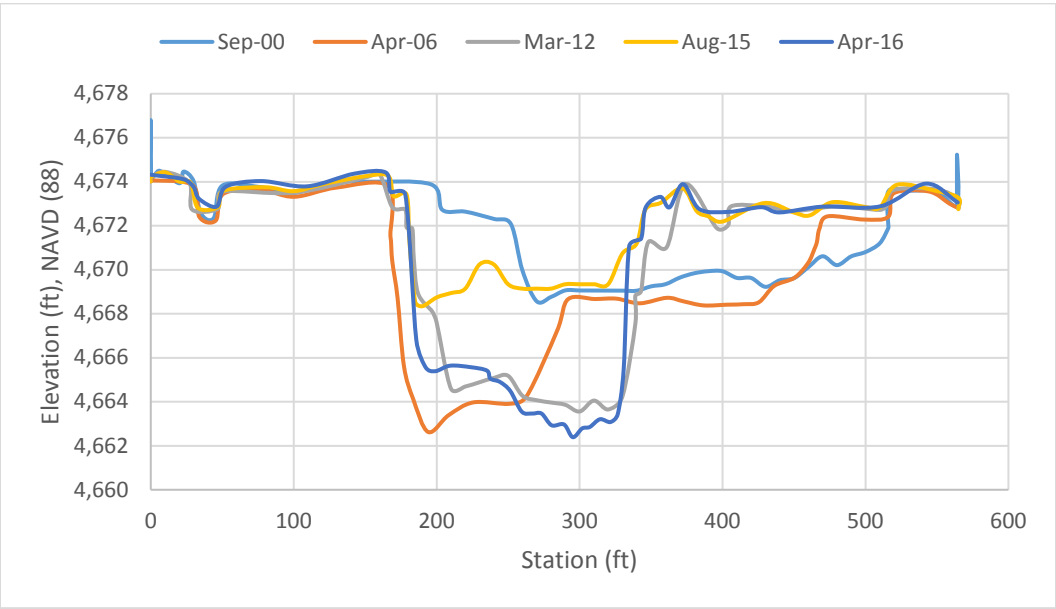

Figure 70. Rio Puerco (RP-1201) cross section survey comparison.

RP-1202.5

Between April 2006 and March 2012 the thalweg shifted inwards 50 feet from the right riverbank and narrowed slightly. Sediment deposition raised the thalweg bed by four feet from 2012 to 2015, and within the next year the thalweg had reverted back to incising to its original 2012 invert elevation. There are no impacts to riverside infrastructure at this location.

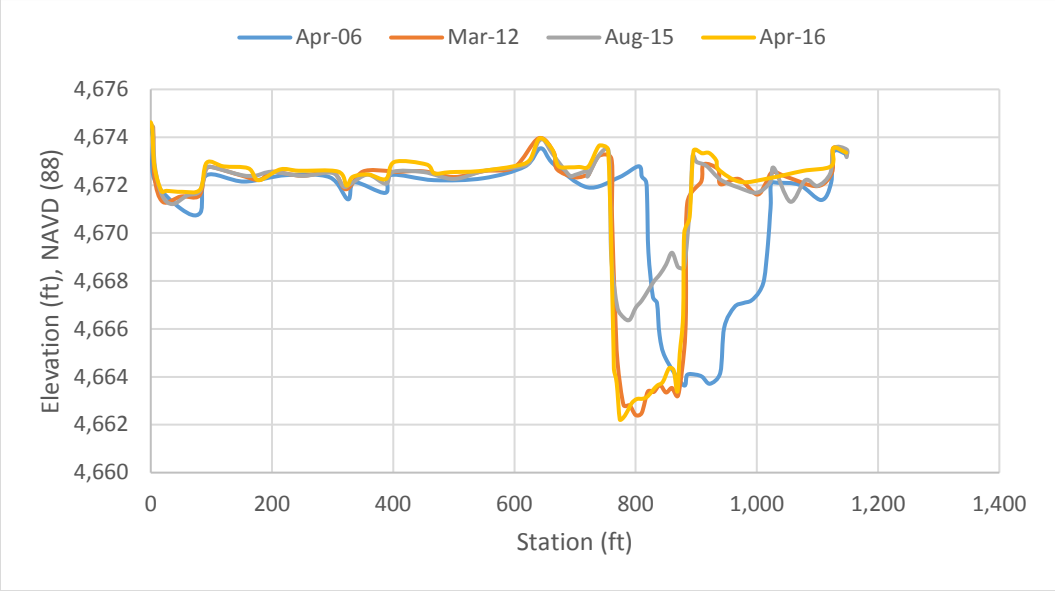

Figure 71. Rio Puerco (RP-1202.5) cross section survey comparison.

RP-1203.7

The thalweg shifted 118 feet towards the right riverbank from April 2006 to March 2012. Since 2012 the thalweg has remained at this location within the cross section and cycled through periods of sediment deposition and channel incision, with the most recent being a drop in its invert elevation of five feet. Migration of the channel thalweg towards the center cross section would be preferred to prevent any detrimental impacts to the nearby Drain Unit 7 Extension that leads into the San Acacia Diversion structure.

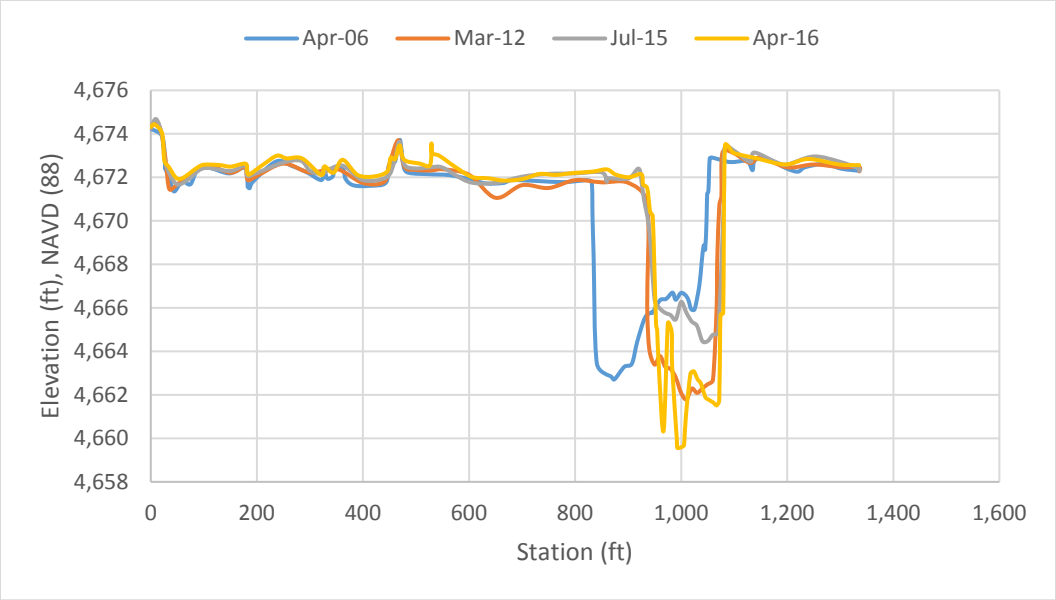

Figure 72. Rio Puerco (RP-1203.7) cross section survey comparison.

RP-1204.5

Sediment accumulation within the river left section has forced flows to concentrate at the river right. The main channel has narrowed by 60 feet since 2006 and its bed has cycled between raising and lowering elevations just as those have done immediately upstream. Channel incision from 2015 to 2016 lowered the thalweg invert by two feet. The current location of the main channel does threaten the integrity of the Drain Unit 7 Extension levee and direction of the channel towards the central cross section would relieve this hydraulic pressure.

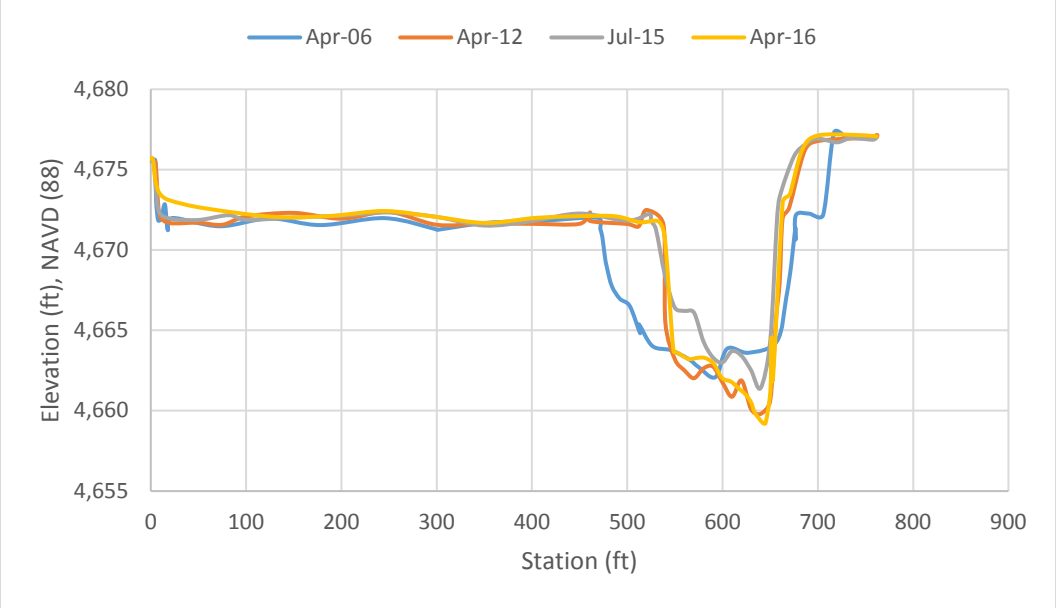

Figure 73. Rio Puerco (RP-1204.5) cross section survey comparison.

RP-1205

Sediment accumulation on the river left bank again has forced flow to concentrate at the river right and directly adjacent to the Drain Unit 7 Extension levee. The channel bed incised here from 2000 to 2012 by six feet, filled back in with four feet of sediment until 2015, and incised again by 2016 to its 2006 depth. From 2006 to 2012 the main channel shifted inwards by 25 feet and has widened towards the section center with each subsequent survey.

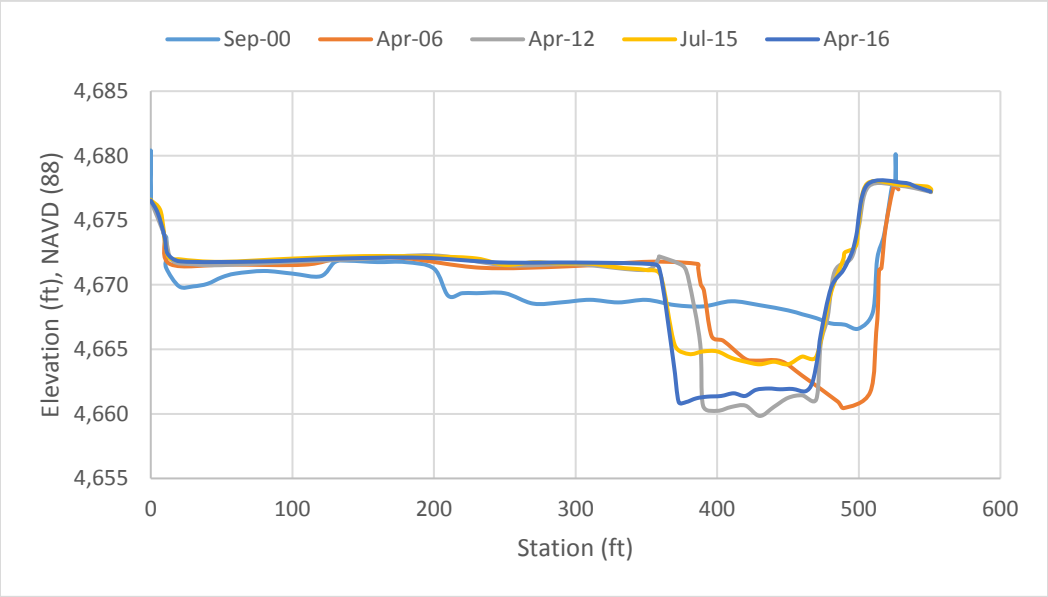

Figure 74. Rio Puerco (RP-1205) cross section survey comparison.

RP-1205.8

This section lies directly upstream of the San Acacia Diversion Dam. Since 2006 the channel has widened by 58 feet and experienced both sediment deposition and incision within the bed. The most recent incision by the thalweg lowered the bed elevation by up to seven feet at some locations.

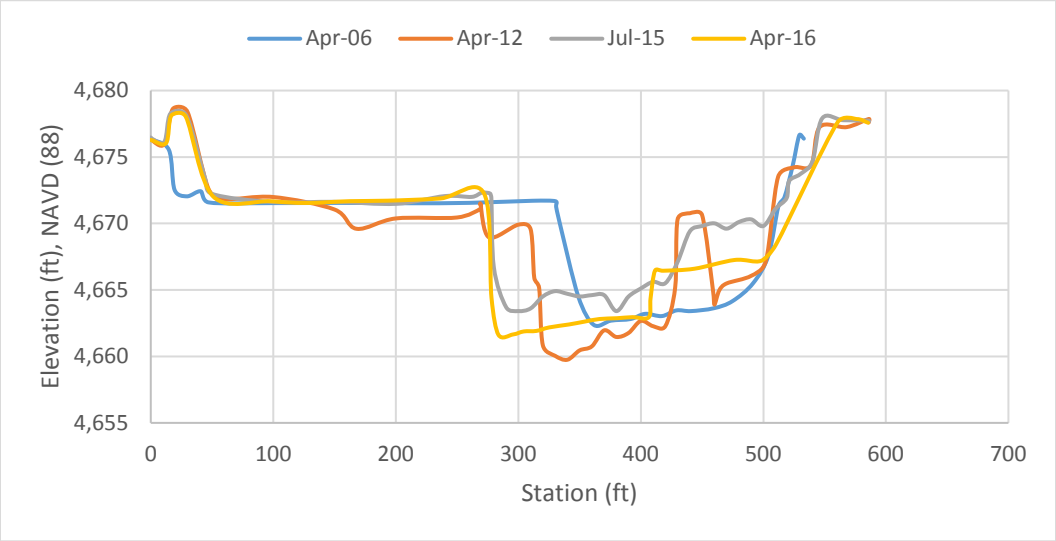

Figure 75. Rio Puerco (RP-1205.8) cross section survey comparison.